REPORT NO.
UCB/EERC-90/21
DECEMBER 1990

EARTHQUAKE ENGINEERING RESEARCH CENTER

OBSERVATIONS AND IMPLICATIONS OF TESTS ON THE CYPRESS STREET VIADUCT TEST STRUCTURE

by

MARTIN E. BOLLO
STEPHEN A. MAHIN
JACK P. MOEHLE
ROY M. STEPHEN
XIAOXUAN QI

Report to the California Department of Transportation

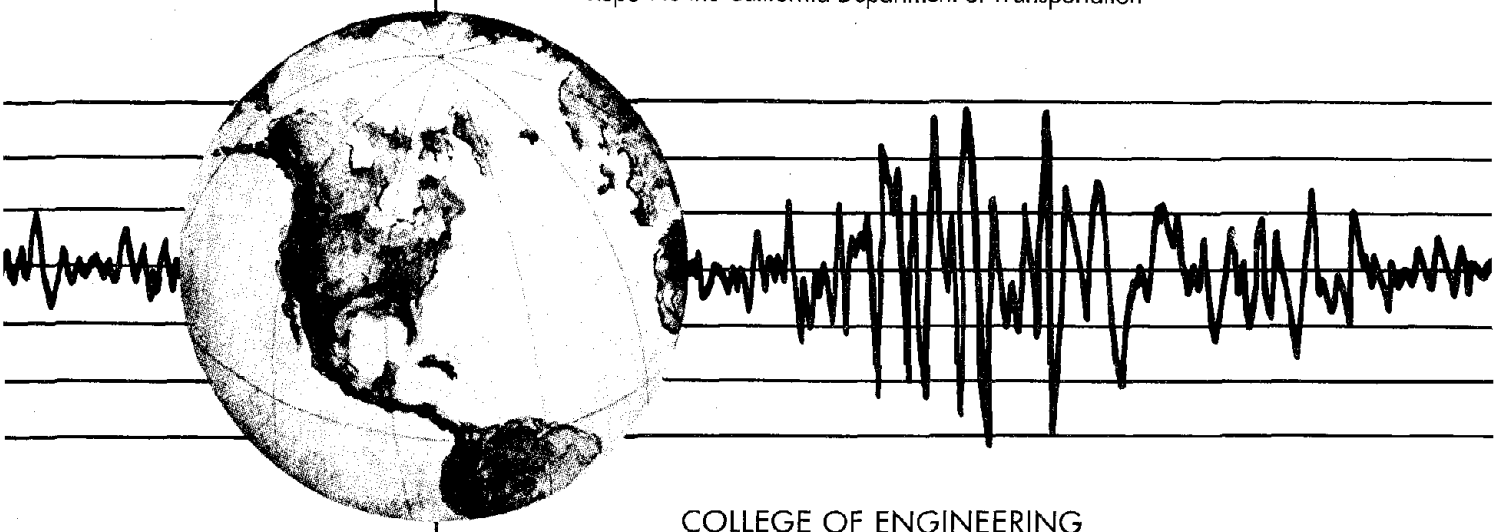

COLLEGE OF ENGINEERING

UNIVERSITY OF CALIFORNIA AT BERKELEY

For sale by the National Technical Information Service, U.S. Department of Commerce, Springfield, Virginia 22161

See back of report for up to date listing of EERC reports.

DISCLAIMER

Any opinions, findings, and conclusions or recommendations expressed in this publication are those of the authors and do not necessarily reflect the views of the Sponsors or the Earthquake Engineering Research Center, University of California at Berkeley.

50272-101

REPORT DOCUMENTATION PAGE	1. REPORT NO. UCB/EERC-90/21	2.	3. PB93-114775

4. Title and Subtitle
Observations and Implications of Tests on the Cypress Street Viaduct Test Structure

5. Report Date
December 1990

6.

7. Author(s)
M.E. Bollo, S.A. Mahin, J.P. Moehle, R.M. Stephen, and X. Qi

8. Performing Organization Rept. No.
UCB/EERC-90/21

9. Performing Organization Name and Address
Earthquake Engineering Research Center
University of California, Berkeley
1301 So. 46th Street
Richmond, Calif. 94804

10. Project/Task/Work Unit No.

11. Contract(C) or Grant(G) No.
(C)
(G)

12. Sponsoring Organization Name and Address
Earthquake Engineering Research Center
University of California, Berkeley
1301 So. 46th Street
Richmond, Calif. 94804

13. Type of Report & Period Covered

14.

15. Supplementary Notes

16. Abstract (Limit: 200 words)

During the October 17, 1989 Loma Prieta earthquake, a 3/4-mile length of the upper deck of the viaduct collapsed suddenly onto the lower deck. Following the earthquake, a series of experiments was carried out on an undamaged portion of the viaduct in order to identify the structural causes of the collapse as well as to study ways of retrofitting other similar freeways. Results of these tests are reported, analyzed and interpreted in this report. Experiments conducted include low amplitude forced vibration tests to determine the dynamic characteristics of the structure and high amplitude static load tests to assess the strength, stiffness and toughness of the structure. Both sets of tests focused on response in the transverse direction and were conducted on the structure in its original configuration as well as following partial retrofit. Three different partial retrofits were attempted to mitigate problems with the lower joint region. These (1) added a steel strongback to the columns, (2) encased the pedestal in a steel jacket, and (3) reinforced the joint with steel anchors grouted in inclined holes drilled through the joint/pedestal region. The final tests of the retrofitted structure were carried out cyclically to deformation levels resulting in severe damage. The test results indicate the importance of considering the strength and deformability of joints when evaluating and retrofitting such highway structures and of identifying the likely hierarchy of member and joint failures. Simply repairing and strengthening damaged elements is not a guarantee of satisfactory behavior. In such cases, damage may shift to other undesirable locations. Design implications resulting from these tests are identified.

17. Document Analysis a. Descriptors

b. Identifiers/Open-Ended Terms

c. COSATI Field/Group

18. Availability Statement:	19. Security Class (This Report)	21. No. of Pages
Release Unlimited	unclassified	289
	20. Security Class (This Page) unclassified	22. Price

(See ANSI-Z39.18) See Instructions on Reverse

OPTIONAL FORM 272 (4-77)
(Formerly NTIS-35)
Department of Commerce

OBSERVATIONS AND IMPLICATIONS OF TESTS ON THE CYPRESS STREET VIADUCT TEST STRUCTURE

by

Martin E. Bollo
Stephen A. Mahin
Jack P. Moehle
Roy M. Stephen
Xiaoxuan Qi

Department of Civil Engineering

and

Earthquake Engineering Research Center

University of California at Berkeley

Report No. UCB/EERC-90/21
December 1990

/B

ABSTRACT

The Cypress Street viaduct was a double deck portion of Interstate 880 located in the western part of Oakland, California. The reinforced concrete structure was designed in the early 1950's and construction was completed in 1957. During the October 17, 1989 Loma Prieta earthquake, a 3/4-mile length of the upper deck of the viaduct collapsed suddenly onto the lower deck, resulting in 42 fatalities and scores of injuries. Following the earthquake, a series of experiments was carried out on an undamaged portion of the viaduct in order to identify the structural causes of the collapse as well as to study ways of retrofitting other similar freeways. Results of these tests are reported, analyzed and interpreted in this report.

Experiments conducted include low amplitude forced vibration tests to determine the dynamic characteristics of the structure and high amplitude static load tests to assess the strength, stiffness and toughness of the structure. Both sets of tests focused on response in the transverse direction and were conducted on the structure in its original configuration as well as following partial retrofit. Three different forms of partial retrofit were considered. The final tests of the retrofitted structure were carried out cyclically to deformation levels resulting in severe damage.

The tests confirmed that collapse in the typical bent was likely triggered by a local failure involving the short pedestal that connected the upper level columns to the lower bent cap - column joint. Shear forces in the columns resulted in inclined cracks at the base of the pedestal which extended downward and outward through the joint. As was common at the time of construction, transverse reinforcement was not placed in the joint to resist shear or to provide confinement. As a result, the joint was the weak link for the shear resistance of the column and pedestal. Tests during demolition, and subsequent analyses, clearly indicate that an inclined shear failure in the pedestal/joint region would be sufficient to produce collapse of the upper deck.

The tests indicate that the typical bent would likely be able to resist an effective base shear equal to approximately 32% of its weight before failure. This value is far greater than the 6% working stress coefficient employed in the original design. Simple elastic and plastic static analyses used in conjunction with conventional design formulae were able to predict the location of the failure in the typical bent, as well as the approximate load at which this failure occurred. Elastic dynamic analyses of the test structure indicate forces and displacements 60% greater than those needed to initiate failure for a ground motion recorded during the Loma Prieta earthquake near the viaduct. While other factors (such as traveling seismic waves, soil-structure interaction, configuration irregularities, and detailing used for atypical bents) all likely contributed to the failure of the viaduct, this study shows that elementary deficiencies in the transverse structural framing were sufficient to explain the observed failure.

Three different partial retrofits were attempted to mitigate the problems with the lower joint region. These (1) added a steel strongback to the columns, (2) encased the pedestal in a steel jacket, and (3) reinforced the joint with steel anchors grouted in inclined holes drilled through the joint/pedestal region. Retrofitting had little effect on the overall lateral stiffness. However, retrofitting increased the apparent strength by 184%, and deformability by 1150%. Stable hysteretic loops were developed through a ductility of 2.5, and a single excursion to a displacement ductility of about 6 was achieved.

The first two retrofit types were unable to maintain composite action and areas of severe local distress were observed. The grouted joint anchors proved effective for the loading imposed, but construction problems and their behavior under different loading conditions suggest the need for further investigation. During the retrofit tests the upper joints of all bents suffered failures, with wide diagonal cracks developing and large portions of the concrete cover spalling by the end of the test. The tests indicate that a majority of the global inelastic deformations achieved by the retrofitted structure is associated with this shear distress, rather than with ductile flexural yielding of retrofitted members.

Because of the severity of this damage, it is unlikely that the retrofitted structure could have sustained additional load cycles in its final damaged condition.

The test results indicate the importance of considering the strength and deformability of joints when evaluating and retrofitting such highway structures and of identifying the likely hierarchy of member and joint failures. Simply repairing and strengthening damaged elements is not a guarantee of satisfactory behavior. In such cases, damage may shift to other undesirable locations.

Design implications resulting from these tests are identified in this report. However, it is not possible on the basis of a single test program to make far ranging and comprehensive recommendations for evaluation and retrofit of reinforced concrete bridge structures. Issues requiring further investigation are identified in the concluding remarks.

ACKNOWLEDGMENTS

The work reported herein could not have been carried out without the extraordinary efforts of many individuals and organizations. The authors owe a tremendous debt of gratitude to all of those who gave generously of their time, effort and advice.

The California Department of Transportation must receive special acknowledgment for the vision to initiate these tests and for providing the fiscal and manpower resources to see them completed. Especially appreciated are the leadership and support provided by James Roberts, Chief of the Division of Structures, and Burch Bachtold, until recently, Director of District 4.

Robert M. Jones and Irving A. Schroeder, Caltrans Associate Bridge Engineers, were an integral part of the research team and their continuous presence on-site during the planning and execution of the tests is greatly appreciated. Their efforts in designing the loading frame and retrofits, and in helping with the construction and test logistics, were vital to the success of the project.

In addition, Steve MacLennan, Caltrans Senior Bridge Engineer, and David Bruder, Associate Bridge Engineer, provided invaluable assistance in preparing and carrying out the field tests. Albert Sequeira, Senior Electronics Engineer, and his staff from the Caltrans Division of New Technology provided essential help in calibrating and installing some of the instrumentation. The assistance of numerous staff engineers from the Caltrans' District 4 Maintenance Office is also appreciated, especially the efforts of Camilo Abreu, Vince Ramirez and Werner Stephenson. The guidance of James Gates, Caltrans project manager for these investigations is gratefully acknowledged.

In order to complete the tests on schedule, a high level of dedication, professionalism and cooperation was required on the part of the contractor and the construction trades. Special thanks are given to W. Bourke Harris, President, and Alan Straub, Vice President, of Christie Constructors, Inc. for

the fine efforts of their team. In addition, members of Iron Workers Local 378 in Oakland are commended for their part in carrying out a difficult and sometimes tedious assignment with precision, dispatch and good humor.

The authors especially wish to thank the many staff and students of the University of California at Berkeley who participated in the research program. Staff members Richard Parsons and William MacCracken were almost continuously involved with performing the tests. Numerous graduate students helped instrument, analyze and observe the tests. These include Mark Aschheim, Ruben Boroschek, Luis Bozzo, Victor Cheng, Joel Conte, Jose Martinez-Cruzado, Allah-Nawaz Qaisrani, Robert Sarnoff and Stephen Welch. Dr. I. Takewaki, Dr. Yin Changyin, and Dr. J.W. Wallace helped with the tests. The assistance of Patricia Alvarez in preparing the manuscript is greatly appreciated.

The financial support of the California Department of Transportation to conduct and interpret the tests is gratefully acknowledged. The National Science Foundation provided supplemental funds to assist in the analysis of the results.

The findings, opinions and conclusions presented in this report are those of the authors. They do not necessarily represent the recommendations or policy of the sponsors or other individuals involved with the research program.

PREFACE

To assist other investigators in evaluating and analyzing the test results presented in this report, experimental data is available in digital form. Diskettes containing the test results may be obtained from the National Information Service for Earthquake Engineering at 404A Davis Hall, University of California, Berkeley, CA 94720.

TABLE OF CONTENTS

Page

Abstract i

Acknowledgments iv

Preface vi

Table of Contents vii

List of Tables ix

List of Figures x

1. OVERVIEW OF THE TEST STRUCTURE AND TEST PROGRAM 1

1.1 Description of the Cypress Street Viaduct Structure 1
1.2 The Loma Prieta Earthquake 2
1.3 Performance of the Viaduct during the Loma Prieta Earthquake 3
1.4 Object and Scope of the Cypress Street Viaduct Test Program 4

2. DESCRIPTION OF THE TEST STRUCTURE AND EXPERIMENTS 5

2.1 Introduction 5
2.2 Description of the Test Structure 5
2.3 Description of Retrofits 8
2.3 (a) Original Structure 8
2.3 (b) Retrofitted Structure 9
2.4 Test Program 12
2.4 (a) Dynamic Tests 12
2.4 (b) Static Tests 13
2.4 (c) Instrumentation and Data Acquisition 14

3. TEST RESULTS 16

3.1 Introduction 16
3.2 Dynamic Properties of the Original Structure 16
3.3 Static Test of the Original Structure 17
3.4 Dynamic Properties of the Retrofitted Structure 19
3.5 Static Test of the Retrofitted Structure 19
3.5 (a) Load Cycle to 900 Kips (Cycle 1) 20
3.5 (b) Load Cycles to 1800 Kips (Cycles 2 to 5) 20
3.5 (c) Load Cycles to 2700 Kips (Cycles 6 to 8) 23
3.5 (d) Load Cycles to 3300 Kips (Cycles 9 to 13) 27
3.5 (e) Final Load Cycles to 4000 Kips (Cycles 14 to 16) 35
3.5 (f) Final Damage Condition 44
3.5 (g) Summary 45

4. ANALYSIS OF EXPERIMENTAL RESULTS 50

4.1 Introduction 50
4.2 Original Structure 50

4.2 (a) Strength 50
4.2 (b) Stiffness and Dynamic Characteristics 58
4.2 (c) Expected Response During Loma Prieta Earthquake 59
4.3 Retrofitted Structure 60
4.3 (a) Global Strength 60
4.3 (b) Behavior of Retrofitted Bents 63
4.3 (c) Behavior of Upper Joints 68

5. CONCLUDING REMARKS 70

5.1 General 70
5.2 Construction and Test Issues 71
5.3 Original Structure 71
5.4 Retrofitted Structure 72
5.5 Recommendations for Future Research 75

REFERENCES 76

TABLES 78

FIGURES 92

APPENDIX A 196

APPENDIX B 198

APPENDIX C 262

LIST OF TABLES

Table		Page
2.1	Testing and construction schedule	78
2.2	Calculated deck, bent-cap and column weights	79
2.3	Original structure transducer locations	80
2.4	List of instruments	83
3.1	Lateral load test: original structure	88
3.2	Lateral load test: retrofitted structure	89
3.3	Concrete core test results	90
3.4	Rebar sample locations	90
4.1	Calculated section strengths	91

LIST OF FIGURES

Figure		Page
1.1	Map showing the location of the epicenter of the viaduct	92
1.2	Map of the Cypress Street viaduct area	93
1.3	Typical deck section and reinforcement	94
1.4	Bent reinforcing details	95
1.5	Bent reinforcement and pedestal detail	96
1.6	Reinforcing steel stress-strain curve	97
1.7	Cypress viaduct soil profile	98
1.8	Locations of accelerometers near the Cypress Street viaduct	99
1.9	Recorded accelerations obtained at Emeryville office building	99
1.10	Recorded accelerations obtained at Oakland 2-story office building and response spectra	100
1.11	Recorded accelerations obtained at Oakland Wharf and response spectra	101
1.12	Collapse of the I-880 Cypress St. viaduct	102
1.13	Collapse of the I-880 Cypress St. viaduct	102
1.14	Close-up view of failed column	103
1.15	Standing deck span at 26th street	103
1.16	Joint cracking indicative of incipient failure	104
1.17	Joint cracking	104
1.18	View of failed upper column	105
1.19	Fallen upper column	105
2.1	Cypress St. viaduct test structure	106
2.2	South end of test structure showing ragged edge of deck	107
2.3	Ground level photo showing Bents 47-48	107
2.4	Ground level photo showing separation of test specimen from off-ramp	108
2.5	Aerial photo showing test specimen and adjacent off-ramp	108
2.6	Photo showing hole in lower deck for loading frame	109
2.7(a)	Original crack locations on Bent 45	110
2.7(b)	Original crack locations on Bent 46	111
2.7(c)	Original crack locations on Bent 47	112
2.8(a)	Existing cracks in joint regions of Bent 45	113
2.8(b)	Existing cracks in joint regions of Bent 46	114
2.8(c)	Existing cracks in joint regions of Bent 47	115
2.9(a)	Original crack locations on east face	116
2.9(b)	Original crack locations on west face	117
2.10	Photos of typical crack locations prior to testing	118
2.11	Original structure retrofit (typical)	119
2.12	Photo of original structure retrofit	120
2.13	Original structure retrofit close-up	120
2.14(a)	Bent 45 retrofitting plans	121

2.14(b) Bent 45 retrofitting plans 122
2.15(a) Bent 46 retrofitting plans 123
2.15(b) Bent 46 retrofitting plans 124
2.16(a) Bent 47 retrofitting plans 125
2.16(b) Bent 47 retrofitting plans 126
2.16(c) Bent miscellaneous details 127
2.17 Bent 45 retrofit details 128
2.18 Bent 46 retrofit details 129
2.19 Bent 47 retrofit details 130
2.20 Forced vibration test 131
2.21 Forced vibration generator 132
2.22 Vibration generator housing on top deck 132
2.23 Vibration force vs. speed non-counter balanced 133
2.24 Loading frame photo 134
2.25 Loading frame 135
2.26 Loading frame details 136
2.27 Hydraulic jacking system schematic 137
2.28 Linear potentiometer locations, original strucutre 138
2.29 Bent 46 linear potentiometer locations 139
2.30 Additional instrument locations 140
2.31(a) Wire pot locations: all bents 141
2.31(b) Bent 45: strain gage locations 141
2.31(c) Bent 45: wide flange strain gage locations 142
2.31(d) Bent 45: linear pot locations 142
2.31(e) Bent 45: coupler locations 143
2.31(f) Bent 46: strain gage locations 143
2.31(g) Bent 46: linear pot locations 144
2.31(h) Bent 46: west end linear pot locations 144
2.31(i) Bent 46: east end couplers 145
2.31(j) Bent 46: west end couplers 145
2.31(k) Bent 47: strain gage locations 146
2.32 Bent 46 lower joint and pedestal instrumentation 147
2.33 Bent 46 top joint instrumentation 148
2.34 Rebar strain gages 148

3.1 Forced vibration responses measured from original structure 149
3.2 Normalized displacements derived from forced vibration of the original structure 150
3.3 Load-displacement relationships for original structure 151
3.4 Load-drift relationships for original structure 152
3.5 Damage to the west end of Bent 46 during static load tests on the original structure 153
3.6 Damage to the west end of Bent 46 after the original tests 153
3.7 Forced vibration responses measured from retrofitted structure 154

3.8	Normalized displacements derived from forced vibration tests	155
3.9	Measured mode shapes of retrofit structure	156
3.10	Loading pattern: original structure	157
3.11	Displacement history of retrofitted structure	158
3.12	Bent 45 load-displacement relationship	159
3.13	Bent 46 load-displacement relationship	160
3.14	Bent 47 load-displacement relationship	161
3.15	Comparison of original load-displacement relationships	162
3.16	Bent 45 load-drift relationship	163
3.17	Bent 46 load-drift relationship	164
3.18	Bent 47 load-drift relationship	165
3.19	Ratio of average lower to upper deck deflections	166
3.20	Bent-top deflection ratios for different bents	166
3.21	Inclined cracks in lower joint of NE face of Bent 45 after Cycle 7	167
3.22	Diagonal crack formation in the top east joint of Bent 45 after Cycle 7	167
3.23	Bent 46 after Cycle 7	168
3.24	Crack formations in lower joint of the west end of Bent 45 after Cycle 8.	168
3.25	Coupler-force joint-displacement relationship in lower joint of Bent 45	169
3.26	Column shear cracks formed on the west end column of Bent 46 during Cycle 8.	170
3.27	West end, Bent 46 upper joint shear angle	171
3.28	Diagonal crack formation in the top east joint of Bent 45 after Cycle 9.	172
3.29	Diagonal crack formation after Cycle 10, upper east joint, Bent 45	172
3.30	Separation of wide flange retrofits from columns	173
3.31	Inclined cracks formed after Cycle 12, upper joint of NW face of Bent 46	174
3.32	Bent 45, west column. Shear key horizontal crack under last (4000 kip) load cycle	174
3.33	Bent 46, west column. Deflected shape under 4000 kip load	175
3.34	Bent 47, west column deflected shape under 4000 kip load	175
3.35	Bent 46, west column shear key opening and horizontal flexural crack at lower deck level (bottom of upper column) under 4000 kip load	176
3.36	Buckled HSS-section, top west joint of Bent 47	176
3.37	Damage to the east end of Bent 45	177
3.38	Damage to the west end of Bent 45	178
3.39	Damage to the east end of Bent 46	179
3.40	Damage to the west end of Bent 46	180
3.41	Damage to the east end of Bent 47	181
3.42(a)	Damage to the west end of Bent 47	182
3.42(b)	Damage to the top joints on the east end of Bent 47	183
3.43	Core drill locations	184
4.1	Bent collapse mechanisms	185
4.2	Local collapse mechanism internal forces	186
4.3	Lateral force needed to resist tendency of outward motion of roller support	

	on a simple portal frame	187
4.4	Moments and shears due to gravity alone	187
4.5	Potential critical shear crack locations as a function of end conditions	188
4.6	Pedestal shear failure stick model collapse mechanism	189
4.7	Computer analysis model	189
4.8	Measured and calculated load-displacement relationship	190
4.9	Calculated mode shapes of analytical model	191
4.10	Top displacement history	192
4.11	Top acceleration history	192
4.12	Base shear history	192
4.13	Load-displacement relationships: original and retrofitted	193
4.14	Comparison between load-displacement relationship and measured and calculated strength levels	194
4.15	Composite forces on Bent 45	195
4.16	Maximum shear stress in joint	195

1. OVERVIEW OF THE TEST STRUCTURE AND TEST PROGRAM

1.1 Description of the Cypress Street Viaduct Structure

The Cypress Street viaduct was a double-deck portion of Interstate 880 located in the western part of Oakland, California (Figs. 1.1 and 1.2). The structure extended in an approximately north-south orientation for a length of about 1.5 miles. The viaduct had been designed in accordance with the 1953 AASHTO specifications [1.3], and was constructed between 1955 and 1957. For over thirty years the structure served as a major freeway linking the northern and southern regions of the San Francisco Bay Area.

The roadway structure consisted of multi-cell reinforced concrete box girders supported on either reinforced concrete or combined reinforced/prestressed concrete bents. Figure 1.3 illustrates the most common box girder cross section and supporting bent elevation. The typical box girder had a width of 54 feet and a span of approximately 70 feet. Deck expansion joints were provided typically every third span.

The majority of bents along the viaduct had the configuration illustrated in Fig. 1.4 [1.4]. This typical bent consisted of reinforced concrete bent caps framing rigidly into reinforced concrete columns. The upper columns were connected at their base to the lower bent cap through 27-in. tall pedestals. Hinged joints were provided between the pedestals and upper level columns as shown in Fig. 1.5. The columns in the lower level were also connected through hinged joints to reinforced concrete pile caps.

Bents of different configuration were also used along the length of the viaduct, primarily at locations where ramps entered and exited the freeway, and where the upper and lower decks merged and diverged at either end of the viaduct length. A complete description of the viaduct geometry is presented elsewhere by Nims, et al. [1.2].

Concrete in the structure was specified to be normal weight with a design working stress of 1250 psi. Mild reinforcement was specified to be Grade 40. Tests of materials in November and December 1989 [1.5] indicated an average concrete compressive strength of 6275 psi and a reinforcement yield

strength of 43 ksi (Fig. 1.6). Additional material tests have been performed by a variety of investigators and are summarized in Ref. 1.6.

The structure was supported on pile foundations. Pile lengths and soil conditions varied considerably along the viaduct length (Fig. 1.7). In the northern half, the structure was supported on fill underlain by soft clay and slightly compact clayey silts or sands, with firmer material located at a depth of approximately 40 to 60 ft. In the southern half, the structure was supported on a layer of loose to dense material, with dense bearing material at a depth of approximately 20 ft. Depth to bedrock was in excess of 500 ft. along the entire length. Soil characteristics to bedrock have been identified in detail and reported [1.8] for two locations along the viaduct (near Bents 44 and 89). Lateral load tests of two pile caps were reported in Ref. 1.9.

1.2 The Loma Prieta Earthquake

The Loma Prieta earthquake occurred at 5:04 pm on 17 October 1989 [1.10]. The epicenter was near Santa Cruz, about 60 miles southwest of the Cypress Street viaduct. The surface wave magnitude was 7.1. The duration of strong ground shaking was between 10 and 15 sec in the epicentral region, which is relatively short for this intensity of earthquake.

No instrumental response records for the Loma Prieta earthquake are available at the Cypress Street viaduct. However, ground motion records were obtained at four sites within 2-1/2 miles of the viaduct (Fig. 1.8). Peak recorded accelerations ranged between 18 and 29 percent of gravity at these sites. Recorded ground motions and computed linear elastic response spectra for three nearby sites are shown in Figs. 1.9 through 1.11. Considering general similarities in soil conditions and proximity, the Oakland Wharf and Emeryville records might be considered representative of possible records occurring in the northern section of the Cypress Street viaduct.

1.3 Performance of the Viaduct during the Loma Prieta Earthquake

During the earthquake a 3/4-mile length of the upper deck of the Cypress Street viaduct collapsed onto the lower deck (Figs. 1.2, 1.7 and 1.12 through 1.15). The collapse extended from the northern end of the viaduct to 26th Street, at which location two bents and one deck span remained standing (Fig. 1.15), and from there south to 18th Street. South of 18th Street, the viaduct sustained visible damage ranging from none (no apparent cracking) to severe (joint cracking indicative of incipient joint failure and possible collapse (Fig. 1.16)). A detailed description of the collapse has been reported elsewhere [1.2, 1.13].

Based on damage observations (e.g., see Figs. 1.16 through 1.19), it appears that the collapse of the typical bent was triggered by failure of the reinforced concrete section that includes the lower beam-column joint and the upper column pedestal just above the joint. Beam-column joints just to the south of the collapsed portion of the viaduct showed cracking damage suggestive of the type of failure observed in the northern portion (Fig. 1.16). The damage shown in Fig. 1.16 occurred in a typical bent of the type illustrated in Fig. 1.4. Other types of frames are likely to have sustained damage and collapse modes different from that shown in Fig. 1.16. However, in all types of frames the collapse appears to have involved failure of the connection between the lower bent cap and the upper column [1.2]. Collapse of the structure is believed to have resulted in several secondary failures such as shear failures in columns, and connection failures in the upper beam-column joints. Demolition photos (Appendix A) demonstrate how local damage to a column could have contributed to a progressive collapse of the structure.

The basic causes and precise sequence of collapse have been the subject of considerable speculation and discussion. The failure of the structure was surely the result of a combination of several factors, and the relative importance of each of these is currently not completely known. Among the unresolved issues are the importance of transverse and longitudinal motions, of variable soil conditions, of traveling seismic and response waves, of global structural configuration and of local structural details. More detailed investigations are needed to assess the relative importance of these and other factors relative to the collapse of the Cypress Street Viaduct and the retrofit of other similar structures.

1.4 Object and Scope of the Cypress Street Viaduct Test Program

A length of the Cypress Street viaduct remained apparently undamaged following the Loma Prieta earthquake. A series of experiments was carried out on a portion of the undamaged viaduct in order to provide an indication of the structural causes of the collapse during the earthquake, as well as to study ways of retrofitting similar freeway structures located in California. The portion of the viaduct between 13th Street and 14th Street in Oakland (i.e., Bents 45 through 47) was selected for testing [Fig. 1.2]. All of the bents within the test structure had the same geometry and detailing as illustrated in Figs. 1.3 through 1.5.

The experiments conducted included low amplitude forced vibration tests and high amplitude static tests, both focusing on response in the transverse direction. The tests were conducted on the structure in its original configuration and following partial retrofit. The final tests on the retrofitted structure were carried out to deformation levels resulting in severe damage to the structure.

This report presents results of the experimental study and associated preliminary analytical work. The report is designed to illustrate the main features of the experiment as well as some of the implications that are believed to be important in conducting seismic evaluations and in planning retrofits of similar structures.

2. DESCRIPTION OF THE TEST STRUCTURE AND EXPERIMENTS

2.1 Introduction

This chapter describes the field tests that were conducted on a portion of the Cypress Street viaduct. Section 2.2 describes the configuration, structural details, and initial condition of the test structure. Section 2.3 describes retrofits that were carried out in the course of the test program. Section 2.4 presents details of the test program. A schedule of the testing program is provided in Table 2.1.

2.2 Description of the Test Structure

A segment of the Cypress Street viaduct structure between 13th and 14th Streets in Oakland was selected for destructive field tests following the Loma Prieta earthquake. The segment included three bents (Bents 45, 46 and 47) plus upper and lower decks spanning between and cantilevering beyond the bents (Fig. 2.1). Preliminary visual surveys of the viaduct indicated that this portion of the freeway had not been significantly damaged by the earthquake. Ambient vibration tests had been conducted at this location shortly following the earthquake, as reported by Nims, et al. [1.2].

Prior to testing, the test structure was isolated from the surrounding portions of the viaduct using conventional demolition techniques. To the south of Bent 45, the upper and lower decks were partially removed, leaving a ragged-edged cantilever spanning approximately 15 feet beyond Bent 45 (Fig. 2.2). A deck expansion joint was located 12 feet to the north of Bent 47. The upper deck was removed beyond that joint. The lower deck beyond that joint and the lower column of Bent 48 were retained (Fig. 2.3). During lateral load tests of the structure the lower deck north of the expansion joint was isolated from the rest of the structure by jacking it upward and shoring it away from the main test structure. During the test program an expansion joint seat extender detail was tested by Caltrans using this lower deck expansion joint. The hinge restrainer test is not described in this report (see Dubovik et al. [2.1]).

An off-ramp leading from the upper deck was located to the west of the test structure. The ramp was physically isolated from the main test structure and the separation was increased prior to testing by

partial demolition of the offramp. The offramp was retained as an observation and access deck (Figs. 2.4 and 2.5).

The three bents of the test structure (Bents 45, 46, and 47) were of the type shown in Figs. 1.3 through 1.5. Both the upper and lower bent caps are of reinforced concrete, framing rigidly into supporting reinforced concrete columns. The upper columns were supported on "hinges" located 27 inches above the top of the lower deck. The hinges were formed by placing a half-inch thickness of soft expansion joint material around the column perimeter at this location, leaving a 20-in. by 36-in. section of concrete continuous vertically through the joint (Figs. 1.4, 1.5). The continuous section of concrete was reinforced with four 52-inch lengths of vertical #11 bar. Similarly formed hinges connected the lower columns and the pile caps.

Each of the bents was supported on pile caps. A cap was in turn supported on 19 piles having an average length of 16.7 feet at the test site.

The main longitudinal reinforcement in the bent caps consisted of #11 and #18 Grade 40 bars. At the intersection with the inside face of the supporting columns, the longitudinal reinforcement ratio was 0.0028 (top) and 0.0044 (bottom) for the upper bent cap and 0.0071 (top) and 0.0035 (bottom) for the lower bent cap. Bent cap longitudinal reinforcement at the top face was developed in the joint using 90-degree hooks. Bottom face longitudinal reinforcement (#18 bars) had a straight development length of approximately 40 inches (18 bar diameters) into the joint. Two sets of #5 bars were placed at intermediate elevations along each side face of the bent caps.

Bent cap transverse reinforcement consisted of pairs of U-shaped #6 stirrups (Fig. 1.5). At the face of the joints, the transverse reinforcement ratio was 0.0071. The product of that ratio and the nominal steel yield stress of 40,000 psi is 285 psi.

Column longitudinal reinforcement consisted of straight #18 Grade 40 bars (Fig. 1.5). With the exception of the inner layer of reinforcement in the upper column, all bars terminated at the upper end of a column within the beam-column joint 12 inches below the upper surface of the deck. Column longitudinal reinforcement ratios (ratio of total longitudinal steel area to gross concrete area at the top of the column) were 0.052 for the upper columns and 0.021 for the lower columns.

Column transverse reinforcement consisted of single #4 perimeter ties with 90-degree hooks. These ties were spaced 12 inches on center along the clear height of the columns. The corresponding transverse reinforcement ratio was 0.00069. The product of that ratio and the specified steel strength is 28 psi, 56% of the minimum value currently stipulated for nominal shear reinforcement in flexural members.

A 27-inch tall reinforced concrete pedestal was located between the top of the lower deck and the upper column hinges (Fig. 1.5). None of the main upper or lower column longitudinal reinforcement extended into this stub. Rather, the stub was reinforced vertically with fourteen 5-foot lengths of #11 bar that extended from the top of the pedestal downward into the lower beam-column joint. These overlapped the column reinforcement by approximately sixteen #11 bar diameters. In addition, the #11 dowels that reinforced the column hinge extended longitudinally down into the pedestal. Transverse reinforcement in the pedestal consisted of four pieces of #4 perimeter ties having 90-degree hooks.

Beam-column joints contained the bent cap and column longitudinal reinforcement as described in the preceding paragraphs. Transverse reinforcement consisted of C-shaped ties spaced at 18 inches on center along the exterior face of the joints (Fig. 1.5). The legs of these cap ties had a length of 6 inches.

The roadway was supported on seven-cell reinforced concrete box girders (often referred to as decks in this report) that spanned continuously between the bent caps. Details are shown in Fig. 1.3. To accommodate the loading frames used in the static lateral load tests, openings were made in the lower deck on each side of each bent (Fig. 2.6).

Calculated weights of decks, bent caps (including joints), and columns (including the stub above the top of the lower bent) are listed in Table 2.2. Normal weight concrete having a density of 150 pcf and nominal dimensions are assumed in these calculations. Actual density and dimensions were found to be effectively the same as the nominal values. The total calculated weight of the upper deck, upper bent caps, and upper halves of columns was nearly 2780 kips. The total calculated weight of the entire structure above the piles caps was 5700 kips.

Crack patterns and maximum crack widths were observed visually and recorded before testing. These are presented in Figs. 2.7 through 2.10. Damage was observed to increase, especially in the lower

joint regions, during the demolition process. Consequently, the test structure had significant inclined cracking in the lower joints on the east side of the structure at the time of the tests.

2.3 Description of Retrofits

The test structure was retrofitted in two phases. The first phase retrofits were relatively minor and were intended to increase safety during tests of the original structure, but otherwise to have little effect on observed response. The second phase retrofits were more extensive and were intended to increase the strength and toughness of the structure as might be done in a partial field retrofit. These retrofits are described separately below under headings "Original Structure" and "Retrofitted Structure," respectively.

2.3(a) Original Structure

Minor modifications were made to the original structure so that tests to determine the original structure strength could be carried out safely. The modifications involved removal of the lower deck concrete guard rail adjacent to each column and placement of external shear reinforcement over the column pedestal and lower beam-column joint (Figs. 2.11 - 2.13).

The external shear reinforcement consisted of steel rectangular tube sections strapped onto the pedestal or lower joint using 1-3/8-inch diameter Dywidag threaded post-tensioning rods (Fig. 2.12). Above the beam-column joint, the rods were anchored to the outer steel tubes, extended across the column section, and were there anchored to steel tubes at the inner column face. Within the depth of the joint, the rods passed through drilled holes in the box girder and were anchored to the first interior web of the girder (Fig. 2.11).

With the exception of the west end of Bent 46, the post-tensioning rods described in the paragraph above were tensioned to a load of 55 kips (95 kips for the rods at the level of the bent-cap below the deck). At the west end of Bent 46, the lowest pair of post-tensioning rods was snugged tight using wrenches, and the other rods were all left loose (gaps between the tubes and the concrete were visible). The steel tubes above the lowest tube were propped on top of the lowest tube using wood blocks. During

the first cycle of the static tests, the rods were checked and found to be insufficiently loose. They were further loosened for the second cycle. All rods were tightened for the third cycle.

Using couplers, the upper two pairs of post-tensioning rods of each bent on either side of the roadway were interconnected across the deck. The rods were propped up using wood blocks during testing so as to reduce the tension carried by them.

With the modifications described above, lateral load tests were conducted by loading the upper deck toward the west. The intent of the modifications was to ensure that joint failure could occur only in the west connection of Bent 46 (for which tubes and post-tensioning rods were in place, but left loose) and not in the other joints. It is believed that the modifications had negligible effect on the overall lateral stiffness of the structure.

Prior to testing, an attempt was made to repair the cracks present in the lower joints by injecting epoxy. Cores taken from Bent 46 during preparations for the subsequent retrofit test showed that the epoxy had not penetrated across the full width of the joint.

Steel and timber shoring was installed in both levels of the test structure to ensure safety in the event of a brittle failure. The tops of the shores were separated from the deck to be supported by a gap of 1 to 2 inches. It is not believed that the shoring had any effect on the measured lateral resistance of the structure.

2.3(b) Retrofitted Structure

Following tests of the "original" structure, the test structure was extensively modified to enhance its strength and, more importantly, its toughness. Three different partial retrofit schemes were attempted, one each for Bents 45, 46, and 47. The retrofit concepts and details as finally selected were the result of a complex set of compromises arising from time, personnel, and funding constraints as well as a general restriction that the retrofits investigated should be of the "semi-permanent" type then being considered for the retrofit of the other Bay Area double deck viaducts. Reinforced concrete retrofits were not considered due to insufficient time available to fabricate the retrofits and cure the concrete prior to testing. Details of the selection process are not relevant here, and therefore are not presented.

No attempt is made in the following text to cover all details of each retrofit. Instead, only the main features are described. Complete details of the retrofits are contained in the structural drawings presented in Figs. 2.14 through 2.16.

A feature common to each retrofit was the addition of external post-tensioning rods to each bent cap (Figs. 2.14 through 2.19). The objectives of this post-tensioning were (a) to improve confinement of the column longitudinal reinforcement within the joints, (b) to improve joint confinement and strength, and (c) to improve continuity of bentcap longitudinal reinforcement. As noted previously, the joints of the original structure effectively had no transverse reinforcement, and bentcap bottom reinforcement had an anchorage length within the joint of approximately 18 bar diameters. Within the depth of the box girder, the external post-tensioning rods were anchored at the first interior web of the box girder, resulting in a span of 12 ft. These rods were prestressed to 55 kips on Bents 45 and 47, and to 50 kips on Bent 46. Rods within the depth of the joint, but below the box girder, had longer lengths (Figs. 2.14 - 2.16), and were prestressed to 50 kips on Bent 46 and 95 kips on Bents 45 and 47. The prestressing of the rods resulted in an average compressive stress at the end of the bent cap of approximately 87 psi on Bent 46 and 130 psi on Bents 45 and 47.

Another feature common to all the retrofits was the placement of external shear reinforcement over the column clear height. The shear reinforcement consisted of rectangular steel tubes post-tensioned to the column using 1-in. and 1-3/8-in. diameter threaded Dywidag rods tensioned to 55 and 95 kips each, respectively. On Bent 45, several of the rods were not tightened, as indicated in Fig. 2.14. On Bent 46, the rods on the upper columns were not initially tightened. When inclined cracking was observed during testing, the rods of Bent 46 were tightened, as described in Section 2.3. On Bent 47, rods were tightened over the full height of the upper column. The rods provide a supplementary transverse reinforcement ratio of 0.0013. The product of this ratio and the nominal capacity of the rods (130 ksi) is 170 psi. Because of the short length of these and other post-tensioning rods, seating and other losses made precise determination of forces in the rods difficult.

In addition to the retrofit features described previously, Bent 45 was retrofitted with four steel wide flange (W10 x 112) sections placed on the outer and inner faces of the columns (Figs. 2.14 and

2.17). On the east side of the structure, the outer "strongback" wide flange sections were continuous over their full height. On the west side, the outer wide flange sections extended over the full height of the structure, but they were discontinuous at the elevation of the bottom of the upper bent cap. The wide flange sections on the inside faces of the east and west side columns were discontinuous at the bottoms of the bent caps and at the top of the pedestal in the upper column (i.e., at the column hinge). The inside face of both column pedestals was reinforced using a 1-1/2-in. thick steel plate over 3/8-in. thick plywood. The wide flange sections and steel plates were held in place using steel rectangular tubes and post-tensioning rods.

Bent 46, in addition to the common retrofit features described previously, had four 1-3/8-in. diameter threaded Dywidag rods inserted in 2-in. diameter cored holes (Fig. 2.15). Grout was used to anchor the rods on the east side of Bent 46, and epoxy was employed on the west side. The holes extended from the outer face of the pedestal (just above its base) toward the bent cap, at a downward angle of 30 degrees. External anchorage for the inclined post-tensioning rods was provided by a rectangular tube section cut on a bevel and Dywidag nuts snugged tight with a wrench. In addition, steel plates were attached on the outer faces of the pedestal and joint using rectangular tubes and post-tensioning rods (Fig. 2.18). Some additional confinement was provided on the side faces of the pedestal by means of rectangular tubes and post-tensioning rods.

Bent 47, in addition to the common retrofit features described previously, had as its main retrofit feature the placement of a steel collar around the pedestal and lower portion of the upper level column (Figs. 2.16 and 2.19). The collar around the pedestal was fabricated from 2-1/2-in. thick steel plates. To facilitate construction, the collar was fabricated as two L-shaped sections which were post-tensioned together in the field using rectangular tubes and Dywidag bars. Shrinkage compensating grout was placed under the collar to account for the variable dimensions of the concrete sections at this location. Steel flanges, 1-in. thick, extended downward from the collar on the north and south sides of the lower joint. These side plates were clamped to the joint using longitudinally-oriented, 1-3/8-in. diameter, post-tensioning rods that passed through approximately 2-in. diameter holes drilled through the joints near the box girder. These holes were not grouted. One-half-inch thick steel plates extended over the full

height of the inner and outer faces of the columns in much the same way as did the wide flange sections on Bent 45. The plates were held in place using steel rectangular tubes and external post-tensioning rods.

All of the retrofit steel plates located on the west side of Bents 45, 46 and 47 had 3/8-in. thick plywood placed between the steel and the concrete columns. Plywood strips were also added on the east side of Bent 46. This plywood was introduced to reduce the composite action that could be developed by the steel retrofits on this side of the test specimen. Some composite action between the concrete and steel elements was expected for columns on the east side of Bents 45 and 47.

2.4 Test Program

A series of static and dynamic tests was performed on the original and retrofitted test structure. The test procedures are described below.

2.4(a) Dynamic Tests

Two vibration generators were attached to the upper deck (Fig. 2.20) to impart sinusoidally-varying dynamic loads in the transverse direction. A vibration generator consisted of a pair of weights that were rotated synchronously in opposite directions about a vertical axis (Fig. 2.21). The resultant centrifugal force from a generator thus varied sinusoidally as a function of speed of rotation and weight. The two generators were electronically controlled. They were placed symmetrically on the upper deck and operated simultaneously (Figs. 2.20 and 2.22). The two generators could be operated in phase to impart predominantly transverse translation, or 180 degrees out of phase to impart predominantly torsional motion. The magnitude of the applied force could be controlled by varying the total weight being reciprocated by the generator, and the rate at which it was reciprocated (Fig. 2.23).

Dynamic tests were conducted at various stages during the test program. A given test had as its objective identification of the frequency, mode shape, and equivalent viscous damping of a single dynamic response mode. For a typical test, the weight reciprocated by the vibration generator was held constant, and the frequency was varied, starting at a frequency below the estimated natural frequency of the structure, and increasing the frequency in steps. For a given frequency step, the forcing function was held

constant until the structure reached steady state, after which time response data were recorded. The frequency was then increased and the process was repeated for the next step.

In a test, the natural frequency of vibration was estimated as that frequency for which maximum response was obtained. Equivalent viscous damping was obtained using the half-power bandwidth method [2.2].

The maximum total lateral force applied by the generators in the dynamic forced vibration tests was approximately 6 kips. Assuming damping at two percent of critical in the lowest mode, with a resulting dynamic amplification of approximately 25 for steady state harmonic response, the maximum effective dynamic force is estimated to have been approximately 150 kips. This is approximately 2.6% of the total structure weight of 5700 kips.

2.4(b) Static Tests

Static lateral load tests involved externally applied loads oriented solely in the transverse direction. The lateral loads were applied to the underside of the upper deck (box girder) at each of the three bents. No lateral load was applied to the lower deck. In contrast with the dynamic tests described in Section 2.4(a), the load rate was sufficiently low as to qualify the test as being static. The magnitude of the total lateral load was as high as 4,000 kips in the final tests.

Loading was achieved using six steel loading frames, one positioned on each side of each bent (Figs. 2.24 through 2.26). A loading frame consisted of two inclined wide flange members that extended from the base of the structure (just above the pile caps) upward through holes that had been opened in the lower deck to an apex just beneath the bottom of the upper deck. Lateral load was applied between the top of the loading frame and the bottom of the upper deck using 330-ton hydraulic jacks. The jacks reacted against steel blocks that were attached to the bottom of the upper deck using post-tensioning rods that passed through the deck (Figs. 2.25 and 2.26).

The inclined members of the loading frame were attached at the base to steel sections that had been post-tensioned against the lower columns just above the pile caps (Figs. 2.24 and 2.26). Horizontal tie beams were attached just above grade level to resist the horizontal thrust developed at the base of the

frame. Thus, the loading frame was effectively internal to the structure itself. It is unlikely that significant external reactions in the form of pile forces were generated in the course of the static tests. Effects of foundation movements are therefore not included as part of the static tests.

The hydraulic jacks used in the static tests were capable of compressive loading only. Special arrangements were thus needed in order to achieve lateral deformation reversals representative of seismic loading. Six jacks (one on each side of each bent) were positioned to achieve loading to the east, and another six jacks were positioned to achieve loading to the west. The hydraulic supply was provided by a dual stage, 10,000 psi, manually controlled hydraulic pump. The jacks were connected to a common manifold so that the force applied to each jack was virtually identical. The hydraulic system used is illustrated schematically in Fig. 2.27.

A system of removable steel reaction blocks was developed to enable the jacks to be used alternately in the east and west directions without having to remove and replace the jacks (Fig. 2.26). The system greatly facilitated testing; nonetheless, each reversal of load required significant physical effort which, in turn, limited the number of load reversals possible in the time available for the tests.

2.4(c) Instrumentation and Data Acquisition

Instrumentation for the forced vibration tests consisted of accelerometers and seismometers. For determining vibration frequencies and damping properties, four accelerometers were placed in the positions shown in Fig. 2.20. For determining mode shapes, seven accelerometers and one seismometer were placed as also shown in Fig. 2.20. To ensure accurate determination of mode shapes, all accelerometers were previously cross-calibrated by fixing them adjacent to one another on the top deck of the structure while it was being vibrated at the resonant frequency. During dynamic testing, data were recorded at a rate of 50 samples per second using a microcomputer based data acquisition system.

Instrumentation for the static tests prior to retrofitting was restricted to a few instruments. The applied load from each jack was monitored using pressure gages inserted in the hydraulic lines close to each jack. Lateral displacements at both upper and lower deck levels at each bent were measured using wire potentiometers (locations are indicated in Fig. 2.28). Additional instruments were placed to monitor

deformations of the west side of Bent 46, especially in the upper column, pedestal and joint regions (Figs. 2.29 and 2.30). Information on data channel number, transducer type and transducer location is listed in Table 2.3.

Instrumentation for the retrofitted structure included the instruments used to measure the applied load and total lateral displacements described in the preceding paragraph. In addition, a variety of other instruments were installed as described below and in Fig. 2.31. A tabulation of data channel number, transducer type, and transducer location is included in Table 2.4. Instrumentation is depicted in the following figures: Figure 2.31(a) shows locations and channel numbers of pressure gages and global displacement transducers; Figures 2.31(b), (f) and (k) depict rebar strain gages (gages were welded to the exposed surface of selected rebar near beam-column interfaces); Figures 2.31(d) and (h) depict linear potentiometers used to monitor local joint and pedestal displacements; Figures 2.31(e), (i), and (j) depict post-tensioning rod couplers instrumented to record rod force; Figure 2.31(c) depicts wide flange strain gages; and Figure 2.31(g) depicts linear potentiometers used to measure column deformations. Some of the instrumentation is shown in Figs. 2.32 through 2.34.

Strain gages were applied directly to reinforcing bars in their pre-strained state. Because initial strains are not known, absolute strains can not be determined.

Data from all tests were recorded at intervals using a micro-computer based data acquisition system. During data sampling, loads on the test structure were held constant.

Deformations in Bent 47 were optically measured by Motion Analysis, Inc. The technique used and results obtained are reported elsewhere [2.3].

Whitewash was applied to the reinforced concrete joints along with some of the steel attachments and wide flange sections in order to help identify cracking and steel yielding. A visual record of cracking was logged during the test by observers equipped with binoculars. Observers were usually situated on the north and south sides of each column. Templates showing various crack widths were attached to each joint to assist in estimating crack sizes. Crack locations were marked on the structure following each major load cycle.

3. TEST RESULTS

3.1 Introduction

Basic test data and observations are presented in this chapter. More detailed analysis and interpretation of the results are contained in Chapter 4. The measured dynamic and static characteristics of the "original" structure are described in Sections 3.2 and 3.3, respectively. Section 3.4 presents information on the dynamic properties of the retrofitted structure. The behavior of the retrofitted structure when subjected to static cyclic lateral loads is described in Section 3.5.

3.2 Dynamic Properties of the Original Structure

Power spectra obtained from the accelerations recorded during the forced vibration frequency sweep tests (see Section 2.4(a)) are shown in Fig. 3.1 as a function of response frequency. These sets of data contain the first two translational vibration modes of the test structure. The magnitude of the forcing function during these tests varies with the square of the input vibration frequency. Peak acceleration response data can be normalized to correspond to peak displacement values expected for a constant magnitude sinusoidal forcing function as:

$$\text{Normalized displacement response} \approx \text{constant x measured accel. response} / (f^4) \qquad (3.1)$$

in which f is the frequency at which the measured response is recorded. This relationship accounts for the frequency-squared relation between centrifugal force and forcing frequency, and the frequency-squared relation between accelerations and displacements.

Figure 3.2 presents the resulting normalized displacement responses. The individual curves drawn in parts a) and b) of the figure show the results of each individual frequency sweep.

The first and second mode translational frequencies (periods) of the test structure are estimated from the peaks on the normalized response curves (Fig. 3.2) to be 2.4 Hz (0.42 sec.) and 7.0 Hz (0.14 sec). The equivalent viscous damping was estimated using the half-power bandwidth method to be 2.3

percent of critical in the first mode. Because of potential errors in smoothing the normalized response curves in Fig. 3.2, estimates of frequency and damping are subject to error.

Because of time limitations and technical difficulties, mode shapes were not obtained during the forced vibration tests of the original structure.

Nims, et al. [1.2] report data for ambient vibration tests conducted on the same portion of the freeway before the demolition of adjacent viaduct segments. They report transverse translational frequencies (periods) of 2.5 Hz (0.39 sec.) and 4.5 Hz (0.22 sec.) in the first and second modes, respectively. The first and second mode shapes in the transverse translational directions were reported to be (1.00, 0.45) and (1.00, -0.51). The first value in parentheses represents the ordinate at the upper deck, and the second value represents the ordinate at the lower deck level.

3.3 Static Test of the Original Structure

As described in Section 2.3(a), the static test of the original structure was carried out after five of the lower beam-column joints and the concrete pedestals just above the joints had been clamped to prevent failure. The joint and pedestal at the west end of Bent 46 were not clamped tight, although the clamping devices were in place. The purpose of this test was to assess the initial stiffness and strength of the original structure.

Static loading consisted of three cycles of load in the west direction only. Because of the potential brittleness of the non-retrofitted structure, testing was stopped at the onset of significant cracks in the lower joint/pedestal region. No load reversals were attempted.

Figure 3.3 presents the measured relations between total applied load and the displacements at the upper and lower deck levels for each bent. Figure 3.4 plots the applied load versus the average bent drift in the upper level. This drift is obtained by subtracting the transverse displacements at the two levels. The lower level deformed up to 0.092 % of its height (here taken as 23 ft - 0 in.). Drifts in the upper level were as much as 0.28% of the difference in elevation between the two decks (taken as 23 ft - 0 in.). Thus, drifts in the upper level contributed between 70 and 75% of the total displacement measured at the upper deck for the loading used in this test.

During the test the pressures applied to each hydraulic jack were effectively the same. Consequently, nearly equal load was applied to each bent. The load resisted by each bent, however, could not be measured. Lacking a clear indication to the contrary, it is assumed that each bent resists about one-third of the total applied lateral load.

As indicated in Table 3.1, three load cycles were applied. No cracking was apparent during the first cycle. Following the peak of the first cycle, the load was reduced, and clearances between the clamping devices and the concrete joint and pedestal at the west end of Bent 46 were checked. The clearances were found to be virtually non-existent at some locations. Consequently, all post-tensioning rods at this connection were loosened at this time until an approximately one-quarter inch wide gap could be observed between the clamping device hardware and the concrete.

During the second load cycle, hairline cracking at the interface between the deck and the concrete pedestal was observed along with an inclined crack in the pedestal directly below the hinge in the upper column. Loading was continued to a total load of 1410 kips. At approximately this load, cracks began to widen significantly without increasing load. The second load cycle was stopped at this stage. This load corresponds to approximately 25% of the total weight of the test structure.

The progression of cracking at the end of Cycle 2 is indicated in Fig. 3.5. Because cracks during periods of intense loading had to be observed from a distance using binoculars, it was not possible to monitor crack widths accurately.

Prior to the third load cycle (Fig. 3.3), the clamping devices in the pedestal area only (i.e. top two levels) on the west end of Bent 46 were prestressed to reduce the progression of the inclined cracks that had developed during the previous cycle. Loads were increased to a maximum of 1796 kips, or 1.27 times the maximum load reached during the second cycle. Fig. 3.6 shows the crack development at the pedestal height of Bent 46 after removal of the joint retrofit. Minor flexural cracking was observed in the upper columns.

3.4 Dynamic Properties of the Retrofitted Structure

Following application of the retrofitting measures described in Section 2.3(b), forced vibration tests were conducted again. Figures 3.7 and 3.8 present acceleration and normalized displacement response curves (normalized as described in Section 3.2). Based on the normalized response curves, the first and second transverse translational frequencies (periods) are estimated to be 2.6 Hz (0.38 sec) and 7.6 Hz (0.13 sec). Damping values in the same two modes are estimated to be 4.4 and 1.8 percent of critical based on the half-power bandwidth method. The first two torsional modes were similarly determined to have frequencies (periods) of 3.0 Hz (0.33 sec) and 8.0 Hz (0.13 sec).

Mode shapes were also identified from the dynamic tests. These are plotted in Fig. 3.9. The first mode shape is relatively linear, consistent with ambient vibration test results obtained by Nims, et al. [1.2] for this portion of the viaduct. Static test results for the original and retrofitted structure indicate that only 25 to 30% of the top displacement develops at the lower levels. During the forced vibration tests the foundation of the structure translated and rotated (Fig. 3.9). These deformations were not significant in the static tests because of the way the reaction frames were attached to the test structure. In addition, in the dynamic tests inertia forces are induced on the mass of both the upper and lower deck. Consequently, deformed shapes for the dynamic and static tests would be expected to be different.

3.5 Static Test of the Retrofitted Structure

The data from the static tests of the retrofitted structure are described in this section. Complete basic data recorded for these tests are provided in Appendix B. The data channel numbers, instrument types, and instrument locations for these data can be identified in Table 2.4 and Fig. 2.31.

The static load tests of the retrofitted structure followed the schematic load and displacement histories indicated in Figs. 3.10 and 3.11. This load pattern, involving several cycles in one direction followed by several in the reversed direction, was selected based on an estimate of the number of times the direction of loading could be changed during the time available for testing. In all, 16 load cycles were

imposed and the load direction was reversed five times. The history is not intended to be representative of any particular seismic excitation.

Results are reported below for groups of load cycles corresponding to five major target load levels: 900, 1800, 2700, 3300 and 4000 kips. Actual loads and displacements achieved in each cycle are listed in Table 3.2.

Typically, for each group of load cycles a brief discussion of the overall lateral load-displacement relations developed is provided below. This is followed by a discussion of the physical damages observed in each bent. Results for selected instruments are then examined to help characterize the damage. In addition, the chronology of damage is summarized and comments on the effectiveness of the retrofits are offered in Section 3.5(g).

3.5(a) Load Cycle to 900 Kips (Cycle 1)

A load cycle to a total force of 900 kips was initially imposed in the west direction. This loading direction was the same as that employed in the static test of the original structure. This initial test was conducted to seat the loading apparatus and to verify proper operation of the instrumentation. No structural distress was apparent as a result of this load cycle.

3.5(b) Load Cycles to 1800 Kips (Cycles 2 to 5)

The structure was next subjected to two cycles of 1800-kip (nominal) total lateral load in the west direction, followed by two similar cycles in the east direction. This load level exceeded the level at which damage in the original test structure had been observed (Section 3.3), and approximately matched the lateral load level achieved in the third cycle of the static load tests of the original structure after all of the pedestals had been clamped.

Measured relations between total lateral load and lateral displacement (Figs. 3.12 through 3.18) indicate effectively linear elastic response at this stage. Comparison of these load-displacement responses with those obtained for the original structure (see Fig. 3.15) indicates that the retrofits may have had an

increase in overall initial structural stiffness. However, on closer examination this increased stiffness appears to be due to a seating problem that existed up to a load of about 100 kips.

Upper level displacements during these cycles were approximately 0.85 in., for an overall drift index of 0.15%. Displacements at the lower deck during these cycles averaged about 28% of those measured at the upper deck (Fig. 3.19). This displacement ratio differs from the first dynamic mode shape (Fig. 3.9), which showed a lower deck displacement of 41% of the upper deck displacement. This difference is apparently associated with the differences between the static and dynamic loading used and the flexibility of the foundations which is included in the forced vibration tests and does not contribute to the deformations during the static load tests.

The loading apparatus was designed to apply the same external lateral force to each bent of the test structure. The internal distribution of forces is not known. The resulting displacements of each bent indicate that each bent displaced nearly equally at all stages of testing (Fig. 3.20).

Minor damage was noted at this stage in each of the bents. Very limited nonlinear response was recorded during these cycles by the instrumentation (see Appendix B). Detailed illustrations of cracking and other damage can be found in Appendix C. A brief narrative description of the behavior of each bent follows.

Bent 45. -- In Bent 45 small inclined cracks were noticed in the lower joint on the west side during loading to the west. These cracks initiated during Cycle 2; starting from the eastern (inside) face of the pedestal where it joined the top of the lower deck and running diagonally downward into the joint. This crack grew to have a length of about 20 in. during Cycle 3. This type of inclined cracking was consistent with that observed in the earthquake damaged portions of the viaduct (Fig. 1.16) and in the static load tests of the original structure.

When loads were applied towards the east, small cracks were detected at the inside of the base of the pedestal on the east side of the structure. At this stage, these cracks were nearly horizontal in orientation. An inclined crack also initiated on the east side of the north face in the lower joint at the level of the deck. This crack ran diagonally upwards from the top of the lower deck corner towards the west. On the west side of the bent, previously formed cracks closed.

The instruments installed on Bent 45 generally indicated elastic response at this stage. Some minor nonlinear response can be detected in the strain gages attached to the wide flange sections (Figs. B.40 (Channel 65), B.42 (Channel 67) and B.44 (Channel 77)) and in the linear potentiometers measuring slip between the wide flanges and the concrete (Fig. B.35 (Channel 30)).

Bent 46. -- The small inclined cracks formed in the lower joint on the west side of Bent 46 during the test of the original structure reopened slightly as load increased towards the west during Cycle 2. No new cracks formed during Cycle 3.

Cracks on the west side of the structure closed during Cycles 4 and 5. However, inclined cracks were observed to open during these cycles to the east at the base of the pedestal on the east side of the structure. The location of these cracks coincided with the location of epoxy repaired cracks formed during the demolition and site preparation. As noted at the end of Section 2.3(a), the epoxy did not appear to penetrate completely over the entire cracked surface. Nonetheless, the cracks remained relatively narrow and did not propagate significantly beyond the level of the bonded post-tensioning rods embedded in the joint.

For cycles toward the east, nonlinear strain excursions were detected in the strain gage attached to the nut at the end of one of the inclined rods embedded in the lower eastern joint in Bent 46 (Fig. B.47 (Channel 88)). In this direction of motion the rods on the east side should carry tension. The nonlinearity of the strain reading at such small strains may be associated with slip and bending of the attachment plates as well as with joint shear. For Cycles 2 and 3, during which the gaged rod should have been in compression, the strain gage detected only minor linear straining.

Bent 47. -- Sudden and relatively loud noises were periodically emitted from Bent 47. These noises appeared to be caused by slippage or relocation of the retrofit steel and post-tensioning rods relative to the concrete. Visual inspection failed to locate any fracture or buckling of steel plates or connections. No concrete cracking was observed, though it must be noted that the pedestal and lower joint were sheathed in steel. During the first load to the east (Cycle 4) a loud snapping sound was heard as the load approached 1770 kips. Shortly thereafter, inclined cracks were observed in the upper joint region above the west column. At this time the drift in the upper level was 0.65-in., resulting in a drift index of 0.24%.

3.5(c) Load Cycles to 2700 Kips (Cycles 6 to 8)

(i) Cycles 6 and 7

The next set of load cycles began with two more cycles toward the east, but with the nominal total load level intensified to 2700 kips. New damage was observed in the structure during these cycles. These cycles were followed by an additional 2700-kip excursion to the west. The increasing levels of damage in the structure during Cycles 6 through 8 is reflected in the minor nonlinearity in local responses monitored by the instrumentation (Appendix B). Behavior during Cycles 6 and 7 will be described in this sub-section, followed in the next sub-section by a discussion of results obtained during Cycle 8. Patterns of cracking developed in Cycles 6 through 8 are shown in Appendix C. The locations of cracks shown are approximate.

As indicated in Figs. 3.12 through 3.18, the global load-displacement response of the structure diverged only slightly from linear during Cycle 6. Response in Cycle 7 was essentially linear with only small hysteresis. Maximum inter-level drift indices were 0.47 % for the upper level and 0.16 % for the lower level.

Bent 45. -- During these excursions to the east, Bent 45 developed flexural cracks (cracks essentially at right angles to the longitudinal axis of the member) at the bottom of the upper bent cap near the inside face of the west column. These cracks extended upward over nearly half of the depth of the cap (Fig. C.2).

Consistent with previous behavior, little cracking was observed during cycles to the east in the pedestal and lower joint regions on the west side of the structure. However, the corresponding regions on the east side of the structure developed distinctive inclined cracks that roughly followed the surface projection of the hook of the top rebar in the cap (as well as other irregularly spaced inclined cracks) during these cycles (Fig. 3.21). Flexural cracks were observed along the boundaries of the upper joint region, extending vertically from the top of the upper bent cap along the face of the upper deck, and extending horizontally from the outer face of the column at the elevation of the bottom of the upper cap (Fig. 3.22).

The increased damage in the structure was detected by the instrumentation attached to Bent 45. For example, nonlinear relations are recorded for the strain gages attached to the wide flange sections adjacent to the pedestal (Figs. B.40 (Channel 65), B.42 (Channel 67), B.44 (Channel 77) and B.45 (Channel 78)) and in the displacement transducers measuring slip between the concrete and the wide flange sections (Fig. B.30 (Channel 25)). The strains measured on the wide flanges are far less than the yield values. It is likely that a significant amount of the nonlinearity is due to slip between the steel and concrete that is associated with breakdown of composite action. The differences in the shapes of the curves in Figs. B.39 and B.40 (Channels 64 and 65) and Figs B.43 and B.44 (Channels 76 and 77) could be a consequence of the plywood that was inserted between the steel wide flanges and the concrete column on the west side in order to reduce the effectiveness of the composite action as well as of the differing senses of the change in column axial forces induced by overturning effects.

Flexural cracking in the column and bent caps did not extend directly through the instrumented sections. Opening (rotation) of the hinge at the top of the west pedestal was detected by the attached displacement transducers (Figs. B.36 and B.37 (Channels 31 and 32)).

Bent 46 -- On the west side of Bent 46 flexural cracks formed over the lower half of the upper cap near the face of the deck.

On the east side of Bent 46 cracks occurred along the diagonal of the upper joint. These ran from the east (outside) face at the top of the joint to the west (inside) face at the lower boundary. It is important to note that the direction of these cracks is nearly orthogonal to that of the inclined cracks occurring in the lower joint during this cycle (Fig. 3.23). Small flexural cracks were also observed at the top of the bent cap at its east end where the deck butted up against the joint. The previously formed inclined cracks in the lower joint reformed, became slightly wider, and extended somewhat further along the epoxy repair line.

Nonlinearity is apparent in the instrumentation installed on Bent 46. For example, significant nonlinearity was observed in the strain gage readings for the west face longitudinal steel of the east column (Fig. B.10 (Channel 81)) and in the strains measured in the nut at the end of the inclined

post-tensioning bars grouted in the lower joint on the west side (Fig. B.47 (Channel 88)). In the latter case, relative strains are again seen to be very small, though highly nonlinear.

The west pedestal on Bent 46 develops some nonlinearity (Fig. B.25 (Channel 20)). Some permanent offset is retained in the pedestal at the end of Cycle 7. In addition, some opening (rotation) of the hinge just above the pedestal was measured at the west face of Bent 46 (Figs. B.32 and B.33 (Channels 27 and 28).

Bent 47. -- On the west side of Bent 47, diagonal cracks that had initiated during Cycles 4 and 5 in the upper joint reformed, widened and extended, especially during Cycle 7. Flexural cracking occurred at the bottom face of both upper and lower bent caps at their west ends. Several loud snapping noises were heard as the load approached 2700 kips. This noise was attributed to slippage of steel plating, though no physical manifestation of damage was detected. Any damage that may have occurred in the concrete was hidden by the steel plates used in retrofitting this bent.

On the east side of Bent 47 inclined cracks appeared in the upper joint. These were similar in orientation to those that formed on the east side of Bent 46 and roughly parallel with those formed on the west side of Bent 47. Flexural cracks also appeared at the top of the upper bent cap near the inside face of the east column.

Reinforcement strain gages in Bent 47 recorded only small strains at this stage. Elastic response may be inferred from the lack of cracking near a gaged section as well as from the linearity of the plots in Fig. B.12 (Channels 91 and 92).

(ii) Cycle 8

Following loading to the east, the test structure was loaded to the west through one cycle to a total nominal load of 2700 kips. As in the two preceding cycles to the east, the global lateral load-displacement relations remained nearly linear, although this cycle showed more hysteretic behavior than the two previous 2700-kip loading cycles to the east.

Bent 45. -- The existing inclined cracks in the lower joint on the west side reopened and extended in a diagonal direction roughly following a line corresponding to the position of the hooked top

reinforcement in the lower cap (Fig. 3.24). New flexural cracks formed at the base of the west pedestal. These ran in a nearly horizontal direction. A vertical hairline crack was also noted on the south side of the west pedestal at its top, approximately where the dowels crossed over from the upper column into the pedestal.

On the east side of Bent 45 flexural cracks formed at the bottom of the upper cap near the east column. As a result, cracks had now formed vertically across the entire section. In addition, the hinge between the east pedestal and the upper column opened up visibly at this point.

The incremental damage to the structure during Cycle 8 was apparent in nonlinearity in several instrument readings. For example, Fig. B.35 (Channel 30) indicates that slip between the wide flanges and concrete on the east column in Bent 45 intensified significantly during this cycle. Slip at the same location on the west side was smaller (Fig. B.30 (Channel 25)). Wide flange strain readings were also nonlinear (Figs. B.39 through B.44 (Channels 64, 65, 66, 67, 76 and 77). Because the measured strains are still far below the yield strain of the steel, this nonlinearity is a likely consequence of the slip between the wide flanges and the adjacent concrete. The inclined strain gage on the west column (Fig. B.46 (Channel 79)) indicates that the wide flange sections began to take increasing shears at this load stage.

Nonlinearity of the lower joint response can be seen in Fig. B.48 (Channel 97), which shows the force in the top post-tensioning rod across the lower joint in the west column, and in Fig. B.38 (Channel 33), which shows the lateral deformation across the joint at the elevation of the rod. The second of these figures indicates a small permanent dilation across the joint, while the first shows that the post-tensioning rod begins to resist load at an increasing rate. The behavior of this joint is further illustrated in Fig. 3.25. The nonlinearity of response may be the result of a new horizontal crack extending outward from where the top of the deck met the column as well as the extension of the existing crack along the projection of the hook of the top rebar.

Bent 46. -- In Bent 46 the post-tension rods in the upper columns were not stressed to enhance shear capacity and confinement. Diagonal cracks occurred during Cycle 8 in the upper west side column. These cracks formed suddenly while the load was being held at the nominal 2700-kip level. The cracks (Fig. 3.26) were inclined from the east (inside) on the top to the west (outside) on the bottom. The test

structure was unloaded and the rods on the west column were subsequently stressed to provide increased shear resistance.

During Cycle 8, inclined cracks in the lower west joint also extended and merged to form a continuous crack. On the east side of Bent 46 small flexural cracks formed on the bottom of the upper cap near the west face of the east column.

The onset of inclined cracking in the upper west column of Bent 46 was detected in one of the couplers inserted in the post-tensioning rods near the top of the column (Fig. B.63 (Channel 112)). Apparently, this rod was sufficiently snug to develop force once the column cracked. The other rods, being loose, did not pick up any additional load until the rods were post-tensioned at the completion of Cycle 8.

As indicated by Fig. B.25 (Channel 20) and others, nonlinear deformation apparently continued to increase at an accelerated rate in the pedestal on the west side of Bent 46. Joint shearing deformations can be inferred from the instrumentation placed on the upper west side joint in Bent 46. Shear strains are estimated as:

$$\theta = (Ch11 + Ch17*Tan\beta - Ch42/Cos\beta)/96 \qquad (3.2)$$

in which θ = Shear Angle

β = Angle between Channels 11 and 42

These results are plotted in Fig. 3.27. Some limited nonlinear response is detected in this plot at this stage.

Bent 47. -- Bent 47 continued to make loud popping sounds during Cycle 8. Small flexural cracks were observed near the east column at the bottom of the upper bent cap. The strain gages on Bent 47 indicate virtually elastic behavior at the locations instrumented.

3.5(d) Load Cycles to 3300 Kips (Cycles 9 to 13)

In this load sequence, a series of five cycles with nominal loads between 3300 and 3600 kips were targeted, although Cycle 10 reached a maximum load of 2997 kips (Fig. 3.10). The first of these cycles

loaded the structure toward the west. This was followed by three cycles to the east, and finally by a single cycle to the west.

(i) Cycle 9

During Cycle 9 moderate nonlinearity developed in the global lateral load-displacement relations (Figs. 3.12-3.14 and Figs. 3.16-3.18). Upper deck level displacements increased to about 2.7 in. for an overall drift index of 0.49%. Drift indices equal to 0.73 % and 0.25 % developed in the upper and lower levels, respectively.

Bent 45. -- More diagonal cracks occurred in the upper joint on the west side of Bent 45 (Fig. 3.28). Cracks in the upper joint were orthogonal to those that had occurred in the joint during Cycles 6 and 7. Thus, this joint had X-patterned cracking characteristic of reversed shear. In contrast, inclined cracking in the lower joint was mostly oriented in one direction. Horizontal flexural cracks also appeared during this cycle near the outside face of the top level west column at its upper end.

Inclined cracks were observed to open along the west face of the lower deck in the longitudinal direction. These cracks may have developed along pre-existing shear cracks in the longitudinal webs. However, they appeared to be associated with torsion induced in the deck as a result of transverse motion of the structure.

On the east end of Bent 45, cracks in the upper joint that had developed in the previous cycles merged and enlarged. Relatively little new damage was observed in the lower east joint.

Strain readings obtained for gages on the cap and column rebars continued to indicate linear response when plotted against applied lateral load except for the upper west column. Figure B.4 (Channels 74 and 75) indicates large strains consistent with yielding for rebars on both faces of the upper column during this cycle. Since initial strain conditions in the rebar are not known, accurate assessment of the onset of yielding is not possible.

Bent 46. -- New cracks developed in the upper joint on the west end of Bent 46. This fully developed a X-shaped cracking pattern in this joint. Increased shearing deformation in the upper joint is reflected in Fig. 3.27 and in Figs. B.16, B.17, B.18, B.20 and B.22 (Channels 11 to 13, 15 and 17)). This

first non-linear behavior of Channels 11 and 12 is indicative of the increased size and quantity of diagonal cracks that formed in this cycle. Likewise, the prestressing rods on the upper bent cap of Bent 46 were active (Fig. B.59 (Channel 108)).

Cracks in the lower west joint continued to expand and merge during Cycle 9. However, crack widths remained relatively narrow. Shearing deformations in the joint increased significantly at this time as can be seen by comparing Figs. B.25 and B.28 (Channels 20 and 23).

The inclined cracks in the upper west side columns did not reopen, indicating the efficacy of the retrofit that had been done at the end of Cycle 8. Instrumented couplers installed in the transverse post-tensioning rods placed over the height of this column to increase its shear capacity indicate that rod stress varied with applied lateral load. This suggests that the rods were effective in helping resist shear in the column (see Figs. B.53, B.62 and B.63 (Channels 102, 111 and 112)).

On the east side of Bent 46, diagonal cracks developed in the upper joint. Again, these were approximately perpendicular to the previously formed cracks at this location, forming an X-shaped crack pattern.

The east pedestal developed an inclined crack. This crack initiated at the top of the pedestal near the dowels that connected the pedestal with the upper column and inclined downward to the western (inside) face of the pedestal. This inclined crack thus was oriented opposite to those observed following the earthquake.

Flexural cracking occurred at the bottom of the lower east bent cap near the face of the east column. Inclined cracks in both bent caps, associated with pre-existing cracks caused by gravity loading, opened noticeably during these cycles.

Strain gages attached to the rebars indicated strains lower than the value associated with yield. Again, it must be noted that the strain gages were placed on the bars for these tests and it is not known what strain existed in the bars prior to these tests. However, as was the case with Bent 45, gages at the top of the west column indicated strains consistent with yielding on both the tension and compression faces of the column (Fig. B.7 (Channels 86 and 87)). The low strain readings for the reinforcing bars in the bent caps seems inconsistent with the observed damage. However, it appears that cracking and

yielding did not occur in the immediate vicinity of the gages, especially at the top face, since the strain gages were installed on the bentcap away from the joint. The maximum strain recorded in the bottom bar on the east end (this bar was in tension for this direction of loading) was very close to the yield strain and plots of rebar strain vs. lateral load exhibited significant nonlinearity during the next cycle to the west, Cycle 13 (Fig. B.5 (Channel 82)). The displacement transducer located at the top of the west joint region (this crosses the flexural cracks in the bent cap) indicated significant nonlinearities beginning during this cycle (Fig. B.16 (Channel 11)).

Bent 47. -- The upper west joint in Bent 47 developed inclined cracks to produce an overall X-shaped pattern. A new flexural crack occurred at the top of the lower bent cap near the pedestal face. This was visible between the steel plating on the sides of this joint and the deck. Strain gages attached to the top of the west column recorded strains in excess of the yield level for bars on the east and west faces (Fig. B.15 (Channels 95 and 96)).

On the east side of the structure cracks in the upper joint region formed and joined together, and the joint exhibited signs of overall distress. A distinct X-shaped pattern of cracks had now formed on the east end of Bent 47. No new cracks were noted in the lower joint or bent cap regions.

(ii) Cycle 10

The post-tensioning rods along the mid-height of the upper east column of Bent 46 were loose at the beginning of this load cycle. At a total load of 2997 kips, inclined cracking suddenly formed in this column. This load corresponds to approximately 53% of the total weight of the test structure. The displacement at this point was 2.0 in. to the east at Bent 46, corresponding to an overall drift index of 0.3%. The cycle was terminated and the load was released when the inclined cracks formed. The post-tensioning rods on the column were then stressed and loading was resumed with Cycle 11 (to be described later).

The lateral load-deformation relations for this cycle were essentially linear with relatively little permanent offset. Bent 47 started to exhibit slightly more nonlinearity at this stage (Figs. 3.12 to 3.14 and Fig. 3.20). The increased damage in the upper level resulted in an increasing concentration of drift

in the upper level. At this stage (Table 3.2 and Fig. 3.19) about 25% of the drift occurred in the lower level (compared with approximately 30% for the early cycles).

Bent 45. -- The existing cracks in the upper west joint region extended and joined. Small inclined cracks were observed to form in the upper west column. The location of the couplers on the column were such that they did not detect the formation of these cracks. However, strain gages and displacement transducers indicate continued nonlinearity associated with slip between the steel wide flange sections and the concrete columns.

The existing cracks in upper joint on the eastern side also extended and widened during Cycle 10. The lower joint formed additional inclined cracks and existing cracks extended.

Bent 46. -- As mentioned above, inclined cracks developed in the upper column on the east. The cracks ran from about mid-height on the west (inside) face of the column downward diagonally to the east (outside) face near the hinge. The occurrence of cracks coincided with a sudden increase in the tension in the post-tensioning rod coupler at the mid-height of the column (see Fig. B.54 (Channel 103). The load at which these cracks occurred was 11% higher than that required to form similar cracks in the west column (while the structure was loaded toward the west).

Bent 47. -- Inclined cracks in the upper west joint merged. Flexural cracking at the bottom of the upper bent cap near the west column opened. Cracks in the upper east joint extended to form continuous cracks.

(iii) Cycles 11 and 12

Load cycles 11 and 12 in the east direction had a target of 3300 kips total load. Global load-displacement relations for these cycles (Figs. 3.12 to 3.14) exhibit greater nonlinearity. The load-displacement relations appear to be stable for the two cycles. Maximum displacement at the top during Cycle 12 was 3.9 in. in Bent 46. A drift index of 1.1% and 0.39% were achieved in each of the upper and lower levels, respectively. These drift values show a marked increase over those of Cycle 9 (0.73% and 0.25% for the upper and lower levels, respectively) during which a similar load was applied to the

west. The ratio of lower to upper deck level displacements was approximately 0.3 (Fig. 3.19). Table 3.2 contains information related to the deformed state of the structure at this time.

Bent 45. -- Existing flexural and shear cracks in the upper west and east joints widened, extended and joined together, consistent with previous motion to the east. Additional small inclined cracks formed in the upper west column. However, additional load was not detected by the instrumented external post-tensioning rods used for shear reinforcement on this column (Figs. B.50 and B.51 (Channels 99 and 100)). While most of the cracks in the west lower joint closed at this stage, new inclined cracks formed in the lower east joint and existing cracks extended.

Nonlinearities in the plots of rebar strain vs. applied load were detected at the bottom face of the top bent cap at the west end (Fig. B.6 (Channel 73)) and at the western (tension-most) sides of both upper level columns at their top (Figs. B.4 and B.7 (Channels 69 and 74). Recorded strains were consistent with rebar yielding.

Instrumentation also detected some of the first large slips between the wide flange sections and the columns (e.g., see Fig. B.30 (Channel 25)). These slips appear to be linearly related to upper level drifts.

In addition, instrumentation of the hinge on the west pedestal quantifies a rotation of the hinge that could be detected visually (Figs. B.36 and B.37 (Channel 31 and 32)). The western edge of the hinge opened approximately a quarter of an inch at this point. The strain gages on the adjacent wide flange section exhibit response that is related nonlinearly to applied load. The wide flanges on both sides of Bent 45 indicate strains significantly below those that might be associated with overall yielding of the section. As indicated before, it is believed that the apparent nonlinearity in these strain gage readings is related to slip of the wide flange sections over the concrete.

An important aspect of the loss of composite action became visually obvious during these cycles as well. A gap was observed between the exterior steel wide flanges and the adjacent concrete in many places. The distribution of the gap opening is schematically illustrated in Fig. 3.30. It is believed that this effect is associated with excessive stiffness or strength of the wide flange sections relative to the post-tensioning bars used to clamp them to the columns. The stiff wide flange sections used tended to

remain straight as the frame distorted. The result was that the joints and columns were not confined over large areas of their east and west faces. The gap was observed to close and reform during subsequent cycles suggesting elastic action of the wide flanges and post-tensioning rods. The use of more flexible or weaker vertical steel sections may have avoided this problem. Similarly, more transverse post-tensioning might have partially alleviated this situation (see Section 4.3(b)).

Bent 46. -- Additional inclined cracks formed in the upper west joint and these connected in many cases with previously formed cracks to form longer cracks that extended over the full extent of the joint (Fig. 3.31). The shear deformations in the joint are seen to increase significantly during these cycles (Fig. 3.27). In addition, the bent cap lower reinforcement began to yield at this stage as suggested by the crack opening inferred from Fig. B.18 (Channel 13) and the rebar strains shown in Fig. B.8 (Channel 85). This disintegration of the upper joint resulted in tension forces being added to the loads carried by both the upper and lower post-tensioning rods connected to this joint (Fig. B.58 and B.59 (Channels 107 and 108)). During previous cycles incremental forces in these bars would be of opposite sign, consistent with beam bending.

The previously formed inclined crack at the top of the pedestal on the west side of the structure extended and was joined by additional parallel cracks. Instrumentation attached to the top of the pedestal indicated that the shear key began to slip horizontally during these cycles. About a quarter of an inch slip was noted across at this stage (Fig. B.24 (Channel 19)). Rotations measured at this location were comparable to those monitored on Bent 45 (Fig. B.32 and B.33 (Channels 27 and 28)).

On the east side of Bent 46, the diagonal cracks in the upper joint connected and became considerably wider. The concrete cover began to spall from the joint core at this stage. Little instrumentation was placed on this joint. However, it is clear from Fig. B.10 (Channel 81) that the rebar strains measured at the western (compression most) side of the column far exceed the yield value. This column exhibited the largest amount of apparent yielding compared with the other bents. Strains recorded in other reinforcement near the joint remained below the nominal yield value. The disintegration of the joint and local yielding resulted in complex behavior in the lower post-tensioning rod on the cap. For the direction of the applied load, flexural action of the bent cap would tend to result in a decrease in the rod

tensile load. However, as the lateral load exceeded that imposed in Cycle 10, the tension in the rod is seen to increase noticeably, apparently as a result of joint dilation (Fig. B.57 (Channel 106)).

In the lower joint on the east side cracks extended and a complex X-pattern of small inclined cracks was observed. Cracks perpendicular to the inclined post-tensioning rods embedded in the joint, while well formed, remained small in size. The small cracks running roughly parallel to the grouted rods in the joint were apparently associated with joint shear and are oriented in a direction consistent with those observed in the upper joint.

The retrofit applied to the upper columns on the west and east sides of Bent 46 appeared to remain effective. Previously formed cracks remained closed during these (and subsequent) cycles.

Bent 47. -- As in the other upper joints on the west side, cracks at this location in Bent 47 lengthened and widened, forming cracks that extended across the diagonal of the joint. The flexural cracking at the bottom of the upper bent cap near the inside of the west column opened. Some of the cracks exceeded 0.24 inches in width. On the east side existing cracks reformed, extended, and widened. Little could be observed related to damage near the lower joint. However, loud popping noises continued to be emitted from various locations on Bent 47.

(ii) Cycle 13

Following a load reversal, the final 3300-kip load cycle to the west was undertaken. The response features were similar to those noted for Cycle 9, the previous 3000-kip cycle to the west. In general, cracks widened and became more well defined. This was especially true in the upper joints. Deformation transducers attached to the upper west joint in Bent 46 indicated nonlinearities twice as large as those occurring during Cycle 9 (Figs. B.16, B.17 and B.22 (Channels 11,12, and 17)). The incremental load developed in the post-tensioning rod installed at the top of this joint doubled in response to the increased cracking and disintegration in the joint (Fig. B.59 (Channel 108)).

The forces developing in the post-tensioned rods of the lower west joint in Bent 46 were somewhat higher than those that developed during Cycle 9 (Figs. B.60 and B.61 (Channels 109 and 110)).

Strain gage readings obtained for the upper reinforcement in the west column again exhibited nonlinearity when plotted against applied lateral load.

3.5(e) Final Load Cycles to 4000 Kips (Cycles 14 to 16)

The final load cycles included a final cycle to the west with a total nominal load level of 4000 kips, followed by a load reversal with one cycle to 3300 kips and a final cycle to nearly 4000 kips, both toward the east. Maximum displacement to the west was approximately 5.60 in., and maximum displacement to the east was approximately 9.90 in. These values correspond to overall drift indices of 1.0% and 1.8%, respectively.

(i) Cycle 14

During Cycle 14 the severity of damage in the test structure increased. Its distribution was similar to that in Cycle 13. The displacements tended to concentrate in the upper level with more than 78% of the total displacement occurring in the upper level (see Fig. 3.19). This upper level drift index equalled 1.59% for this cycle. Based on the clear length of the upper level columns the drift index would be 2.4%. Bent 47 tended to be somewhat softer than the others with a slight resultant rotation of the test specimen around a vertical axis.

The slope of the force - displacement relations for the bents was considerably reduced during this cycle as loads increased above 3300 kips (Figs. 3.12 to 3.14). However, the reduced stiffness was maintained until the maximum load capacity of the jacks was reached. The full capacity of the test structure was thus not reached in this direction during this cycle. The maximum force reached was 4049 kips, corresponding to approximately 71% of the total weight of the test structure. The tangent stiffness of the test structure, measured near zero applied lateral load, is significantly less at the end of this cycle than at the beginning. This is an indirect indication of the damage suffered during the cycle.

Bent 45. -- The lower west joint was severely damaged at this stage. Rather than developing a number of small parallel inclined cracks, as observed in the upper joints, a single large crack formed roughly following the contour of the hook in the bars at the top of the cap. The lower end of the crack

at this stage was nearly vertical and located within the exterior cover of the lower column section. This cracking pattern was very similar to that developed in the earthquake-damaged portions of the Cypress viaduct.

The wide flange sections were not able to prevent this cracking, although they were well able to resist the loads, as evidenced by the small strains developed in the steel sections and the low force levels induced in the post-tensioning rods (Fig. B.48 (Channel 97)). The incremental load in this rod during this cycle was about 60 kips. When added to the initial prestress of 55 kips, the total load was only approximately 60% of the load capacity of the rod. The horizontal displacement transducer positioned across the top of the lower joint, near the upper post-tension rod, indicated a deformation of about 0.34-in. for this cycle (Fig. B.38 (Channel 33)). By elastic theory the post-tensioning rod would extend approximately 0.23-in. considering the measured incremental force in the rod and an unbonded length of 14 ft - 0 in. Once the concrete cracked, this retrofit was unable to keep the cracks from opening.

In the upper west joint, several new cracks formed and pre-existing ones opened wider as the lateral bent displacement increased. Maximum crack widths at the end of the cycle were estimated to be in excess of 0.4 inches. The deterioration of this joint is reflected in the forces developed in the lower post-tensioning rod running across the joint (Fig. B.49 (Channel 98)). During the beginning of the cycle the incremental forces in the rod were compressive, consistent with the negative bending moment developed at the end of the cap. As the lateral load increased and the joint expanded as a result of inclined cracking, the maximum incremental compression load was reduced by a factor of approximately 2 (i.e., the sense of incremental loading reversed so that the amount of compression in the rod at the point of maximum load to the west was approximately half that registered in the rod during Cycle 13). Strains in the bars on both the east and west sides of the upper west column were measured to be about 0.8% at this stage (Fig. B.7 (Channels 74 and 75)), indicating significant yielding of the column reinforcement had occurred.

The steel wide flange sections were observed to separate from the exterior faces of the concrete columns and joints in several locations consistent with the deflected shape of the bent (see Fig. 3.30). Small shear cracks were observed to form in the upper west column in locations where the wide flange

sections had separated from the concrete. The instrumented couplers on some of the transverse post-tensioning rods on the column indicated an increase in their load for the first time during this cycle (Figs. B.50 and B.51 (Channels 99 and 100)). In addition, vertical slips as much as 0.25 inches were measured between the wide flange sections and the concrete (Fig. B.35 (Channel 30)).

On the east side of the bent, the lower joint developed some horizontal cracks located slightly below the base of the pedestal. These cracks opened to approximately 0.2 inches at the exterior face of the column. In addition, small cracks that were inclined downward toward the east formed in the same region. The joint region just below the pedestal was covered by a series of closely spaced, criss-crossed cracks. These were over the region where the lower column bars lap-spliced the longitudinal reinforcement used for the pedestal.

The upper joint on the east side of Bent 45 developed several new inclined cracks and existing cracks became wider. During this cycle, inclined cracks in excess of 0.16 in. in width were observed. Flexural cracks adjacent to the upper joint opened wide with the crack width at the bottom of the bent cap being approximately 0.25 in. The strain gage on the bottom reinforcement in the bent cap recorded strains in excess of 1%.

Bent 46. -- As in the other bents, inclined cracks in the upper joints extended and widened on the west side. Relatively large deformations were recorded by the displacement transducers located in the upper joint. For example, Fig. B.16 (Channel 11) shows that the growth across the top of the joint was nearly 0.4 in. The force increase in the horizontal post-tensioning rod at this location was approximately 60 kips (Fig. B.59 (Channel 108)). Some new horizontal cracks were also noted near the top of the upper west column. Steel strains in the reinforcing bars at the top of this column were measured to be nearly 1% (Fig. B.11 (Channels 86 and 87)).

The lower west joint exhibited some new horizontal cracks near the east side of the base of the pedestal. The pedestal deflected laterally as a result (compare Figs. B.25, B.26 and B.28 (Channels 20, 21 and 23)). The inclined crack through the lower west joint was well formed at this stage. However, virtually no shear slip was observed.

On the east side of Bent 46 inclined cracks in the upper joint opened to a width of approximately 0.04 in. Flexural cracks in the upper bent cap had widths exceeding 0.25 in. near the bottom of the east joint when the peak load was reached. Steel strains were measured to be about 1.3% in the bottom bars near these cracks (Fig. B.9 (Channel 82)). The horizontal post-tensioning rod at the bottom of the joint developed incremental forces of approximately 110 kips. Combined with the initial prestress the total load in this rod was approximately 160 kips, or nearly 83% of its yield strength.

The lower east joint did not exhibit any new damage. However, the inclined crack developed in Cycle 9 at the top of the pedestal continued to elongate downwards towards the west. The couplers located on the transverse column rod near this location apparently carried some of the column shear developed during this cycle (Fig. B.52 (Channel 101)).

Bent 47. -- The upper west joint developed increased cracking consistent with other bents. On the east side, the upper joint had distinct inclined cracks and adjacent flexural cracks in the bent cap opened to a width exceeding 0.05 in.

At the lower east joint signs of yielding in the steel plates covering the joint were observed by light, but widespread, flaking of the whitewash painted over the steel. This flaking was observed on the south and north exterior faces of the joint below the level of the pedestal.

Loud noises continued to emanate from this bent during the test. A possible source of some of these noises was clearly visible. The steel collar placed around the pedestal was observed to rotate along with the pedestal relative to the lower bent cap and joint. The bottom of the upper column was then bent (kinked) with respect to the lower column. The rotation of the side plates attached to the north and south sides of the lower joint resulted in significant bending distortion of the post-tensioning rods used to attach these plates to the joint. These rods were not grouted in the holes drilled in the joint. The upper and lower rods were bent in opposite directions, but both in a horizontal plane, consistent with a rotation of the cover plates about a horizontal axis.

(ii) Cycles 15 and 16

The direction of loading was reversed following Cycle 14. On loading to a nominal total load of 3300 kips the lateral stiffness of the structure was seen to be considerably reduced in comparison with its original one. The stiffness deterioration exhibited appears to be typical of reinforced concrete structures, with the load path seeking the furthest load point previously achieved in the direction of loading. Little evidence of pinching in the global hysteresis loops was detected.

During the first part of Cycle 15 the structure was unloaded and then reloaded. This allowed shims to be installed in the reaction frames (see Section 2.4(b)) so that the full displacement capacity of the jacks could be realized.

The displacement reached during Cycle 15 was similar to that realized during Cycles 11 and 12 for the same force levels. Thus, in spite of the additional damage observed in the structure the strength characteristics of the structure remained stable. The stiffness properties of the structure had, however, significantly degraded.

During Cycle 16, one of the stages of the hydraulic power supply overheated and broke. The loading of the structure was continued under reduced pumping capacity. As a consequence, it took several hours to achieve the latter two-thirds of the imposed displacement excursion. The maximum displacement reached during Cycle 16 in Bent 46 was 9.90-in. This corresponds to an overall drift index of 1.8%. As noted previously displacements tended to concentrate increasingly in the upper level. At the point of maximum displacement more than 91% of the total displacement occurred in the upper level (see Fig. 3.19, 3.33 and 3.34). The drift index for the upper level equalled 3.25% for this cycle, considering the height of the level to be the difference in elevations between the tops of the decks. Based on the clear length of the upper column and pedestal, the drift index was 5.0%.

The slope of the force - displacement relations for the bents leveled off at a load of approximately 3800 kips (Figs. 3.12 to 3.14), indicating that the maximum capacity of the structure had been achieved. This load corresponds to approximately 67% of the total weight of the test structure. The tangent stiffness near zero load was greatly reduced on unloading compared with the value seen at the beginning of Cycle 15.

Bent 45. -- Existing cracks consistent with eastward motion of the bent reopened during Cycles 15 and 16. However, in some cases cracks associated with prior loading to the west failed to close completely during these eastward cycles.

During Cycle 15 little or no yielding could be discerned from the strain gage readings on the west side of the structure. Apparently, the flexibility of the structure had increased to the point that stresses in the steel were significantly reduced at this displacement level. The lower bar on the east side of the upper bent cap, which had yielded significantly in tension during Cycle 14 to the west, was seen to degrade its stiffness characteristics significantly during Cycle 15 (Fig. B.5 (Channel 70)). It appears that the bar had begun to slip from its anchorage in the joint during the previous cycle, and a degraded and pinched reloading characteristic can be noted.

During Cycle 16 deformations and damage increased considerably. In general, cracking was consistent with prior cracking during previous cycles to the east. Inclined cracks in excess of 0.6-in. width were observed in the upper east joint region. Flexural cracks in the adjacent upper bent cap also opened with cracks as wide as 0.2 in. noted at the bottom of the cap. Strain gage readings (Fig. B.6 (Channel 73)) in the lower reinforcement at this location reached 2%. However, only slight nonlinearity was detected in the plots of strain vs. lateral loads for reinforcement at the top of the west column (Fig. B.7 (Channels 74 and 75)).

The column hinge at the top of the west side pedestal rotated considerably. The opening on the west side of the hinge exceeded 0.87 in. in spite of the wide flange section being clamped to the column (Fig. 3.32 and B.36 (Channel 31)). At the same time the east side of the hinge closed about 1/4 in. (Fig. B.37 (Channel 32)). In addition, the hinge was observed to slip horizontally. Inclined cracks in the column above this pedestal were also observed to open slightly and forces in the transverse post-tensioning rods were seen to increase (Figs. B.50 and B.51 (Channels 99 and 100).

On the east side existing cracks associated with eastward motion opened. At the latter stages of this cycle cracks nearly 2 in. wide were observed in the upper joint. The opening was made possible in part by the increasing separation observed between the joint and the wide flange sections. As noted previously, the stiffness (and strength) of the wide flange sections and the large change in curvature of

the column resulted in a gap forming along the upper part of the east joint. Relatively large pieces of concrete cover began to spall along some of the cracks in the joint.

Steel reinforcement at the inside (west) face of the top of the east column yielded with measured strains reaching nearly 0.9%. The lower bar in the bent cap near the east column did not yield in compression and exhibited pinched behavior associated with bond slip (Fig. B.5 (Channel 70)).

In the lower east joint the well dispersed inclined cracks formed during previous cycles coalesced into a single large diagonal crack that opened to as much as 0.6 in. in width during the initial portions of these cycles. This crack again followed the projection of the hook in the top layer of reinforcement in the bent cap. During the latter portions of Cycle 16 large portions of the cover over the joint became loose just below the pedestal and spalled. This occurred in an area where the steel dowels in the pedestal were lap spliced with the discontinued bars in the lower column. A significant discontinuity in the deflected shape of the east column was noted at this location after the lower joint began to spall.

Bent 46. -- Behavior was similar to that observed in Cycle 12. However, for Cycle 15 instrumentation indicated reduced inelastic strains in the reinforcement. A pinched relation between strain and lateral load (Fig. B.9 (Channel 82)) for the lower bar on the east end of the upper bent cap suggests that bond slip may have accompanied the tensile rebar yielding detected during Cycle 14. The deterioration and dilation of the upper west joint was reflected during Cycle 15 in a large 85-kip increase in the tension load acting on the lower post-tensioning rod that crosses the joint (Fig. B.58 (Channel 107). It should be noted that the upper rod also developed tensile forces (up to 30 kips), rather than compressive ones, during this cycle apparently because the effects of joint disintegration dominated those associated with bending (Fig. B.59 (Channel 108)). Nonetheless, the increment of load in the bottom post-tensioning rod on the eastern upper joint continues to be compressive (Fig. B.57 (Channel 106)) at this stage.

During Cycle 16 large cracks (some nearly 1/2-in. wide) developed in the upper west joint. Figures B.17 and B.18 (Channels 12 and 13) indicated total elongations across the joint between 0.5 and 1.0 in. Both top and bottom horizontal post-tensioning rods used to strengthen the upper bent cap and confine the joint developed significant incremental tensile loads during the cycle, with the lower rod developing incremental forces in excess of 185 kips. Combined with the initial pre-stress the total load

in the rod exceeded 120% of the nominal yield capacity of the rod. The lower reinforcing bar at the west end of the top cap yielded significantly, with the measured strains at the gaged location equaling 2% (Fig. B.8 (Channel 85)). West column reinforcement yielded moderately near the joint (Fig. B.11 (Channels 86 and 87)).

The hinge and pedestal both deformed significantly on the west side. The hinge opened approximately 0.66 in. on the west side, while little closure was noted on the east side (Fig. 3.35). The smaller hinge rotation at this location relative to Bent 45 was attributed in part to the large translation and rotation observed in the pedestal itself. Figure B.25 (Channel 20) indicates that the top of the pedestal translated almost 1/2 in. relative to the lower deck.

A concentrated horizontal slip was noted in the west hinge as well. Figure B.24 (Channel 19) indicates that this slip exceeded 1/2 in. It is interesting to note from this figure that the slip only occurs to the east. This slip is accompanied by a nearly vertical splitting crack at the center of the north and south faces of the pedestal near its top.

In the lower west joint a horizontal crack developed at the base of the pedestal. This crack was about 0.5 in. wide at the west face and extended eastward through the region where the pedestal reinforcement connected to the lower column bars by means of short lap splices. The inclined crack opened slightly, possibly as a result of joint shear. The top horizontal post-tensioning rod on the lower joint initially developed incremental compressive loads (Fig. B.60 (Channel 109)). These are consistent with the positive moment developed at this end of the bent cap. However, by the end of Cycle 16 the incremental load becomes tensile.

On the east side, the upper joint had open cracks along both diagonals. Several cracks approached 1 in. in width. The north and south sides of the joint began to bulge outward as the cycles continued and portions of the cover spalled from these faces. The top part of the upper joint broke loose from the core. The column below the upper bent cap developed distinctive horizontal cracks. Instruments on the reinforcing bars near this location indicated strains as much as 2.0% (Fig. B.10 (Channels 80 and 81)). The strain vs. lateral load plots for the lower bars in the bent cap remained nearly linear during this excursion, in contrast to the large nonlinear excursions during earlier cycles. This provides further

evidence of the likelihood of bond deterioration during Cycle 14. The upper bars in the bent cap were not instrumented near the cracked section. Flexural cracks at the top of the cap remained relatively small.

The shear reinforcement on the east column remained effective. The lowest instrumented transverse post-tensioning rod in the upper column was located just above the hinge. This rod developed significant force during the last cycle in comparison with other rods on the column (compare Figs. B.52 and B.54 (Channels 101 and 103 which had both cracked during previous cycles)). The hinge was observed to translate and instrumentation at this section indicated horizontal displacements of approximately 0.15 in. (Fig. B.34 (Channel 29)).

No large cracks formed in the lower east joint. The inclined cracks that crossed the inclined post-tensioning rods remained narrow. The cracks here were as much as 0.5 in. wide at the deck end but decreased quickly in width as they propagated downwards. Spalling was observed at the east face of the east column near the foot of the inclined crack. This spalling is apparently associated with bending in the pedestal. The spalling occurred at a location where there was a gap of several inches between the two plates used to confine the joint and anchor horizontal post-tensioning rods. Adjustment of the locations of these plates might improve this behavior. Strains measured in the nut at the end of the embedded rod continued to indicate little force as a result of lateral loading. It appears that bond remained effective on these grouted rods.

Bent 47. -- The behavior of this bent during Cycle 15 was similar to that observed during Cycle 12. During Cycle 16 the upper west joint developed large inclined cracks. These cracks had widths of as much as 0.1 in. Flexural cracks at the bottom of the west end of the upper bent cap opened to widths of 0.3 in. One of the rectangular steel tube sections used for anchoring the horizontal post-tensioning rods to the joint suffered large inelastic buckling under the nut (Fig. 3.36). Because this occurred near the end of the test, it was not repaired. Rod forces at this location in Bent 46 equalled or exceeded their nominal yield capacities.

The upper joint on the east side developed large cracks in both inclined directions. The concrete shell on the north and south sides bulged out as the joint began to disintegrate.

Loud popping noises were heard during these cycles. The protruding flanges of the steel collar used to attach the pedestal collar to the lower joint were observed to rotate (slip) during this cycle. As in Cycle 14, this resulted in a sharp discontinuity of the deflected shape of the upper columns at the level of the top of the lower deck (rather than at the column hinge at the top of the pedestal) (Fig. 3.34). In addition, the post-tensioning rods used to clamp the flanges to the lower joint were observed to bow in opposite orientations from those seen in Cycle 14. The bending of the rods became a safety concern by the end of the cycle.

3.5 (f) Final Damage Condition

Following Cycle 16 testing was stopped in order to vacate the test site on schedule. In addition, the structure was considered to be unsafe for continued testing. The structure was jacked back to the west so that little permanent displacement remained when the structure was shored and dismantled. The shoring under the test structure was shimmed to bring it into contact with the structure. Instrumentation, loading apparatus and other experimental equipment were then removed. Photographs in Figs. 3.37 to 3.42 indicate the final damage state of the test structure.

Some of the retrofit steel was removed to permit closer inspection of the damages. It was possible to remove by hand substantial amounts of the concrete cover from the upper joints in all frames and from the lower joint on the eastern side of Bent 45. The concrete inside the main reinforcement in these locations was highly fractured and probably could have been removed by hand if there had been more access space available between the longitudinal column bars. Close inspection around many of the hooked #18 cap bars indicated significant splitting distress in the concrete. In the vicinity of the hook the concrete had separated by up to an inch or more from the steel. Virtually no concrete was in place around the column lap splice in the lower joint on the east side of Bent 45.

The steel flanges were removed from the lower joint region from the east side of Bent 47. The lower joint was cracked along the #18 top bar hook, but relative to other bents there were a greater number of thin, well dispersed cracks. The region within the collar was inspected during demolition and found to be largely pulverized. It could be completely broken apart by hand.

Material Samples -- Concrete cores were removed from each bent just prior to demolition for possible testing. Locations of the cores are shown in Fig. 3.43, and test results are indicated in Table 3.3. Straight pieces of reinforcing bar were removed from the structure following demolition. The locations of these bars are indicated in Table 3.4.

3.5(g) Summary

The test specimen was designed primarily to assess the effectiveness of various partial retrofit techniques in preventing the catastrophic type of failure observed in the Cypress Street viaduct during the Loma Prieta earthquake. As such, attention focused on strengthening the pedestal/lower joint region under loading transverse to the roadway. The tests indicated that the retrofits used were able to prevent a sudden brittle failure of the upper deck, at least for the loading history imposed. However, significant damage developed during the test. The progression of damage can be summarized as follows:

1. The lower joints of the retrofitted structure developed inclined cracks similar to those observed in the damaged portions of the viaduct during the Loma Prieta earthquake. These cracks initiated very early in the tests and became more extensive and distinct as testing progressed, generally following the contour of the hook in the top #18 bars in the lower cap.

The relatively flexible unbonded post-tensioning bars and wide flange sections provided in Bent 45 were unable to prevent these cracks from opening wide. The bonded post-tensioning rods grouted in Bent 46, while not preventing the formation of these cracks, limited adjacent crack widths to less than 0.25 inches (see Fig. 3.35). The steel jacket used in Bent 47 prevented direct visual observation of concrete cracking during the test. However, the collar rotated significantly with respect to the lower joint in later cycles and the concrete in the joint and pedestal was observed during demolition to be highly cracked and pulverized.

2. The upper joints developed diagonal cracks at an early stage (Bents 45 and 46: during 2700-kip cycles with an upper level drift of 0.47%, and Bent 47 : during 1800-kip cycles with a drift of 0.23%). Diagonal cracking in the joints occurred in an orthogonal direction during load reversal, resulting in a

distinct X-shaped cracking pattern. The upper joints all eventually began to disintegrate, with cracks as wide as 0.25-2.0 inches forming, and with the concrete bulging and spalling. Early in the tests incremental loads in the cap post-tensioning rods varied consistent with beam-bending theory (i.e. tension forces developed on one side while compression forces developed on the other). Later in the tests all cap post-tensioning rods were observed to carry incremental tension forces as they were called on to resist crack opening and joint dilation.

3. Bent caps developed vertical cracks near their ends. At the top the cracks were located in the narrow interface between the edge of the deck and the joint. The deck proved sufficient to suppress any significant extension of the plastic hinge into the deck. At the bottom, cracks divided and some inclined away from the column, consistent with the shear in the cap. Strains in both top and bottom bars exceeded the yield level. In some cases strains of as much as 2% were recorded. Evidence, however, exists that during later stages of testing the bond broke down between the concrete and the straight bottom rebars in the upper cap. The development length provided for these bars was only 18 bar diameters.

4. In Bent 46, the upper columns did not initially have increased shear capacity in order to measure their shear strength. Shear cracks formed in the west column at a total load of 2694 kips (Cycle 8) towards the west and in the east column at a total load of 2997 kips (Cycle 10) towards the east. Once columns were strengthened by tightening the loose external post-tensioning rods, no further shear distress was noted.

5. Flexural cracking and yielding were noted in the upper level columns just below the upper bent caps. Nonlinearity in plots of rebar strain vs. lateral load were noted during Cycle 9 for columns in all bents. The column bars exhibited strains in excess of 1.8% in tension and compression during the later test cycles.

6. The built-in column hinges at the top of the upper level pedestals were observed to rotate and slip. Instrumentation on the hinge indicated that the vertical opening of the hinge was as much as 0.65 inches. This was most severe for Bent 45 in spite of the wide flange sections clamped to the pedestal and column. Instruments in both Bents 45 and 46 detected horizontal slips between the column and pedestal in excess of 0.45 inches during the last cycles.

Distinct splitting and inclined cracks developed at the tops of the pedestals in Bents 45 and 46. These initiated during load excursions in which the pedestals were displaced towards the interior of the structure. The cracks propagated from the top center of the pedestal (where the dowels extended from the column into the pedestal) and inclined downward toward the interior of the test structure. In Bent 46 the pedestal developed significant flexural deformations with large flexural cracks opening at its base.

The pedestal in Bent 47 was not visible during testing. However, the concrete within the collar was observed after the tests to be pulverized. Because of slip between the steel flanges used to connect the pedestal steel collar to the lower joint and the lower joint a significant discontinuity developed in the lateral displaced shape at the elevation of the top of the lower deck.

It is also important to observe from these tests that damage tended to concentrate with cycling in the upper level. During the initial cycles drifts in the lower level were approximately 30% of the overall deformation. During the last cycle, less than 10% of the total displacement at the upper level was contributed by displacements in the lower level.

The drift indices for the structure during the last cycle were 1.8% overall, but 3.3% for the upper level considering the distance between the tops of the decks. Upper level drift indices would increase to 5.0%, if the clear distance between the upper and lower decks were considered in the calculations.

Each of the bent retrofits behaved in a different fashion. Brief comments regarding each retrofit scheme are offered below.

Bent 45. Bent 45 had steel wide flange sections clamped to the columns by means of horizontal unbonded post-tensioning rods. The clamping force provided for the east side was inadequate to prevent slip between the steel sections and the adjacent concrete (the westside columns had plywood inserted between the concrete and steel so composite action was not expected). Significant local nonlinearities were observed in the instrumental results from nearly the first cycle of testing.

An important consequence of using relatively long (14 ft.) unbonded post-tensioning rods at the joints was that the rods did not take much load until the joint cracked (due to

relative rigidities). Once cracking occurred, the rods stretched significantly, which translated directly to opening of the cracks.

Another problem arose because of the incompatible deflected shapes of the steel wide flange sections and the concrete frame. The post-tensioning rods were unable to maintain contact between the steel and concrete. Significant gaps developed, especially near the joint regions where confinement was desired (see Fig. 3.30). This behavior accentuated damage in the joints. More flexible or weaker steel sections used in conjunction with balanced post-tensioning forces would have been preferable in retrospect.

As a result of these phenomenon the lower joint began to disintegrate at the level of the top hooked bar in the lower cap. This is consistent with observed earthquake damages in the viaduct. However, the actual failure mode observed in the test specimen was heavily influenced by the bond stresses developed in the upper portion of the joint where the longitudinal steel in the pedestal is lap spliced with the discontinuous lower column reinforcement. The area suffered extensive spalling, following formation of a dense criss-crossed cracking pattern over these lap splices.

As indicated earlier the upper joint suffered severe distress. The hinge at the top of the pedestal was observed to open and slip in spite of the attached wide flange sections.

Bent 46. Bent 46 had inclined (untensioned) post-tensioning rods grouted or epoxied in the lower joints. These did not prevent the formation of the characteristic inclined joint crack, but the bond between the bar and adjacent concrete limited crack opening. Instrumentation at the nut on the end of the rod indicated that bond remained effective and load had not been transferred to the external anchorage. An X-pattern of narrow inclined cracks was noted lower in the joint on the east side of the bent. These cracks appear characteristic of the onset of joint shear cracking.

The pedestal acted like a flexural element, eventually forming a large horizontal flexural crack at its base and crushing concrete on the compression face. The eventual

behavior of this response mode was not investigated in these tests and the adequacy of the confinement provided and the resistance of the lap splices at the base of the pedestal to maintain ductile flexural behavior under additional cycling need to be assessed.

In addition, splitting initiated in the hinge at the top of the pedestal and inclined shear cracks were developed near the hinge. Significant rotations and slipping deformations were measured at the hinge.

Bent 47. Bent 47 had a steel collar placed around the pedestal and steel plates were placed over other elements. These details made loud popping noises from nearly the beginning of the tests. No physical source of these noises was detected, but it is presumed that the noise resulted from slippage of the steel plates relative to the concrete members.

The steel plates prevented contemporaneous observation of the damage to the concrete. Upon removal of some of the plates following the tests, the concrete was found to be highly cracked and locally pulverized.

The collar also rotated significantly with respect to the lower joint. The transverse post-tensioning provided to clamp the flanges to the lower joint was inadequate to prevent this slippage and rotation. Because of this rotation, the post-tensioning bars severely distorted during the final cycles of the tests and the pedestal and upper column developed a kink in its deflected shape at the top of the lower deck (compare Figs. 3.33 and 3.34).

4. ANALYSIS OF EXPERIMENTAL RESULTS

4.1 Introduction

In this chapter the experimental results are analyzed and interpreted. Emphasis is placed on reconciling observed behavior with calculated results obtained using analysis methods and design formula commonly employed in engineering practice. In Section 4.2, the strength, stiffness and dynamic characteristics of the original structure are assessed and a simple dynamic analysis is presented to help understand the behavior of the viaduct during the Loma Prieta earthquake. In Section 4.3, the effects of the retrofits on the overall strength and stiffness of the test structure are evaluated and the local behavior of various members and retrofits are studied in detail.

4.2 Original Structure

The measured strength and stiffness characteristics of the reinforced concrete bents prior to retrofitting are compared in this section with results of numerical analyses. Based on the results of these analyses and of supplemental elastic dynamic analyses, the likelihood of collapse due to simple transverse response during the Loma Prieta earthquake is evaluated.

4.2(a) Strength

The strength of the original structure was examined experimentally during the static load test conducted prior to retrofitting. As described in Section 2.3(a), five of the six pedestals of the test structure were clamped during this test. The west pedestal of Bent 46 was not clamped so that the onset and development of damage in the pedestal and lower joint region could be observed. Lateral load was applied toward the west until the onset of well-defined inclined cracking in the pedestal. The total load applied to the test structure at this point was 1410 kips.

The load resisted by each bent was not measured directly. However, given that the columns had nominally identical construction and nearly equal axial loads, and furthermore that the load and displacement applied at the upper deck of each bent were effectively equal, it is reasonable to assume that

each bent resisted one-third of the total lateral load. Thus, the load per bent at onset of well-defined pedestal cracking was approximately 1410 kips/3 = 470 kips.

Estimated Member Strengths. -- To evaluate whether the observed failure mode is consistent with the mode that would be calculated using conventional methods, strengths of members in flexure and shear, and of the entire structure under vertical and lateral load have been calculated. Results of member stiffness and strength calculations are summarized in Table 4.1.

In member strength calculations, steel has been assumed to have an elasto-plastic stress-strain relation with a yield stress of 40 ksi. Effects of inadequate longitudinal rebar anchorage lengths in tension (l_d) were taken into account by assigning a reduced yield stress to the bar. The reduced yield stress was taken equal to the quantity 40 ksi x $l_d/(30d_b)$, which assumes development of the full yield stress for an anchorage length of 30 bar diameters (d_b). The compressive strength of the concrete was taken to be 6 ksi. Standard equivalent rectangular (Whitney) stress blocks were used to represent concrete compression stress zones in the flexural strength calculations. Shear strengths were taken as the quantity

$$V_n = 2\sqrt{f'_c}bd + A_v f_y d/s \qquad (4.1)$$

The effects of axial load on shear strength were disregarded. Nonetheless, the effects of the relatively low axial forces present in the columns due to gravity loads were included in the computation of column flexural strengths, as these effects were expected to be more significant.

The quantities in Table 4.1 indicate that the columns at both levels were stronger in flexure than the bent caps framing into them, despite the relatively large size of the bent caps. Flexural yielding, if it could occur, would be expected on the basis of the relative strengths shown in Table 4.1 to initiate and concentrate in the bent caps. Thus, column yielding and inadequate flexural ductility capacity of the columns were not likely initiators of collapse.

Plastic Collapse Mechanism. -- The distribution of forces that might have existed in the structure at the point of collapse was investigated considering several possible plastic collapse mechanisms. The

collapse models and associated calculation results of Fig. 4.1 were used to evaluate the strength of a typical bent of the test structure subjected to a single lateral load applied at the centroid of the upper deck. Only flexural yielding was considered in these computations, and all members and joints were assumed to have sufficient deformation capacity to develop the mechanisms indicated. The finite dimensions of the joints have been considered in computing these forces. Based on these calculations, a flexural collapse load of 590 kips per bent was determined.

The distributions of moment and shear corresponding to the collapse mechanism are shown in Fig. 4.2. The critical flexural mechanism consists of plastic hinges at each end of the upper bent cap. The lower bent cap and the columns at both levels are stressed below their flexural capacities. Thus, a partial collapse mechanism, consisting of plastic hinges and built-in pin connections in the upper level, would be expected considering flexural action alone.

The critical collapse mechanism requires a total load of 590 kips applied to the upper cap (assumed towards the right) and requires shears of 287 kips and 303 kips in the upper level left and right side columns, respectively. The difference in required column shears is attributable to the difference between the positive and negative moment strengths of the upper bent cap. Because of the larger strengths of the lower columns, and because a single lateral load is applied at the top of the bent, the upper columns are clearly more critical in shear than the lower ones. The shear strength of the upper columns (Table 4.1) is estimated to be 390 kips, greater than that needed to develop a flexural collapse mechanism. The computed shear strength of the pedestal is 320 kips, which is only slightly greater than that required for a flexural failure of the bent. The computed shear strengths of the pedestal and column may be overestimated by Equation 4.1. Several factors could contribute to a reduction in strength. For example, the dowel action required to transfer shear forces across the built-in pin by shear friction induces splitting forces that could reduce strength. In addition the ACI [4.1] stipulates that the quantity $A_v f_y/bs$ be at least 50 psi when transverse reinforcement is provided to resist shear. Computed values of this quantity equal 28 psi for the column and 43 psi for the pedestal. As a result, it would be prudent to disregard the contribution of the ties to the shear strength of the columns and pedestal. The pedestal is weaker than the column and would have a strength of 245 kips based on the concrete contribution alone. This value is

below that required to develop a flexural collapse mechanism and a shear failure in the pedestal might be expected prior to yielding of the bent cap.

Further justification for reducing the shear capacity of the pedestal may be found by examining the detailing of the joint region near the base of the pedestal. ACI provisions for computing shear demands on members have indicated that critical design shears may be taken at a distance "d" from the support, if the support is in a region of compression. The term "d" represents the effective depth of the member. The reasons for this provision are illustrated in Figure 4.5 which has been adapted in part from the ACI Commentary [4.1]. Tests have indicated that arch action and other mechanisms can be counted on to directly transfer to such supports the loads applied near the ends of a properly detailed member. However, when a compression support is not provided, the ACI requires that the full tributary load on the member be considered explicitly for the shear design and that the joints be detailed to transfer the anticipated loads. This condition is illustrated in Fig. 4.5(b).

Considering the lower joint/pedestal in a transverse bent on the side towards the direction of loading (the right side in this example) one can by analogy see that shear cracks would tend to form not only in the pedestal, but also could extend downward into the joint as schematically illustrated in Fig. 4.5 (c). While there is no additional tributary load that needs to be considered in this case, detailing of the pedestal/joint interface region clearly becomes critical. While some transverse steel was provided in the pedestal to help resist shear, reference to Fig. 1.5 shows that the region of the joint into which a pedestal shear crack might propagate was devoid of transverse (horizontal) reinforcement. The top bars in the lower cap were hooked downwards at this location, generally following the likely inclination of a shear crack extending from the pedestal into the joint. Thus, the cap bars cannot be considered effective in restraining such potential shear cracks. Moreover, the bond stresses generated by the hook (the hook is in tension for loads applied to the right in this example) would also tend to split the concrete in the same area.

Detailed finite element analyses can be used to provide quantitative information on the extension of column shear cracks downward into the joint region. However, a simple estimate of the load required can be obtained by computing the shear strength of the pedestal assuming it had no transverse

reinforcement. The concrete contribution alone is estimated, using methods outlined previously, to be 245 kips. This is approximately 78 kips less than listed in Table 4.1.

These revised shear strengths indicate that neither the upper column nor the pedestal would possess sufficient shear strength to develop a flexural plastic mechanism in the test structure. The pedestal is the weaker element and failure would be expected to initiate in the pedestal. The expected failure mode would be brittle because of the low amounts of transverse reinforcement provided in the pedestal and the absence of reinforcement in the lower joint.

Capacity Estimates Based on Elastic Analysis. -- The preceding calculations of lateral capacity are based on plastic analysis. However, the required shear forces in the critical column and pedestal exceeded the capacities of these elements. The simplicity of the structural system and the expected brittle nature of the failure mode makes it possible to estimate the lateral load needed to bring the pedestal to its shear strength by performing an elastic analysis of the bent.

To make this estimate, one needs first to estimate the shears present in the pedestal as a result of gravity loading. While there is no net shear applied laterally to the structure under gravity loading and moments at the tops of the pedestals are negligible due to the built-in pins, significant shears may develop in the columns and pedestals. These shears develop because pin, rather than roller, connections were provided. To restrain the tendency of the base of the columns to splay outward, an inward thrust must be applied by the pedestal to the base of each column (see Fig. 4.3).

Using a simple elastic stick model having non-prismatic sections and rigid beam-column joints, the calculated internal actions are as shown in Fig. 4.4. The initial pedestal shear due to gravity loads is estimated to be 176 kips. The shear acting at the time of testing is not known, because of the uncertain effects of construction activities and over 30 years of service life.

The shear that can be applied to a pedestal due to lateral load is its total shear strength modified by the gravity load induced shears. For lateral loads applied towards the right, gravity load induced shears would increase the shear that can be taken by the left pedestal and decrease the apparent strength of the right pedestal.

Thus, for the critical right side pedestal the incremental shear that can be applied due to lateral loading is approximately 245 kips - 176 kips = 69 kips. Assuming further that under lateral load the two columns of a bent share equally the applied lateral load, the expected lateral load per bent at the onset of shear failure in the right pedestal is 2 x 69 kips = 138 kips. This value is 70% less than the load of 470 kips per bent measured at the onset of inclined pedestal cracks in Bent 46.

One might reasonably argue that creep, shrinkage, cracking, bond deterioration and slip, and other factors may have significantly reduced the initial gravity load related shears in the pedestals. If one assumes that the gravity load induced shears were zero, the lateral load needed at the top cap to induce shear cracking at the base of the pedestal would be 2 x 245 kips = 490 kips per bent, slightly higher than the observed value. While considerable scatter exists in experimental data on shear strength, this result would tend to indicate that a substantial proportion of the gravity induced thrusts may have been relieved over the 32 year service life.

Modified Plastic Collapse Mechanism. -- It can be shown with the aid of some simple additional calculations that the lateral load required to initiate shear cracking in the pedestal/lower joint region, 470 kips per bent, provides a fair measure of the actual collapse load for the structure as a whole. To assess this assertion, consider the simplified stick model collapse mechanism shown in Fig. 4.6. For this idealized mechanism the pedestal shear failure has been included and is represented as a 45-degree inclined failure plane having a horizontal resistance of 245 kips, the computed nominal shear strength of the concrete in the pedestal. The critical collapse mechanism for the upper level can be completed by introducing a flexural plastic hinge at the opposite end of the upper bent cap. The flexural resistance at this location is taken as the positive moment strength of the bent cap considering the inadequate anchorage of the bottom bars. External loads considered in the analysis include the approximate average upper level weight per bent (W = 1085 kips total) and a horizontal load applied to the top level of each bent, H.

For the depicted mechanism, a lateral force H having a direction **opposite** to that shown in Fig. 4.6 is required. This solution indicates that once a shear failure commences in one of the pedestals along an inclined failure plane, gravity load alone is sufficient to drive the global failure to its conclusion.

Refinements to the above analytical collapse model are undoubtedly possible, but not likely to alter this basic conclusion. The progressive collapse depicted in the demolition photo sequence shown in Appendix A further demonstrates the ability of a local failure in the pedestal region to produce a total collapse of the upper level.

Lateral Shear Coefficients. -- A typical upper level bent including a 70-ft deck span weighs 1085 kips. Thus, the measured load capacity of 470 kips per bent corresponds to an upper deck shear coefficient (lateral load/weight) of 0.43.

If lateral loads during dynamic response are assumed to distribute in a ratio 2:1 (upper:lower deck) corresponding to a linear mode shape and equal deck masses, the effective base shear corresponding to the upper deck strength of 470 kips is 1.5 x 470 kips per bent = 705 kips per bent. A typical two-level bent including a 70-ft deck span weighs 2215 kips. Thus, the effective base shear coefficient is 0.32. Had premature shear failures been prevented by adequate detailing, the calculated effective base shear coefficient increases to 1.5 x 590 kips/2215 kips = 0.40. These coefficients are well in excess of the design base shear coefficient of 0.06 required by the 1953 AASHTO specification to which the viaduct was designed.

Shear Strength of Columns. -- The tests on the retrofitted structure provide data on the shear strength of the upper level columns in their original state. During these tests, the post-tensioning rods over the mid-height of both upper columns in Bent 46 were not initially tightened. As described in Section 3.5(c), inclined cracking indicative of distress in shear in the two columns began during different cycles, but in each case lateral loads were approximately 900 kips per bent. Shearing distress was initially observed in a column when lateral load was applied toward the column relative to the center of the test structure. Assuming that the initial column shear due to gravity load effects was equal to 176 kips (calculated as described above using elastic theory), the shear in the critical column at the onset of inclined cracking was approximately 176 + 900/2 = 626 kips. Based on the average column effective depth of 42 inches, and assuming a concrete compressive strength f'_c of 6000 psi, the corresponding average nominal

shear stress was 626/(42 x 48) = 311 psi, or approximately $4.0\sqrt{f'_c}$. If one discounts the initial gravity load induced shear (because of prior service conditions), the nominal shear stress reduces to 223 psi, or approximately $2.9\sqrt{f'_c}$.

Current ACI and AASHTO recommendations regarding the shear strength of columns suggest that the nominal contribution of the concrete may be taken as:

$$V_c = 2[1+N_u/(2000A_g)]\ \sqrt{f'_c}b_w d \qquad (4.2)$$

where N_u is the axial load. The axial force due to dead load in the upper columns is approximately 1085 kips/2 = 543 kips. The axial load in the columns corresponding to 900 kips lateral load per bent can be estimated by statics assuming that the built-in pins at the base of the upper columns develop no moment. For this condition, the axial load due to overturning moment effects is approximately 253 kips. The critical column then has a total axial compressive load of 543 + 253 = 796 kips. This value is relatively low (less than 5.8% of the gross area of the column times the compressive strength of the concrete). Nonetheless, substituting this value into Eq. 4.2 suggests that the concrete contribution is approximately $2.4\sqrt{f'_c}$bd, or approximately 20% more than permitted for zero axial load. Steel transverse reinforcement would also be expected to contribute somewhat to the shear resistance. This contribution is almost $0.4\sqrt{f'_c}$bd according to standard design provisions. By summation, the total nominal shear resistance of the column should be $2.8\sqrt{f'_c}$bd, which is very close to the observed range of 2.9 to $4.0\sqrt{f'_c}$bd.

The small discrepancy may be partially due to uncertainties in estimating the distribution of shear forces between the two columns in the bent. These are expected to be influenced by the different axial loads present in the columns as a result of overturning moment and other effects. Because of these and other uncertainties, prudence is warranted in evaluating the shear strength of columns. In particular, the rapid deterioration under cyclic inelastic loading of the shear strength of columns with low axial load intensities has prompted many design codes (ACI and partially AASHTO) to discount entirely the contribution of the concrete to shear strength. These tests shed little light on this broader problem.

However, they provide additional confidence that conventional procedures can provide reasonable estimates of cracking loads in shear-critical elements.

4.2(b) Stiffness and Dynamic Characteristics

The test structure was modeled analytically as an elastic three-dimensional structure using the SAP90 series of computer programs [4.2]. In the model, columns and bent caps were modeled using line elements coincident with member centerlines and the multi-cell box girders were modeled using shell elements located at the mid-depth of the box girder. Beam-column joints were assumed to be rigid and as such were modeled using relatively stiff line elements to interconnect the more flexible beam, column, and box-girder elements. The base of the analytical model was assumed to be fixed (i.e., soil-structure interaction was not considered). The built-in shear key/pin connections at the tops of the pile caps and pedestals were modeled as ideal pin connections. Figure 4.7 depicts the assembled finite element model of the structure.

Element properties of the analytical model were based on nominal gross concrete sections of the test structure (cracking was assumed to not occur). For the beam and column elements, flexural and shear stiffness in both principal directions, and axial and torsional stiffness along the axis of the member were considered. For the shell elements, both membrane and plate bending actions were included. Based on measurements from a concrete core taken from an undamaged portion of the Cypress Street viaduct [1.5], concrete modulus and Poisson's ratio were assumed to be 3,700 ksi and 0.15, respectively. Corresponding modulus values of cores from the test structure averaged 3440 ksi (Table 3.3).

Figure 4.8 compares measured and calculated relations between lateral load and lateral displacement at the mid-depth of the upper deck. The measured relations were obtained during the static lateral load tests of the test structure prior to retrofitting (see Section 3.3 for a description of the test). The calculated load vs. displacement relation was obtained by applying a lateral load just below the deck level, on the two edge nodes of each bent of the analytical model described previously. The calculated stiffness slightly exceeds the measured stiffness.

Mode shapes and frequencies were also calculated using the analytical model described above. The two lowest calculated transverse translational modal periods (frequencies) are 0.382 sec. (2.62 Hz) and 0.144 sec. (6.96 Hz). These values compare with periods (frequencies) of 0.42 sec. (2.4 Hz) and 0.14 sec. (7.0 Hz) measured during forced vibration tests of the original structure. The calculated mode shapes, shown in Fig. 4.9, were < 1.0, 0.269 > for the first mode, and < 1.0, -3.44 > for the second mode.

4.2(c) Expected Response During Loma Prieta Earthquake

It is not possible given the simple model of Fig. 4.7 to represent fully the response of the viaduct during the Loma Prieta earthquake because the model does not consider the complete 1.5-mile length of the structure and supporting soil. However, it is possible given the simple model to obtain a rough estimate of structural response in the transverse direction, and with that estimate to draw a conclusion as to whether simple transverse response of this bent would be sufficient to explain the collapse of the structure during the earthquake.

For the response analysis, three ground motion records obtained in the vicinity of the structure were considered (Figs. 1.9 through 1.11). Based on considerations of proximity and similarity in soil conditions, the record obtained at the Oakland Wharf (Fig. 1.11) was selected to represent the base motion under those portions of the viaduct that collapsed.

The analytical model of Fig. 4.7 represents the stiffness and mass of the test structure. As such, it includes the stiffness of three typical bents, but less than the mass of three typical bents because the two short deck cantilevers on either end of the test structure did not compose the full tributary span (Fig. 2.1). In order to better represent the typical mass of the viaduct, the deck cantilevers were lengthened in the analytical model used for the dynamic analysis. Viscous damping was assumed equal to 2 percent of critical. The 035 component of the Oakland Wharf motion was applied in the transverse direction of the Cypress viaduct analytical model.

Response histories of computed upper deck displacement, upper deck acceleration, base shear, and input base acceleration are plotted for the analytical model in Figs. 4.10 through 4.12. The waveforms indicate that significant response lasted for a duration of approximately 14 seconds. A maximum displacement of 1.29 in. (0.24 percent of total height), maximum base shear of 1230 kips per bent (56 percent of total weight), and a maximum upper deck shear per bent equal to 752 kips were obtained from the elastic analysis.

As indicated in Table 3.1, inclined cracking of the non-retrofitted structure occurred near the base of the pedestal (at the end of Cycle 2) at a load of 470 kips per bent and at an upper level lateral displacement of 0.79 in. Thus, the dynamic analyses for this ground motion indicate forces and displacements more than 60% greater than the structure could resist. The accelerations in Fig. 4.11 suggest that forces (mass times acceleration) exceeding the shear strength of the pedestal joint region would have developed at least nine times had the structure remained elastic. Analyses presented in Section 4.2(a) demonstrated that initiation of pedestal cracking and failure would be sufficient to cause overall instability and collapse of the upper deck level.

Thus, simple dynamic response analyses for the transverse direction of motion (as considered here) are sufficient to account for collapse of the viaduct. Other factors (such as longitudinal response, traveling waves, and earlier failures in other bent types) may have contributed to the failure, but were not necessary for collapse to develop.

4.3 Retrofitted Structure

An evaluation of the behavior of the retrofitted bents is made in this section. The evaluation is based on experimental and numerical analyses, and includes an evaluation of the overall strength and deformation characteristics of the retrofitted structure and of the local behavior of retrofit details.

4.3(a) Global Strength

Static lateral load tests of the retrofit test structure were continued until the effective lateral load strength was developed. During the final cycle of load toward the west, lateral load continued to increase

at a relatively low rate with increasing displacement, indicating that the strength was nearly realized. During the final cycle of loading toward the east, the structure was displaced laterally under effectively constant lateral load, indicating the effective strength had been reached (Table 3.2 and Fig. 3.12).

Figure 4.13 compares load - displacement relations measured before and after retrofitting. The maximum applied lateral load following retrofit was approximately 4000 kips, or nominally 1333 kips per bent. Thus, the retrofits strengthened the test structure by a factor of 2.84 relative to the strength achieved (470 kips per bent) prior to retrofitting. More significantly, the maximum displacement achieved following retrofitting was 12.5 times the maximum displacement corresponding to inclined cracking of the pedestal.

Lateral Stiffness and Displacement Ductility. -- Figure 4.13 also indicates that the overall initial elastic stiffness of the retrofitted structure was virtually unchanged by the retrofitting. Figure 3.15 compares results for the original and retrofitted structures obtained during the initial loading cycles. Once a load of 150 kips is reached the tangent stiffnesses obtained during the two tests are essentially identical. Detailed calculations of the lateral load stiffness of the retrofitted structure have not been carried out. Numerous practical difficulties exist in calculating the effective stiffness of the various composite and prestressed sections.

A nominal yield displacement for the retrofitted structure may be calculated by assuming a lateral load stiffness equal to the measured value for the retrofitted structure, K = 2495 k/in. and a strength equal to 4,000 kips. The nominal yield displacement thus calculated is 1.60 in. at the upper deck. The maximum displacement achieved during the tests was 9.90 in., corresponding to a displacement ductility of 9.90/1.6 = 6.2. The test structure attained this displacement ductility for a single cycle, and sustained significant damage in the process. Stable response was apparently obtained for displacements on the order of 4 in., corresponding to a displacement ductility of 2.5.

Ultimate Lateral Shear Coefficients. -- The maximum total lateral load applied to the retrofitted test structure was approximately 4000 kips in each direction. Given that a typical upper level bent weighs 1085 kips, the effective upper deck lateral shear strength coefficient was 4000/(3 x 1085) = 1.23.

If lateral loads during dynamic response are assumed to develop in a ratio of 2:1 (upper:lower decks), the effective base shear strength is 1.5 x 1300 kips per bent = 1950 kips per bent. Two levels of a typical bent weighed 2215 kips. Thus, the effective base shear coefficient was about 0.90.

During the tests, effectively equal loads were applied by the jacks to each bent of the test structure. However, the strength and stiffness characteristics of each bent were different, so that each bent resisted different loads. Statics alone cannot be used to resolve the load distribution between the bents (or for that matter within a bent). To help estimate the force distribution, measurements from strain gages attached to reinforcing steel in the bent cap and columns of each bent were analyzed. Unfortunately, because each bent had different crack locations and unknown initial strains, strain gage readings could not be reliably interpreted to estimate the distribution of forces.

Estimated Retrofitted Member Strengths. -- Member flexural strengths were calculated assuming both composite and non-composite flexural action between the retrofit steel and the original reinforced concrete sections. Sufficient transverse reinforcement was provided in the columns and pedestals to prevent a shear failure during testing. Thus, shear strengths are not computed or reported here for the retrofitted structure. Table 4.1 lists the calculated cross-sectional flexural strengths.

In the calculations, reinforced concrete material properties were the same as those described in Section 4.2(a). Steel plate and wide flange sections used for the retrofits were assumed to develop 36-ksi yield stress and to have a modulus of elasticity equal to 30,000 ksi.

For the non-composite calculations, the cross-sectional flexural strength and stiffness were taken as the sum of the separately calculated values for the reinforced concrete and steel sections. Conventional assumptions were made to compute reinforced concrete flexural strengths, as described in Section 4.2(a). Steel sections were assumed to develop plastic strengths equal to the product of the yield stress and their plastic section modulus.

For the composite calculations, the steel was assumed to act as additional reinforcement for the reinforced concrete sections, with strengths calculated as described in Section 4.2(a). Differences in details on the east and west sides of the structure result in strength differences not reflected in Table 4.1.

Plastic Collapse Mechanism. -- The expected lateral load strength of each bent was calculated for the flexural mechanisms shown in Fig. 4.1. The calculated critical non-composite and composite strengths for the entire test structure are 2340 kips and 4610 kips, respectively.

Figure 4.14 compares the measured load-displacement relation following retrofitting with the calculated strength levels. In this figure, the lines denoted "Original Structure" correspond to the load measured during the static tests before retrofitting. The lines marked "Non-composite" correspond to strengths calculated for the retrofitted structure assuming the retrofit steel and the concrete sections did not act compositely in flexure. The lines marked "Composite" correspond to the strengths calculated assuming fully composite behavior in flexure. It is clear that the retrofitted structure developed a strength significantly higher than the original structure. The measured strength of the retrofitted structure was between calculated strengths corresponding to the non-composite and composite assumptions.

4.3(b) Behavior of Retrofitted Bents

The behavior of the various retrofits will be examined in this section. Emphasis will be placed on the lower joint region where distress was observed during the Loma Prieta earthquake. The behavior of the upper cap-column joint will be examined in Section 4.3(c).

Bent 45. -- To develop the plastic composite strength of a combined steel and concrete section subjected to shear requires that a frictional force be developed between the two sections. Figure 4.15 illustrates this requirement for a typical column of Bent 45, which had large steel wide flange sections prestressed to the east and west faces of the reinforced concrete columns. The total frictional force required along the height of the column in Fig. 4.15 is approximately equal to the tensile strength of the steel sections. For lateral loading in the opposite sense the required friction force would approximately

equal this value, corresponding to tensile yielding of the wide flange section at one end of the column and compressive yielding at the other.

The minimum friction force required for composite action is then approximated by 36 ksi x 4 x 32.9 $in.^2$ = 4740 kips. In the retrofit of Bent 45, the steel sections were clamped in place using 1-3/8-in. diameter post-tensioning rods. Assuming a friction coefficient of 0.5, each level (pair) of clamping rods could develop the prestress force in one of the rods in friction. So the fifteen levels of 55-kip prestressed rods and four levels of 95-kip prestressed rods could develop a total of 1205 kips friction force, well below the value of 4740 kips required. The prestressing provided (Fig. 2.14) was clearly inadequate to achieve full composite action for this bent.

As indicated in Section 3.5, slip between the steel retrofits and the concrete was observed almost from the beginning of the tests. Figure B.35 (Channel 30) illustrates the resulting nonlinear behavior. The breakdown of composite action also appears to be the cause of the complex nonlinear response recorded (Figs. B.39 through B.44 (Channels 64, 65, 66, 67, 76 and 77)) by the strain gages attached to the wide flanges.

The prestress in the rods used to clamp the steel sections to the reinforced concrete sections must be sufficient to maintain contact under the imposed lateral deformations. Contact over much of the columns and especially the joints was lost during the tests. This behavior is illustrated schematically in Figs. 3.30 and 4.15. During the final stages of testing, the gap between the steel and concrete sections at the lower, east joint of Bent 45 was approximately 3/8-in. wide.

The opening of the gap is attributable to (a) the large flexural stiffness of the steel wide-flange and concrete sections, (b) the incompatibility of the deflected shapes of the reinforced concrete structure and the steel wide flange sections and (c) insufficient prestress force and axial stiffness provided by the prestressing rods that clamped the wide-flanges in place. As illustrated in Fig. 2.14 and 2.17, the prestressing rods were external to the reinforced concrete sections. Over the depth of the bent cap these rods were anchored to the first internal web of the box girder (for those rods within the box girder depth) or across the full bent cap span for those below the box girder. The long unbonded lengths of the rods adjacent to the bent caps resulted in relatively low effective stiffness of the post-tensioning rods. Once

the initial prestress was overcome, the axial flexibility of the rods allowed the wide flange sections to separate from the concrete joints with relative ease.

The external post-tensioning rods within the depth of the joints provided a small amount of joint confinement in the initial undeformed condition of the structure. Under lateral deformations, as described above and illustrated in Figs. 3.30 and 4.15, the steel sections of Bent 45 tended to separate from the joint, rendering completely ineffective the intended joint confinement.

In addition, once the lower joints cracked, the low effective stiffness of the long unbounded post-tensioning rods resulted in large crack openings within the joint. A quantitative example of this is presented in Section 3.5(e) for the lower west joint where elastic stretching of the post-tensioning rods was shown to contribute the majority of the crack opening displacement in the lower joint.

Damage sustained in the lower east joint of Bent 45 (Fig. 3.37) attests to the final cumulative consequences of these effects. The lack of well-distributed cracking within the joint is attributed to the nearly complete lack of bonded transverse joint reinforcement. Clearly, more flexible and weaker steel wide flange section retrofits and a stiffer post-tensioning system would have improved the observed behavior. Nonetheless, details of the final severe damage condition in this joint are also significantly influenced by the bond stresses around the lap splices between the pedestal and column longitudinal reinforcement in the joint.

Bent 46. -- In contrast with the behavior of the Bent 45, the lower joint of Bent 46 did not sustain significant damage by the end of the test. The improved performance is attributed to the presence of the internally bonded post-tensioning rods (Fig. 2.15) which reinforced the upper portion of the joint so that the pedestal shear cracks which extended down the joint were no longer the weak link in the system. In addition, the small bearing plates (rather than the wide flange sections employed in Bent 45) used to anchor the external post-tensioning on the lower bent cap were able to maintain their confining action throughout the tests.

The effectiveness of bonded rods combined with steel wide flange sections was not tested in this test program. However, given the higher stiffness of the bonded rods, and the ability of bonded

reinforcement to better distribute concrete cracking, it is speculated that the addition of bonded rods to the steel wide flange retrofit would result in a significant improvement of joint behavior.

As noted in Section 3.5(e), a large, nearly horizontal, crack developed across the bottom of the pedestal on the west side of Bent 46 where the longitudinal bars from the pedestal lapped the discontinued longitudinal steel from the lower column. It is not certain if this crack was associated with tensile yielding of reinforcement or with anchorage slip. On the east side, spalling initiated on the exterior face of the pedestal/joint region where there was a gap between confinement plates. Thus, by the end of the test this retrofit began to develop localized flexural/anchorage distress that may have worsened during additional cycles. This aspect of the behavior requires further study.

In addition, this joint was the only one to exhibit evidence of apparent shear distress in the lower portion of the joint. While the embedded bars proved very effective in resisting the propagation of the pedestal inclined cracks down into the joint, their orientation was ineffective against orthogonally directed diagonal cracks. Thus, means of reinforcing the joint by additional embedded bars or other techniques remain to be examined. The lower joints in the test structure were not as severely loaded as the upper joints. Because the test structure was loaded only at the upper level, the lower bent cap remained elastic. Thus, these tests did not produce critical loading conditions for the retrofits used on the lower joints.

Bent 47. -- Concrete in the pedestals and lower joints in Bent 47 was not visible during the tests. However, loud popping noises were heard from the vicinity of the joints, starting as early as Cycle 2. It was assumed that these noises were associated with the slip of the retrofit steel relative to the concrete. During the later cycles, a discontinuity in the deformed shape was noted just above the lower bent cap. The steel flanges connecting the restraining collar of the pedestal to the lower joint rotated visibly, severely distorting the post-tensioning bars used to clamp the flanges to the joint.

A simple estimate of the lateral load needed to cause the flanges to rotate can be made by analogy to the analysis of bolt groups. In this case, a pin will be assumed at the top of the pedestal, the shear and flexural resistance of the concrete in the pedestal will be disregarded, gravity load induced shears in the pedestal will not be considered, and additional column axial loads due to global overturning moment

effects will be neglected. From the geometry of the pedestal and the locations of the post-tensioning rods, it can be shown that the frictional force resisted by the most severely loaded post-tensioning rod clamping the flange to the joint is approximately 140% of the lateral shear applied at the top of the pedestal.

Assuming the 1-in. diameter post-tensioning rods are stressed to 50 kips and that a friction coefficient of 0.5 can be developed between the steel and concrete, slip would initiate for pedestal shears near 36 kips. Assuming each pedestal resists the same load, the total lateral load is 6 x 36 kips = 220 kips. This result is highly approximate. Factors such as the resistances of the concrete in the pedestal and the distributed friction developed under the flanges would tend to increase this value. However, factors such as incremental axial loads due to overturning moments would tend to decrease the value.

Slip would be unlikely until the concrete in or below the pedestal cracked in shear. This cracking occurred in the tests of the original structure at a load of 1410 kips. Assuming loads are uniformly distributed between columns at this point and that the strength of the concrete pedestal and steel retrofit are additive, one might estimate the load needed to cause initial slip to be 1410 + 220 = 1630 kips. Once the pedestal cracked slipping would be expected at the lower value of 220 kips.

The estimated 1630-kip pedestal shear needed to initiate slip between the collar flanges and the joint is consistent with experimental observations. The first popping sounds from the joints in Bent 47 were noted towards the end of Cycle 2 as total loads approached 1800 kips. The noises were not detected during Cycle 1 for which the maximum load was 900 kips.

It is clear that the retrofit used on Bent 47 had a high composite ultimate strength, but the clamping forces were insufficient to maintain composite action. Moreover, the relative slip of the collar and the joint resulted in severe distress to the joint and pedestal. During demolition, much of the pedestal region was observed to have been pulverized by prior cycling, and the joint region had a fully developed set of narrow, but closely spaced, inclined cracks. Similarly, it should be recognized that the retrofit does not address potential joint shear problems in the lower joint.

4.3 (c) Behavior of Upper Joints

Each of the upper joints developed significant inclined cracking indicative of shear distress before lateral loads reached the 2700-kip level. By the end of testing, severe cracking and dilation of the joint regions was obvious, with large sections of concrete within these regions having been completely dislodged from the rest of the joint.

The extent of inelastic action within the upper bent cap-column joints can be evaluated from the instrumentation monitoring local deformations of the upper west joint of Bent 46. Using the displacement transducers indicated by Channels 11, 12, and 17 in Fig. 2.31(h), the shear deformation in the joint can be estimated from Eq. 3.1. The plot of lateral load vs. joint shear distortion shown in Fig. 3.27 indicates that shear deformations are relatively low for lateral loads less than approximately 3350 kips. The shear deformations increase substantially beyond that load level. Significant inelastic deformations of the entire structure become apparent at approximately the same load level (Figs. 3.12 through 3.14).

The observations of the preceding paragraph suggest that a primary source of inelastic deformation in the structure was the bent cap-column joints in the upper level, and that these joints were the weak link of the retrofitted framing system. Retrofit of a structure such as the Cypress Street viaduct should explicitly consider the limiting strength of the joints. These results also indicate that it is generally insufficient to fix only one portion of a structure without examining the hierarchy of potential failure mechanisms.

Although it is not possible to determine precisely the shear strength of the joints (because the load per column is not known), it is possible to calculate an upper bound to the joint shear strength. Considering the connection illustrated in Fig. 4.16, the maximum shear force that can develop within the joint is equal to the tensile strength of the top reinforcement in the upper bent cap. In the test structure, the total area of reinforcement was equal to 15.6 in.^{2}, and the maximum stress was likely to be near the yield stress of 43 ksi. Thus, the maximum joint shear is 15.6 in.^{2} x 43 ksi = 670 kips . This corresponds to an average nominal joint shear stress of 670 kips/(48 in. x 48 in.) = 291 psi, or $3.8\sqrt{f'_c}$, based on a

6000-psi concrete strength. This value compares with an ultimate joint shear stress of $3.5\sqrt{f'_c}$ suggested by ACI Committee 352 in 1976 for unconfined joints [4.2].

It is significant to note that the post-tensioning provided in the upper bent cap was unable to prevent disintegration of the joint. The post-tensioning introduced an average prestress of 130 psi to the bent cap. Initially, incremental forces in the upper and lower post-tensioning bars were of opposite sign consistent with stress variations associated with bending of the adjacent bent cap. However, in later cycles only tensile force increments developed as a result of the expansion of the joints during cycling, and the forces in some of the rods reached or exceeded their nominal capacities.

The deteriorated condition of the bent cap-column joints (Fig. 3.37 through 3.42) when the maximum displacement was achieved suggests that sustained cycling at this deformation level would not have been possible. Thus, for a design earthquake requiring several deformation cycles to a given displacement amplitude, a smaller allowable displacement (i.e. displacement ductility) would be desirable. It is not possible given the available test data to define this allowable value. However, it is clear that a displacement, corresponding to the final displacement cycle, is inappropriate. This conclusion applies to bents for which inadequate provisions are made for strengthening the bent cap-column joints to avoid inelastic action within the joints.

5. CONCLUDING REMARKS

5.1 General

Tests on a undamaged portion of the double deck Cypress Street viaduct following the October 17, 1989 Loma Prieta earthquake have provided considerable information regarding the seismic behavior of such structures and the efficacy of various partial retrofit techniques. It is naturally tempting to generalize the results of such tests. However, it must be recognized that the structure incorporated many unique features and that the many assumptions and idealizations introduced in the test program limit the general applicability of the results. Nonetheless, the studies reported herein provide insight into some of the general modes of behavior expected of existing non-ductile concrete freeway structures, the approaches that might be taken in their seismic evaluation and retrofit, and the various pitfalls that might be encountered along the way.

It should also be noted that the intent of this research program was not to investigate comprehensively the specific causes and extent of the failures observed in the Cypress Street viaduct. Indeed, these studies have only considered the transverse behavior of a small undamaged portion of the viaduct. As a consequence, this study has not addressed a number of important issues that may have affected the overall details of the observed failure. These issues include the effects of traveling waves in the soil and in the structure, soil-structure interaction, variability of the supporting soil and foundation systems, access ramps, and alignment changes. Significantly, this study has not addressed issues associated with the longitudinal motion of the viaduct. It was understood in designing these tests that any overall retrofit system would incorporate a mechanism for limiting longitudinal motion.

With these limitations in mind, some general observations are offered below regarding the behavior of the original and retrofitted viaduct as assessed from analysis of the tests reported herein. More detailed observations and interpretations of the data can be found in Chapters 3 and 4.

5.2 Construction and Test Issues

Inspection of the test structure following the earthquake indicated that construction was generally in close conformance with the design drawings. The structure was generally free of corrosion or other signs of deterioration. Material tests indicated in-situ properties exceeded minimum design specifications.

While the structural system used for the viaduct gave the outward appearance of being simple, this appearance was deceptive. A variety of complex bent types were necessitated to accommodate right-of-way, alignment and other requirements. The structural system incorporated numerous built-in pins, apparently in an attempt to minimize secondary stresses due to creep (in post-tensioned bents) and differential settlement, to facilitate future widening of the viaduct, to reduce moments transferred to the foundations, and to simplify analysis efforts. These pins resulted in a system with little or no redundancy. Inspection of construction drawings indicated that the structure was detailed consistent with design practices common at the time of its design. Major deficiencies relative to current design practices included inadequate transverse shear reinforcement (especially in joints and columns), insufficient development lengths of bars terminating in joints, and the general absence of ductile details.

The research program has demonstrated the feasibility of large scale structural testing. The test structure is among the largest tested to date in the world. No insurmountable technical or logistic problems were encountered. The loading and data acquisition systems performed satisfactorily. It should be recognized that a number of factors contributed to the success of the project, including excellent logistics support and management, the proximity of the test site to the host research organization, and the unusually good weather experienced during testing. The tight test schedule was the only major factor restraining the scope of the research program.

5.3 Original Structure

The tests confirmed that collapse of the structure was likely triggered by a local failure involving the short pedestal used to support the upper columns and the lower bent cap-column joint. Shear forces in the columns resulted in inclined cracks at the base of the pedestal that extended downward and outward into the joint, roughly following the projection of the hook at the ends of the top bars in the lower bent

cap. These cracks formed at a lateral load equal to approximately 43% of the weight of the upper deck and at overall lateral drifts of approximately 0.14% of the total height.

As was common at the time of construction, transverse reinforcement was not placed in the joints to resist shear or to provide confinement. As a result, the lower joint was the weak link for the shear resistance of the column and pedestal. Simple elastic and plastic static structural analyses and conventional design formulae used to assess member capacities were able to identify the location of the initial failure and the approximate load at which failure occurred. Tests during demolition and subsequent analyses demonstrated clearly that a failure in the pedestal/joint region would precipitate collapse of the upper deck without the need for any additional lateral load.

Not withstanding the above observations, tests indicate that the typical bent would likely be able to resist a base shear equal to approximately 31% of its weight before failure (assuming inertial forces at the upper level during dynamic response are twice those at the lower level). This value is far greater than the 6% working stress coefficient employed in the original design.

Simple elastic dynamic analyses of a model of the test structure indicate forces and displacements 60% greater than those needed to initiate failure for a ground motion recorded during the Loma Prieta earthquake near the viaduct. While this study did not address all of the factors that could have contributed to the collapse, it is clear that elementary structural deficiencies were by themselves sufficient to explain the observed failure.

The calculated first mode period for the test structure was approximately 9% less than the measured value. There are significant discrepancies between measured and calculated mode shapes. These discrepancies may be due to soil and foundation flexibility.

5.4 Retrofitted Structure

Three different retrofits were attempted to mitigate the problems identified at the lower joint region. In Bent 45, these consisted of steel wide flange sections clamped to the exterior faces of the columns. In Bent 46, the lower joint was reinforced with steel rods grouted or epoxied in holes drilled at an angle through the joint/pedestal region. In Bent 47, the pedestal was confined within a steel jacket

clamped to the lower joint. In addition, the columns were reinforced to provide additional confinement and shear strength, and the bent caps were post-tensioned longitudinally to help confine and strengthen the joints, improve anchorage of bars extending into the joint from the columns, and provide well-anchored longitudinal reinforcement for the cap beams.

These retrofits were all able to maintain the vertical load integrity of the structure through relatively large lateral deformations. Retrofitting had little effect on overall lateral stiffness, but increased strength by 184% and deformability by 1150% relative to the original structure. A single excursion to a displacement ductility of approximately 6 was achieved. Visible damage at this deformation level was severe. Stable lateral load-displacement relations were achieved for cycles of reversed deformation up to displacement ductilities of nearly 2.5.

The retrofits in Bents 45 and 47 were unable to maintain composite action without evidence of large slip between steel and concrete. Areas of severe local distress were observed in these bents. Relative slip between the retrofit steel and the concrete was detected in both bents as early as Cycle 2. Simple calculations performed after the tests identified the likelihood of non-composite behavior. This situation indicates that retrofits must consider not only ultimate strength, but the compatibility and relative deformability of the original and retrofit systems as well.

Retrofits employing steel cladding may not be fully effective until the underlying concrete structure cracks or fails, and thereafter the deformations (and local damage to the concrete skeleton) are controlled by the flexibility of the retrofit system. In these retrofit tests, the long unbonded post-tensioning rods in Bent 45 permitted the opening of wide cracks in the concrete joints and of large gaps between the retrofit steel and the concrete. The bonded tendons embedded in Bent 46 performed much better in this regard. Crack opening at the critical shear surface was effectively limited. However, construction problems associated with drilling holes through heavily congested joints and uncertainties regarding retrofit behavior under different loading conditions suggests the need for further research.

Retrofits, such as those used in Bent 45 and 47, which encase the original concrete structure in steel, make inspection of damage difficult. In the case of Bent 47, concrete within the pedestal was

pulverized by the end of the test. While the load carrying capacity was not jeopardized, non-destructive methods need be developed for detecting such damage following earthquakes.

The upper joints on both sides of all bents suffered apparent shear failures, with accompanying wide diagonal cracks and spalling of large portions of the concrete cover. The test results indicated that a substantial portion of the global inelastic deformations achieved by the structure was associated with this shear distress in the upper joints, rather than with ductile flexural yielding of retrofitted members. It is unlikely that the retrofitted structure could have sustained additional load cycles in its final damaged condition.

None of the joints in the test structure were explicitly reinforced to enhance their shear capacity. The absence of significant joint shear distress in the lower bent cap - column connection should not be taken as an indication of adequate shear capacity in these joints. Rather, it is a consequence of the fact that the base of the retrofitted pedestal (with the possible exception of Bent 46) remained the weak link in the system and that, by loading the test structure only at the top level, it was not possible to develop the full plastic moment capacity of the lower bent cap. As a result, the lower joints did not experience their maximum shear demand. A more effective pedestal retrofit and a more realistic lateral loading distribution could have resulted in joint shear distress at the lower level as well.

The test results clearly indicate the importance of considering the strength and deformability of joints and of identifying the likely hierarchy of member and joint failures during the retrofit design process. Simply retrofitting damaged elements is not a guarantee of satisfactory behavior.

Instruments attached to the built-in pin connections indicated that these connections slipped in some cases nearly a half inch and opened significantly as a result of pin rotations. Local splitting cracks were noted in the vicinity of the connection dowels in spite of local supplemental confinement. In damaged portions of the viaduct, large splitting cracks were observed at this location. The behavior of these connections, especially for situations requiring high shear transfer and multiple cycles, needs further investigation.

5.5 Recommendations for Future Research

These tests were an important first step in understanding the seismic behavior of existing and retrofitted double deck viaducts. However, further research is needed to provide additional insight into the behavior of these structures and to increase our understanding of the reliability of other types of retrofits. Laboratory tests to permit direct comparison of various retrofits under carefully controlled and instrumented conditions should be carried out. Clearly, some of the retrofits used in the test structure could be substantially improved on the basis of the observed performances and additional analyses. The more promising of these schemes should be investigated further. The behavior of existing cap-column joints needs to be better understood and effective strengthening and toughening strategies are required. The factors that control the vertical load integrity of columns that sustain shear distress needs further study.

The behavior of double deck viaducts in the longitudinal direction needs to be investigated. In particular, studies are required to assess the effectiveness of various longitudinal bracing systems and the torsional resistance of the bent cap as it relates to the load carrying system in the longitudinal direction.

Additional analytical studies are needed to assess in greater detail the behavior of the original and retrofitted test structure. Such studies will provide greater understanding of the factors contributing to the response and will provide a benchmark for validating the accuracy of analytical modeling techniques. Studies are also needed to assess the global behavior of long viaducts and to determine the contribution to the response of factors such as soil-structure interaction, traveling waves, variations in soil and foundation properties, local nonlinearities, and expansion joints.

References

1.1 Astaneh, A., Bertero, V.V., Bolt, B.A., Mahin, S.A., Moehle, J.P. and Seed, R.B., "Preliminary Report on the Seismological and Engineering Aspects of the October 17, 1989 Santa Cruz (Loma Prieta) Earthquake," Report No. UCB/EERC-89/14, Earthquake Engineering Research Center, University of California, Berkeley, October 1989.

1.2 Nims, D.K., Miranda, E., Aiken, I.D., Whittaker, A.S. and Bertero, V.V., "Collapse of the Cypress Street Viaduct as a Result of the Loma Prieta Earthquake," Report No. UCB/EERC-89/16, Earthquake Engineering Research Center, University of California, Berkeley, 1989.

1.3 The American Association of State Highway Officials, "Standard Specifications for Highway Bridges," 6th ed. published by the Association, 1953.

1.4 State of California, Department of Public Works, Division of Highways, "As-Built Plans of the Cypress Street Viaduct," June, 1957.

1.5 Monteiro, P.J.M., Asselanis, J. and MacCracken, B., "Preliminary Information on the Mechanical Properties of the Cypress Overpass Concrete," Department of Civil Engineering, University of California, Berkeley, 1989.

1.6 Bailey, S., "Material Study Report on the Cypress Street Viaduct - October 17, 1989 Earthquake," CRTI/Bailey Engineering, Sacramento, CA, 1990.

1.7 Jackura, Ken, California Department of Transportation, "Cypress Viaduct Soil Profile," 1990.

1.8 Heyes, David G., California Department of Transportation, "Geology and Soils in the vicinity of the San Francisco-Oakland Bay Bridge and Cypress Structure Site," 1990.

1.9 Abcarius, J., "Lateral Load Test on Driven Pile Footings," Internal Report, California Department of Transportation, Division of Structures, 1990.

1.10 "The Loma Prieta Earthquake of Oct. 17, 1989," Earthquakes and Volcanoes, Vol.21, No.5, 1989.

1.11 State of California, Division of Mines and Geology, "Plots of the Processed Data for the Interim Set of 14 Records from the Santa Cruz Mountains (Loma Prieta) Earthquake of October 17, 1989."

1.12 United States Geological Survey, "U.S. Geological Survey Strong-Motion Records From the Northern California (Loma Prieta) Earthquake of October 17, 1989," U.S. Department of the Interior, U.S. Geological Survey, Report 89-568, 1989.

1.13 Housner, G.W., Chairman, the Governor's Board of Inquiry on the 1989 Loma Prieta Earthquake, "Competing Against Time," State of California, Office of Planning and Research, May 1990.

2.1 Dubovic, A., "Tests of Pipe Restrainers," Internal Report, California Department of Transportation, Division of Structures, 1990.

2.2 Clough, R.W. and Penzien, Joseph, "Dynamics of Structures," McGraw-Hill Book Co., 1975.

2.3 Motion Analysis Corporation, "Comparing Video-Based Motion Analysis to Traditional Methods - A Case Study on the Earthquake Damaged Interstate 880 Viaduct, Oakland, California," 1990.

4.1 ACI Committee 318, "Building Code Requirements for Reinforced Concrete (ACI 318-89) and Commentary - ACI 318R-89," American Concrete Institute, November 1989.

4.2 ACI Committee 352, "Recommendations for Design of Beam-Column Joints in Monolithic Reinforced Concrete Structures," ACI Journal, Proceedings V.73, No.7, July 1976, pp.375-393.

DATE	CONSTRUCTION ACTIVITIES	TESTS	DATE	CONSTRUCTION ACTIVITIES	TESTS
Wednesday 12/6/89	1) Complete jacking frames 2) Complete epoxy injection of East pedestals 3) Erection of pedestal confinement plates and safety system for Phase 1 SLT 4) Construction of falsework shoring for Bents 45 and 47 for Phase 1 SLT 5) Instrumentation for Phase 1 SLT	Phase 1 FVT	Thursday 12/14/89	1) Retrofitting continues	Hinge Test
			Friday 12/15/89	1) Retrofitting Bents 45,46 & 47 continus 2) Instrumentation by TRANSLAB for hinge test 3) Completion of jacking frames for hinge test 4) Columns @ Bent 48 pinned at top 5) Shoring lowered under long hinge span	Hinge Test
Thursday 12/7/89	1) Complete pedestal confinement plate assemblies and safety system for Phase 1 SLT 2) Completion of instrumentation for Phase 1 SLT 3) Placement of falsework shoring @ Bents 45&47	Complete Phase 1 FVT	Saturday 12/16/89	1) EQ test frame isolated from hinge long span. Timber falsework placed, steel shoring removed. Testing equipment and test weights removed prior to isolation. 2) Retrofitting continues	No Testing
Friday 12/8/89	1) Preassembly of retrofit designs 2) Preassembly of Hinge Test jacking frame	Begin Phase 1 SLT	Sunday 12/17/89	1) Retrofitting continues 2) Site preparation for Phase 2 testing	No Testing
Saturday 12/9/89	1) Preassembly of retrofit designs 2) Preassembly of Hinge Test jacking frame		Monday 12/18/89	1) Retrofitting completed at Bents 45,46 & 47 2) Site preparation for Phase 2 testing	No Testing
Sunday 12/10/89	1) Preassembly of retrofit designs 2) Site preparation for Hinge Test 3) Site preparation for retrofitting 4) Long hinge span lowered with calibrated jacks	Phase 1 SLT ends	Tues/Wed. 12/19/89 12/20/89	1) Site preparation for Phase 2 Static Load Testing	Phase 2 FVT
Monday 12/11/89	1) Retrofitting begins at test site 2) Hinge diaphragms are cored 3) Placement of hinge extenders/restrainers 4) Erection of hinge jacking frame 5) Site preparation for addt'l hinge test	No Testing	Thursday 12/21/89	1) Instrumentation and setup for Phase 2	No Testing
			Friday 12/22/89	No new construction activities	Phase 2 SLT
			Saturday 12/23/89		
Tuesday 12/12/89	1) Retrofitting continues 2) Hinge bolster steel placed 3) Hinge bolsters formed and concrete placed 4) Erection of hinge jacking frame	No Testing	Sun/Mon 12/24/89 12/25/89	CHRISTMAS break	No Testing
Wednesday 12/13/89	1) Retrofitting continues 2) Forms for bolsters stripped 3) Instrumentation for hinge test placed 4) Completion of hinge jacking frame 5) Short cantilver span shored. Long span shores lowered	No Testing	Tuesday 12/26/89	No construction activities	Final Testing Phase 2 SLT
			Wednesday 12/27/89	1) Instrumentation removed	No Testing

SLT = Static Load Test
FVT = Forced Vibration Test

Table 2.1 Testing and Construction Schedule

Element/Component	Weight (kips)
Top Deck	1697
Top Bent Caps	900
Top Columns	185
Lower Deck	1697
Lower Bent Caps	900
Lower Columns	324
TOTAL	5700

Table 2.2 Calculated Deck, Bent Cap, and Column Weights

Channel #	Type of Instrument	Location & Description
(1+2+3)/3	Pressure gage	One third of total applied lateral load
4	Linear pot	Bent 47, horizontal displacement at top of West column
5	Linear pot	Bent 47, horizontal displacement, lower deck level
6	Linear pot	Bent 46, horizontal displacement at top of West column
7	Linear pot	Bent 46, horizontal displacement, lower deck level
8	Linear pot	Bent 46, horizontal displacement, bottom of west column
9	Linear pot	Bent 45, horizontal displacement at top of west column
10	Linear pot	Bent 45, horizontal displacement, lower deck level

Table 2.3(a) Original Structure Transducer Locations

Channel #	Type of Instrument	Location & Description
(1+2+3)/3	Pressure gage	One third of total applied lateral load
11	Linear pot	Bent 46, relative horizontal displacement at top of column
12	Linear pot	Bent 46, relative horizontal displacement at top deck level
13	Linear pot	Bent 46, relative horizontal displacement at inner top deck level
14	Linear pot	Bent 46, relative horizontal displacement at bottom of top deck
15	Linear pot	Bent 46, relative horizontal displacement at 3/4 height of upper west column
16	Linear pot	Bent 46, relative horizontal displacement at 1/2 height of upper west column
17	Linear pot	Bent 46, relative horizontal displacement at 1/4 height of upper west column
18	Linear pot	Bent 46, relative horizontal displacement just above pedestal

Table 2.3(b) Original Structure Transducer Locations

Channel #	Type of Instrument	Location & Description
(1+2+3)/3	Pressure gage	One third of total applied lateral load
19	Linear pot	Bent 46, relative horizontal displacement just below pedestal top
20	Linear pot	Bent 46, relative vertical displacement just below pedestal top
21	Linear pot	Bent 46, relative horizontal displacement at midheight of pedestal
22	Linear pot	Bent 46, relative vertical displacement at midheight of pedestal
23	Linear pot	Bent 46, relative horizontal displacement at bottom of pedestal
24	Linear pot	Bent 46, relative vertical displacement at bottom of pedestal
25	Linear pot	Bent 46, relative vertical displacement at inner part of bottom of pedestal
26	Linear pot	Bent 46, relative horizontal displacement at inner part of bottom of pedestal
27	Linear pot	Bent 46, west end, opening of outside of joint
28	Linear pot	Bent 46, west end, opening of inside of joint

Table 2.3(c) Original Structure Transducer Locations

Channel #	Type of Instrument	Location & Description
1	Pressure Gage	Applied lateral load at bent 46
2	Pressure Gage	Applied lateral load at bent 45
3	Pressure Gage	Applied lateral load at bent 47
4	Wire Pot	Bent 47, upper deck lateral displacement
5	Wire Pot	Bent 47, lower deck lateral displacement
6	Wire Pot	Bent 46, upper deck lateral displacement
7	Wire Pot	Bent 46, lower deck lateral displacement
8	Wire Pot	Bent 46, ground level lateral displacement (West col.)
9	Wire Pot	Bent 45, upper deck lateral displacement
10	Wire Pot	Bent 45, lower deck lateral displacement
11	Linear pot	Bent 46, horizontal deformation at top of west upper beam–column joint
12	Linear pot	Bent 46, diagonal deformation at west upper beam–column joint
13	Linear pot	Bent 46, inclined deformation at bottom of west upper beam–column joint
14	Linear pot	Bent 46, horizontal displacement near top of west upper column
15	Linear pot	Bent 46, vertical deformation at west upper beam–column joint, close to deck
16	Linear pot	Bent 46, horizontal displacement at mid–height of west upper column
17	Linear pot	Bent 46, vertical deformation at west upper beam–column joint, close to edge
18	Linear pot	Bent 46, horizontal displacement near bottom of west upper column
19	Linear pot	Bent 46, shear sliding displacement at west shear key
20	Linear pot	Bent 46, horizontal displacement at top of west pedestal from lower deck

Table 2.4 List of Instruments

Channel #	Type of Instrument	Location & Description
21	Linear pot	Bent 46, horizontal displacement at bottom of west pedestal from lower deck
22	Linear pot	Bent 46, vertical displacement at bottom of west pedestal from lower deck
23	Linear pot	Bent 46, horizontal displacement at west lower beam–column joint from lower deck
24	Linear pot	Bent 46, vertical displacement at west lower beam–column joint from lower deck
25	Linear pot	Bent 45, Slip between RC column and WF section, west colomn at shear key level
26	Linear pot	Bent 45, Slip between RC column and WF section, east colomn at upper beam level
27	Linear pot	Bent 46, west shear key opening, west edge
28	Linear pot	Bent 46, west shear key opening, west edge
29	Linear pot	Bent 46, shear sliding displacement at east shear key
30	Linear pot	Bent 45, Slip between RC column and WF section, east colomn at shear key level
31	Linear pot	Bent 45, west shear key opening, west edge
32	Linear pot	Bent 45, west shear key opening, east edge
33	Linear pot	Bent 45, outward displacement of west side WF sections from lower deck
64	Strain Gage	Bent 45, east column exterior WF section outside flange at pedestal level
65	Strain Gage	Bent 45, east column exterior WF section inside flange at pedestal level
66	Strain Gage	Bent 45, east column exterior WF section outside flange at upper beam level
67	Strain Gage	Bent 45, east column exterior WF section inside flange at upper beam level

Table 2.4 List of Instruments (Cont'd)

Channel #	Type of Instrument	Location & Description
68	Strain Gage	Bent 45, east column east face bar strain at bottom of upper beam
69	Strain Gage	Bent 45, east column west face bar strain at bottom of upper beam
70	Strain Gage	Bent 45, upper bentcap east end top bar strain
71	Strain Gage	Bent 45, upper bentcap east end bottop bat strain
72	Strain Gage	Bent 45, upper bentcap west end top bar strain
73	Strain Gage	Bent 45, upper bentcap west end bottop bat strain
74	Strain Gage	Bent 45, west column west face bar strain at bottom of upper beam
75	Strain Gage	Bent 45, west column east face bar strain at bottom of upper beam
76	Strain Gage	Bent 45, west column exterior WF section outside flange at pedestal level
77	Strain Gage	Bent 45, west column exterior WF section inside flange at pedestal level
78	Strain Gage	Bent 45, west column exterior WF section horizontal on web at pedestal level
79	Strain Gage	Bent 45, west column exterior WF section diagonal on web at pedestal level
80	Strain Gage	Bent 46, east column east face bar strain at bottom of upper beam
81	Strain Gage	Bent 46, east column west face bar strain at bottom of upper beam
82	Strain Gage	Bent 46, upper bentcap east end bottom bar strain
83	Strain Gage	Bent 46, upper bentcap east end top bat strain
84	Strain Gage	Bent 46, upper bentcap west end top bar strain
85	Strain Gage	Bent 46, upper bentcap west end bottop bat strain
86	Strain Gage	Bent 46, west column east face bar strain at bottom of upper beam

Table 2.4 List of Instruments (Cont'd)

Channel #	Type of Instrument	Location & Description
87	Strain Gage	Bent 46, west column west face bar strain at bottom of upper beam
88	Strain Gage	Bent 46, west pedestal rock anchored bar strain
89	Strain Gage	Bent 47, east column east face bar strain at bottom of upper beam
90	Strain Gage	Bent 47, east column west face bar strain at bottom of upper beam
91	Strain Gage	Bent 47, upper bentcap east end bottom bar strain
92	Strain Gage	Bent 47, upper bentcap east end top bat strain
93	Strain Gage	Bent 47, upper bentcap west end top bar strain
94	Strain Gage	Bent 47, upper bentcap west end bottop bat strain
95	Strain Gage	Bent 47, west column east face bar strain at bottom of upper beam
96	Strain Gage	Bent 47, west column west face bar strain at bottom of upper beam
97	Coupler	Bent 45, post–tensioning rod on west column at top of lower deck level
98	Coupler	Bent 45, post–tensioning rod on west column at top of upper deck level
99	Coupler	Bent 45, post–tensioning rod on west upper column at mid–hight
100	Coupler	Bent 45, post–tensioning rod on west upper column above shear key
101	Coupler	Bent 46, post–tensioning rod on east upper column near shear key
102	Coupler	Bent 46, post–tensioning rod on west upper column at mid–height
103	Coupler	Bent 46, post–tensioning rod on east upper column at mid–height

Table 2.4 List of Instruments (Cont'd)

Channel #	Type of Instrument	Location & Description
104	Coupler	Bent 46, post–tensioning rod on east upper column at upper quarter point
105	Coupler	Bent 46, post–tensioning rod on east upper column near upper bentcap
106	Coupler	Bent 46, post–tensioning rod on east column at bottom of lower deck level
107	Coupler	Bent 46, post–tensioning rod on west column at bottom of upper deck level
108	Coupler	Bent 46, post–tensioning rod on west column at top of upper deck level
109	Coupler	Bent 46, post–tensioning rod on west column at top of lower deck level
110	Coupler	Bent 46, post–tensioning rod on west column at bottom of upper deck level
111	Coupler	Bent 46, post–tensioning rod on west upper column near upper bentcap
112	Coupler	Bent 46, post–tensioning rod on west upper column at upper quarter point
113	Strain Gage	Bent 46, crossing steel rod at top of pedestal level

Table 2.4 List of Instruments (Cont'd)

Cycle	Maximum Force Applied (kips)	Lower Deck Maximum Avg. Lateral Displ. (in.) $\delta_{1\ max}$	Upper Deck Maximum Avg. Lateral Displ. (in.) $\delta_{2\ max}$	Upper Level Drift (in.) $(\delta_2 - \delta_1)_{max}$
1	1312.2	0.210	0.691	0.481
2	1410.4	0.212	0.793	0.582
3	1796.1	0.255	1.038	0.784

Table 3.1 Lateral Load Test : Original Structure

Cycle	+ = Westward loading - = Eastward loading F_{target} (kips)	$F_{measured}$ (kips)	Lower Deck Avg. Maximum Lateral Displ. (in.) $\delta_{1\,max}$	Upper Deck Avg. Maximum Lateral Displ. (in.) $\delta_{2\,max}$	Upper Level Drift (in.) $(\delta_2 - \delta_1)_{max}$
1	+900	+891.6	+0.103	+0.357	+0.254
2	+1800	+1817.2	+0.248	+0.844	+0.595
3	+1800	+1810.1	+0.262	+0.851	+0.589
4	-1800	-1795.1	-0.221	-0.850	-0.630
5	-1800	-1807.0	-0.235	-0.885	-0.649
6	-2700	-2687.7	-0.420	-1.649	-1.228
7	-2700	-2702.4	-0.435	-1.719	-1.284
8	+2700	+2693.9	+0.406	+1.408	+1.002
9	+3300	+3343.6	+0.682	+2.697	+2.015
10	-3300	-2997.2	-0.481	-2.009	-1.529
11	-3300	-3520.6	-0.659	-3.308	-2.649
12	-3300	-3659.4	-1.087	-3.856	-2.926
13	+3300	+3349.3	+0.711	+2.811	+2.100
14	+4000	+4049.4	+1.228	+5.604	+4.376
15	-3300	-3304.4	-0.550	-3.142	-2.592
16	-4000	-3932.9	-0.932	-9.900	-8.981

Table 3.2 Lateral Load Test : Retrofitted Structure

Specimen Number	Location (also see Fig. 3.36)	Diam.x Length (in.)	Ultimate Stress[a], f'_c (psi)	Modulus of Elasticity[b], E (ksi)
6	Bent 45	3.75 x 7.52	7490	3580
7	Bent 46	3.75 x 7.64	6760	3100
9	Bent 46	3.75 x 7.52	7200	3900
10	Bent 46	3.75 x 7.44	7100	3060
13	Bent 47	3.75 x 7.52	6420	3340
15	Bent 47	3.75 x 7.48	7220	3140
16	Bent 47	3.75 x 7.44	6400	3560
18	Bent 47	3.75 x 7.48	5980	3840

[a]ASTM testing standard C39
[b]ASTM testing standard C42

Table 3.3 Concrete Core Test Results

Sample Number	Bent	Bar Size	Location
4	45	#11	Pedestal
5	45	#18	East Upper Column
6	46	#18	East Upper Column
7	47	#18	East Upper Column
8	45	#11	Upper Bent Cap
9	45	#18	West Upper Column
10	47	#11	Upper Bent Cap
11	47	#18	West Column

Table 3.4 Rebar Sample Locations

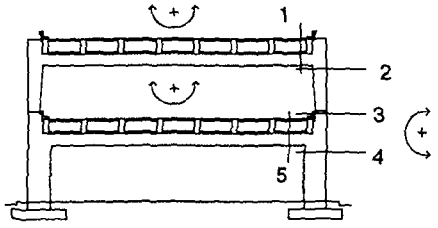

Location	Shear (kips)	Nominal Flexural Capacities (kip·in)					
		Before Retrofit		Following Retrofit * (composite)		Following Retrofit (non-composite)	
		Positive	Negative	Positive	Negative	Positive	Negative
Bent 45							
1. Upper Bent Cap	1780	52700	56000	142000	148000	78800	83000
2. Upper Column	390	106000	106000	156000	302000	127000	127000
3. Pedestal	320	15900	15900	37100	151000	37100	37100
4. 1st Story Column	590	244000	244000	308000	511000	265000	265000
5. Lower Bent Cap	1420	59100	114000	149000	199000	83800	139000
Bent 46							
1. Upper Bent Cap	1780	52700	56000	135000	141000	71000	74900
2. Upper Column	390	106000	106000	106000	106000	106000	106000
3. Pedestal	320	15900	15900	15900	15900	15900	15900
4. 1st Story Column	590	244000	244000	244000	244000	244000	244000
5. Lower Bent Cap	1420	59100	114000	142000	193000	76000	113000
Bent 47							
1. Upper Bent Cap	1780	52700	56000	142000	148000	78800	83000
2. Upper Column	390	106000	106000	111000	140000	106000	106000
3. Pedestal	320	15900	15900	168000	168000	21800	21800
4. 1st Story Column	590	244000	244000	255000	293000	244000	244000
5. Lower Bent Cap	1420	59100	114000	149000	199000	83800	139000

* Details and amount of clamping force employed at many locations were not intended to develop composite action (e.g. Bent 46 and west sides of Bents 45 & 47)

Table 4.1 Calculated Section Strengths Considering Anchorage Length

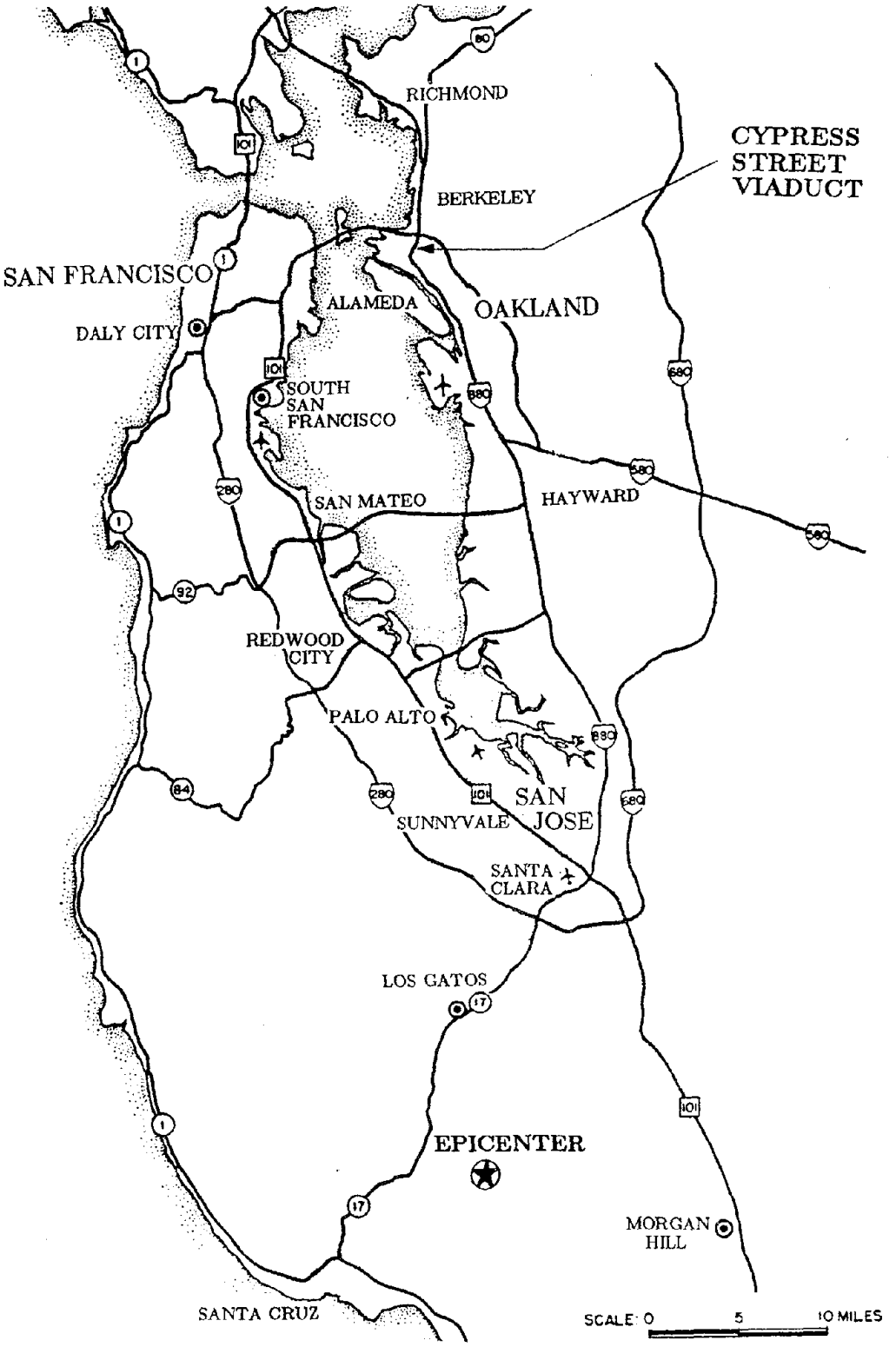

Fig. 1.1 Map showing the location of the epicenter and of the viaduct [after Ref. 1.1].

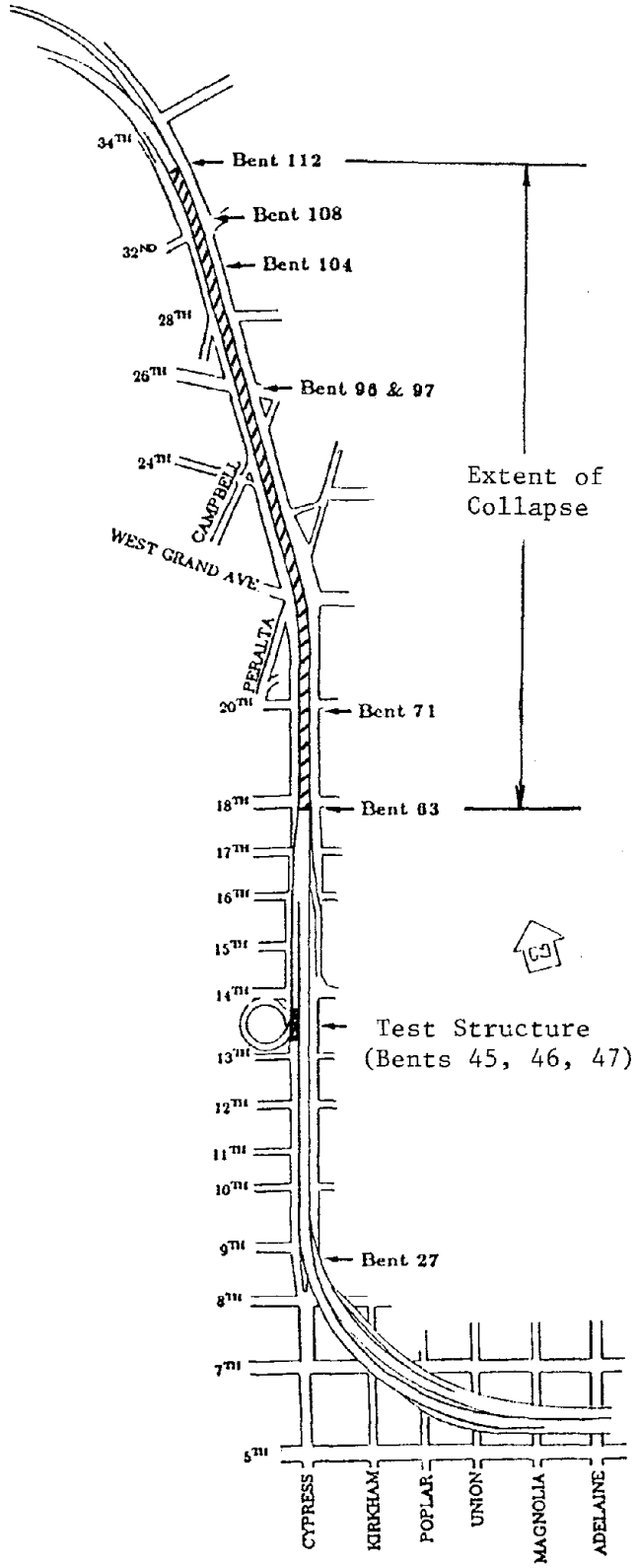

Fig. 1.2 Map of the Cypress Street Viaduct area [after Ref. 1.2].

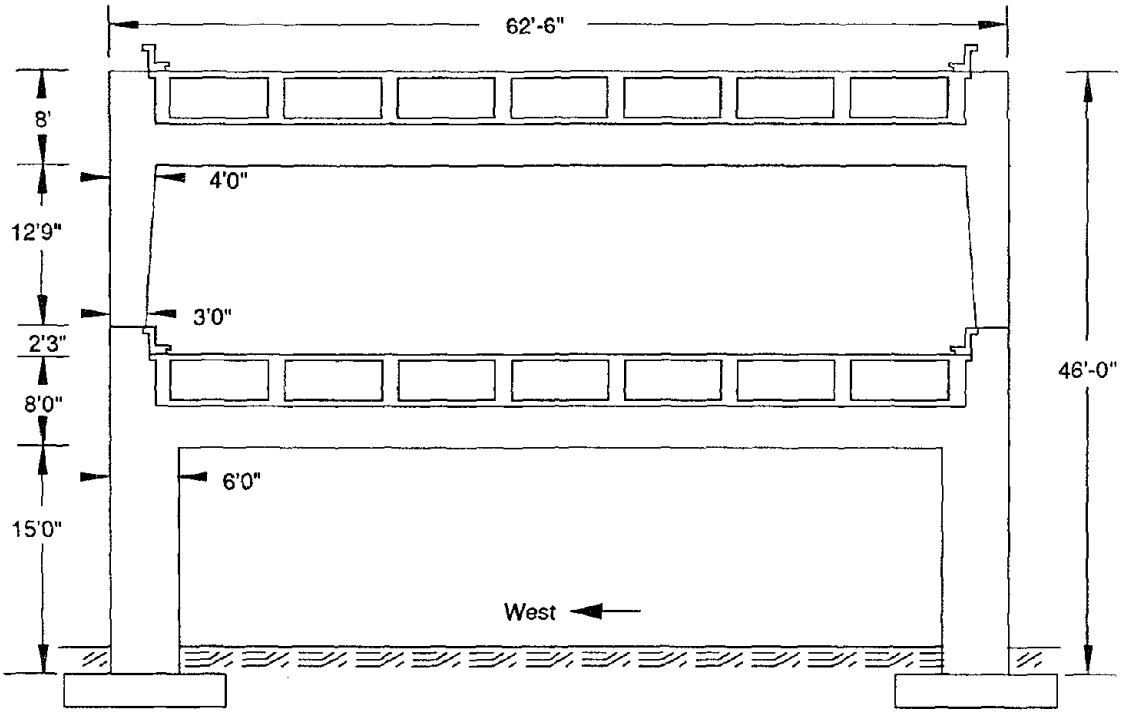

Fig. 1.3(a)

Typical Transverse Bent in Cypress Viaduct

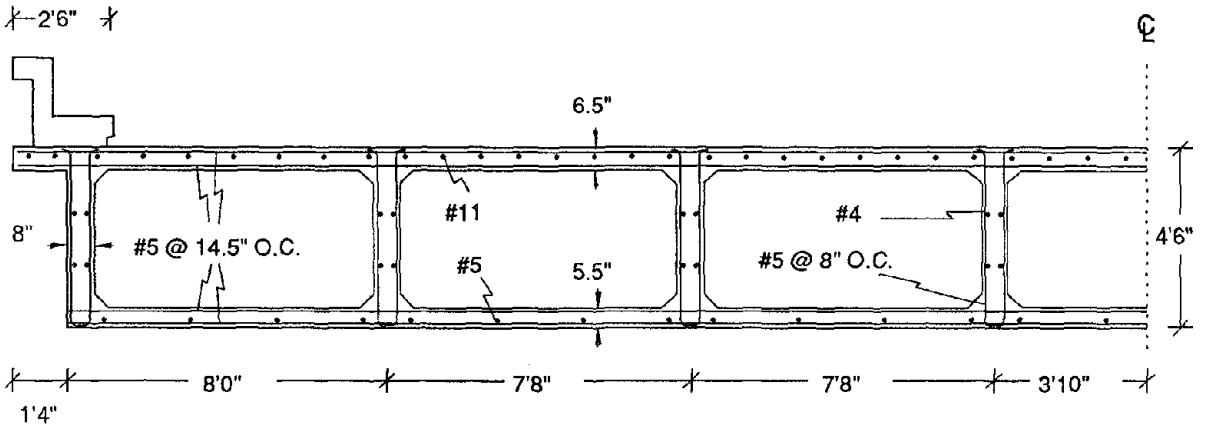

Fig. 1.3(b)

Typical Deck Section & Reinforcement

(This X-section immediately adjacent to Bents 45 & 46)

Fig. 1.3 Typical transverse bent and details

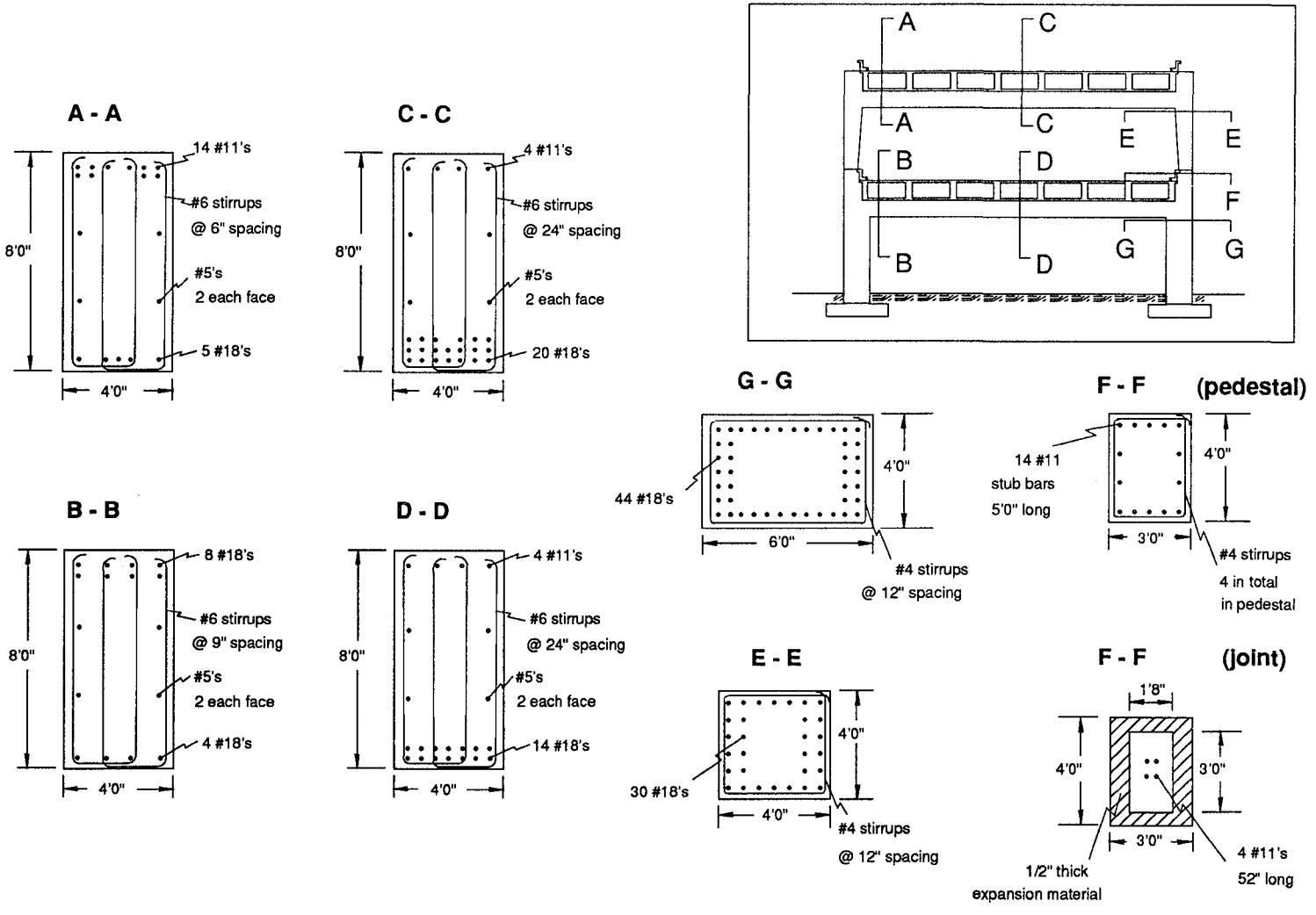

Fig. 1.4 Bent reinforcing details

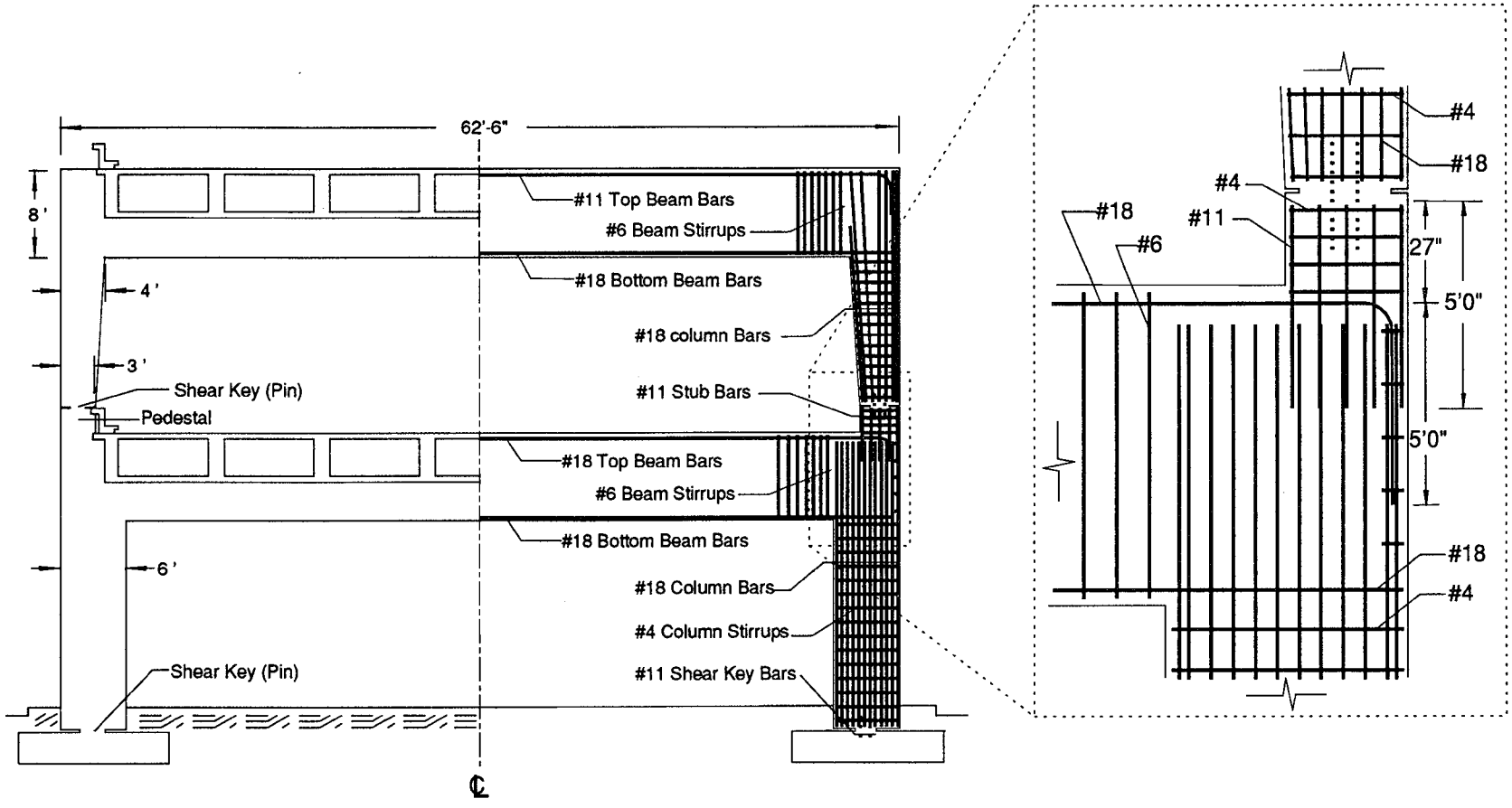

(see Fig. 1.4 for additional pedestal details)

Fig. 1.5 Bent reinforcement and pedestal detail

COMPRESSIVE STRENGTH

Two cores from column 87 were tested. The results were:

Specimen No.	Diam. x Length	Ultimate Stress (PSI)	ASTM Correction*	Compressive Strength (PSI)
87 A	3.75 x 4 in.	7346	0.89	6540
87 D	3.75 x 5.25 in	6322	0.95	6010

*The correction factor is obtained from section 8 of ASTM C39 to compensate for different length to diameter ratios.

a. Measured Concrete Strengths (from Ref. 1.5).

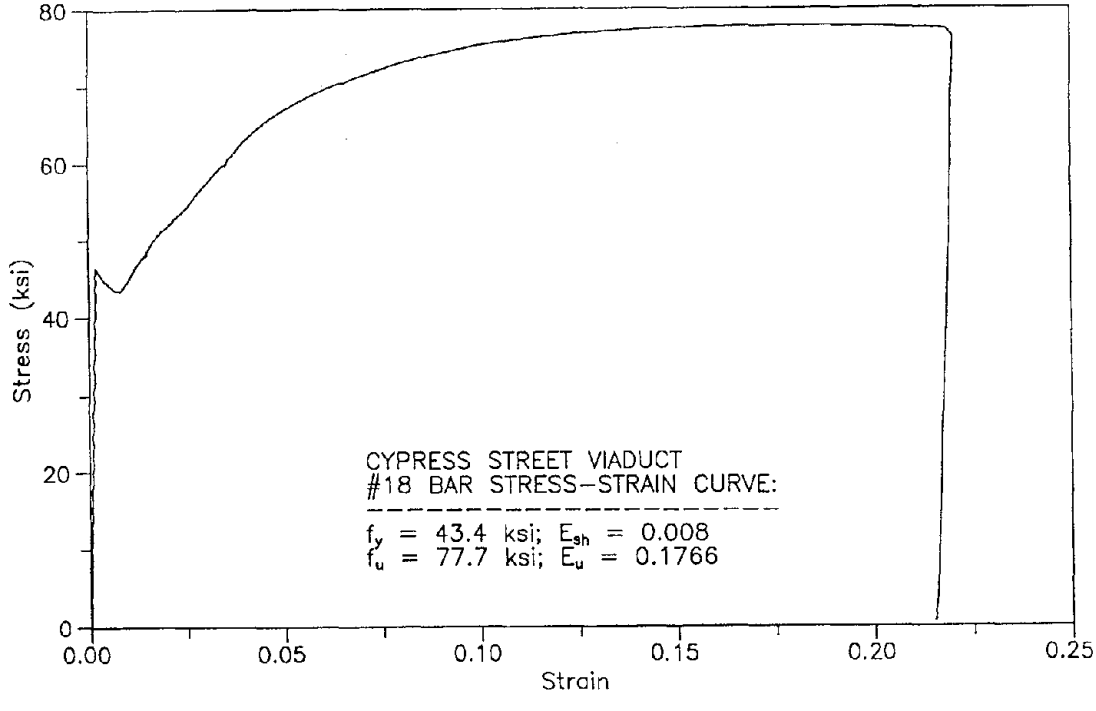

b. Reinforcing Steel Stress-Strain Curve (from Ref. 1.5).

Fig. 1.6 Cypress Street Viaduct material properties.

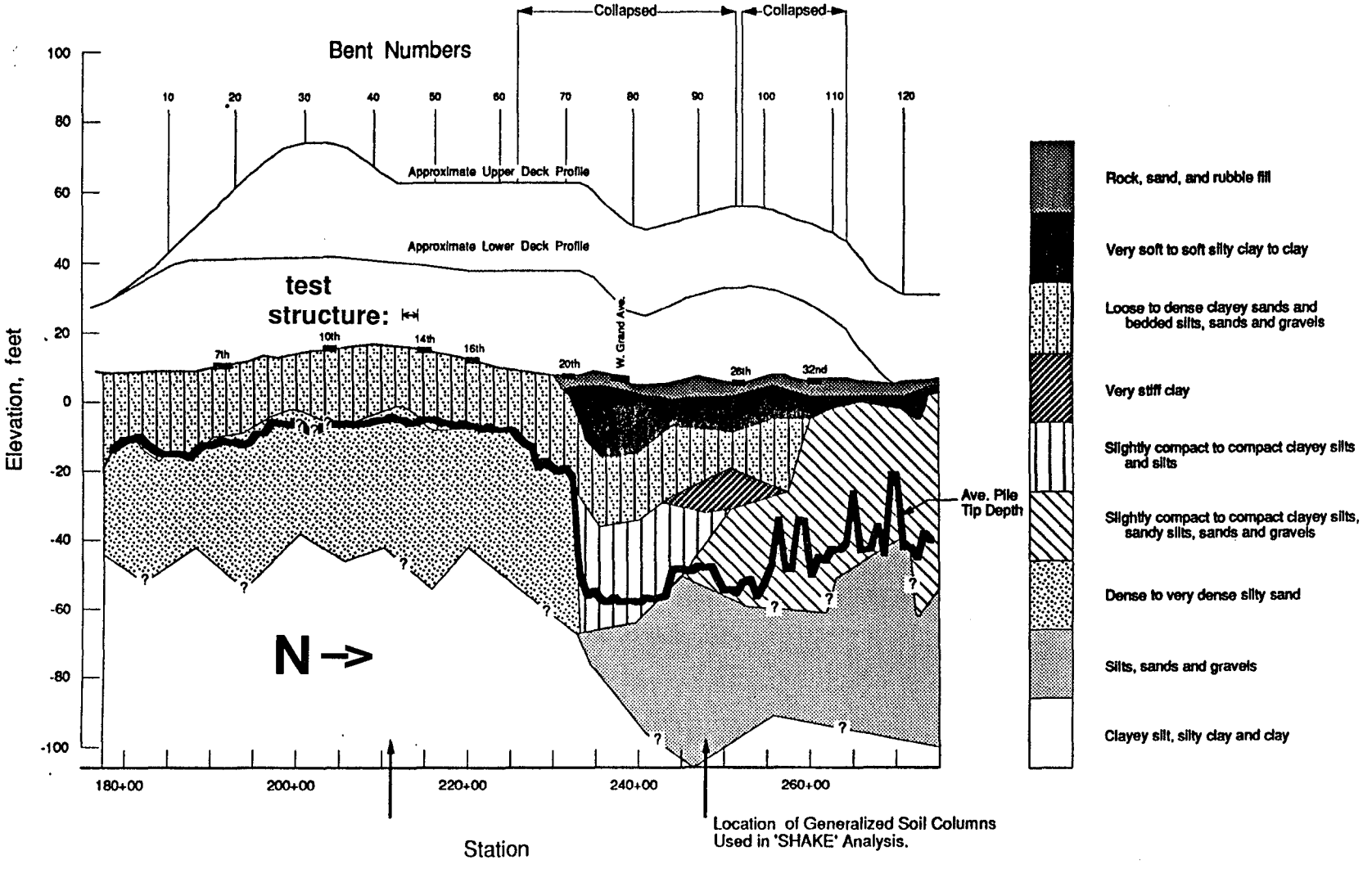

Fig. 1.7 Cypress Viaduct soil profile based on Caltrans boring information from 1953-1990 [after Ref. 1.7].

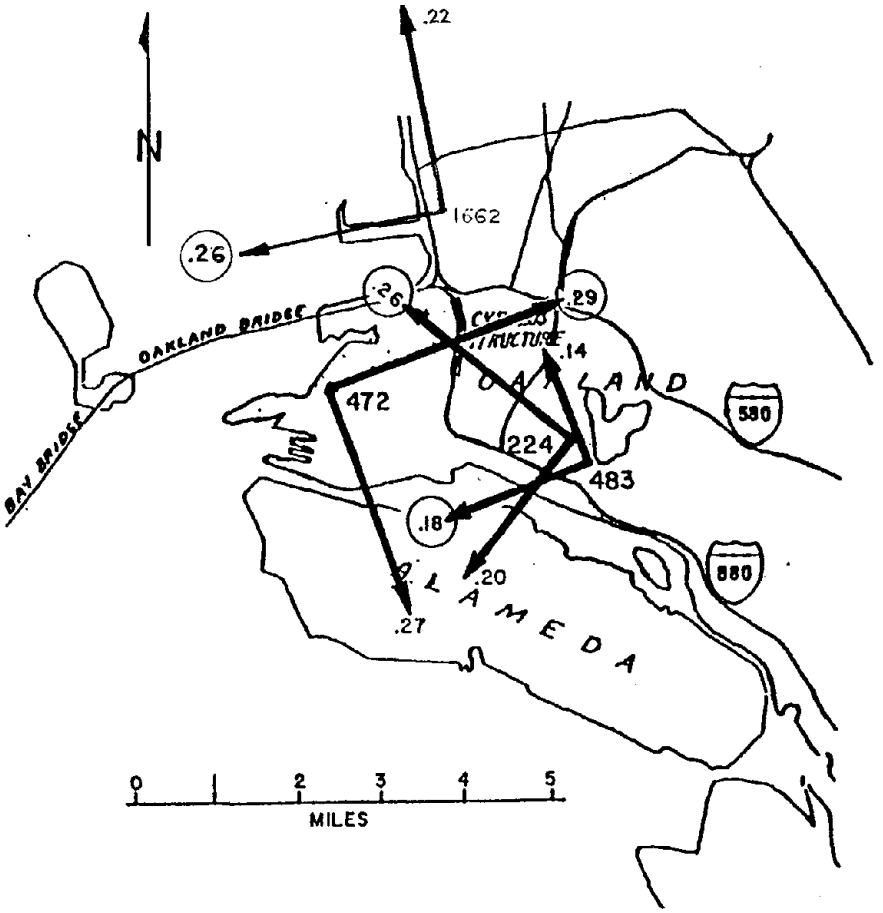

Fig. 1.8 Locations of accelerometers near the Cypress Street viaduct and peak recorded accelerations during the Loma Prieta earthquake [after Ref. 1.7].

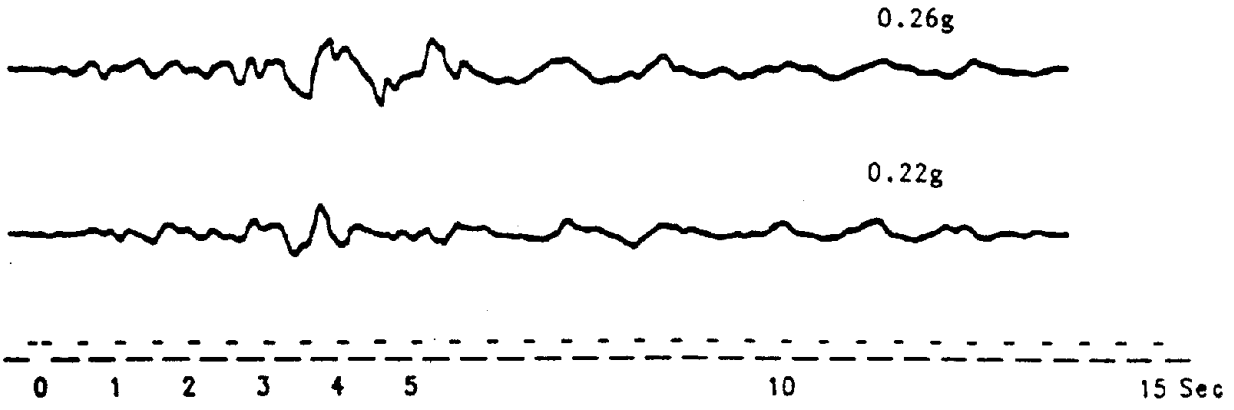

Fig. 1.9 Recorded accelerations obtained at Emeryville office building (USGS Sta. 1662).

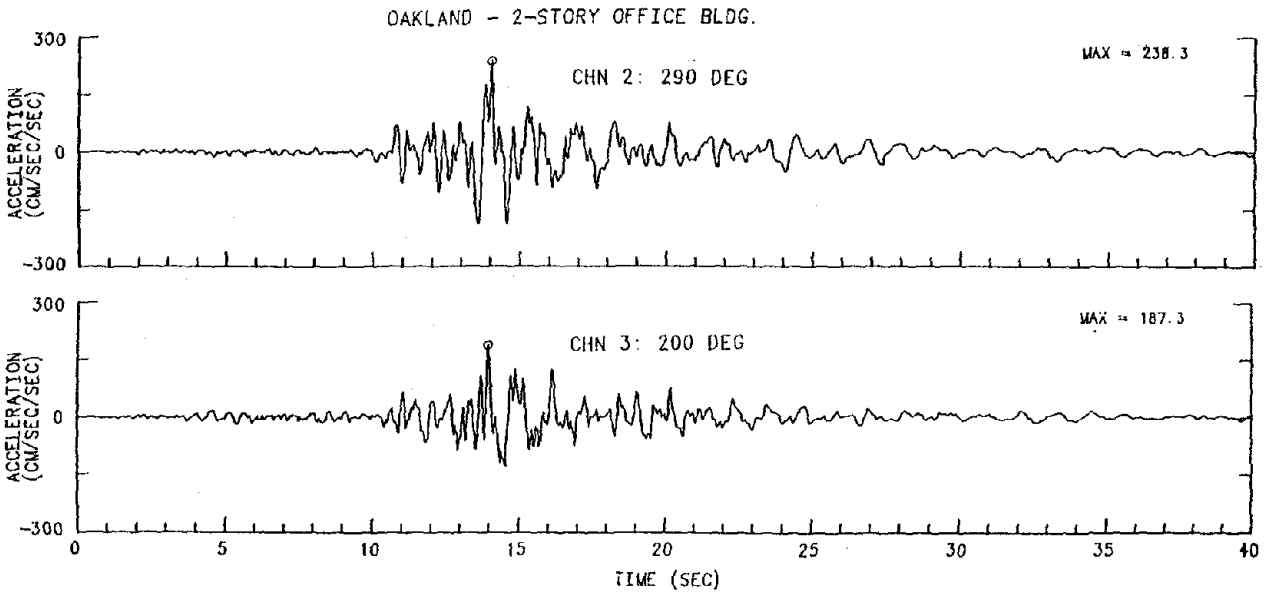

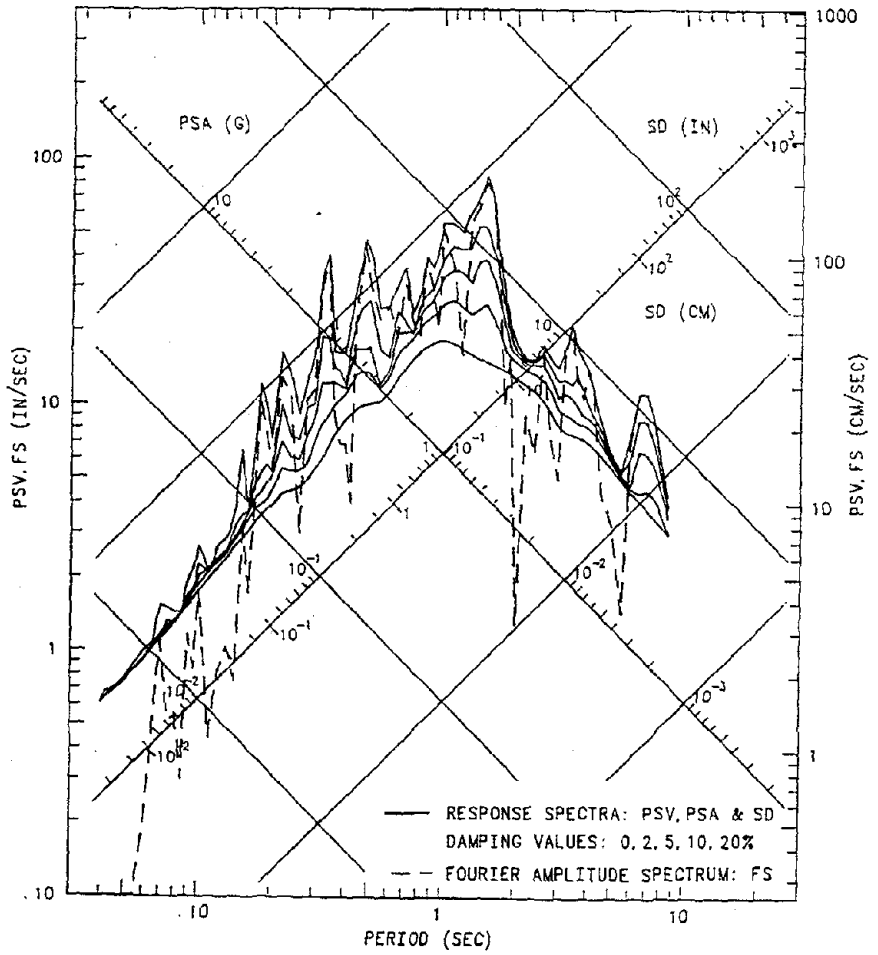

Fig. 1.10 Recorded accelerations obtained at Oakland 2-story office building (SMIP Sta. 224) and response spectra for largest component [from Ref. 1.12].

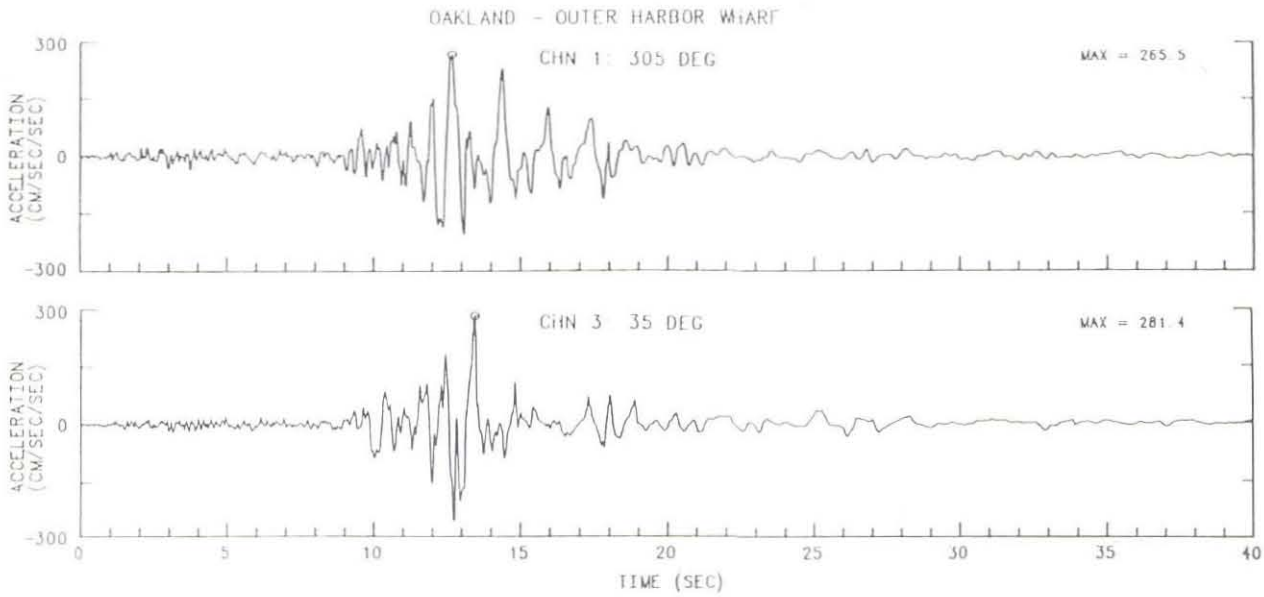

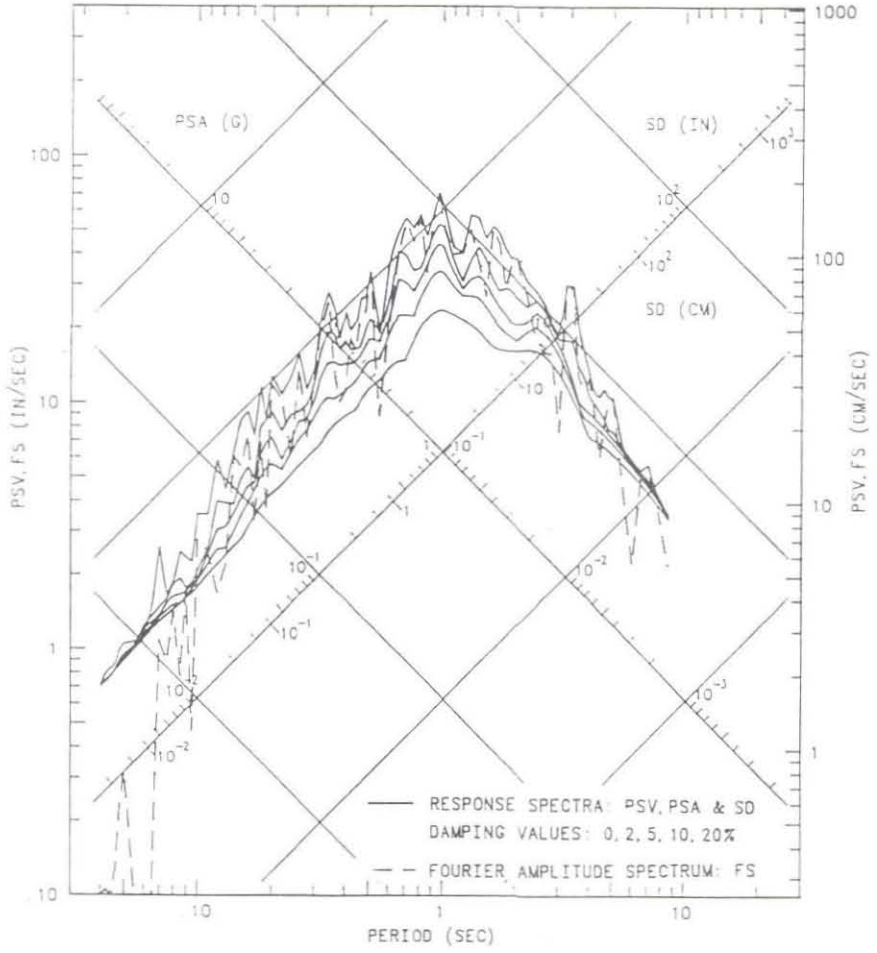

Fig. 1.11 Recorded accelerations obtained at Oakland Wharf (SMIP Sta. 427) and resonse spectra for largest component [from Ref. 1.12].

Fig. 1.12 Collapse of the I-880 Cypress St. Viaduct.

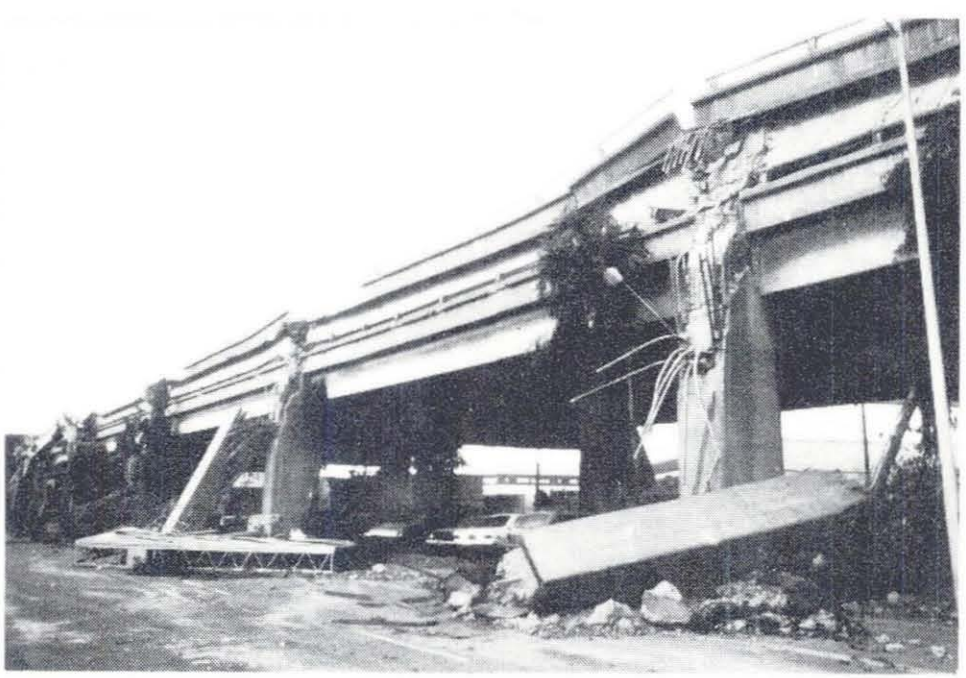

Fig. 1.13 Collapse of the I-880 Cypress St. Viaduct, illustrating the 'popping out' of the second story columns.

Fig. 1.14 Close-up view of failed column.

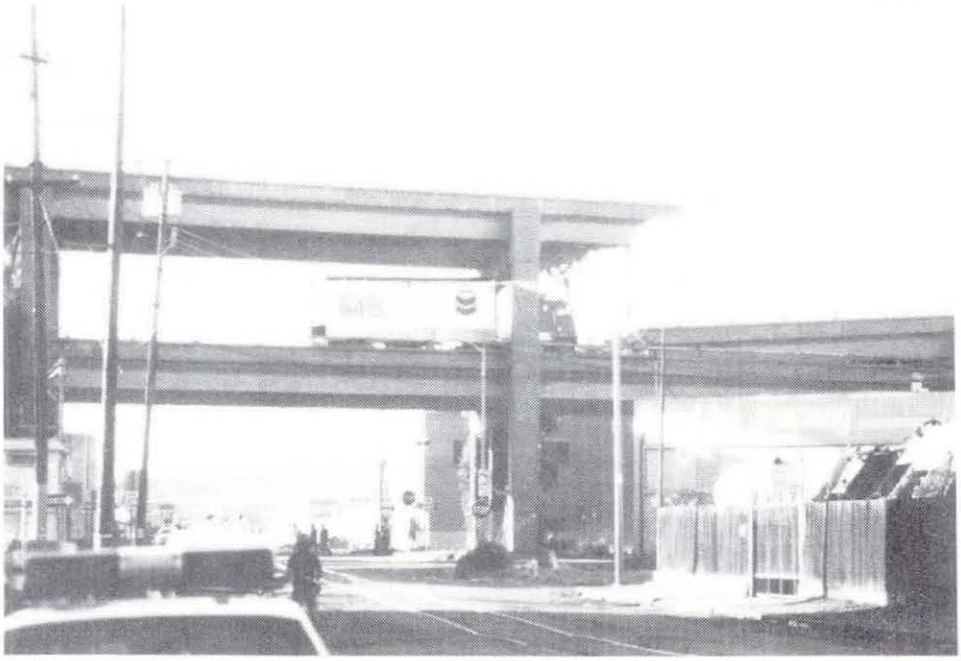

Fig. 1.15 Standing deck span at 26th street.

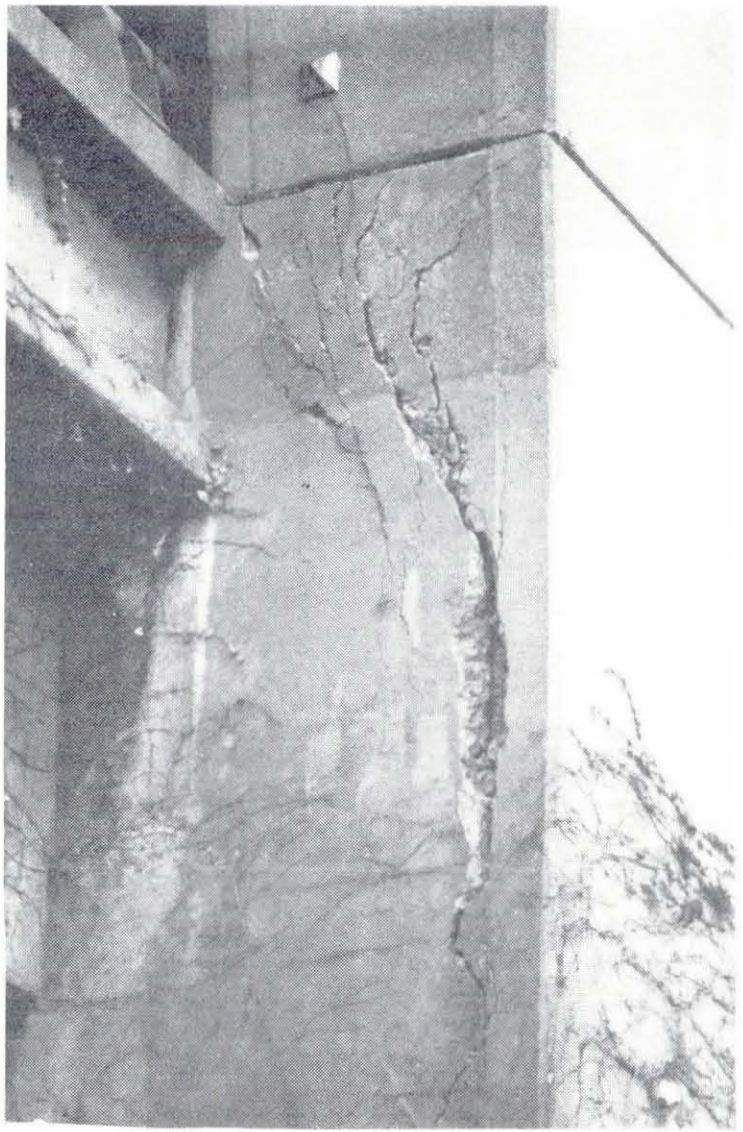

Fig. 1.16 Joint cracking indicative of incipient failure.

[from Ref. 1.2]

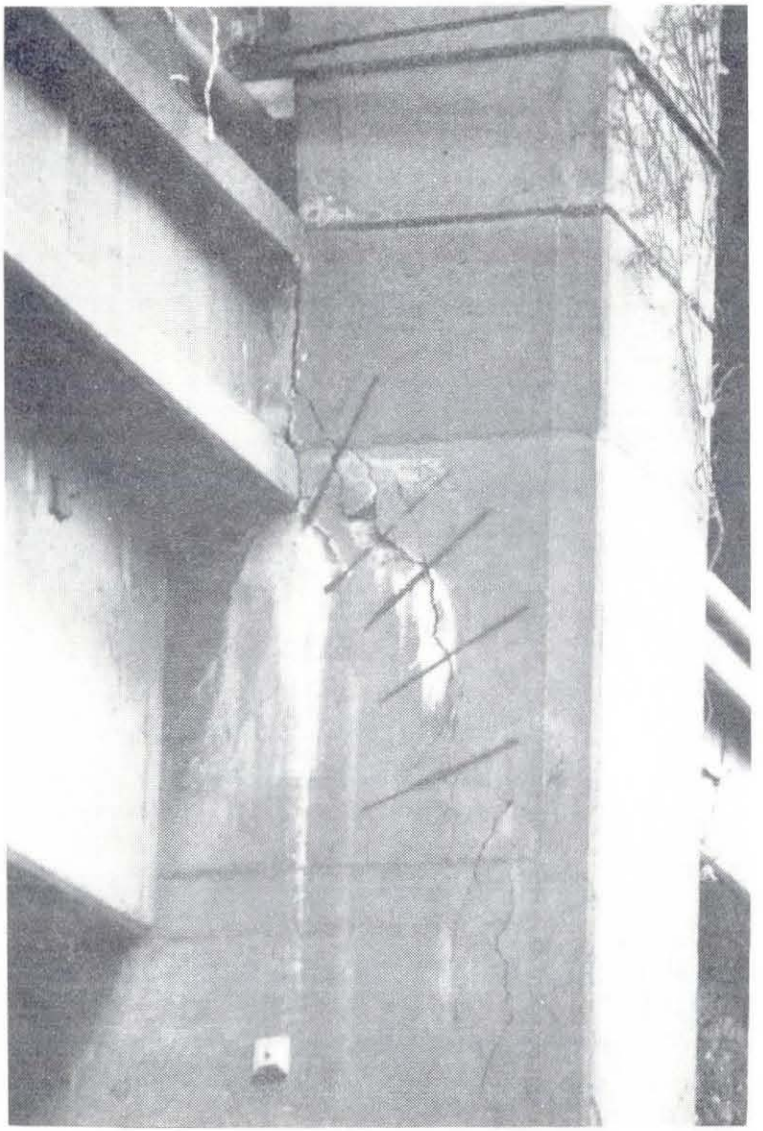

Fig. 1.17 Joint cracking.

[from Ref. 1.2]

Fig. 1.18 Close-up view of failed upper column, illustrating collapse mechanism.

Fig. 1.19 Fallen upper column.

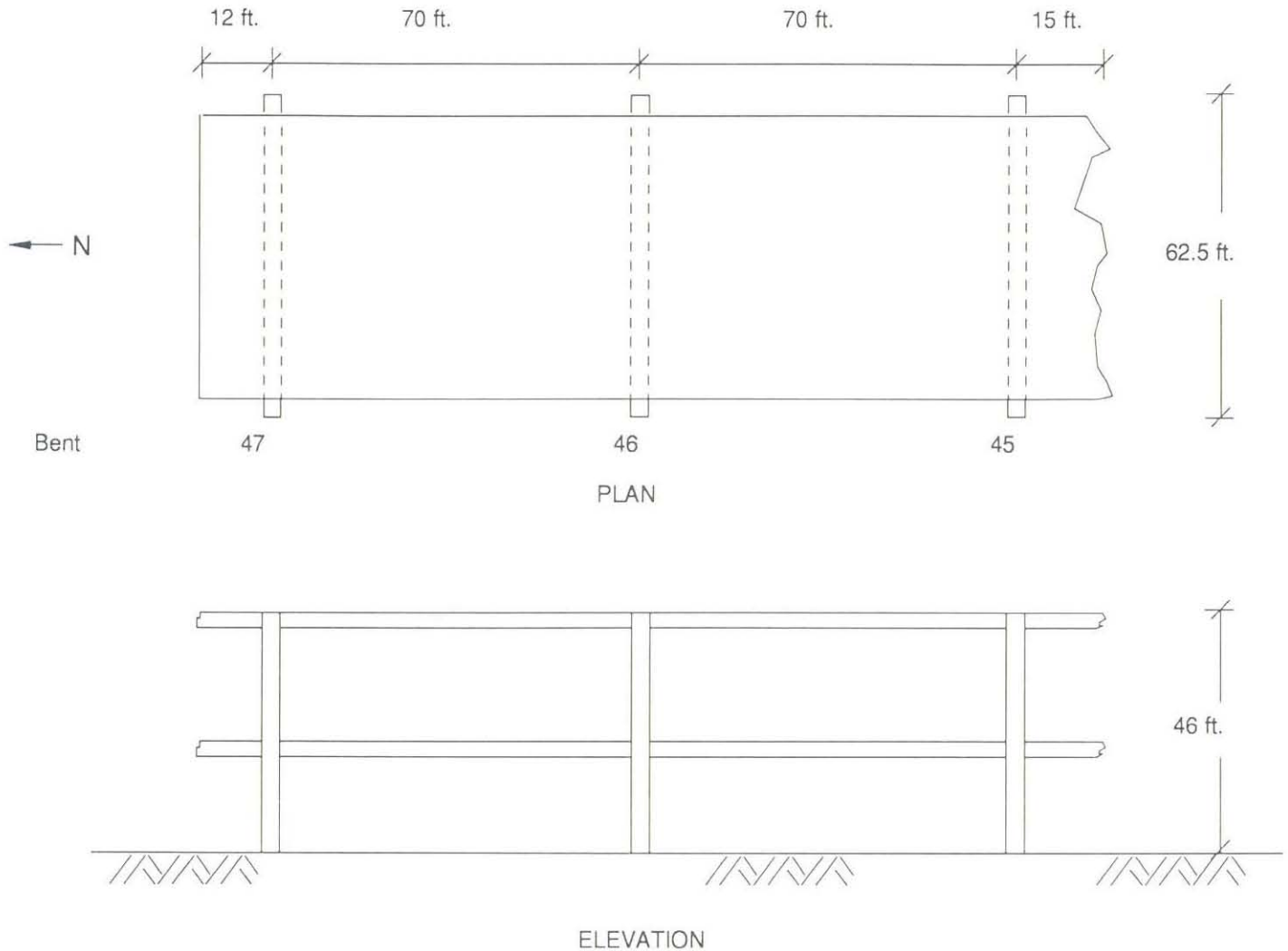

Fig. 2.1 Cypress St. Viaduct test structure

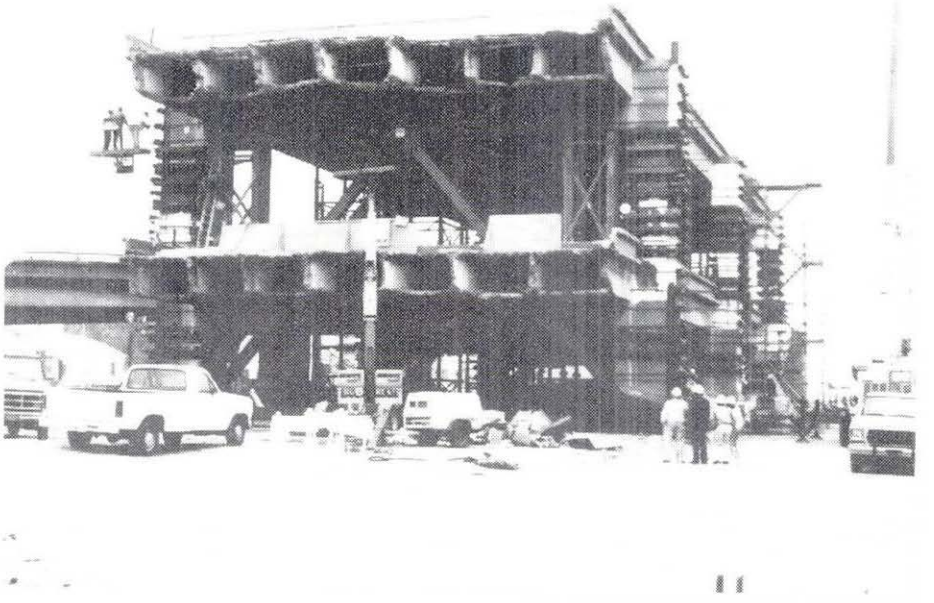

Fig. 2.2 South end of test structure showing ragged edge of deck.

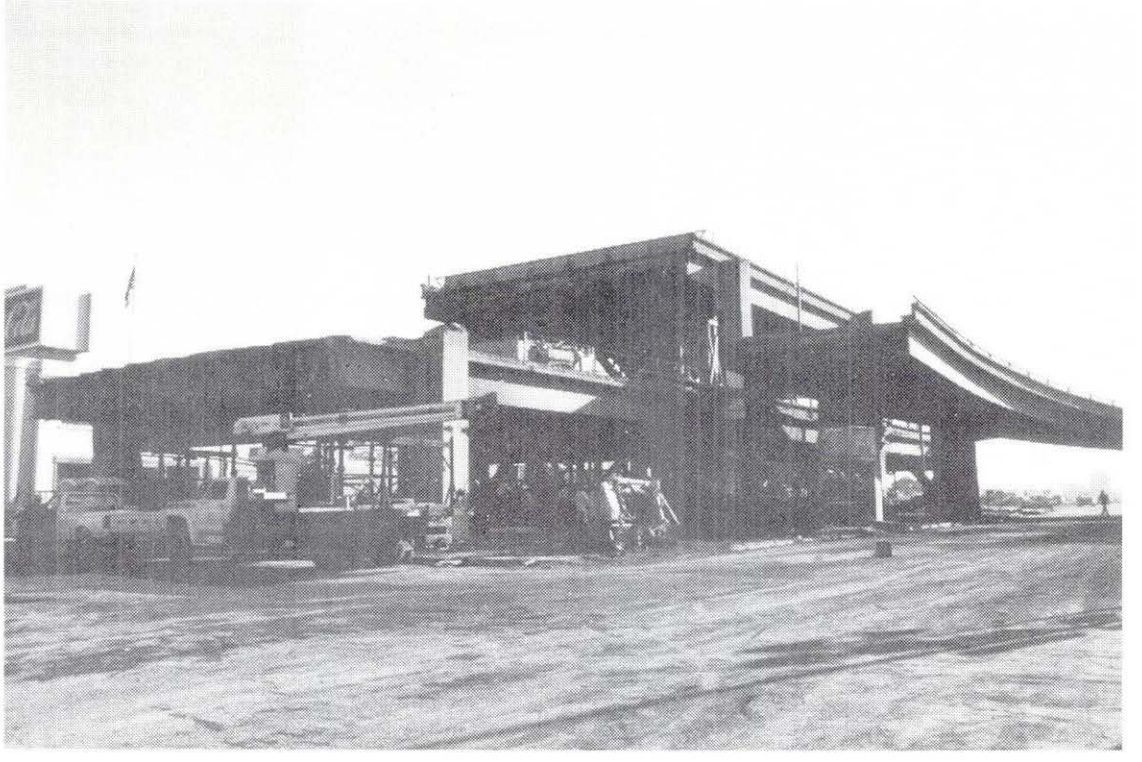

Fig. 2.3 Ground level photo showing Bents 47-48.

Fig. 2.4 Ground level photo showing separation of test specimen from off-ramp.

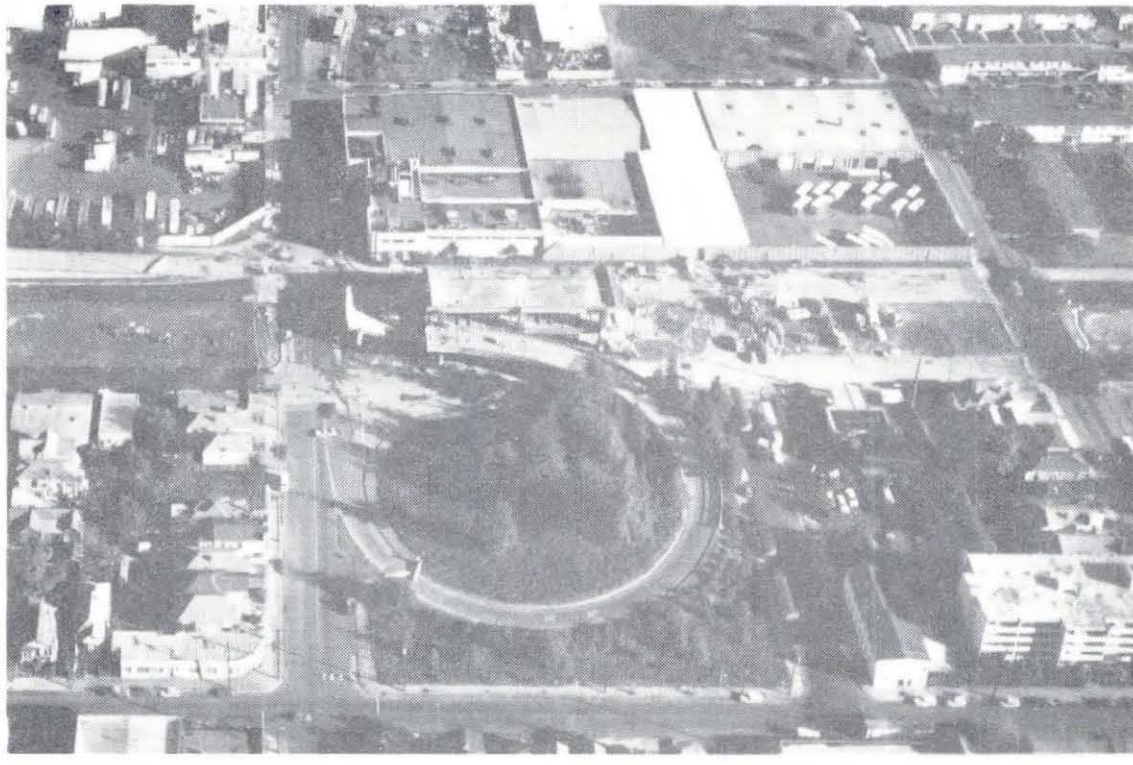

Fig. 2.5 Aerial photo showing test specimen and adjacent off-ramp.

Fig. 2.6 Photo showing hole in lower deck for loading frame.

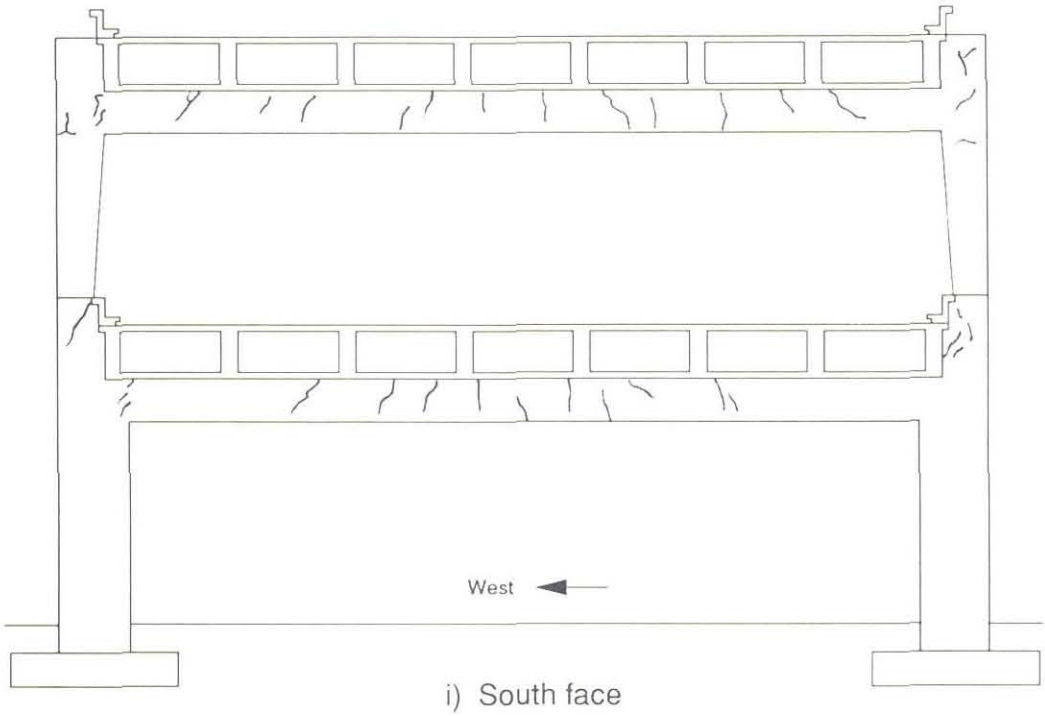

i) South face

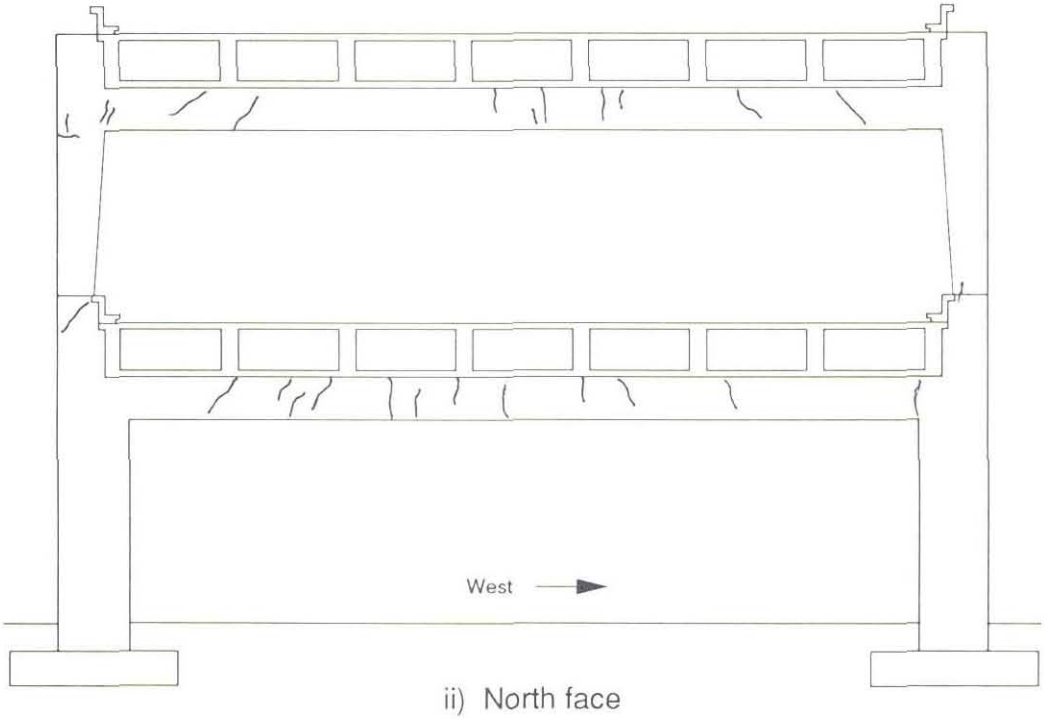

ii) North face

Fig. 2.7(a) Original crack locations on Bent 45

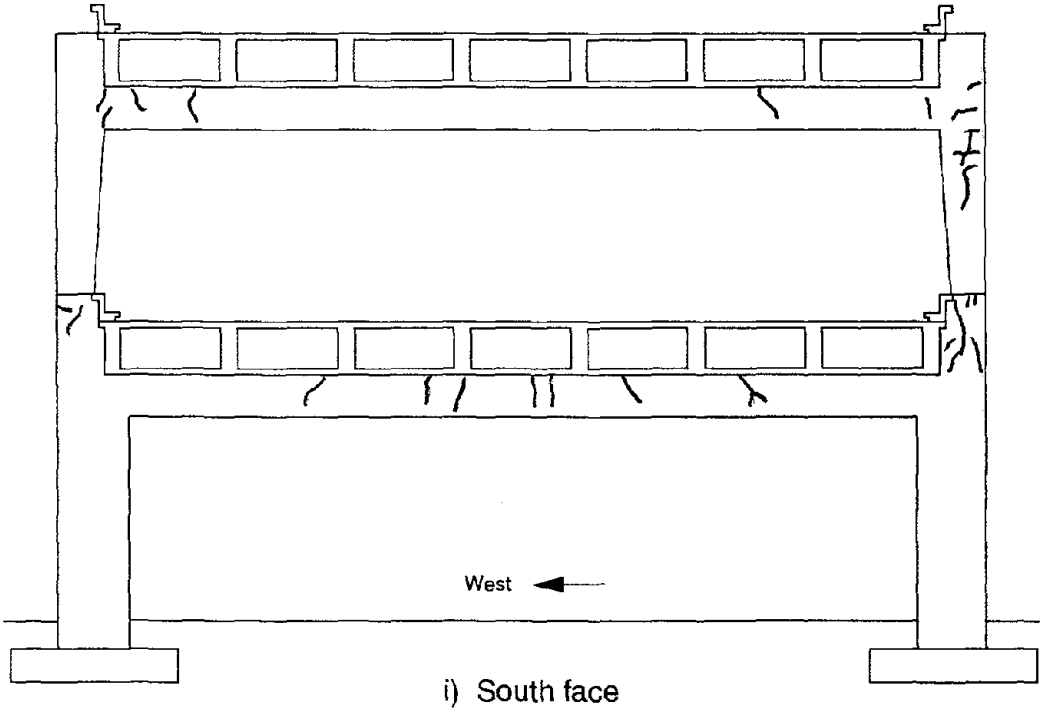

i) South face

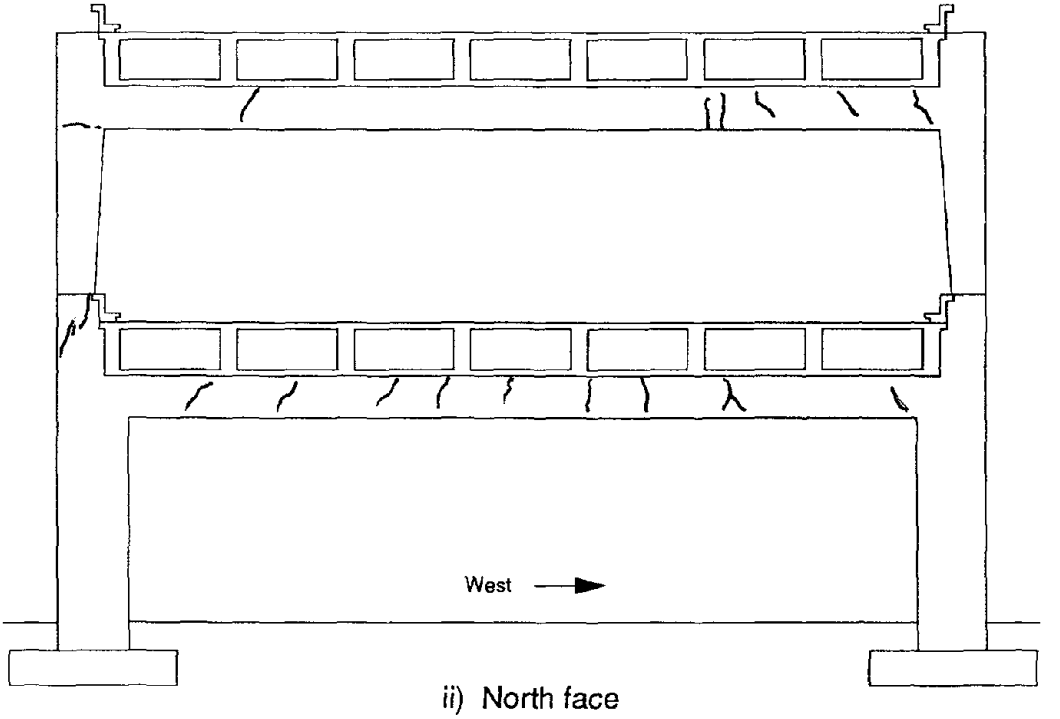

ii) North face

Fig. 2.7(b) Original crack locations on Bent 46

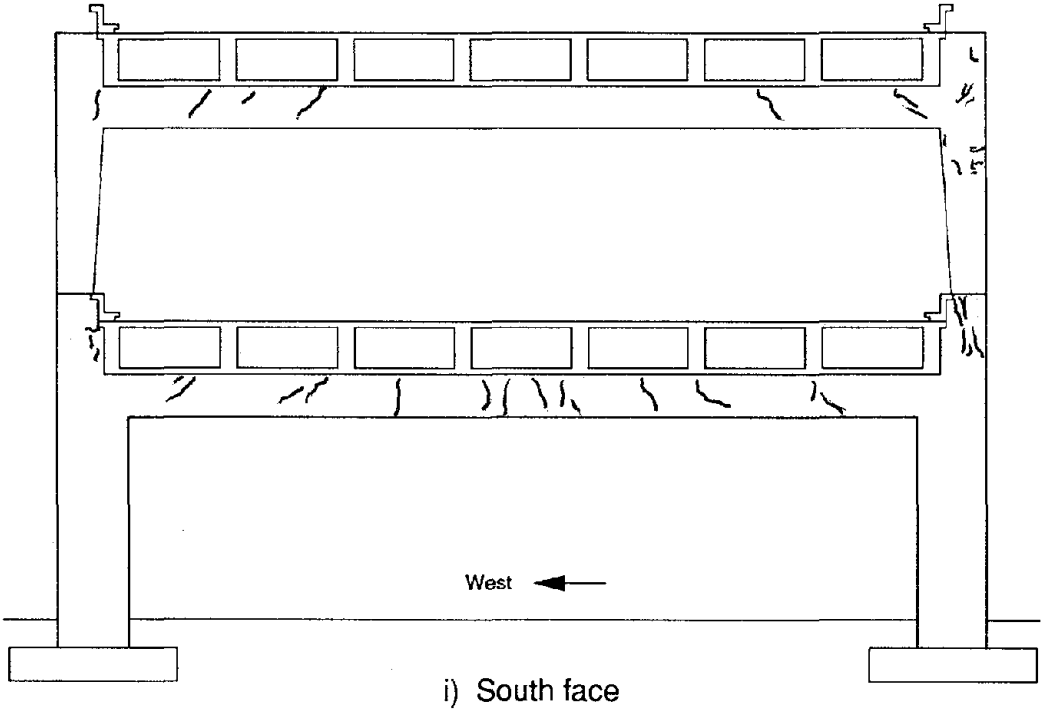

i) South face

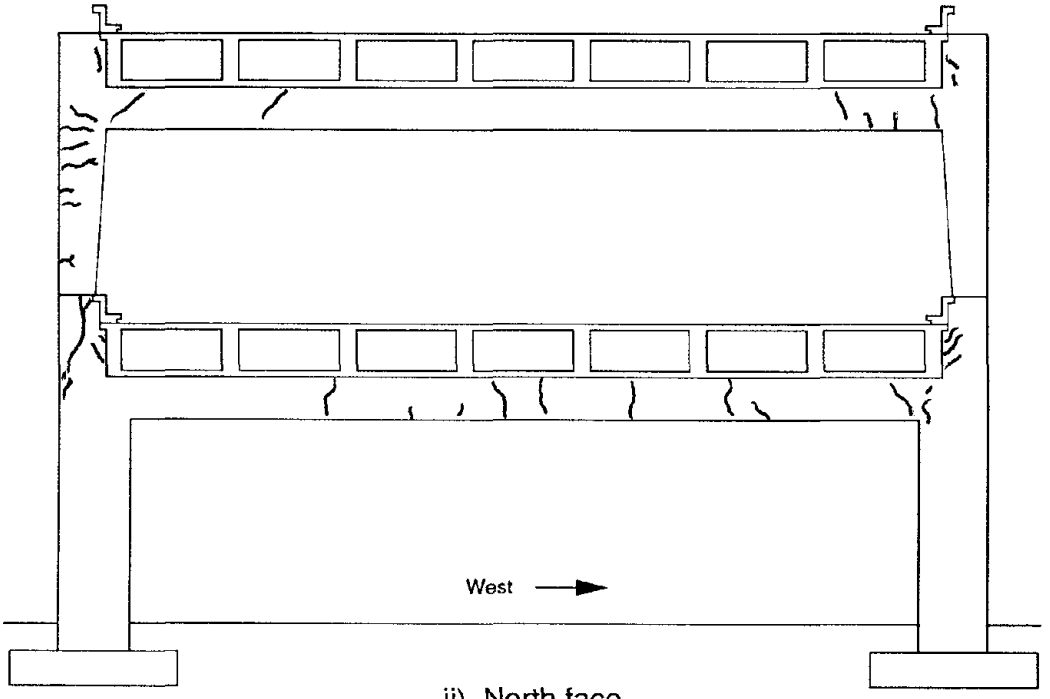

ii) North face

Fig. 2.7(c) Original crack locations on Bent 47

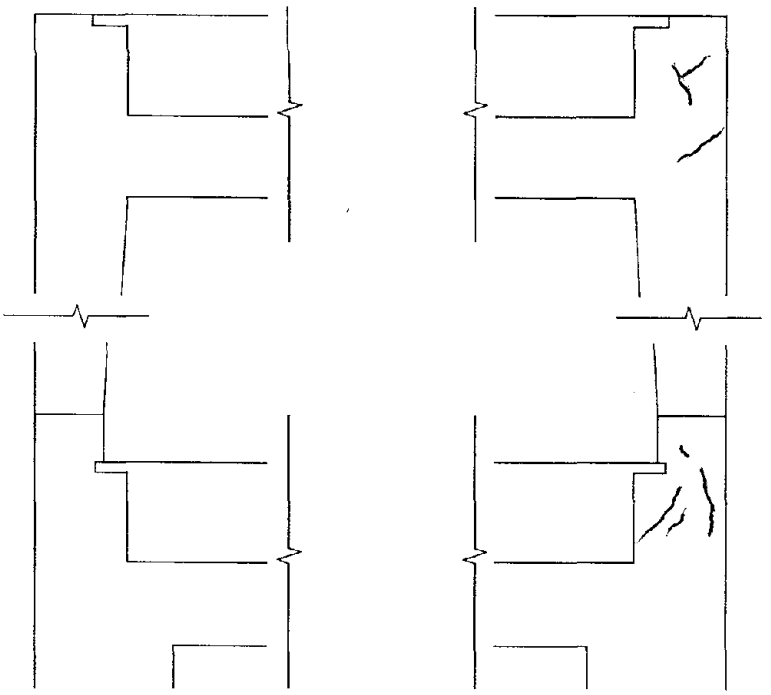

i) South face

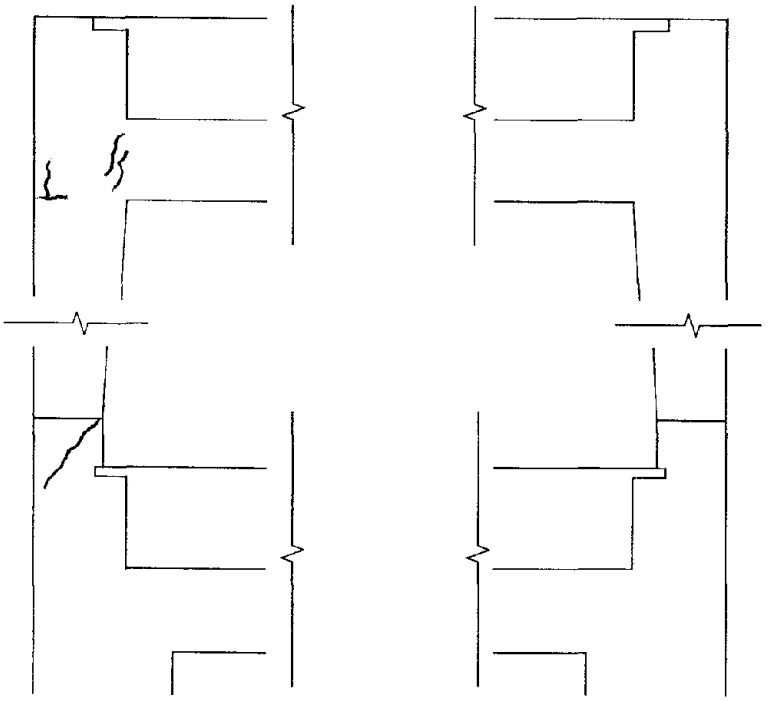

ii) North face

Fig. 2.8(a) Existing cracks in joint regions of Bent 45.

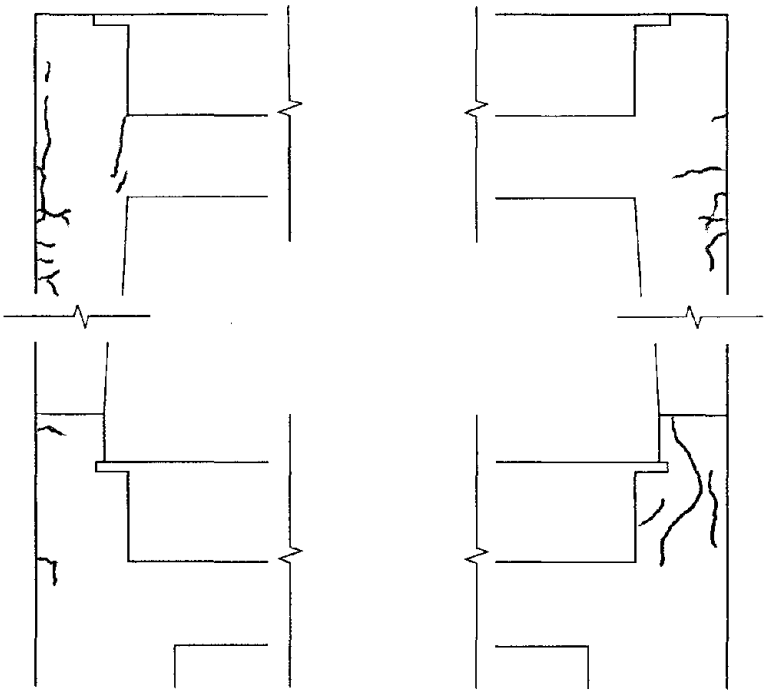

i) South face

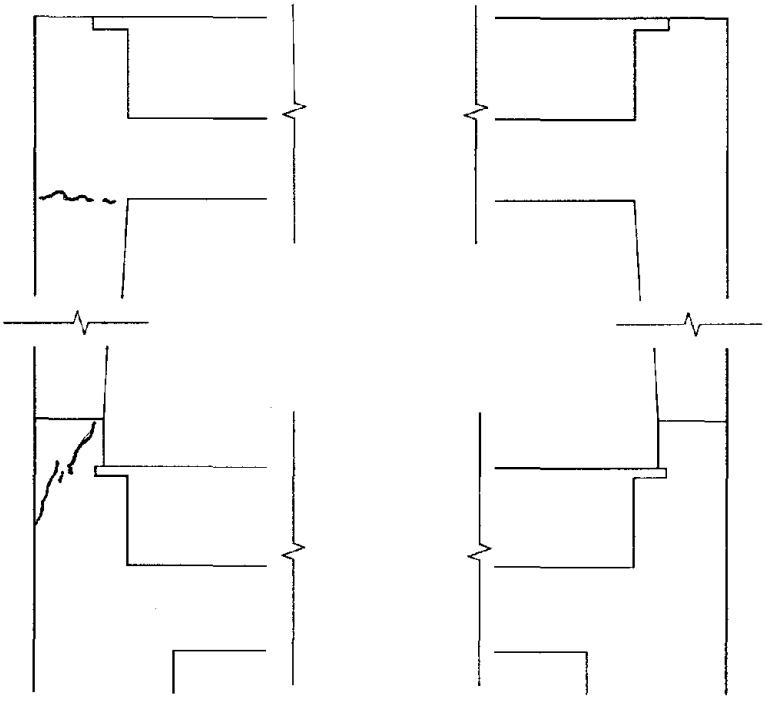

ii) North face

Fig. 2.8(b) Existing cracks in joint regions of Bent 46.

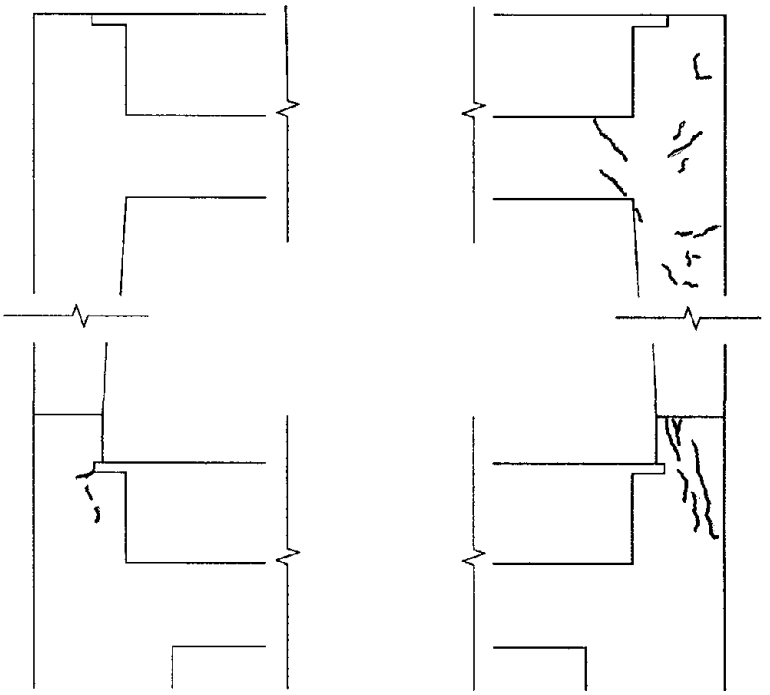

i) South face

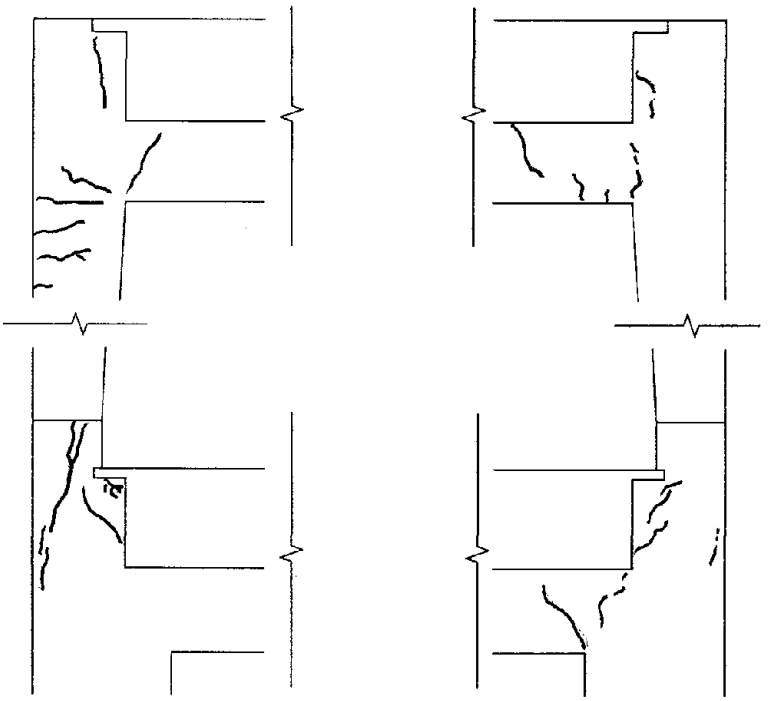

ii) North face

Fig. 2.8(c) Existing cracks in joint regions of Bent 47.

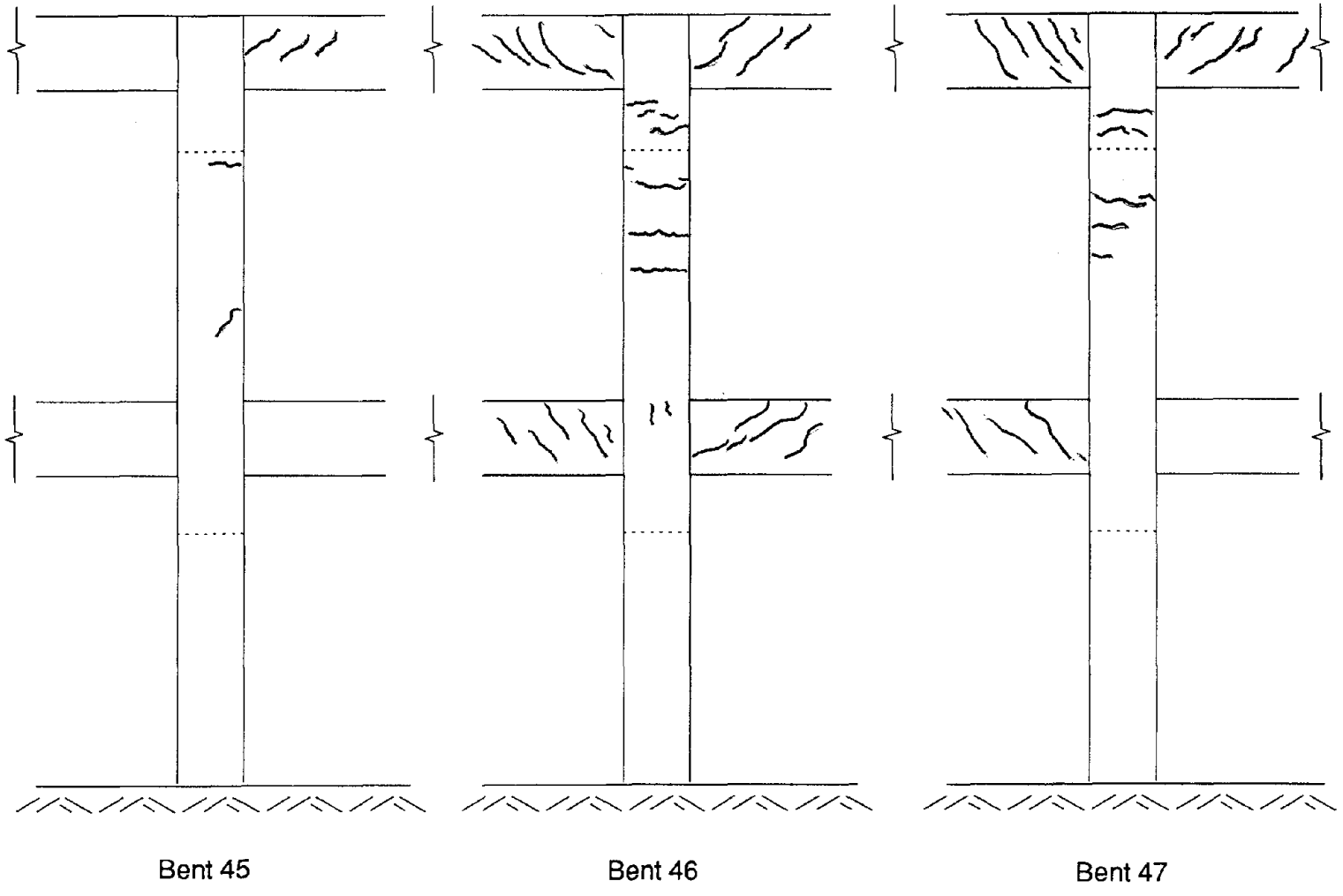

Fig. 2.9(a) Original crack locations on east face

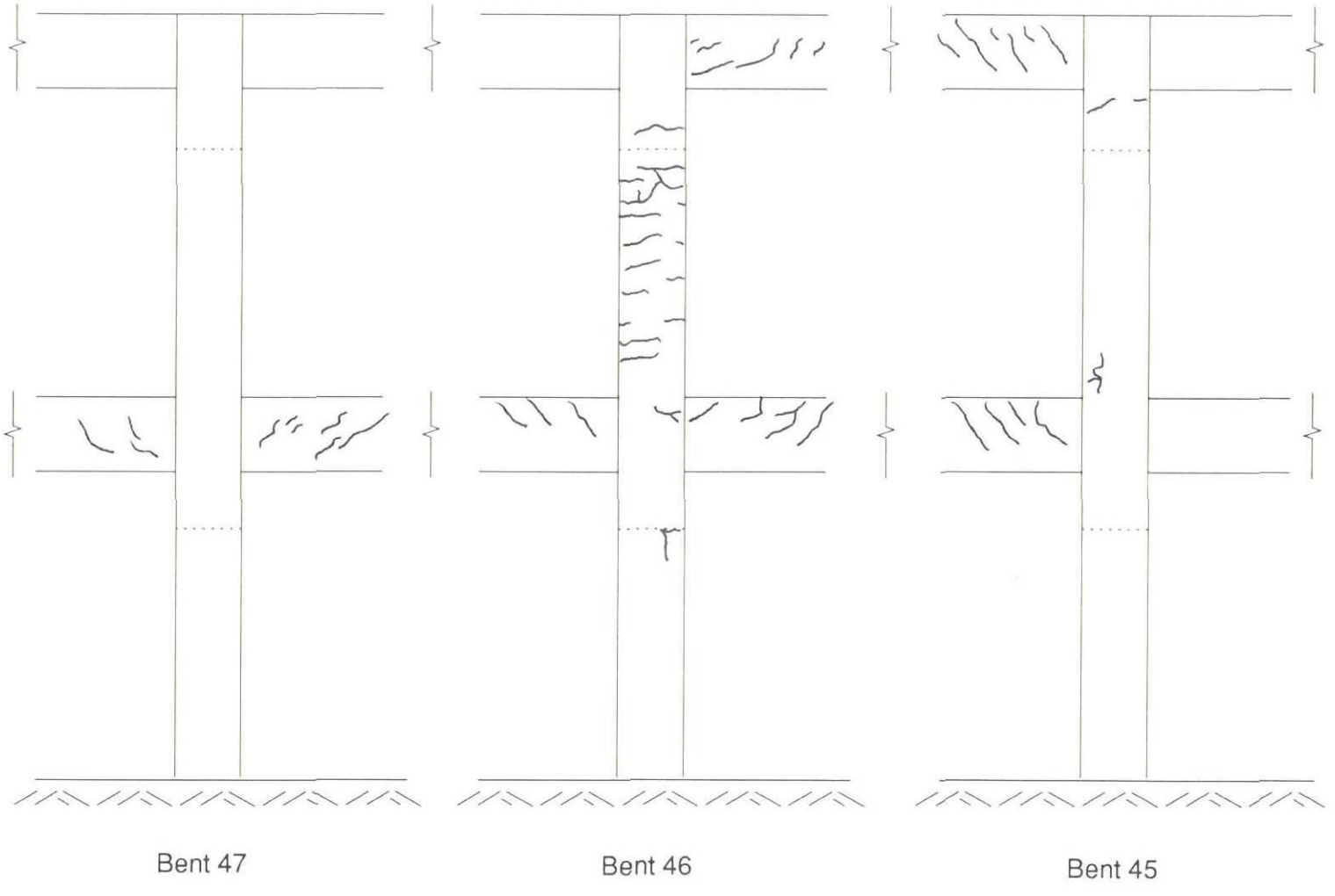

Fig. 2.9(b) Original crack locations on west face

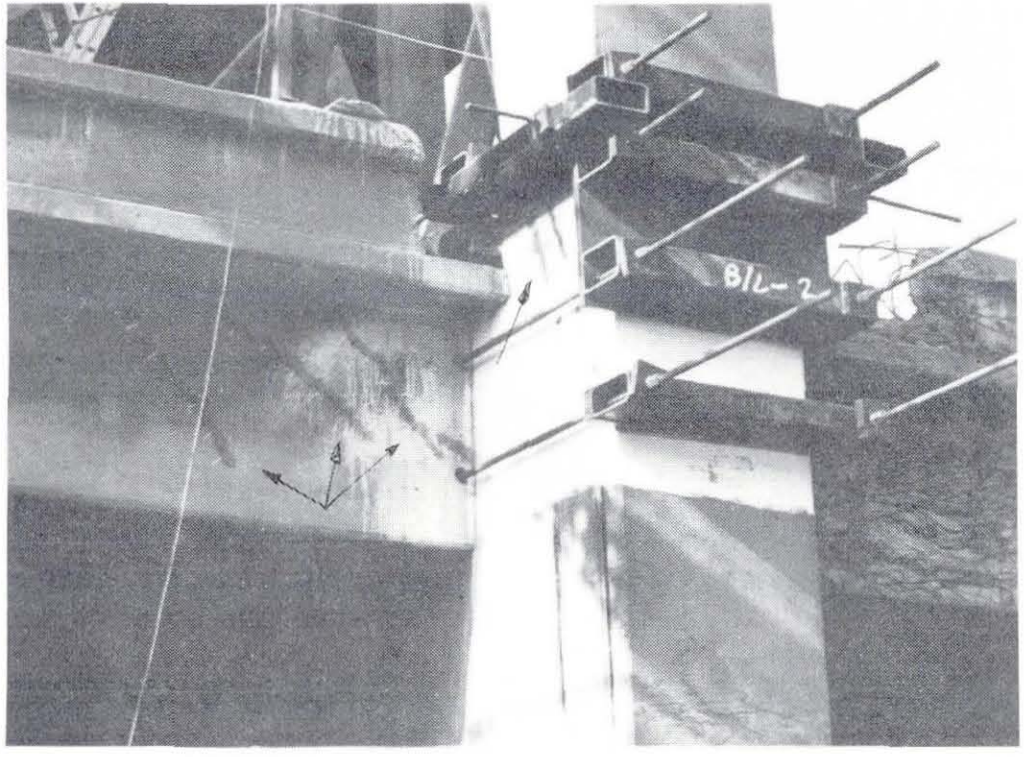

Fig. 2.10(a) Epoxied existing cracks on the east face of Bent 47.

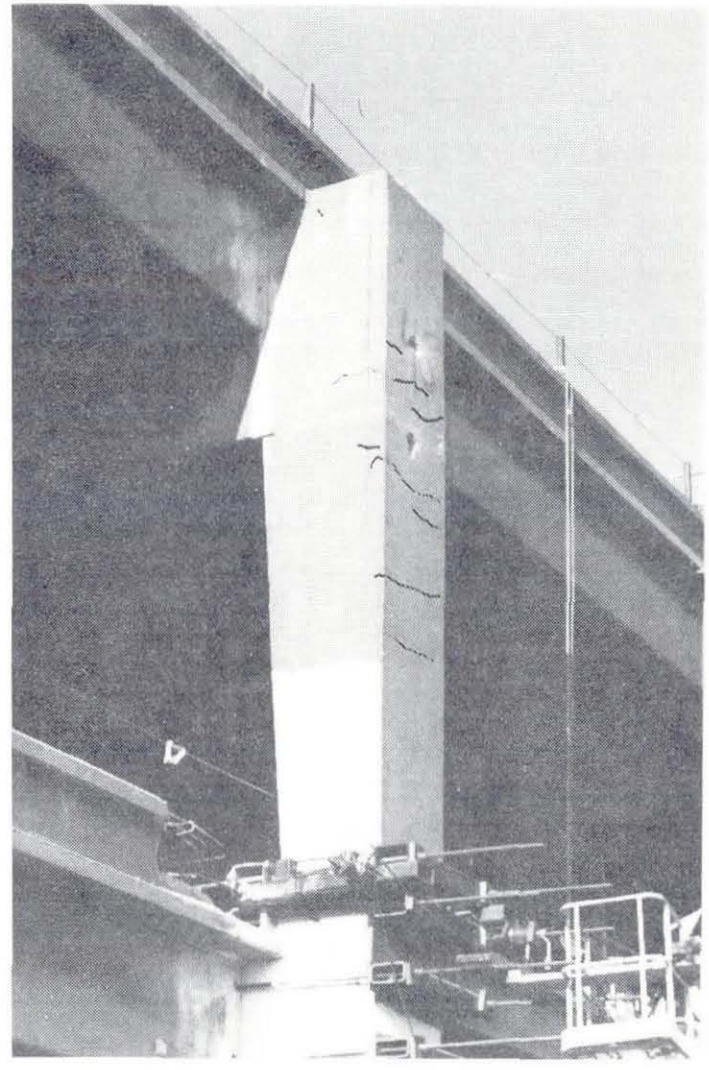

Fig. 2.10(b) Existing hairline cracks on the west face of Bent 46.

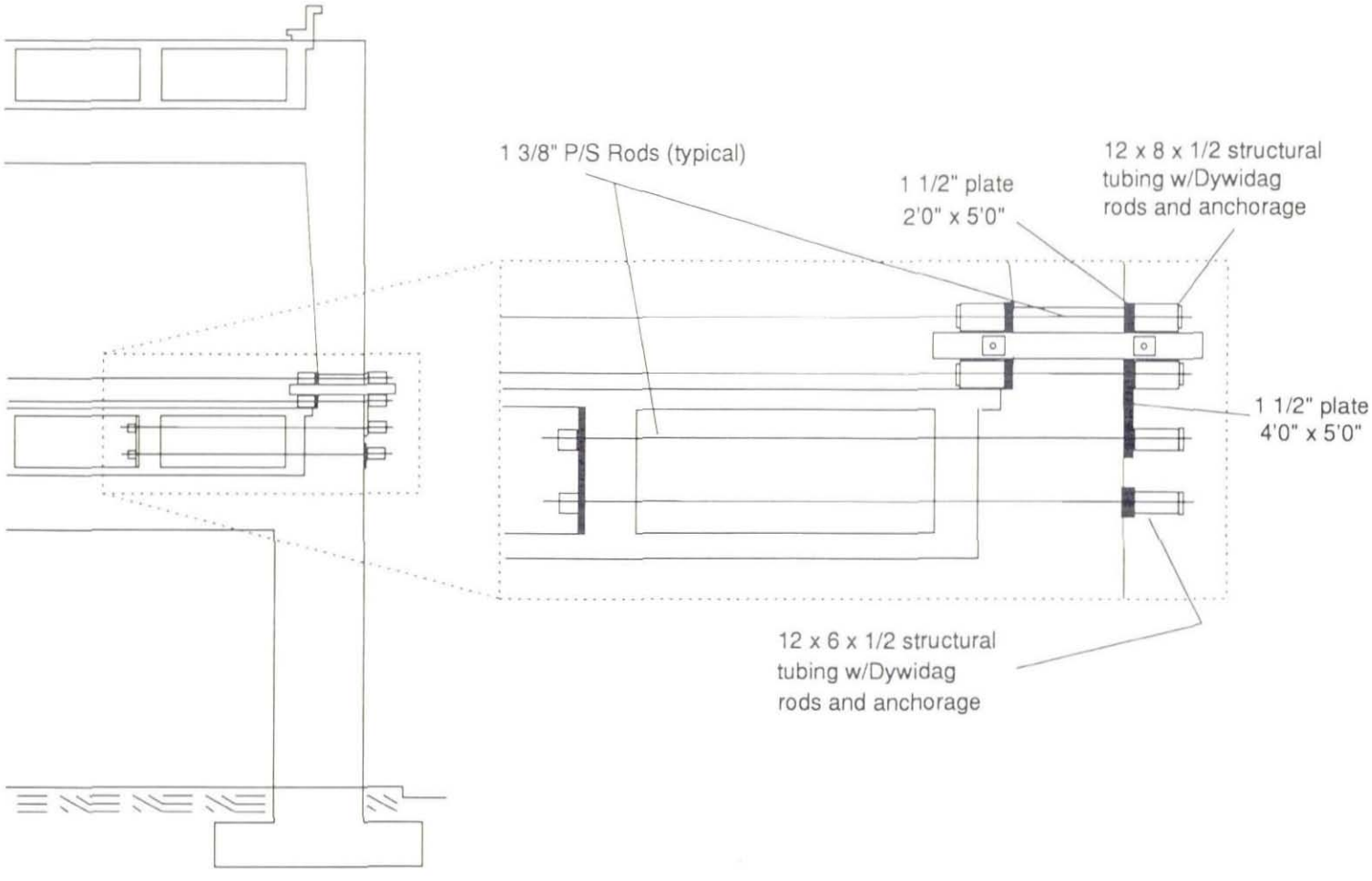

Fig. 2.11 Original Structure Retrofit (Typical)

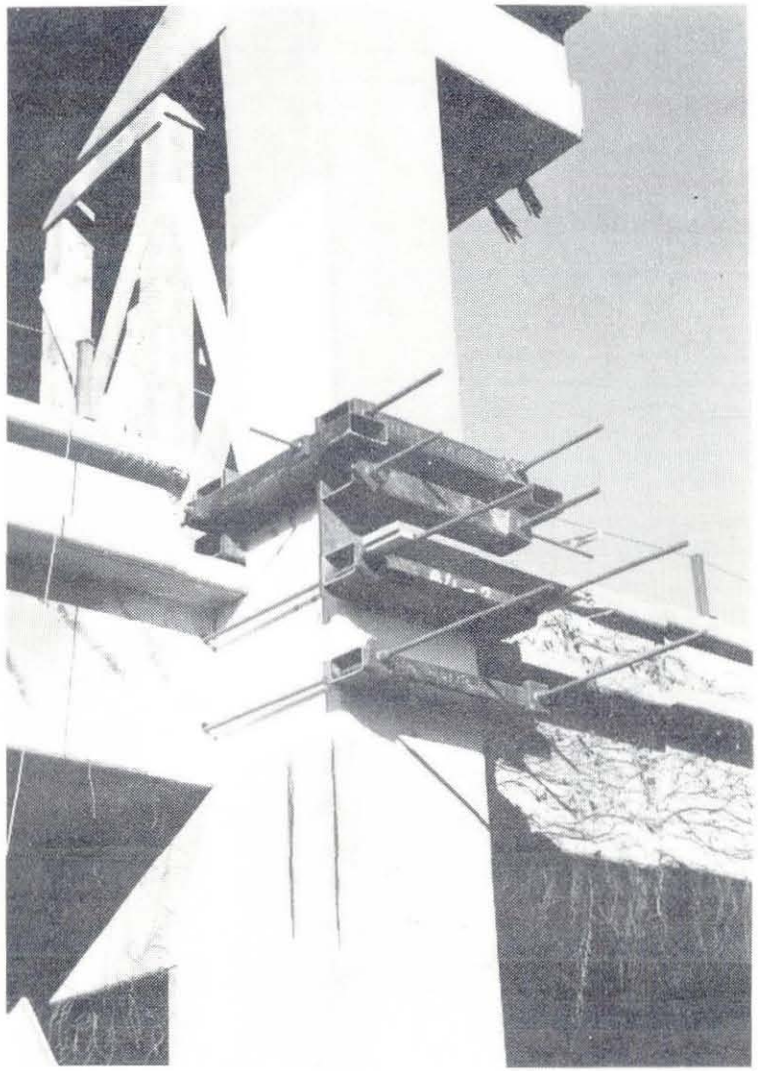

Fig. 2.12 Photo of original structure retrofit.

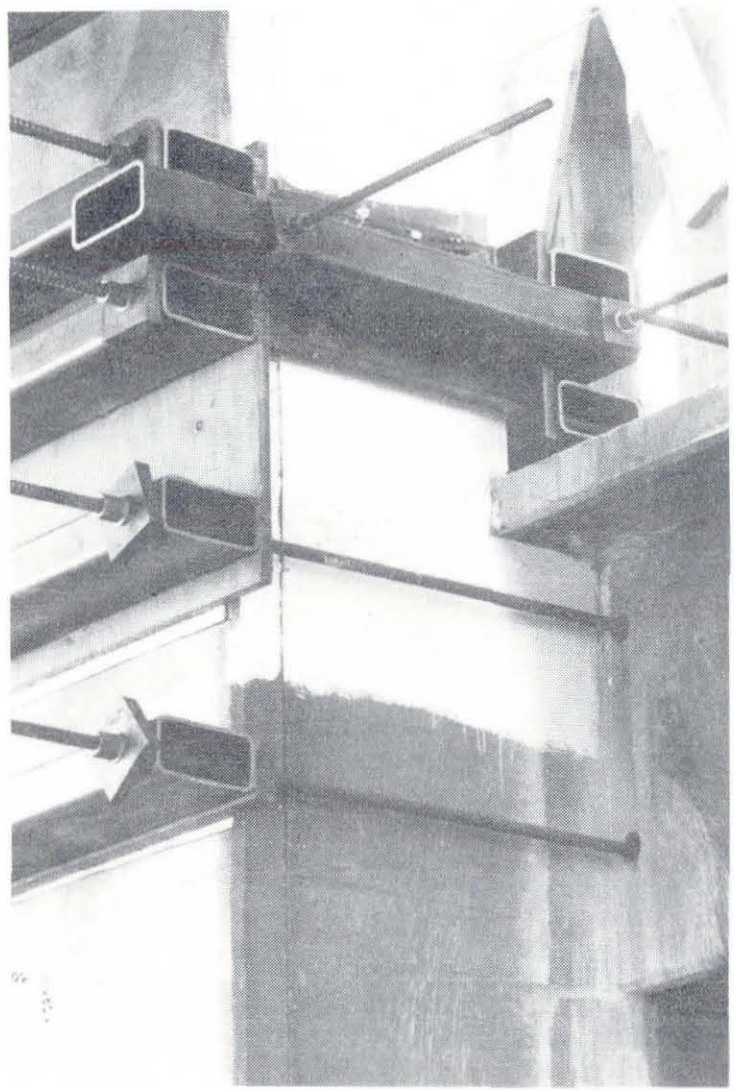

Fig. 2.13 Original structure retrofit close-up.

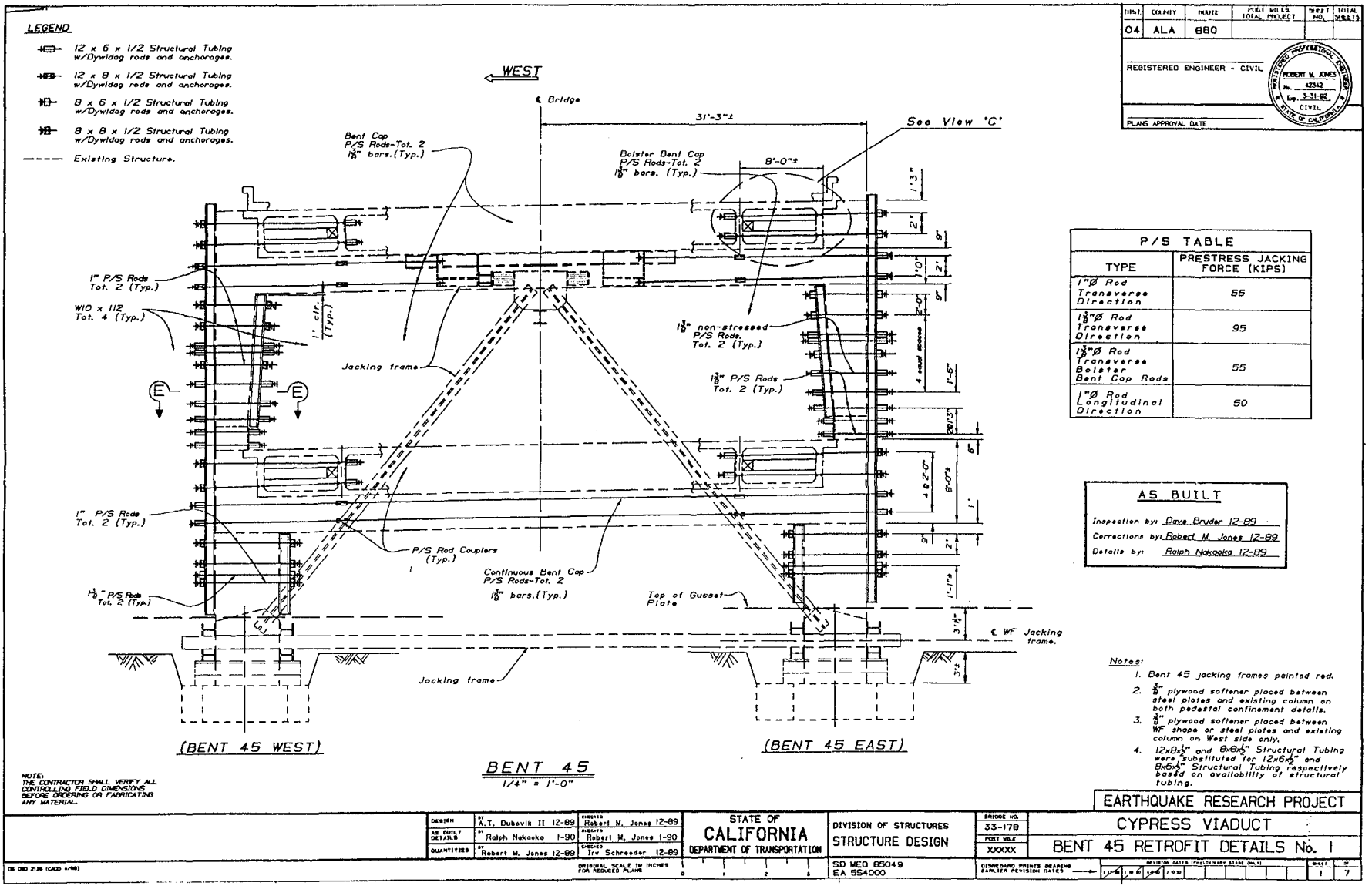

Fig. 2.14(a) Bent 45 retrofitting plans.

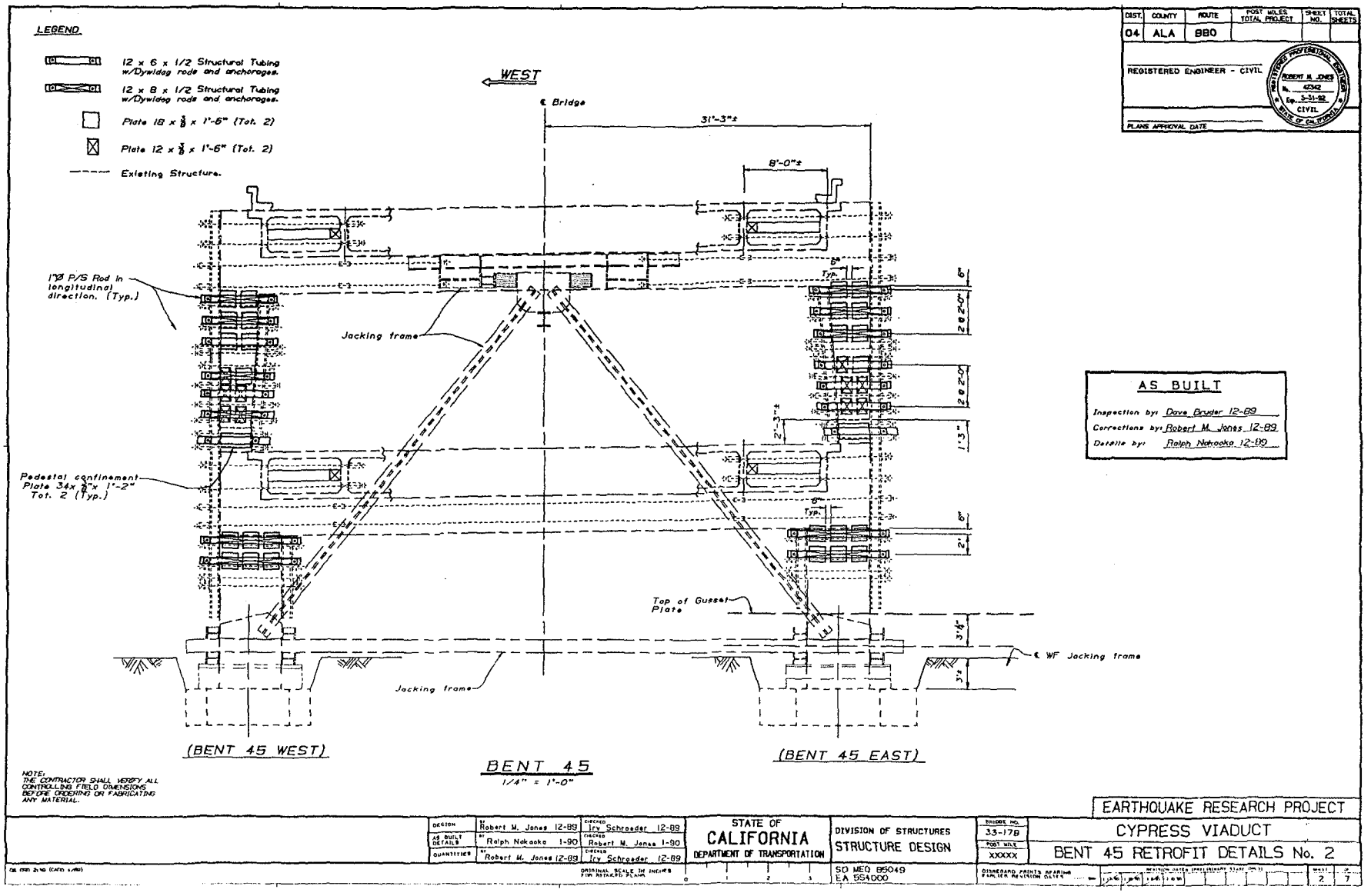

Fig. 2.14(b) Bent 45 retrofitting plans.

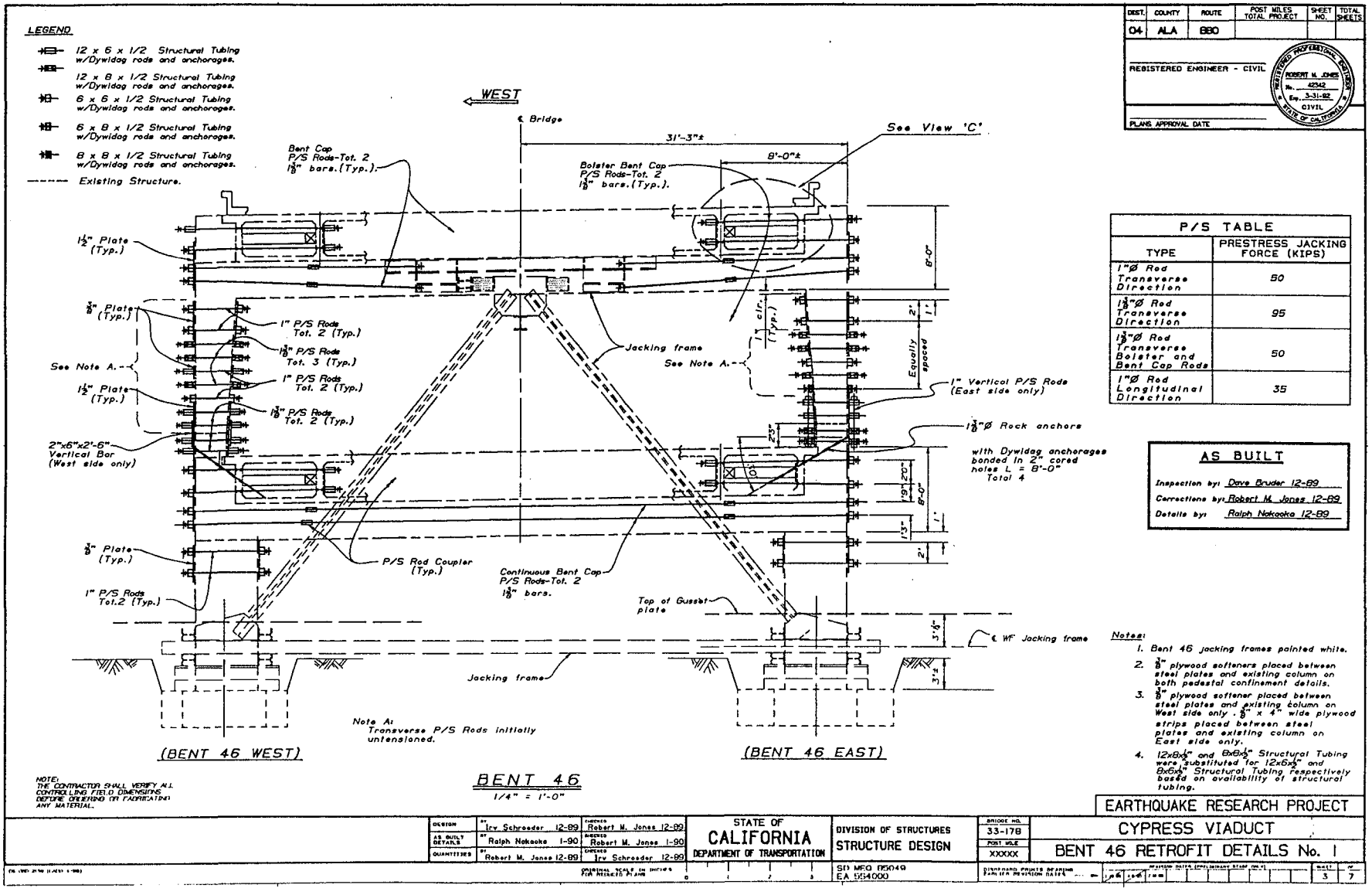

Fig. 2.15(a) Bent 46 retrofitting plans.

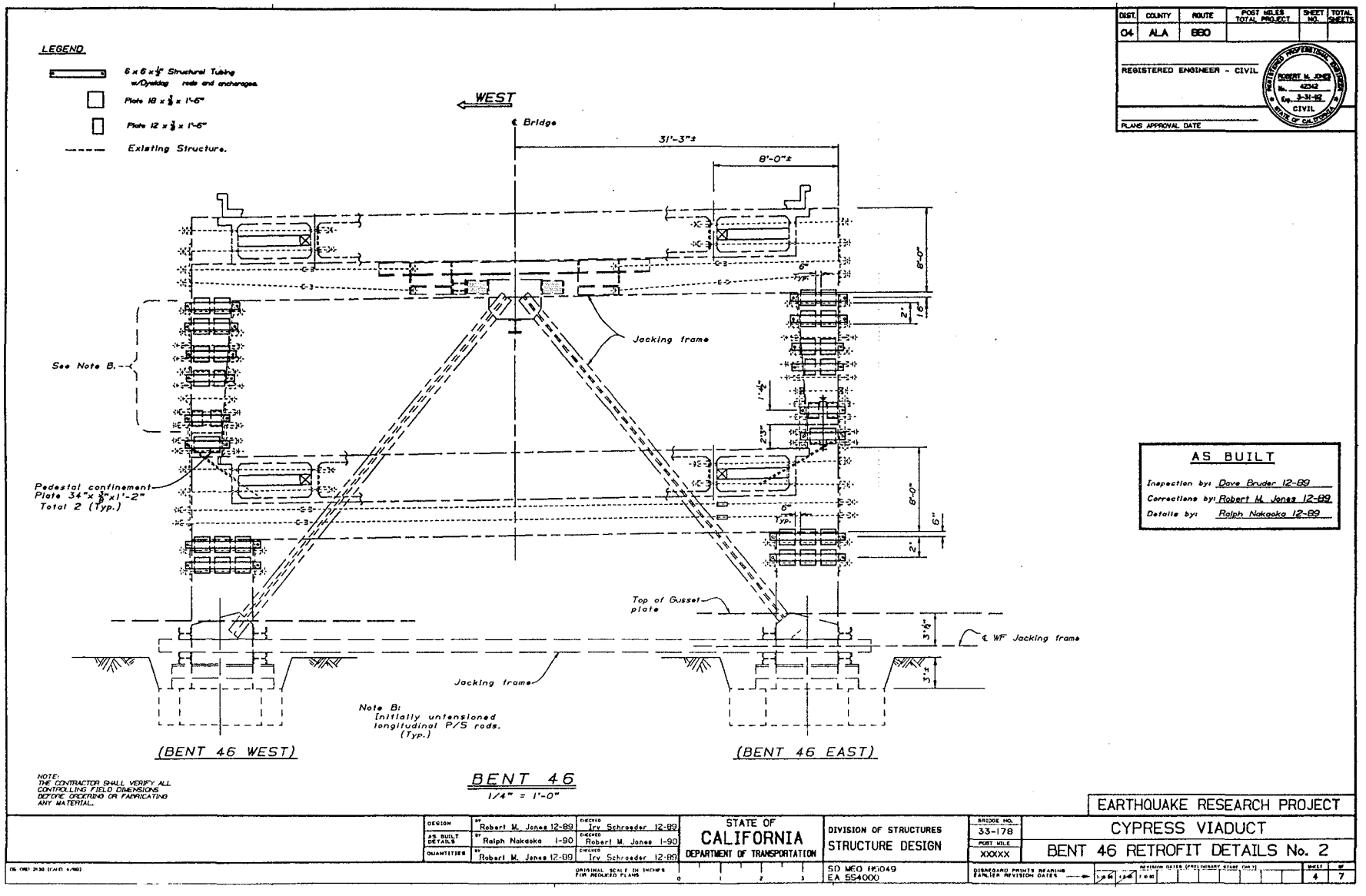

Fig. 2.15(b) Bent 46 retrofitting plans.

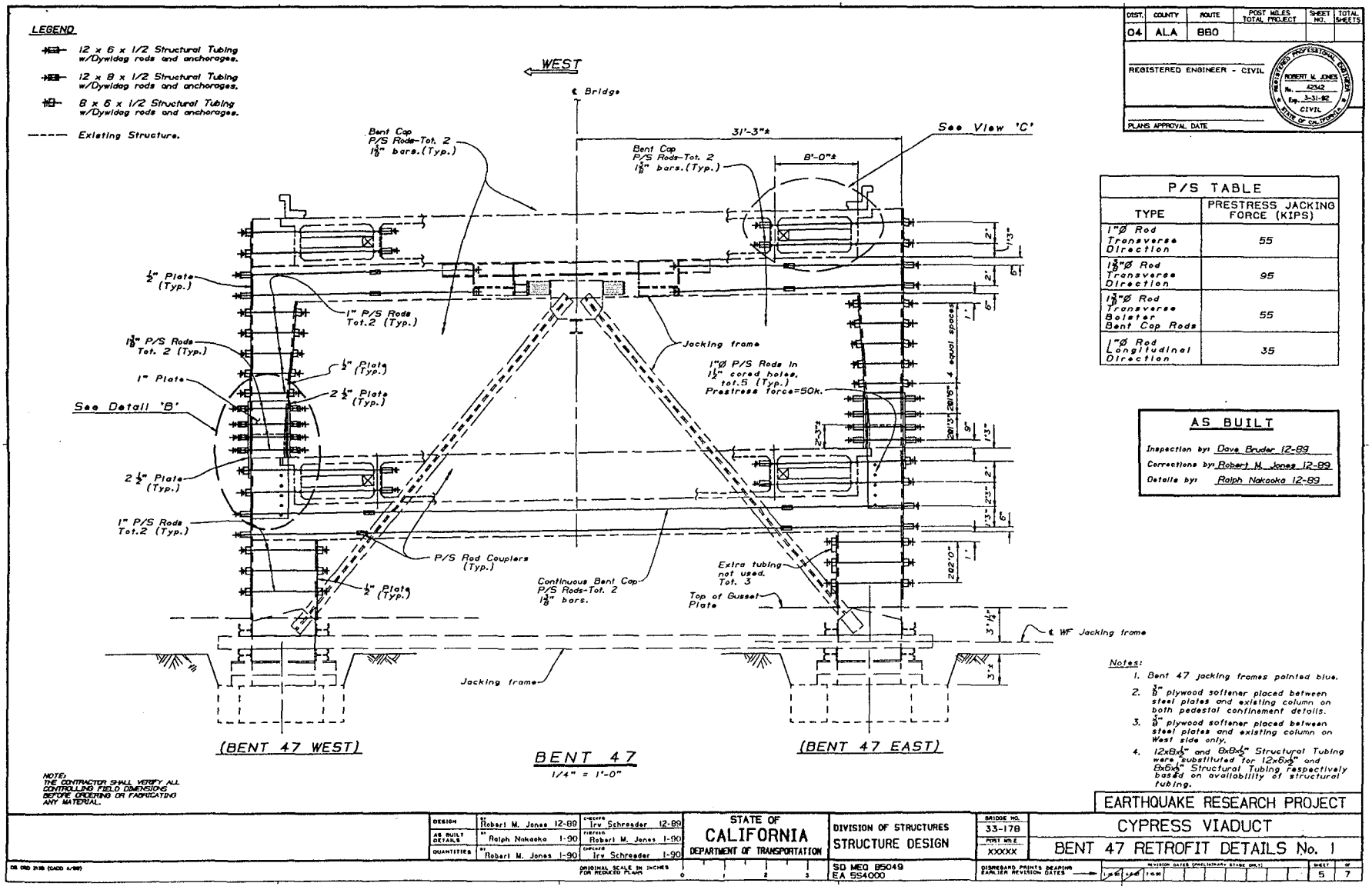

DIST.	COUNTY	ROUTE	POST MILES TOTAL PROJECT	SHEET NO.	TOTAL SHEETS
04	ALA	880			

REGISTERED ENGINEER - CIVIL

ROBERT M. JONES No. 42542 Exp. 3-31-92 CIVIL STATE OF CALIFORNIA

PLANS APPROVAL DATE

P/S TABLE	
TYPE	PRESTRESS JACKING FORCE (KIPS)
1"Ø Rod Transverse Direction	55
1⅜"Ø Rod Transverse Direction	95
1⅜"Ø Rod Transverse Bolster Bent Cap Rods	55
1"Ø Rod Longitudinal Direction	35

AS BUILT

Inspection by: Dave Bruder 12-89
Corrections by: Robert M. Jones 12-89
Details by: Ralph Nakaoka 12-89

Notes:
1. Bent 47 jacking frames painted blue.
2. ⅜" plywood softener placed between steel plates and existing column on both pedestal confinement details.
3. ⅜" plywood softener placed between steel plates and existing column on West side only.
4. 12x8x½" and 8x8x½" Structural Tubing were substituted for 12x6x½" and 8x6x½" Structural Tubing respectively based on availability of structural tubing.

DESIGN	Robert M. Jones 12-89	Irv Schroeder 12-89	STATE OF CALIFORNIA DEPARTMENT OF TRANSPORTATION	DIVISION OF STRUCTURES STRUCTURE DESIGN	BRIDGE NO. 33-178
AS BUILT DETAILS	Ralph Nakaoka 1-90	Robert M. Jones 1-90			POST MILE XXXXX
QUANTITIES	Robert M. Jones 1-90	Irv Schroeder 1-90		SD MEQ 85049 EA 554000	

EARTHQUAKE RESEARCH PROJECT

CYPRESS VIADUCT

BENT 47 RETROFIT DETAILS No. 1

SHEET 5 OF 7

Fig. 2.16(a) Bent 47 retrofitting plans.

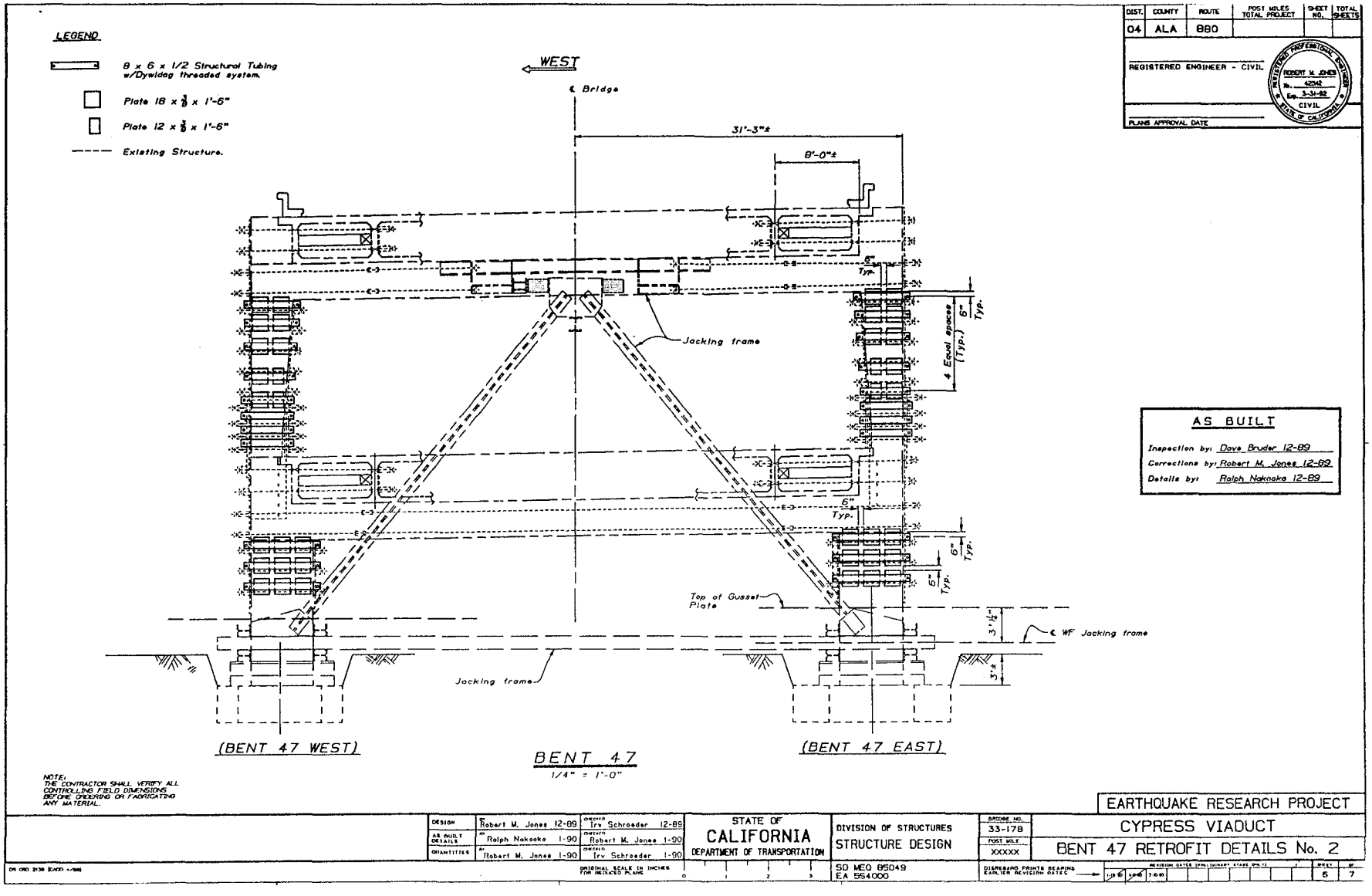

Fig. 2.16(b) Bent 47 retrofitting plans.

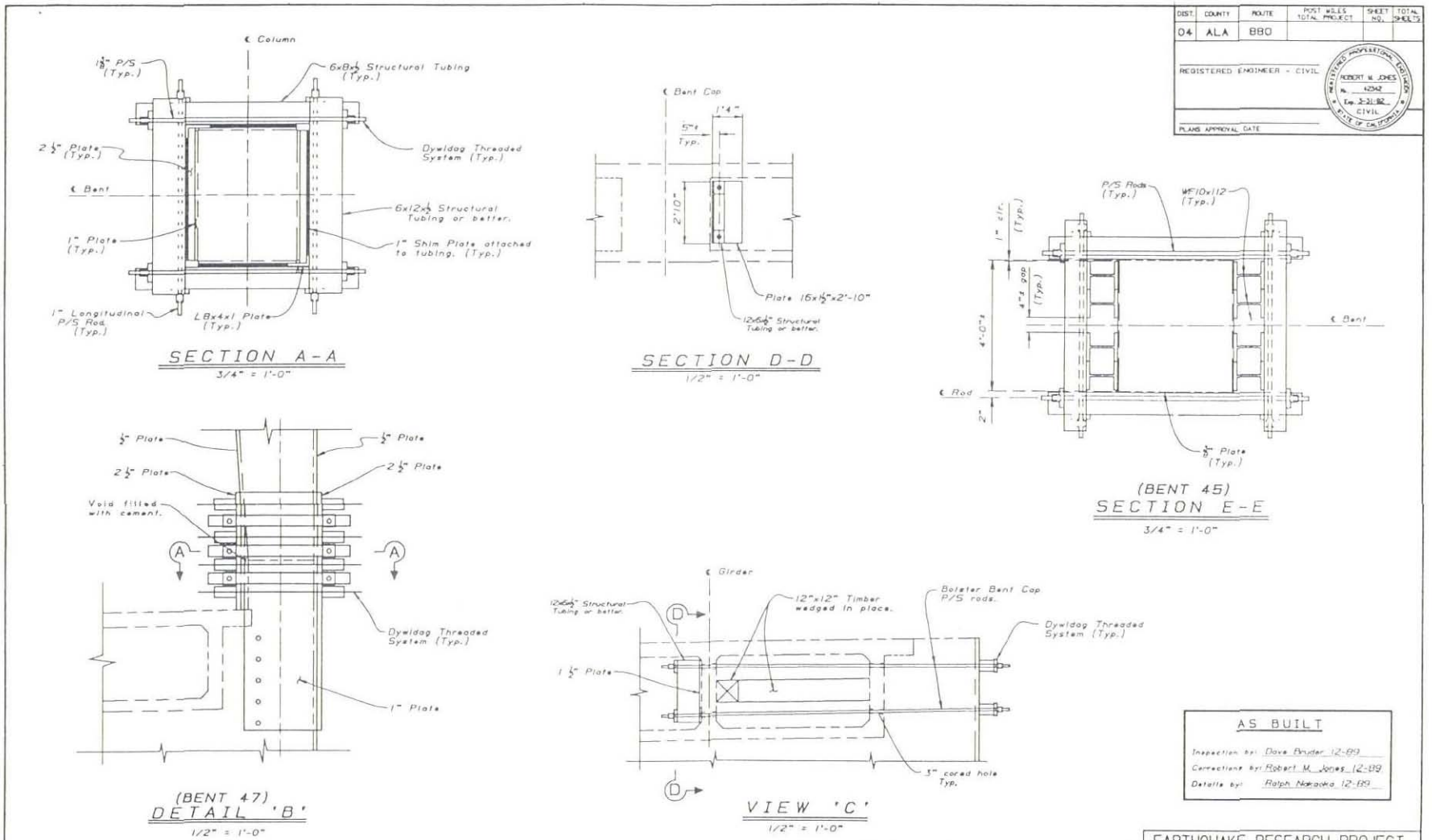

Fig. 2.16(c) Bent miscellaneous details.

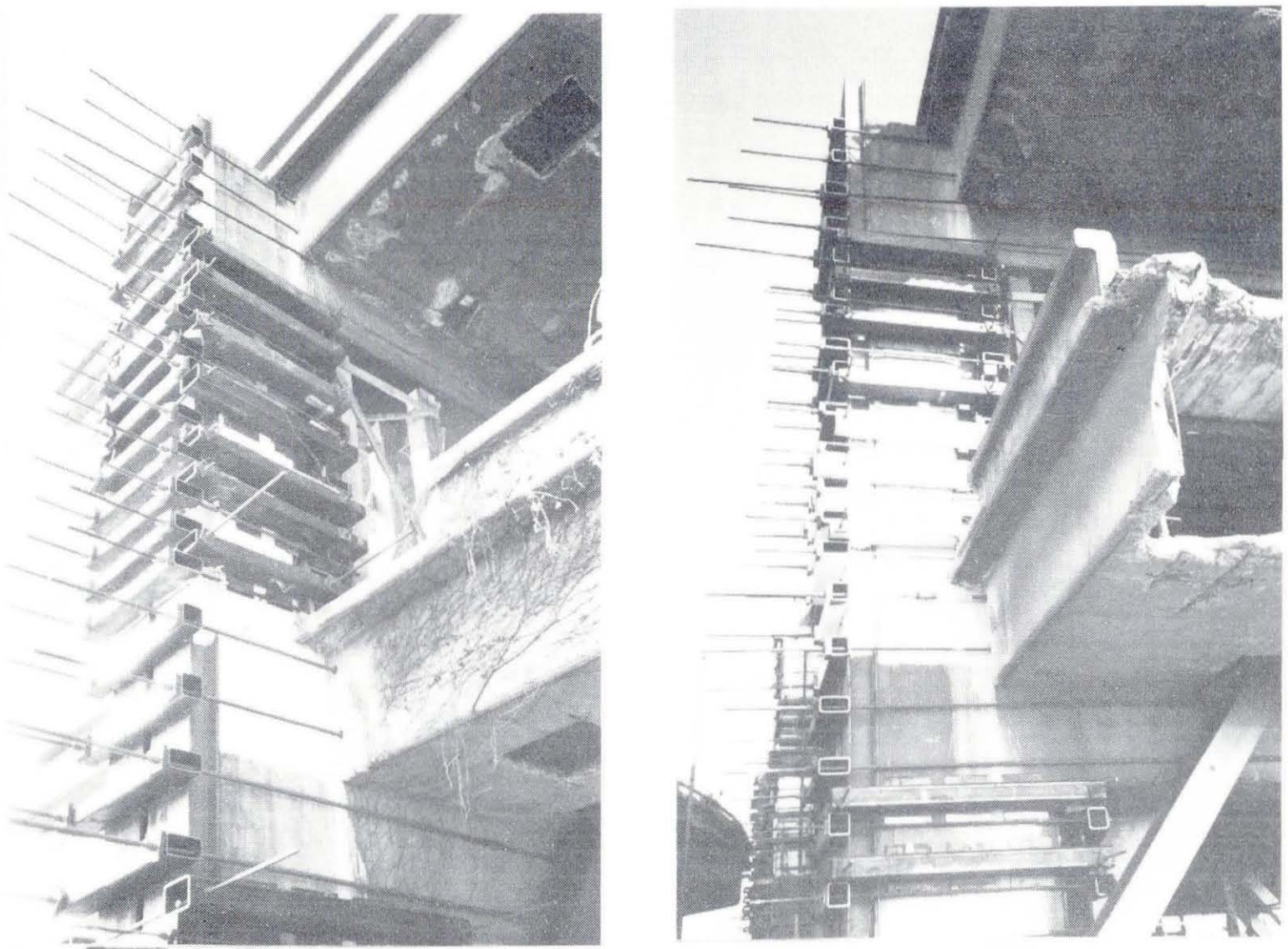

Fig. 2.17 Bent 45 Retrofit details.

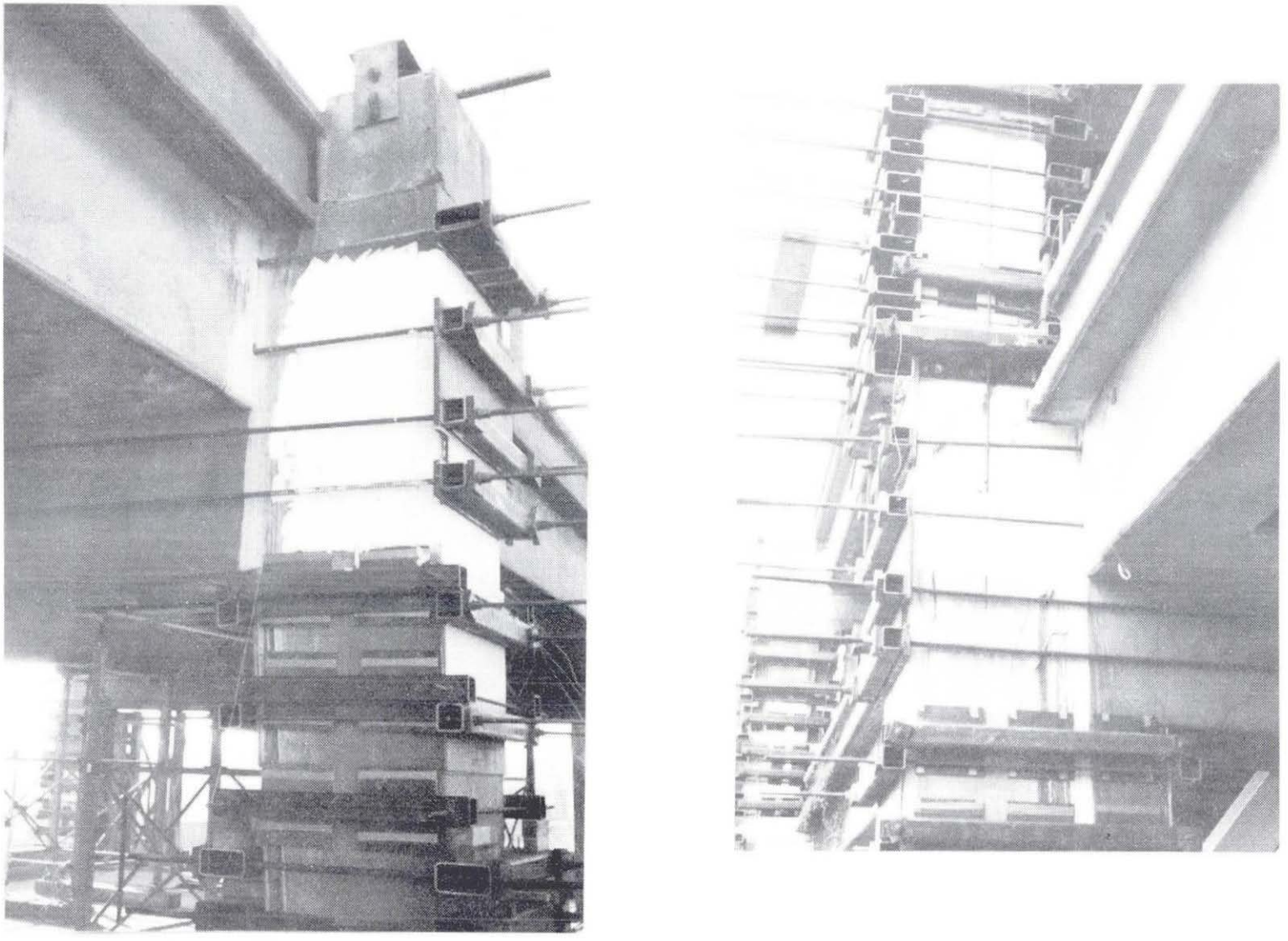

Fig. 2.18 Bent 46 Retrofit details.

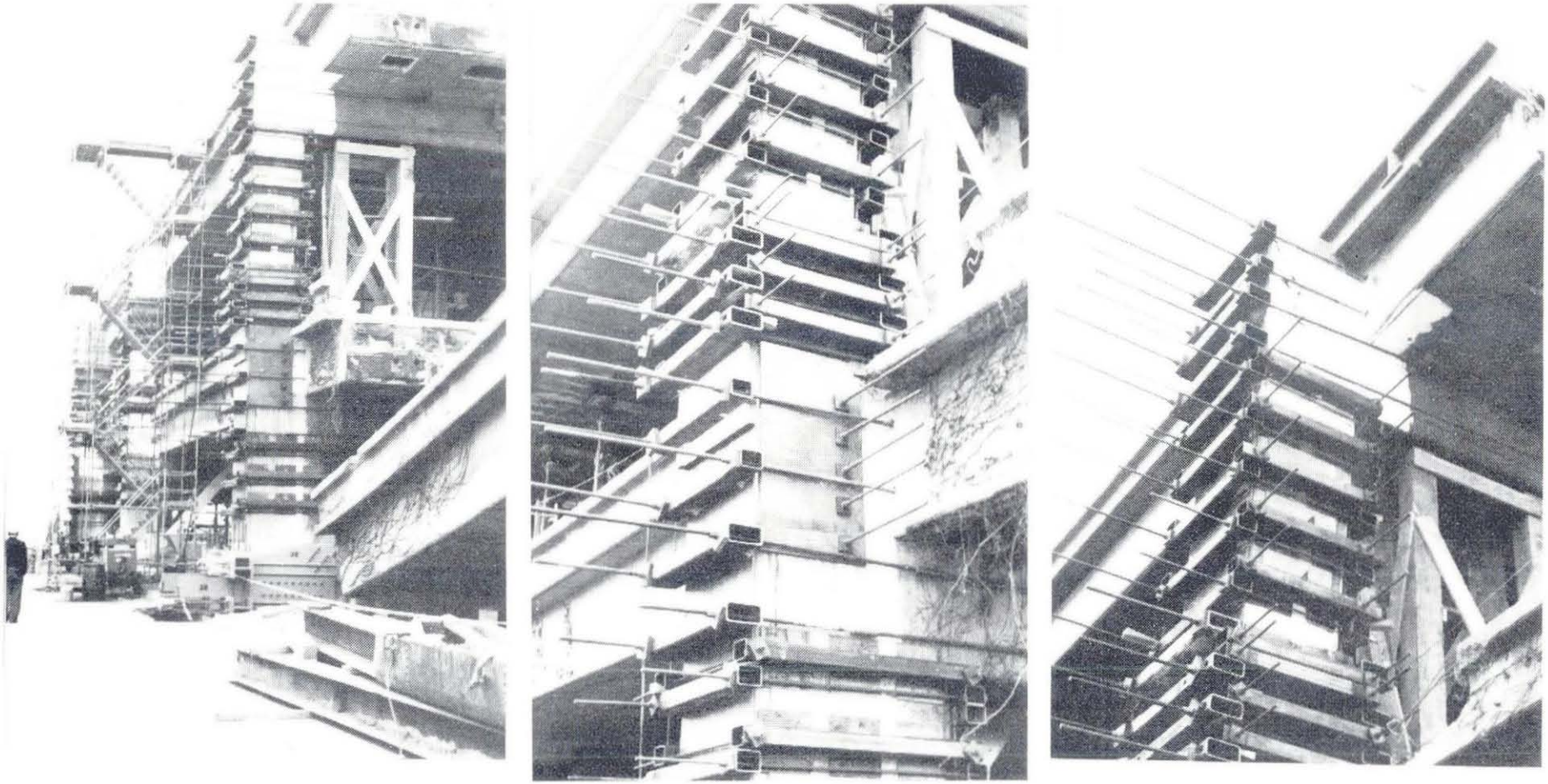

Fig. 2.19 Bent 47 Retrofit details.

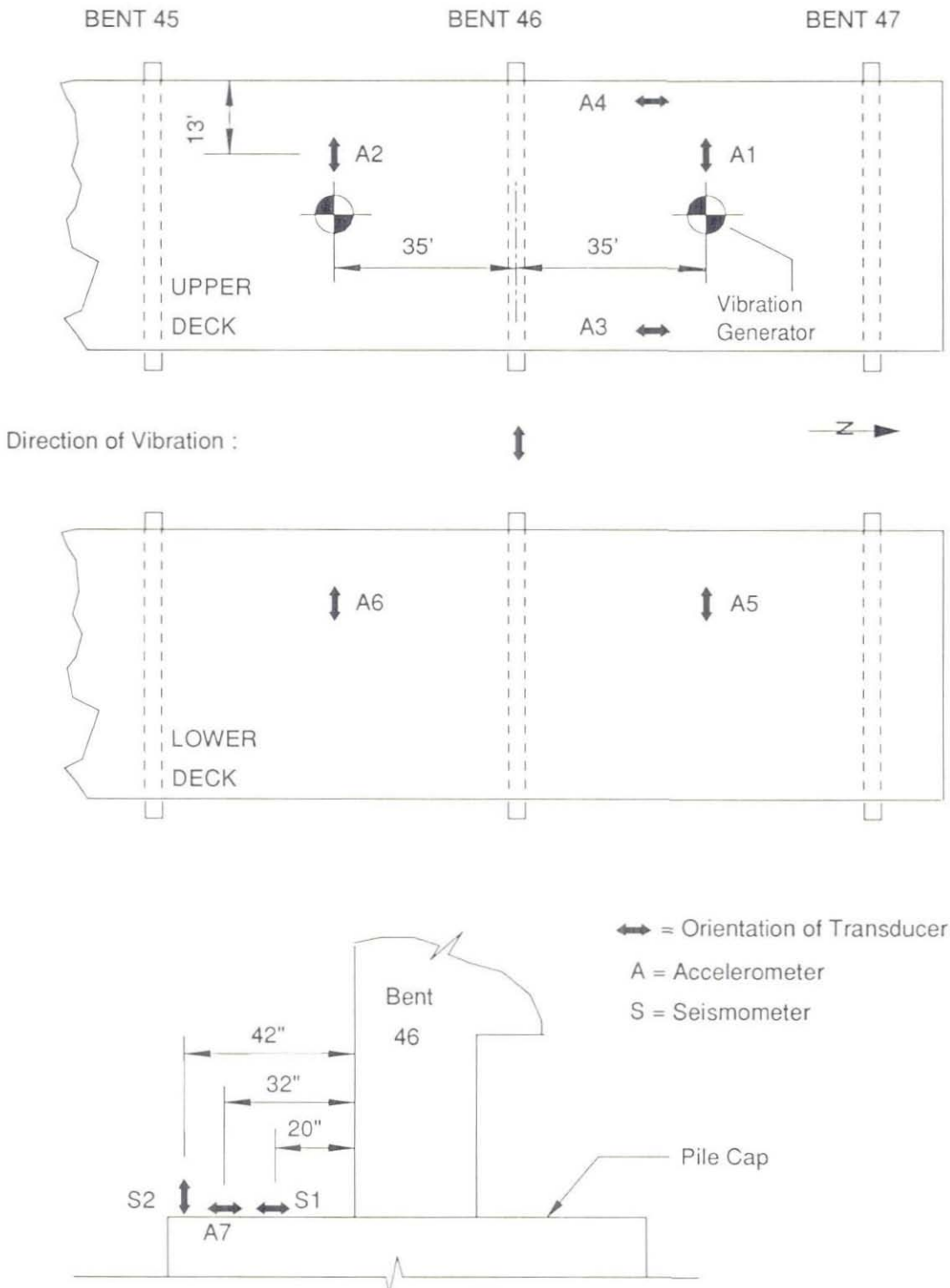

Fig. 2.20 Forced Vibration Test

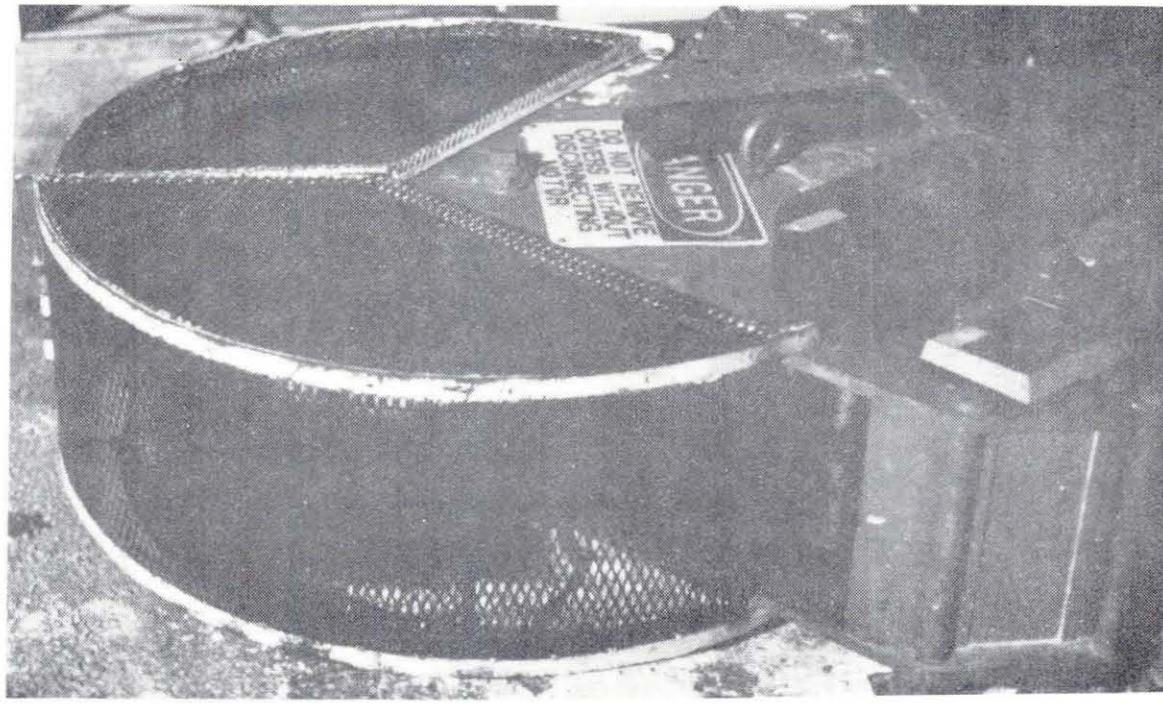

Fig. 2.21 Forced vibration generator.

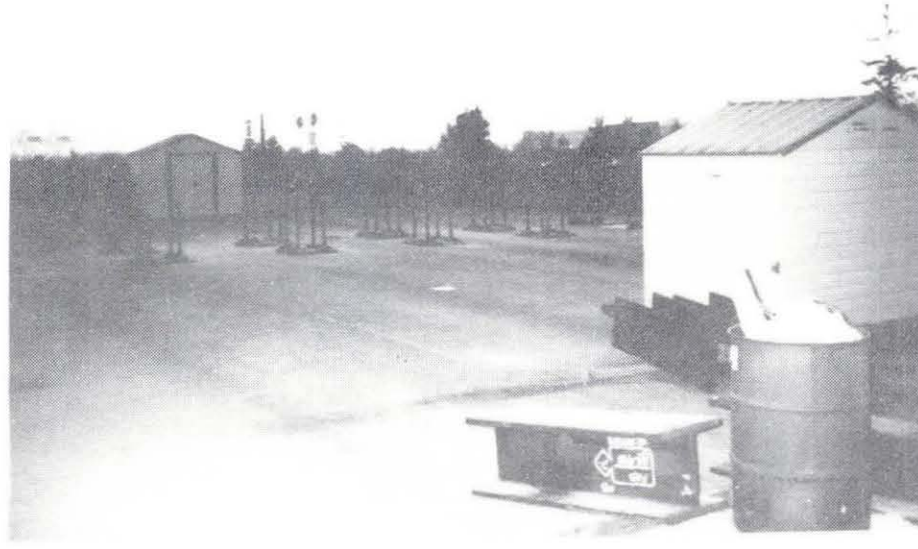

Fig. 2.22 Vibration generator housing on the top deck (installed in metal sheds).

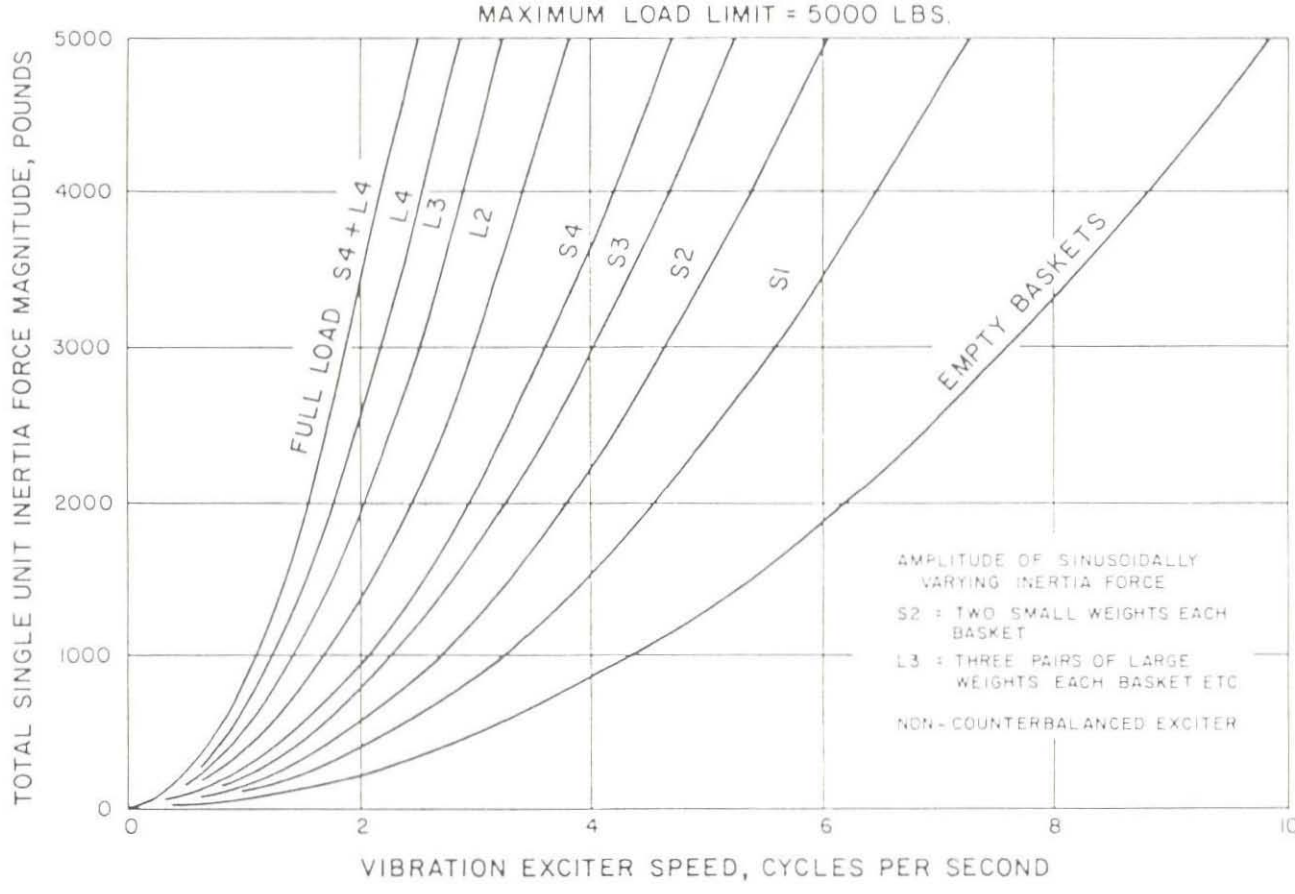

Fig. 2.23 Vibration force vs. speed non-counter balanced.

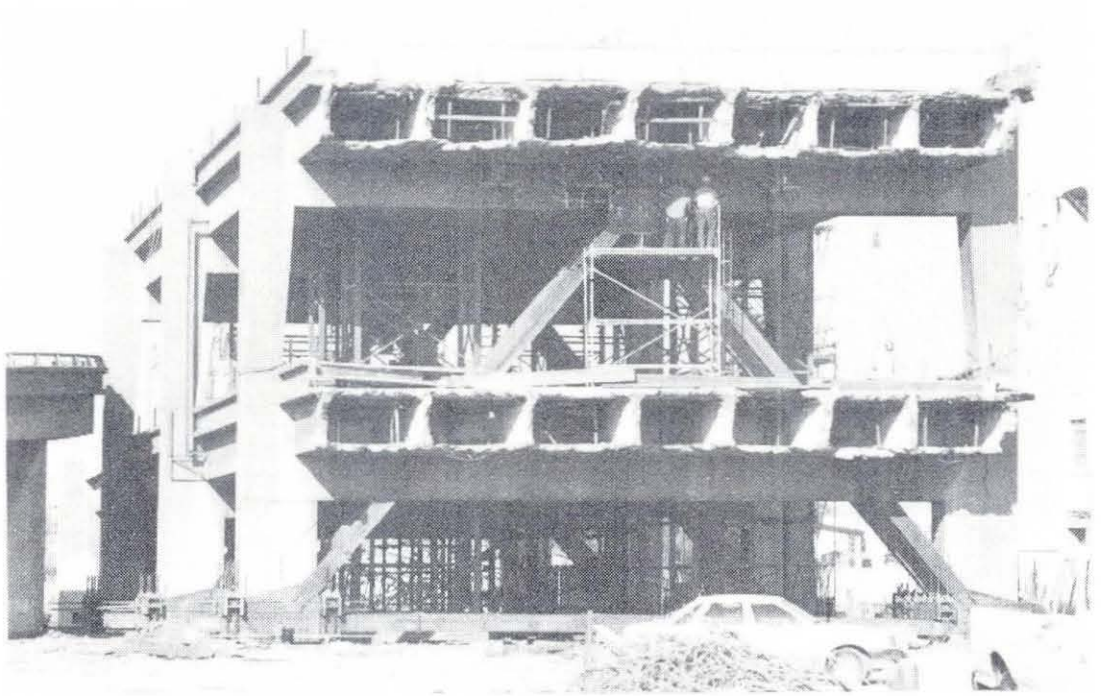

(a) Prior to retrofit.

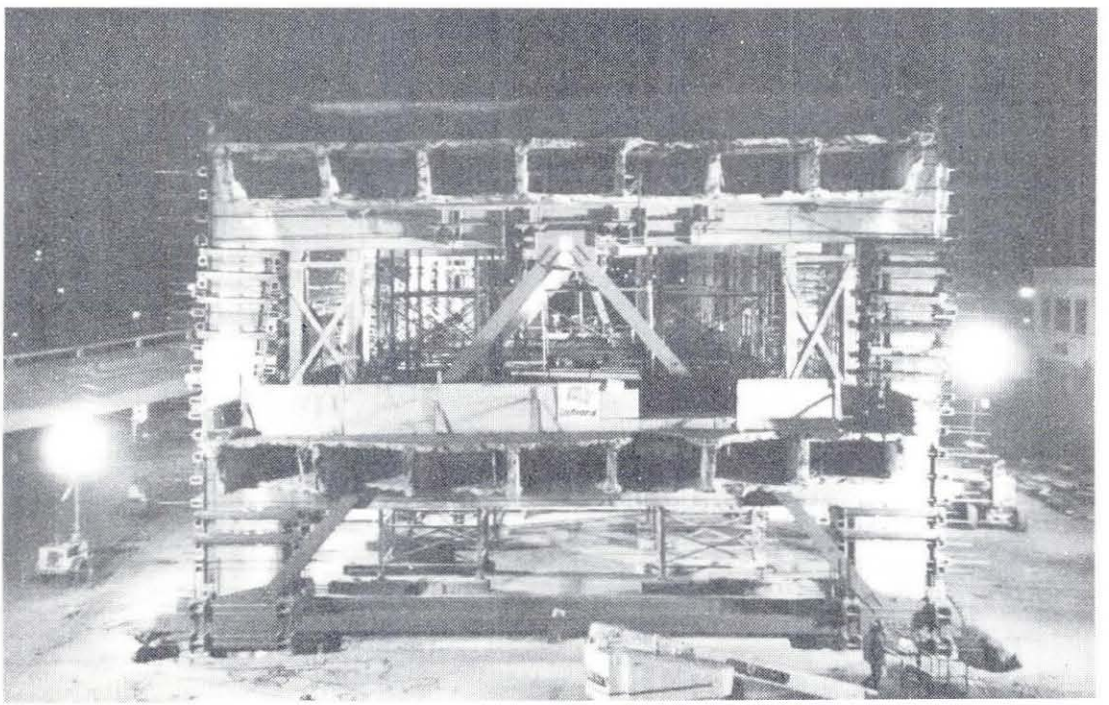

(b) After retrofit.

Fig. 2.24 Loading frame photo.

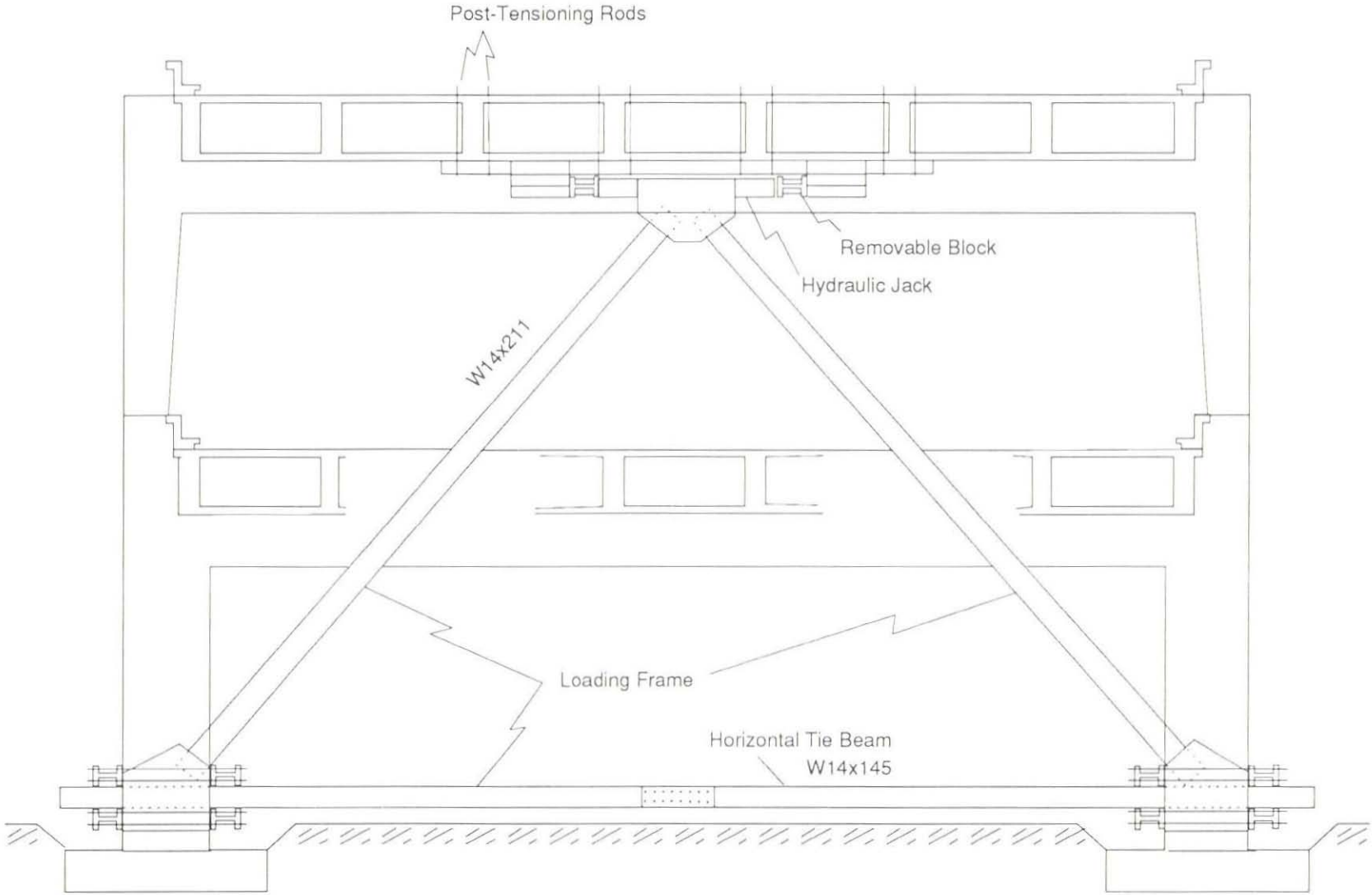

Fig. 2.25 Loading Frame

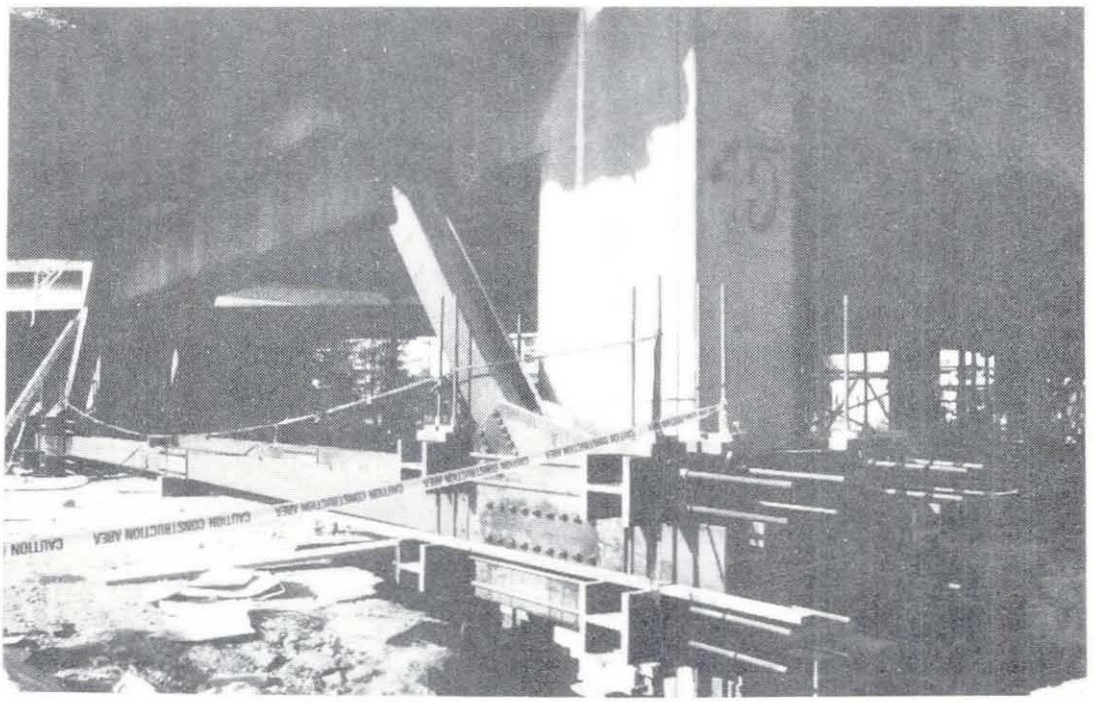

(a) Bottom detail.

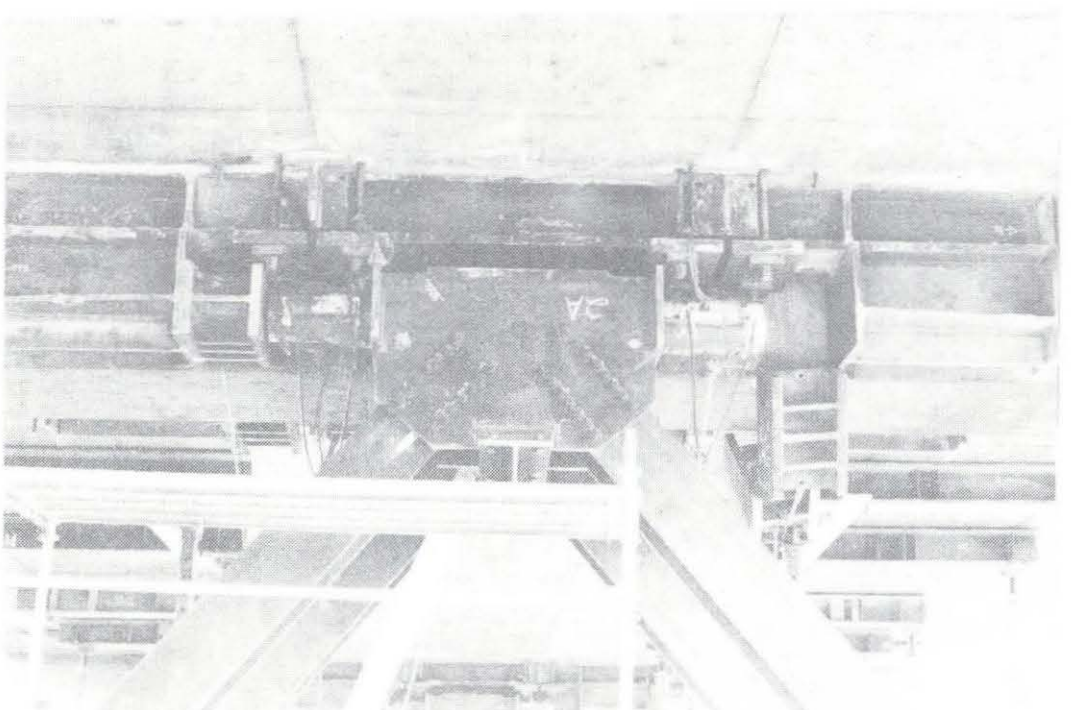

(b) Top detail.

Fig. 2.26 Loading frame details.

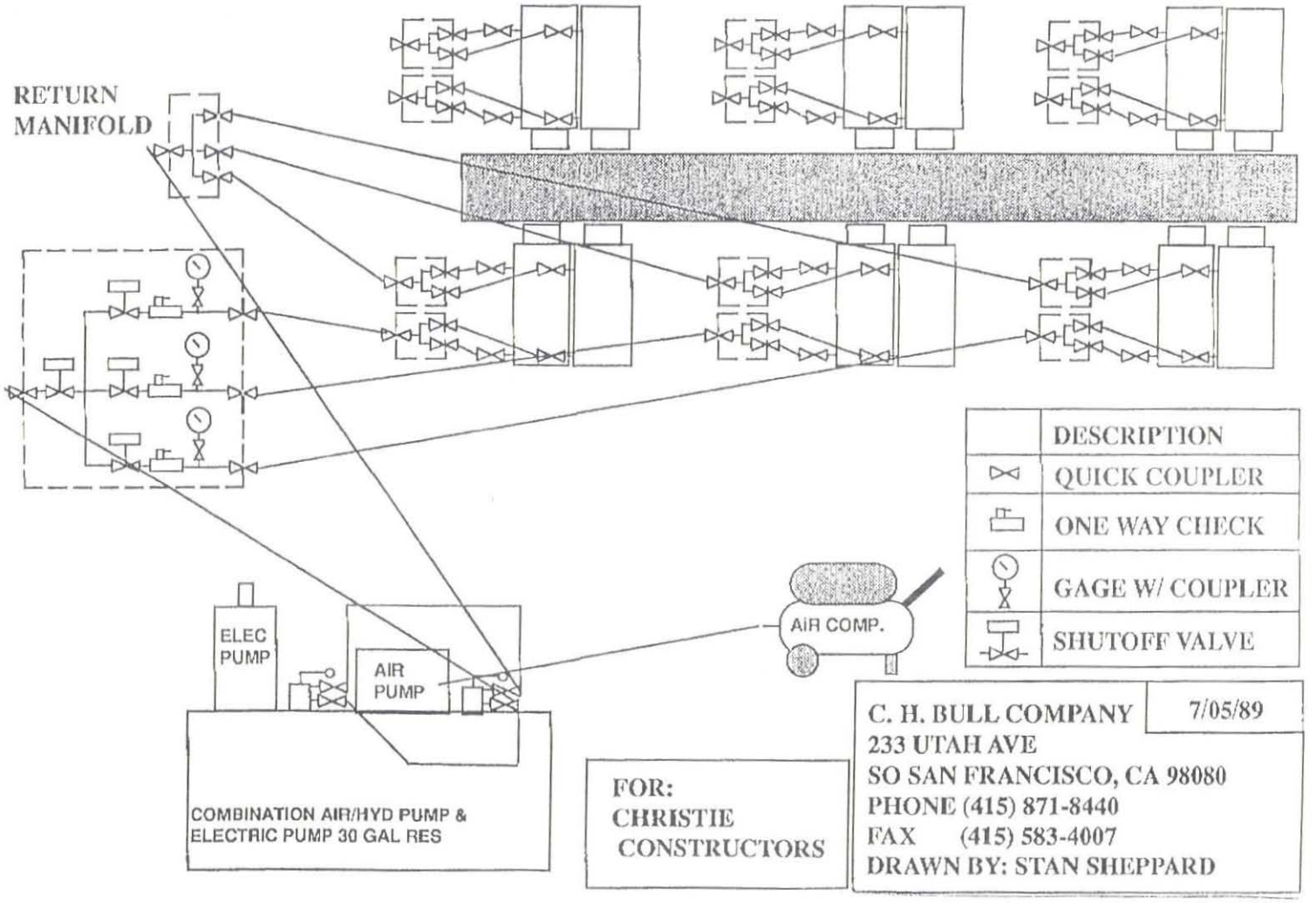

Fig. 2.27 Hydraulic jacking system schematic.

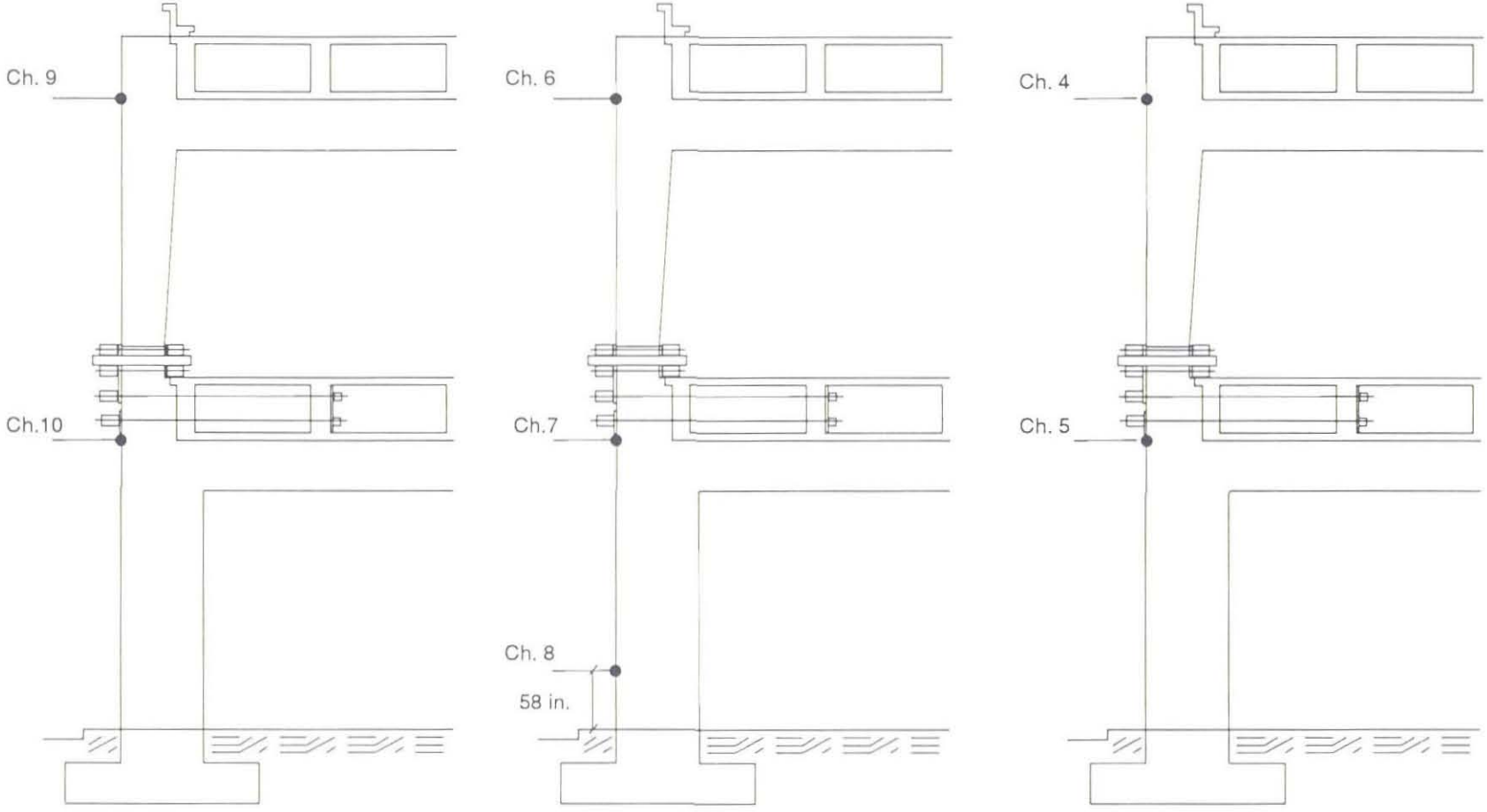

Fig. 2.28 Linear Potentiometer Locations, Original Structure

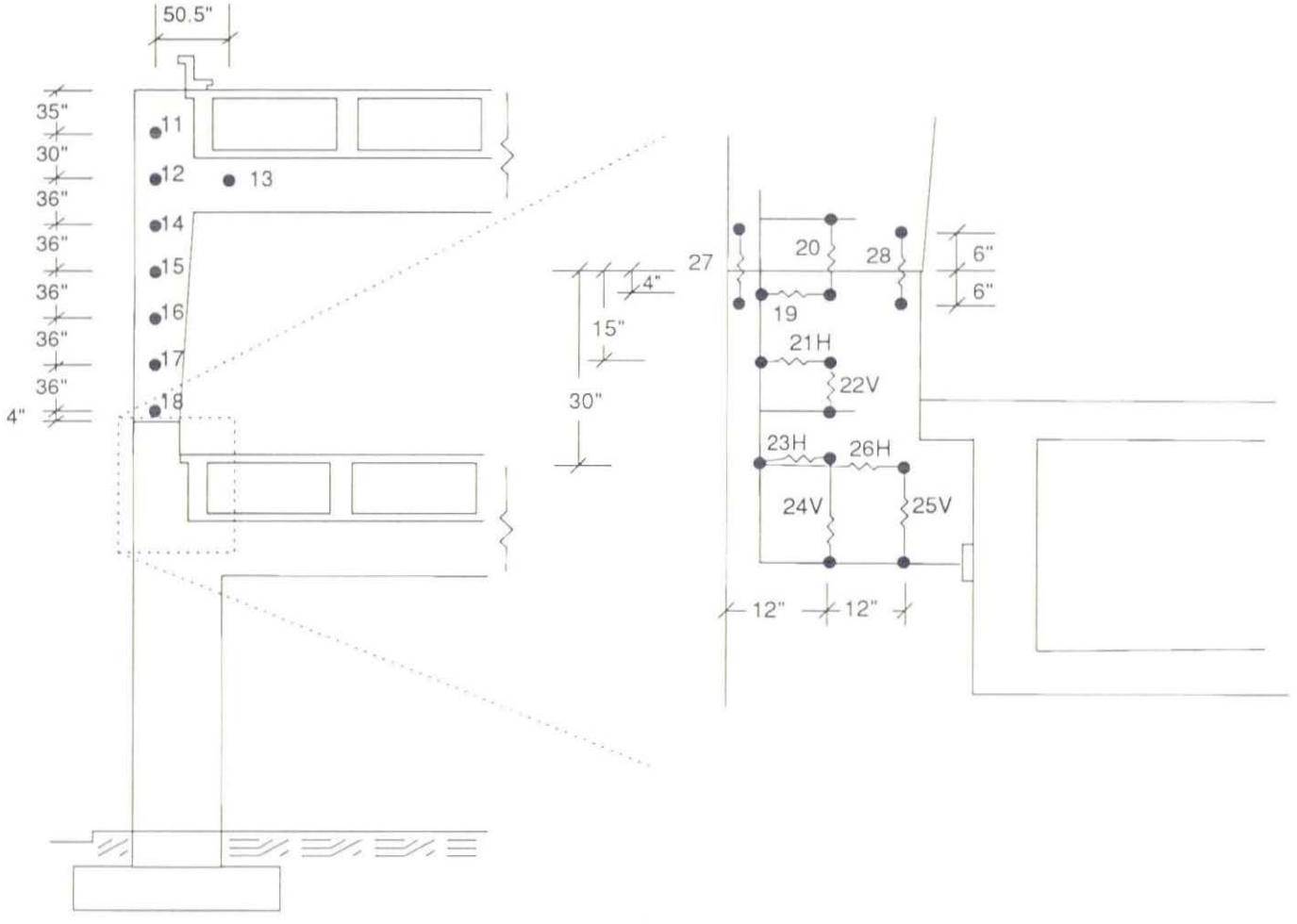

Fig. 2.29 Linear Potentiometer Locations, Original Structure

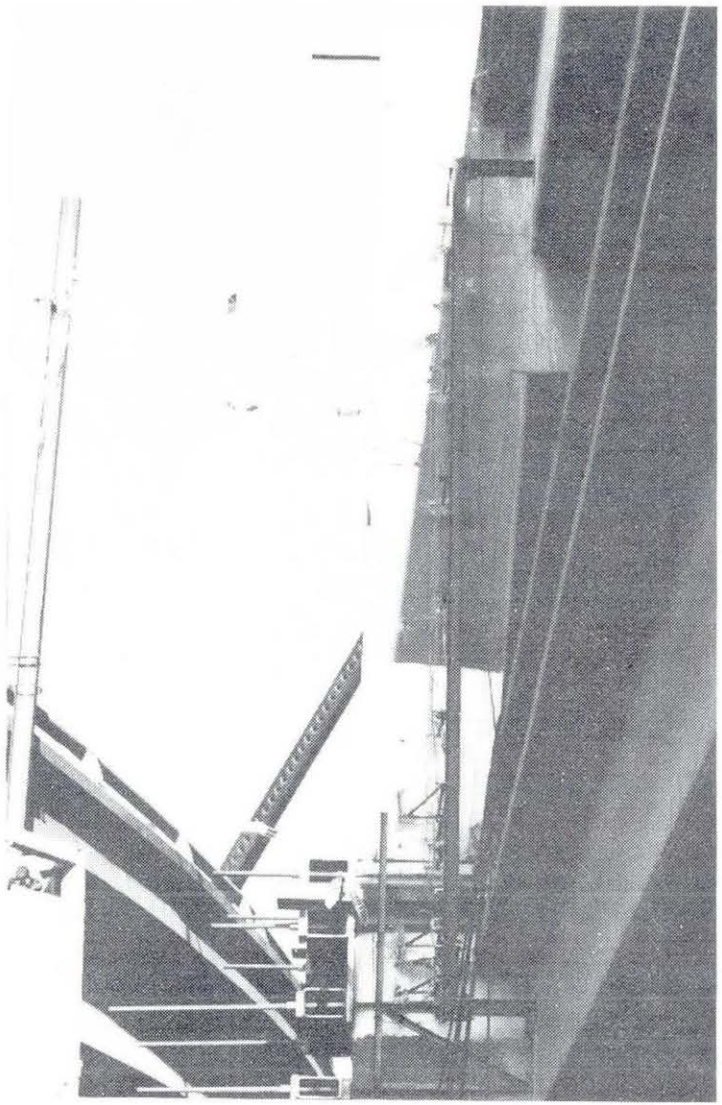

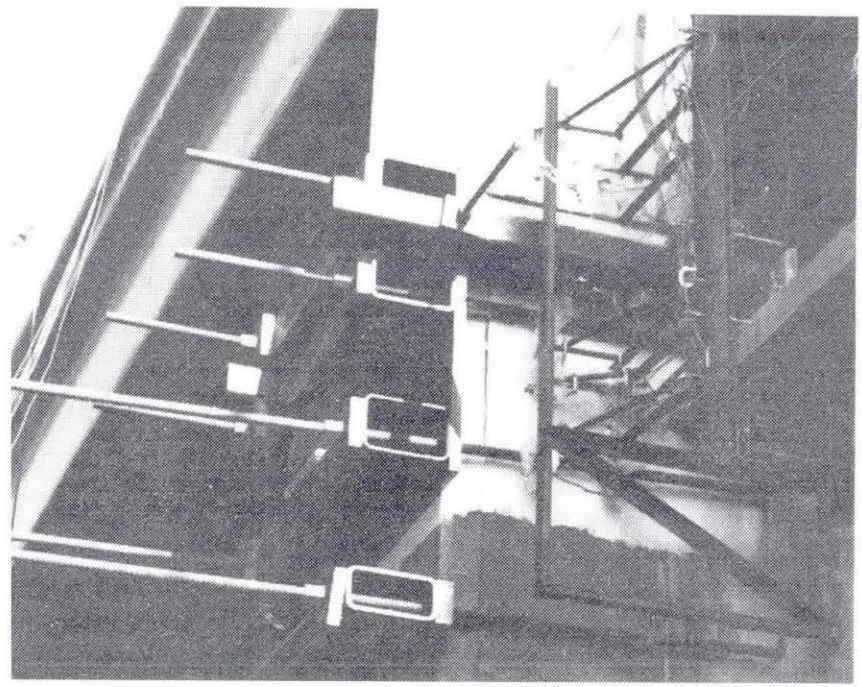

Fig. 2.30 Additional instrument locations on the west side of Bent 46.

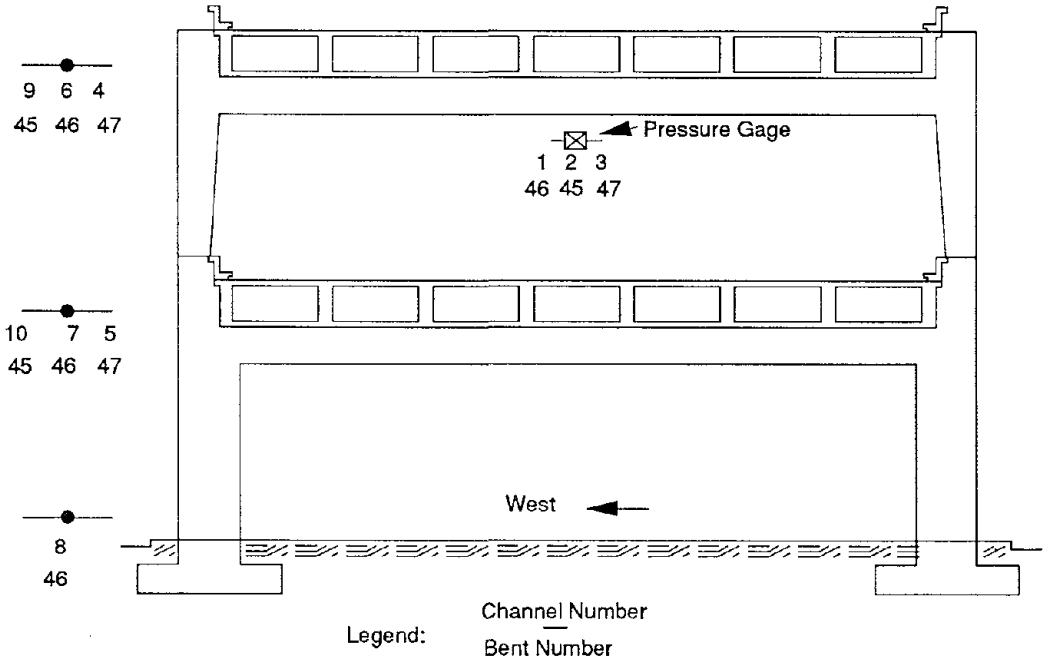

Fig. 2.31(a) Wire Pot Locations: All Bents

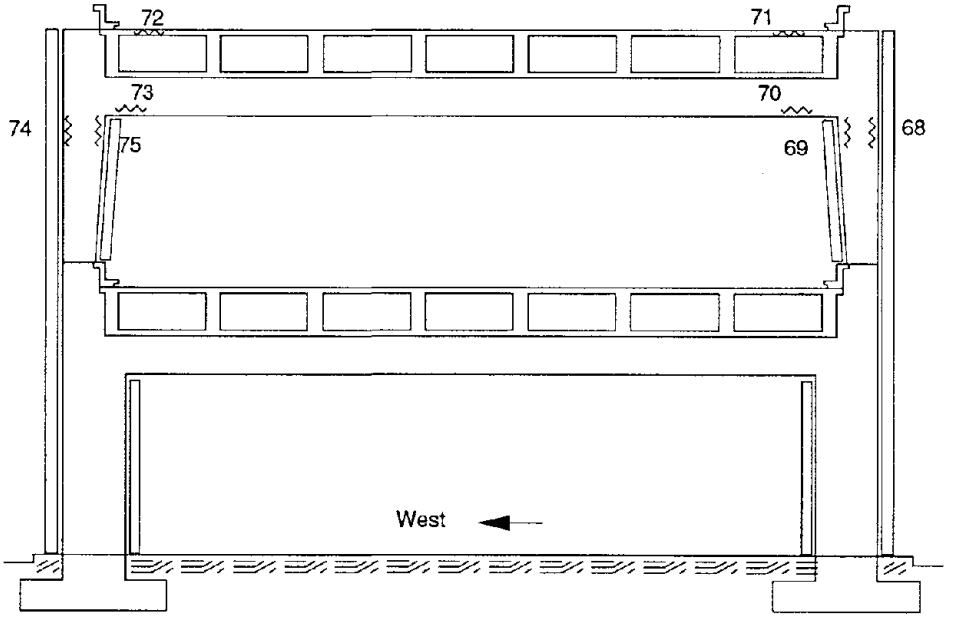

Fig. 2.31(b) Bent 45: Strain Gage Locations

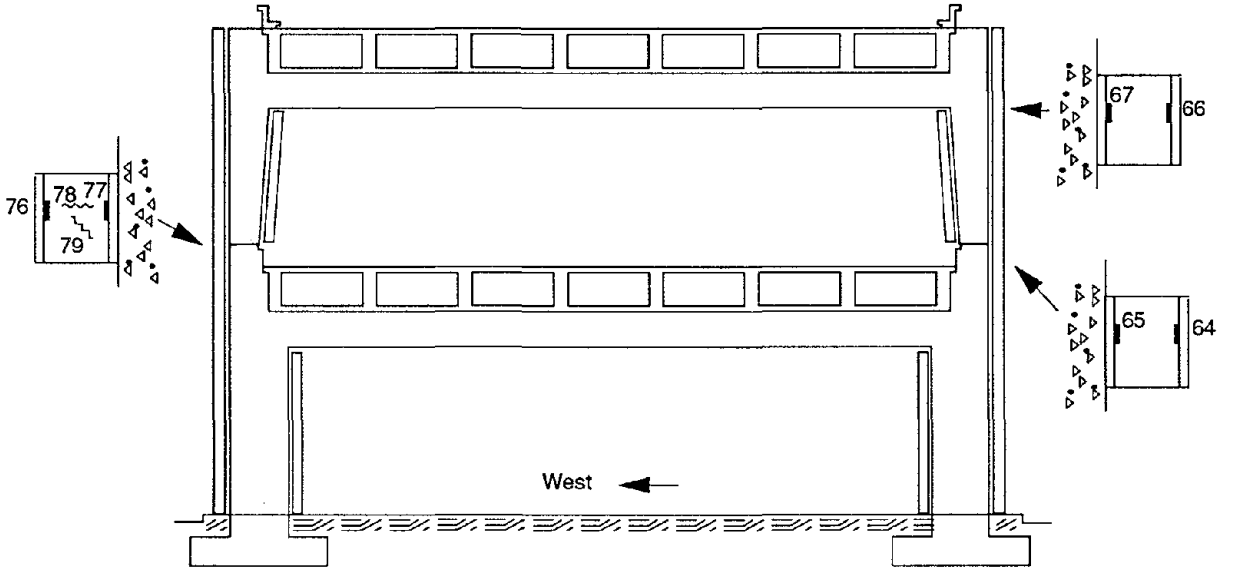

Fig. 2.31(c) Bent 45: WF Strain Gage Locations

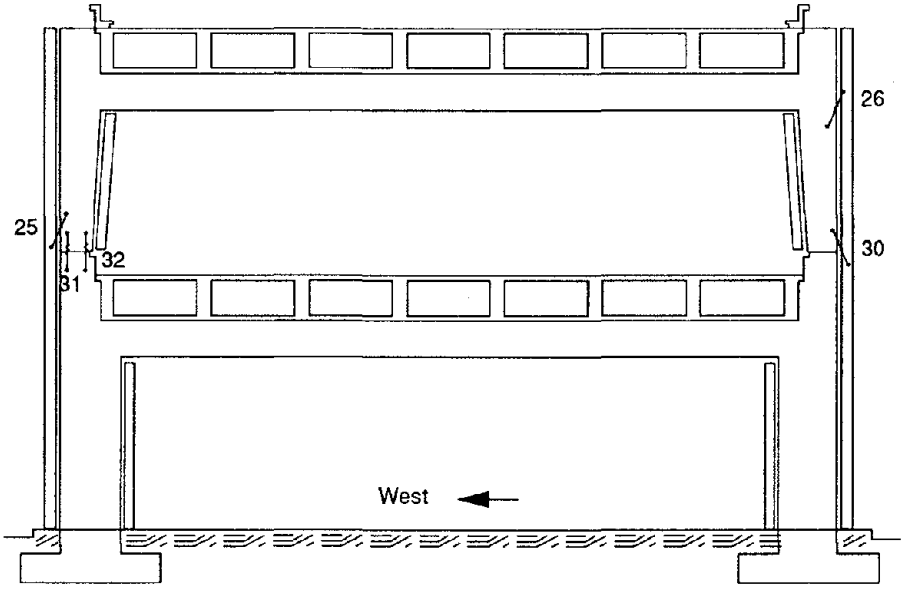

Fig. 2.31(d) Bent 45: Linear Pot Locations

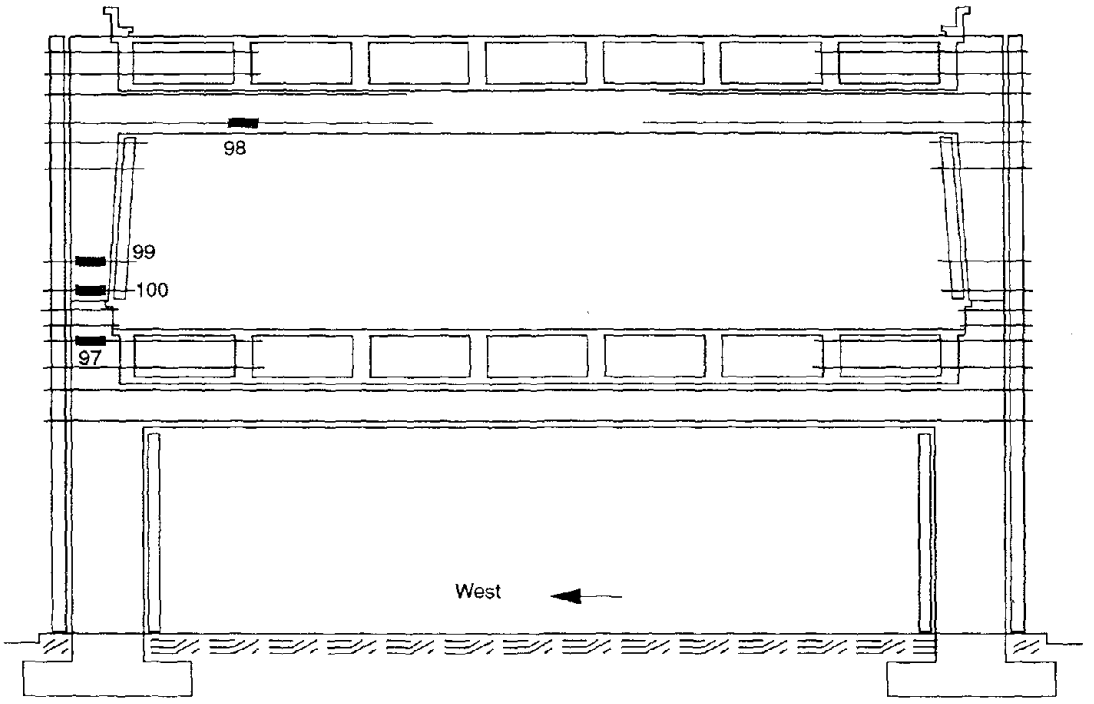

Fig. 2.31(e) Bent 45: Coupler Locations

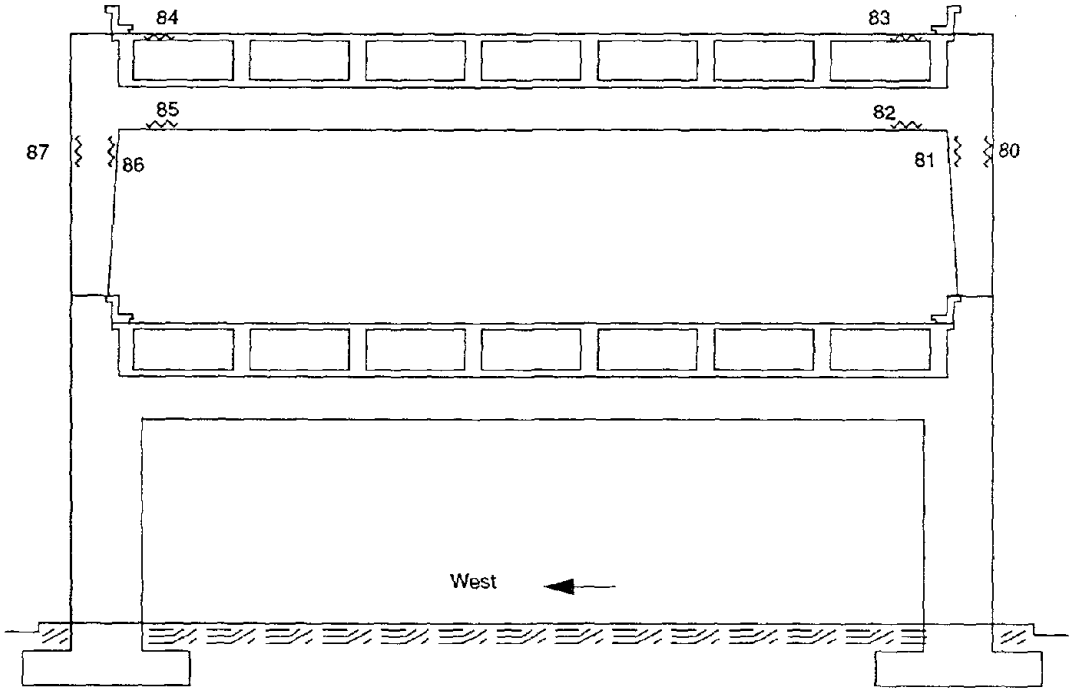

Fig. 2.31(f) Bent 46: Strain Gage Locations

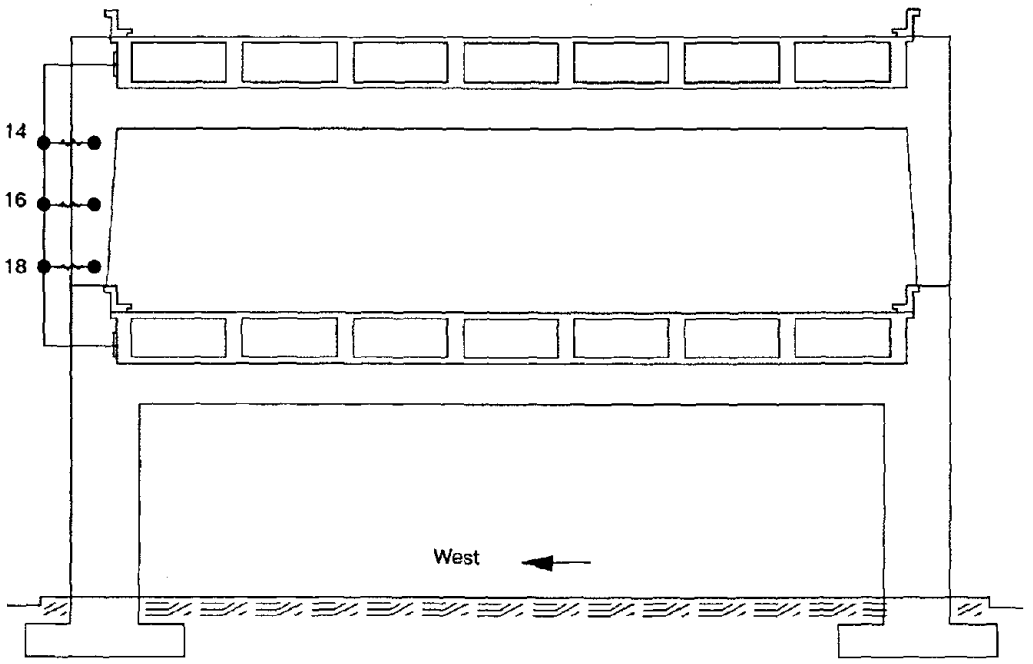

Fig. 2.31(g) Bent 46: Linear Pot Locations

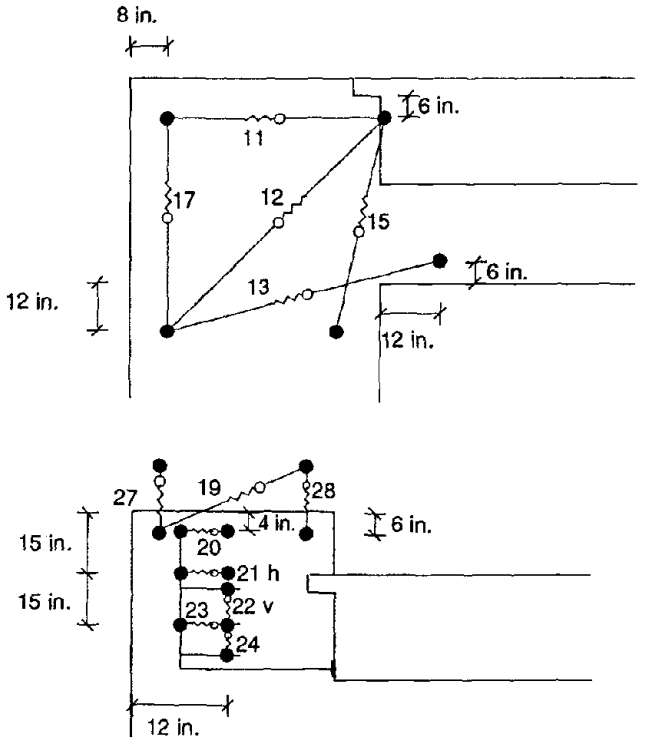

Fig. 2.31(h) Bent 46: West End Linear Pot Locations

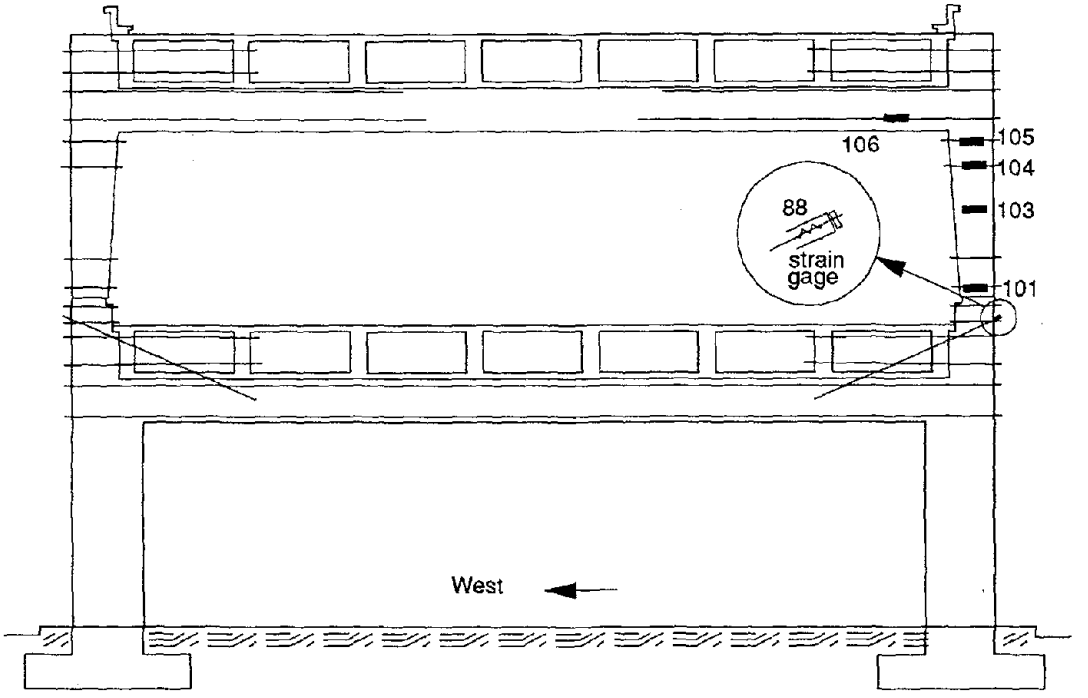

Fig. 2.31(i) Bent 46: East End Couplers

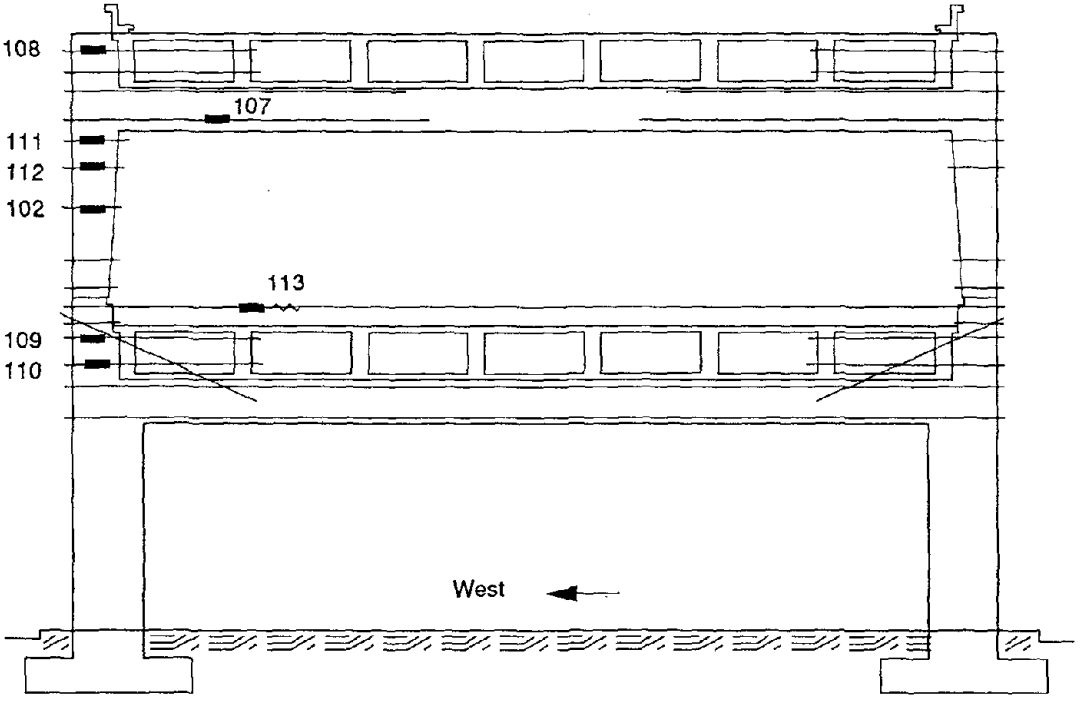

Fig. 2.31(j) Bent 46: West End Couplers

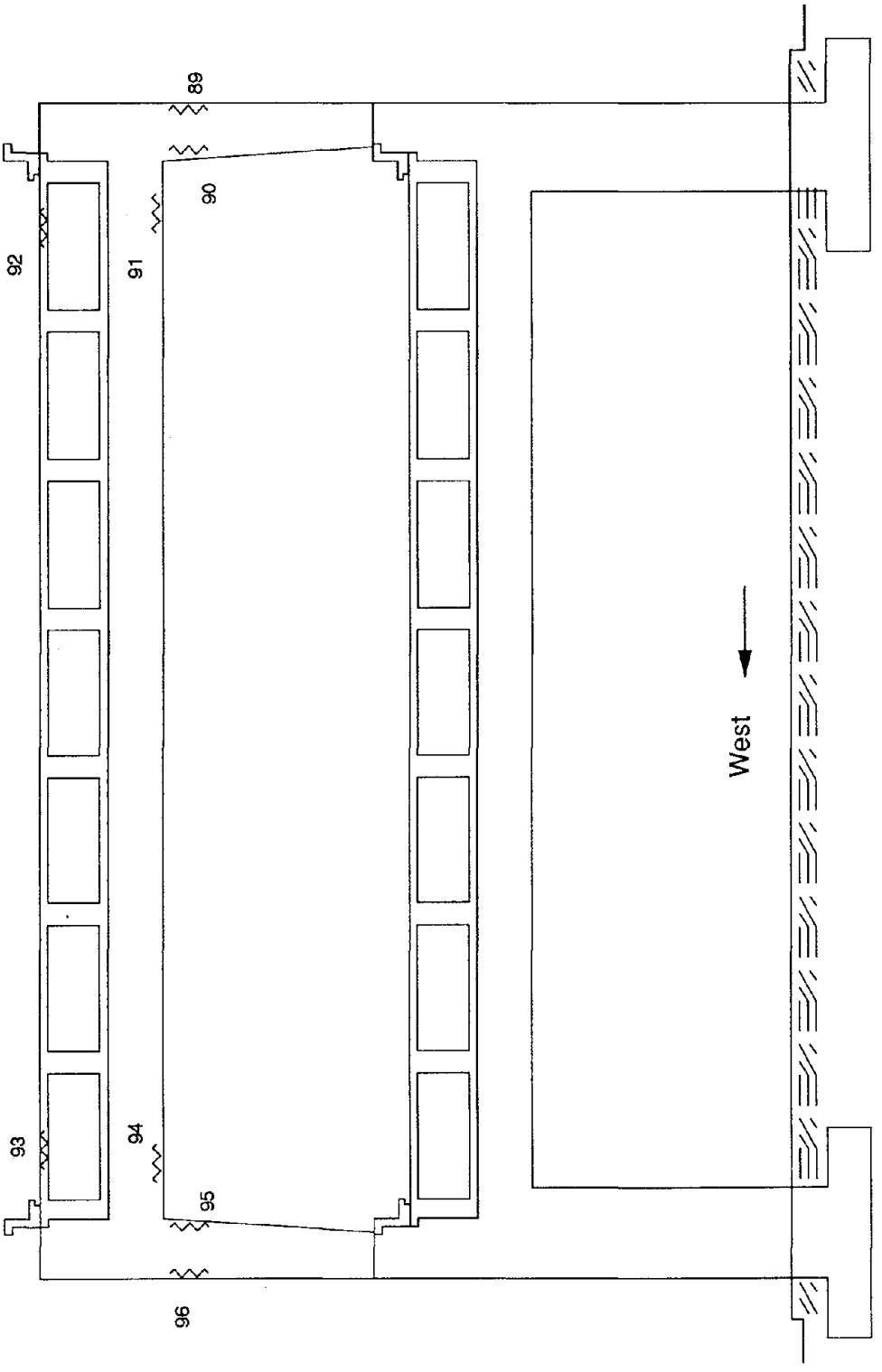

Fig. 2.31(k) Bent 47: Strain Gage Locations

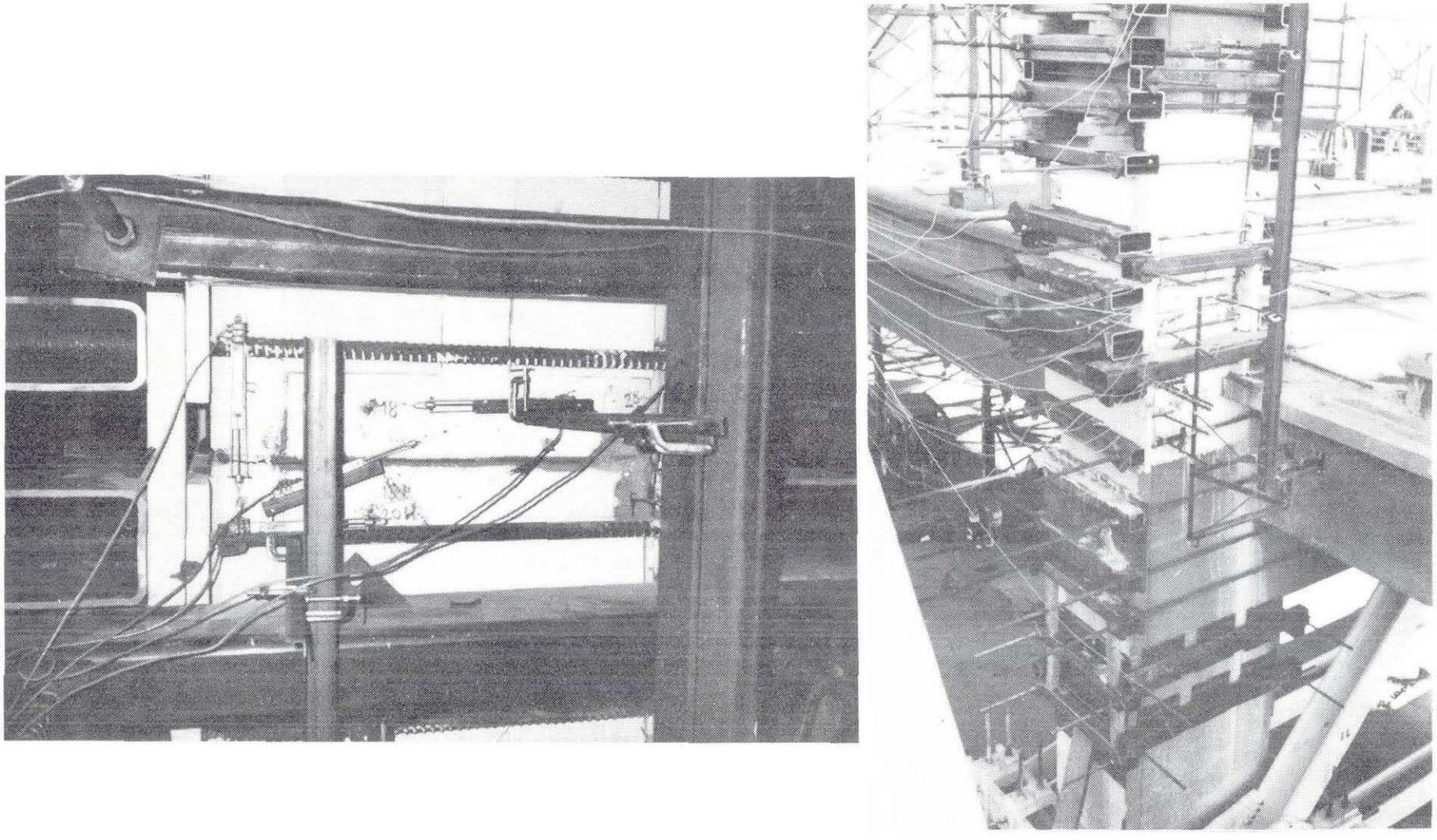

Fig. 2.32 Bent 46 lower joint and pedestal instrumentation.

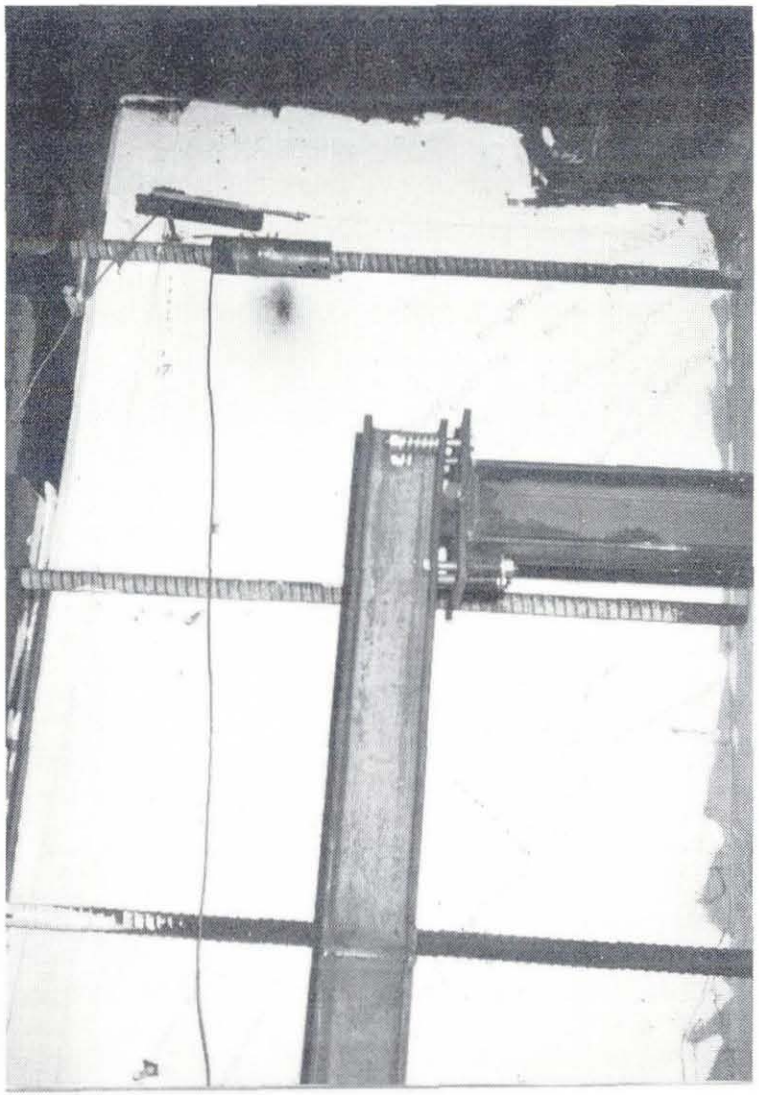

Fig. 2.33 Bent 46 top joint instrumentation.

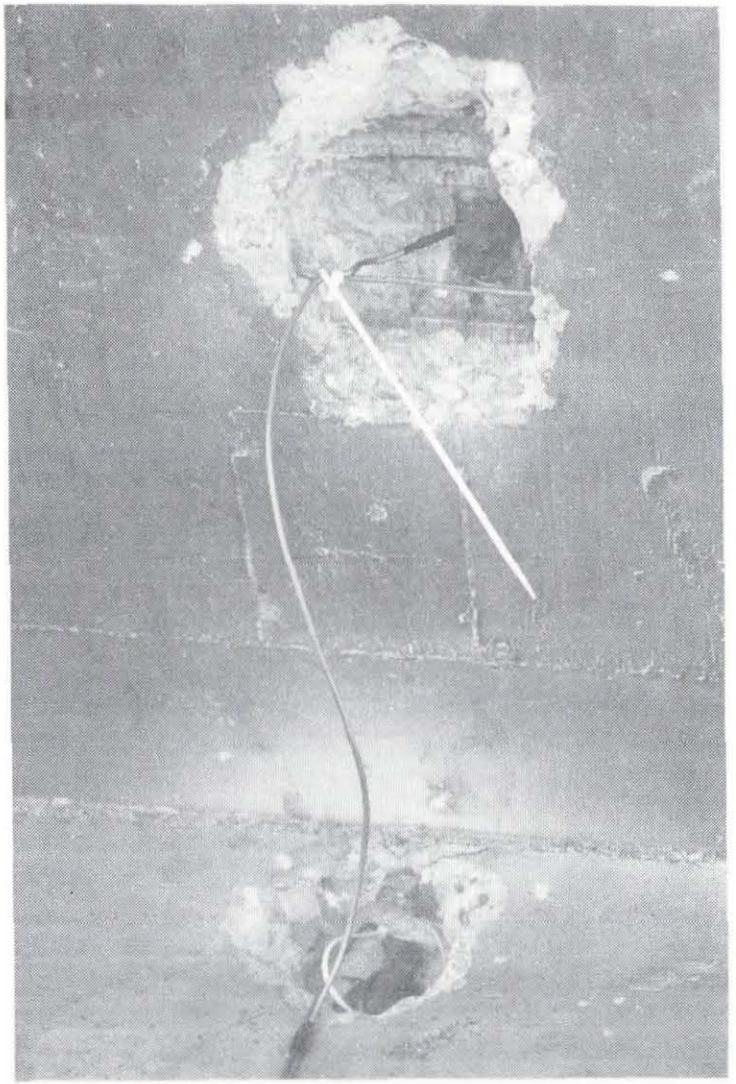

Fig. 2.34 Rebar strain gages.

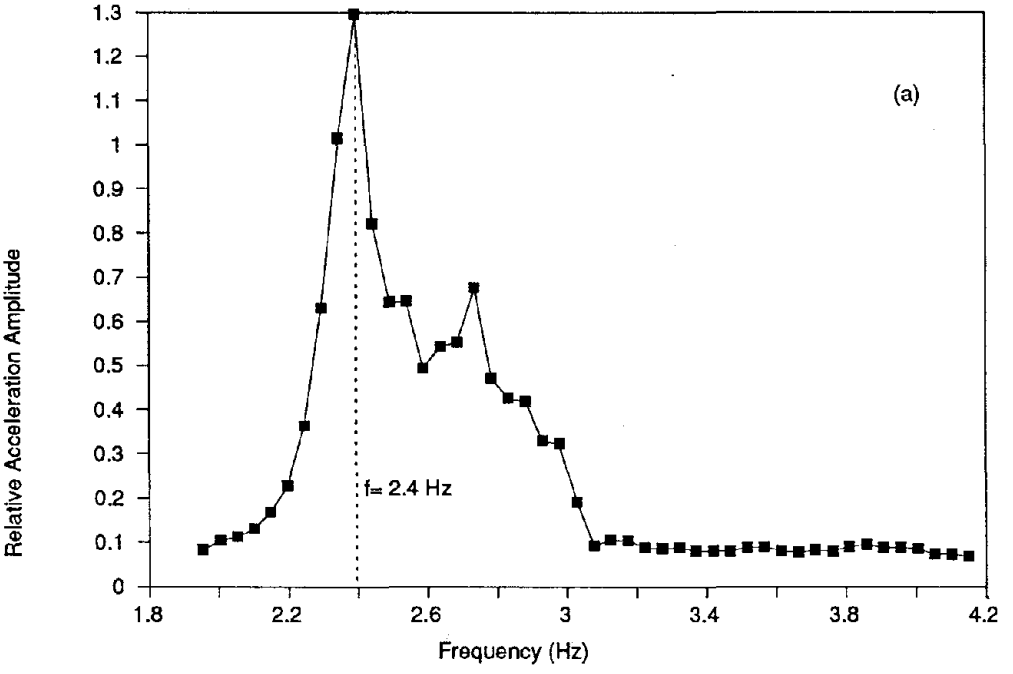

Upper Deck Dynamic Response Spectrum,

Frequency Sweep: First Mode

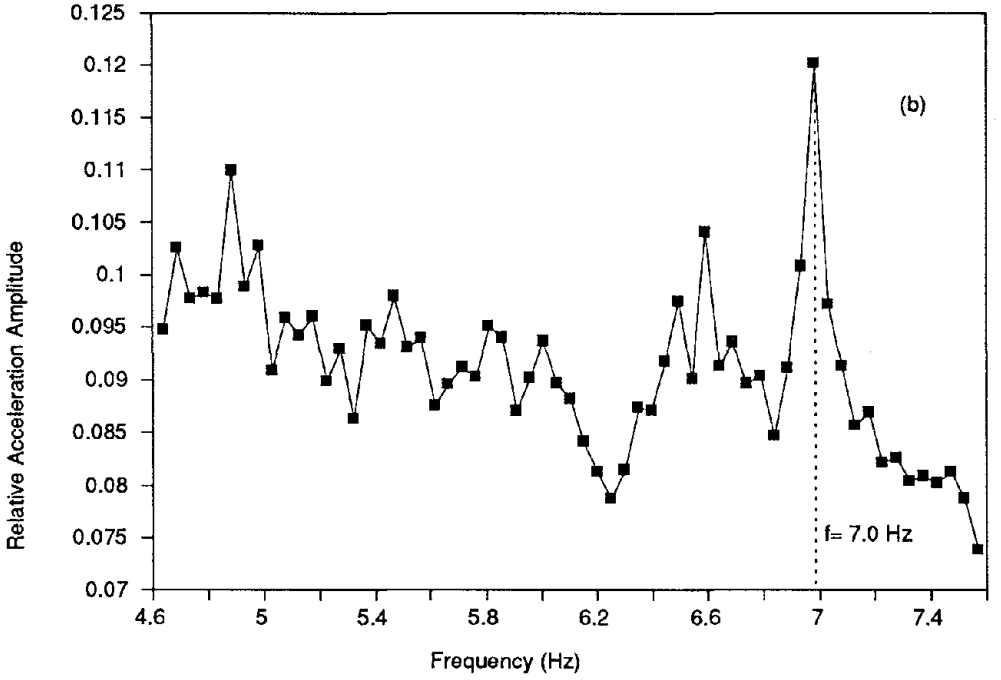

Upper Deck Dynamic Response Spectrum,

Frequency Sweep: Second Mode

Fig. 3.1 Forced Vibration Responses Measured From Original Structure

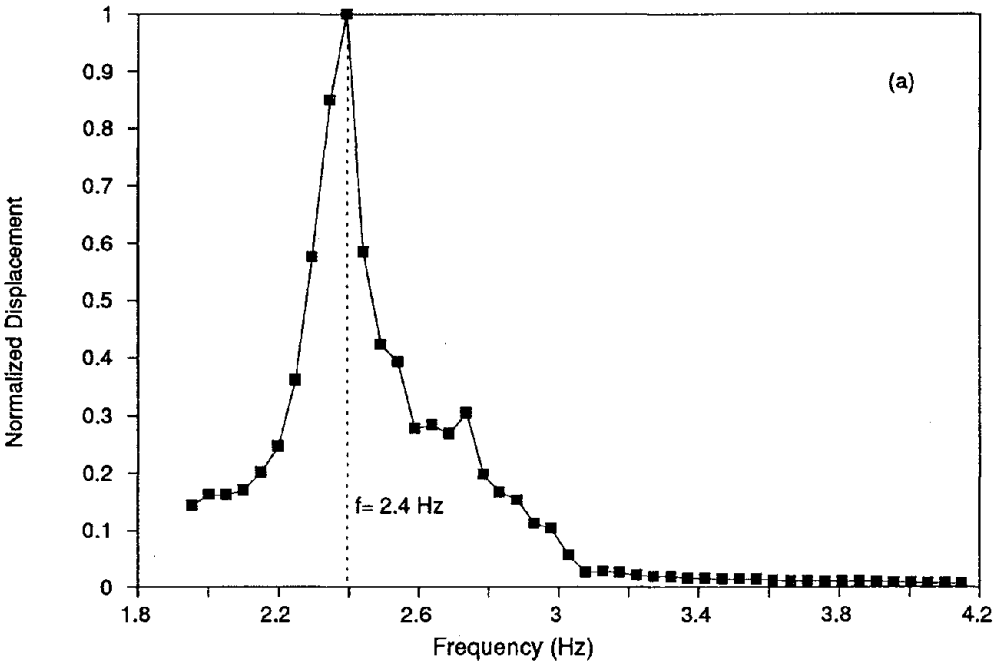

Normalized Dynamic Response Spectrum

Frequency Sweep: First Mode

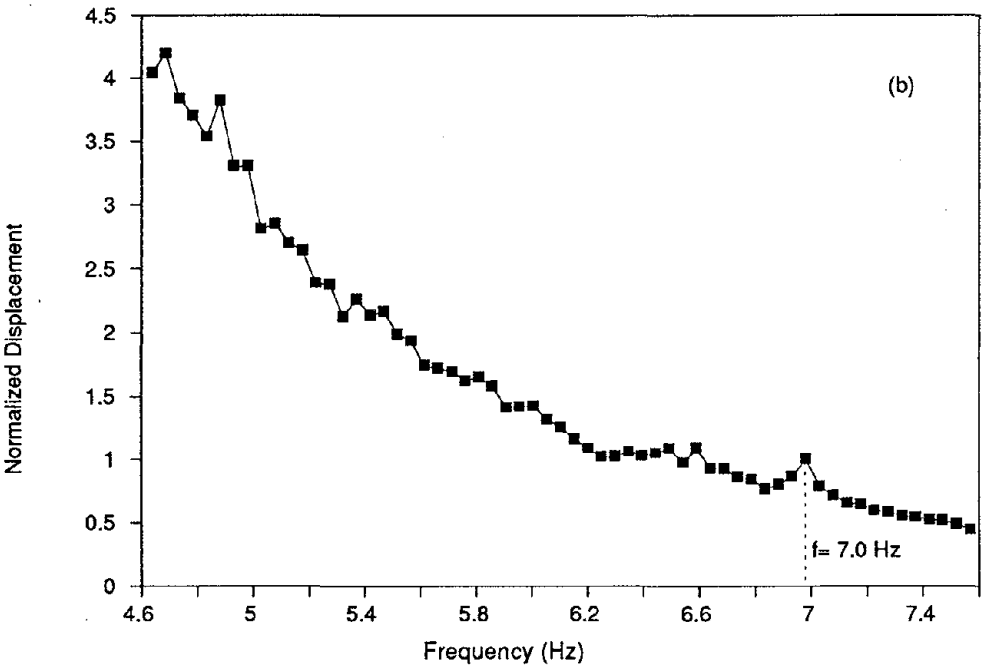

Normalized Dynamic Response Spectrum

Frequency Sweep: Second Mode

Fig. 3.2 Normalized Displacements Derived from Forced Vibration of Original Structure

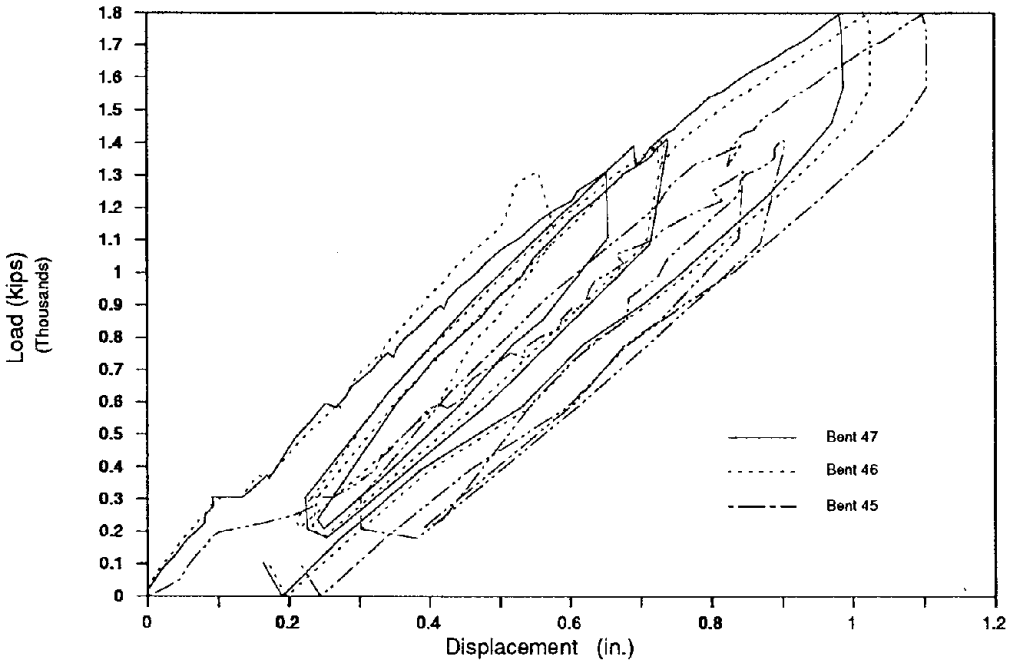

(a) Upper Deck

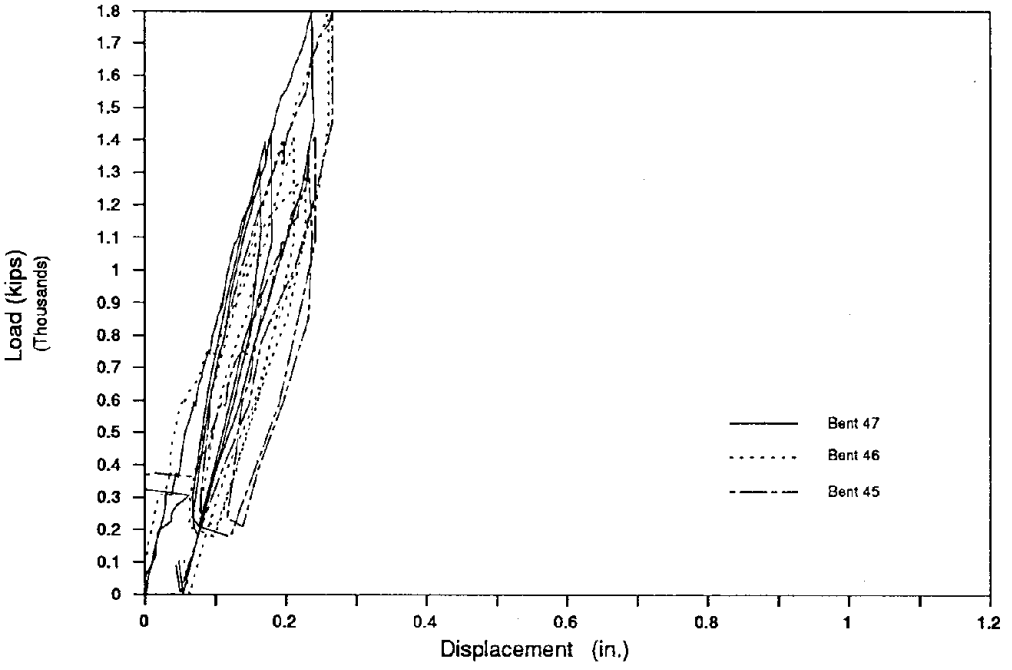

(b) Lower Deck

Fig. 3.3 Load-Displacement Relationships for Original Structure

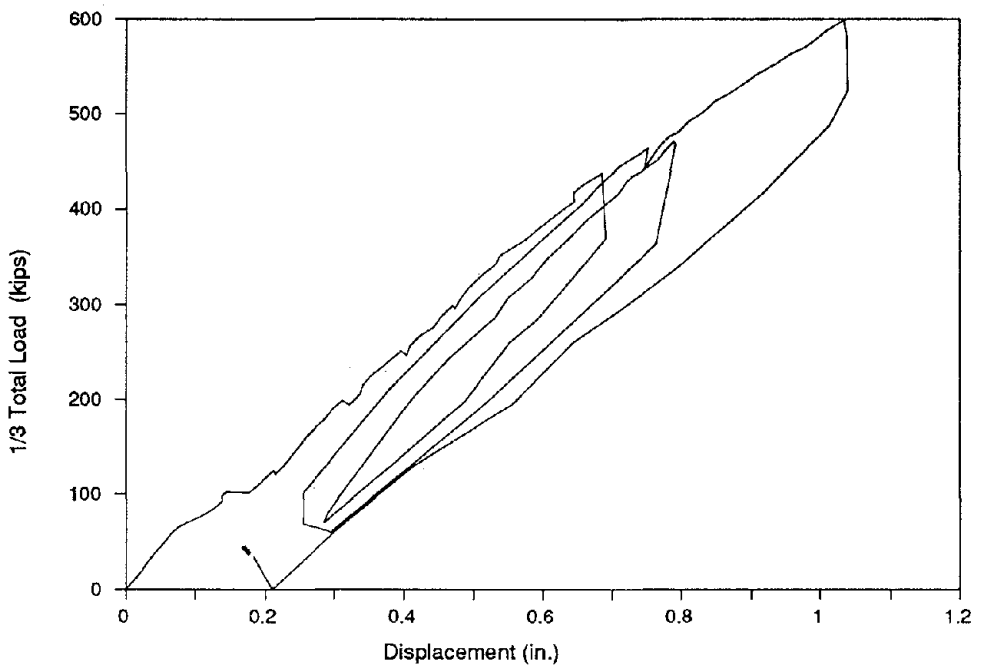

(a) Load vs. Average Bent-top Displacement

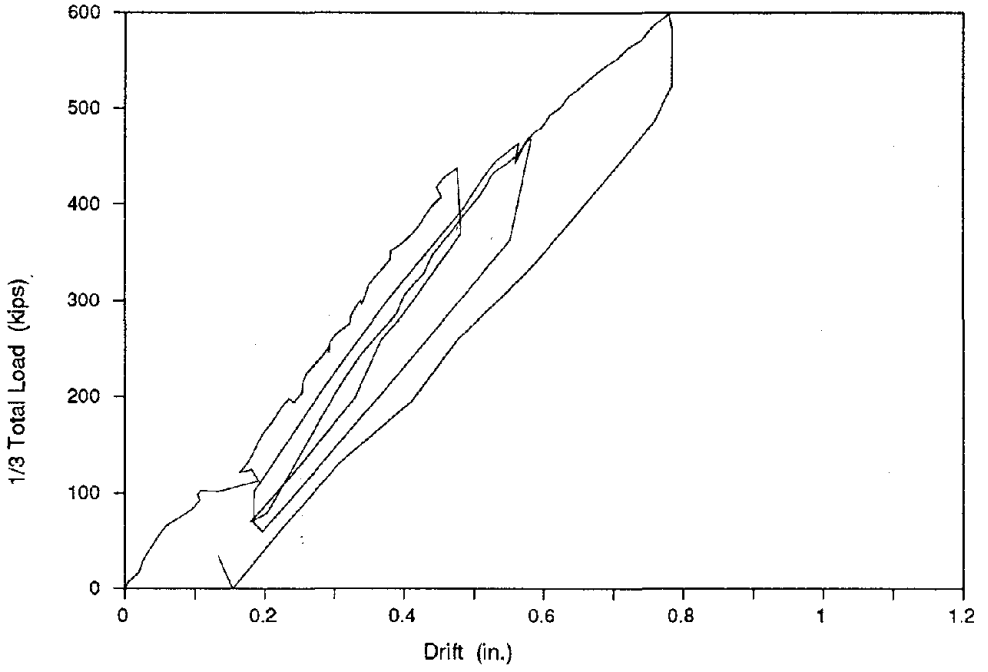

(b) Load vs. Average Upper Level Drift

Fig. 3.4 Load-Displacement Relationships for Original Structure

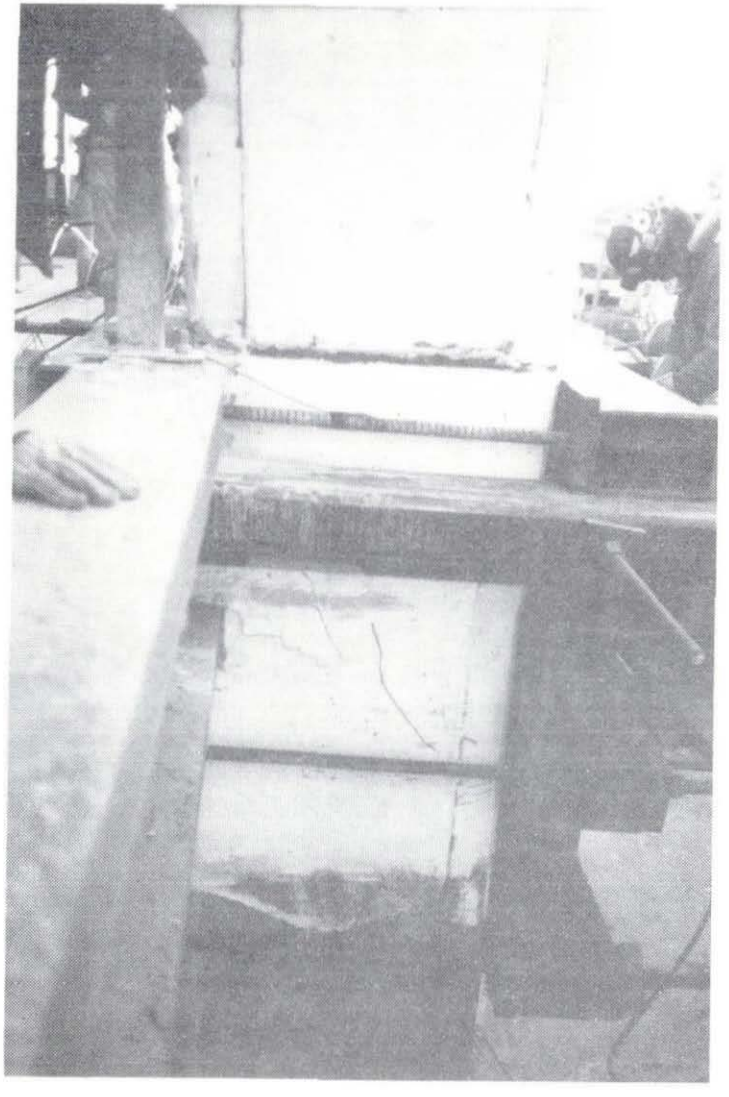

Fig. 3.5 Damage to the lower joint on the west end of Bent 46 during the third load cycle of the static load test on the original structure.

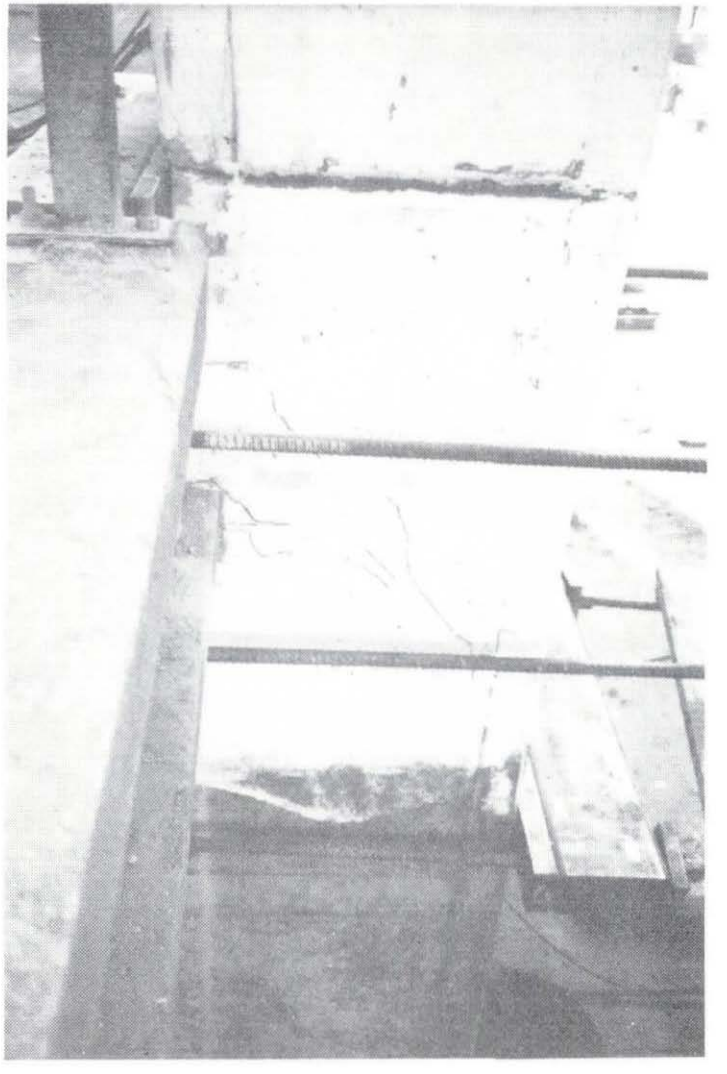

Fig. 3.6 Damage to the west end of Bent 46 after completion of the original structure static load test. The joint retrofit has been removed.

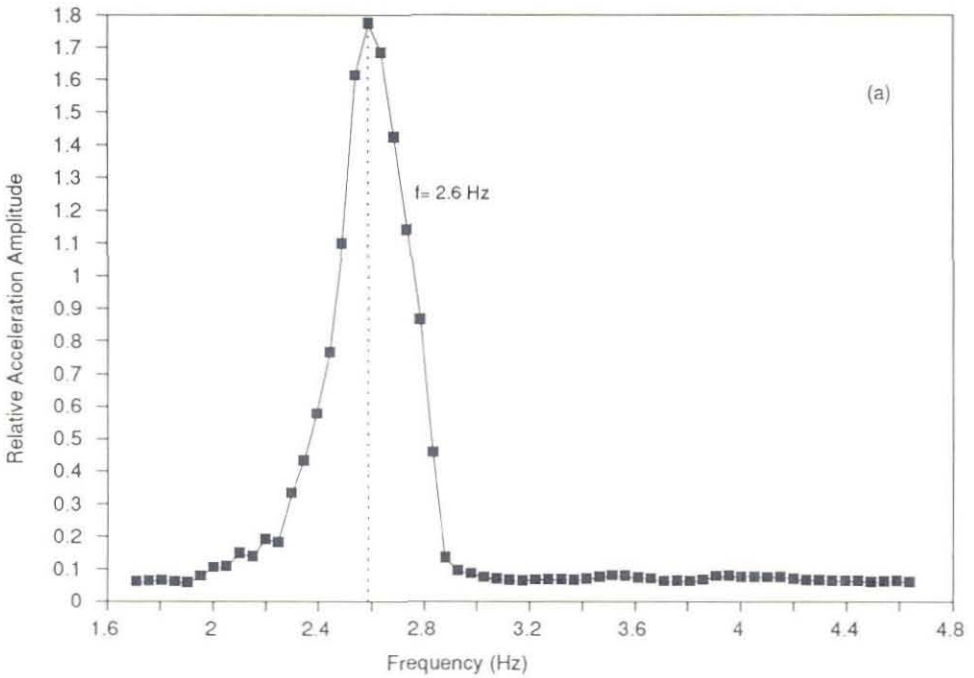

Upper Deck Dynamic Response Spectrum,
First Mode Frequency Sweep

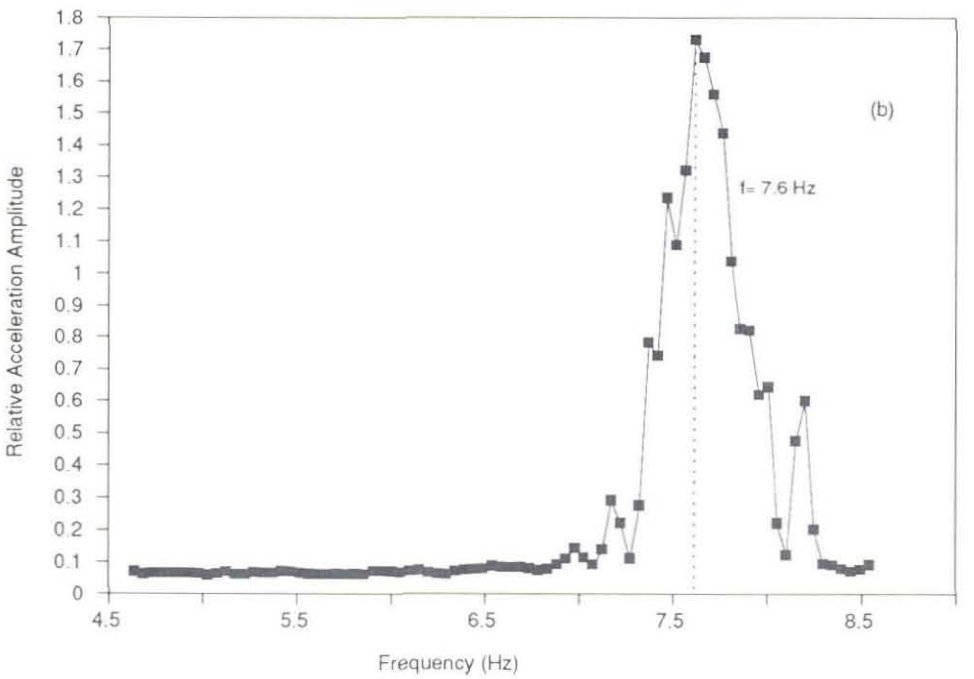

Upper Deck Dynamic Response Spectrum,
Second Mode Frequency Sweep

Fig. 3.7 Forced Vibration Responses Measured from Retrofitted Structure

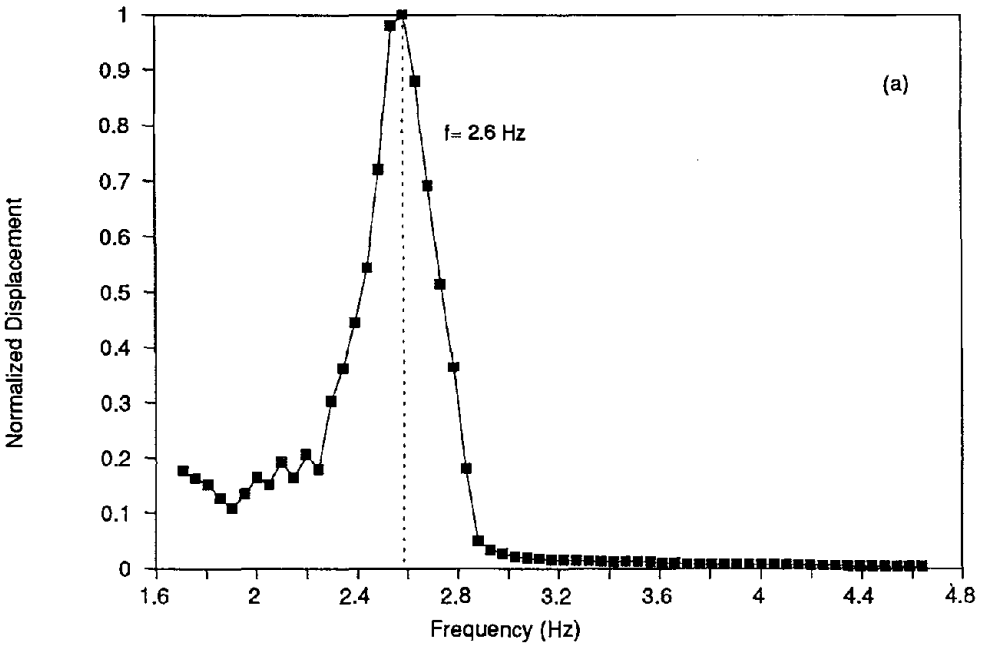

Normalized Dynamic Response Spectrum
First Mode Frequency Sweep

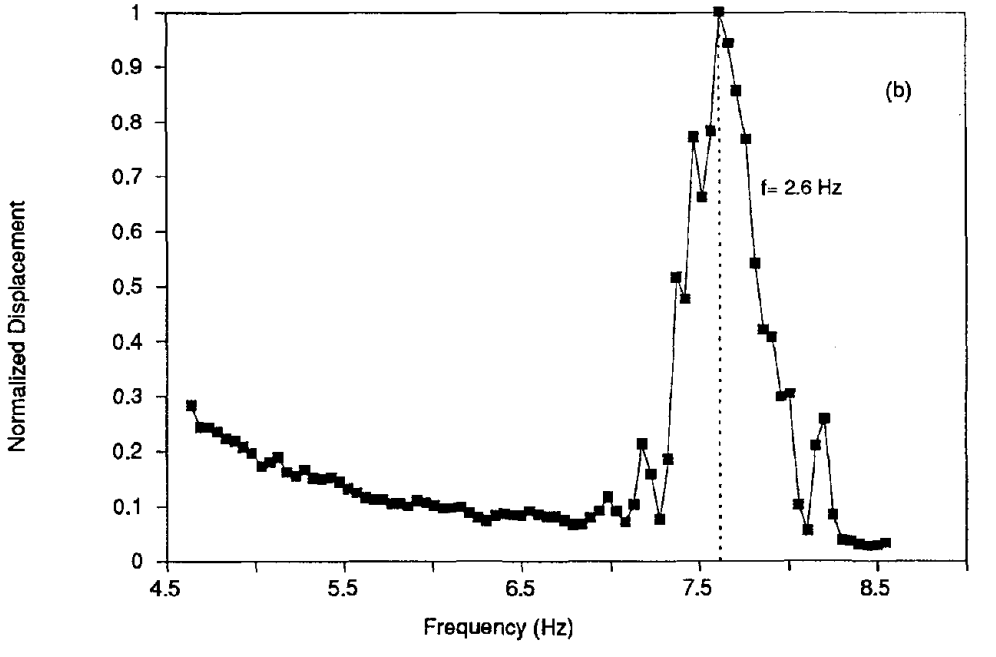

Normalized Dynamic Response Spectrum
Second Mode Frequency Mode

Fig. 3.8 Normalized Displacements Derived from Forced Vibration Tests of Retrofitted Structure

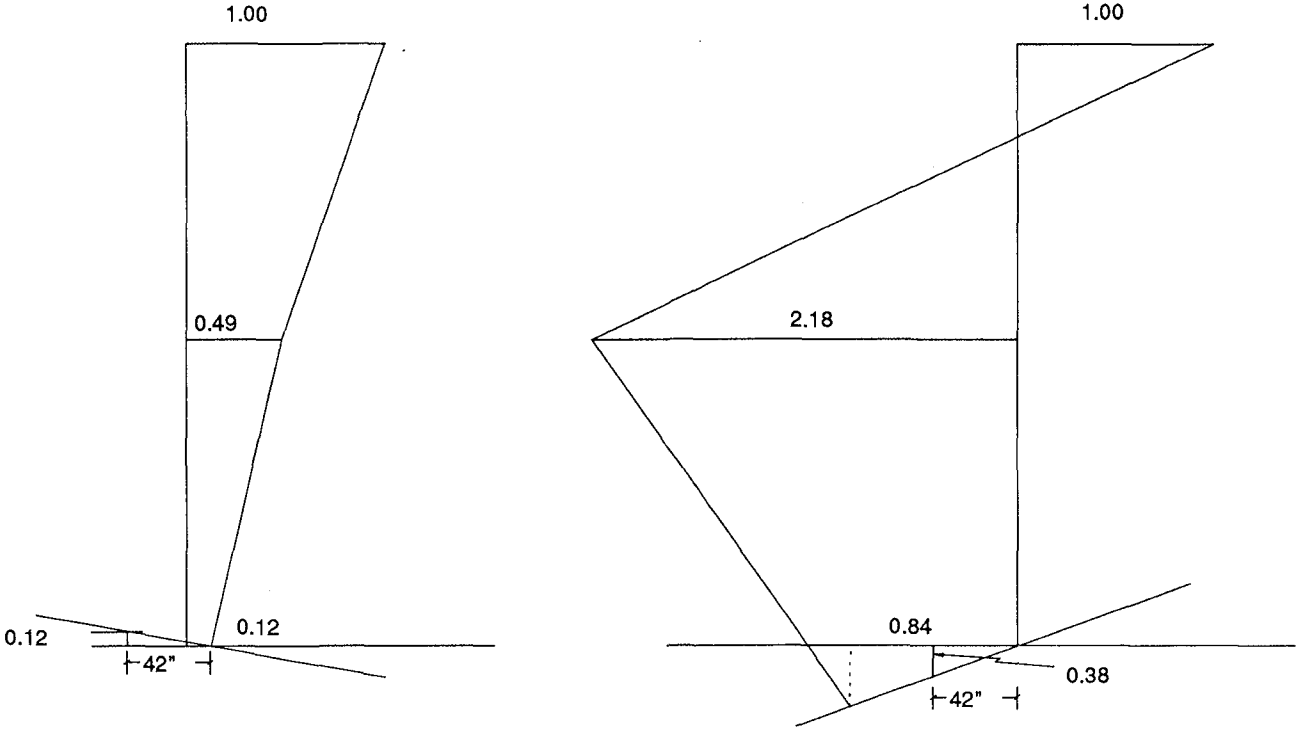

Fig. 3.9 Measured Mode Shapes of Retrofitted Structure

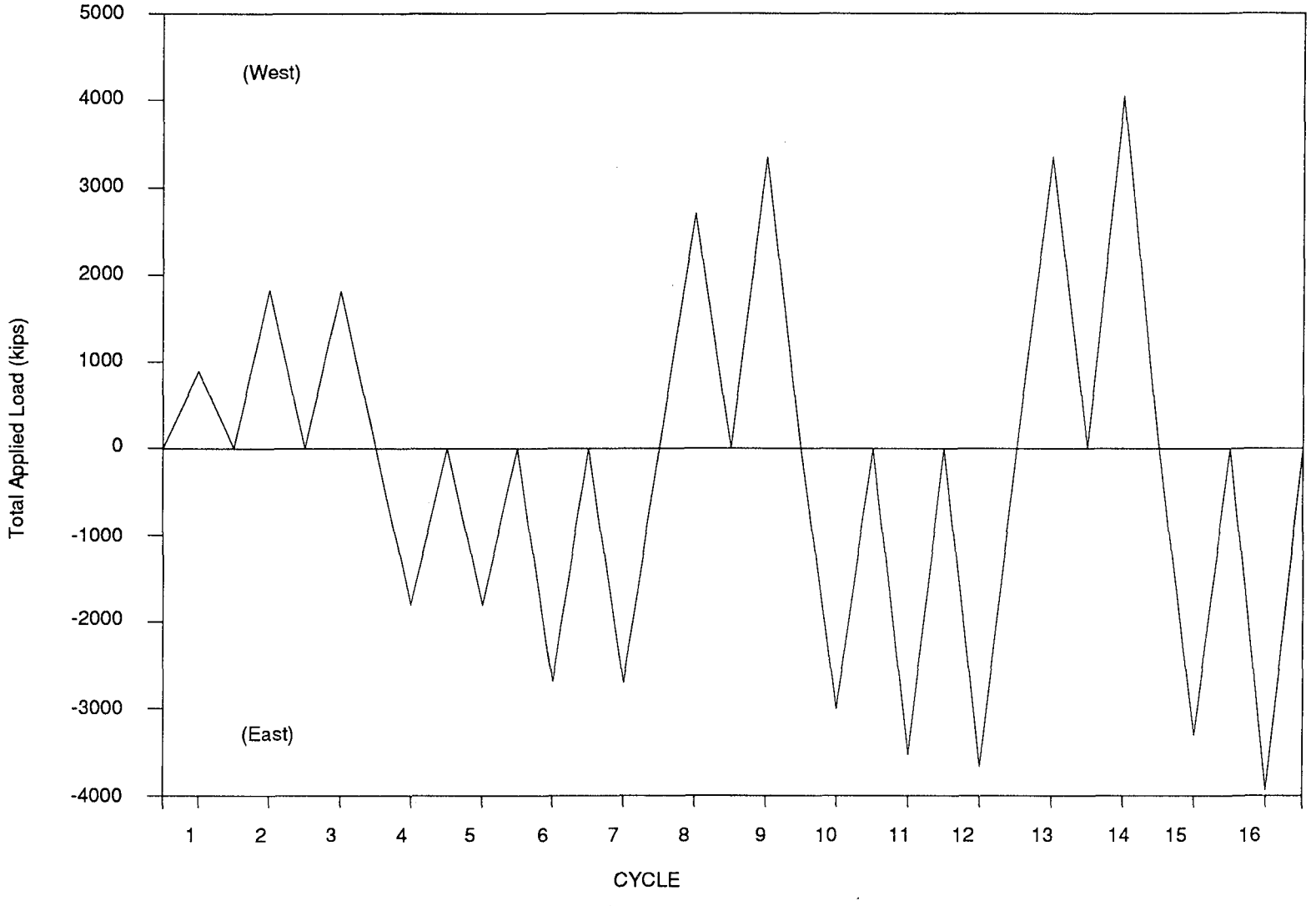

Fig. 3.10 Loading Pattern : Retrofitted Structure

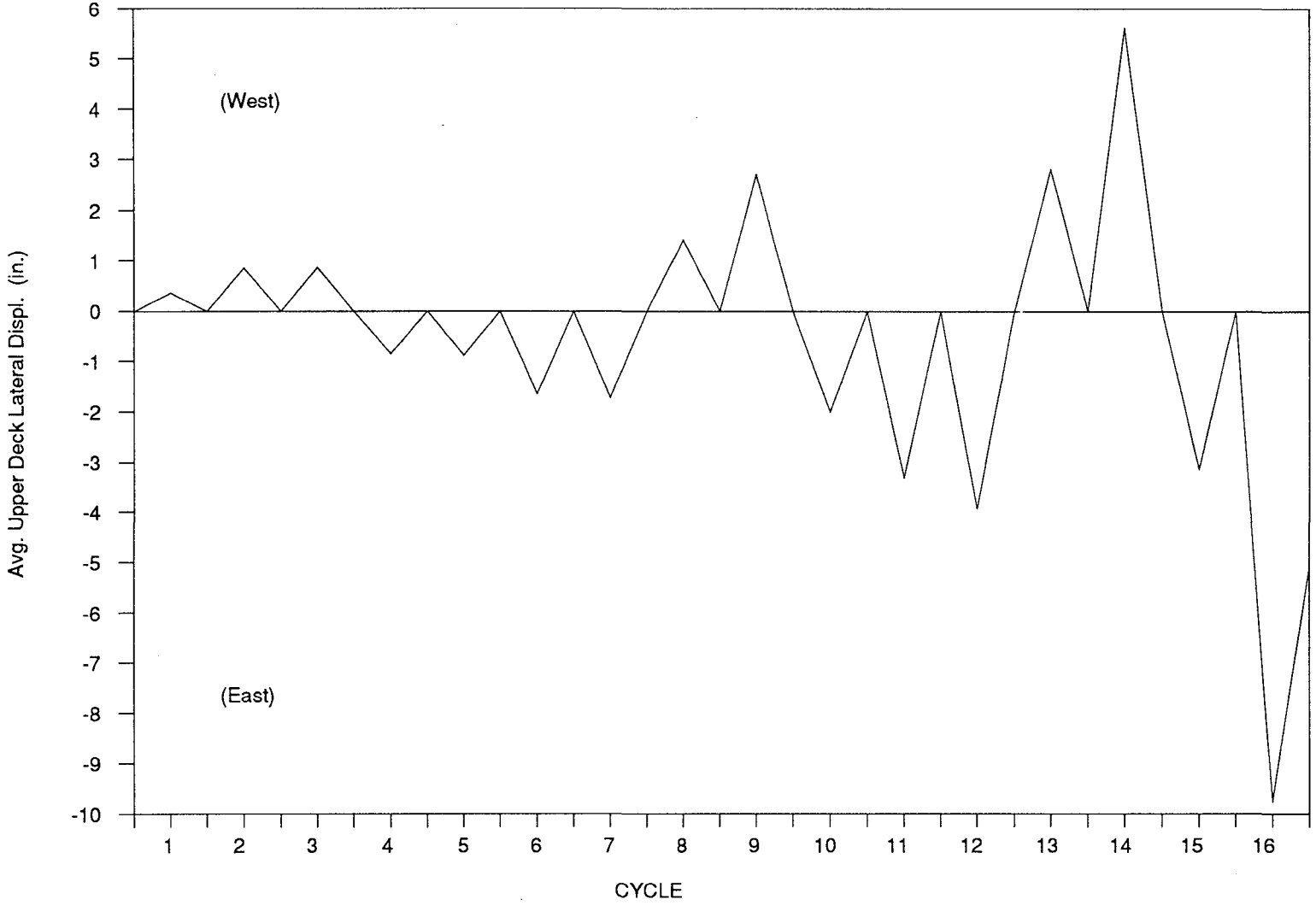

Fig. 3.11 Displacement History of Retrofitted Structure

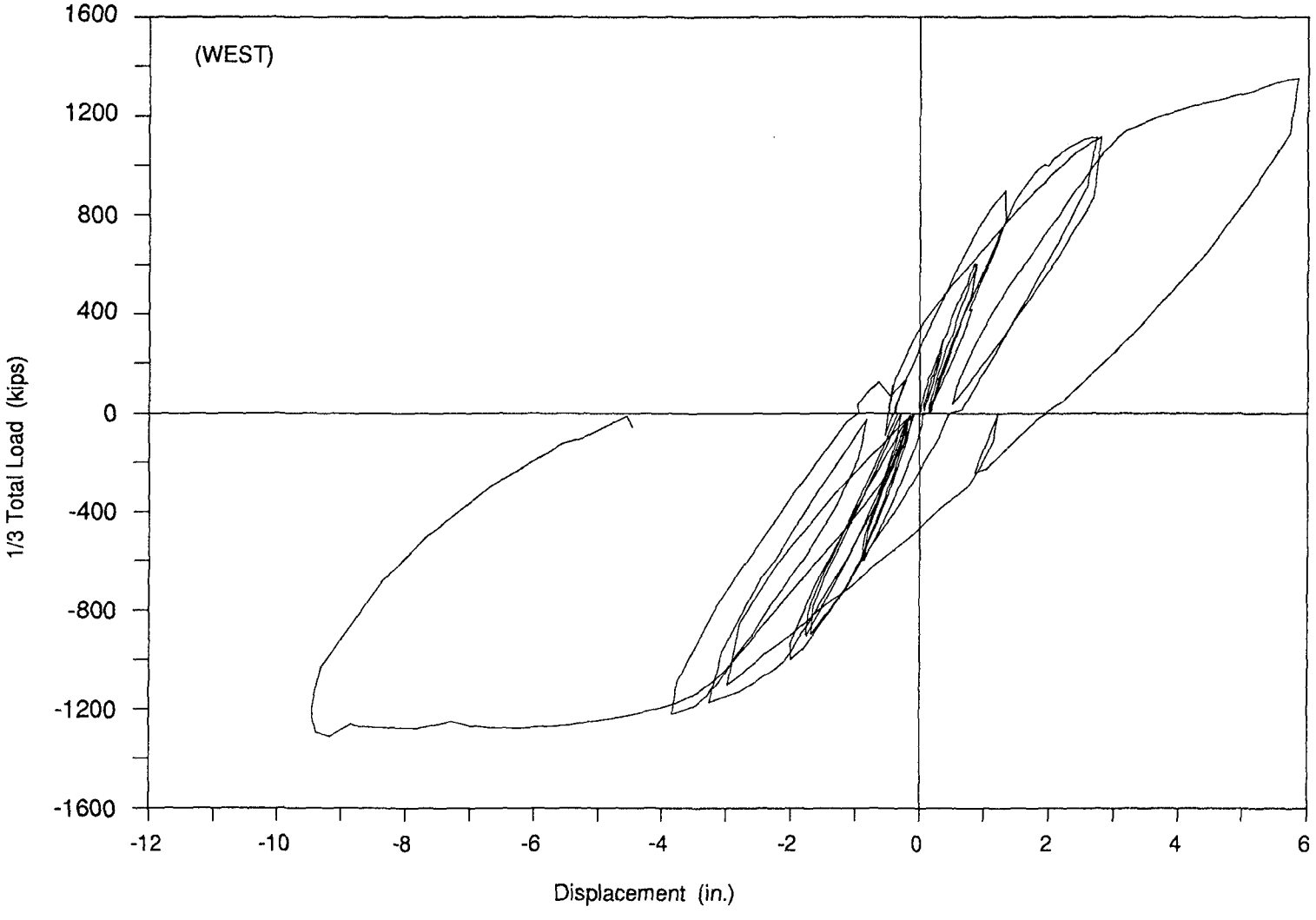

Fig. 3.12 Bent 45, Retrofitted Structure Top Level Load-Displacement Relationship

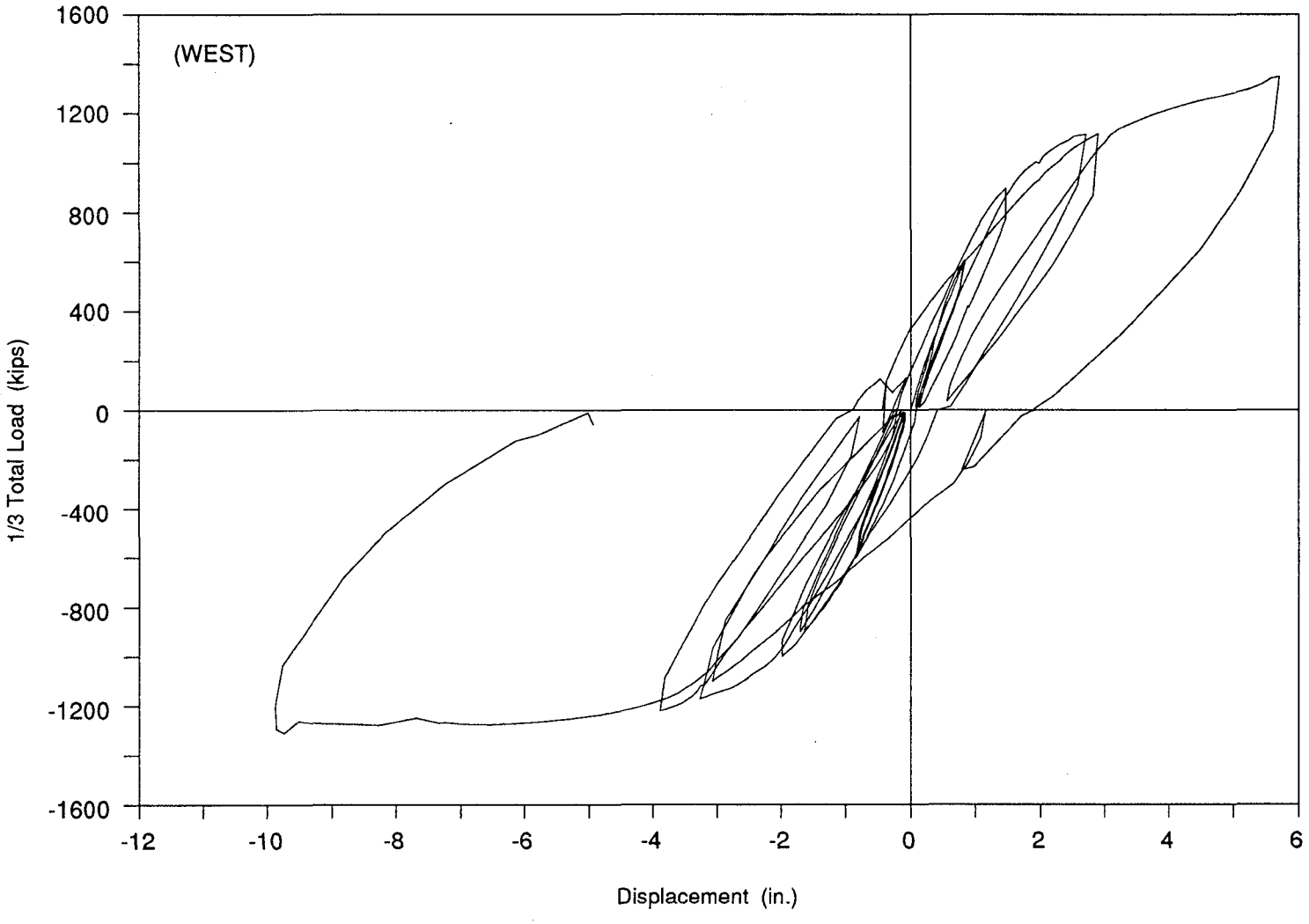

Fig. 3.13 Bent 46, Retrofitted Structure Top Level Load-Displacement Relationship

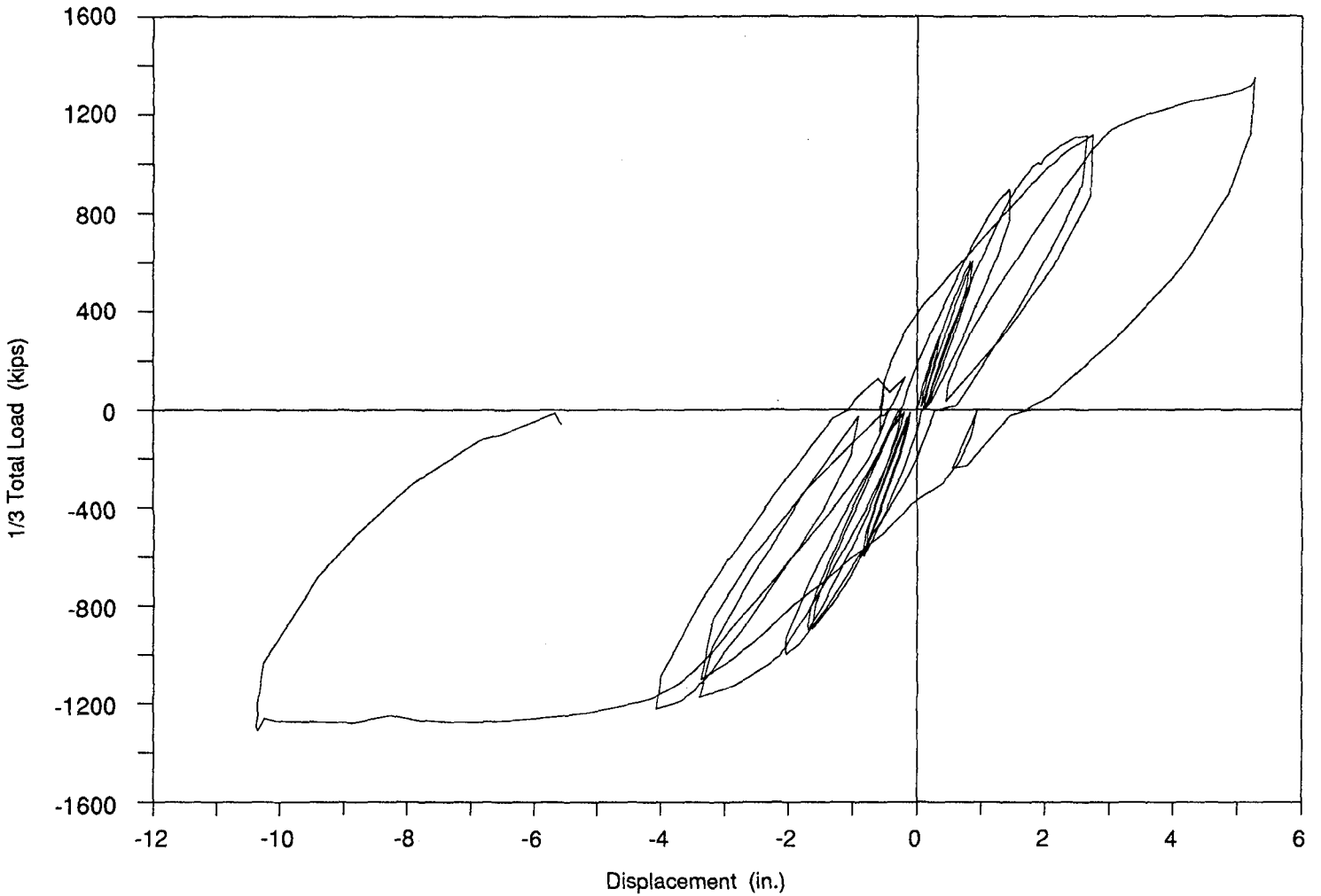

Fig. 3.14 Bent 47, Retrofitted Structure Top Level Load-Displacement Relationship

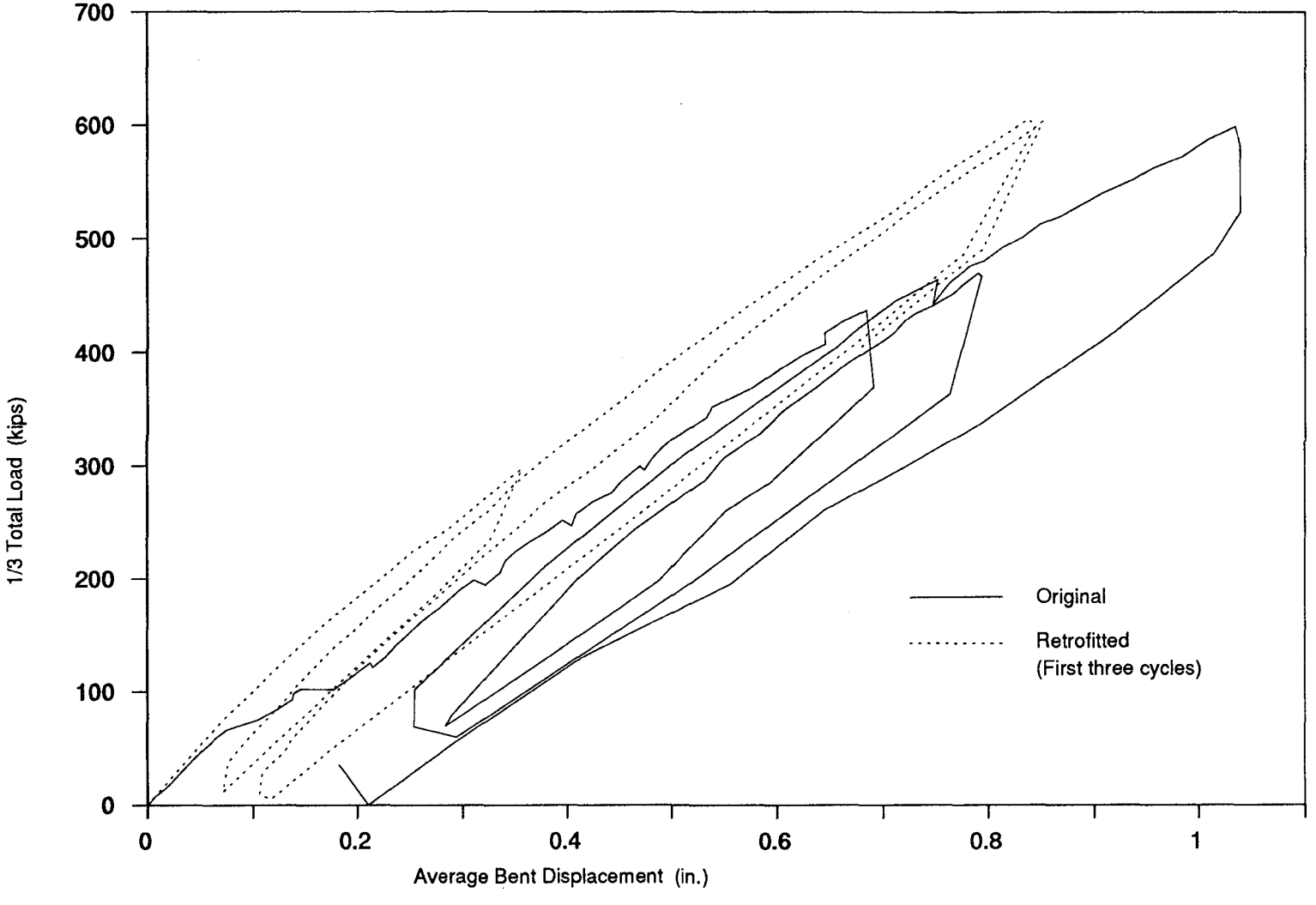

Fig. 3.15 Comparison of Initial Load-Displacement Relationships for Original and Retrofitted Structures

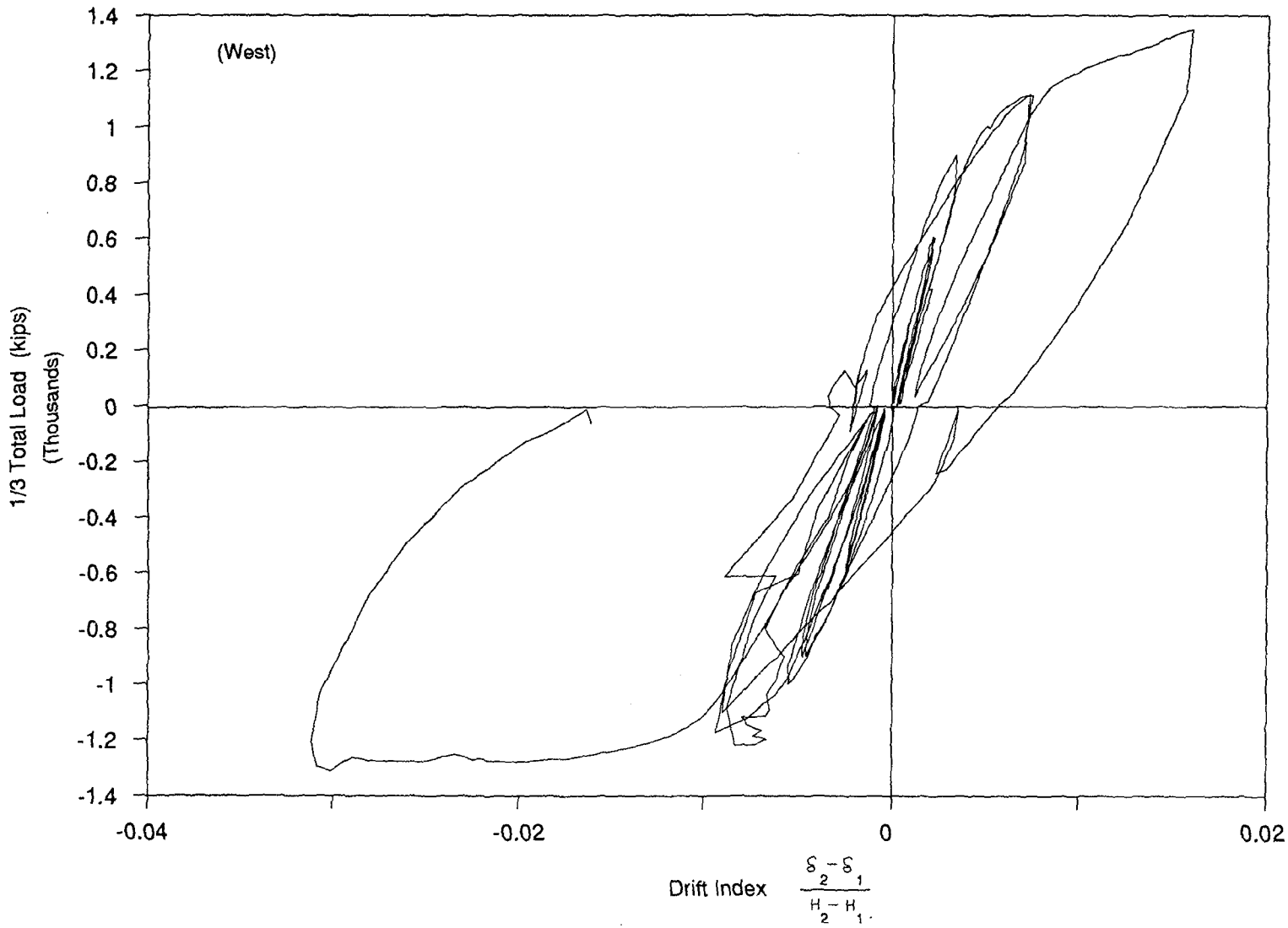

Fig. 3.16 Bent 45 Upper Level Load-Drift Relationship

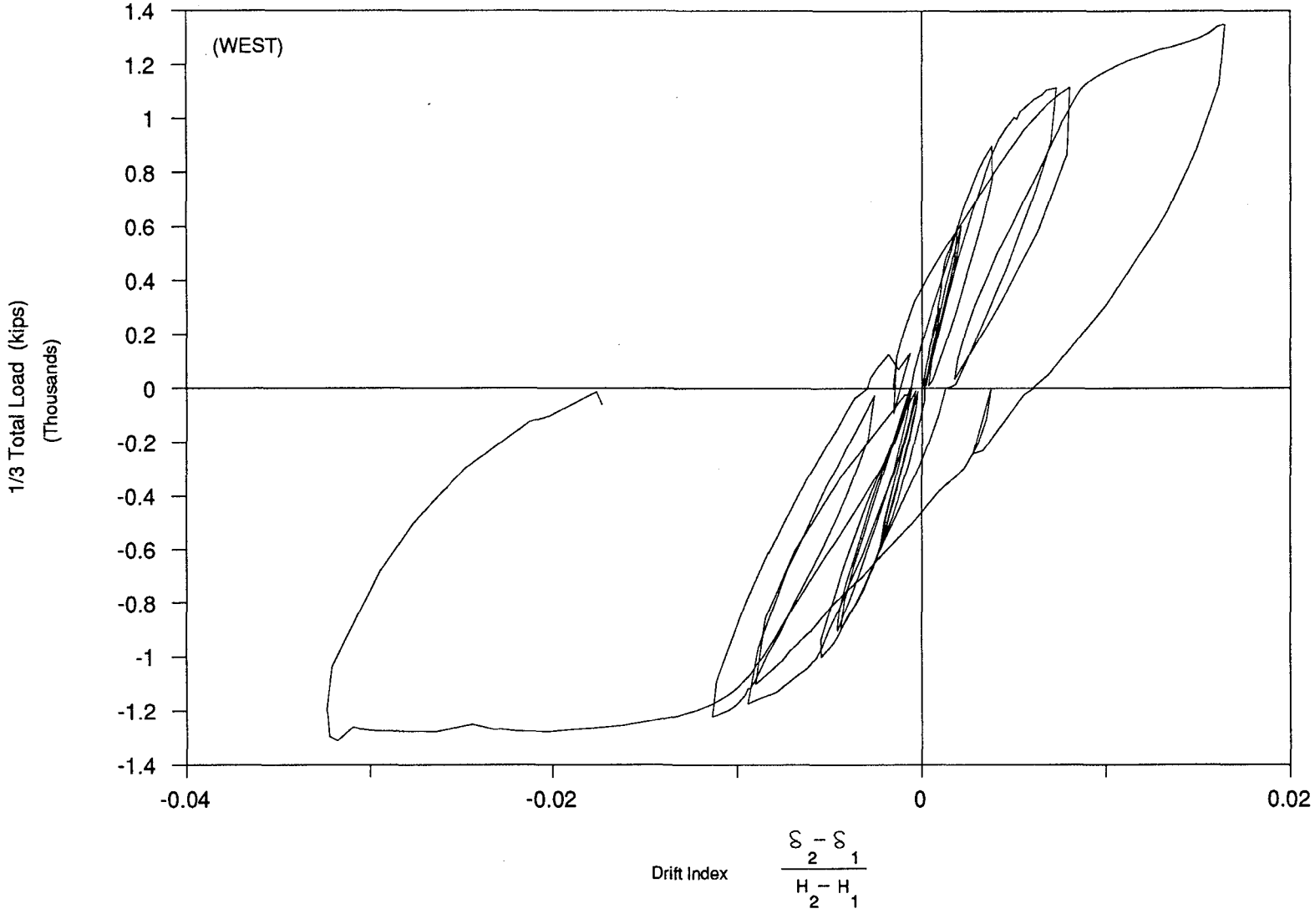

Fig. 3.17 Bent 46 Upper Level Load-Drift Relationship

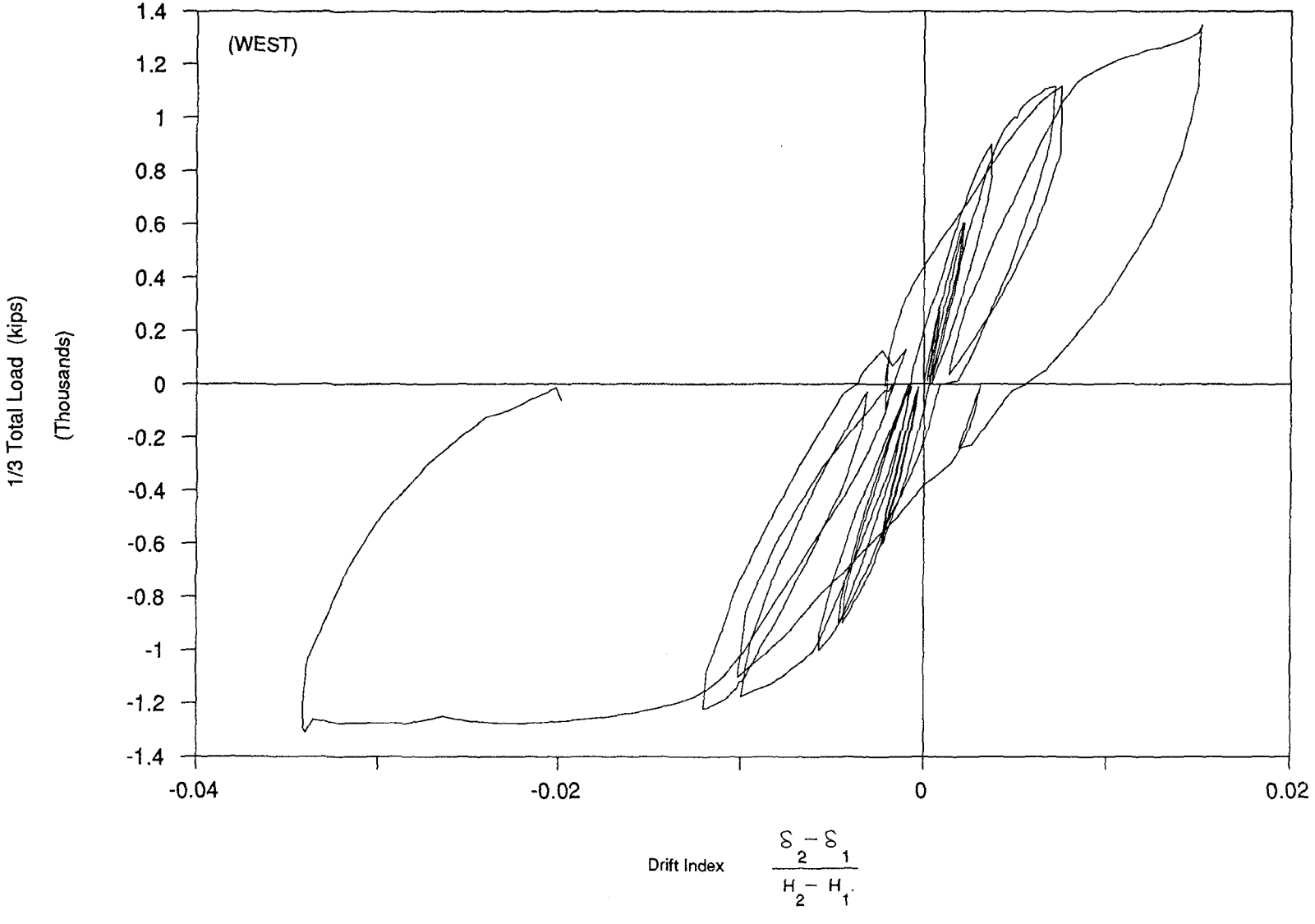

Fig. 3.18 Bent 47 Upper Level Load-Drift Relationship

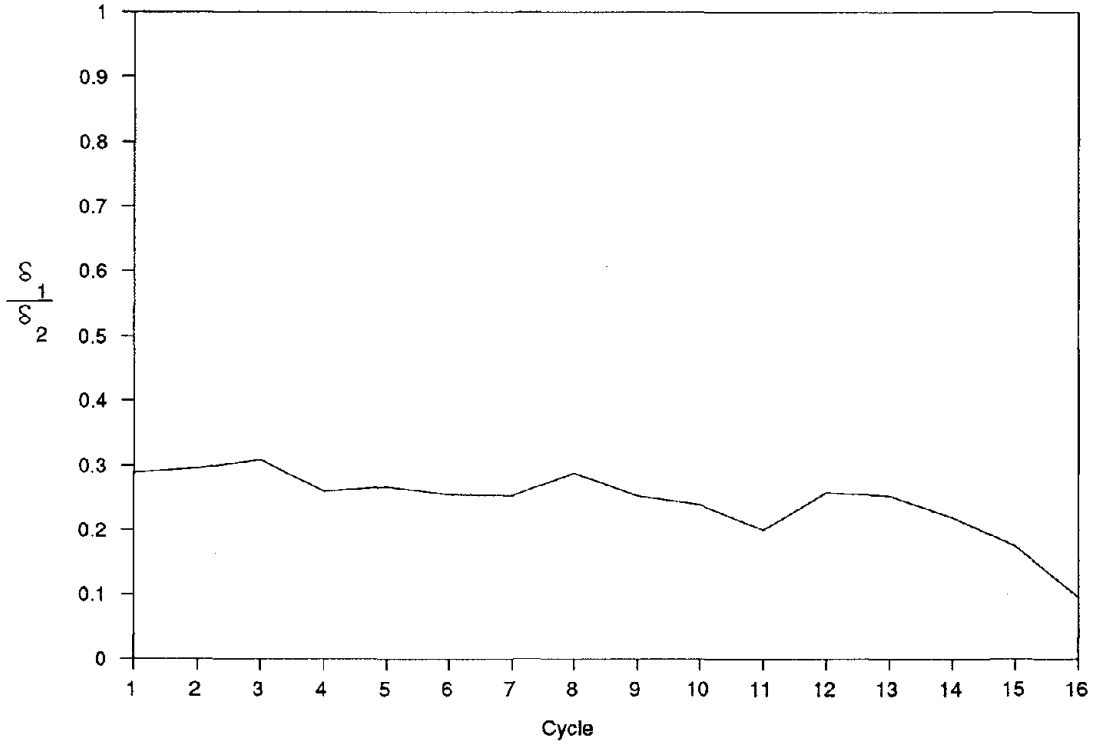

Fig. 3.19 Ratio of Average Lower to Upper Deck Deflections

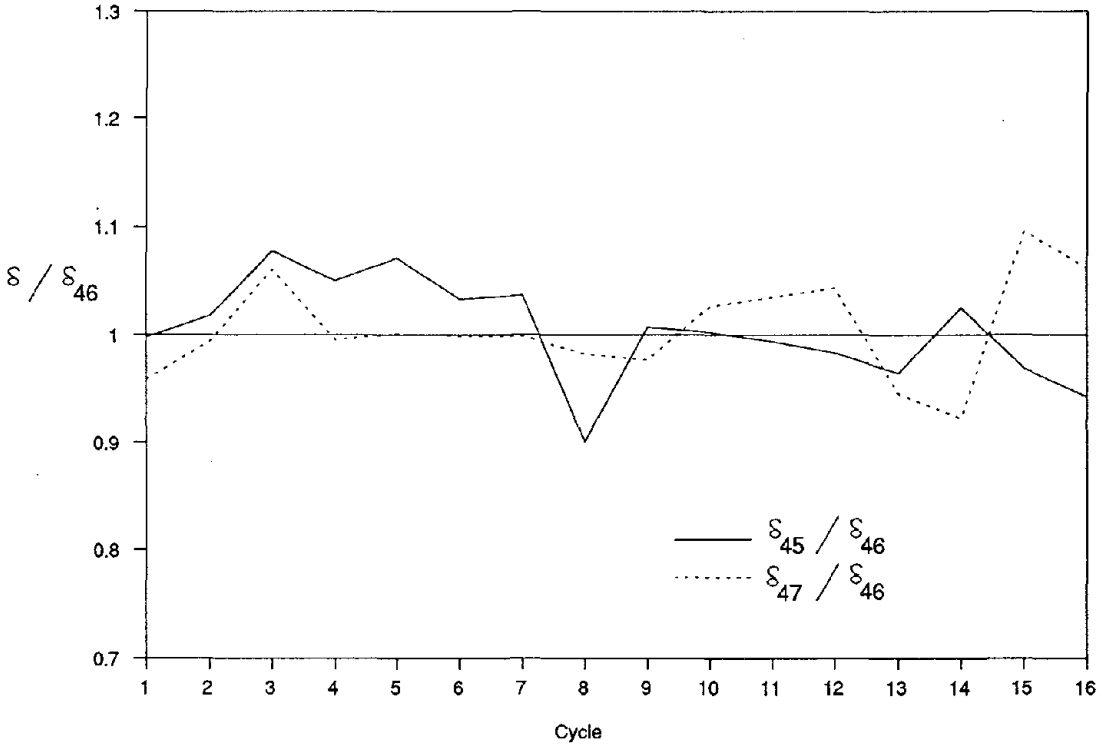

Fig. 3.20 Bent-top Deflection Ratios for Different Bents

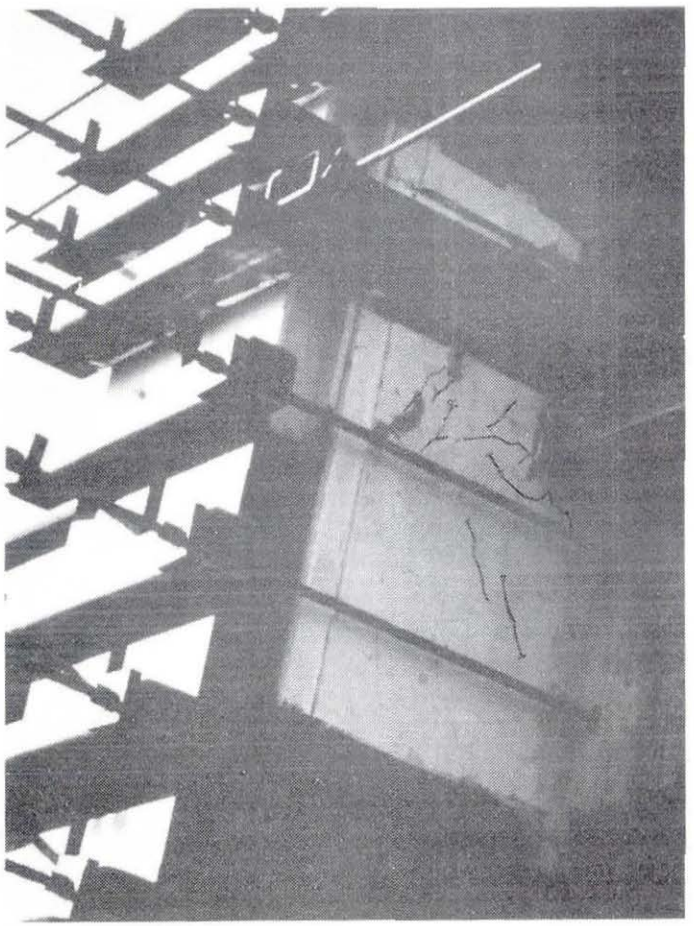

Fig. 3.21 Inclined cracks in the lower joint of the NE face of Bent 45 after Cycle 7.

Fig. 3.22 Diagonal crack formation in the top east joint of Bent 45 after Cycle 7.

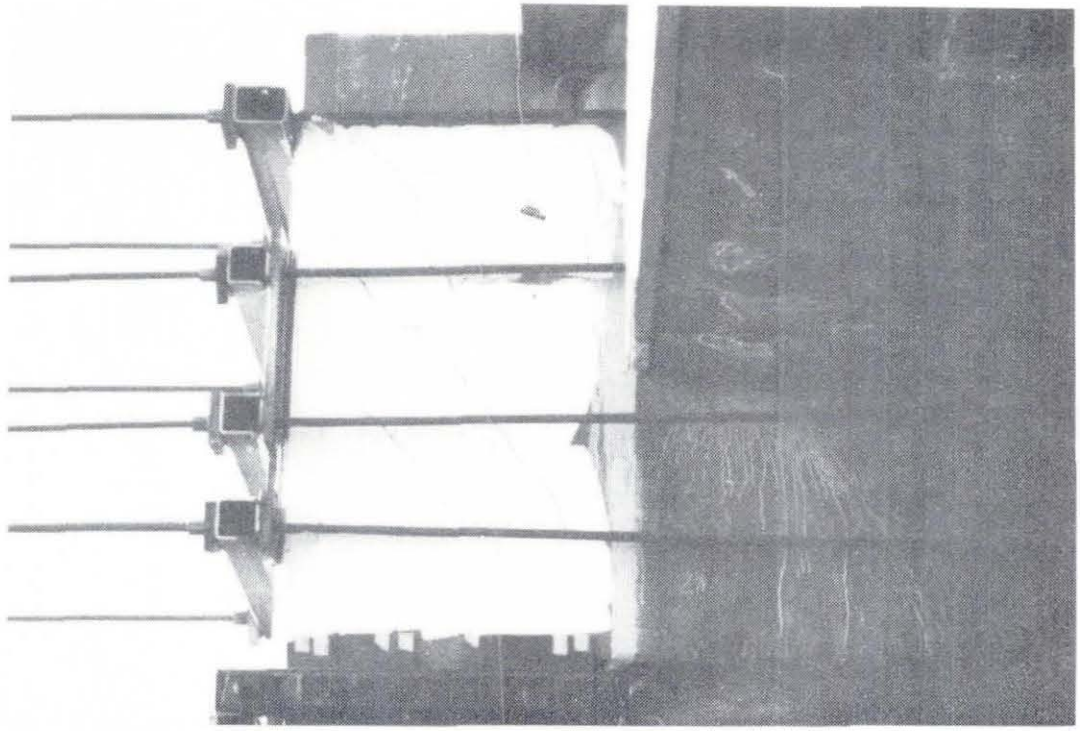

Fig. 3.23 Bent 46 after Cycle 7.

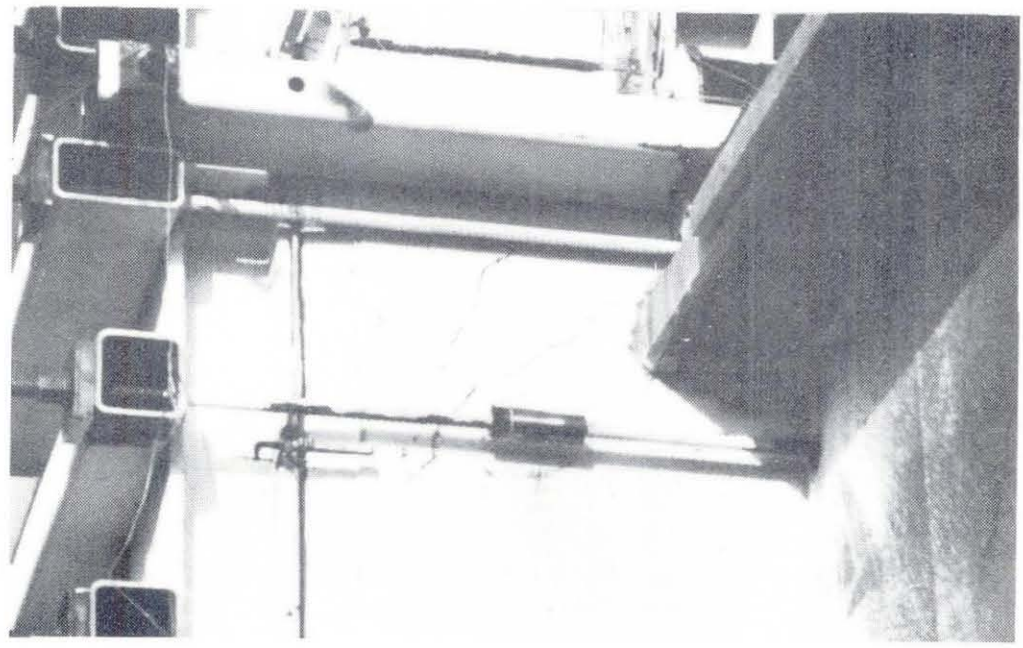

Fig. 3.24 Crack formations in the lower joint of the west end of Bent 45 after Cycle 8.

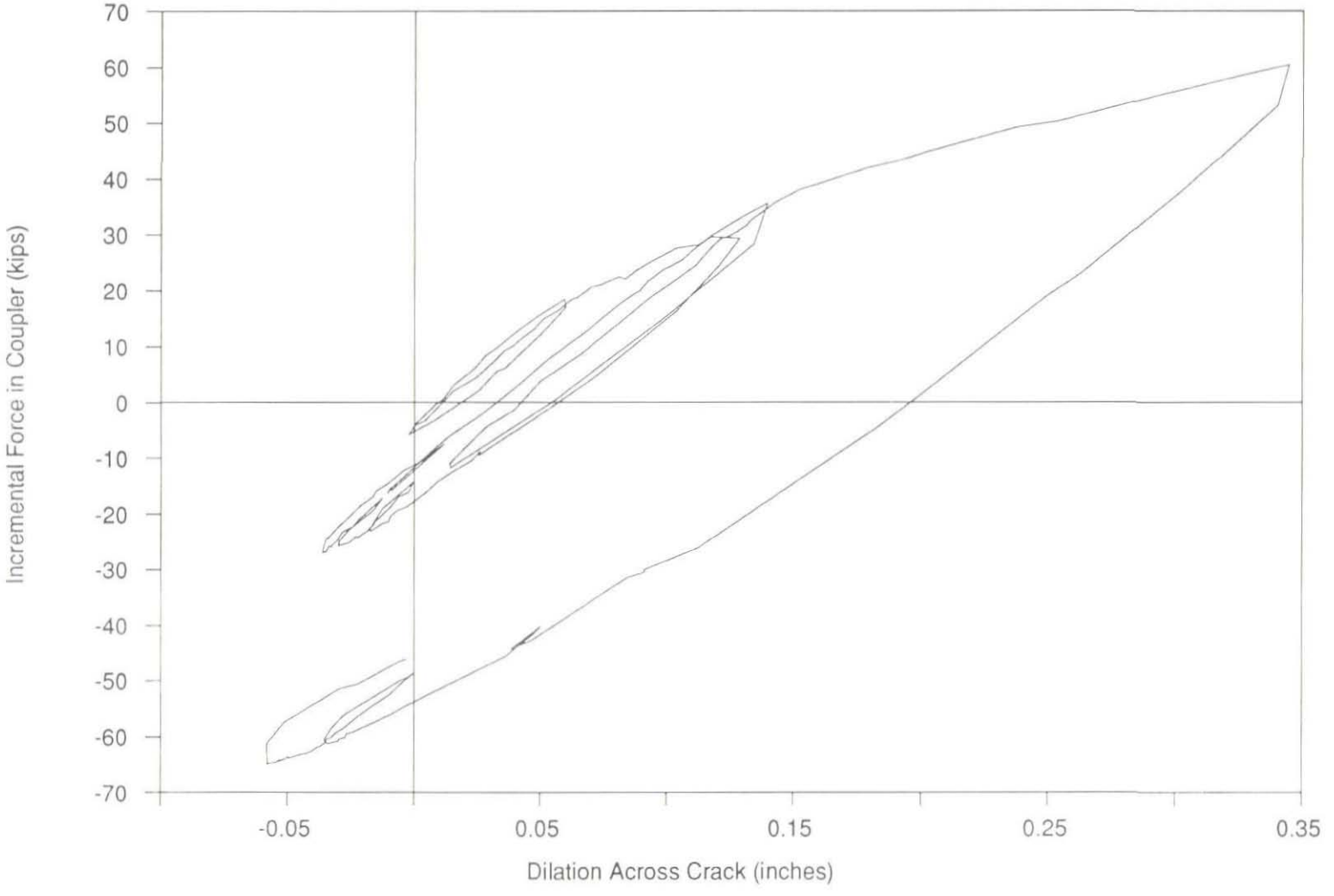

Fig. 3.25 Coupler Force - Joint Displacement Relationship in Lower Joint of Bent 45

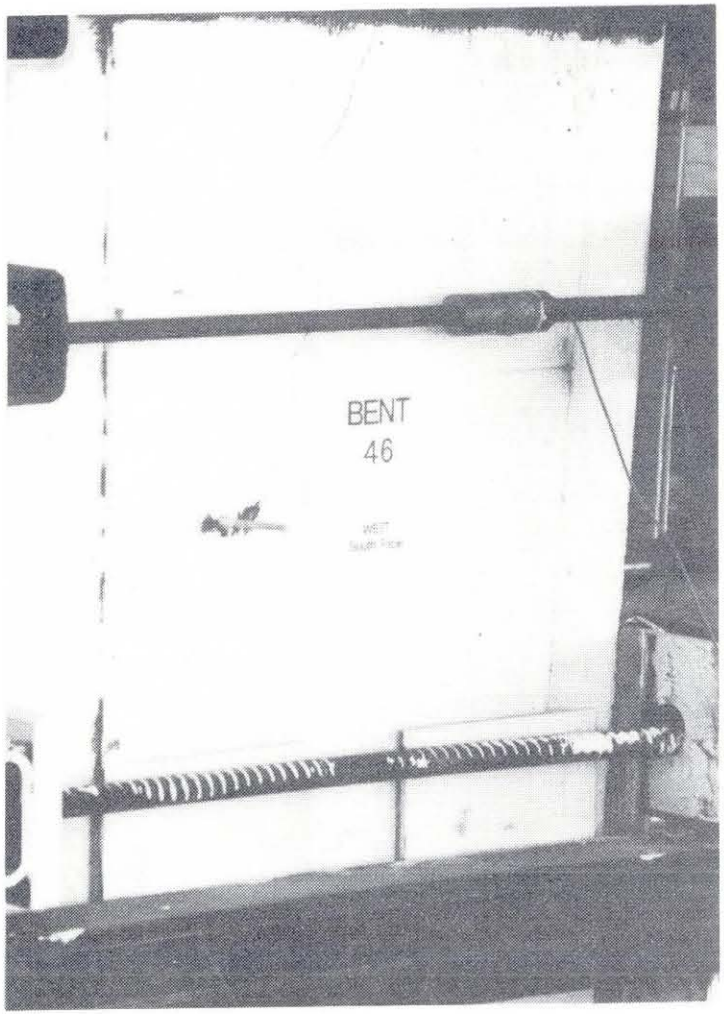

(a) South face.

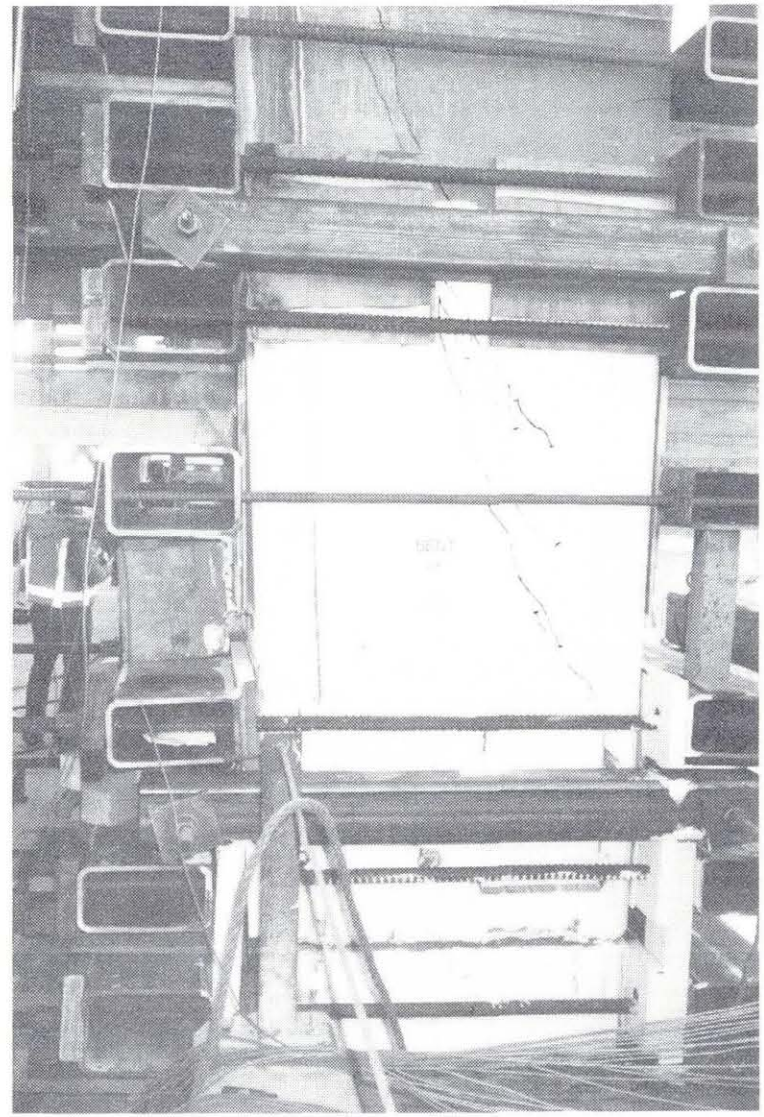

(b) North face.

Fig. 3.26 Column shear cracks formed on the west end column of Bent 46 during Cycle 8.

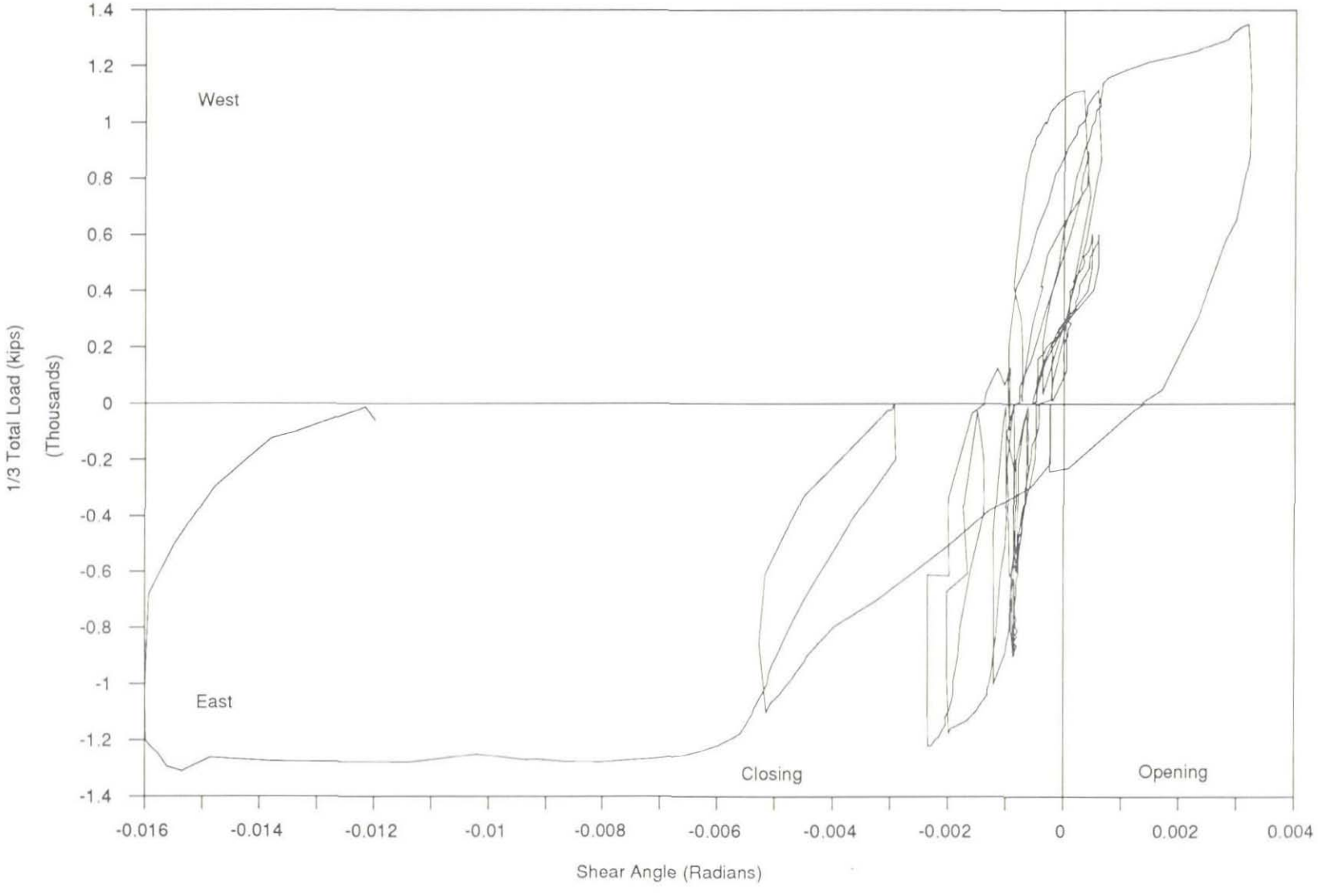

Fig. 3.27 East End, Bent 46: Upper Joint Shear Angle

Fig. 3.28 Diagonal crack formation in the top east joint of Bent 45 after Cycle 9.

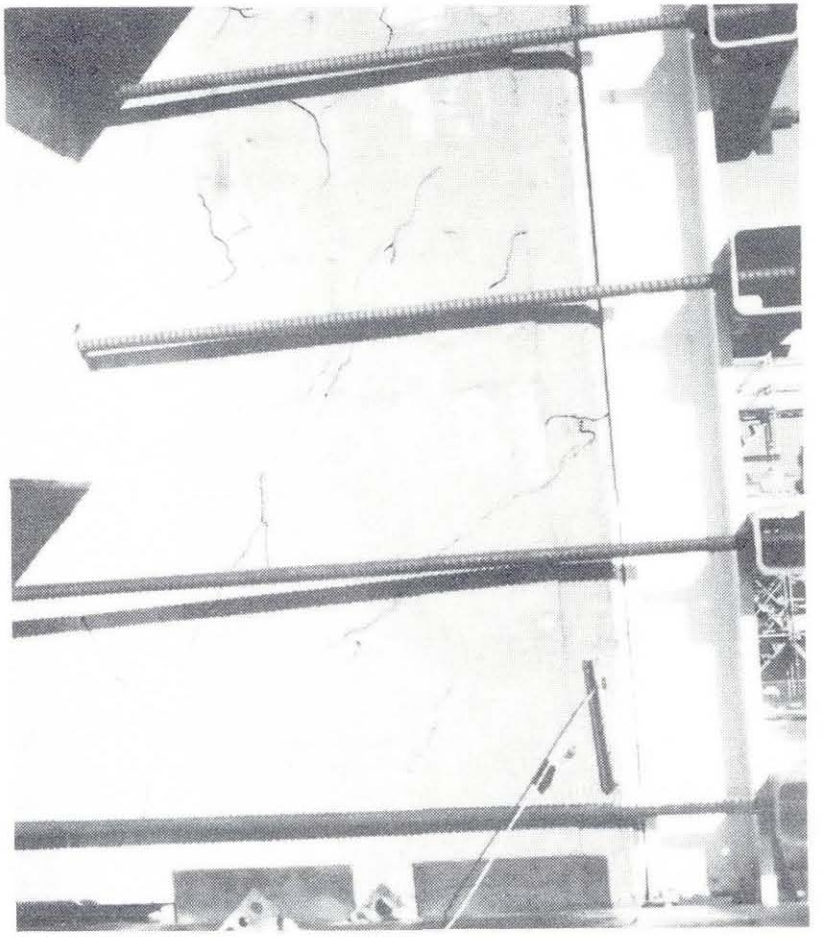

Fig. 3.29 Diagonal crack formation after Cycle 10, upper east joint, Bent 45.

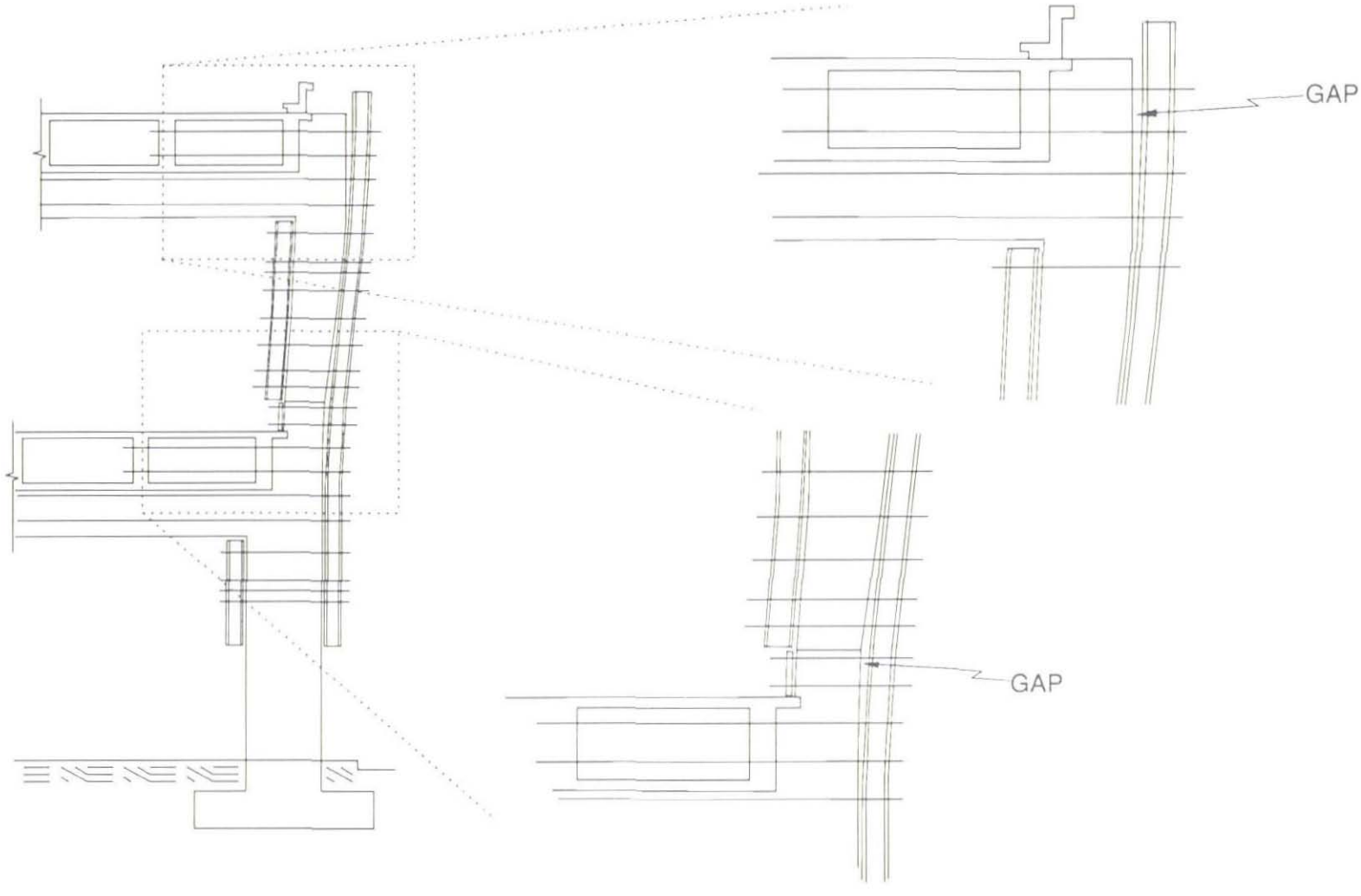

Fig. 3.30 Separation of Wide Flange Retrofits From Columns

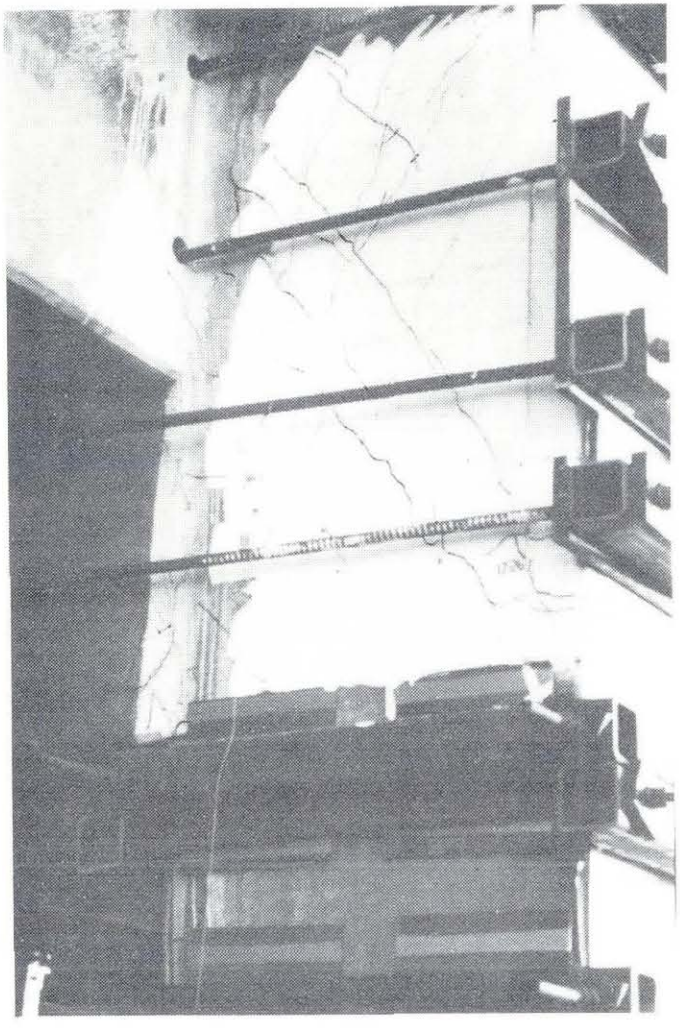

Fig. 3.31 Inclined cracks formed after Cycle 12, upper joint of NW face of Bent 46.

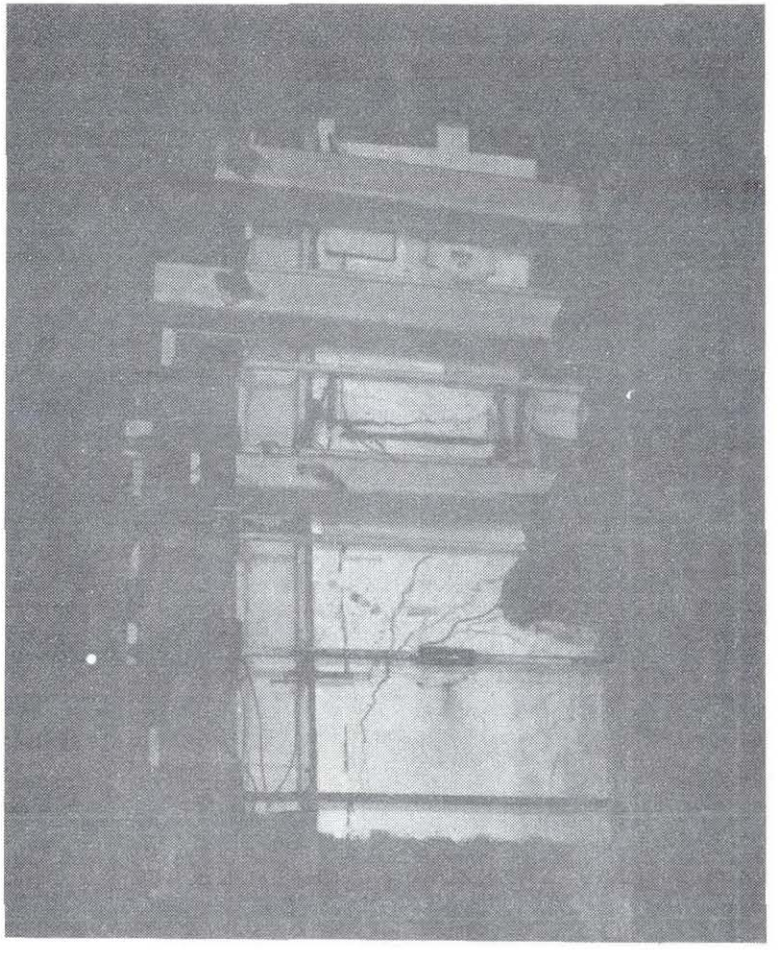

Fig. 3.32 Bent 45, west column. Shear key horizontal crack under last (4000 kip) load cycle.

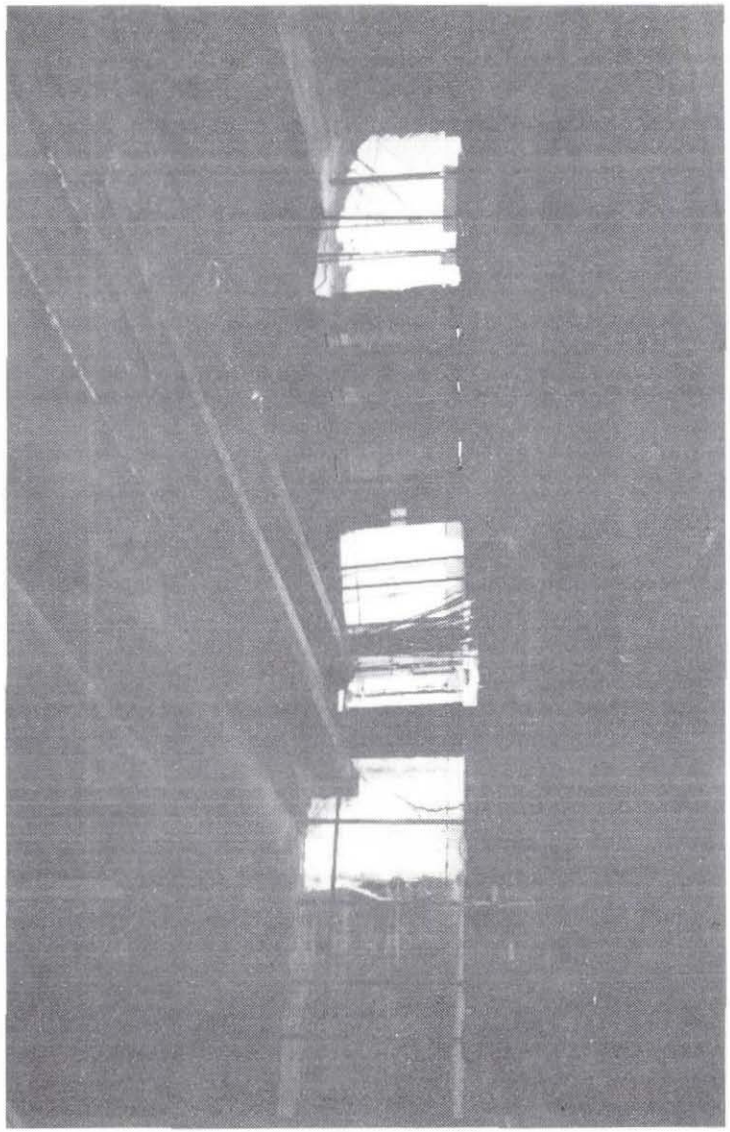

Fig. 3.33 Bent 46, west column deflected shape under 4000 kip load.

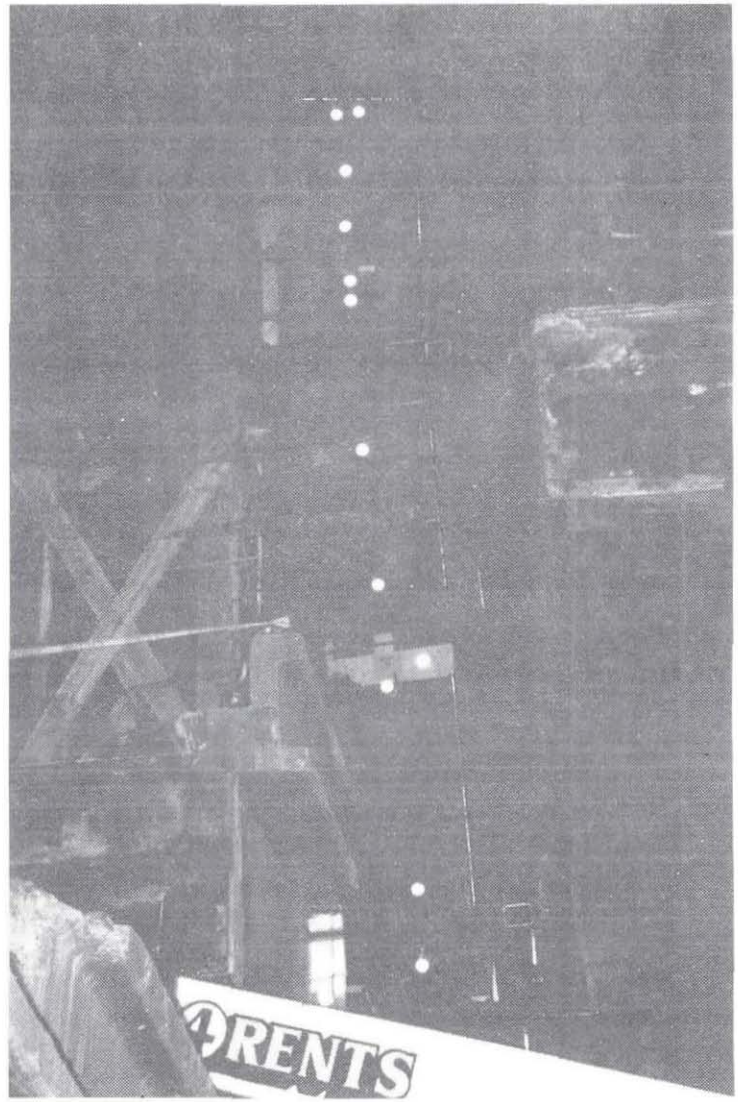

Fig. 3.34 Bent 47, west column deflected shape under 4000 kip load.

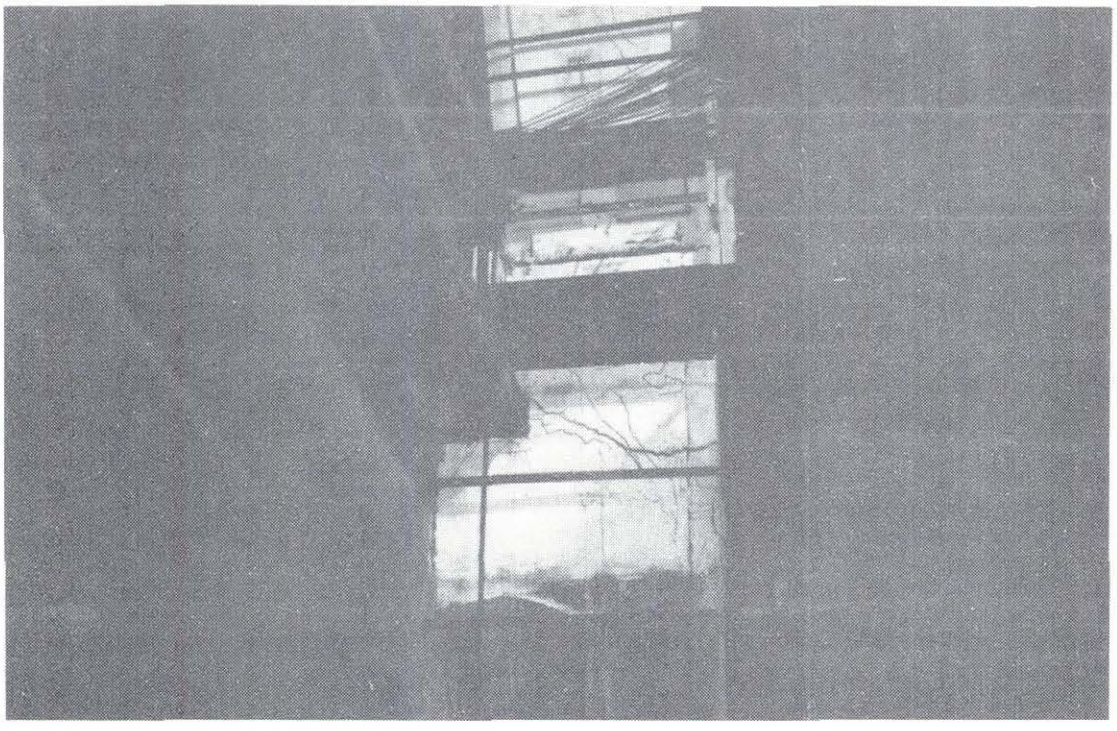

Fig. 3.35 Bent 46, west column shear key opening and horizontal flexural crack at lower deck level (bottom of upper column) under 4000 kip load.

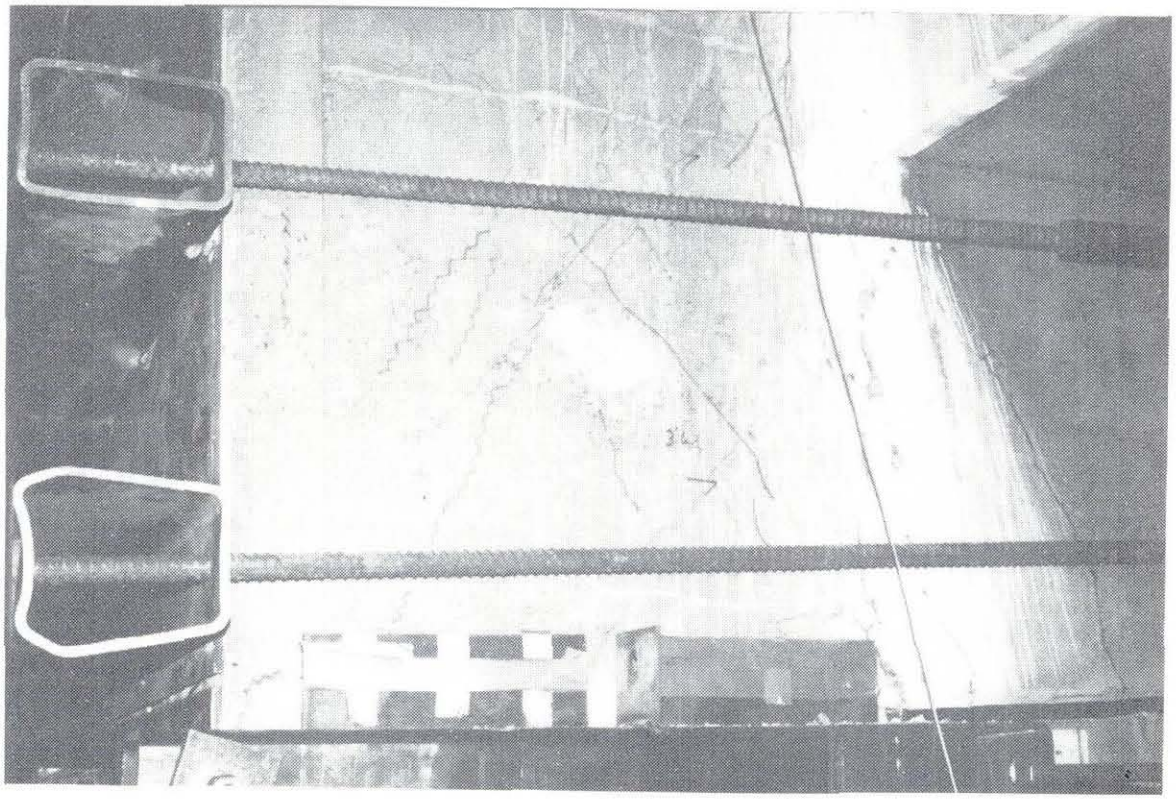

Fig. 3.36 Buckled HSS-section, top west joint of Bent 47.

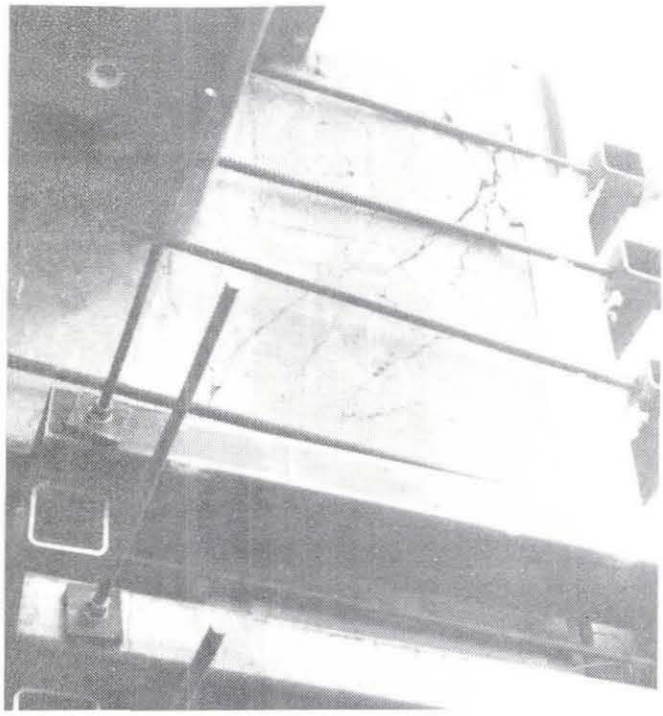

Top joint, south face

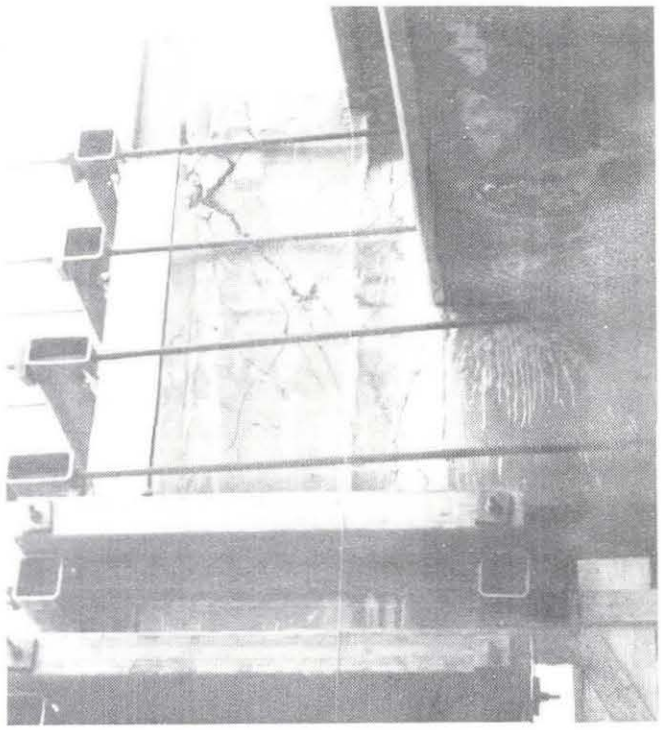

Top joint, north face

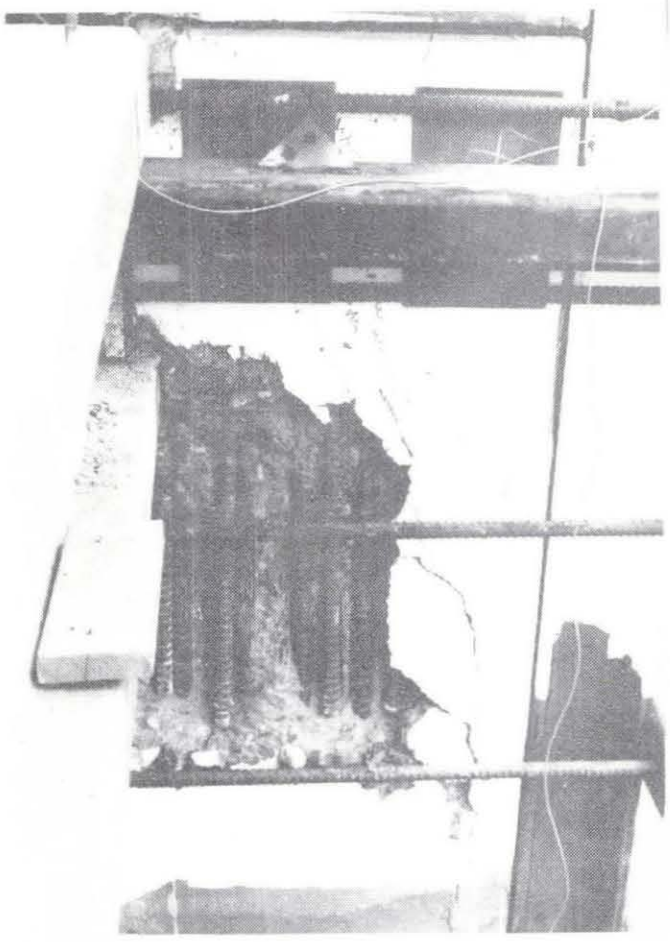

Middle joint, south face

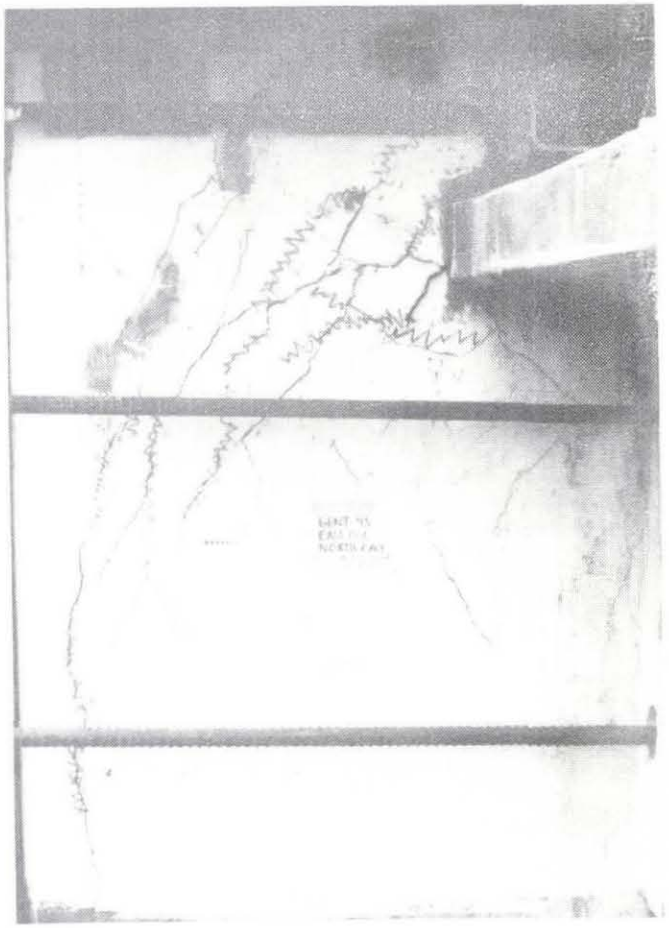

Middle joint, north face

Fig. 3.37 Damage to the east end of Bent 45.

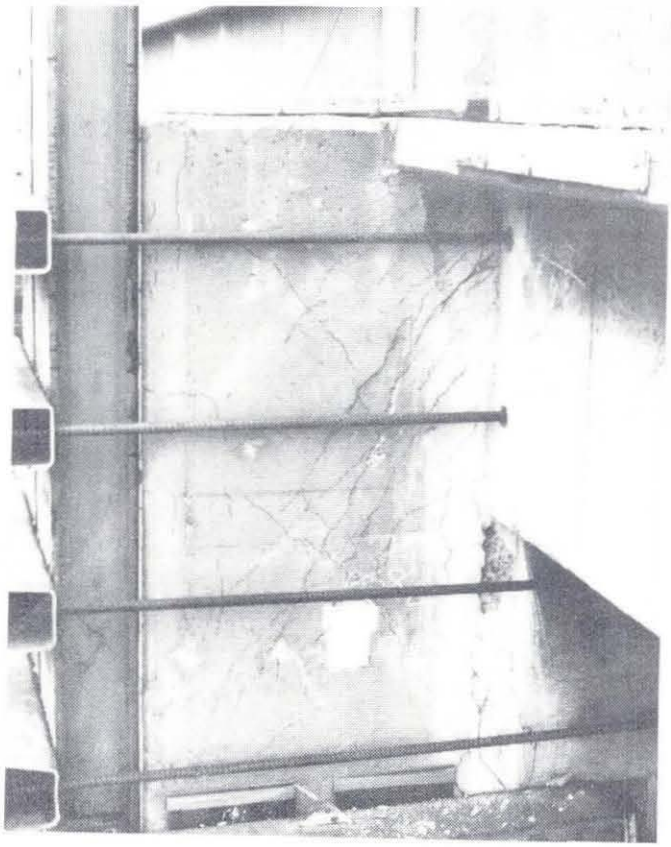

Top joint, south face

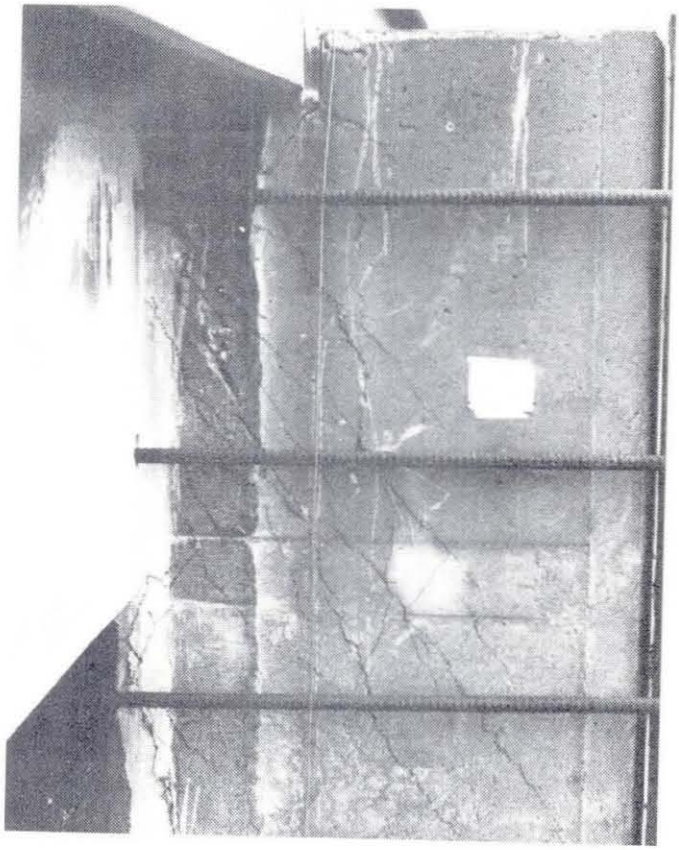

Top joint, north face

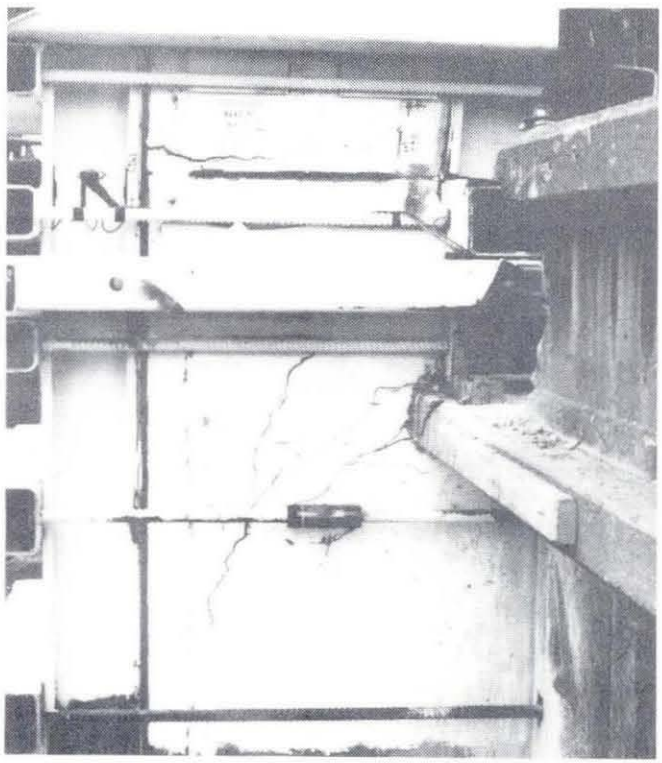

Middle joint, south face

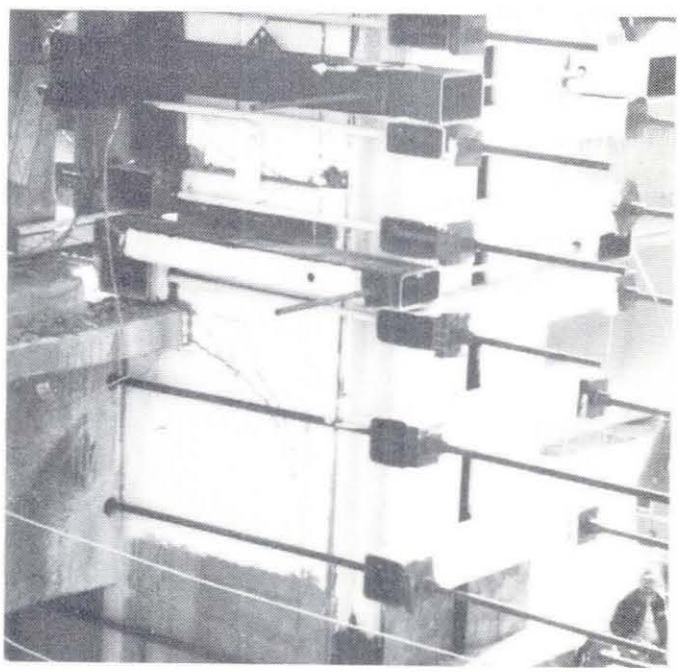

Middle joint, north face

Fig. 3.38 Damage to the west end of Bent 45.

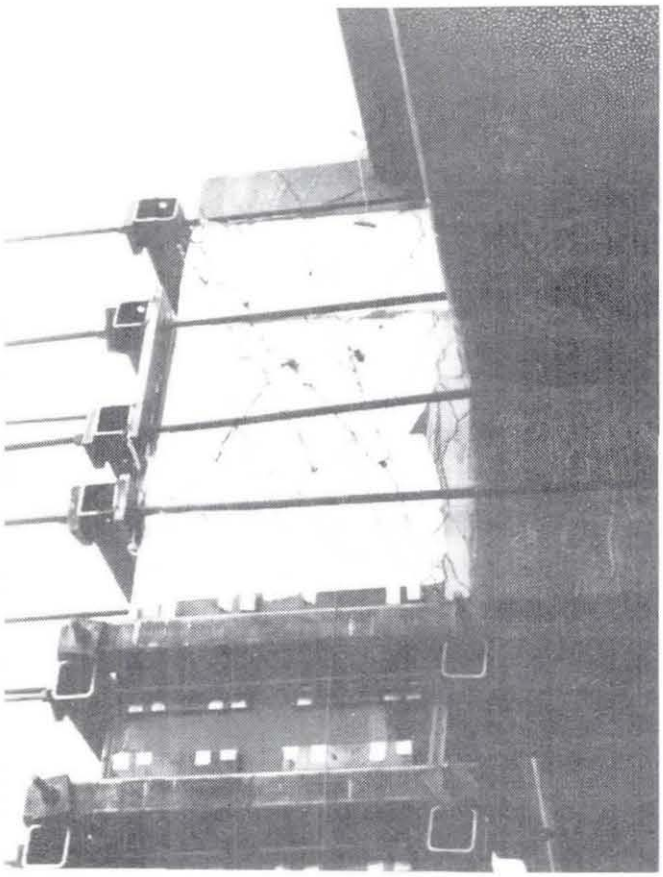

Top joint, north face

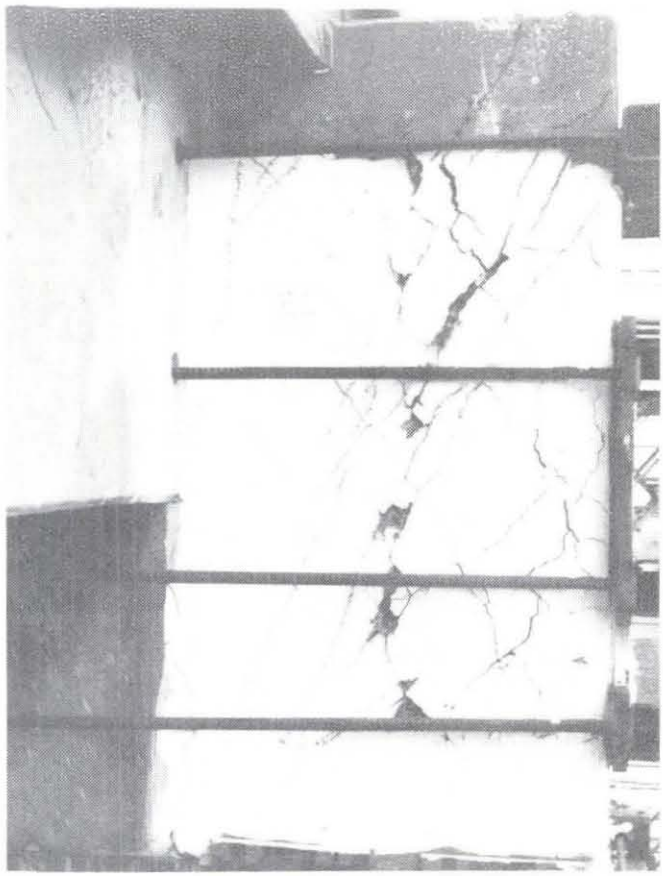

Top joint, south face

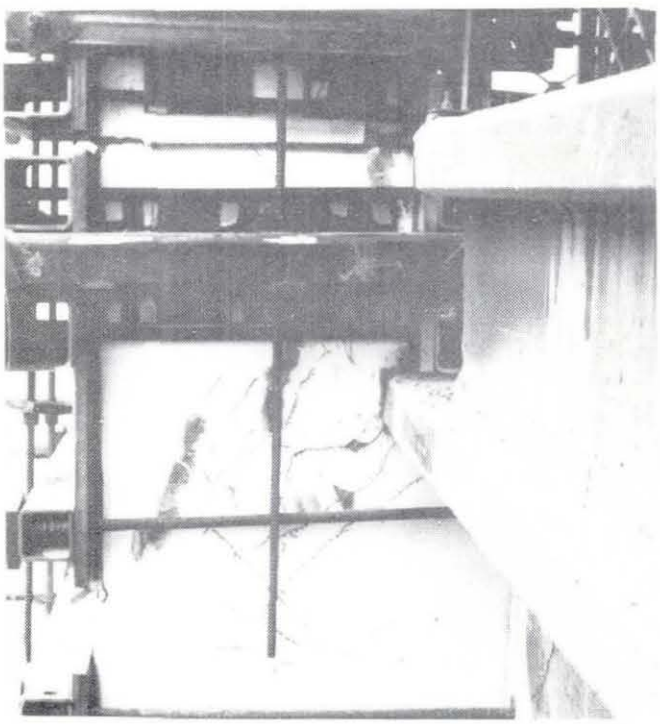

Middle joint, north face

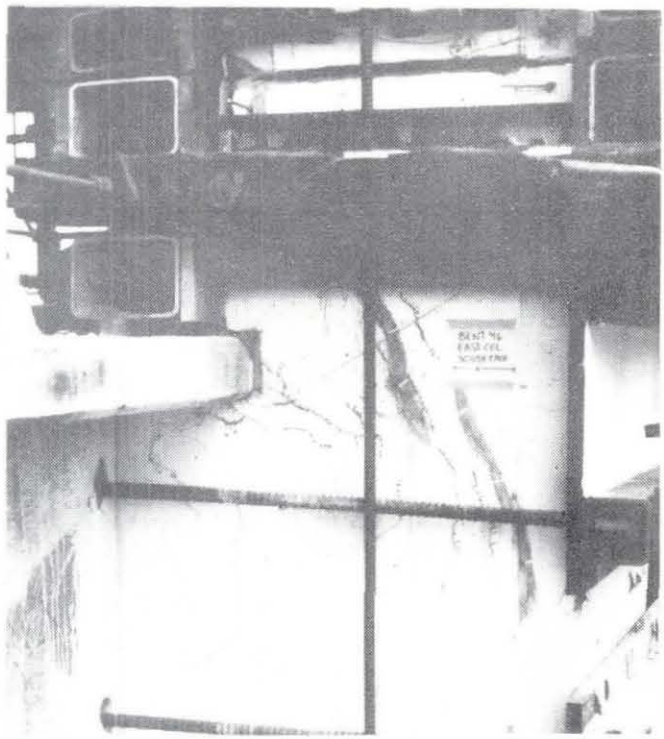

Middle joint, south face

Fig. 3.39 Damage to the east end of Bent 46.

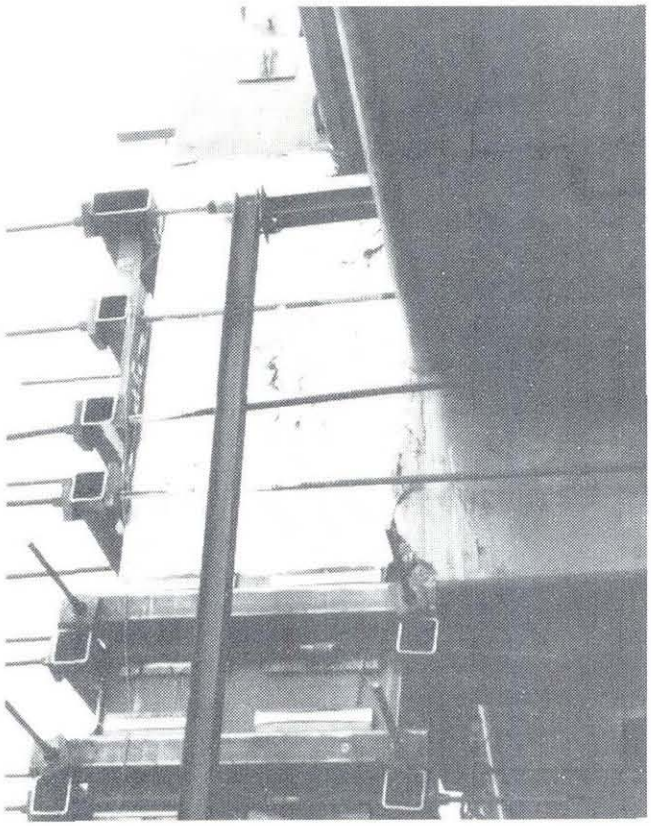

Top joint, south face

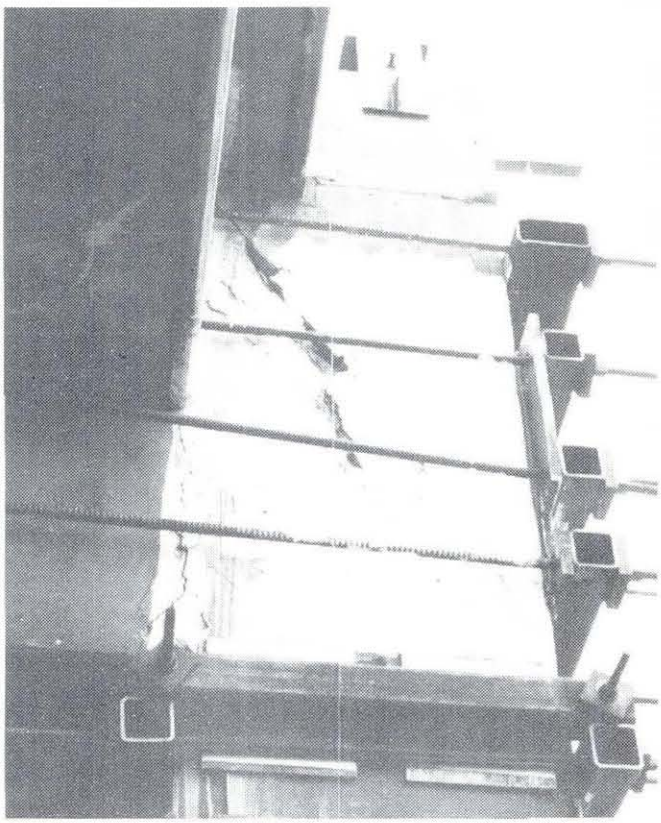

Top joint, north face

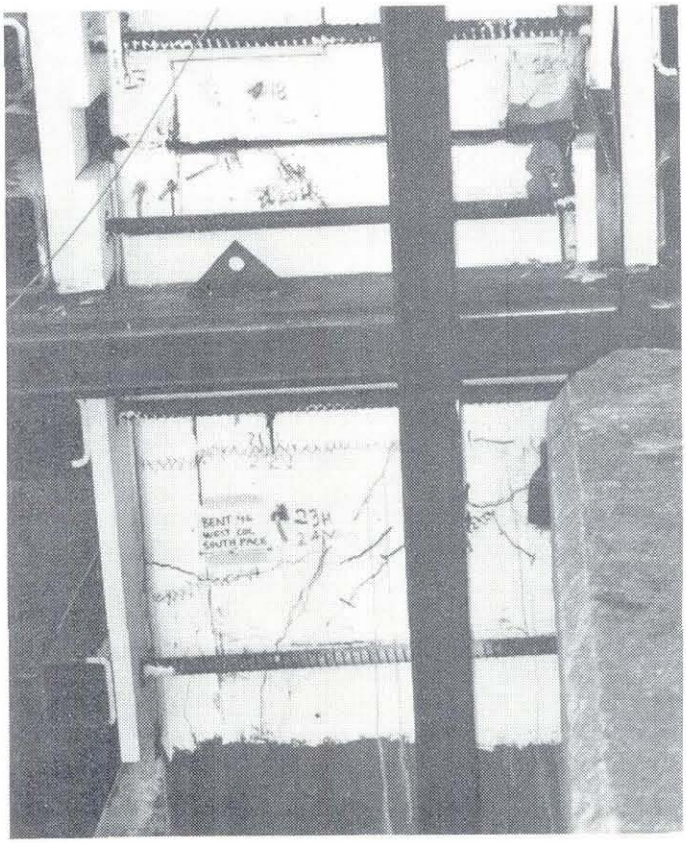

Middle joint, south face

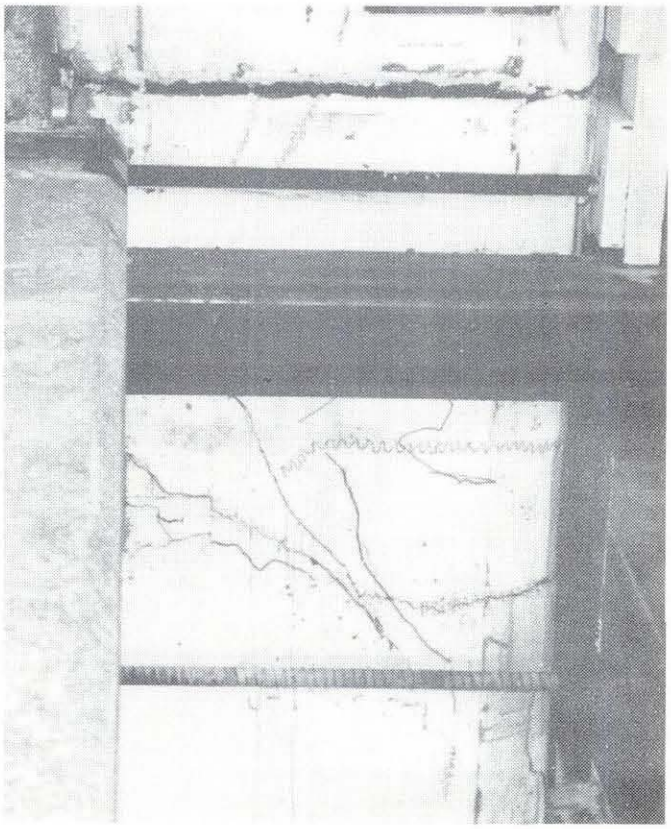

Middle joint, north face

Fig. 3.40 Damage to the west end of Bent 46.

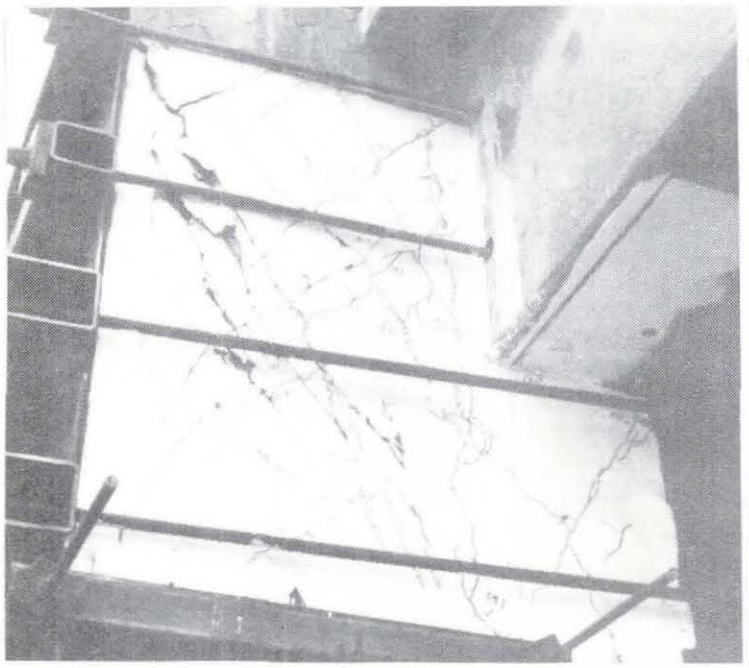

Top joint, north face

Top joint, south face

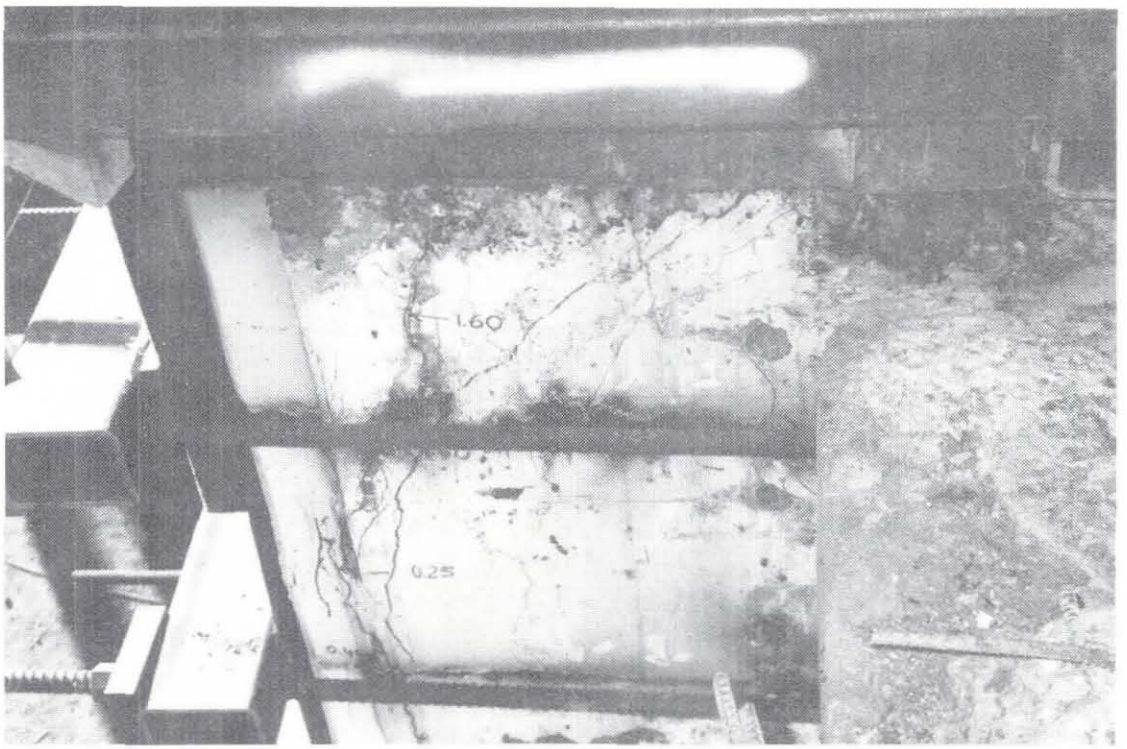

Middle joint, south face

Fig. 3.41 Damage to the east end of Bent 47.

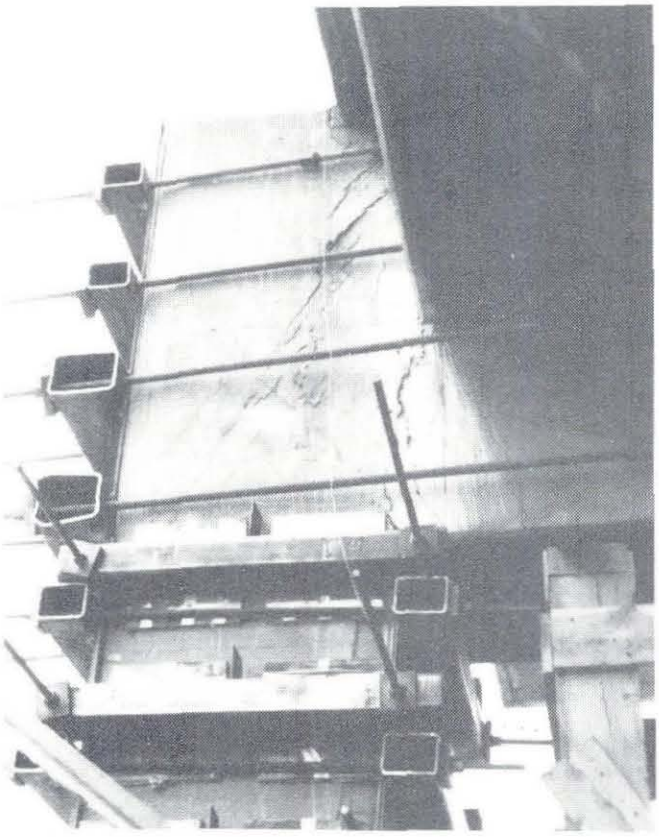

Top joint, south face

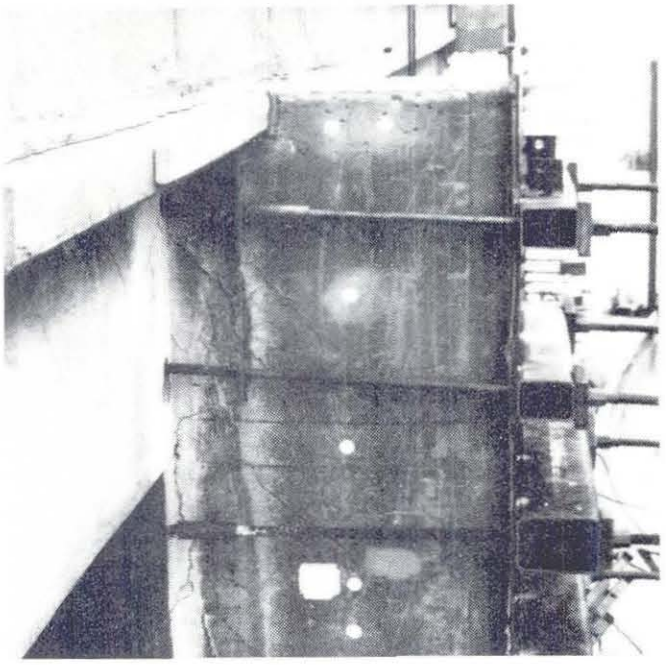

Top joint, north face

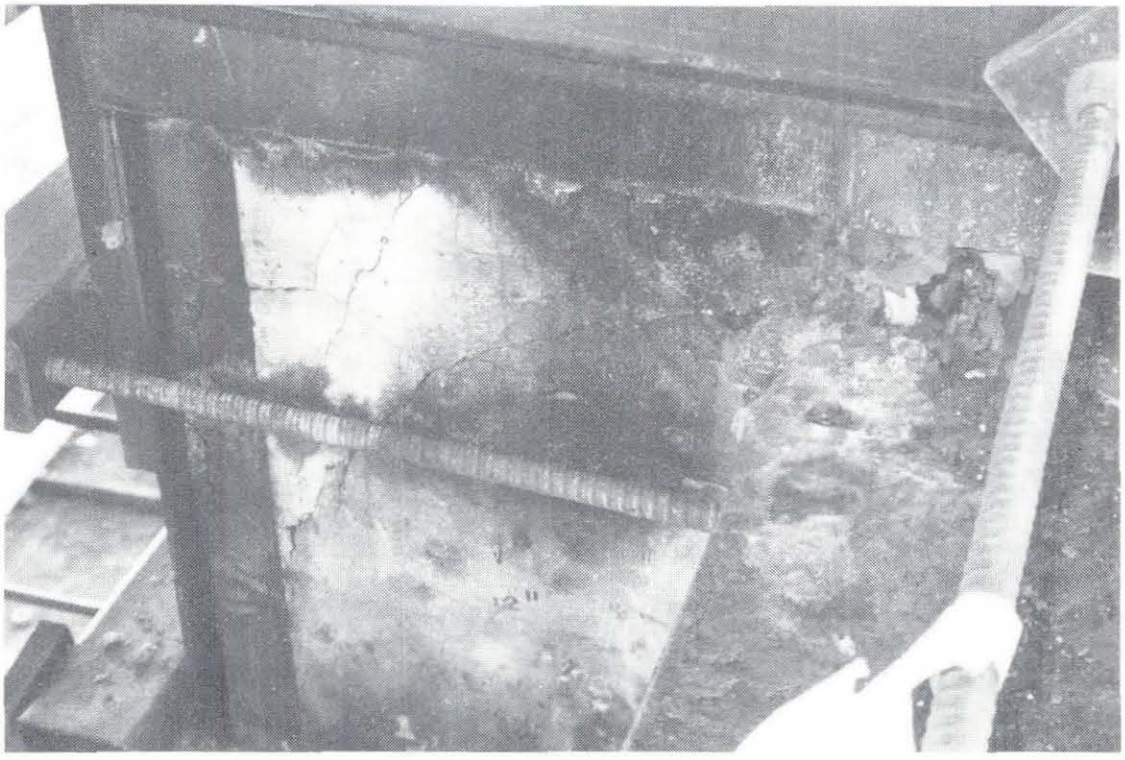

Middle joint, north face

Fig. 3.42(a) Damage to the west end of Bent 47.

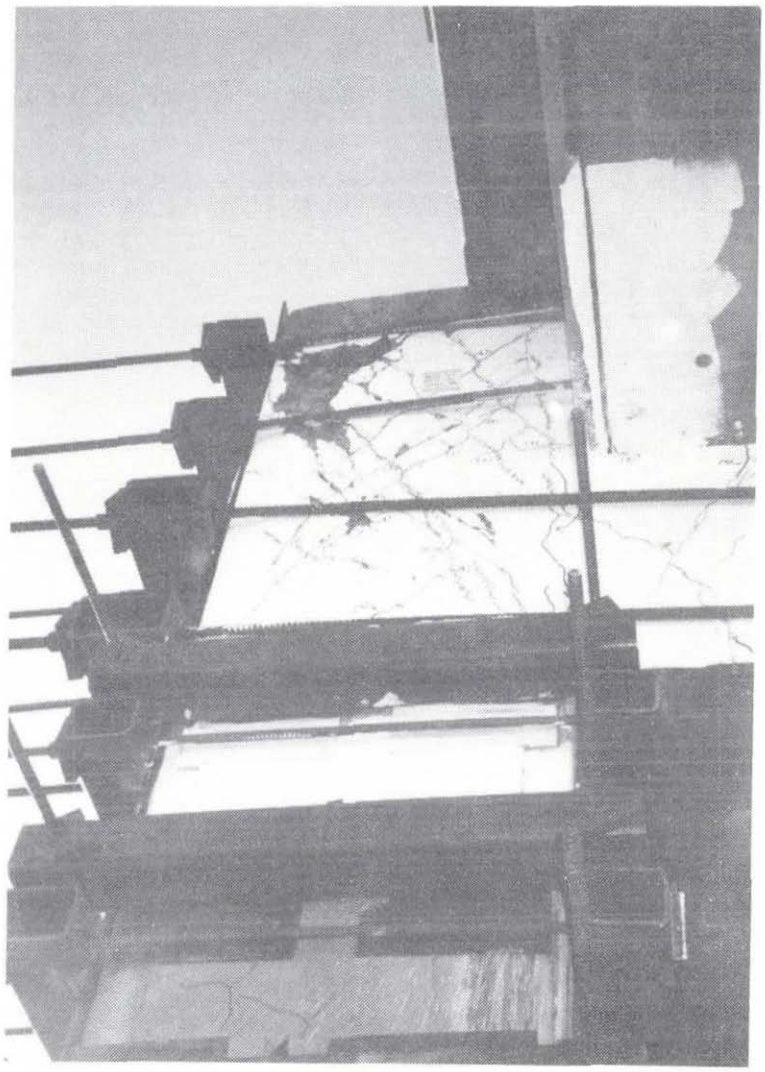

North face

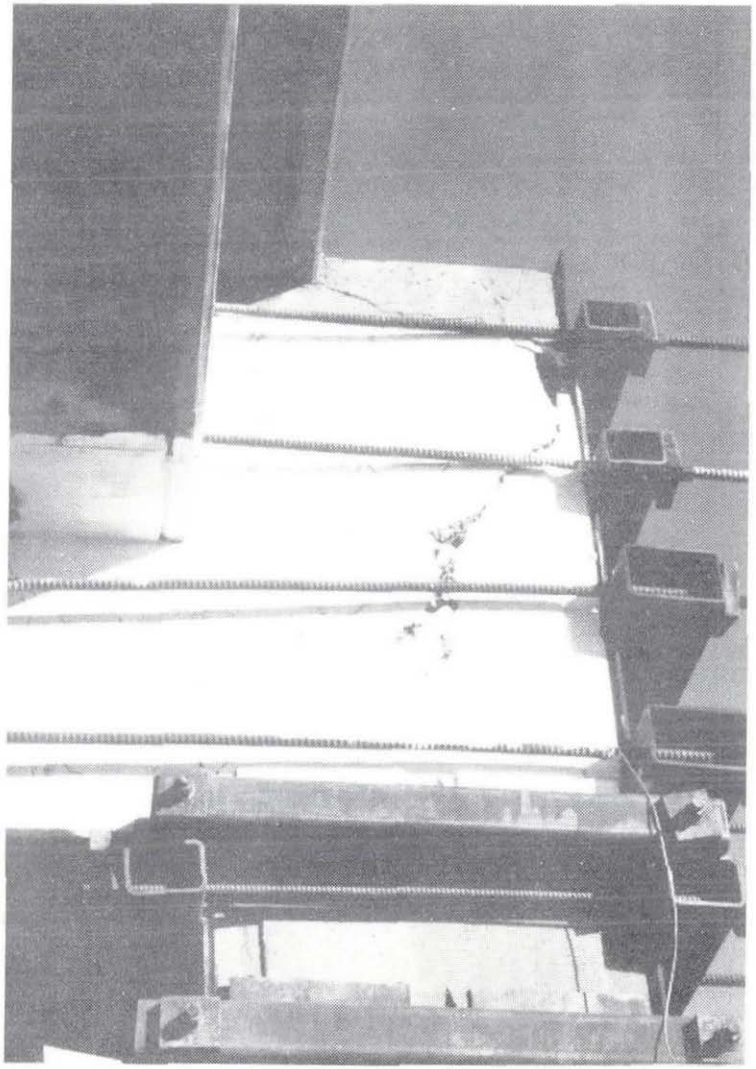

South face

Fig. 3.42(b) Damage to the top joints on the east end of Bent 47.

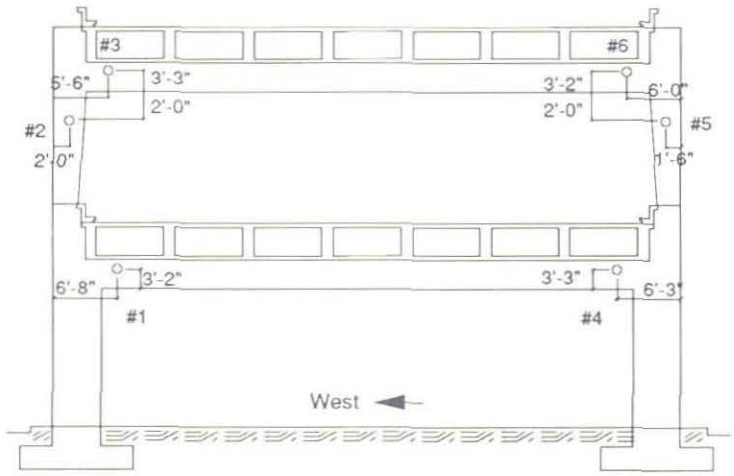

Bent 45
South Face

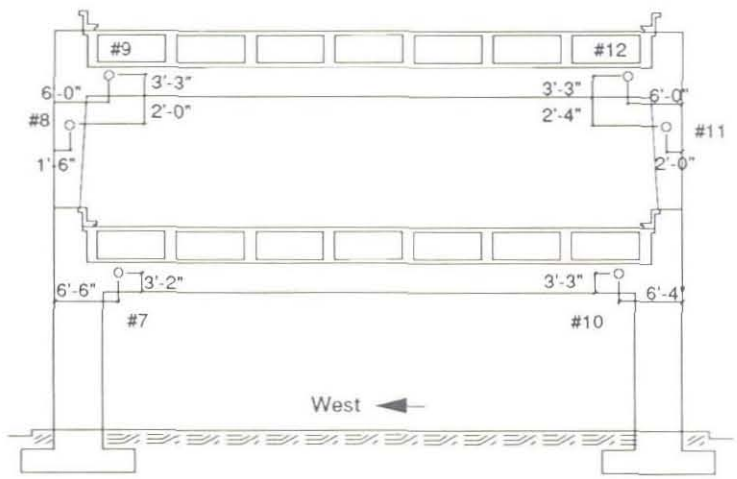

Bent 46
South Face

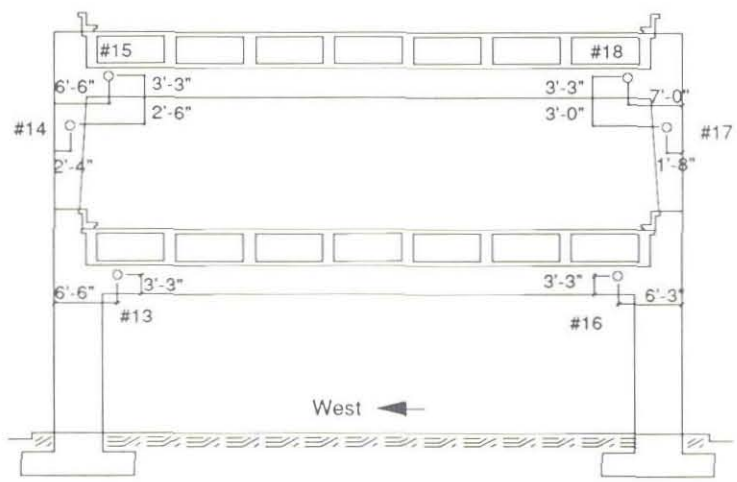

Bent 47
South Face

Fig. 3.43 Core Drill Locations

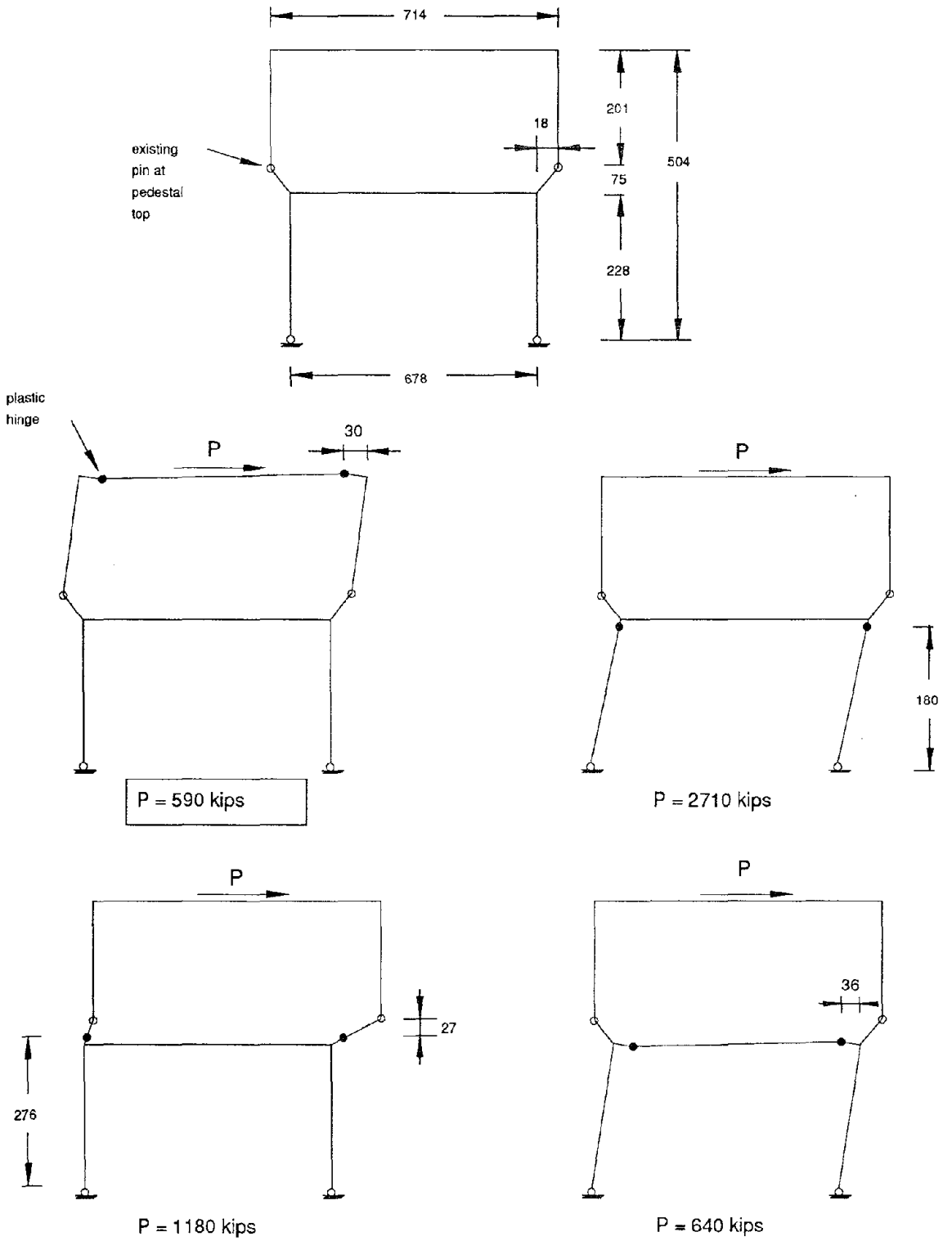

(All dimensions are inches)

Fig. 4.1 Bent Collapse Mechanisms

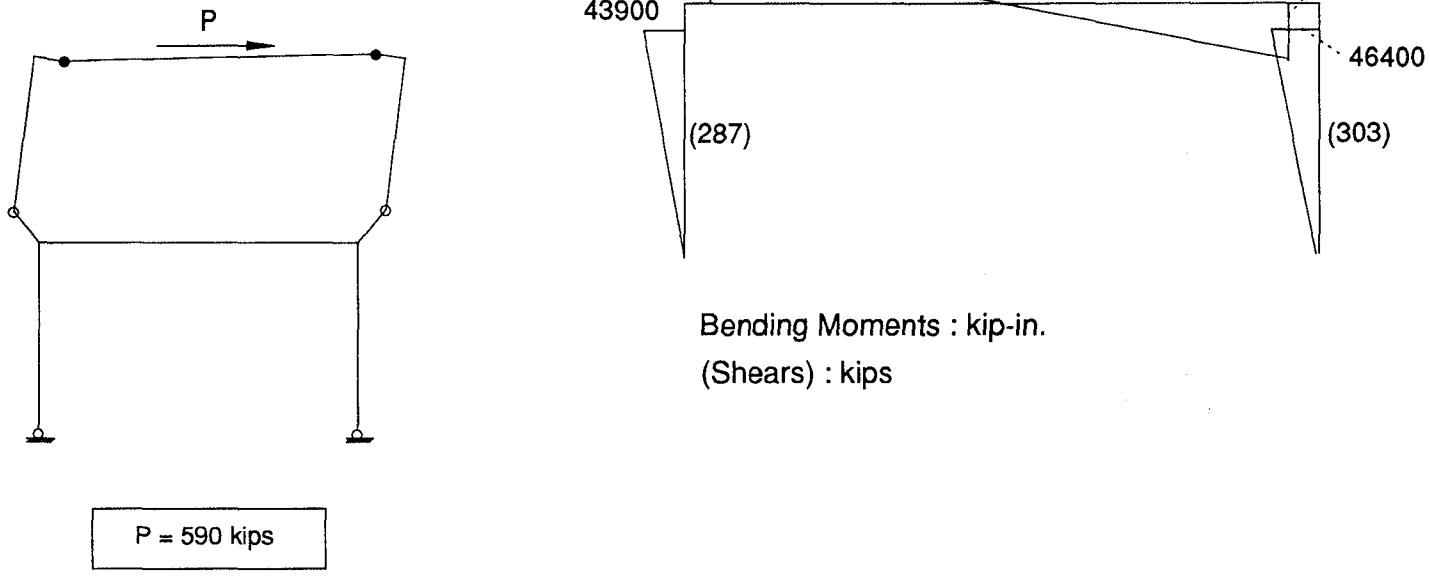

Fig. 4.2 Local Collapse Mechanism Internal Forces

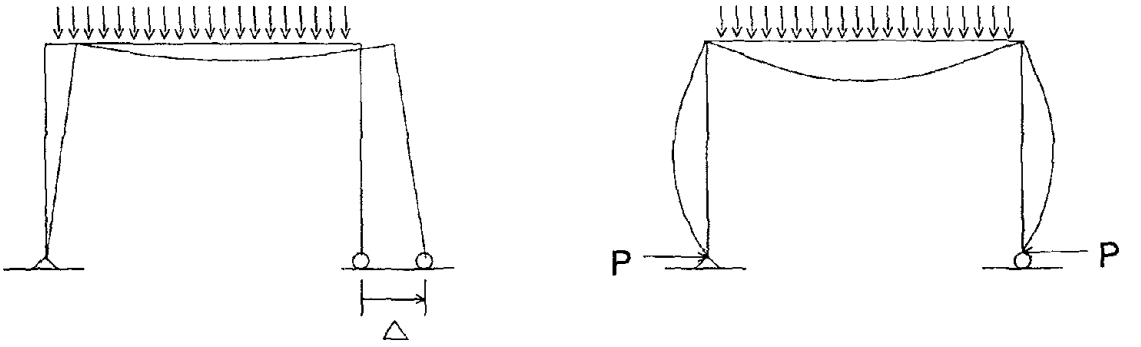

Fig. 4.3 Lateral force needed to resist tendency of outward motion of roller support on simple portal frame.

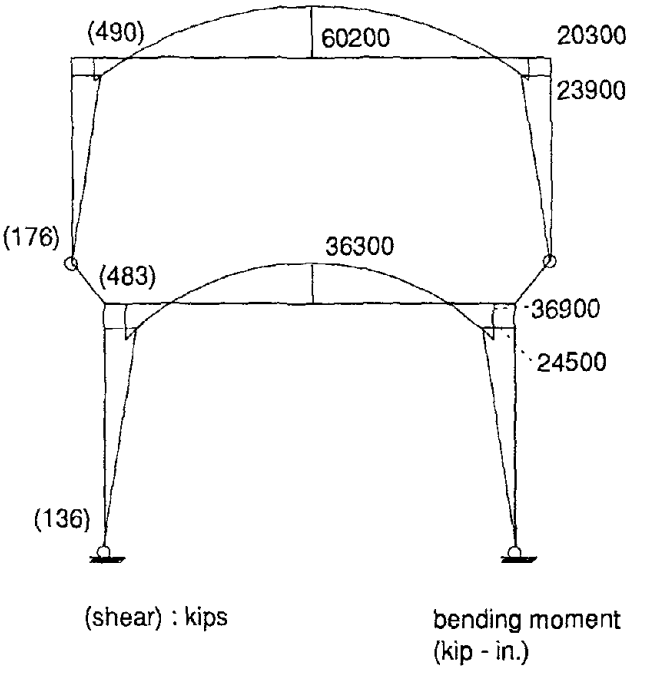

Fig. 4.4 Moments and shears due to gravity alone.

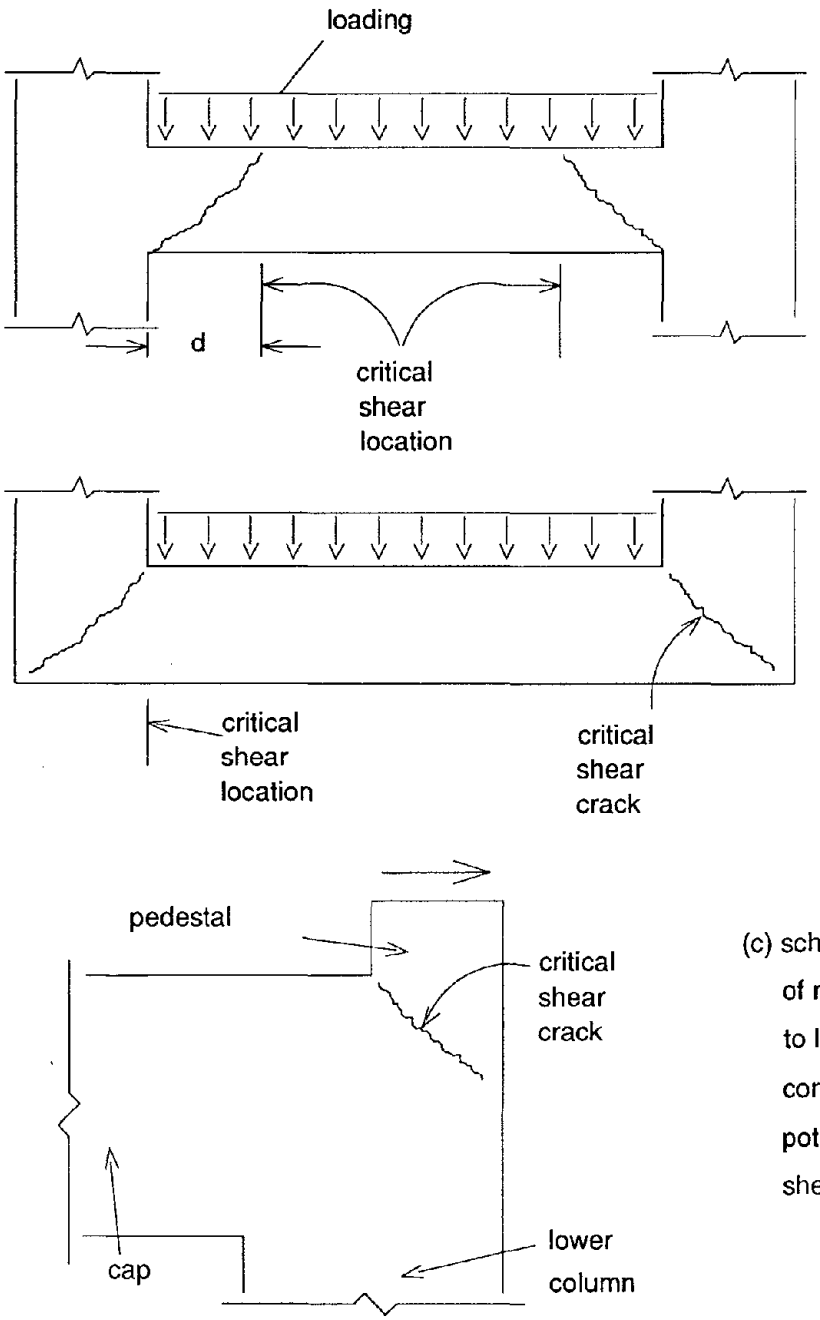

Fig. 4.5 Potential Critical Shear Crack Locations As a Function of End Conditions

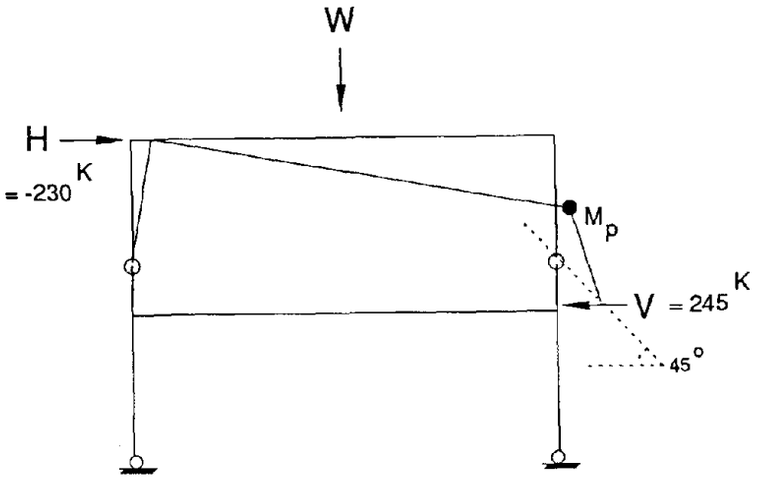

Fig. 4.6 Pedestal Shear Failure Stick Model Collapse Mechanism

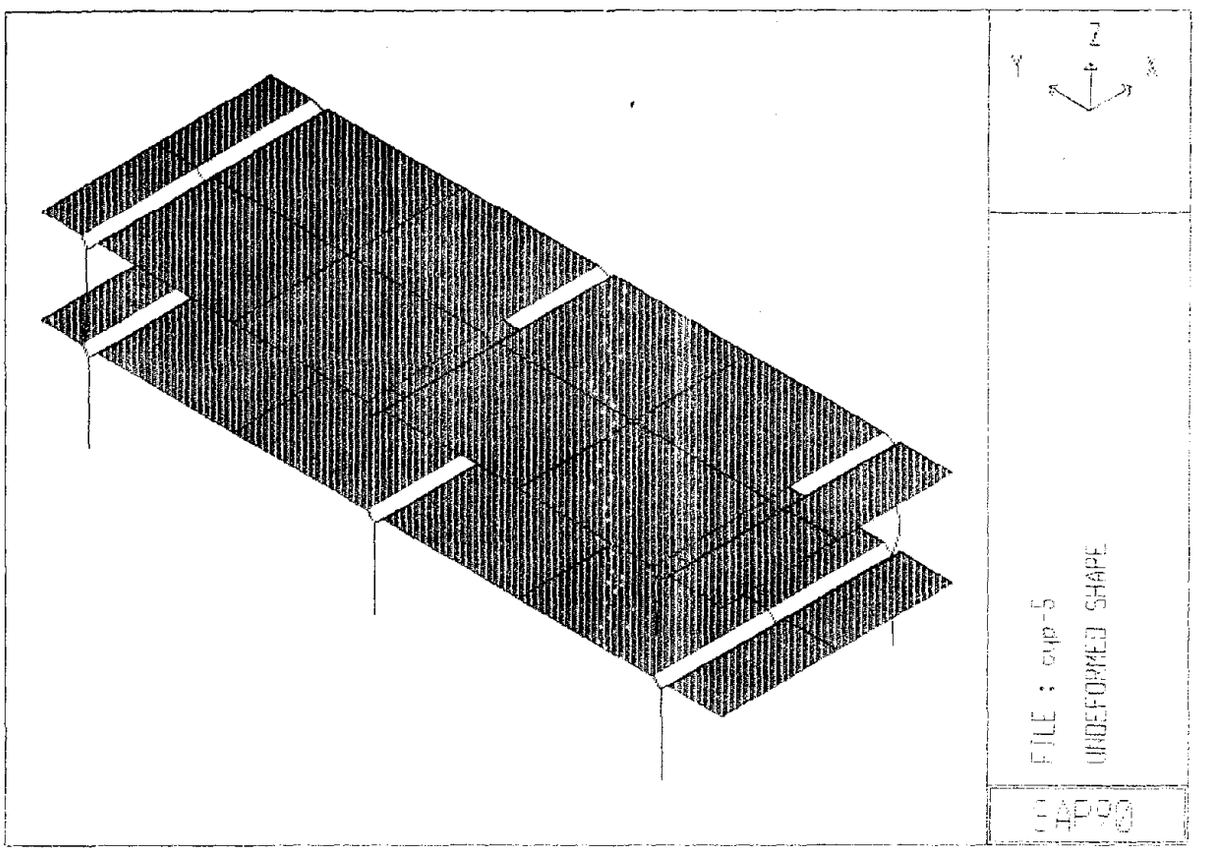

Fig. 4.7 Computer Analysis Model

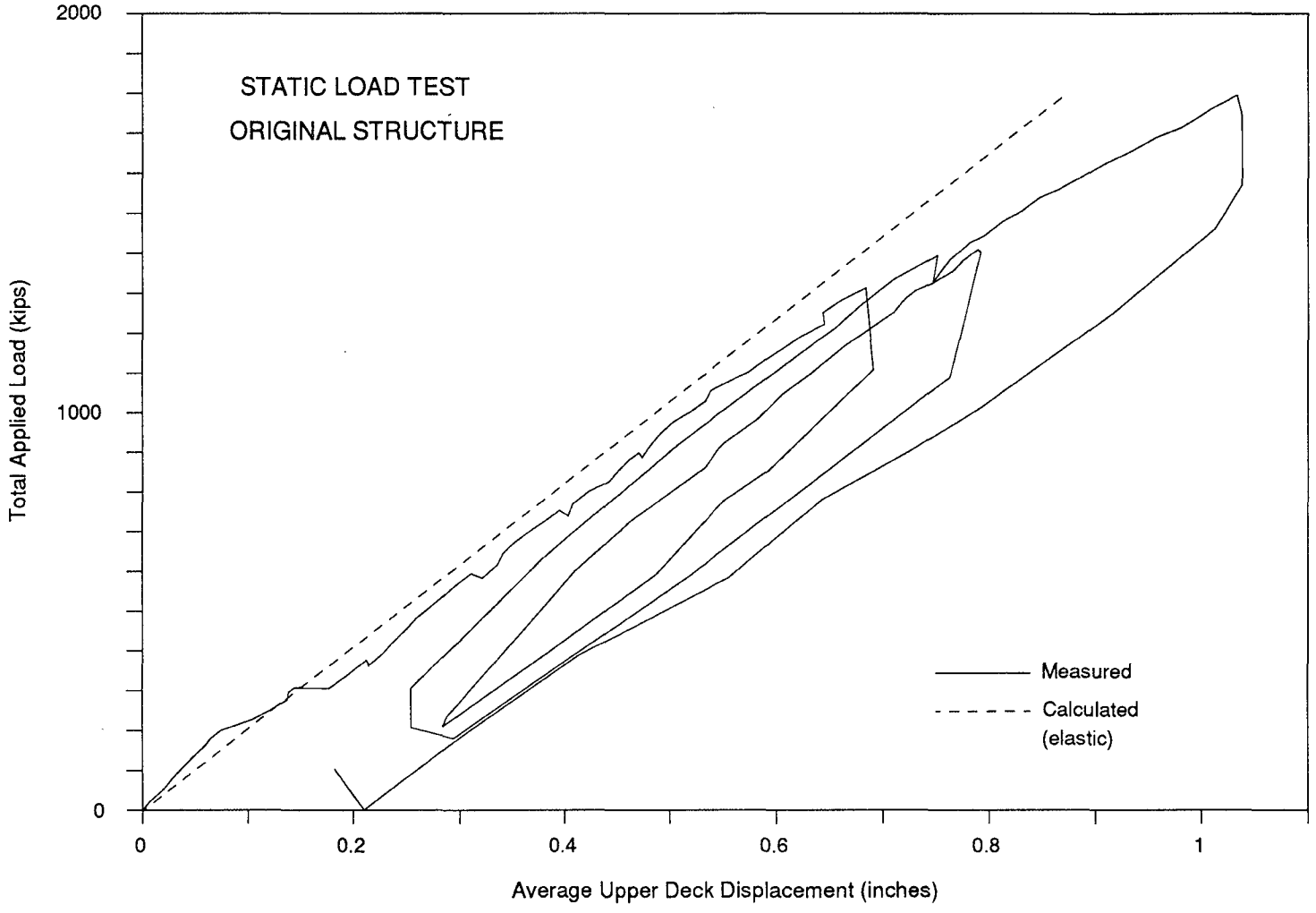

Fig. 4.8 Measured and Calculated Load-Displacement Relationship

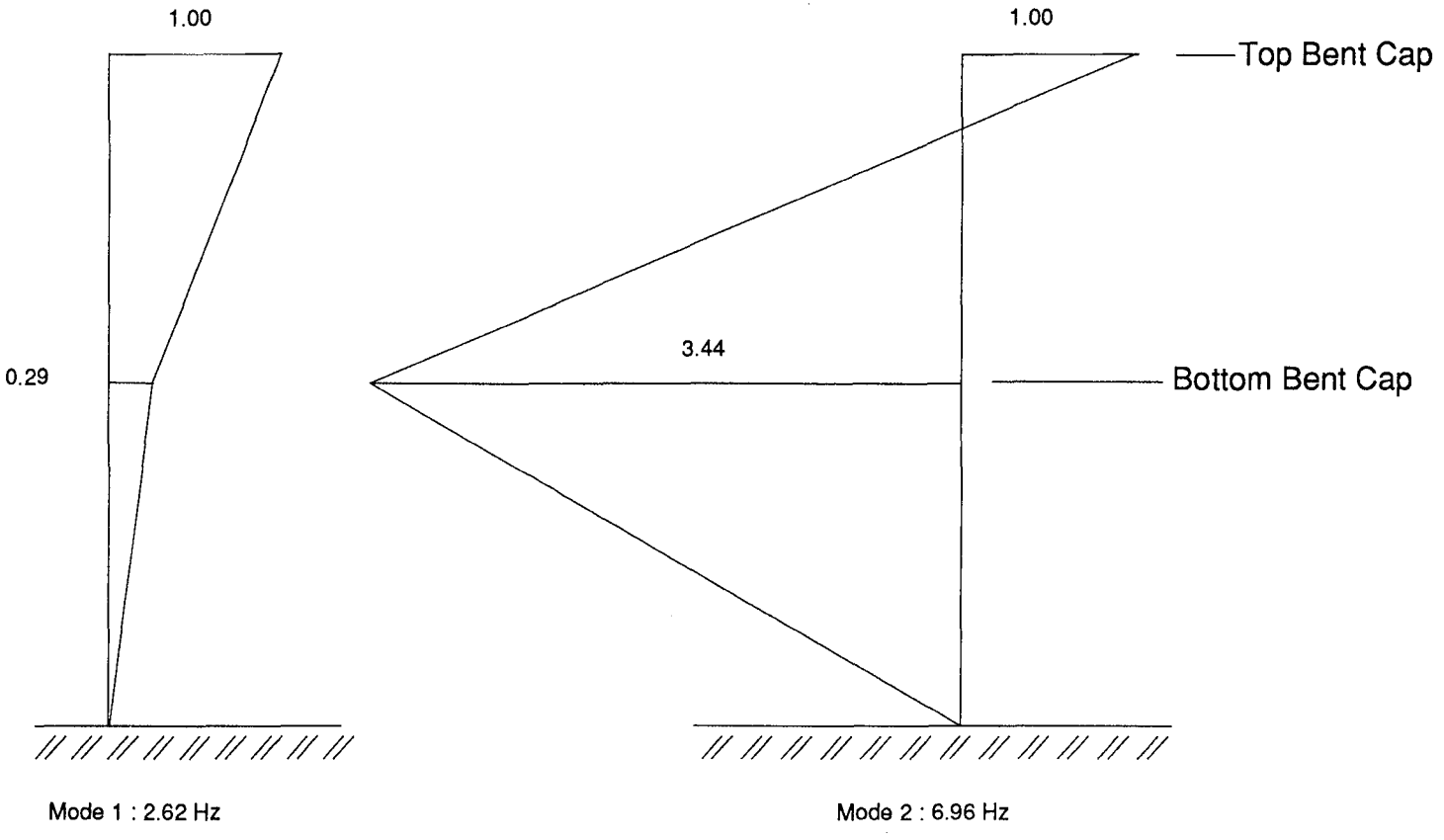

Fig. 4.9 Calculated Mode Shapes of Analytical Model

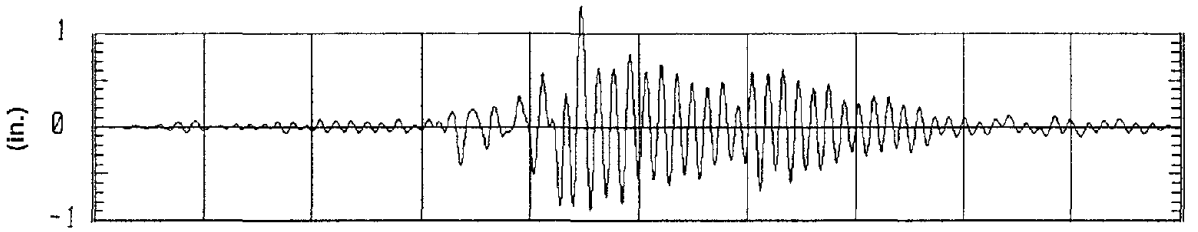

Fig. 4.10 Top displacement history

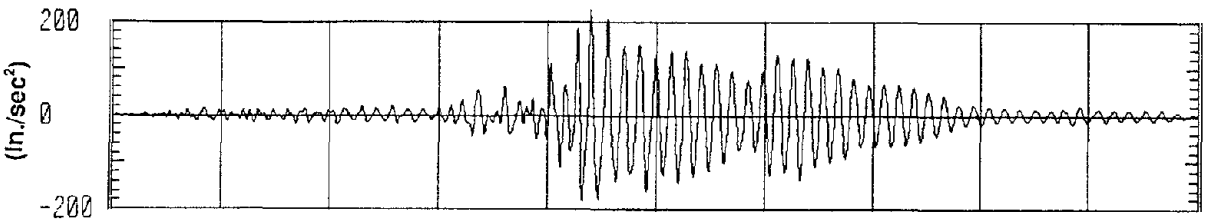

a) Top acceleration history

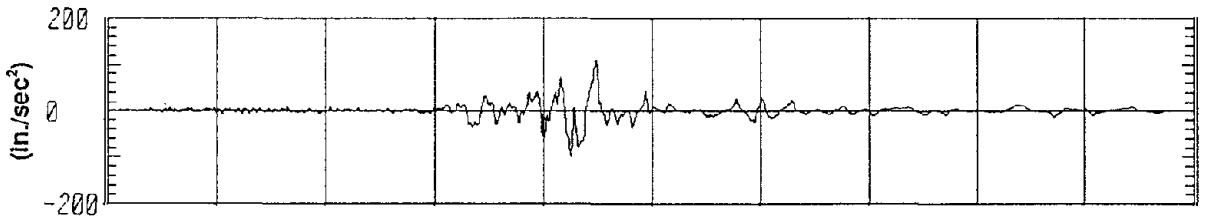

b) Base acceleration history

Fig. 4.11 Acceleration histories

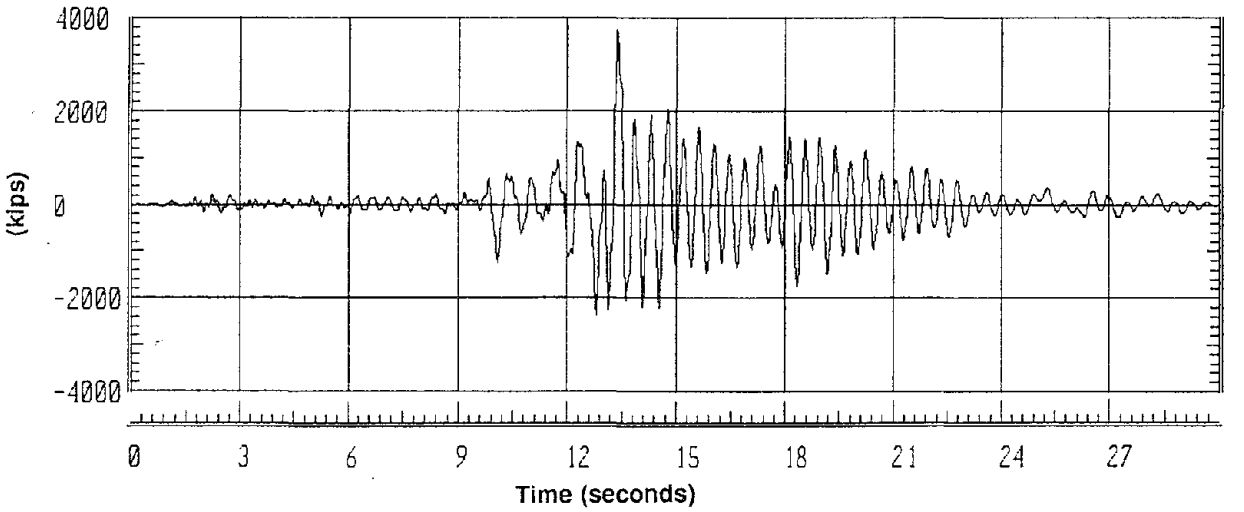

Fig. 4.12 Base shear history

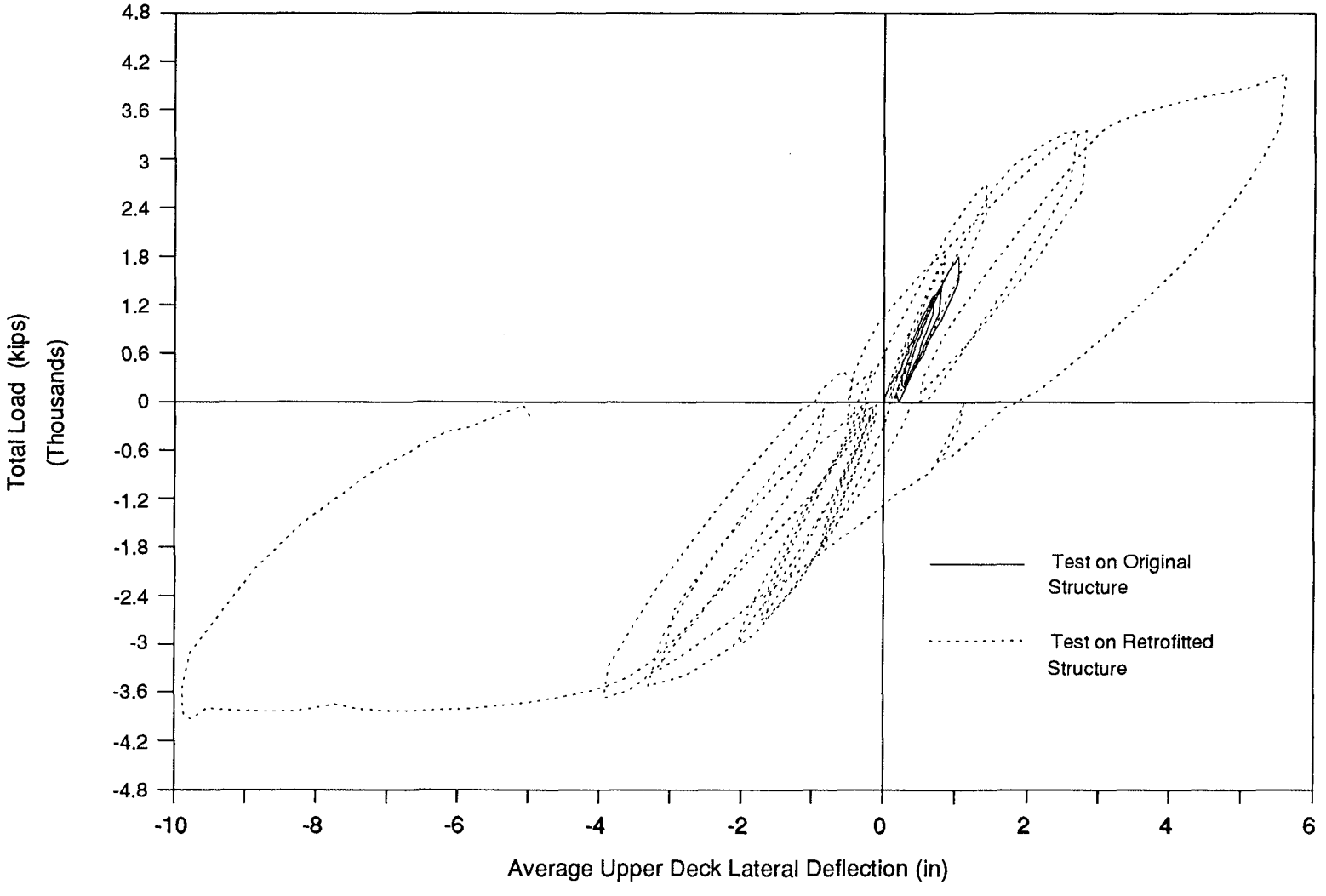

Fig. 4.13 Load-Displacement Relationships: Original and Retrofitted Structures

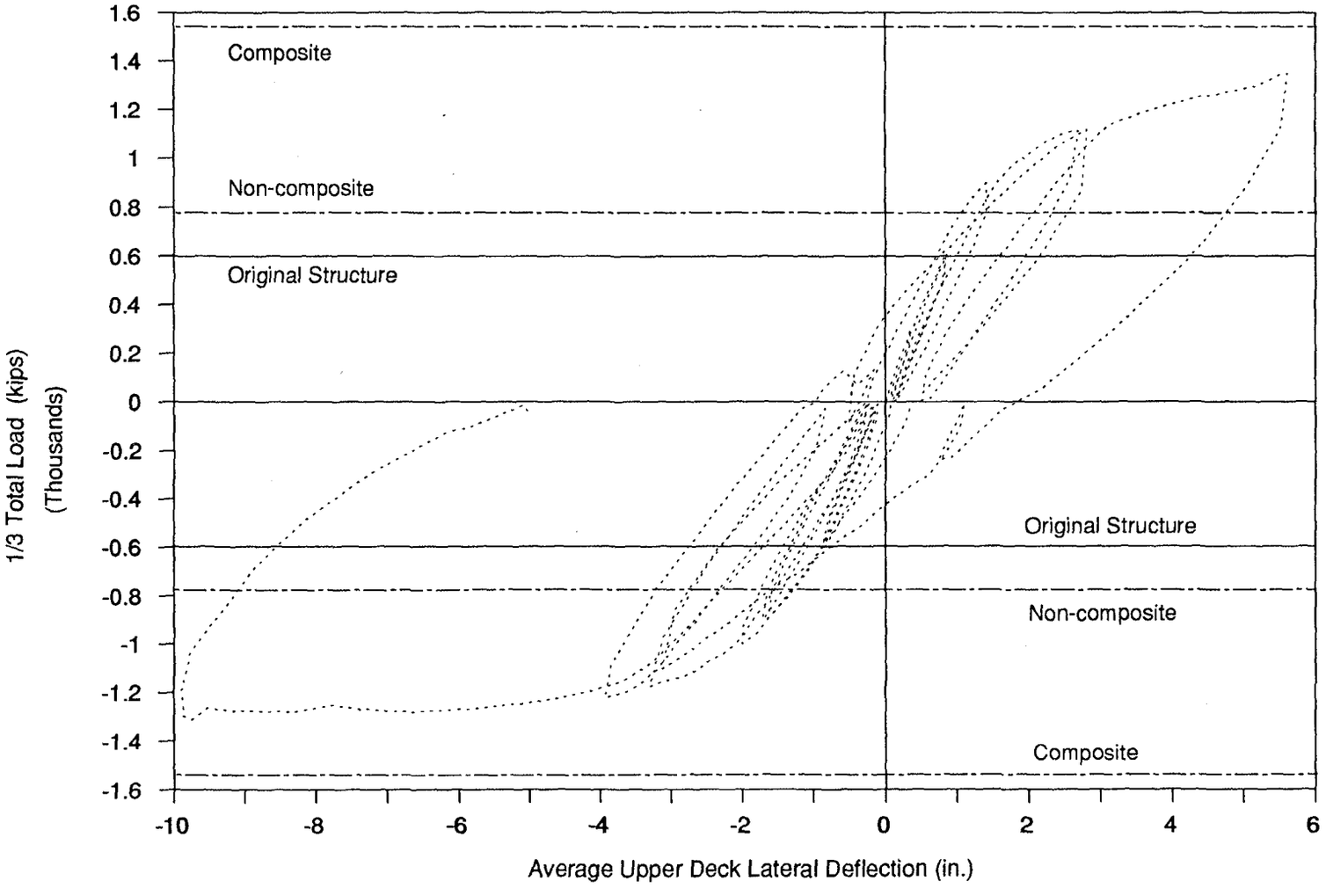

Fig. 4.14 Comparison Between Load-displacement Relationship and Measured and Calculated Strength Levels

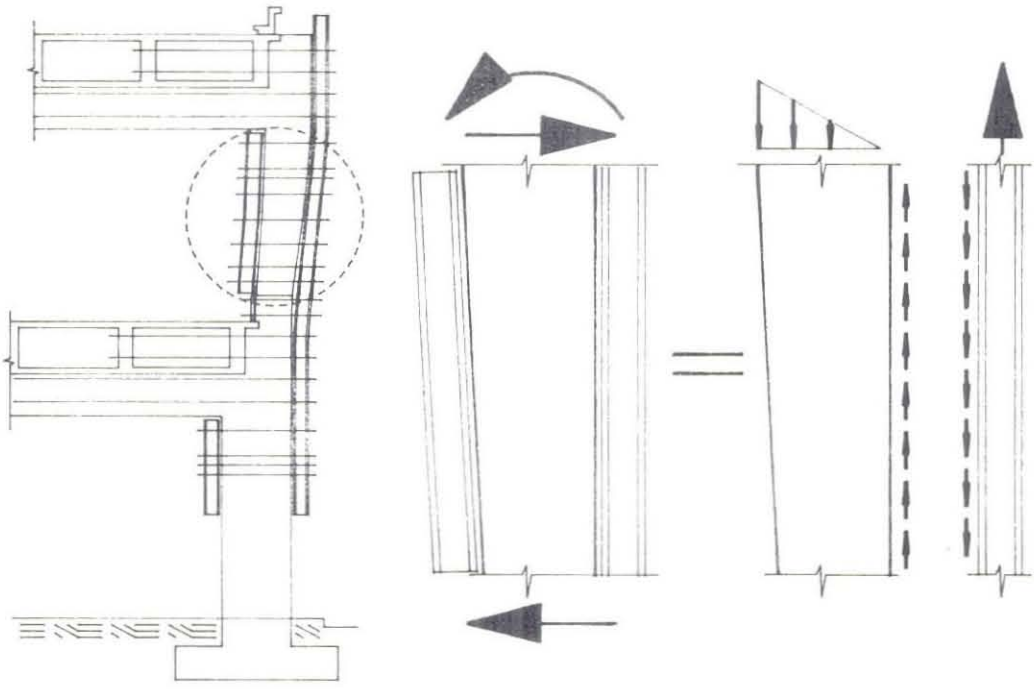

Fig. 4.15 Composite Forces on Bent 45

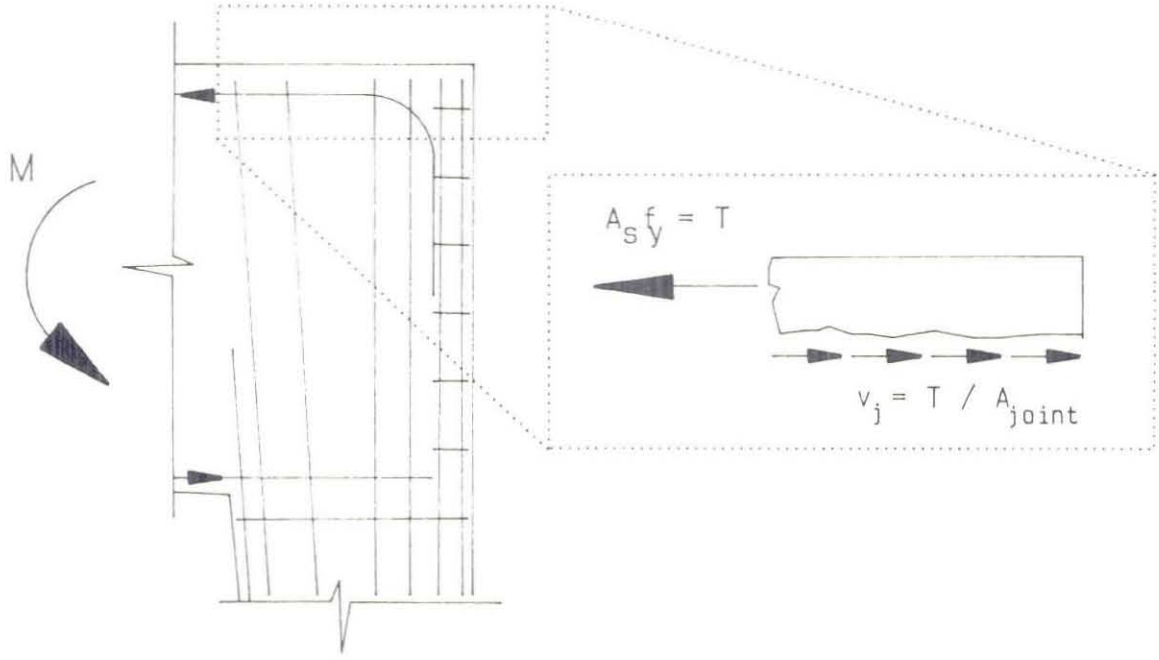

Fig. 4.16 Maximum Shear Stress in Joint

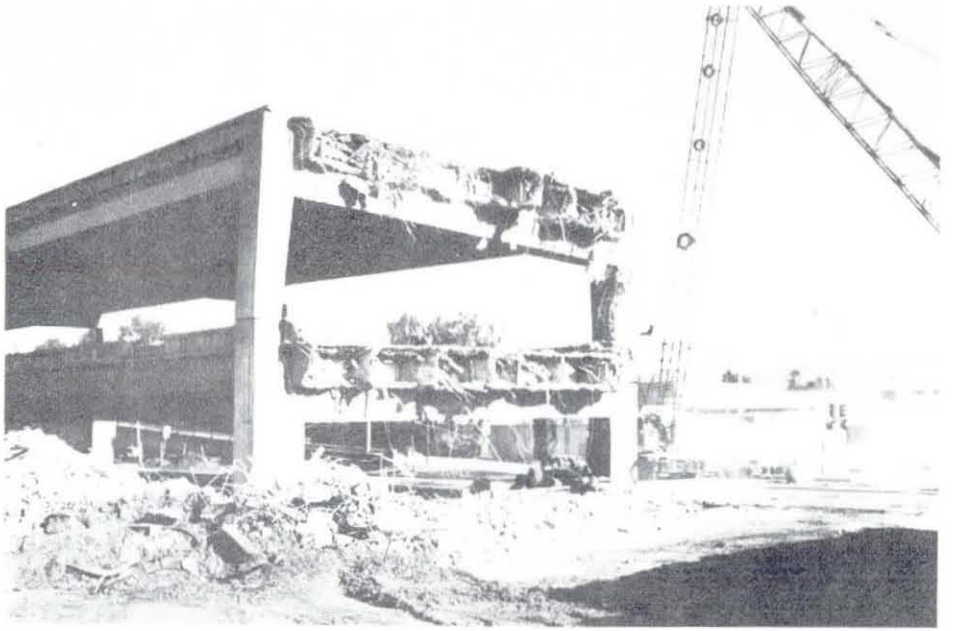

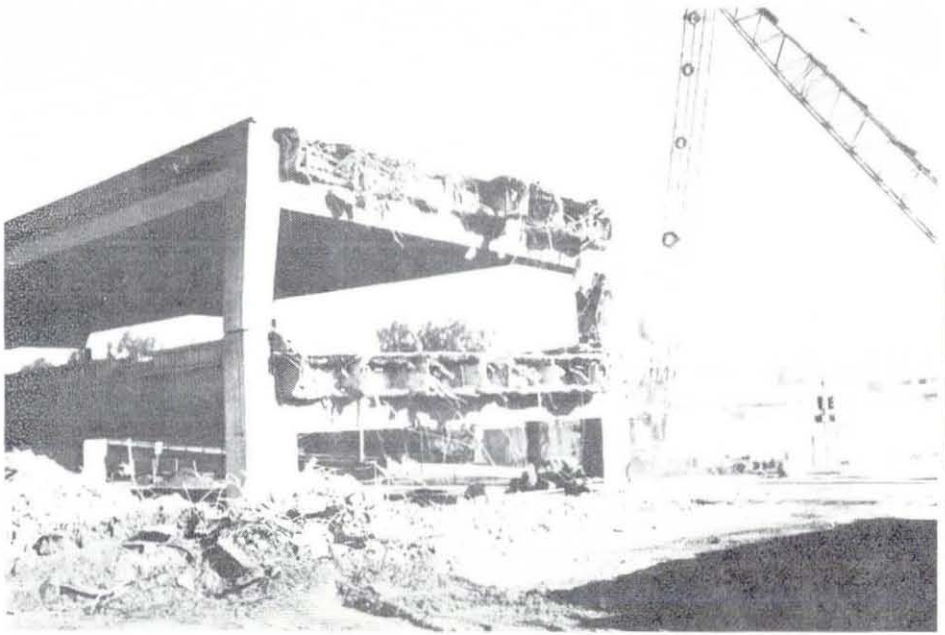

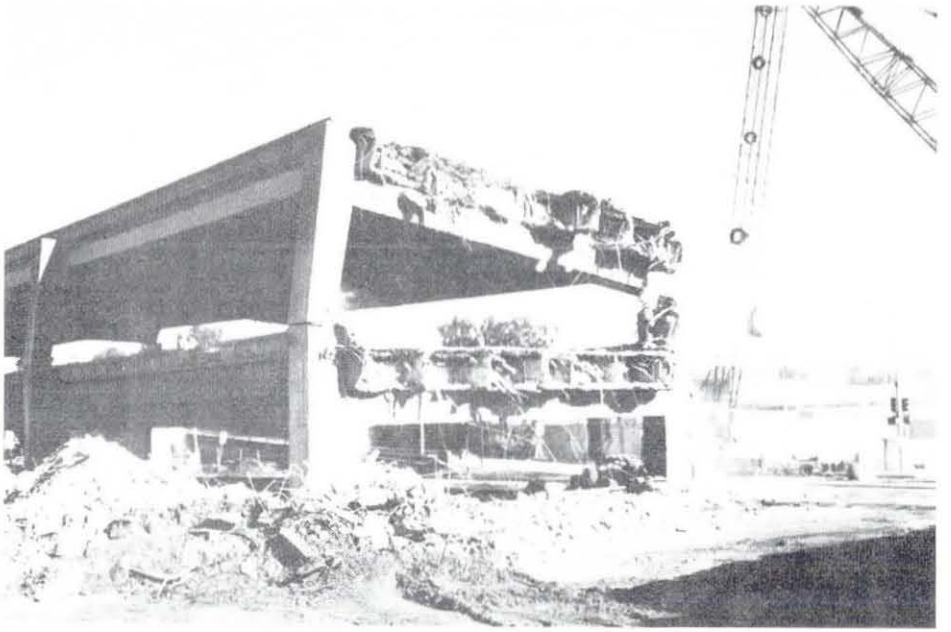

Appendix A: Demolition photo sequence

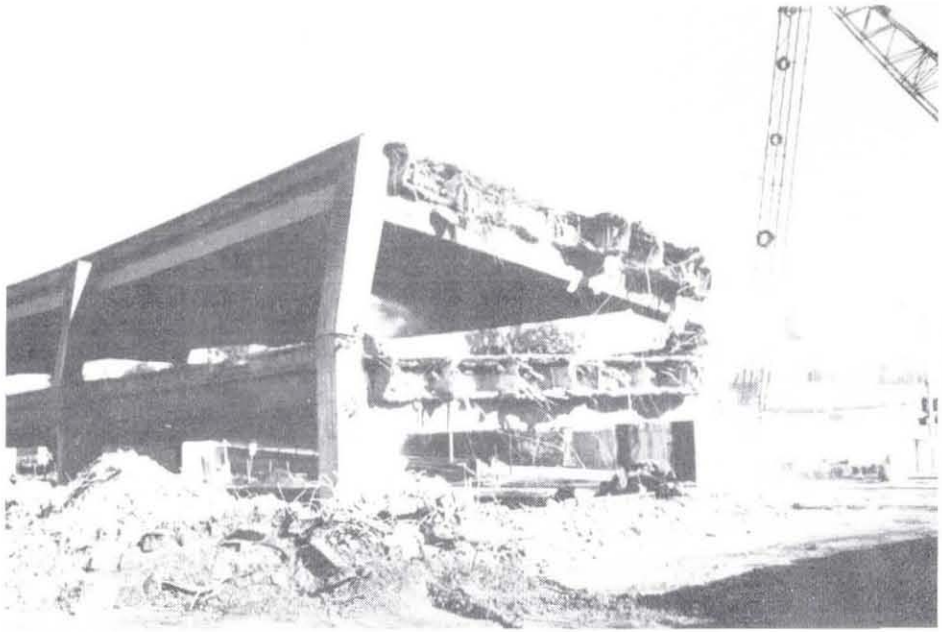

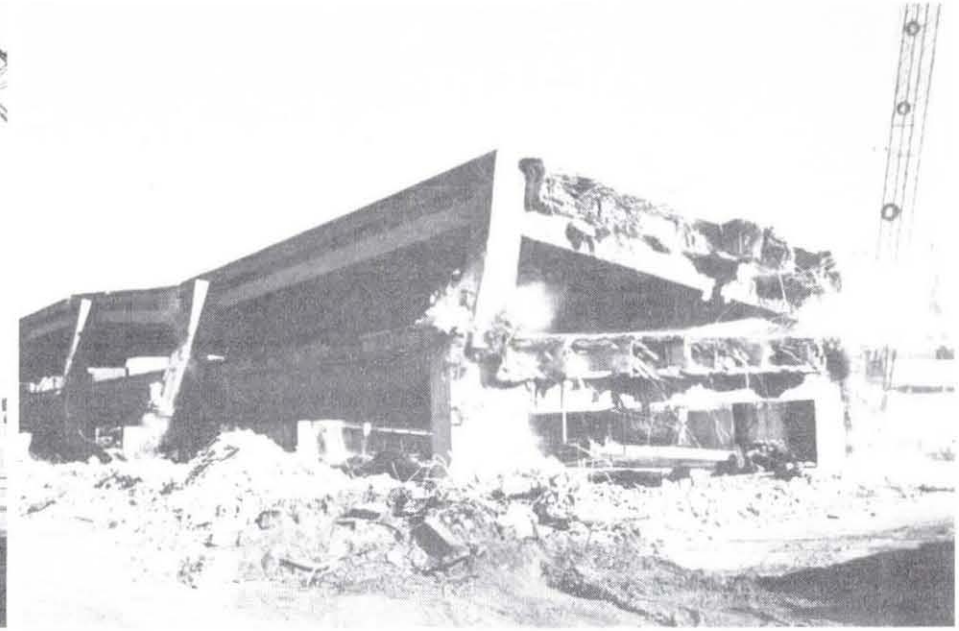

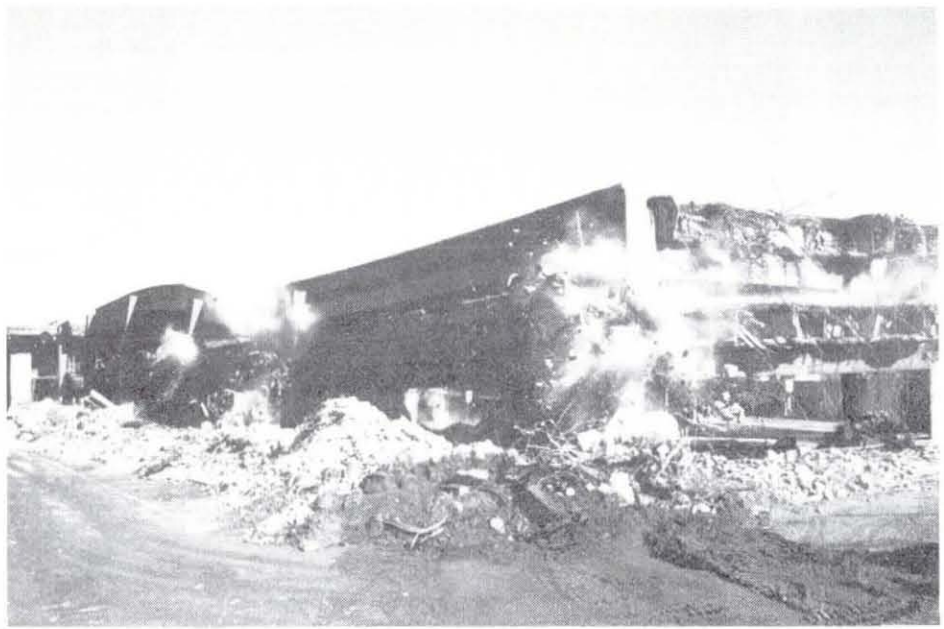

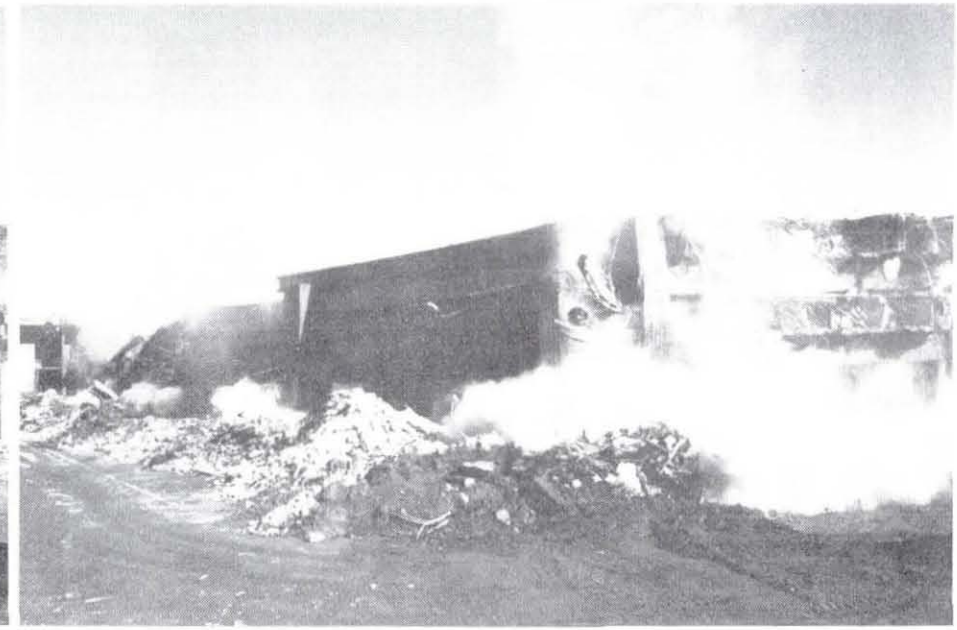

Appendix A: Demolition photo sequence

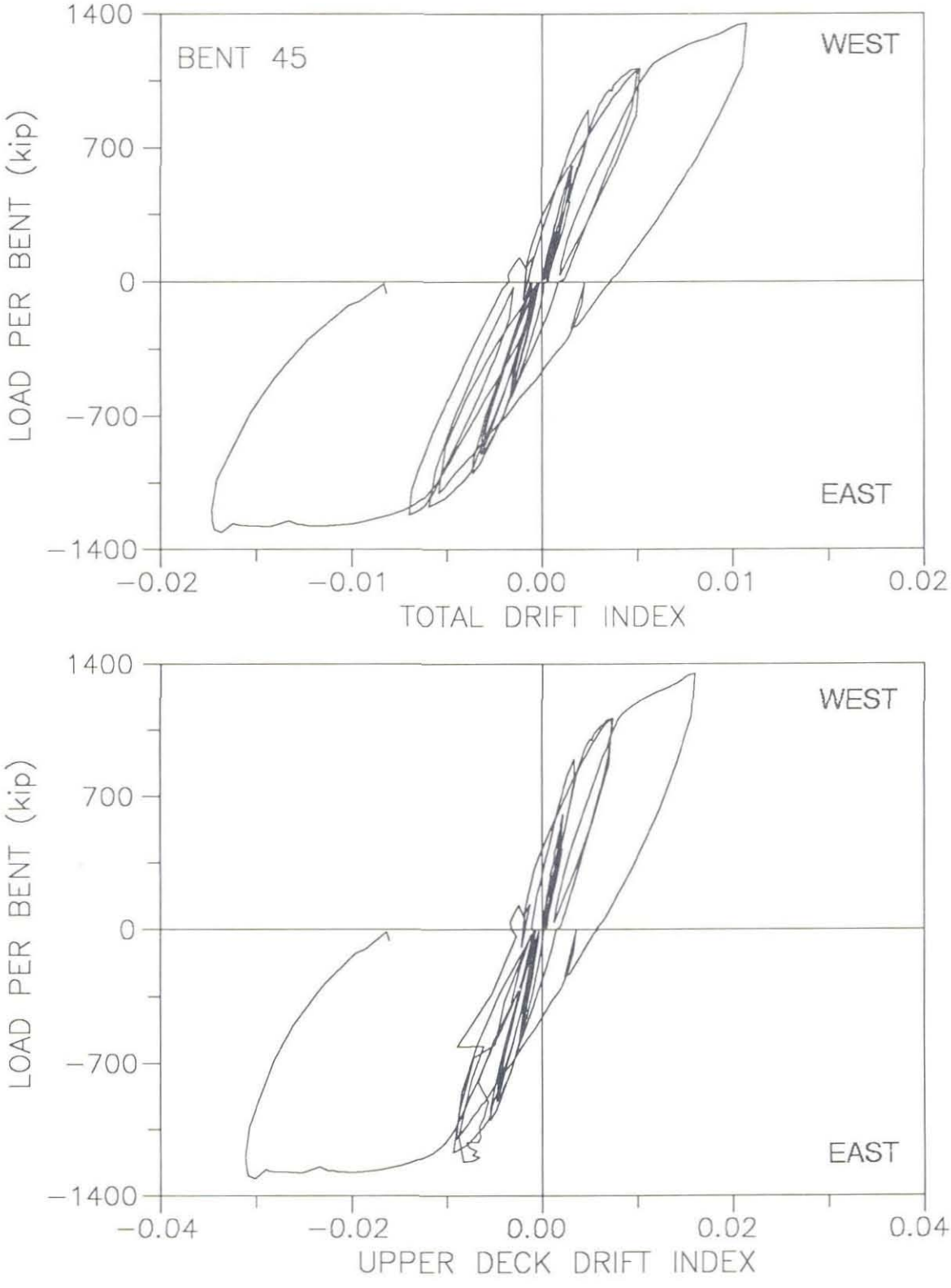
BENT 45
WEST
EAST
1400
700
0
−700
−1400
LOAD PER BENT (kip)
−0.02
−0.01
0.00
0.01
0.02
TOTAL DRIFT INDEX
WEST
EAST
1400
700
0
−700
−1400
LOAD PER BENT (kip)
−0.04
−0.02
0.00
0.02
0.04
UPPER DECK DRIFT INDEX

Fig. B.1

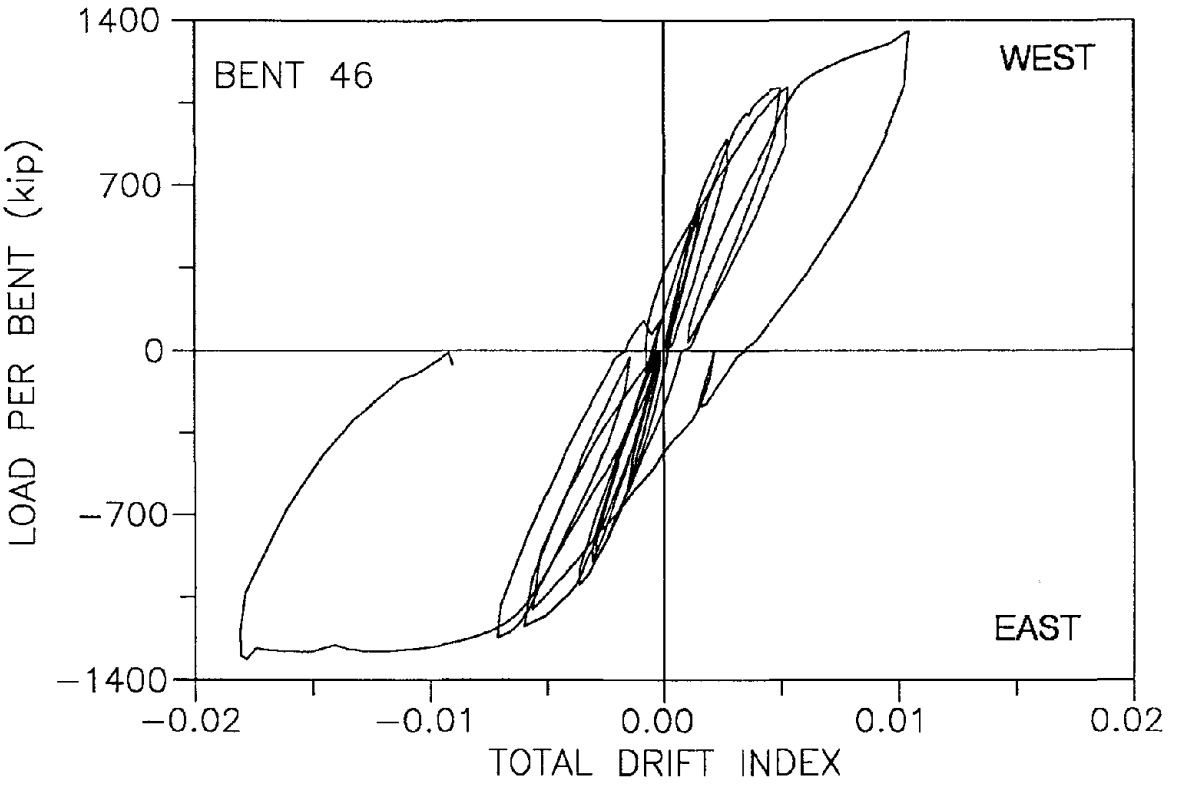
BENT 46
WEST
EAST
1400
700
0
−700
−1400
LOAD PER BENT (kip)
−0.02
−0.01
0.00
0.01
0.02
TOTAL DRIFT INDEX

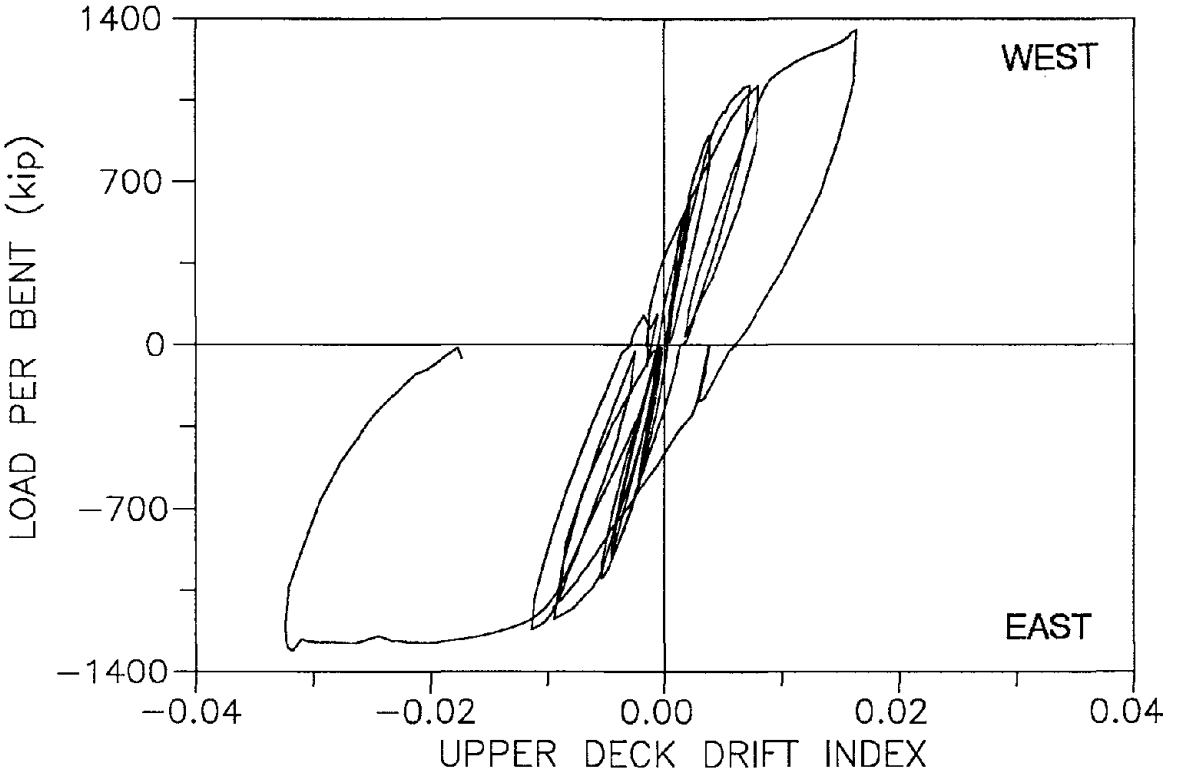
WEST
EAST
1400
700
0
−700
−1400
LOAD PER BENT (kip)
−0.04
−0.02
0.00
0.02
0.04
UPPER DECK DRIFT INDEX

Fig. B.2

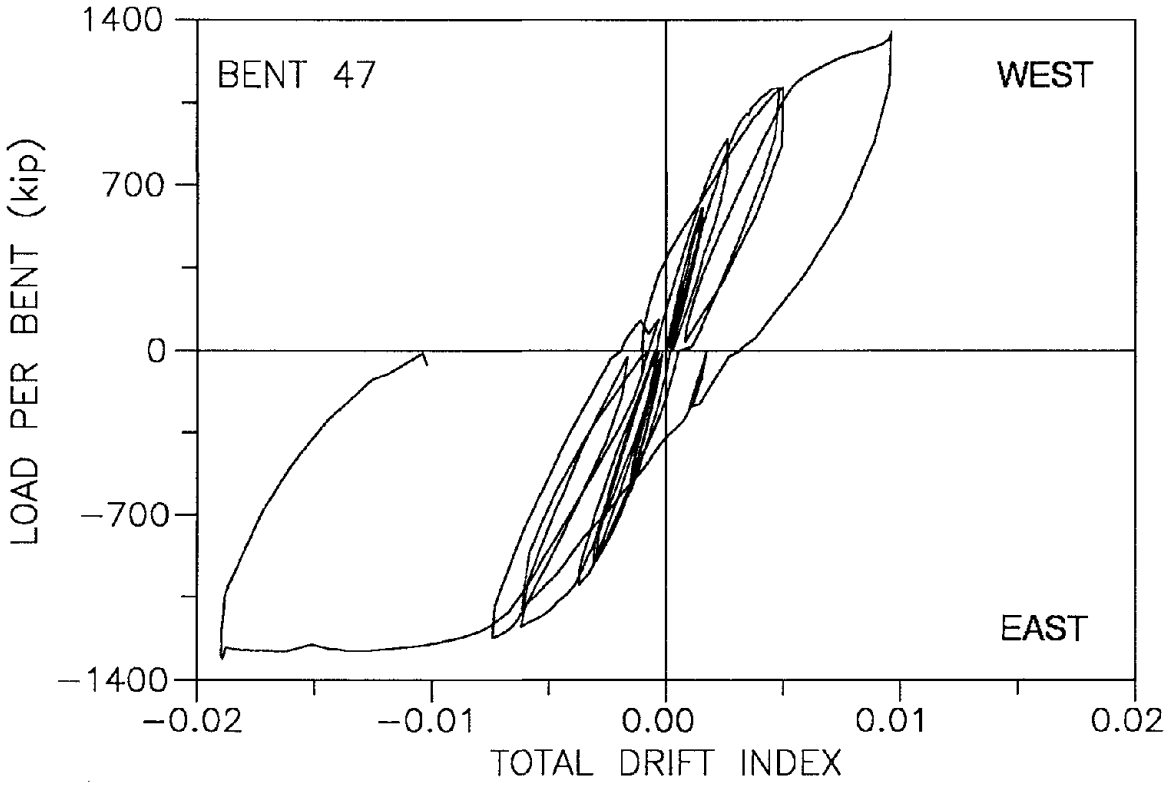
BENT 47
WEST
EAST
1400
700
0
−700
−1400
LOAD PER BENT (kip)
−0.02
−0.01
0.00
0.01
0.02
TOTAL DRIFT INDEX

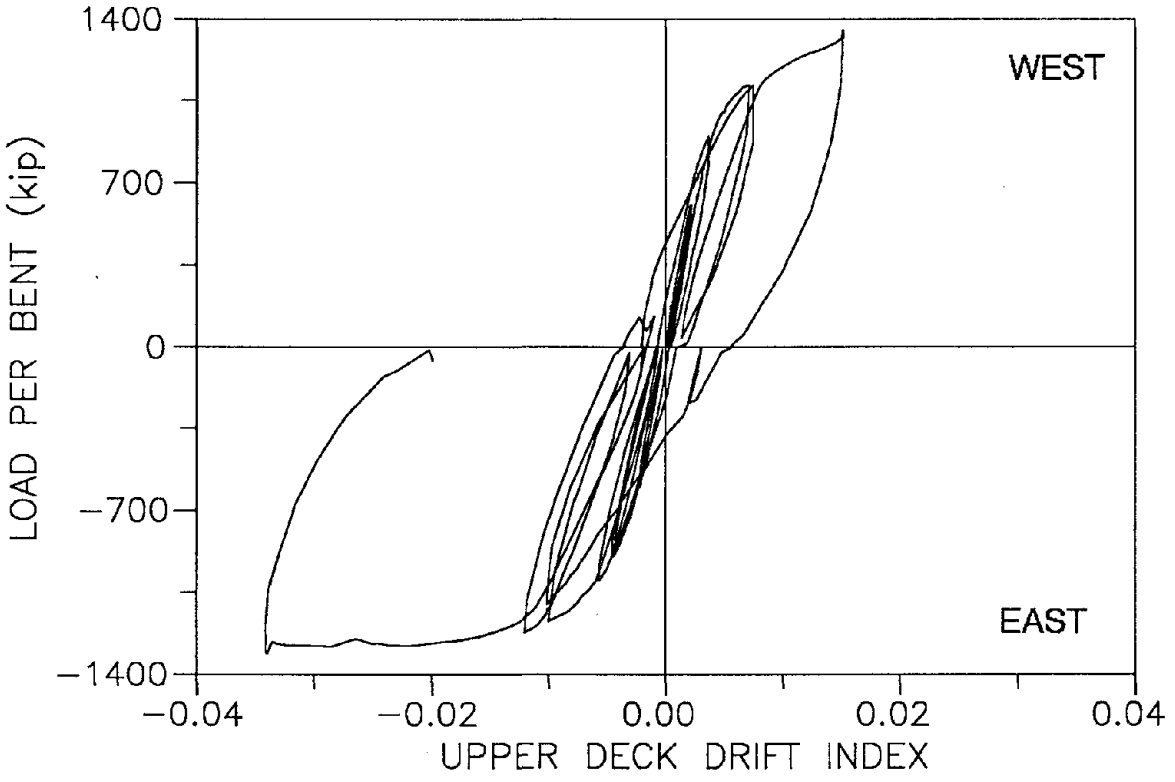
WEST
EAST
1400
700
0
−700
−1400
LOAD PER BENT (kip)
−0.04
−0.02
0.00
0.02
0.04
UPPER DECK DRIFT INDEX

Fig. B.3

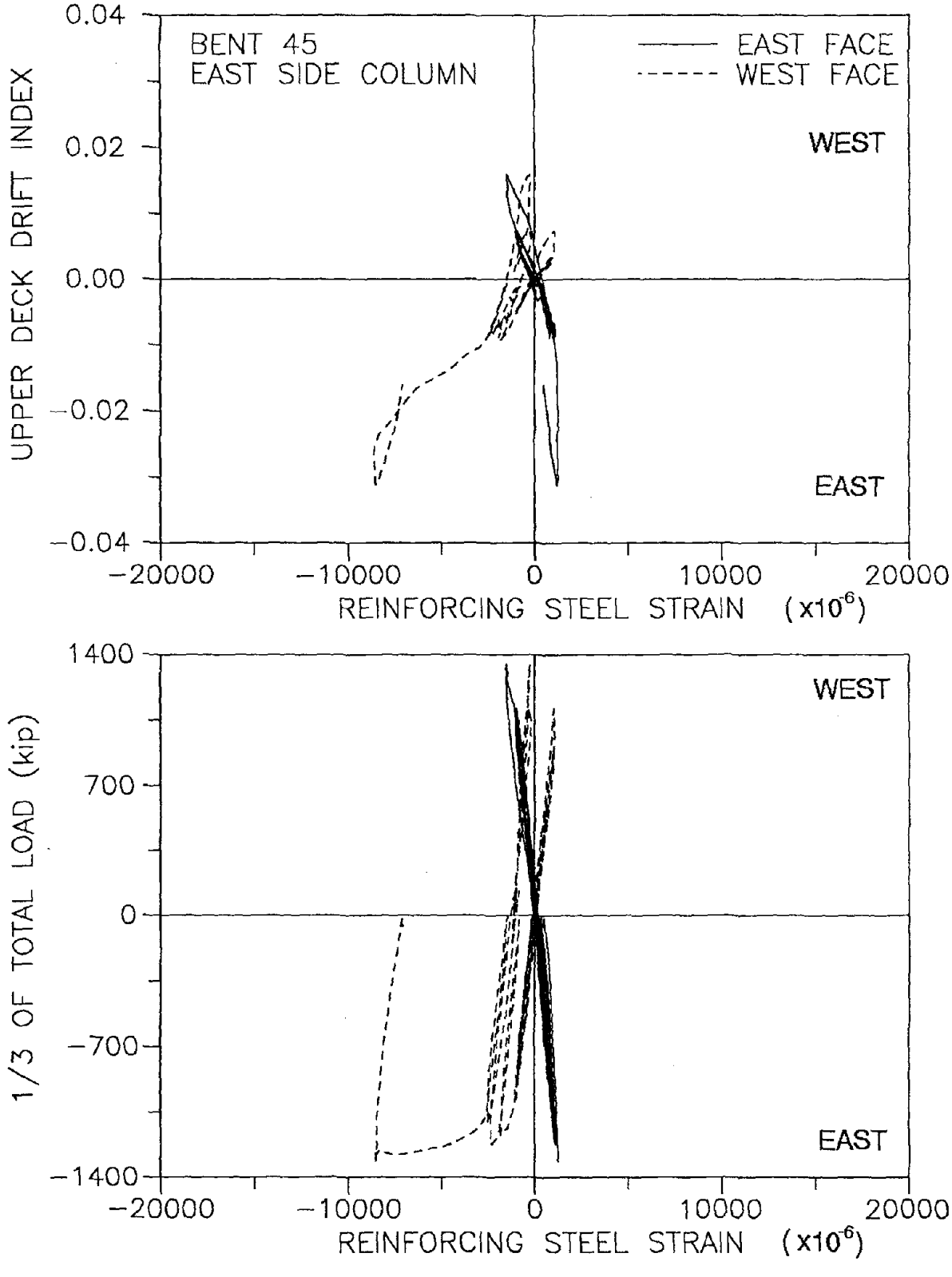
BENT 45
EAST SIDE COLUMN
EAST FACE
WEST FACE
WEST
EAST
UPPER DECK DRIFT INDEX
0.04
0.02
0.00
-0.02
-0.04
-20000
-10000
0
10000
20000
REINFORCING STEEL STRAIN (x10^-6)
1/3 OF TOTAL LOAD (kip)
1400
700
0
-700
-1400
WEST
EAST
-20000
-10000
0
10000
20000
REINFORCING STEEL STRAIN (x10^-6)

Fig. B.4

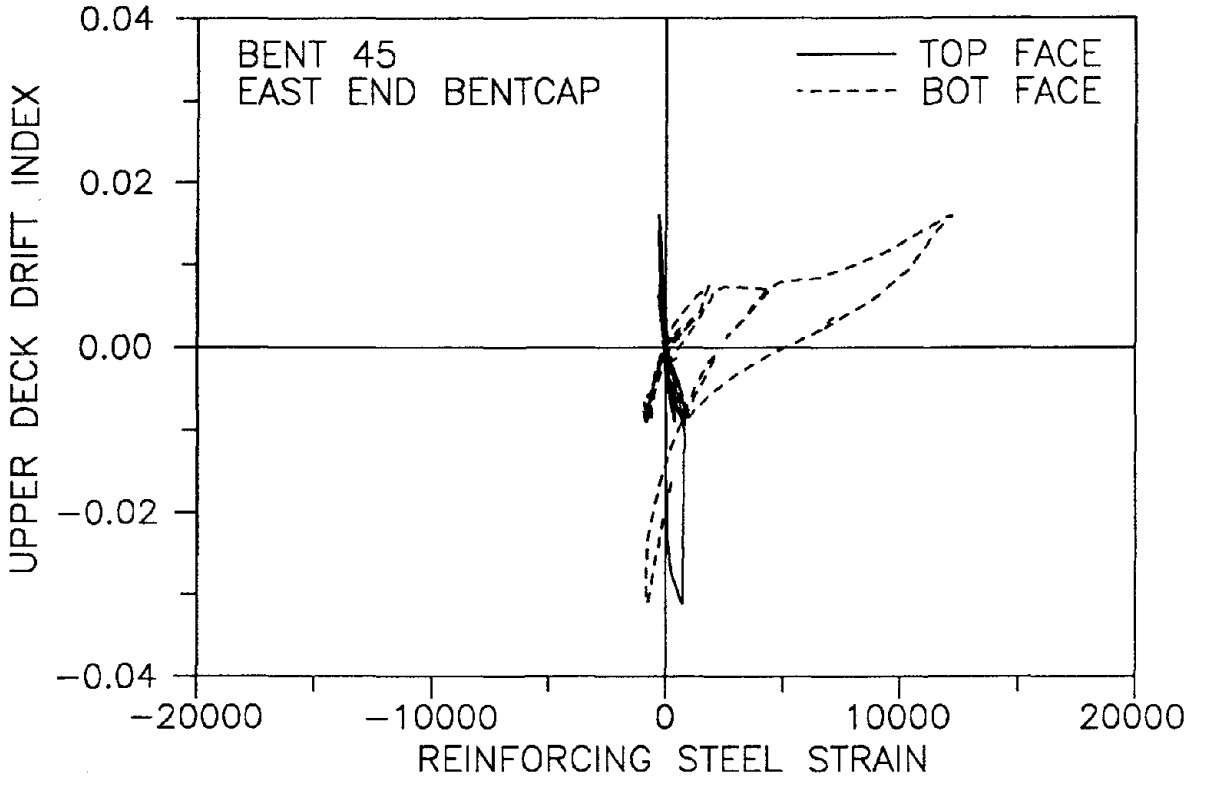
BENT 45
EAST END BENTCAP
TOP FACE
BOT FACE
UPPER DECK DRIFT INDEX
0.04
0.02
0.00
−0.02
−0.04
−20000
−10000
0
10000
20000
REINFORCING STEEL STRAIN

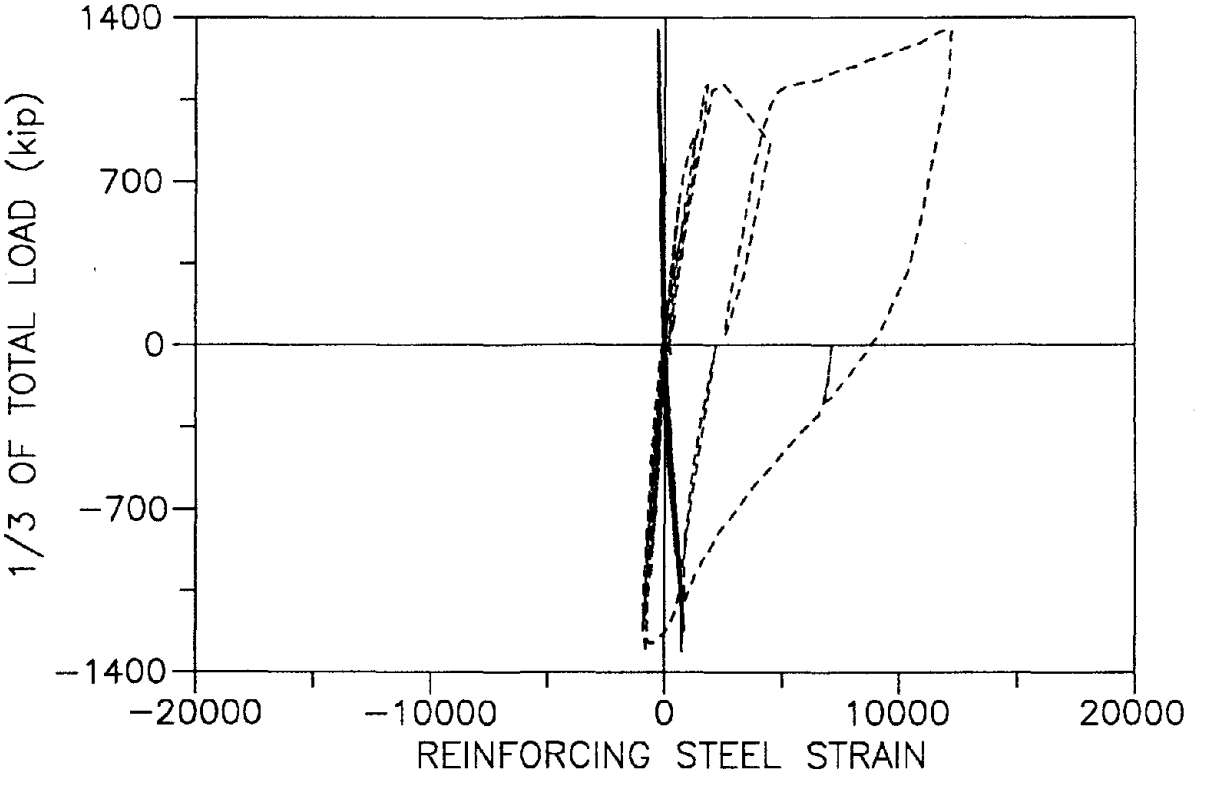
1/3 OF TOTAL LOAD (kip)
1400
700
0
−700
−1400
−20000
−10000
0
10000
20000
REINFORCING STEEL STRAIN

Fig. B.5

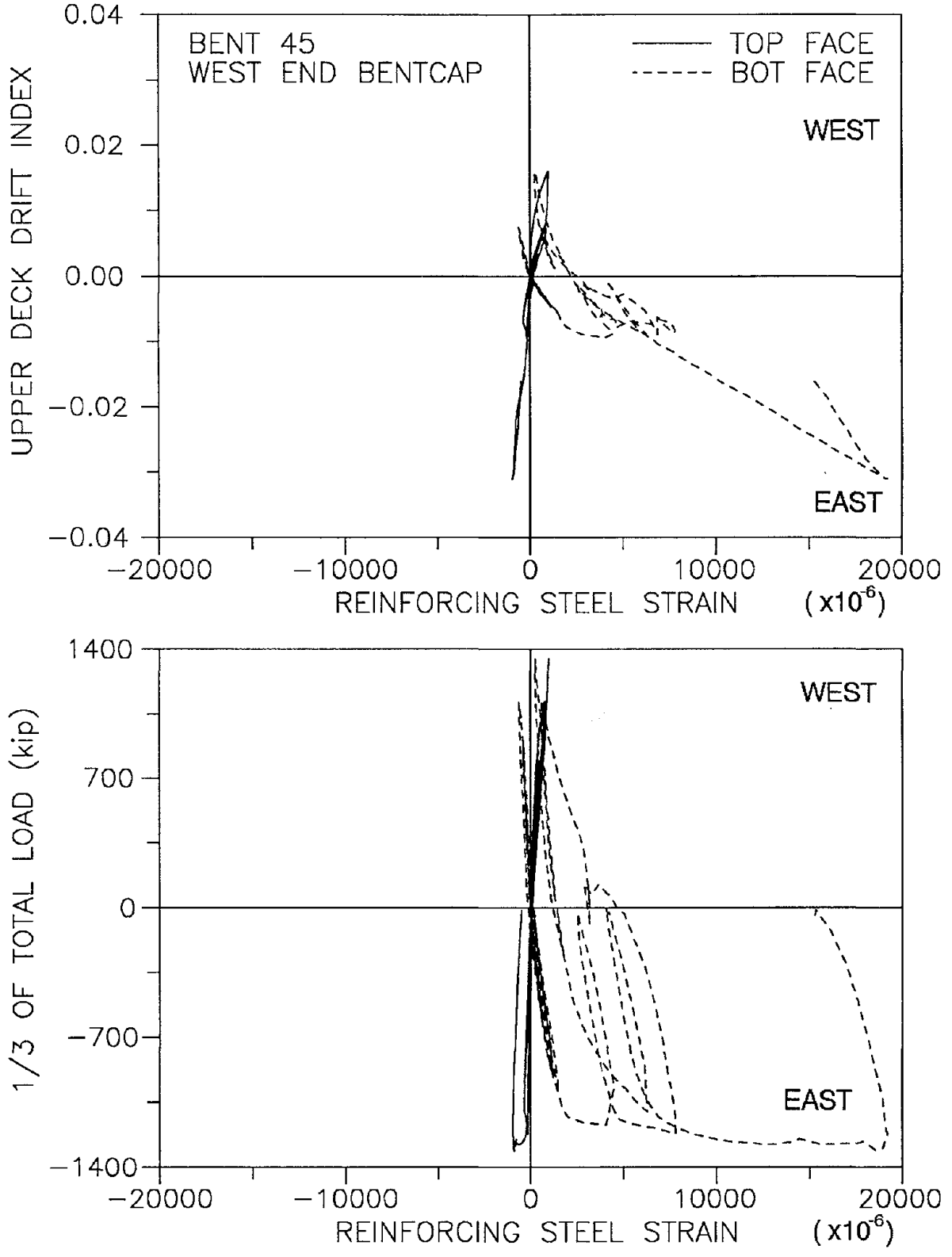
BENT 45
WEST END BENTCAP
TOP FACE
BOT FACE
WEST
EAST
UPPER DECK DRIFT INDEX
0.04
0.02
0.00
−0.02
−0.04
−20000
−10000
0
10000
20000
REINFORCING STEEL STRAIN (x10-6)
1/3 OF TOTAL LOAD (kip)
1400
700
0
−700
−1400
WEST
EAST
−20000
−10000
0
10000
20000
REINFORCING STEEL STRAIN (x10-6)

Fig. B.6

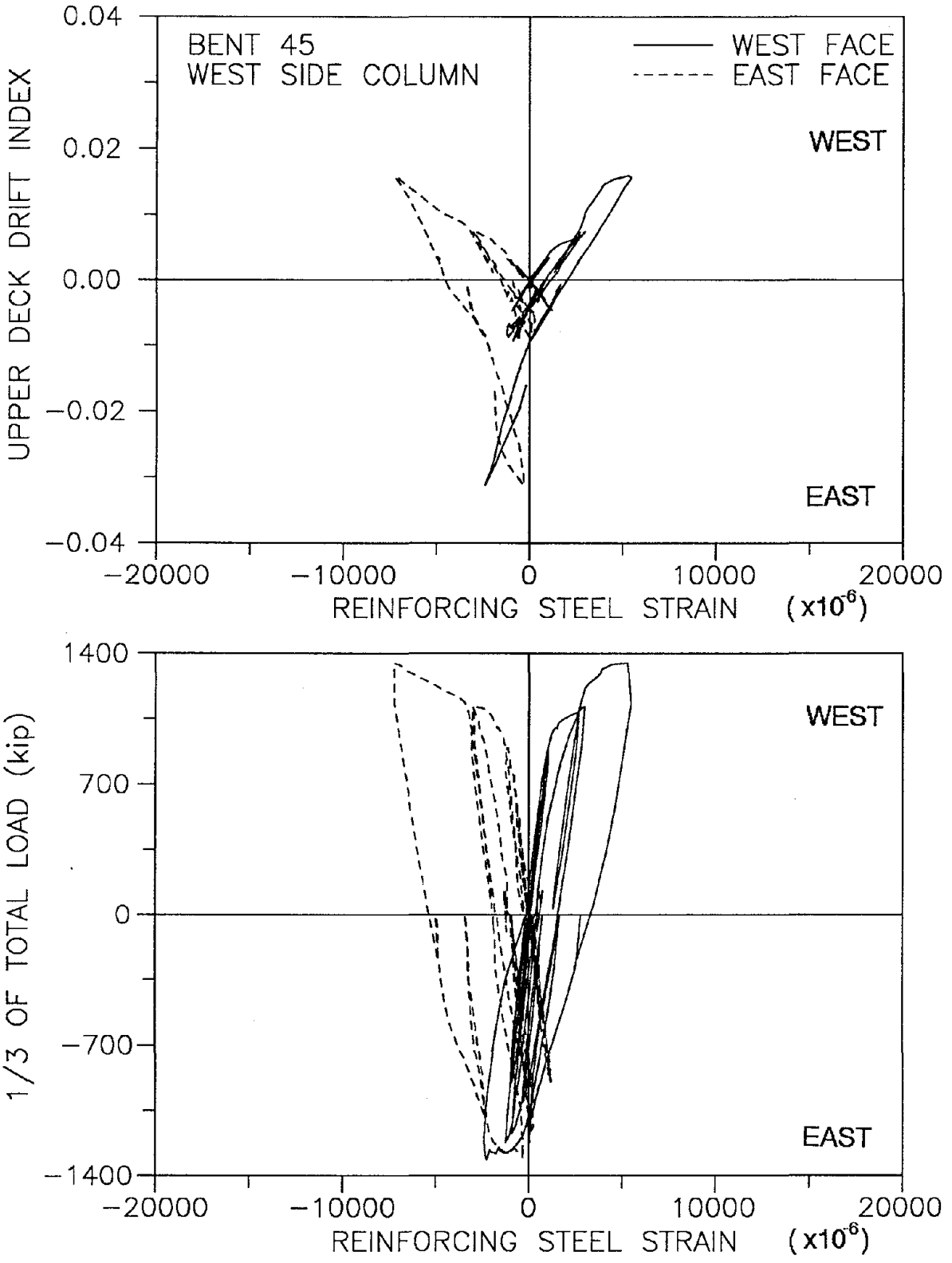
BENT 45
WEST SIDE COLUMN
WEST FACE
EAST FACE
WEST
EAST
UPPER DECK DRIFT INDEX
0.04
0.02
0.00
−0.02
−0.04
−20000
−10000
0
10000
20000
REINFORCING STEEL STRAIN (x10⁻⁶)
1/3 OF TOTAL LOAD (kip)
1400
700
0
−700
−1400
WEST
EAST
−20000
−10000
0
10000
20000
REINFORCING STEEL STRAIN (x10⁻⁶)

Fig. B.7

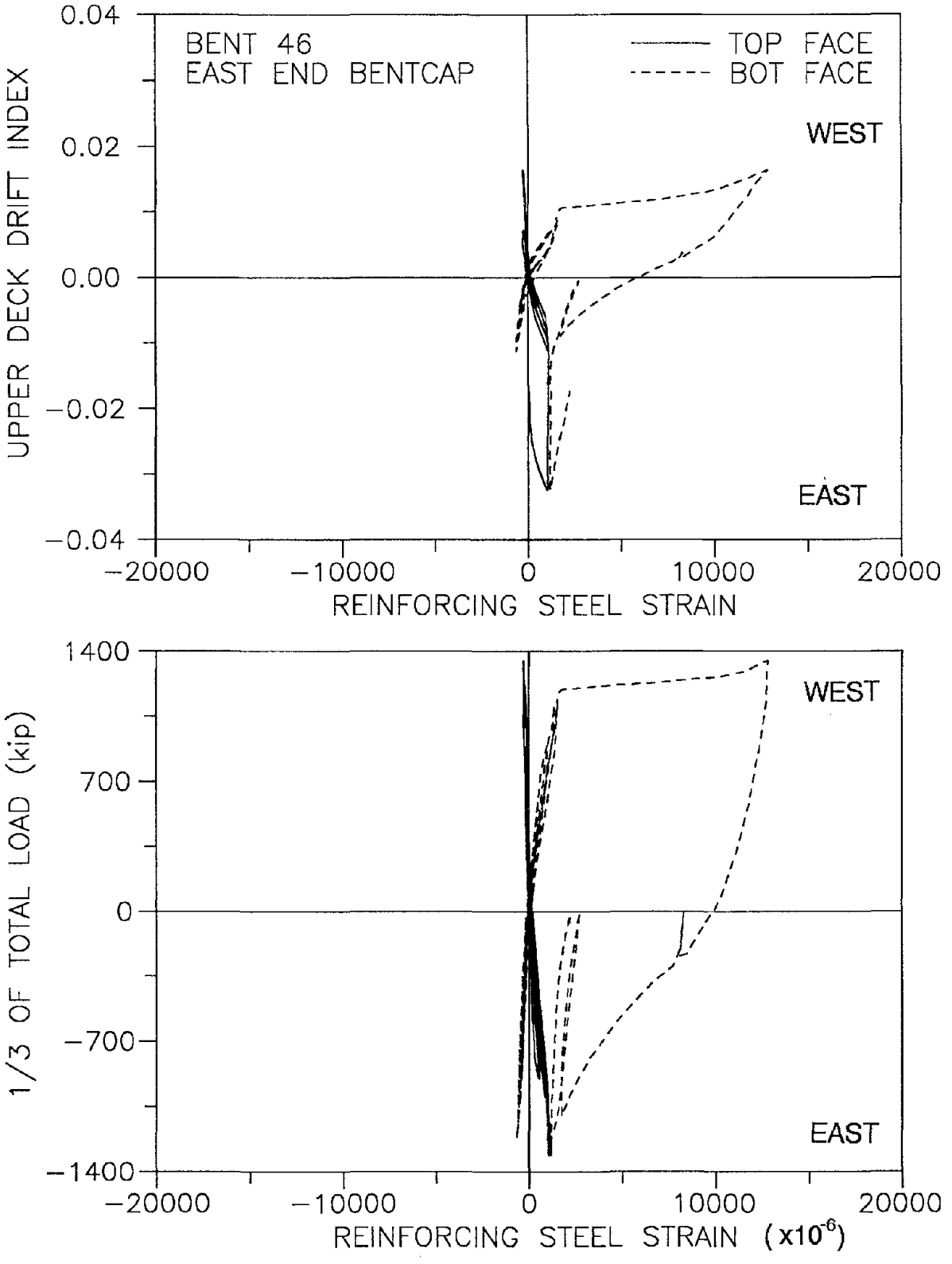
BENT 46
EAST END BENTCAP
TOP FACE
BOT FACE
WEST
EAST
UPPER DECK DRIFT INDEX
0.04
0.02
0.00
−0.02
−0.04
−20000
−10000
0
10000
20000
REINFORCING STEEL STRAIN
1/3 OF TOTAL LOAD (kip)
1400
700
0
−700
−1400
WEST
EAST
REINFORCING STEEL STRAIN (x10-6)

Fig. B.8

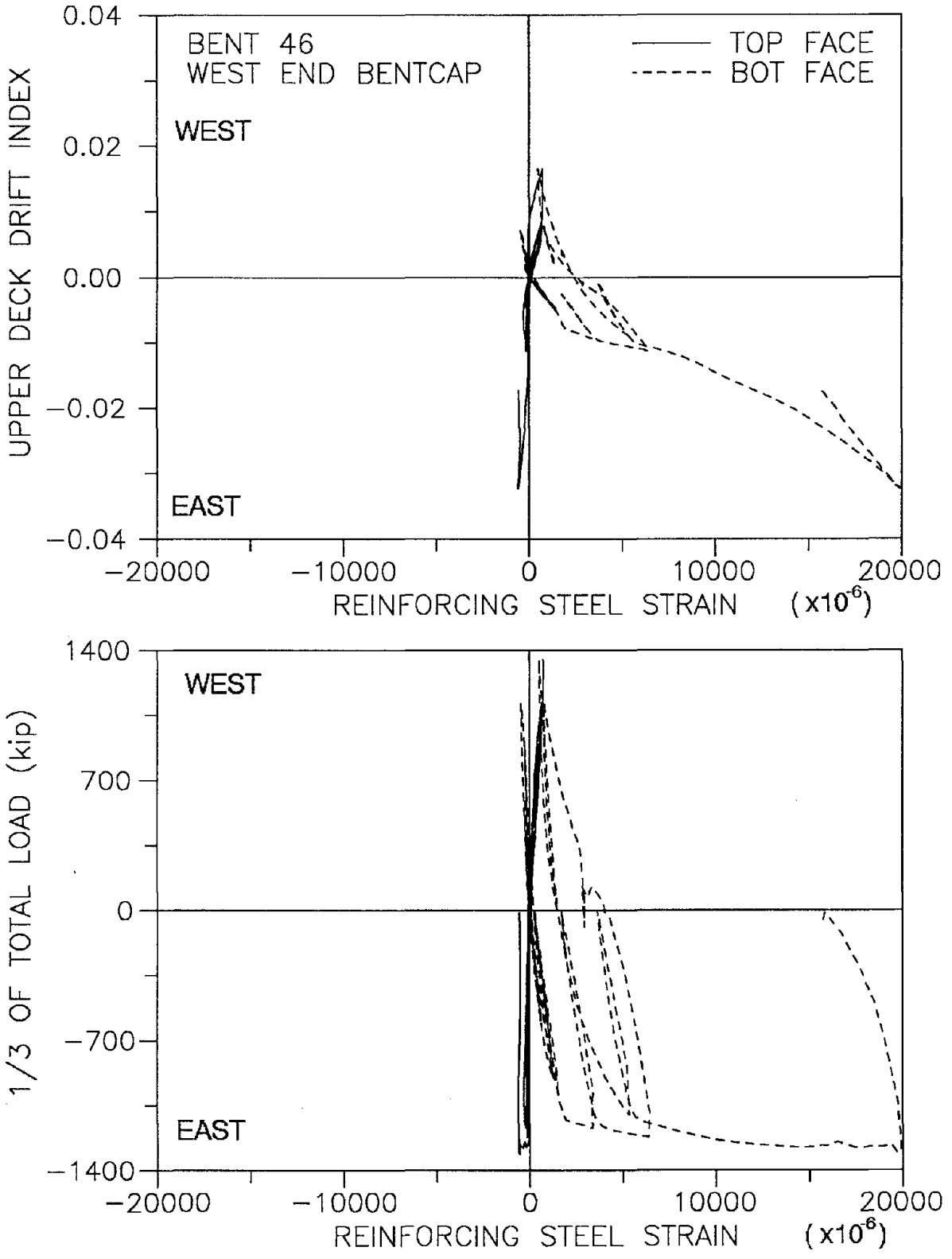
BENT 46
WEST END BENTCAP
TOP FACE
BOT FACE
WEST
EAST
UPPER DECK DRIFT INDEX
0.04
0.02
0.00
−0.02
−0.04
−20000
−10000
0
10000
20000
REINFORCING STEEL STRAIN (x10⁻⁶)
WEST
EAST
1/3 OF TOTAL LOAD (kip)
1400
700
0
−700
−1400
−20000
−10000
0
10000
20000
REINFORCING STEEL STRAIN (x10⁻⁶)

Fig. B.9

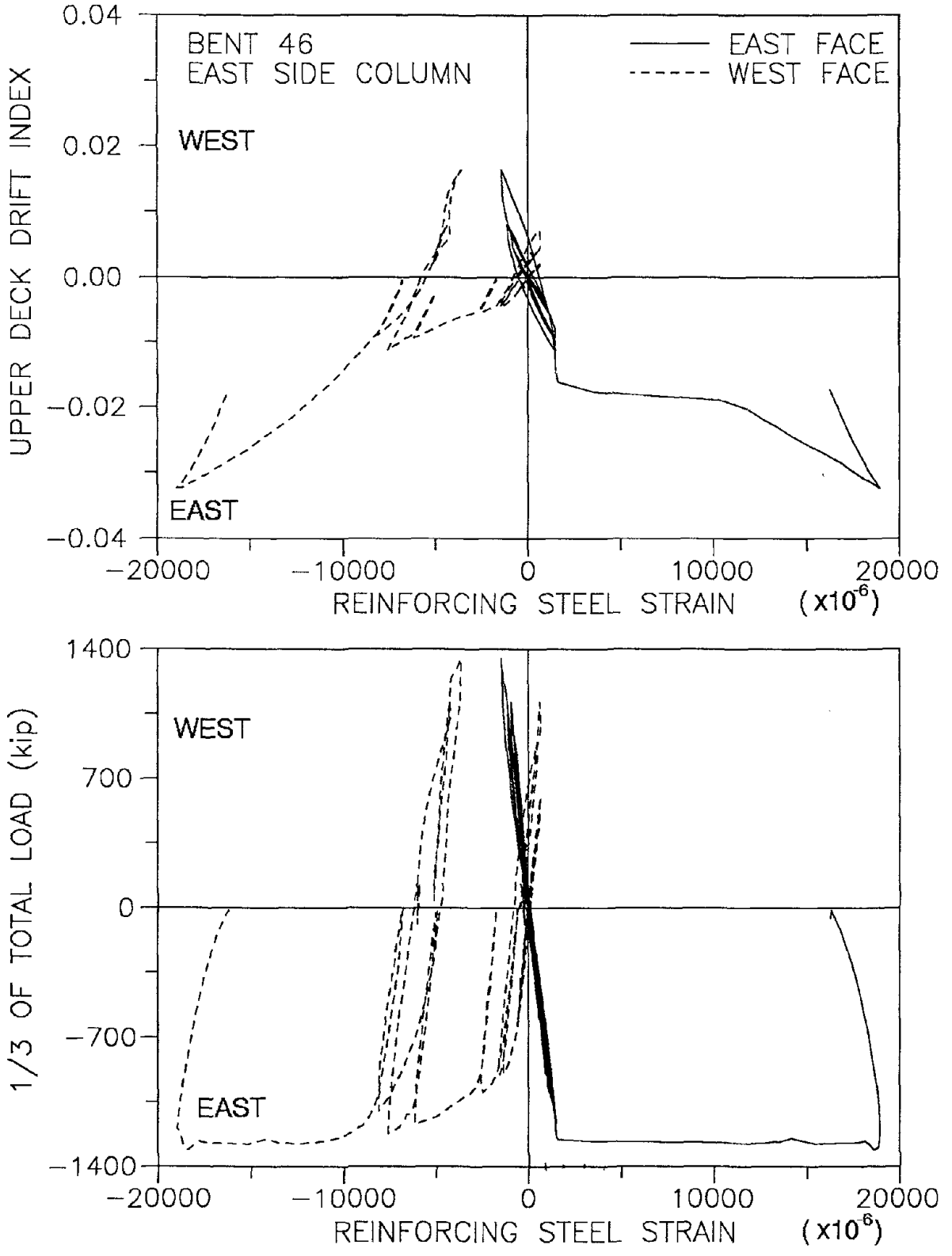
BENT 46
EAST SIDE COLUMN
EAST FACE
WEST FACE
WEST
EAST
UPPER DECK DRIFT INDEX
0.04
0.02
0.00
−0.02
−0.04
−20000
−10000
0
10000
20000
REINFORCING STEEL STRAIN (x10⁻⁶)
1/3 OF TOTAL LOAD (kip)
1400
700
0
−700
−1400
WEST
EAST
−20000
−10000
0
10000
20000
REINFORCING STEEL STRAIN (x10⁻⁶)

Fig. B.10

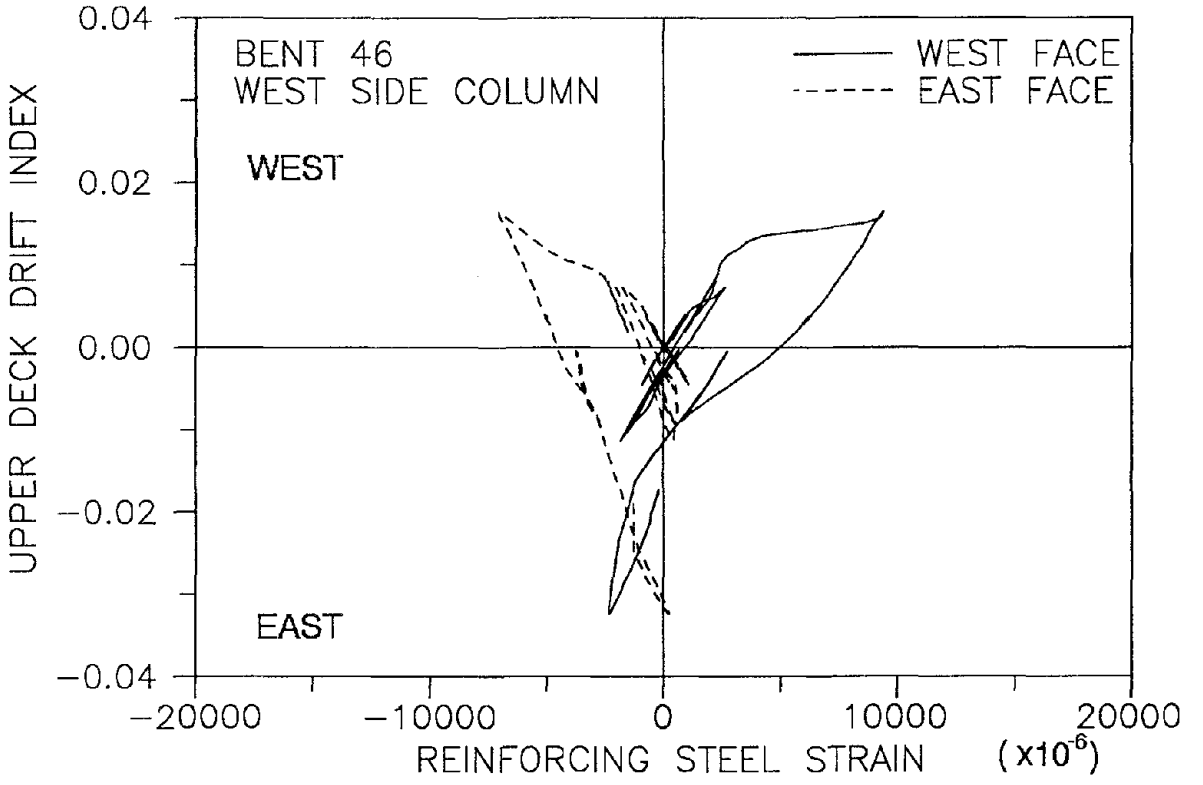
BENT 46
WEST SIDE COLUMN
WEST FACE
EAST FACE
WEST
EAST
UPPER DECK DRIFT INDEX
0.04
0.02
0.00
-0.02
-0.04
-20000
-10000
0
10000
20000
REINFORCING STEEL STRAIN (x10-6)

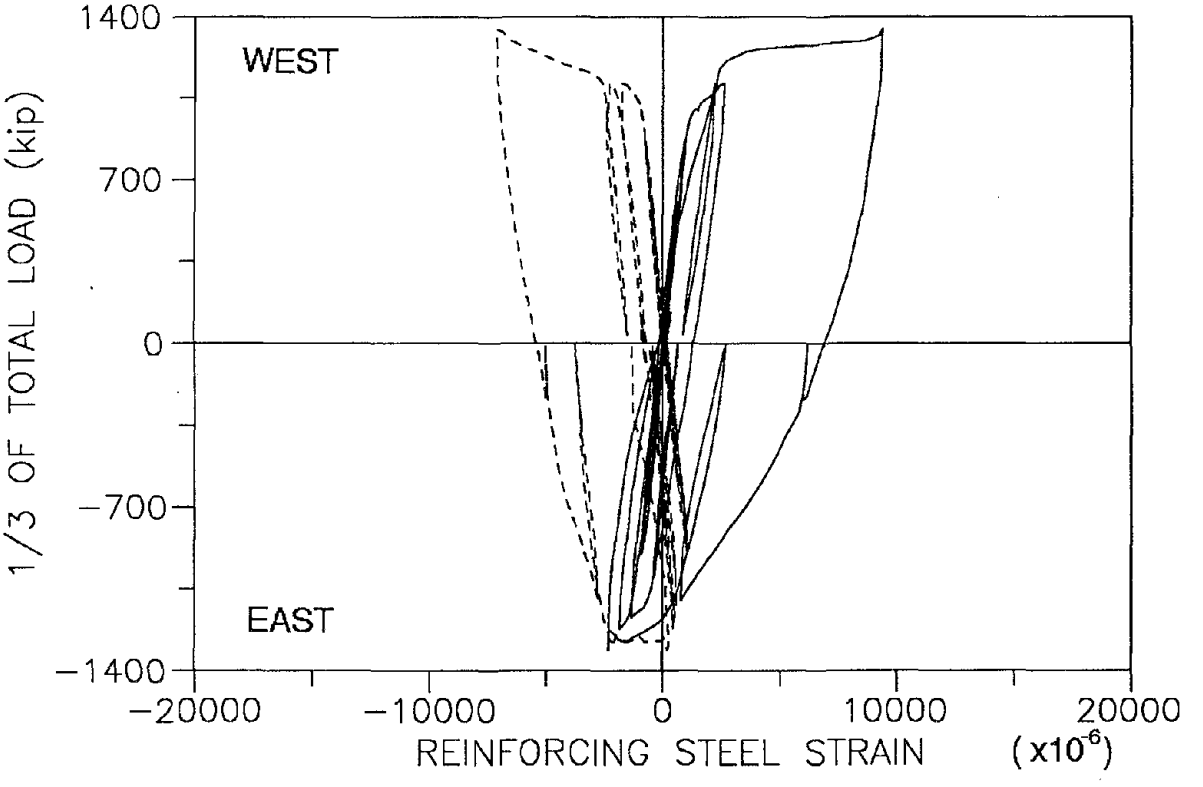
WEST
EAST
1/3 OF TOTAL LOAD (kip)
1400
700
0
-700
-1400
-20000
-10000
0
10000
20000
REINFORCING STEEL STRAIN (x10-6)

Fig. B.11

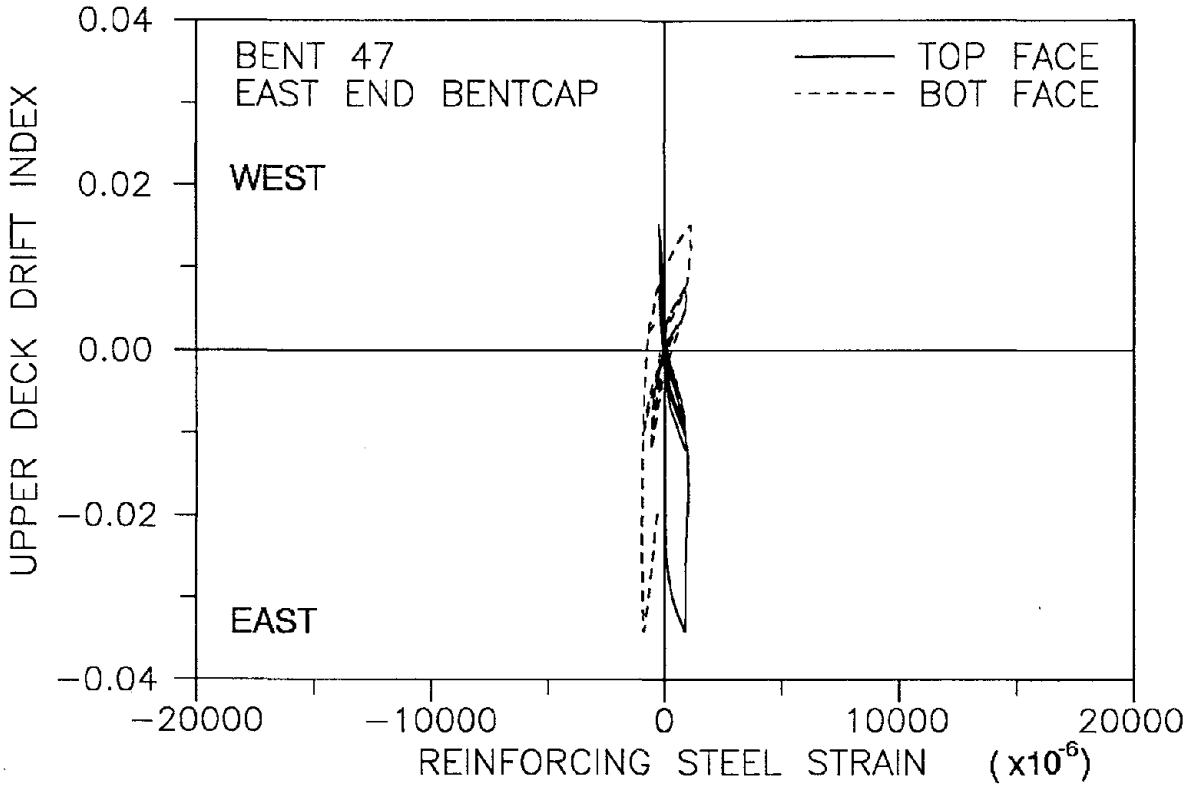
BENT 47
EAST END BENTCAP
TOP FACE
BOT FACE
WEST
EAST
UPPER DECK DRIFT INDEX
0.04
0.02
0.00
−0.02
−0.04
−20000
−10000
0
10000
20000
REINFORCING STEEL STRAIN (x10⁻⁶)

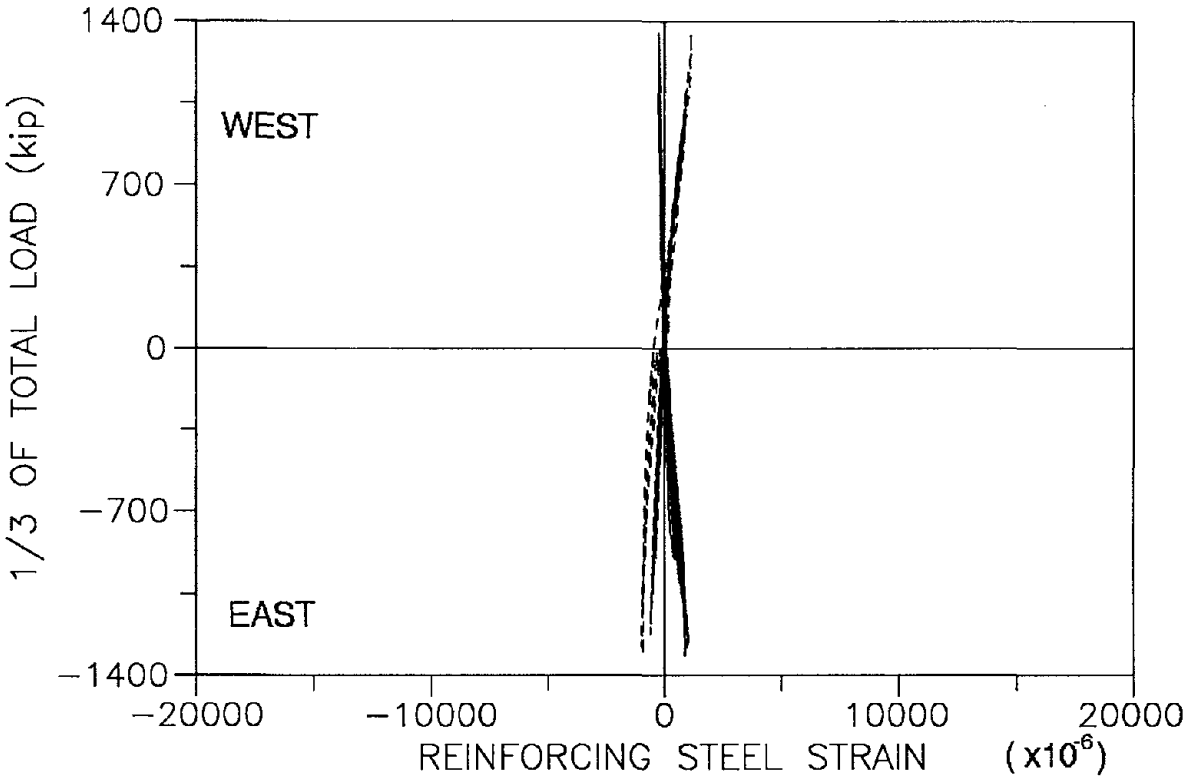
WEST
EAST
1/3 OF TOTAL LOAD (kip)
1400
700
0
−700
−1400
−20000
−10000
0
10000
20000
REINFORCING STEEL STRAIN (x10⁻⁶)

Fig. B.12

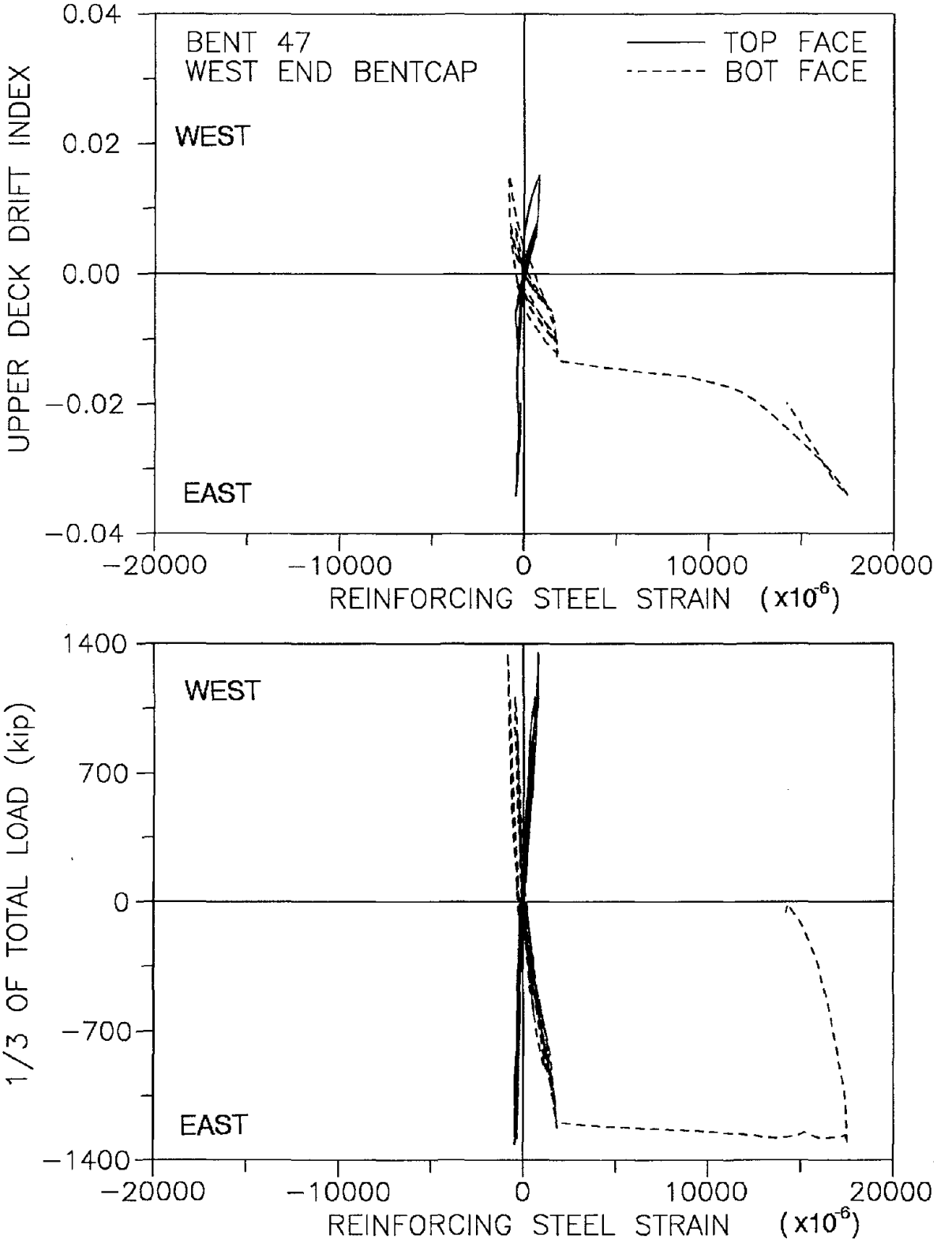
BENT 47
WEST END BENTCAP
TOP FACE
BOT FACE
WEST
EAST
UPPER DECK DRIFT INDEX
0.04
0.02
0.00
−0.02
−0.04
−20000
−10000
0
10000
20000
REINFORCING STEEL STRAIN (x10⁻⁶)
1/3 OF TOTAL LOAD (kip)
1400
700
0
−700
−1400
WEST
EAST
−20000
−10000
0
10000
20000
REINFORCING STEEL STRAIN (x10⁻⁶)

Fig. B.13

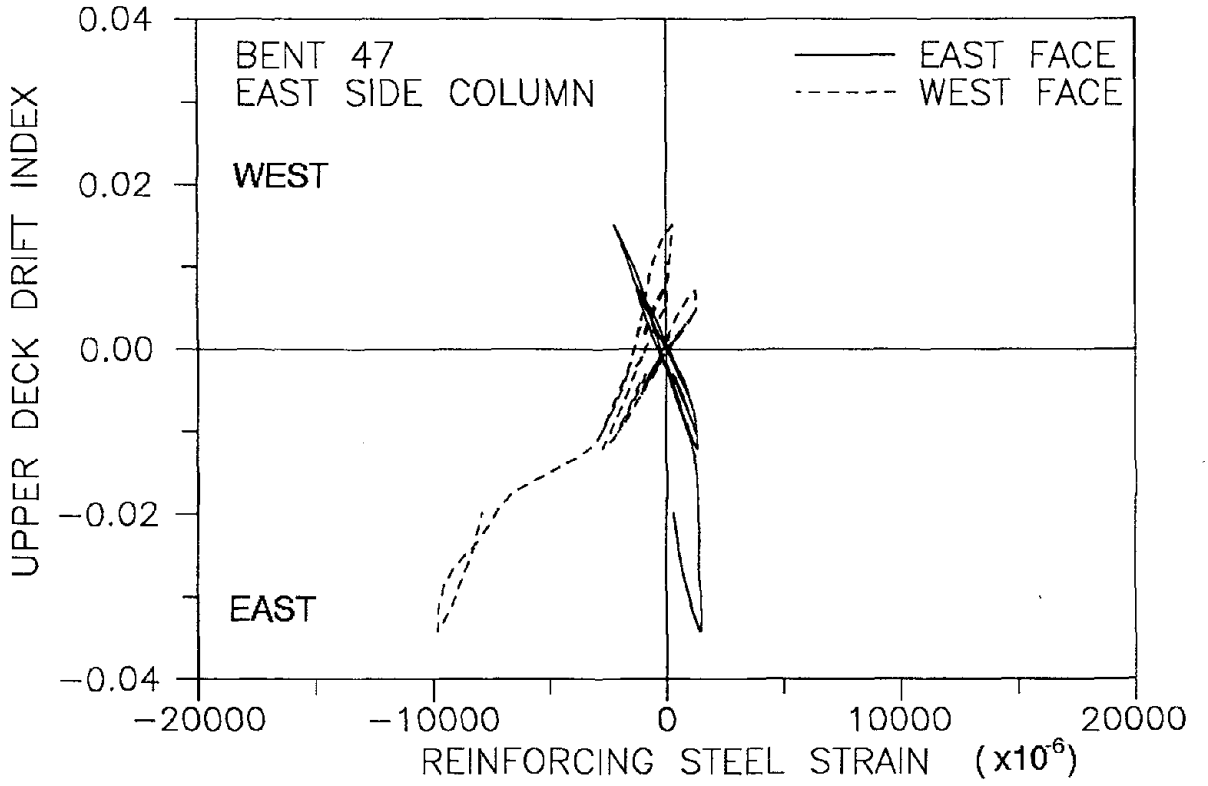
BENT 47
EAST SIDE COLUMN
WEST
EAST
EAST FACE
WEST FACE
UPPER DECK DRIFT INDEX
0.04
0.02
0.00
−0.02
−0.04
−20000
−10000
0
10000
20000
REINFORCING STEEL STRAIN (x10-6)

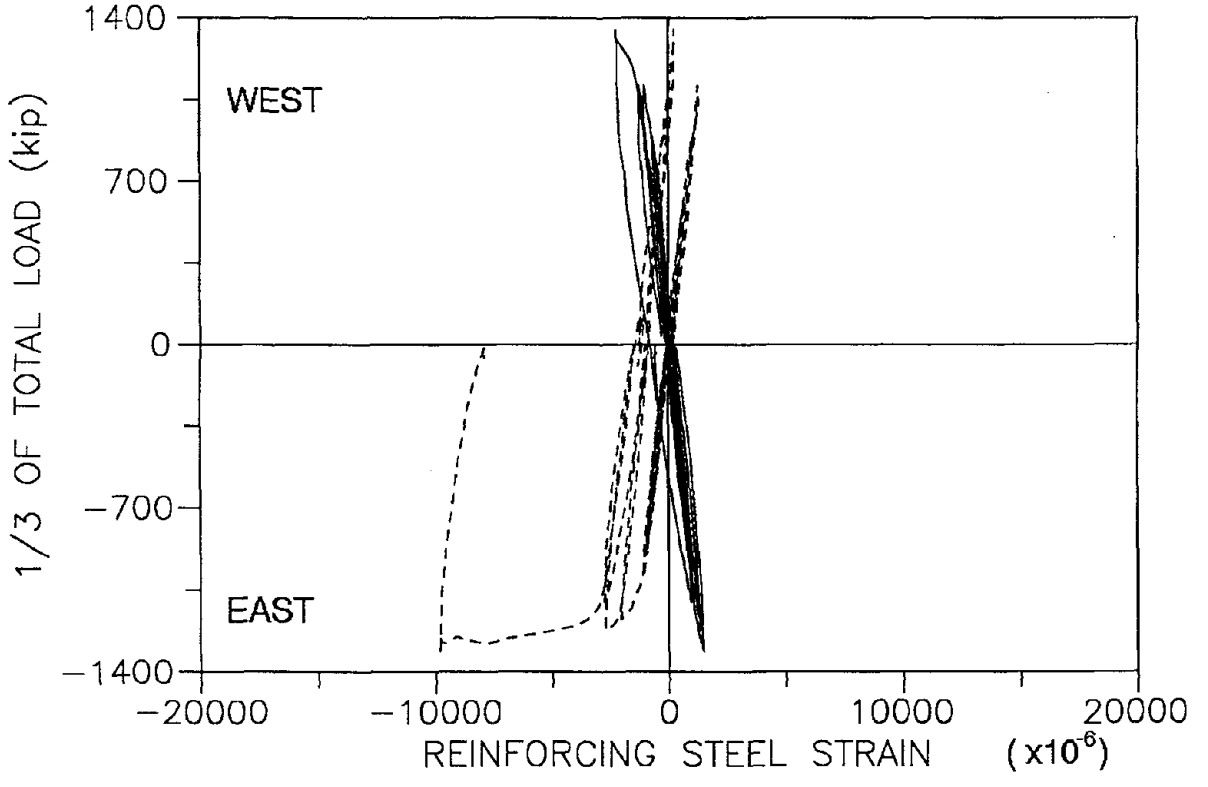
WEST
EAST
1/3 OF TOTAL LOAD (kip)
1400
700
0
−700
−1400
−20000
−10000
0
10000
20000
REINFORCING STEEL STRAIN (x10-6)

Fig. B.14

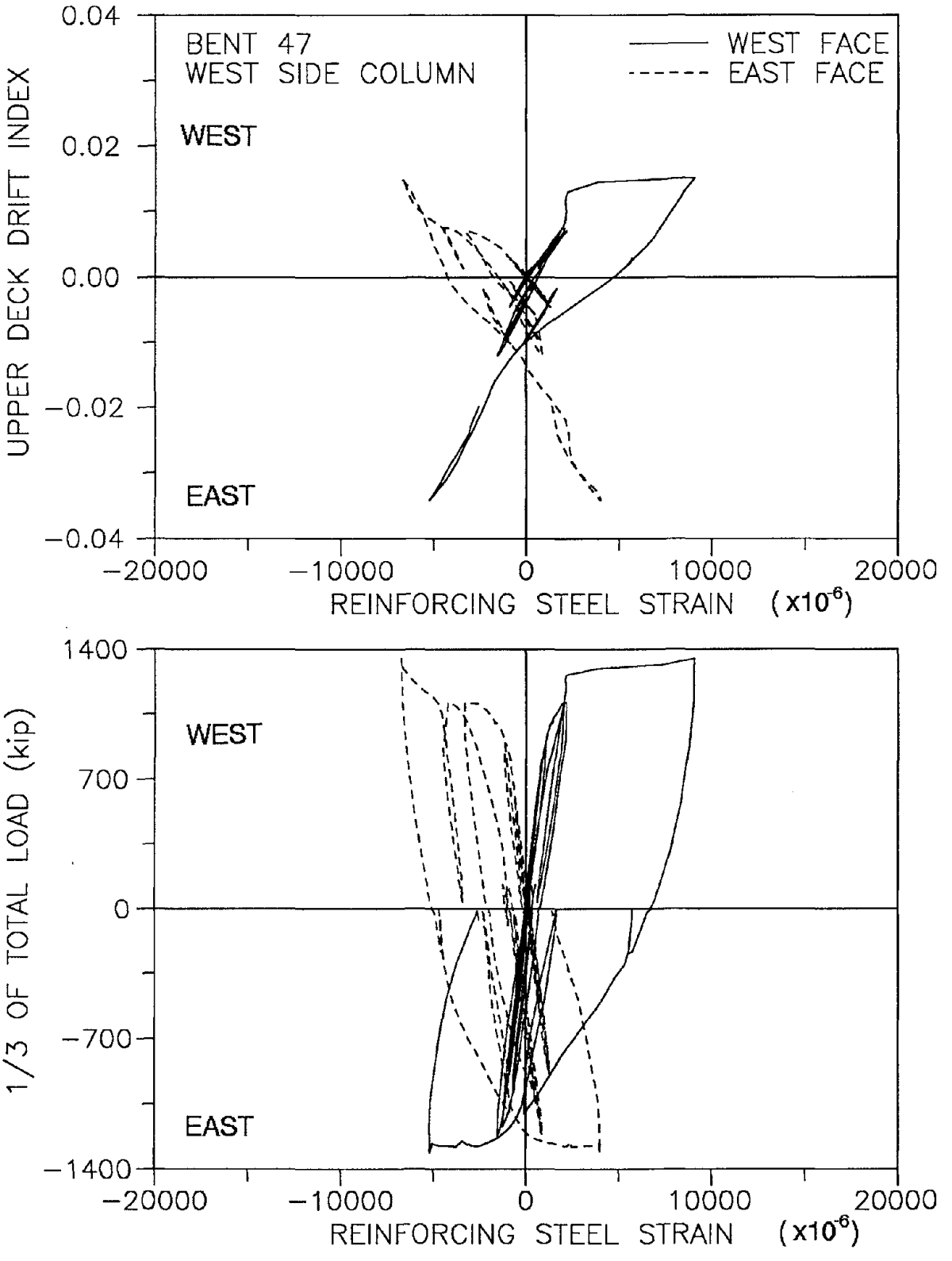
BENT 47
WEST SIDE COLUMN
WEST FACE
EAST FACE
WEST
EAST
UPPER DECK DRIFT INDEX
0.04
0.02
0.00
−0.02
−0.04
−20000
−10000
0
10000
20000
REINFORCING STEEL STRAIN (x10⁻⁶)
1/3 OF TOTAL LOAD (kip)
1400
700
0
−700
−1400
WEST
EAST
−20000
−10000
0
10000
20000
REINFORCING STEEL STRAIN (x10⁻⁶)

Fig. B.15

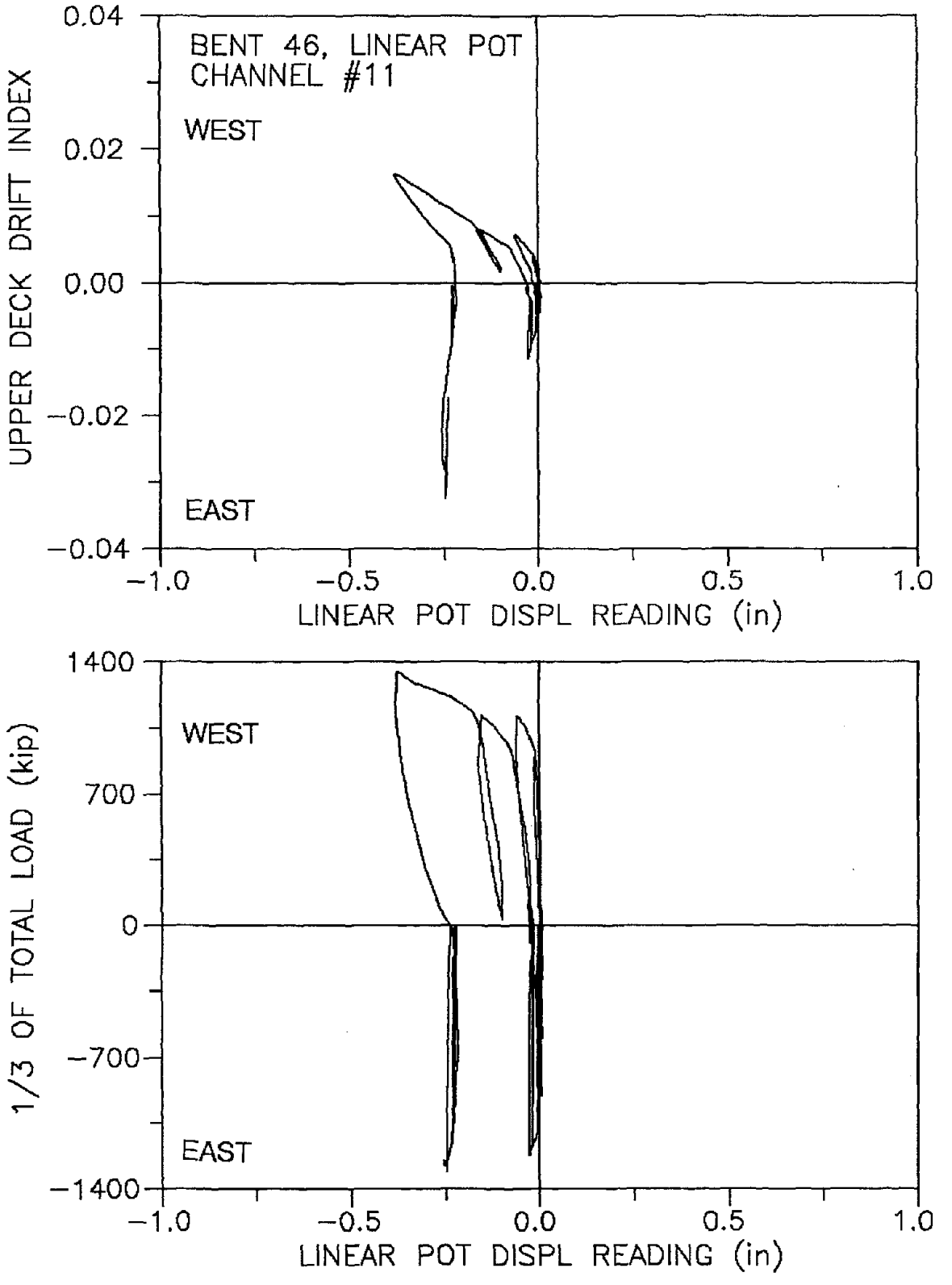
BENT 46, LINEAR POT
CHANNEL #11
WEST
EAST
UPPER DECK DRIFT INDEX
0.04
0.02
0.00
−0.02
−0.04
−1.0
−0.5
0.0
0.5
1.0
LINEAR POT DISPL READING (in)
1/3 OF TOTAL LOAD (kip)
1400
700
0
−700
−1400
WEST
EAST
−1.0
−0.5
0.0
0.5
1.0
LINEAR POT DISPL READING (in)

Fig. B.16

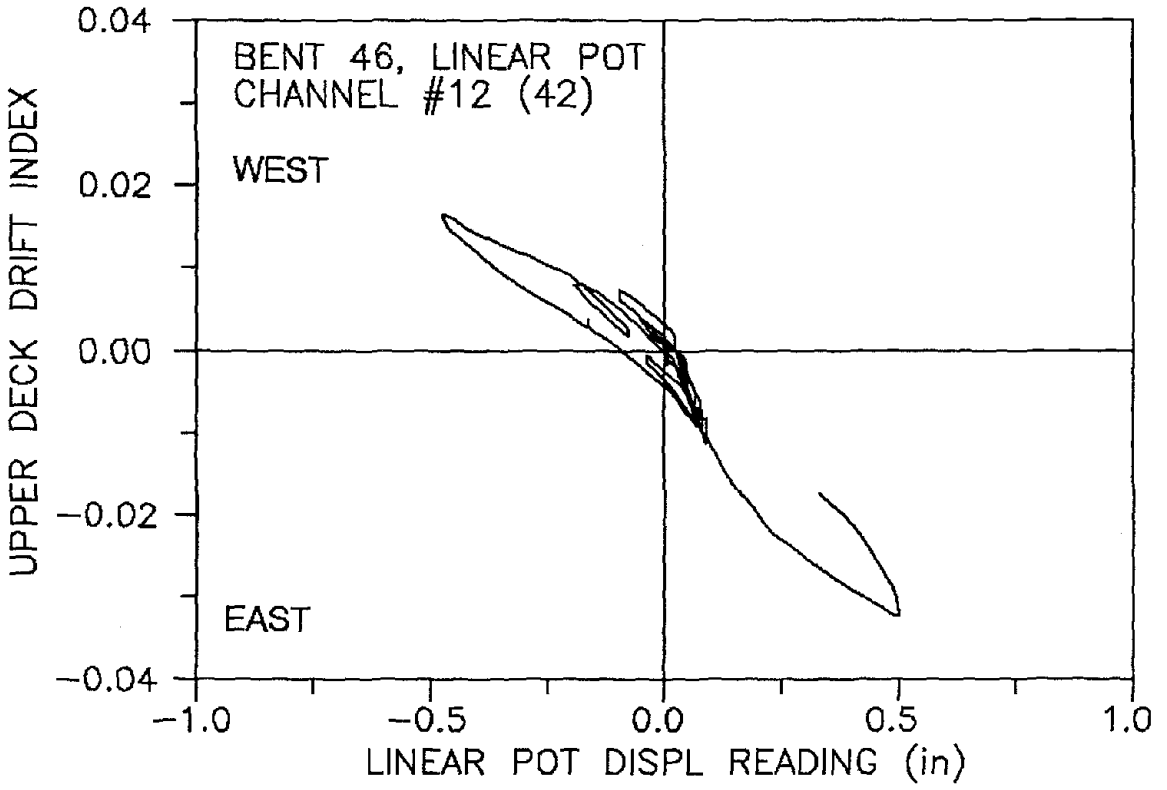
BENT 46, LINEAR POT
CHANNEL #12 (42)
WEST
EAST
UPPER DECK DRIFT INDEX
0.04
0.02
0.00
−0.02
−0.04
−1.0
−0.5
0.0
0.5
1.0
LINEAR POT DISPL READING (in)

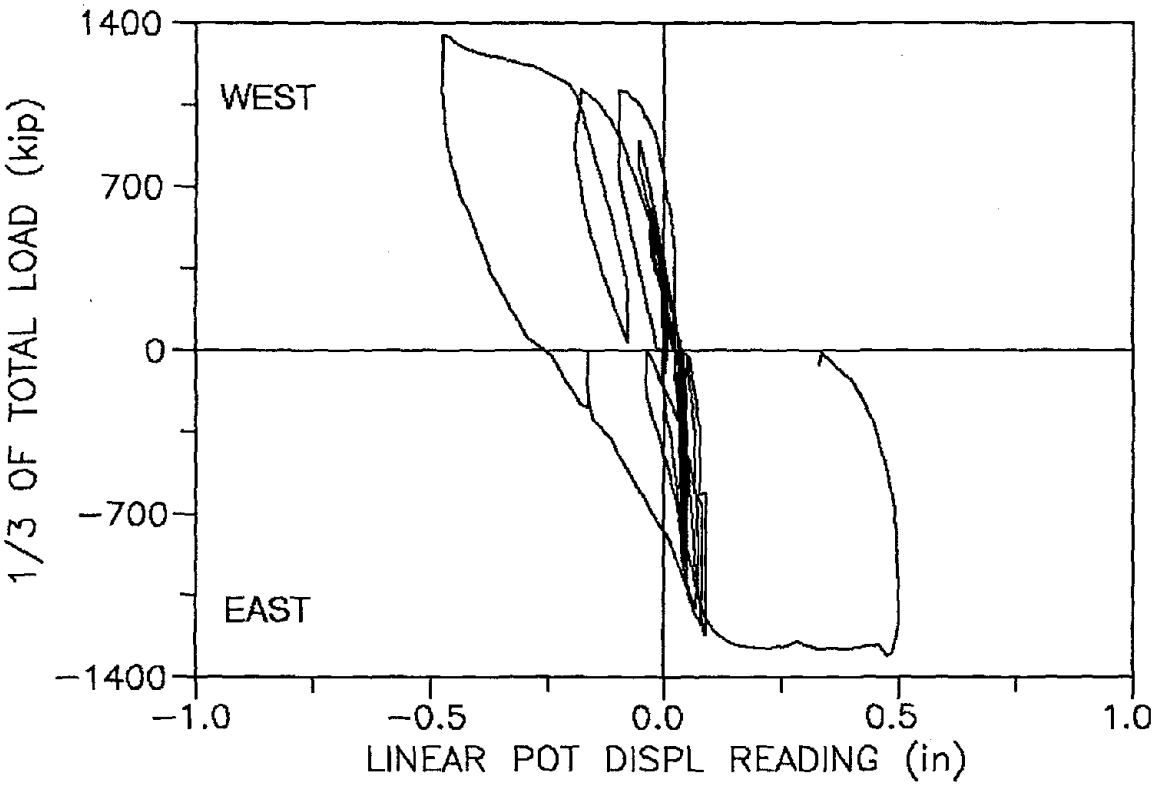
WEST
EAST
1/3 OF TOTAL LOAD (kip)
1400
700
0
−700
−1400
−1.0
−0.5
0.0
0.5
1.0
LINEAR POT DISPL READING (in)

Fig. B.17

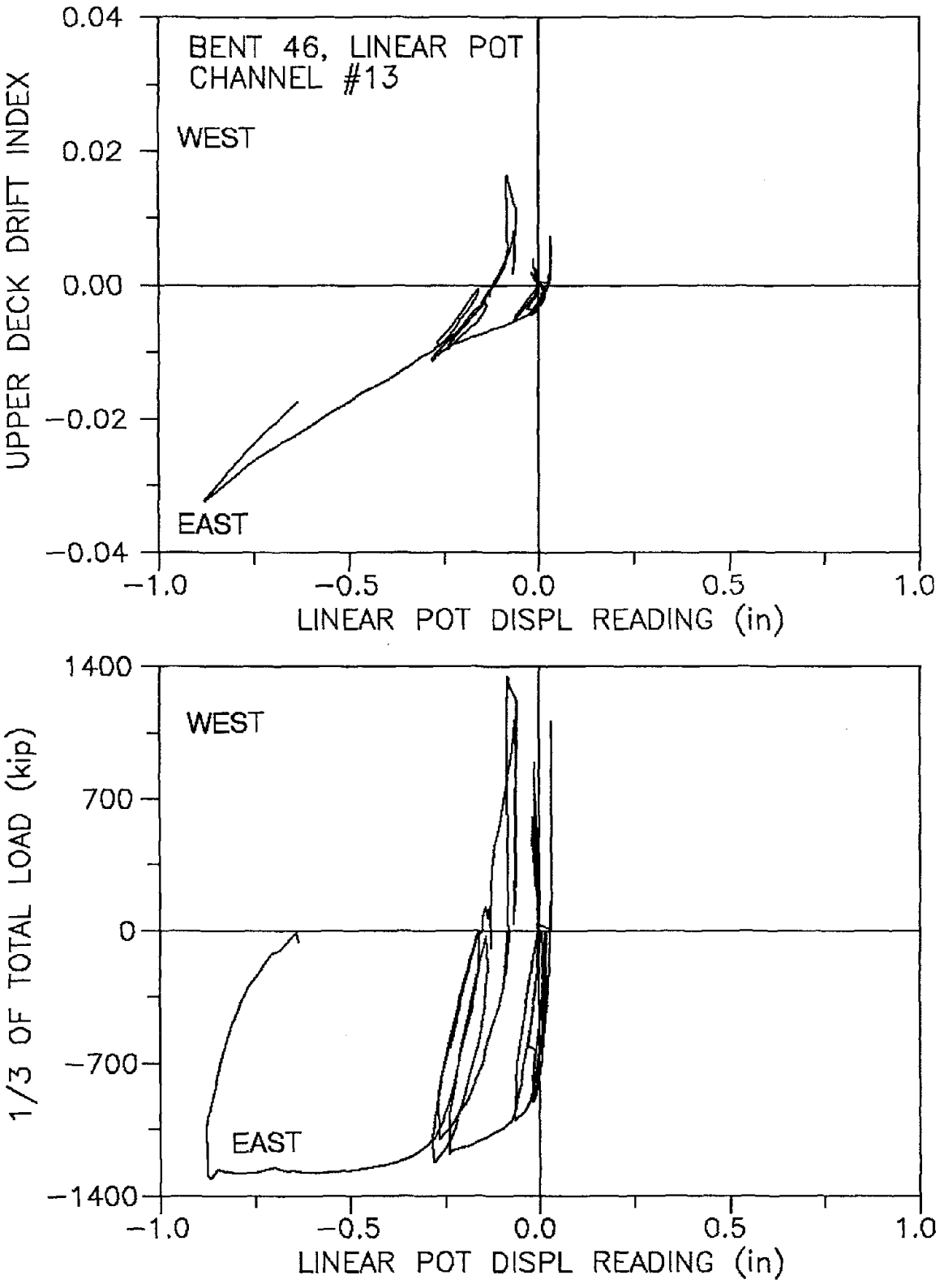
BENT 46, LINEAR POT
CHANNEL #13
WEST
EAST
UPPER DECK DRIFT INDEX
0.04
0.02
0.00
−0.02
−0.04
−1.0
−0.5
0.0
0.5
1.0
LINEAR POT DISPL READING (in)
WEST
EAST
1/3 OF TOTAL LOAD (kip)
1400
700
0
−700
−1400
−1.0
−0.5
0.0
0.5
1.0
LINEAR POT DISPL READING (in)

Fig. B.18

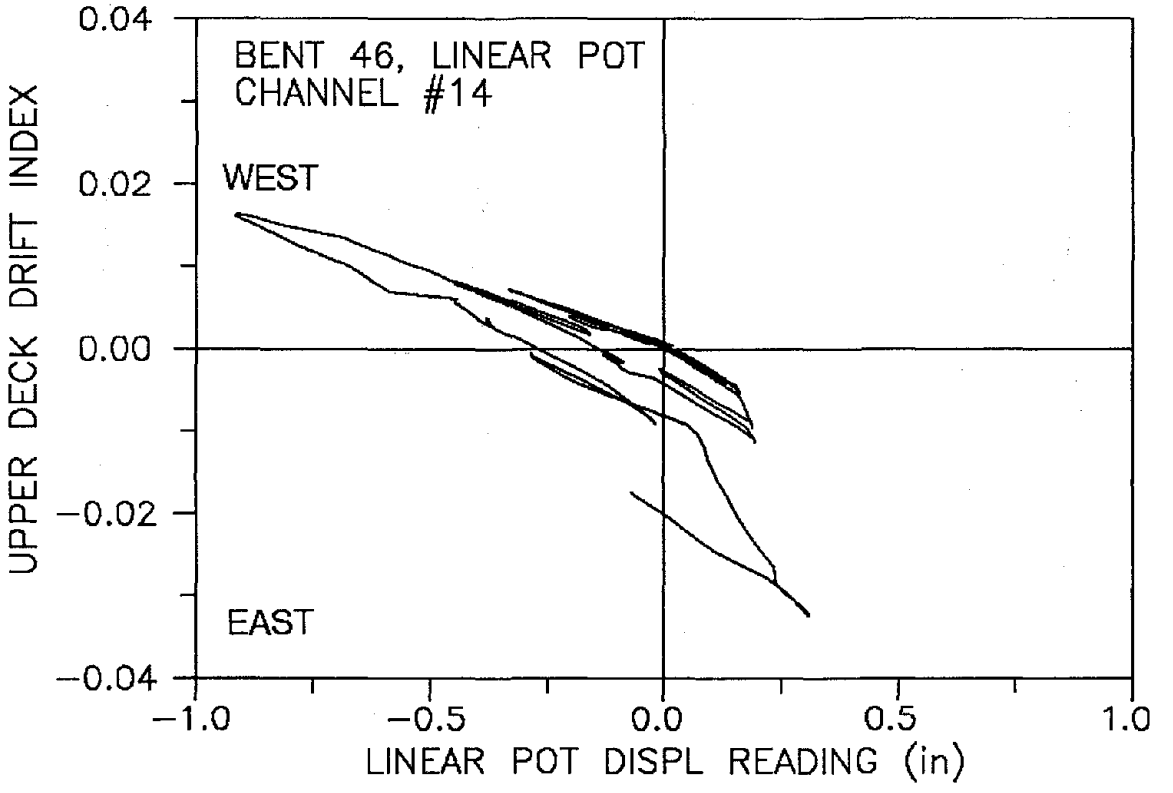
BENT 46, LINEAR POT
CHANNEL #14
WEST
EAST
UPPER DECK DRIFT INDEX
0.04
0.02
0.00
−0.02
−0.04
−1.0
−0.5
0.0
0.5
1.0
LINEAR POT DISPL READING (in)

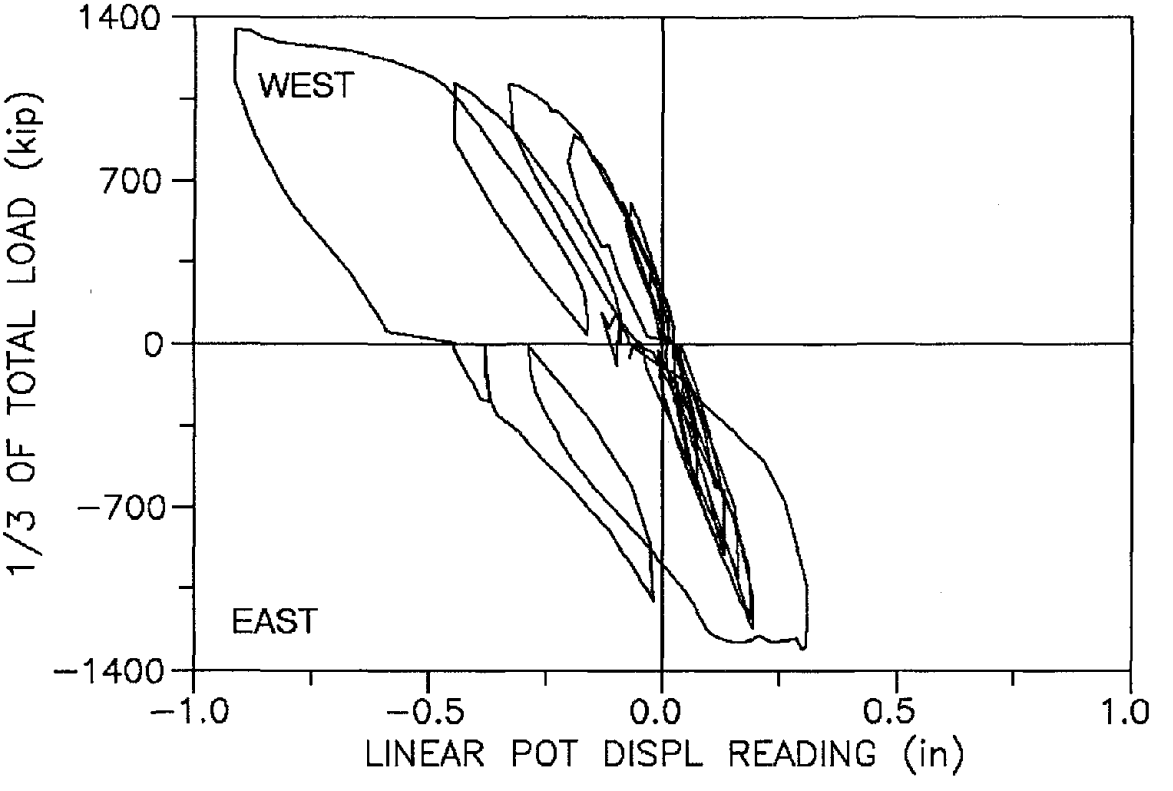
WEST
EAST
1/3 OF TOTAL LOAD (kip)
1400
700
0
−700
−1400
−1.0
−0.5
0.0
0.5
1.0
LINEAR POT DISPL READING (in)

Fig. B.19

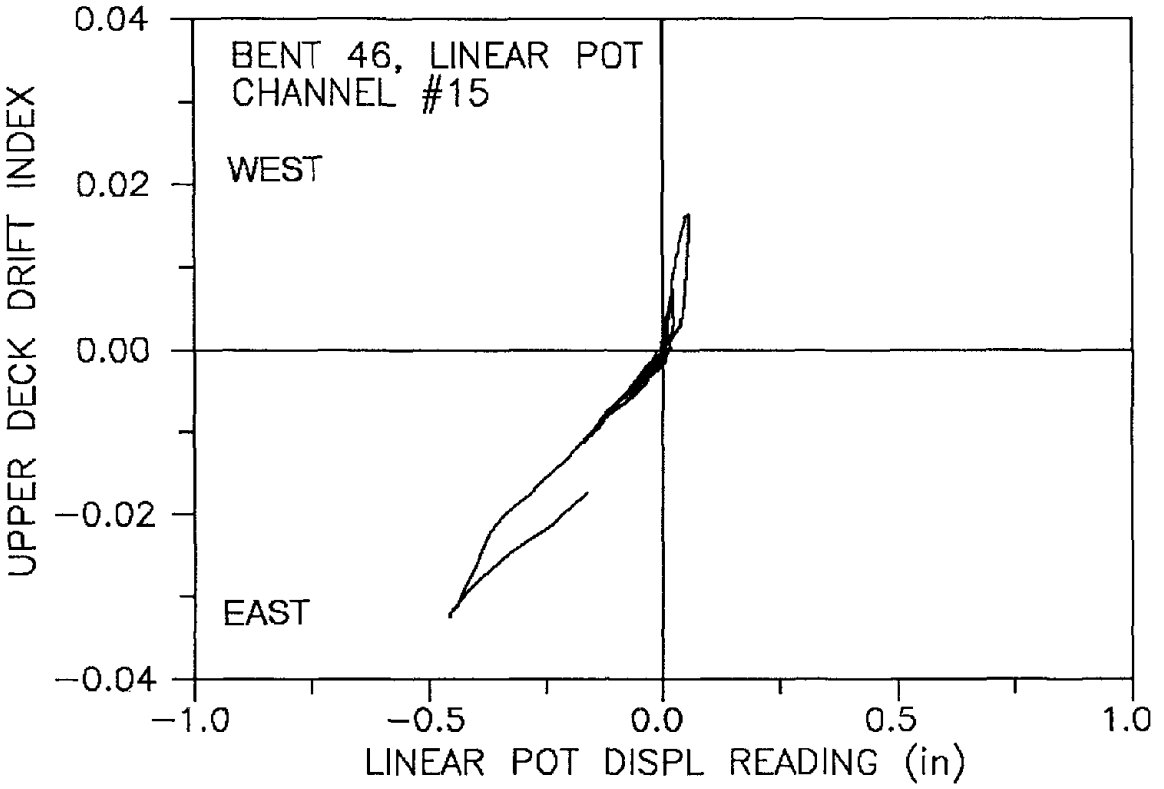
BENT 46, LINEAR POT
CHANNEL #15
WEST
EAST
UPPER DECK DRIFT INDEX
0.04
0.02
0.00
−0.02
−0.04
−1.0
−0.5
0.0
0.5
1.0
LINEAR POT DISPL READING (in)

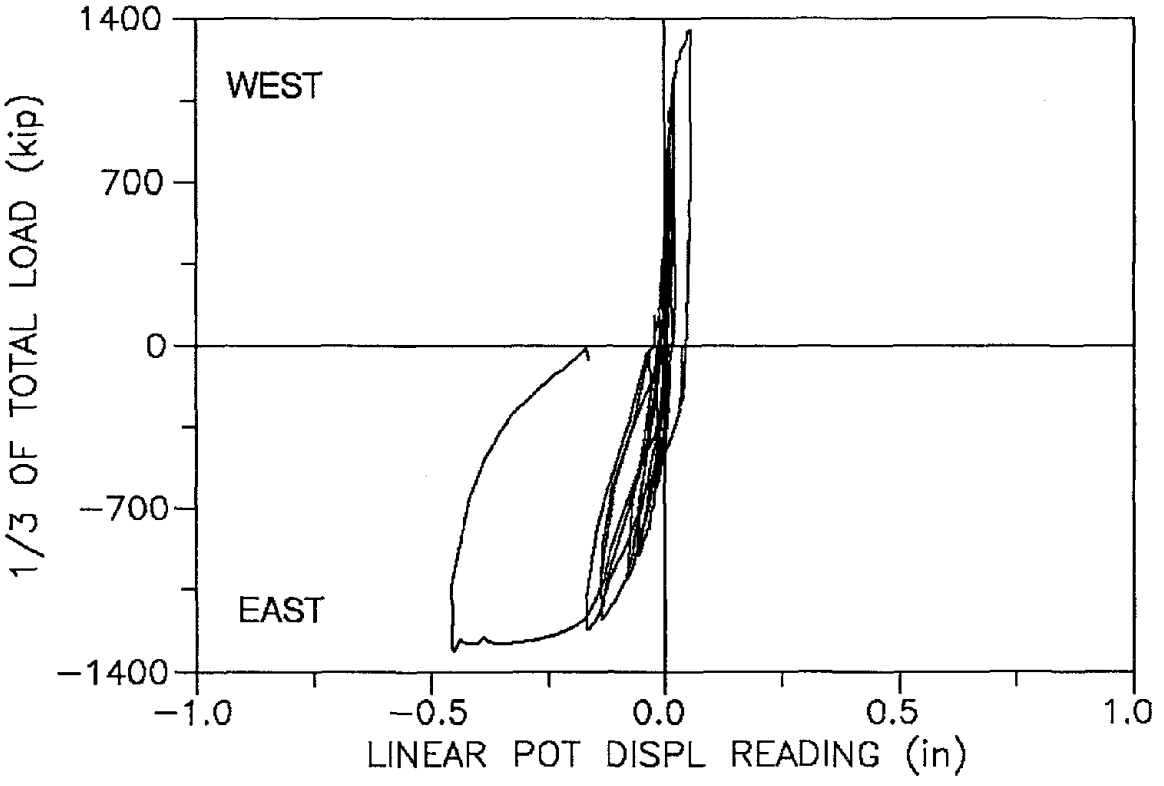
WEST
EAST
1/3 OF TOTAL LOAD (kip)
1400
700
0
−700
−1400
−1.0
−0.5
0.0
0.5
1.0
LINEAR POT DISPL READING (in)

Fig. B.20

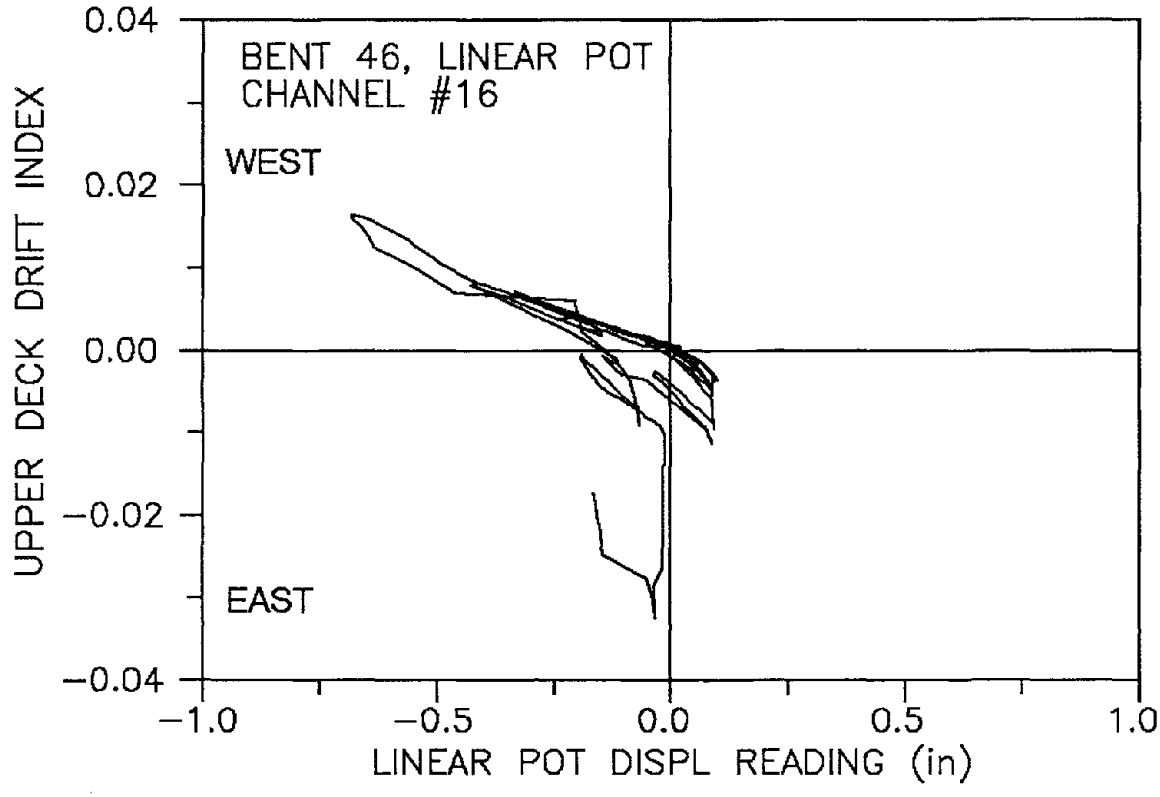
BENT 46, LINEAR POT
CHANNEL #16
WEST
EAST
UPPER DECK DRIFT INDEX
0.04
0.02
0.00
−0.02
−0.04
−1.0
−0.5
0.0
0.5
1.0
LINEAR POT DISPL READING (in)

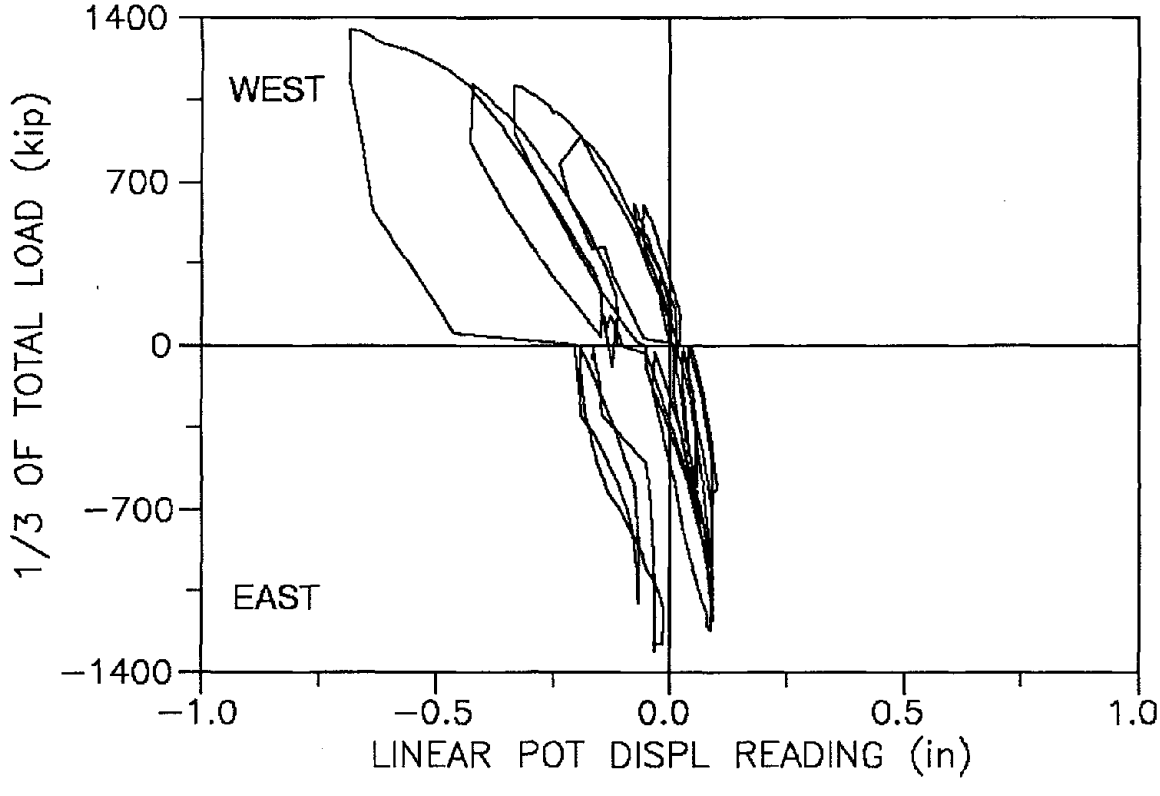
WEST
EAST
1/3 OF TOTAL LOAD (kip)
1400
700
0
−700
−1400
−1.0
−0.5
0.0
0.5
1.0
LINEAR POT DISPL READING (in)

Fig. B.21

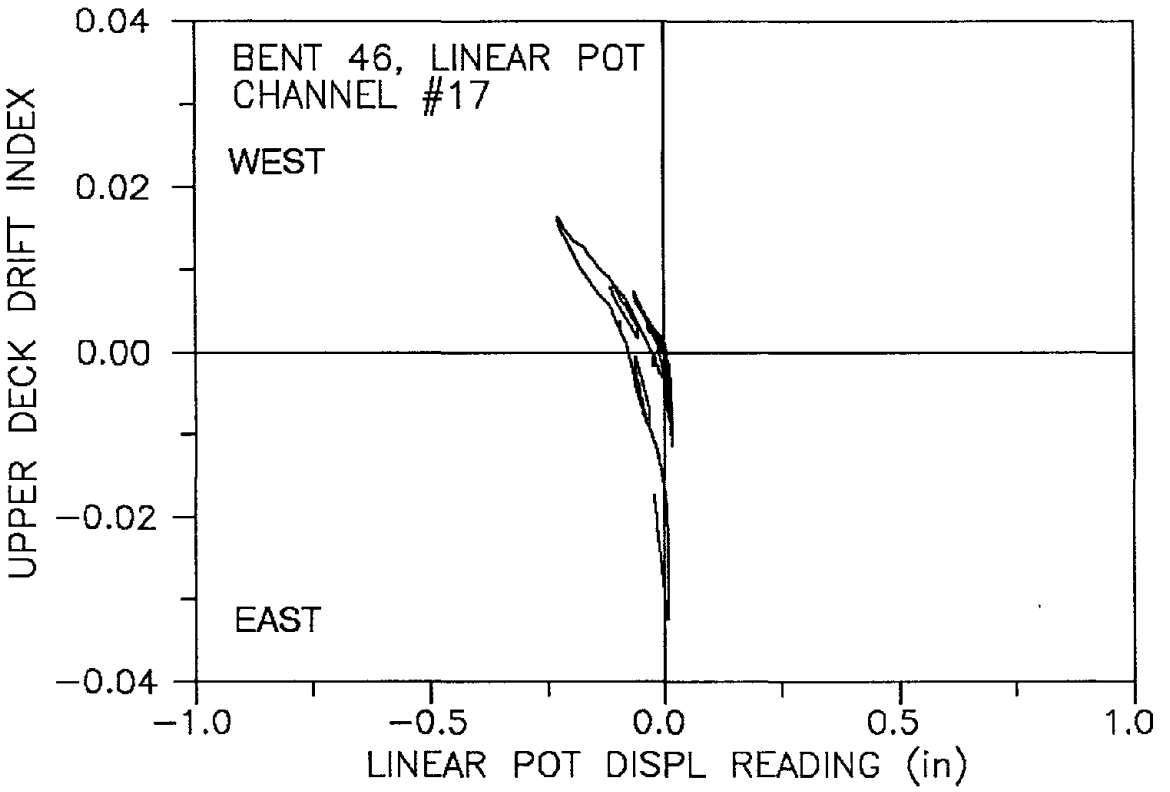
BENT 46, LINEAR POT
CHANNEL #17
WEST
EAST
UPPER DECK DRIFT INDEX
0.04
0.02
0.00
−0.02
−0.04
−1.0
−0.5
0.0
0.5
1.0
LINEAR POT DISPL READING (in)

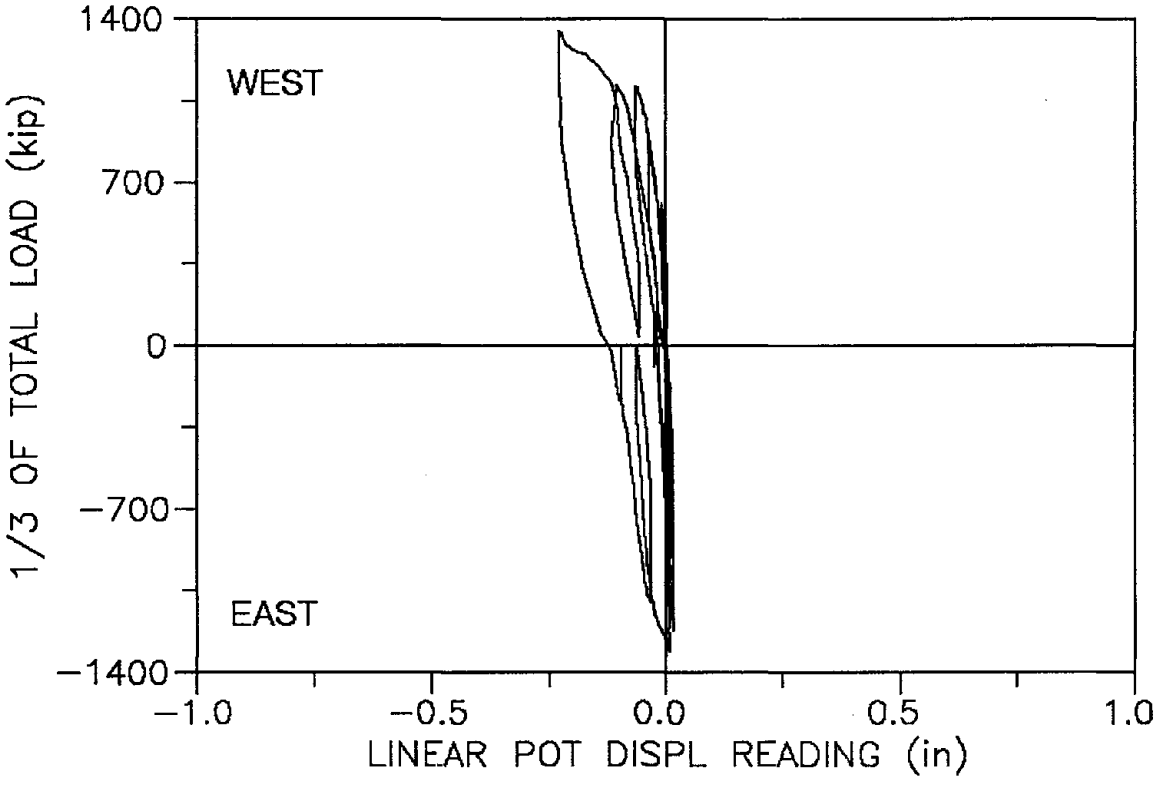
WEST
EAST
1/3 OF TOTAL LOAD (kip)
1400
700
0
−700
−1400
−1.0
−0.5
0.0
0.5
1.0
LINEAR POT DISPL READING (in)

Fig. B.22

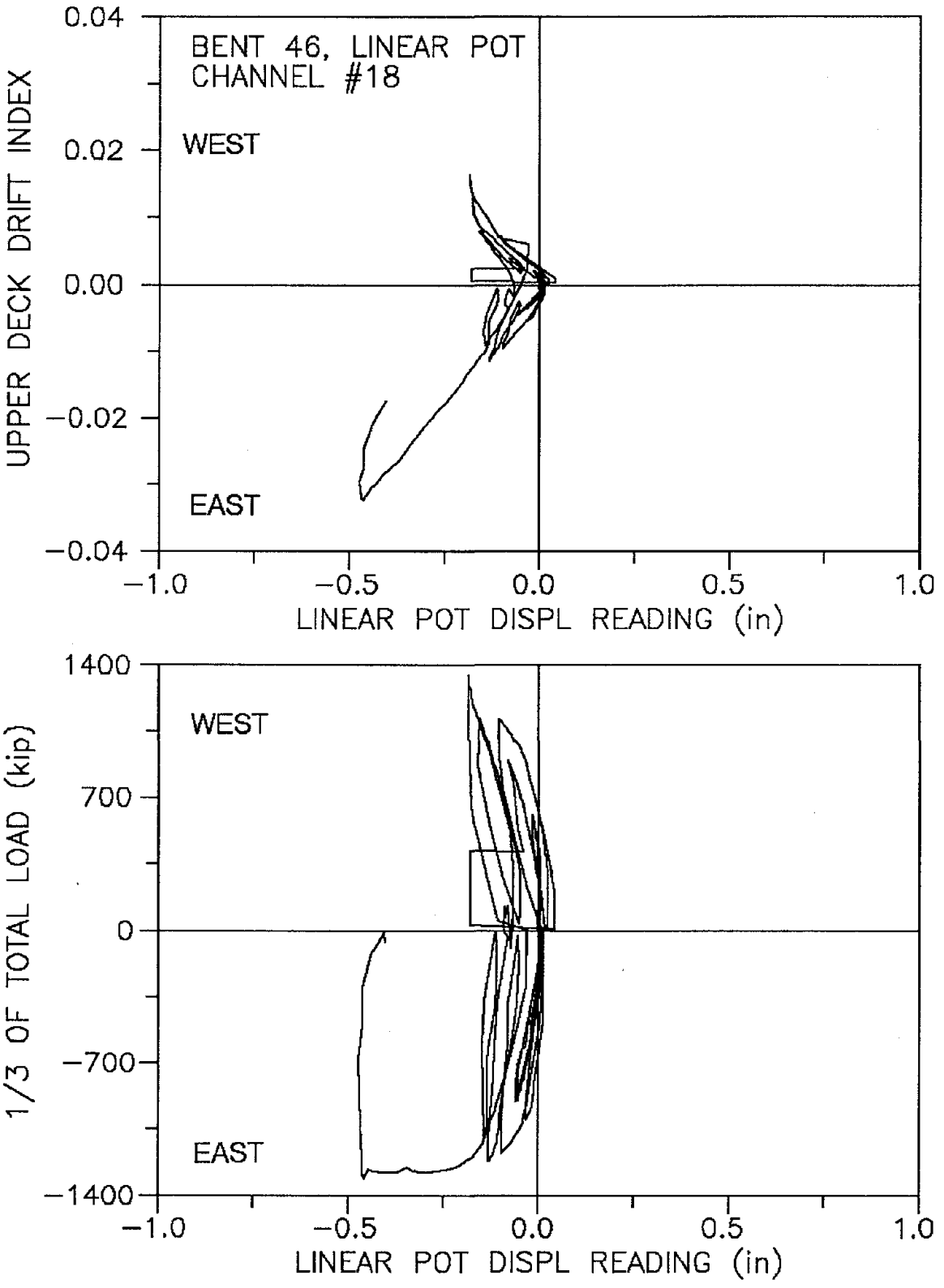
BENT 46, LINEAR POT
CHANNEL #18
WEST
EAST
UPPER DECK DRIFT INDEX
0.04
0.02
0.00
−0.02
−0.04
−1.0
−0.5
0.0
0.5
1.0
LINEAR POT DISPL READING (in)
1/3 OF TOTAL LOAD (kip)
1400
700
0
−700
−1400
WEST
EAST
−1.0
−0.5
0.0
0.5
1.0
LINEAR POT DISPL READING (in)

Fig. B.23

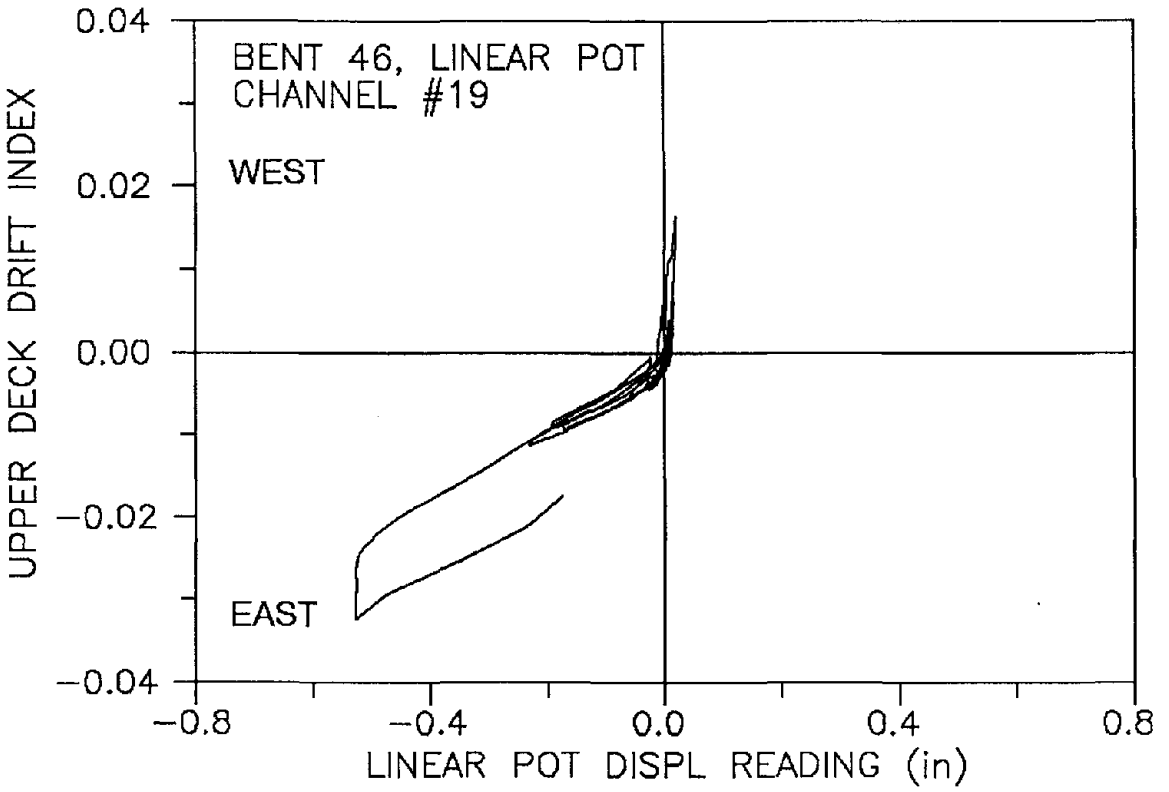
BENT 46, LINEAR POT
CHANNEL #19
WEST
EAST
UPPER DECK DRIFT INDEX
0.04
0.02
0.00
−0.02
−0.04
−0.8
−0.4
0.0
0.4
0.8
LINEAR POT DISPL READING (in)

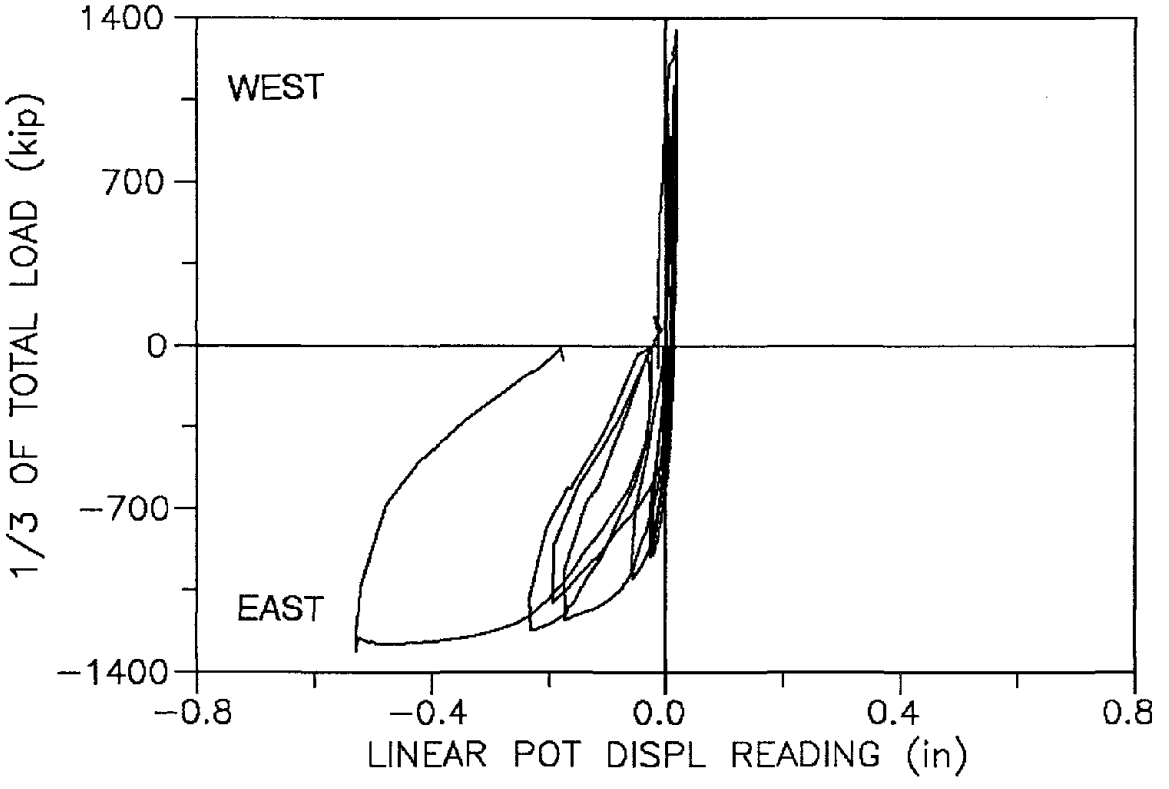
WEST
EAST
1/3 OF TOTAL LOAD (kip)
1400
700
0
−700
−1400
−0.8
−0.4
0.0
0.4
0.8
LINEAR POT DISPL READING (in)

Fig. B.24

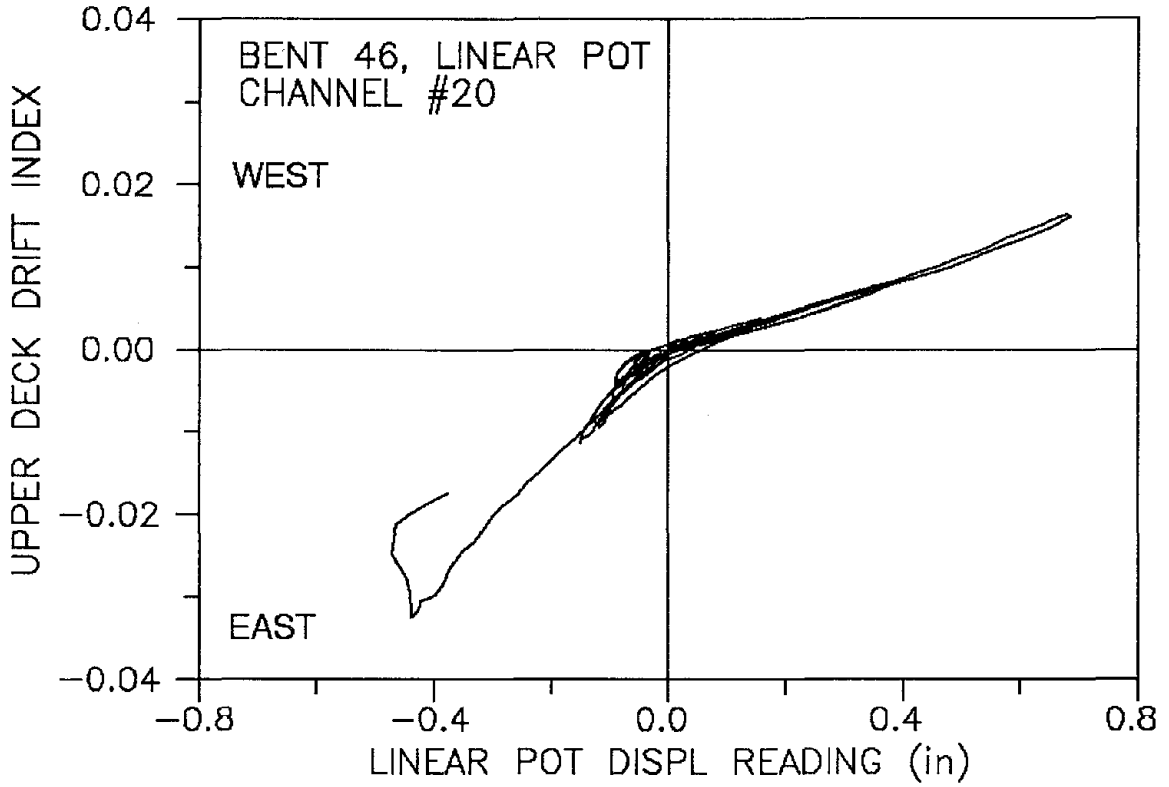
BENT 46, LINEAR POT
CHANNEL #20
WEST
EAST
UPPER DECK DRIFT INDEX
0.04
0.02
0.00
−0.02
−0.04
−0.8
−0.4
0.0
0.4
0.8
LINEAR POT DISPL READING (in)

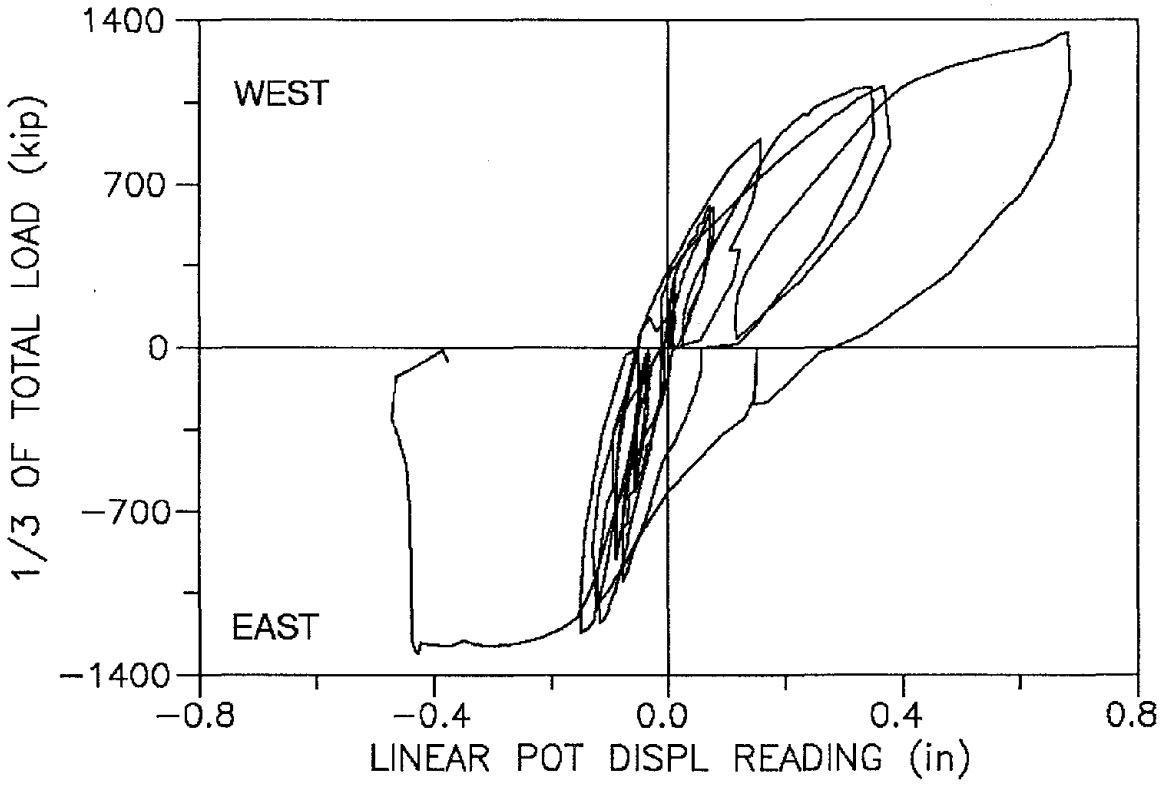
WEST
EAST
1/3 OF TOTAL LOAD (kip)
1400
700
0
−700
−1400
−0.8
−0.4
0.0
0.4
0.8
LINEAR POT DISPL READING (in)

Fig. B.25

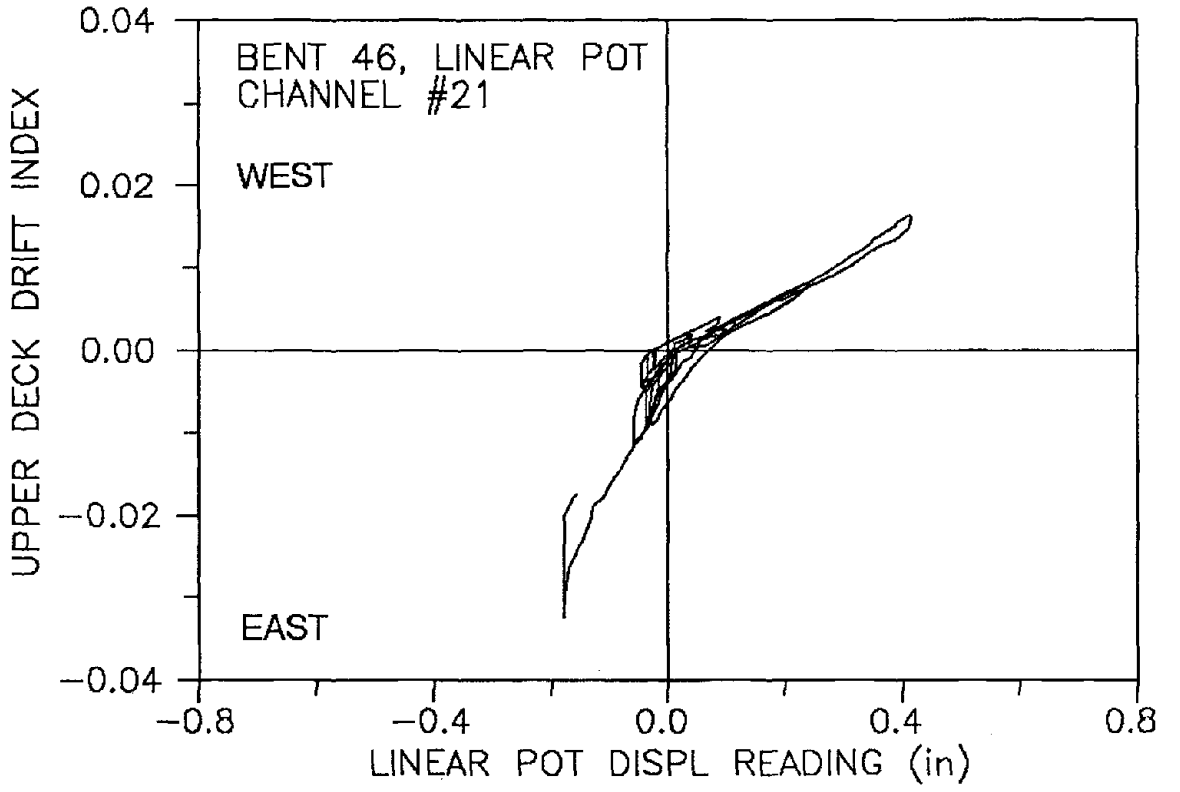
BENT 46, LINEAR POT
CHANNEL #21
WEST
EAST
UPPER DECK DRIFT INDEX
0.04
0.02
0.00
−0.02
−0.04
−0.8
−0.4
0.0
0.4
0.8
LINEAR POT DISPL READING (in)

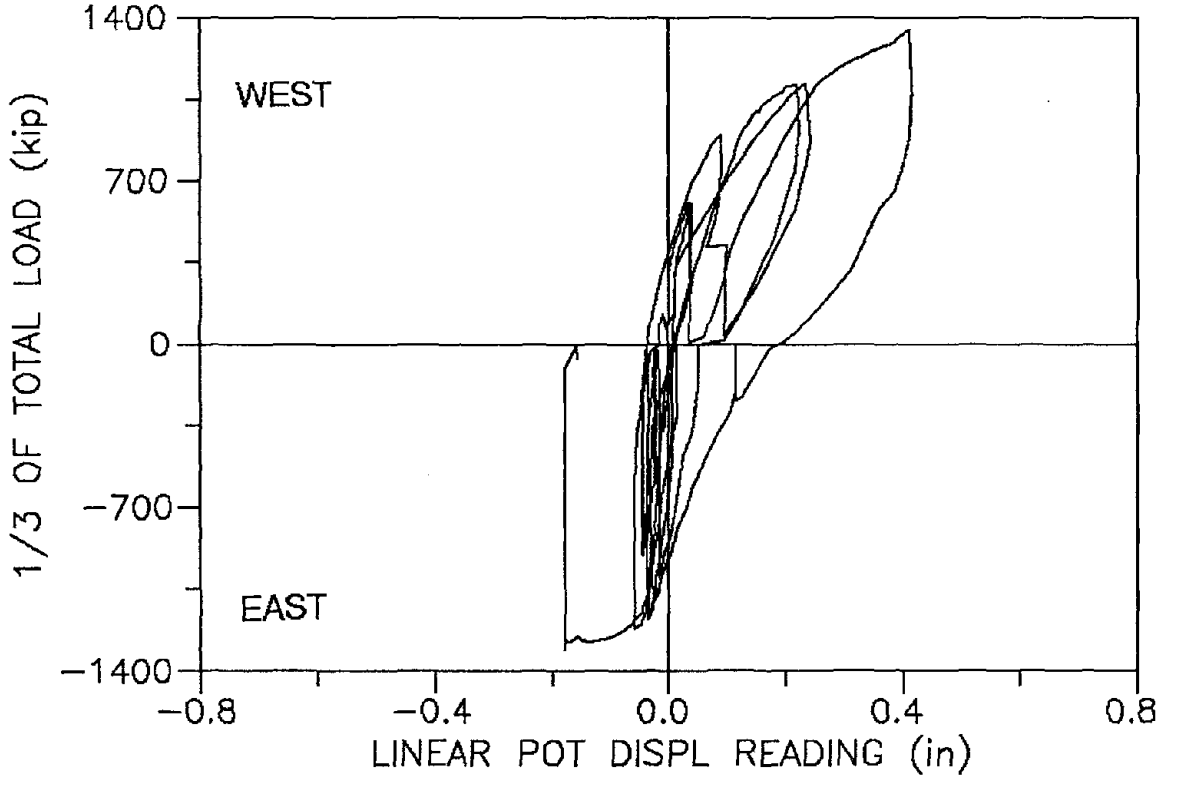
WEST
EAST
1/3 OF TOTAL LOAD (kip)
1400
700
0
−700
−1400
−0.8
−0.4
0.0
0.4
0.8
LINEAR POT DISPL READING (in)

Fig. B.26

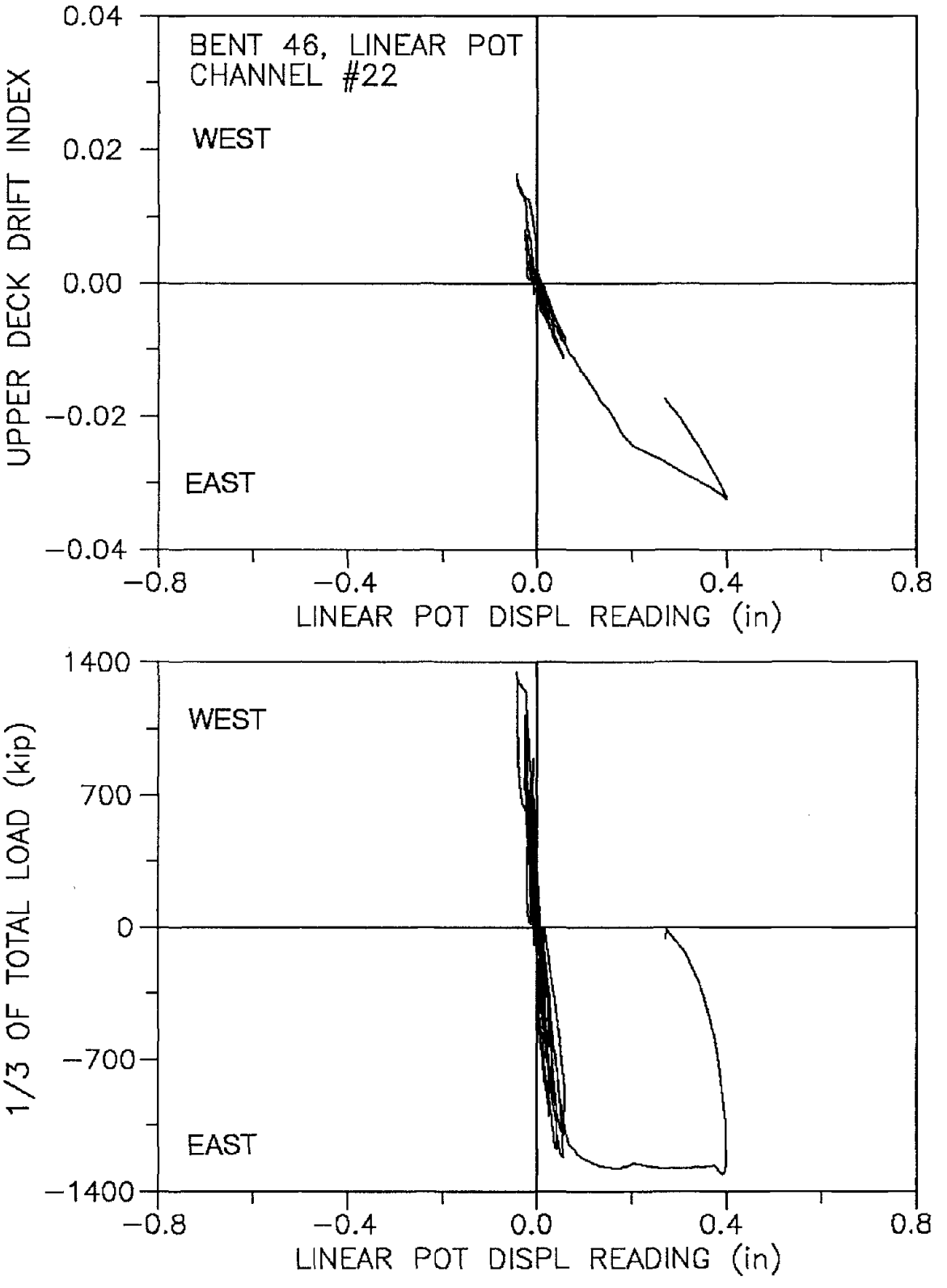
BENT 46, LINEAR POT
CHANNEL #22
WEST
EAST
UPPER DECK DRIFT INDEX
0.04
0.02
0.00
−0.02
−0.04
−0.8
−0.4
0.0
0.4
0.8
LINEAR POT DISPL READING (in)
1/3 OF TOTAL LOAD (kip)
1400
700
0
−700
−1400
WEST
EAST
−0.8
−0.4
0.0
0.4
0.8
LINEAR POT DISPL READING (in)

Fig. B.27

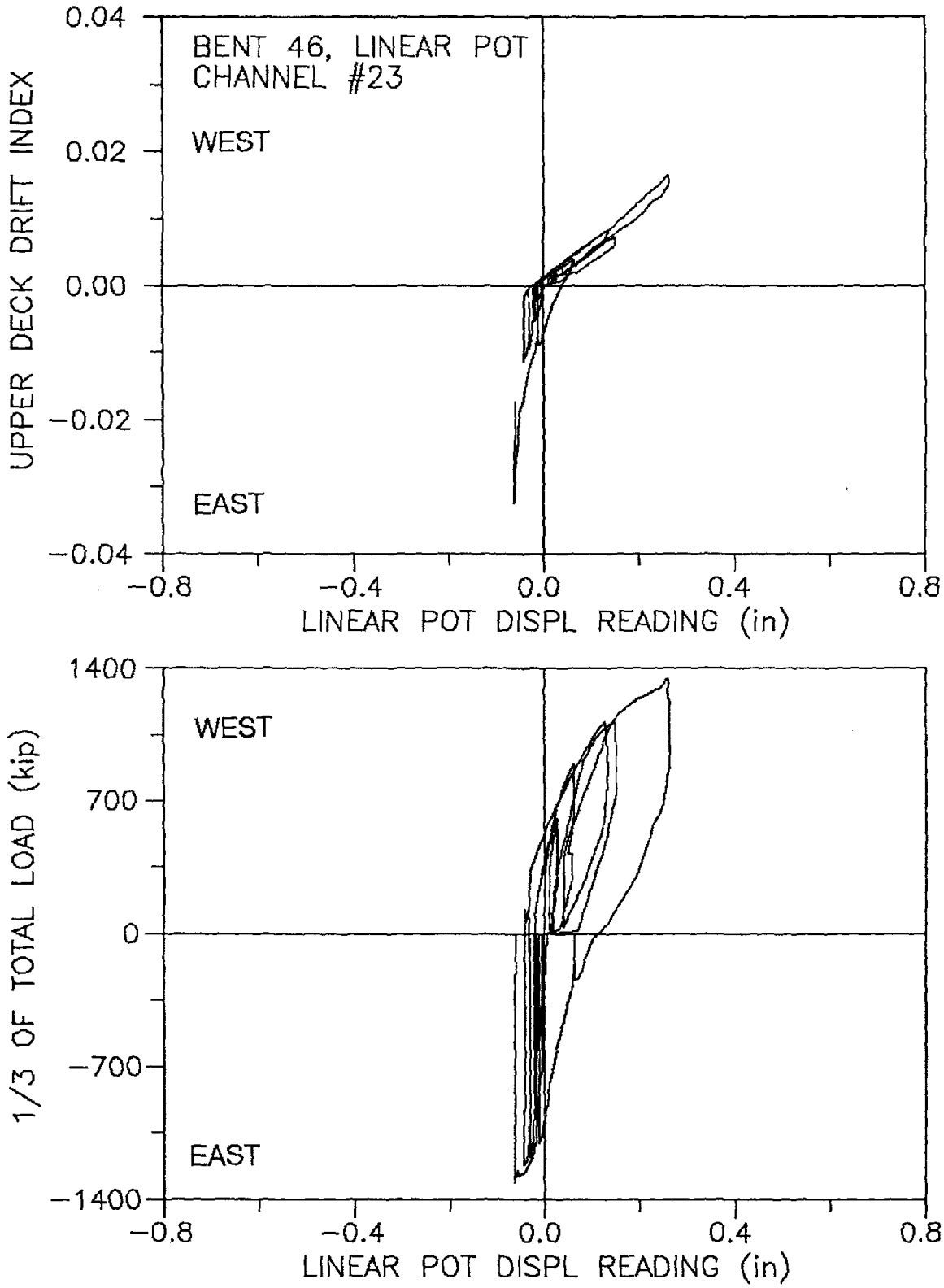
BENT 46, LINEAR POT
CHANNEL #23
WEST
EAST
UPPER DECK DRIFT INDEX
0.04
0.02
0.00
−0.02
−0.04
−0.8
−0.4
0.0
0.4
0.8
LINEAR POT DISPL READING (in)
WEST
EAST
1/3 OF TOTAL LOAD (kip)
1400
700
0
−700
−1400
−0.8
−0.4
0.0
0.4
0.8
LINEAR POT DISPL READING (in)

Fig. B.28

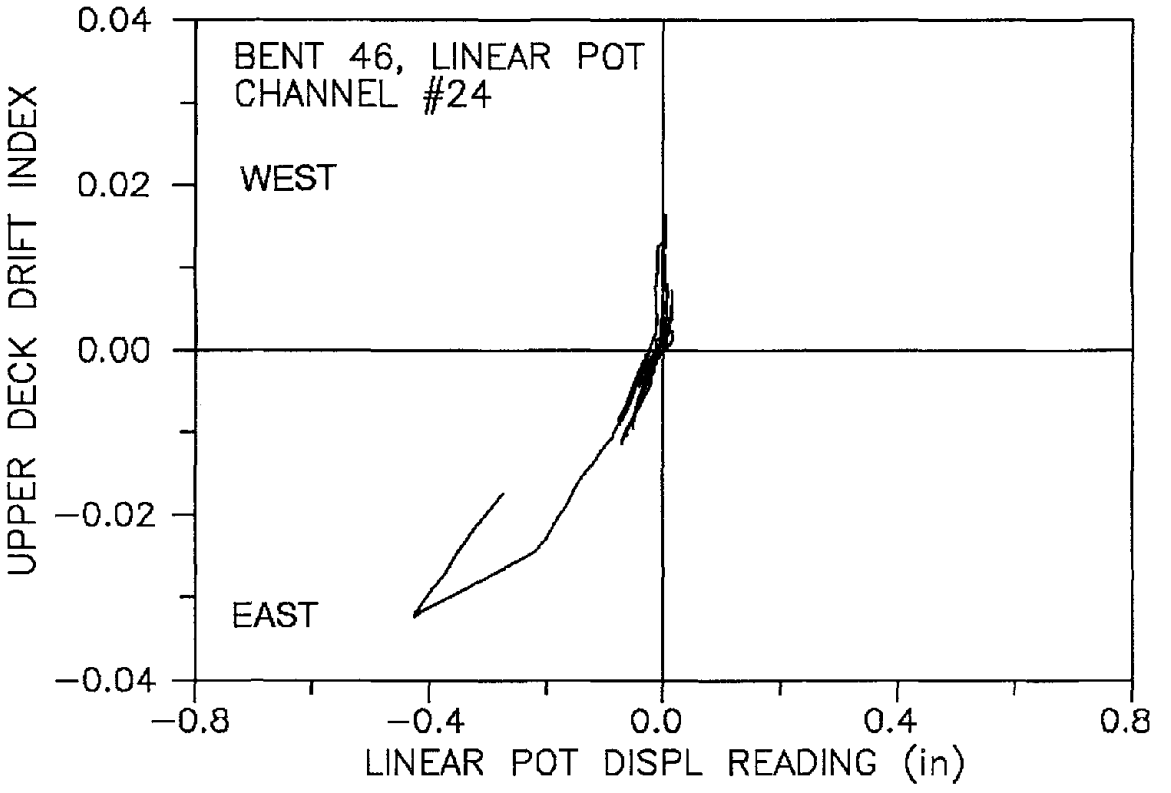
BENT 46, LINEAR POT
CHANNEL #24
WEST
EAST
UPPER DECK DRIFT INDEX
0.04
0.02
0.00
−0.02
−0.04
−0.8
−0.4
0.0
0.4
0.8
LINEAR POT DISPL READING (in)

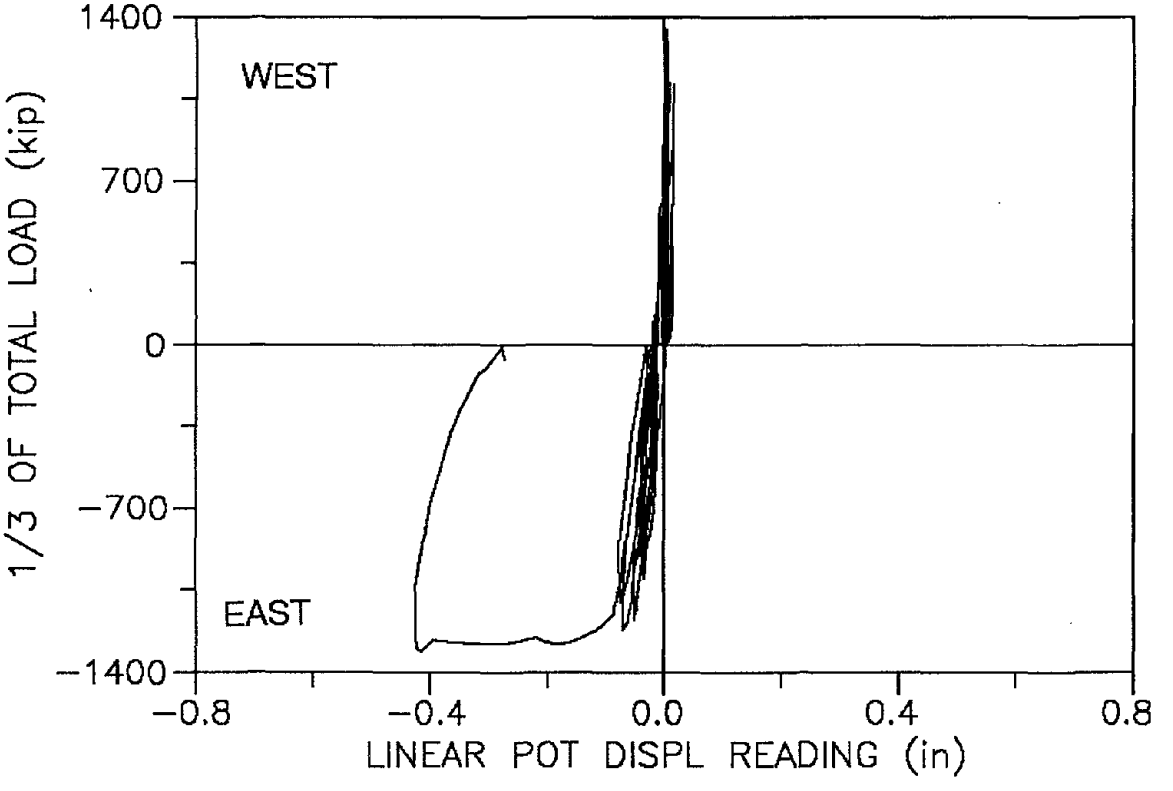
WEST
EAST
1/3 OF TOTAL LOAD (kip)
1400
700
0
−700
−1400
−0.8
−0.4
0.0
0.4
0.8
LINEAR POT DISPL READING (in)

Fig. B.29

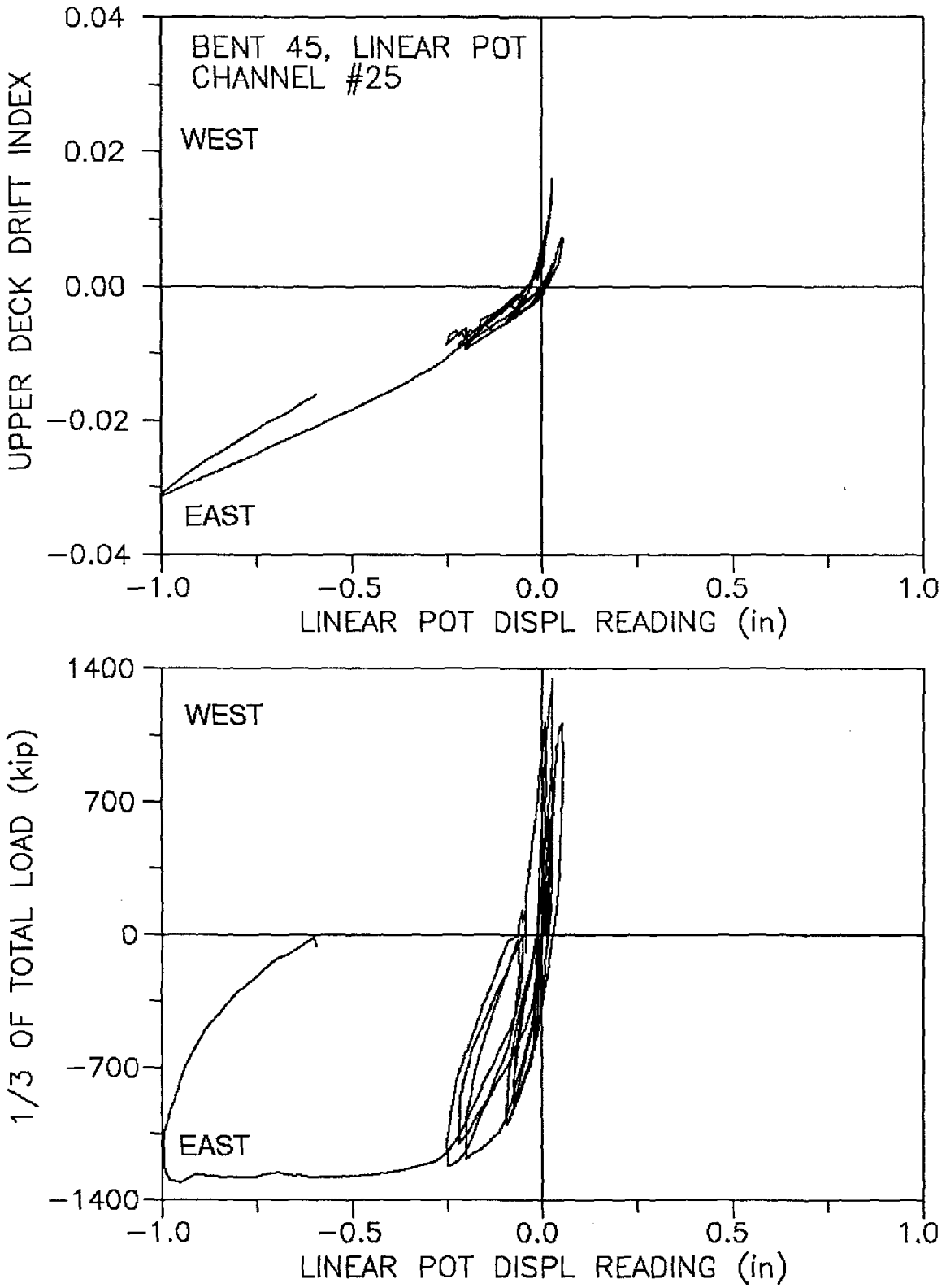
BENT 45, LINEAR POT
CHANNEL #25
WEST
EAST
UPPER DECK DRIFT INDEX
0.04
0.02
0.00
−0.02
−0.04
−1.0
−0.5
0.0
0.5
1.0
LINEAR POT DISPL READING (in)
WEST
EAST
1/3 OF TOTAL LOAD (kip)
1400
700
0
−700
−1400
−1.0
−0.5
0.0
0.5
1.0
LINEAR POT DISPL READING (in)

Fig. B.30

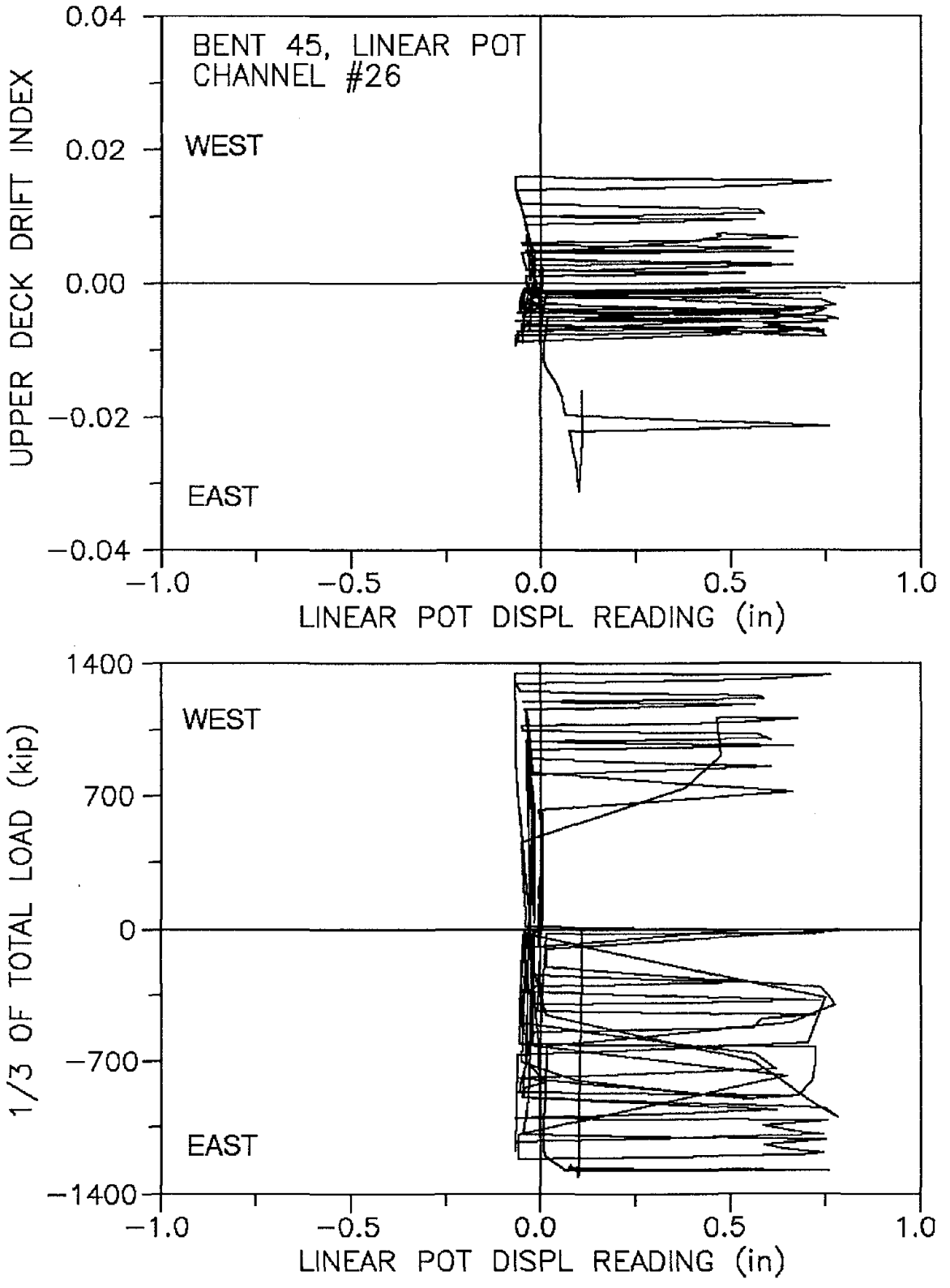
BENT 45, LINEAR POT
CHANNEL #26
WEST
EAST
UPPER DECK DRIFT INDEX
0.04
0.02
0.00
−0.02
−0.04
−1.0
−0.5
0.0
0.5
1.0
LINEAR POT DISPL READING (in)
1/3 OF TOTAL LOAD (kip)
1400
700
0
−700
−1400
WEST
EAST
−1.0
−0.5
0.0
0.5
1.0
LINEAR POT DISPL READING (in)

Fig. B.31

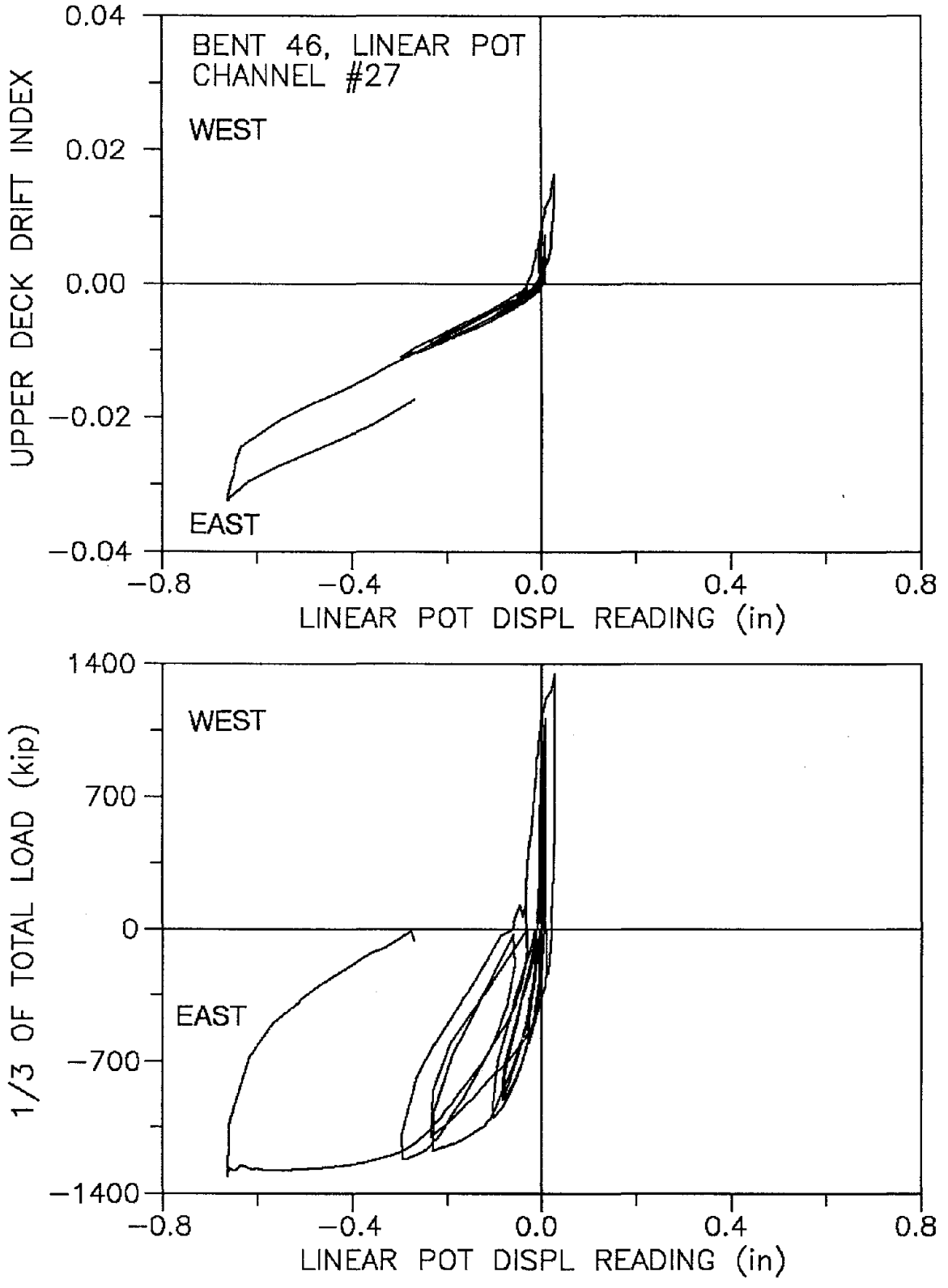
BENT 46, LINEAR POT
CHANNEL #27
WEST
EAST
UPPER DECK DRIFT INDEX
0.04
0.02
0.00
−0.02
−0.04
−0.8
−0.4
0.0
0.4
0.8
LINEAR POT DISPL READING (in)
WEST
EAST
1/3 OF TOTAL LOAD (kip)
1400
700
0
−700
−1400
−0.8
−0.4
0.0
0.4
0.8
LINEAR POT DISPL READING (in)

Fig. B.32

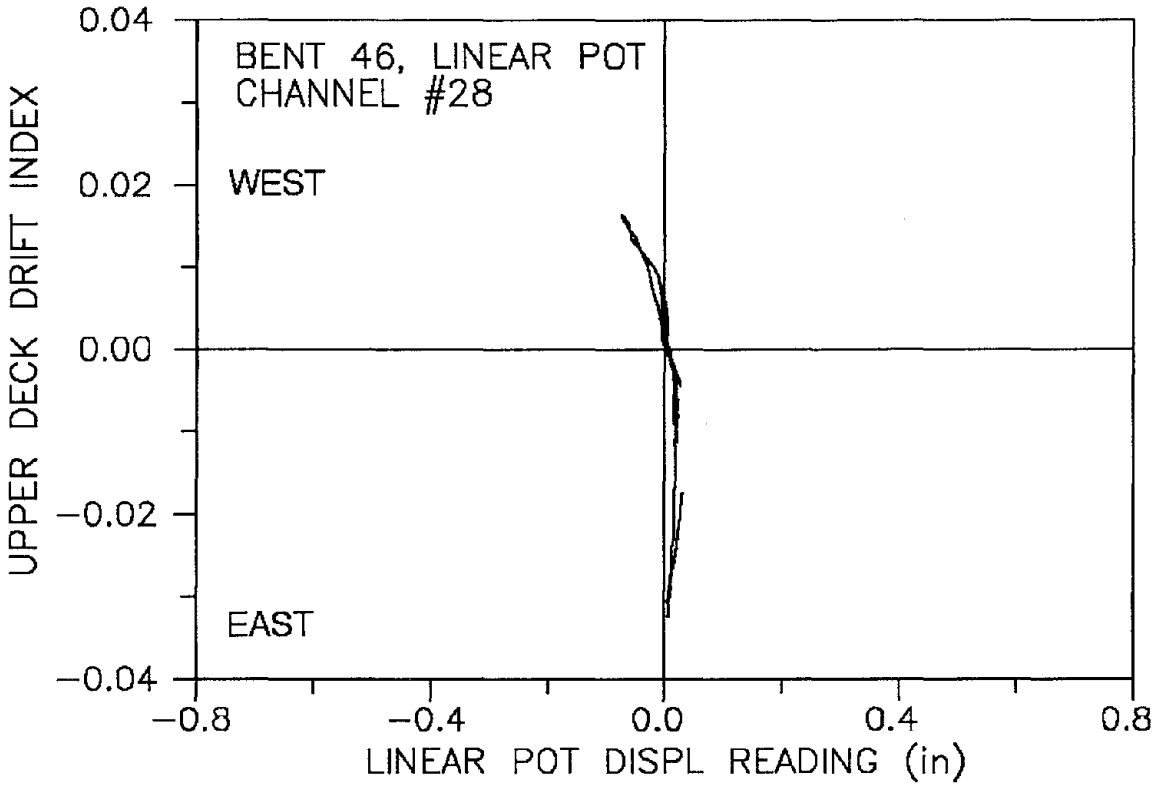
BENT 46, LINEAR POT
CHANNEL #28
WEST
EAST
UPPER DECK DRIFT INDEX
0.04
0.02
0.00
−0.02
−0.04
−0.8
−0.4
0.0
0.4
0.8
LINEAR POT DISPL READING (in)

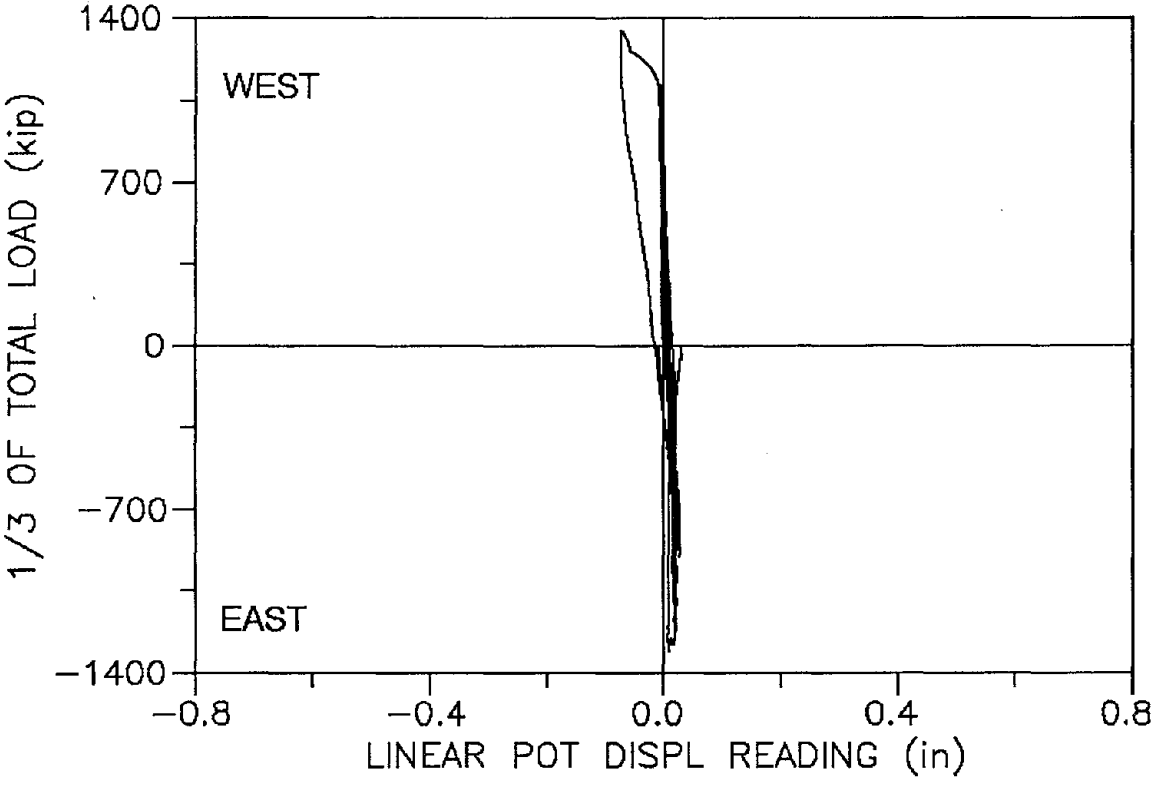
WEST
EAST
1/3 OF TOTAL LOAD (kip)
1400
700
0
−700
−1400
−0.8
−0.4
0.0
0.4
0.8
LINEAR POT DISPL READING (in)

Fig. B.33

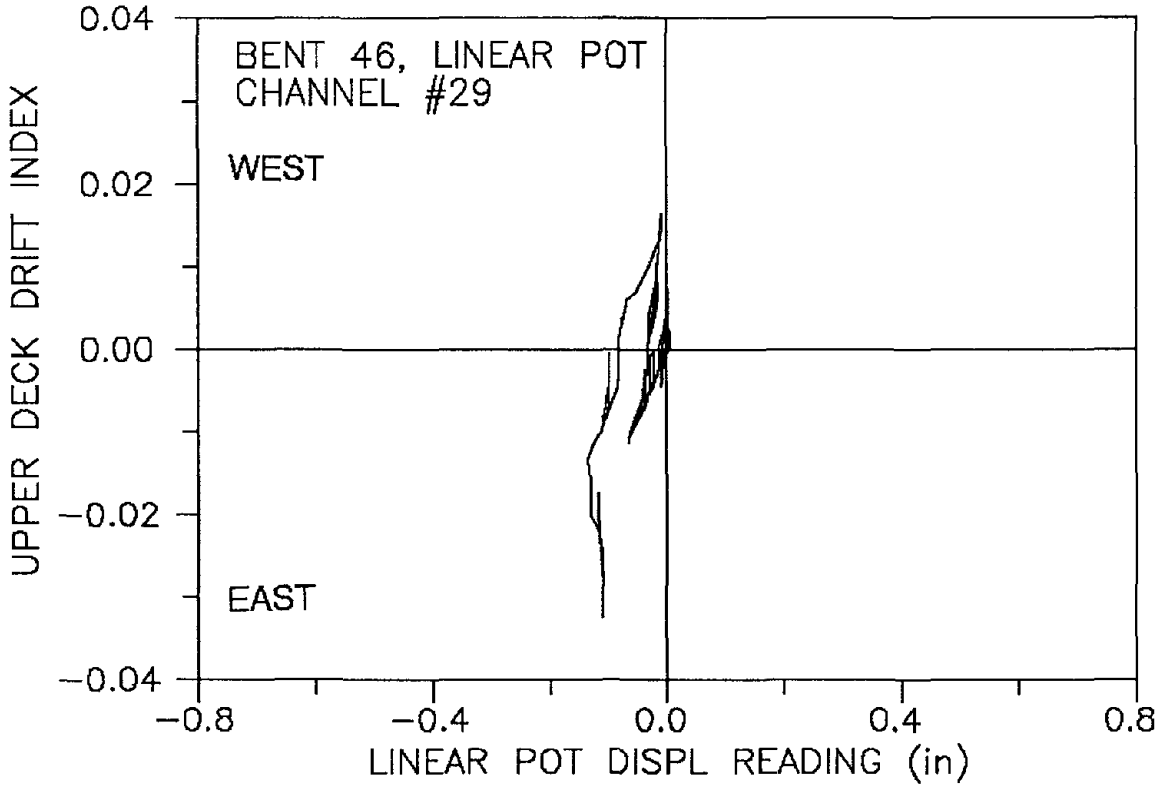
BENT 46, LINEAR POT
CHANNEL #29
WEST
EAST
UPPER DECK DRIFT INDEX
0.04
0.02
0.00
−0.02
−0.04
−0.8
−0.4
0.0
0.4
0.8
LINEAR POT DISPL READING (in)

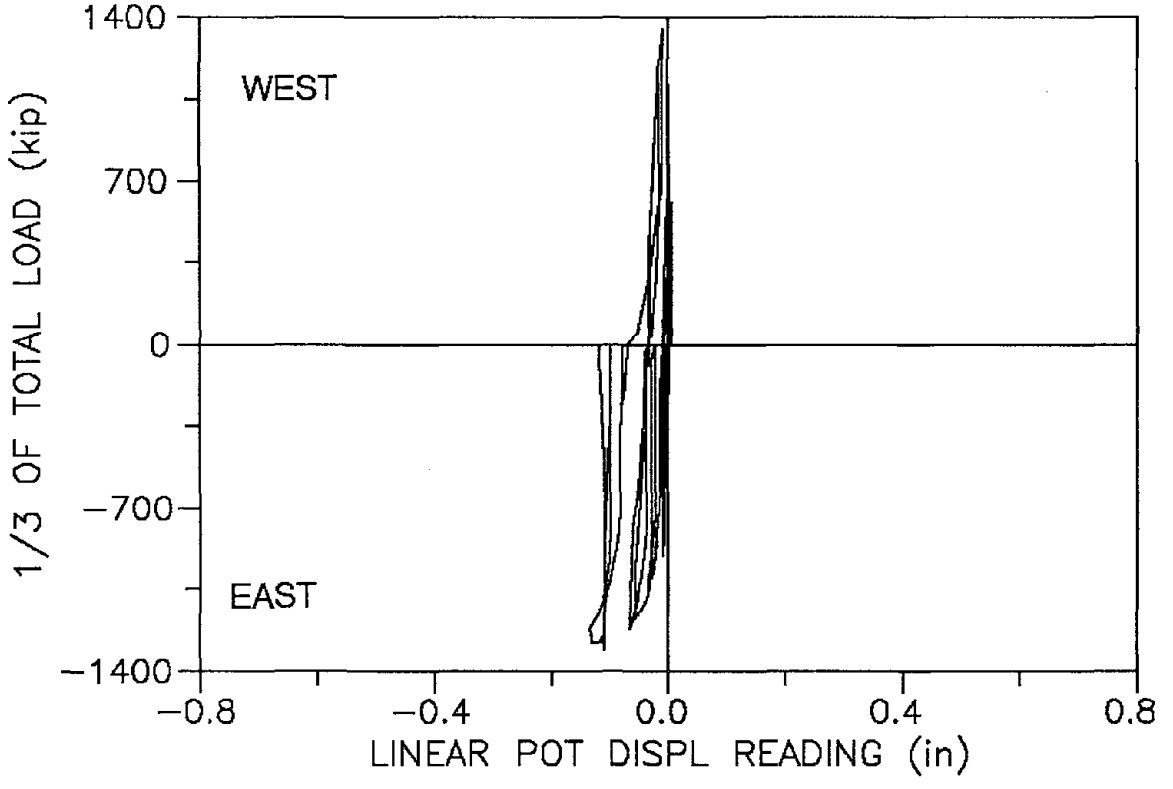
WEST
EAST
1/3 OF TOTAL LOAD (kip)
1400
700
0
−700
−1400
−0.8
−0.4
0.0
0.4
0.8
LINEAR POT DISPL READING (in)

Fig. B.34

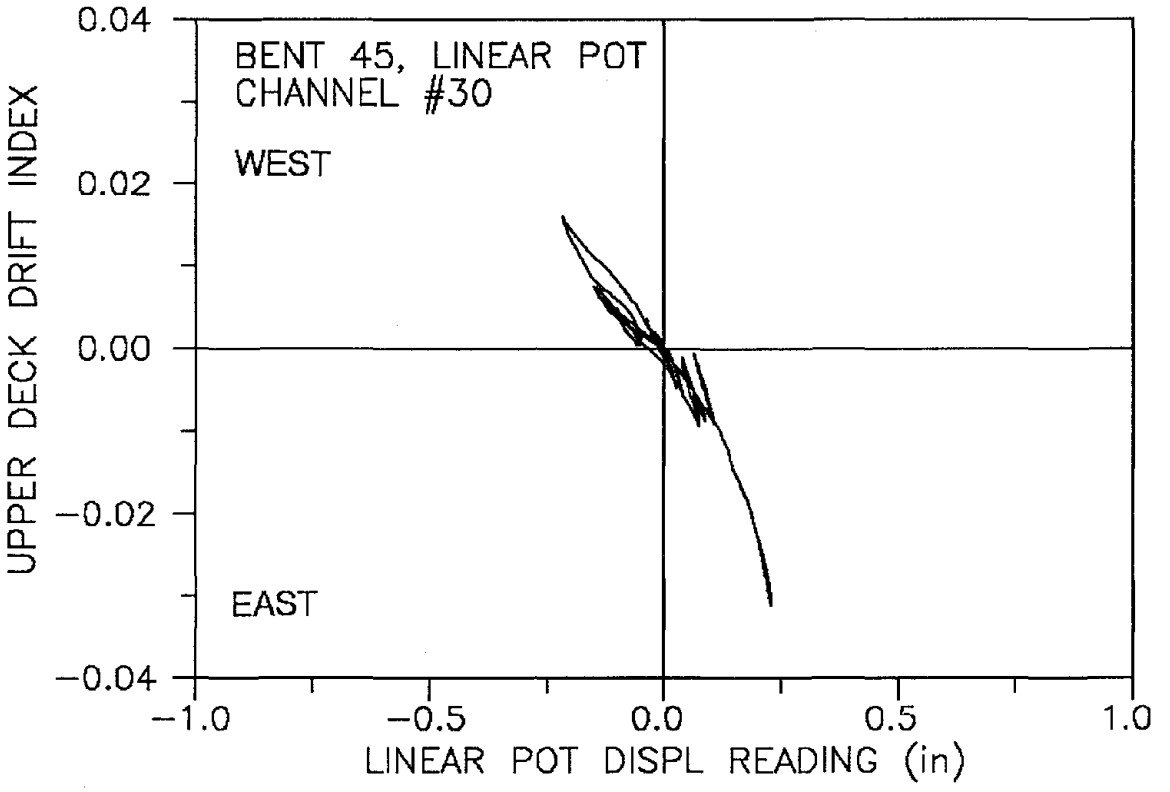
BENT 45, LINEAR POT
CHANNEL #30
WEST
EAST
UPPER DECK DRIFT INDEX
0.04
0.02
0.00
−0.02
−0.04
−1.0
−0.5
0.0
0.5
1.0
LINEAR POT DISPL READING (in)

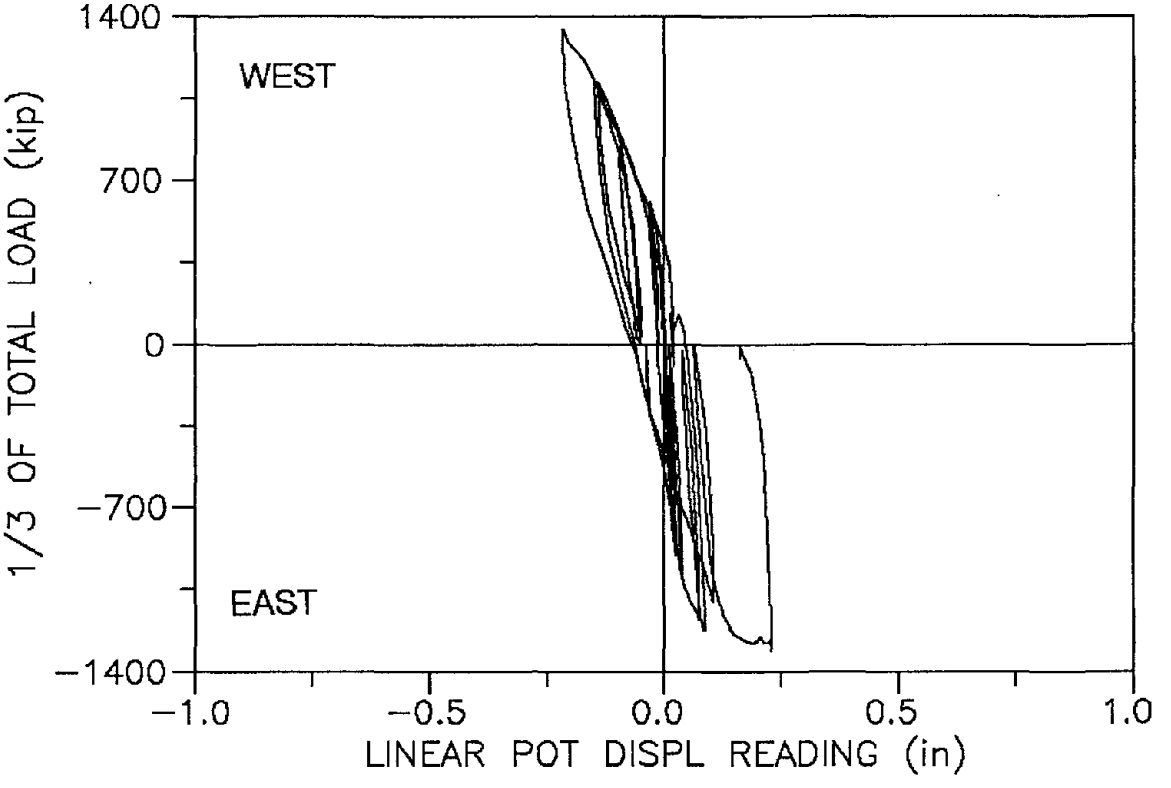
WEST
EAST
1/3 OF TOTAL LOAD (kip)
1400
700
0
−700
−1400
−1.0
−0.5
0.0
0.5
1.0
LINEAR POT DISPL READING (in)

Fig. B.35

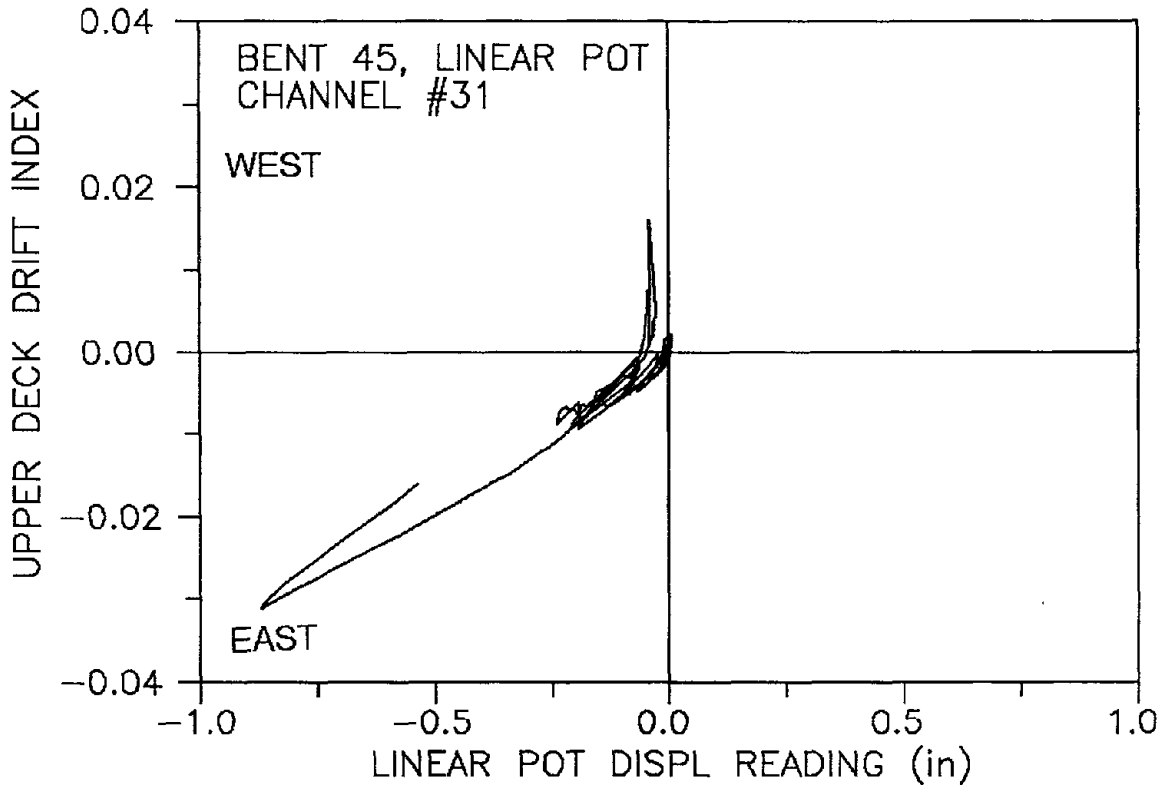
BENT 45, LINEAR POT
CHANNEL #31
WEST
EAST
UPPER DECK DRIFT INDEX
0.04
0.02
0.00
−0.02
−0.04
−1.0
−0.5
0.0
0.5
1.0
LINEAR POT DISPL READING (in)

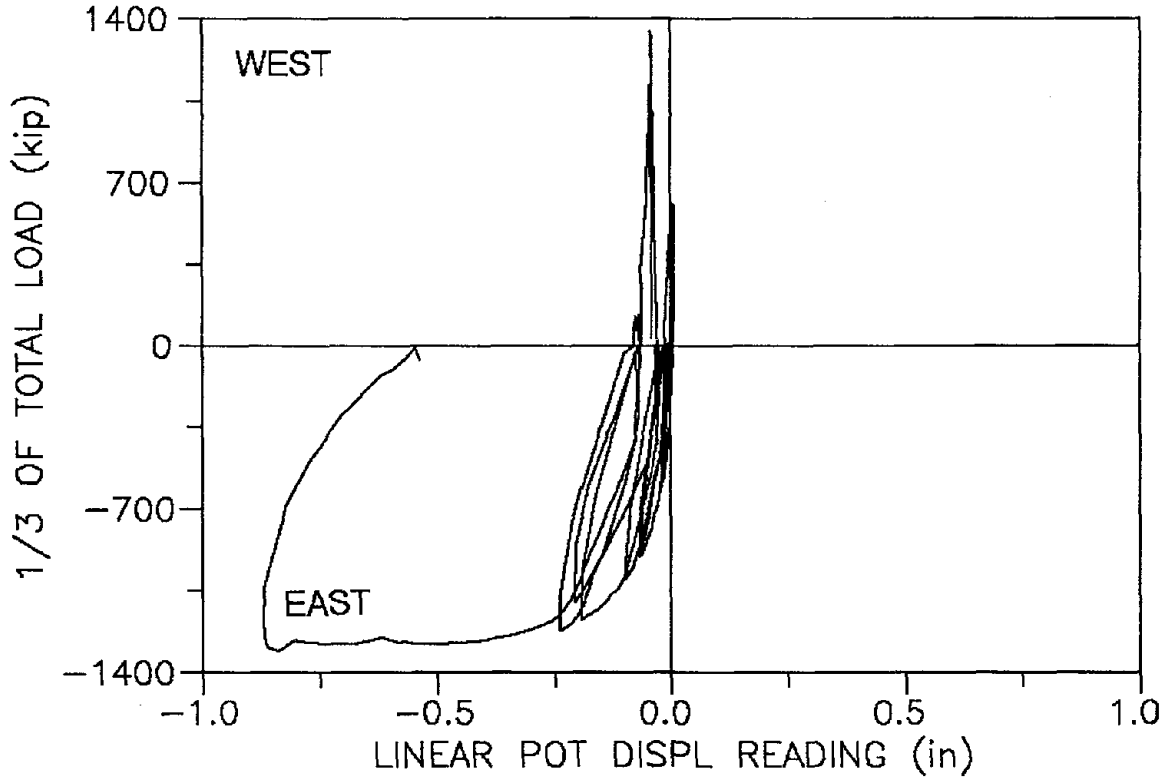
WEST
EAST
1/3 OF TOTAL LOAD (kip)
1400
700
0
−700
−1400
−1.0
−0.5
0.0
0.5
1.0
LINEAR POT DISPL READING (in)

Fig. B.36

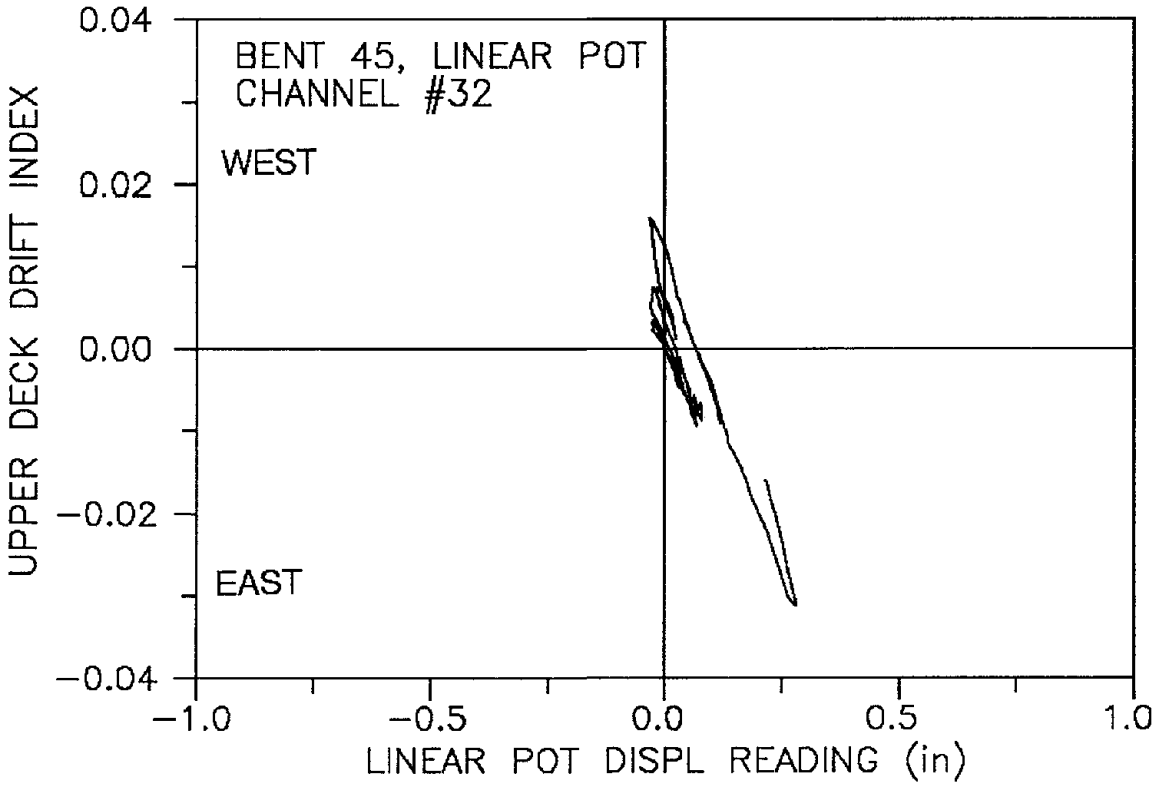
BENT 45, LINEAR POT
CHANNEL #32
WEST
EAST
UPPER DECK DRIFT INDEX
0.04
0.02
0.00
−0.02
−0.04
−1.0
−0.5
0.0
0.5
1.0
LINEAR POT DISPL READING (in)

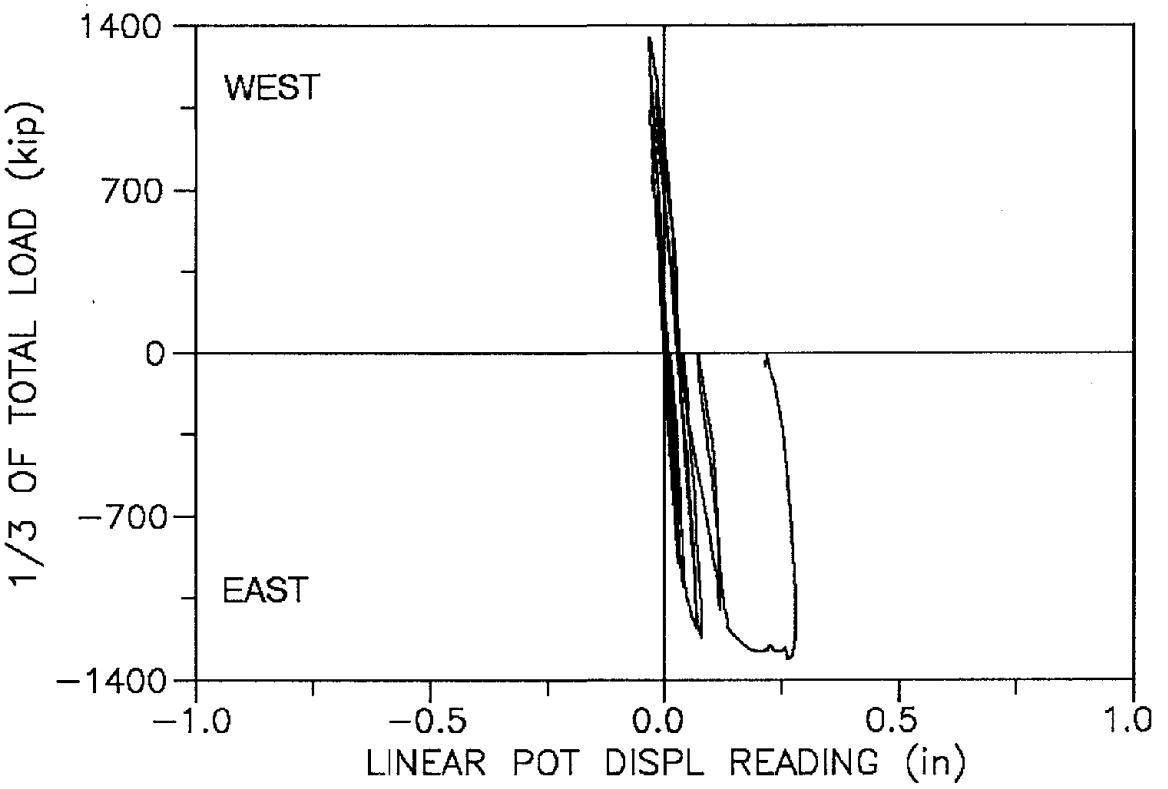
WEST
EAST
1/3 OF TOTAL LOAD (kip)
1400
700
0
−700
−1400
−1.0
−0.5
0.0
0.5
1.0
LINEAR POT DISPL READING (in)

Fig. B.37

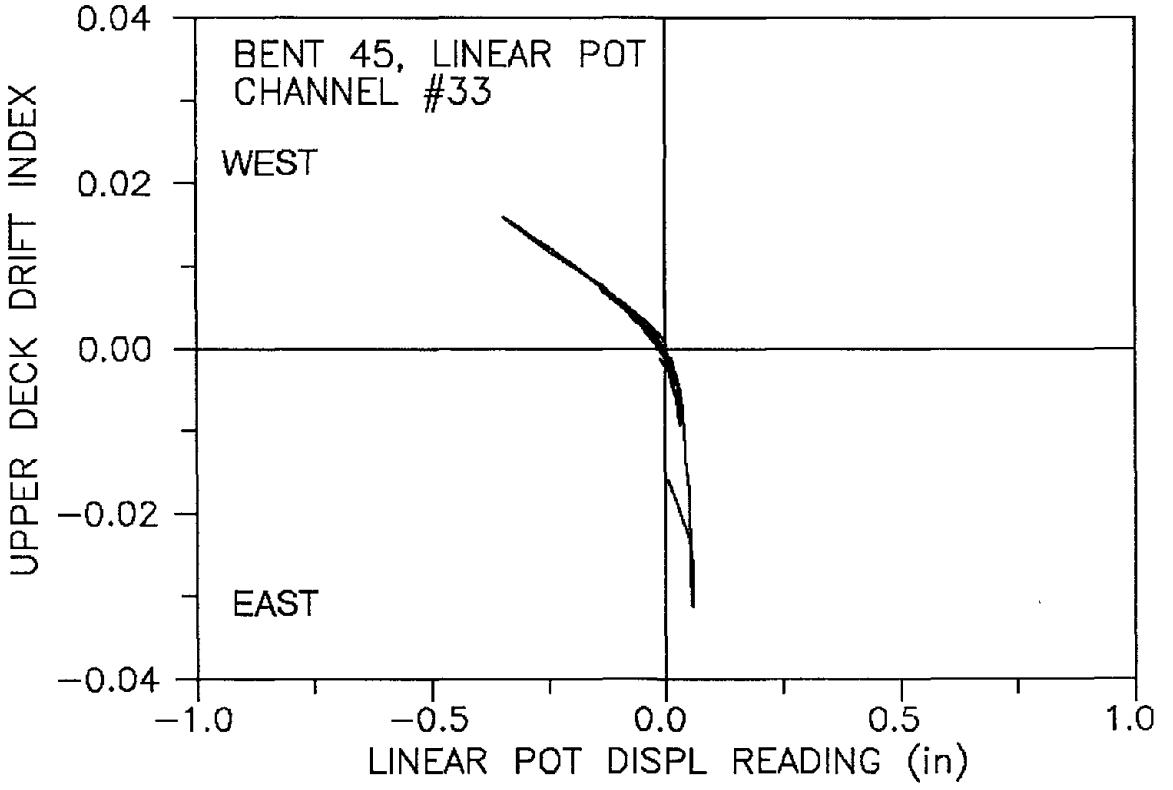
BENT 45, LINEAR POT
CHANNEL #33
WEST
EAST
UPPER DECK DRIFT INDEX
0.04
0.02
0.00
−0.02
−0.04
−1.0
−0.5
0.0
0.5
1.0
LINEAR POT DISPL READING (in)

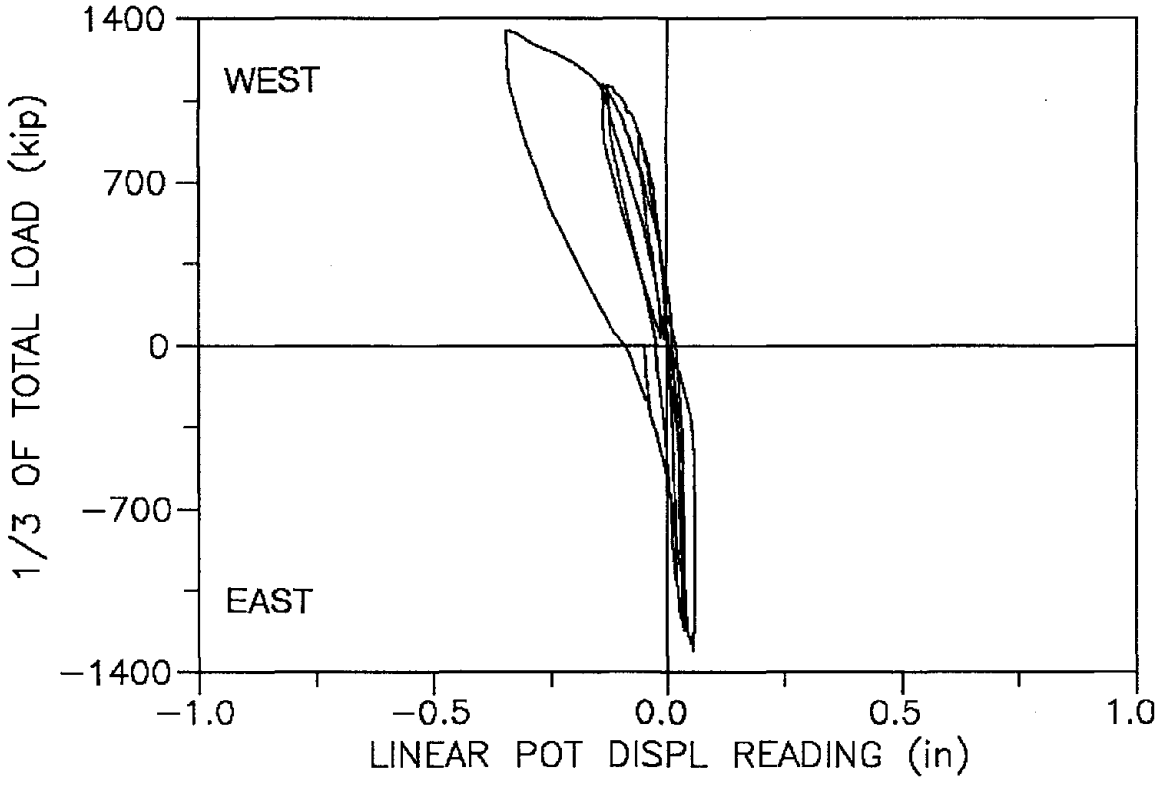
WEST
EAST
1/3 OF TOTAL LOAD (kip)
1400
700
0
−700
−1400
−1.0
−0.5
0.0
0.5
1.0
LINEAR POT DISPL READING (in)

Fig. B.38

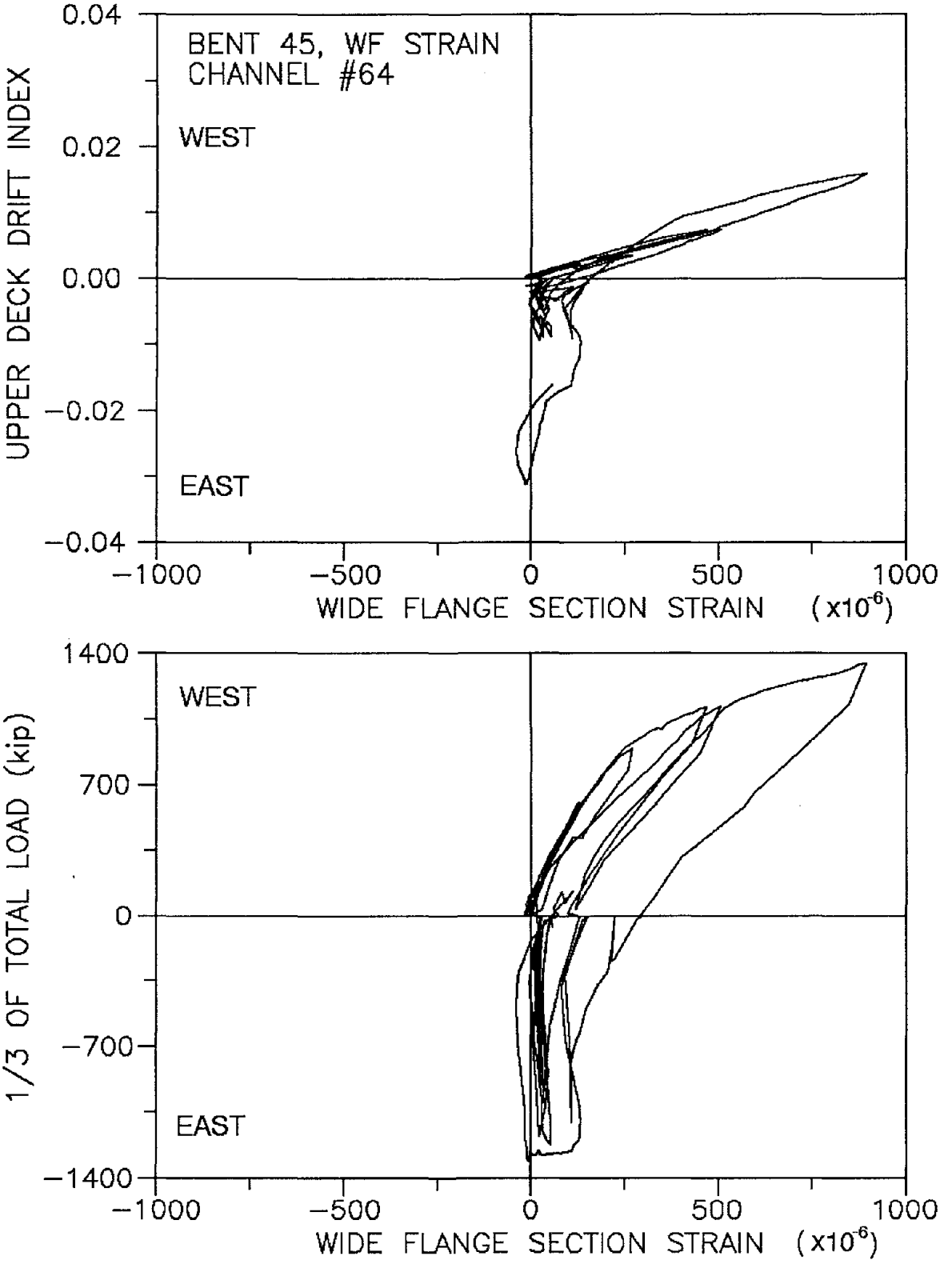
BENT 45, WF STRAIN
CHANNEL #64
WEST
EAST
UPPER DECK DRIFT INDEX
0.04
0.02
0.00
−0.02
−0.04
−1000
−500
0
500
1000
WIDE FLANGE SECTION STRAIN (x10⁻⁶)
WEST
EAST
1/3 OF TOTAL LOAD (kip)
1400
700
0
−700
−1400
−1000
−500
0
500
1000
WIDE FLANGE SECTION STRAIN (x10⁻⁶)

Fig. B.39

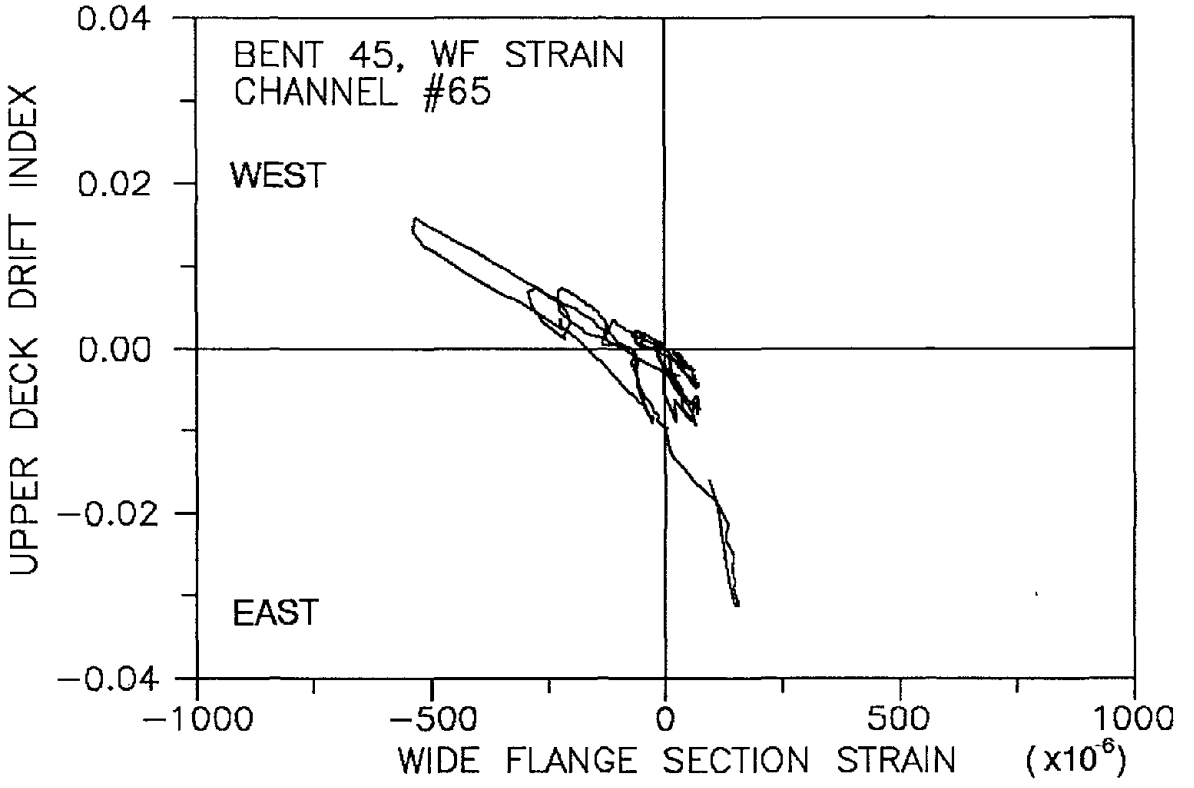
BENT 45, WF STRAIN
CHANNEL #65
WEST
EAST
UPPER DECK DRIFT INDEX
0.04
0.02
0.00
−0.02
−0.04
−1000
−500
0
500
1000
WIDE FLANGE SECTION STRAIN (x10⁻⁶)

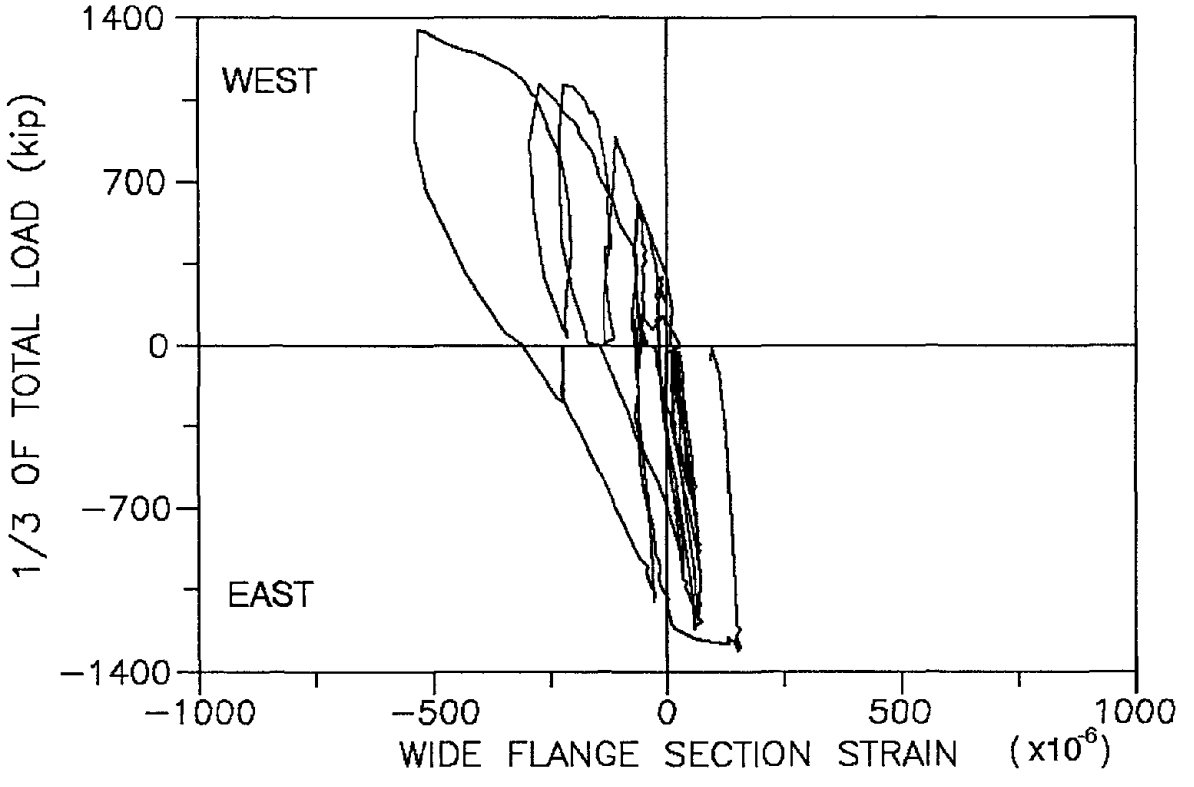
WEST
EAST
1/3 OF TOTAL LOAD (kip)
1400
700
0
−700
−1400
−1000
−500
0
500
1000
WIDE FLANGE SECTION STRAIN (x10⁻⁶)

Fig. B.40

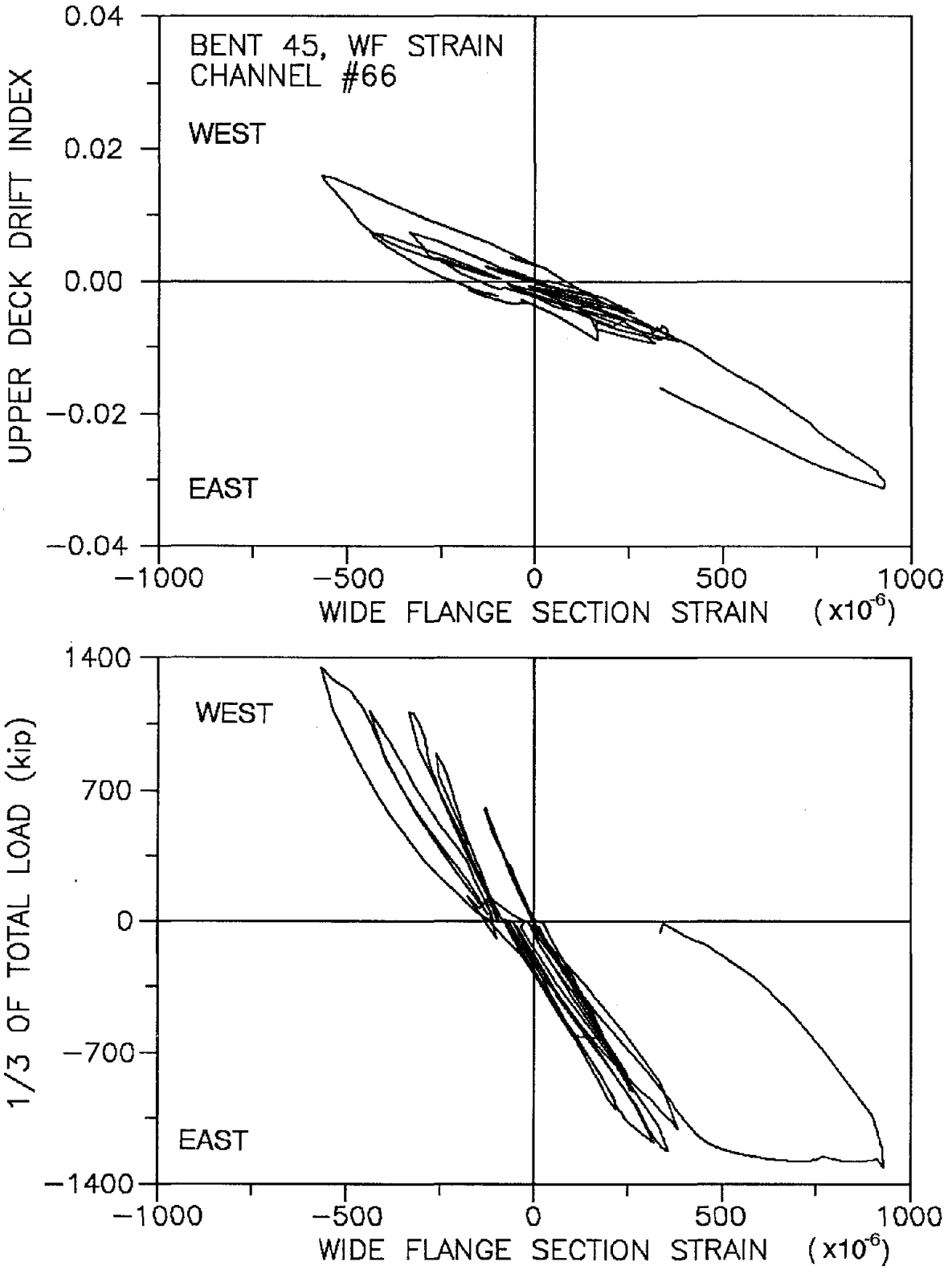
BENT 45, WF STRAIN
CHANNEL #66
WEST
EAST
UPPER DECK DRIFT INDEX
0.04
0.02
0.00
−0.02
−0.04
−1000
−500
0
500
1000
WIDE FLANGE SECTION STRAIN (x10⁻⁶)
WEST
EAST
1/3 OF TOTAL LOAD (kip)
1400
700
0
−700
−1400
−1000
−500
0
500
1000
WIDE FLANGE SECTION STRAIN (x10⁻⁶)

Fig. B.41

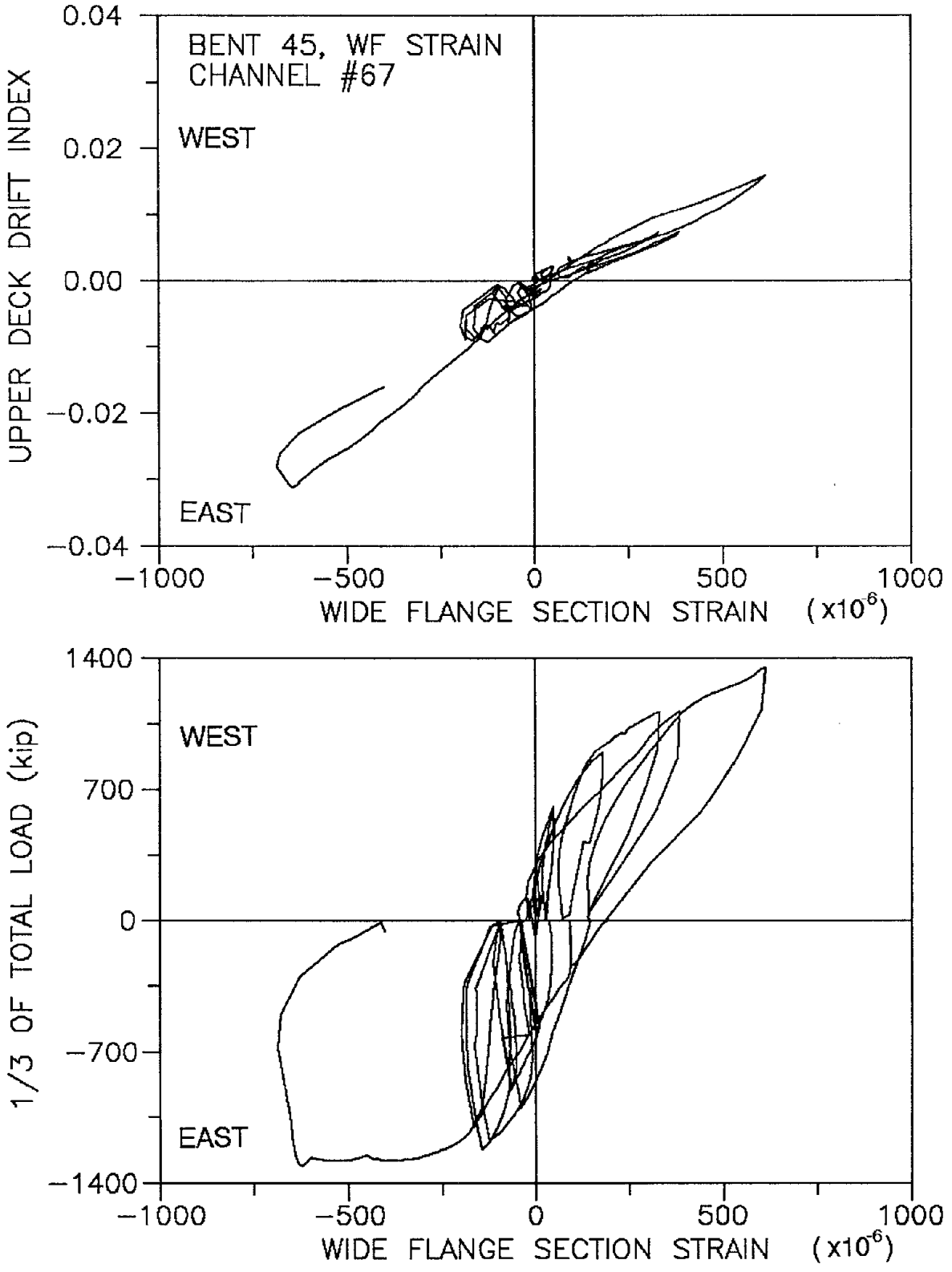
BENT 45, WF STRAIN
CHANNEL #67
WEST
EAST
UPPER DECK DRIFT INDEX
0.04
0.02
0.00
−0.02
−0.04
−1000
−500
0
500
1000
WIDE FLANGE SECTION STRAIN (x10⁻⁶)
1/3 OF TOTAL LOAD (kip)
1400
700
0
−700
−1400
WEST
EAST
−1000
−500
0
500
1000
WIDE FLANGE SECTION STRAIN (x10⁻⁶)

Fig. B.42

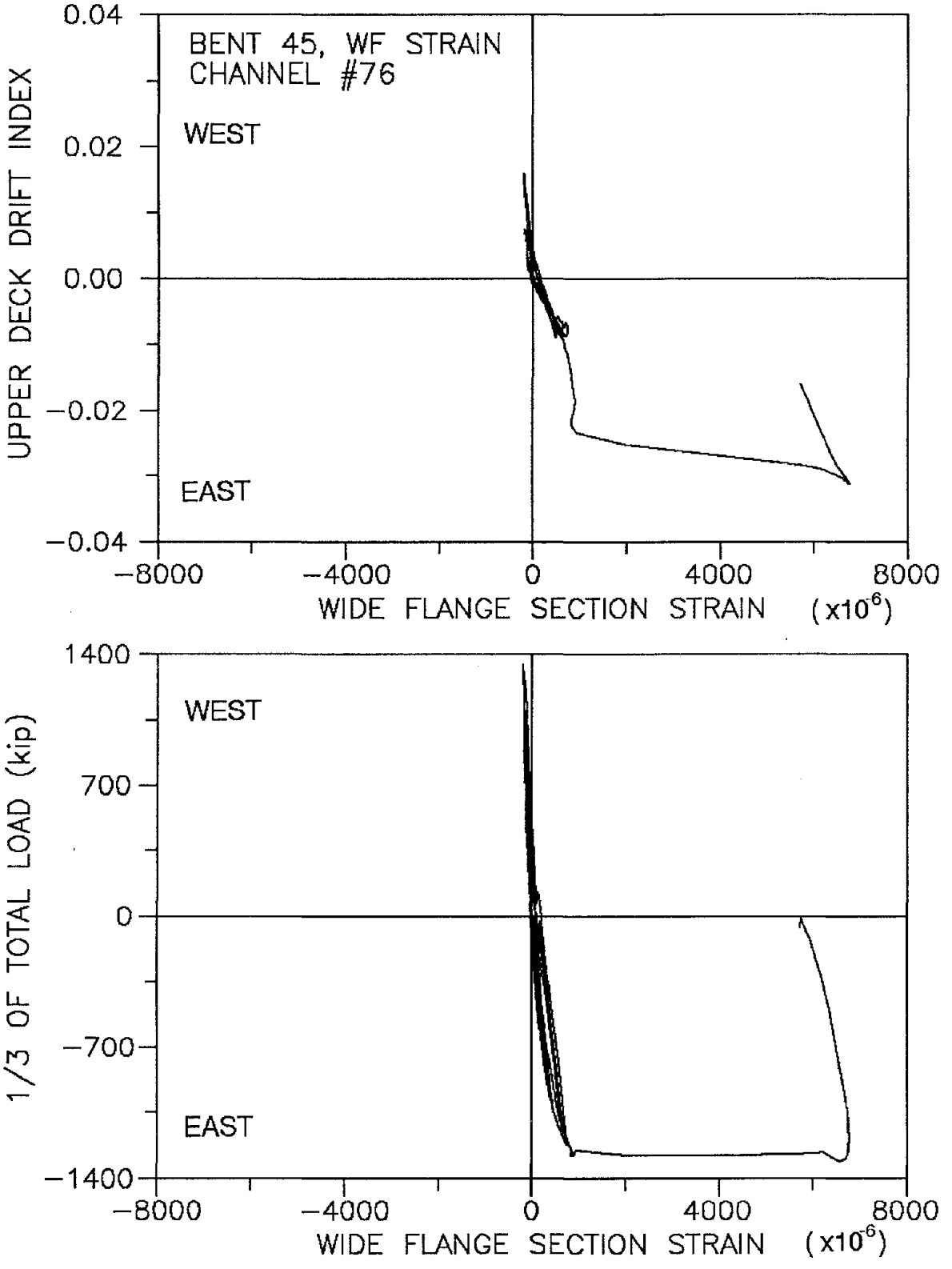
BENT 45, WF STRAIN
CHANNEL #76
WEST
EAST
UPPER DECK DRIFT INDEX
0.04
0.02
0.00
−0.02
−0.04
−8000
−4000
0
4000
8000
WIDE FLANGE SECTION STRAIN (x10⁻⁶)
WEST
EAST
1/3 OF TOTAL LOAD (kip)
1400
700
0
−700
−1400
−8000
−4000
0
4000
8000
WIDE FLANGE SECTION STRAIN (x10⁻⁶)

Fig. B.43

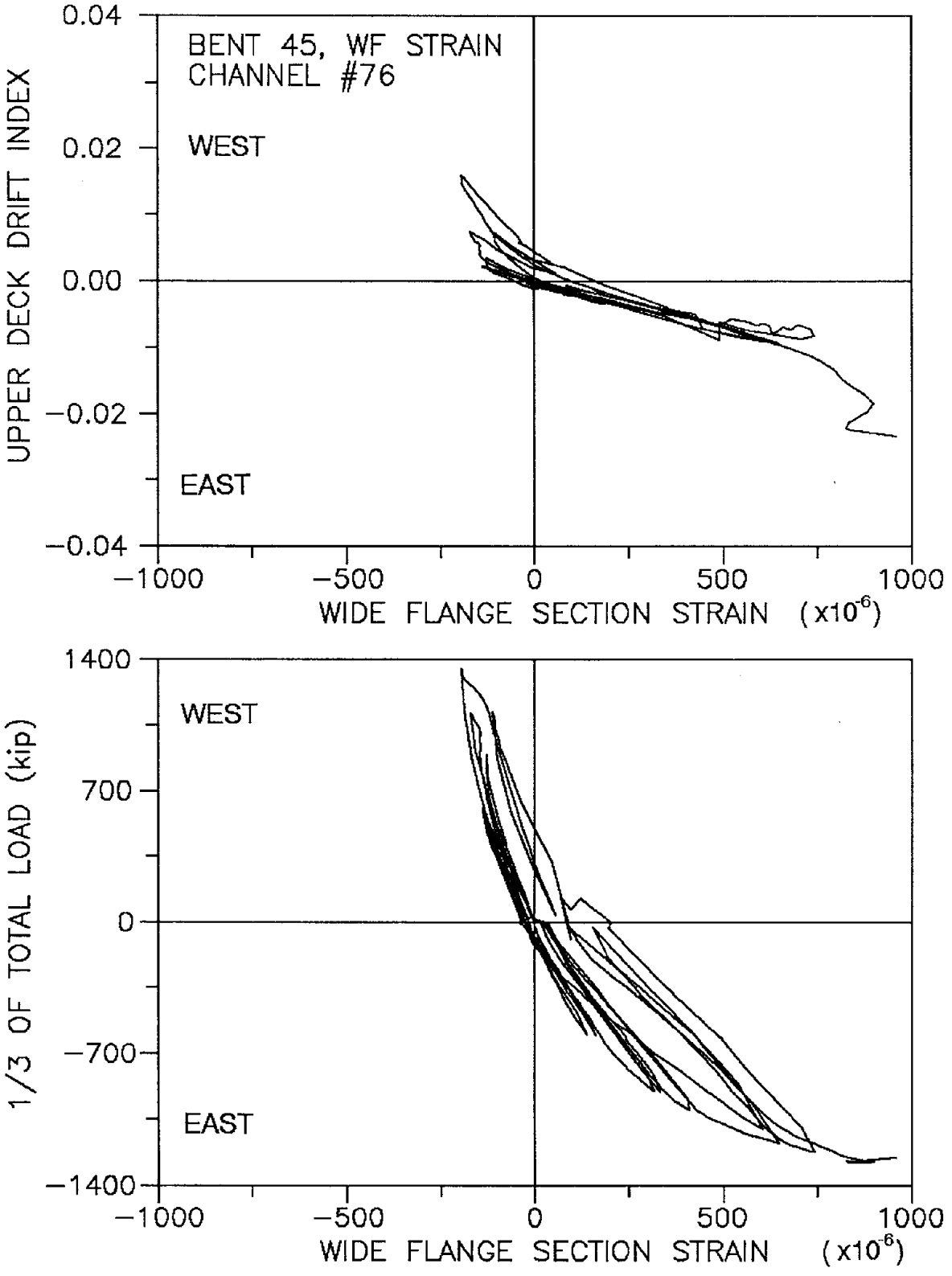
BENT 45, WF STRAIN
CHANNEL #76
WEST
EAST
UPPER DECK DRIFT INDEX
0.04
0.02
0.00
−0.02
−0.04
−1000
−500
0
500
1000
WIDE FLANGE SECTION STRAIN (x10-6)
1/3 OF TOTAL LOAD (kip)
1400
700
0
−700
−1400
WEST
EAST
−1000
−500
0
500
1000
WIDE FLANGE SECTION STRAIN (x10-6)

Fig. B.43

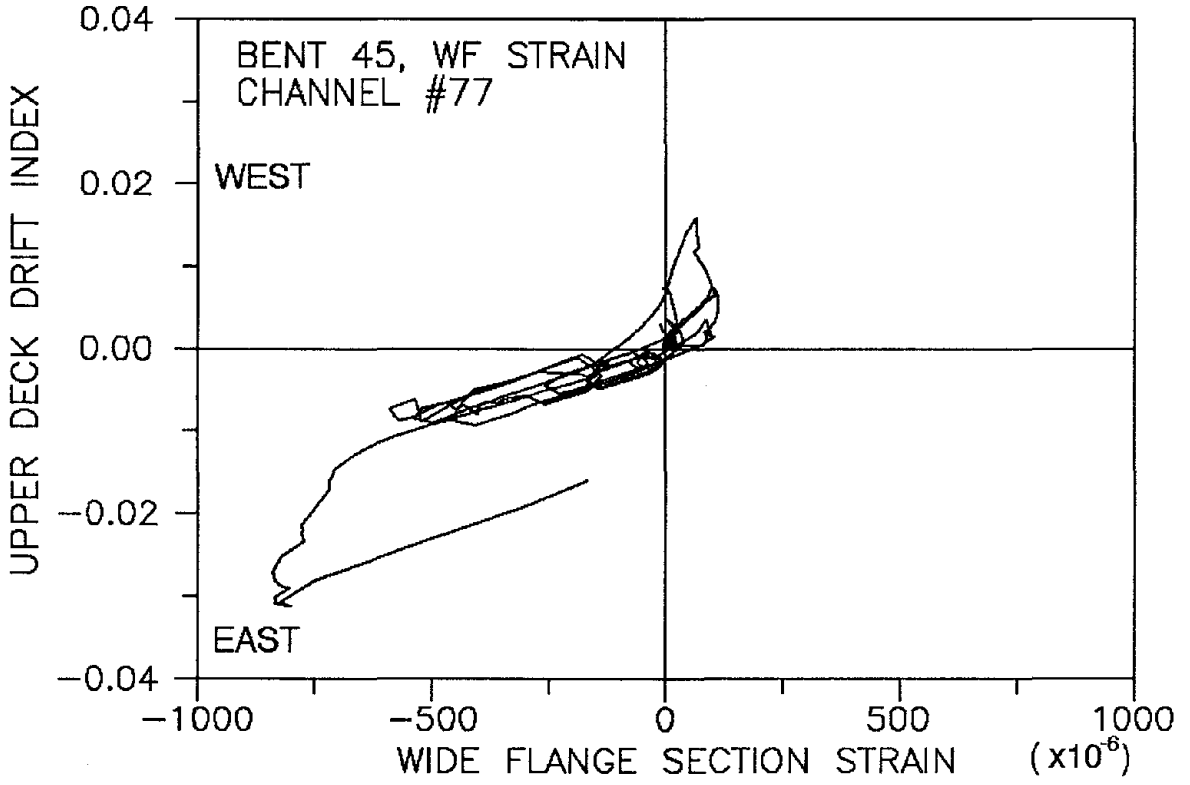
BENT 45, WF STRAIN
CHANNEL #77
WEST
EAST
UPPER DECK DRIFT INDEX
0.04
0.02
0.00
-0.02
-0.04
-1000
-500
0
500
1000
WIDE FLANGE SECTION STRAIN (x10-6)

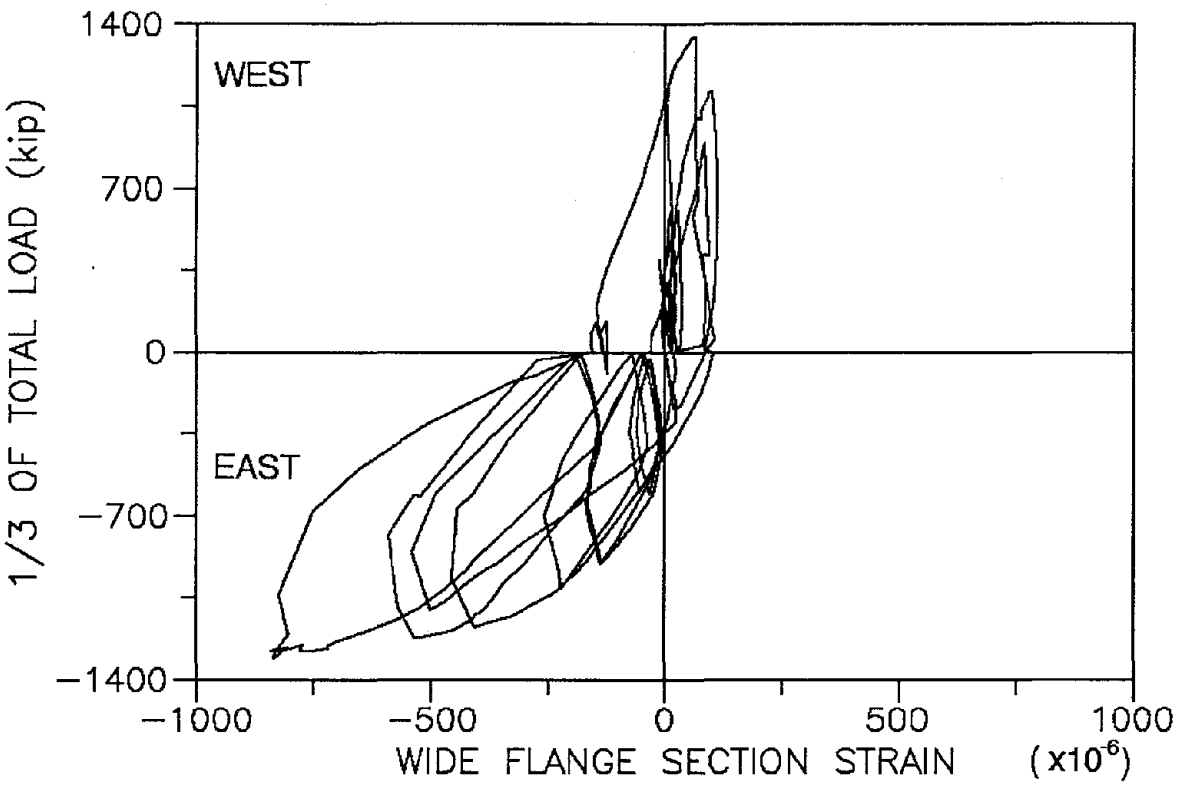
WEST
EAST
1/3 OF TOTAL LOAD (kip)
1400
700
0
-700
-1400
-1000
-500
0
500
1000
WIDE FLANGE SECTION STRAIN (x10-6)

Fig. B.44

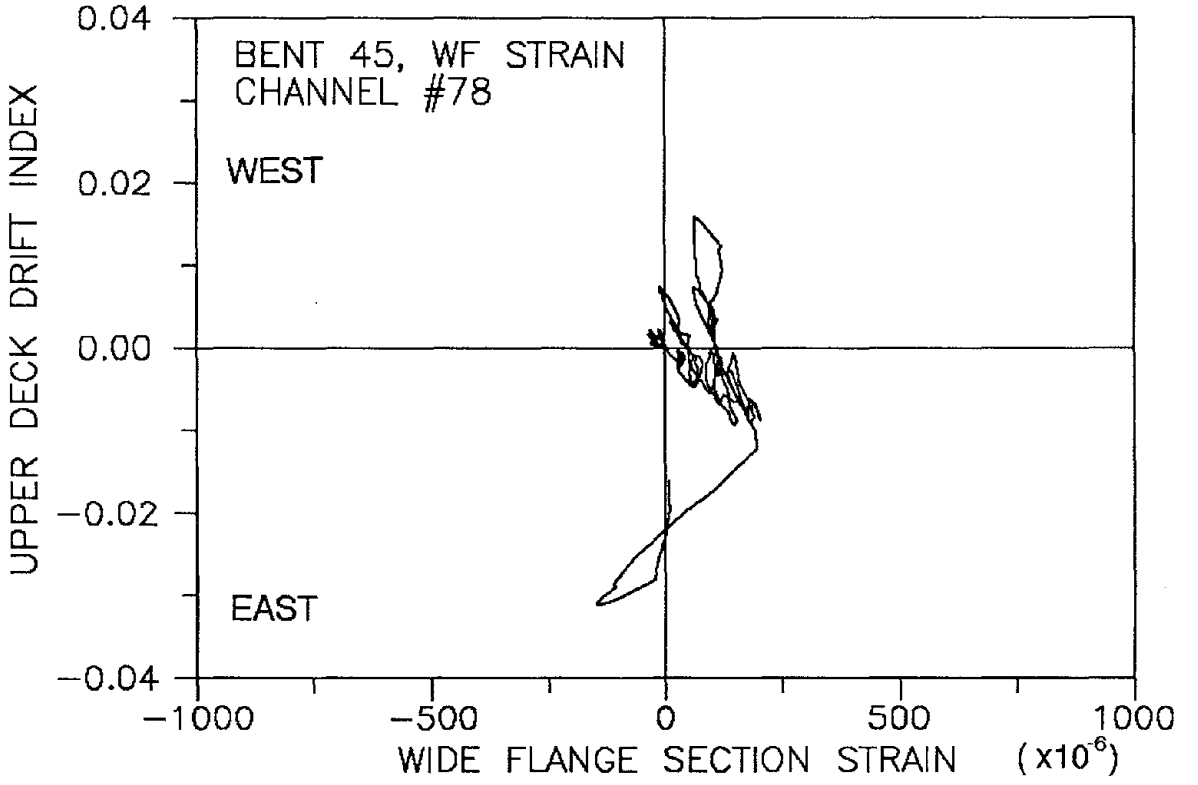
BENT 45, WF STRAIN
CHANNEL #78
WEST
EAST
UPPER DECK DRIFT INDEX
0.04
0.02
0.00
−0.02
−0.04
−1000
−500
0
500
1000
WIDE FLANGE SECTION STRAIN (x10⁻⁶)

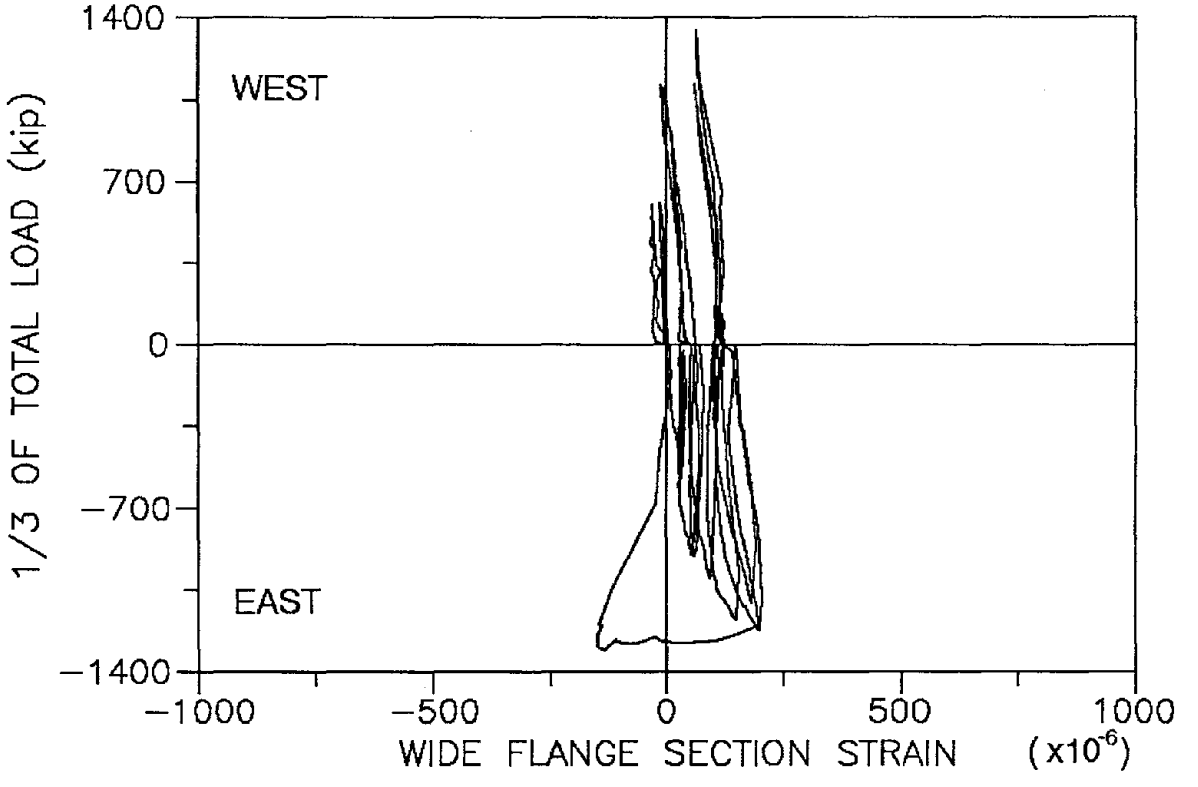
WEST
EAST
1/3 OF TOTAL LOAD (kip)
1400
700
0
−700
−1400
−1000
−500
0
500
1000
WIDE FLANGE SECTION STRAIN (x10⁻⁶)

Fig. B.45

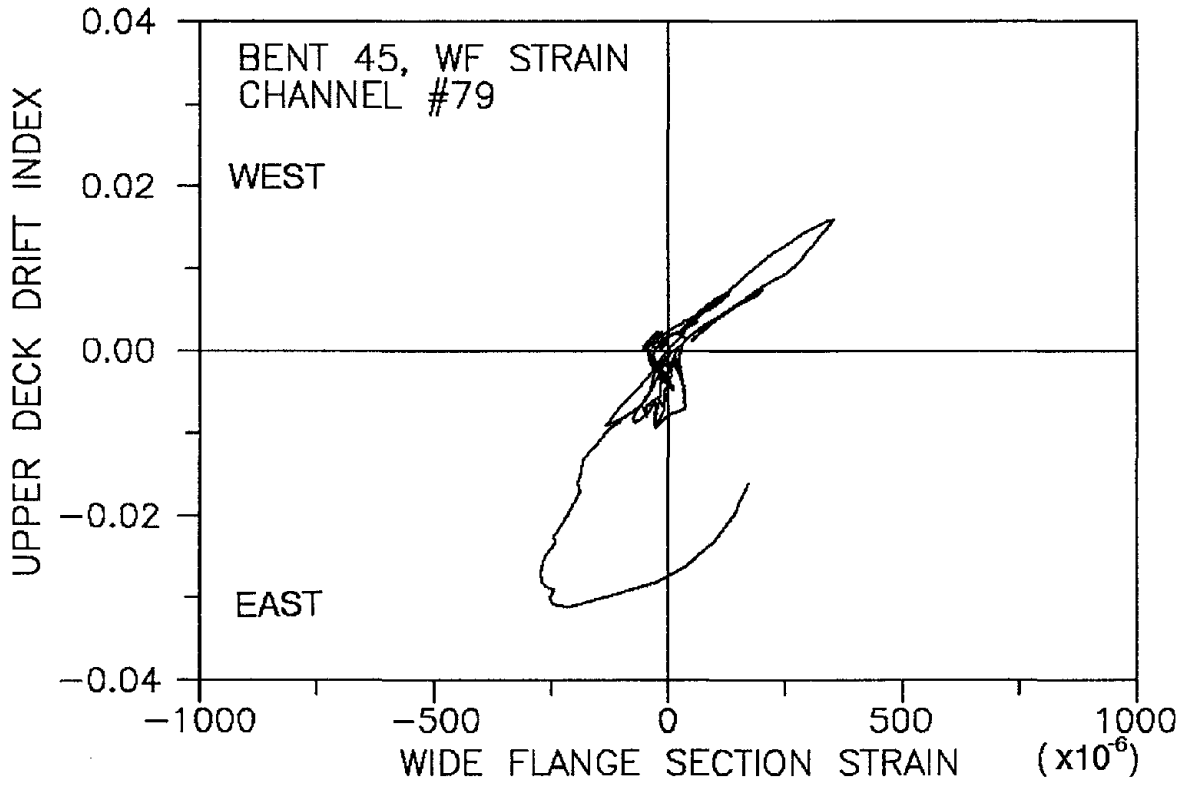
BENT 45, WF STRAIN
CHANNEL #79
WEST
EAST
UPPER DECK DRIFT INDEX
0.04
0.02
0.00
−0.02
−0.04
−1000
−500
0
500
1000
WIDE FLANGE SECTION STRAIN
(x10-6)

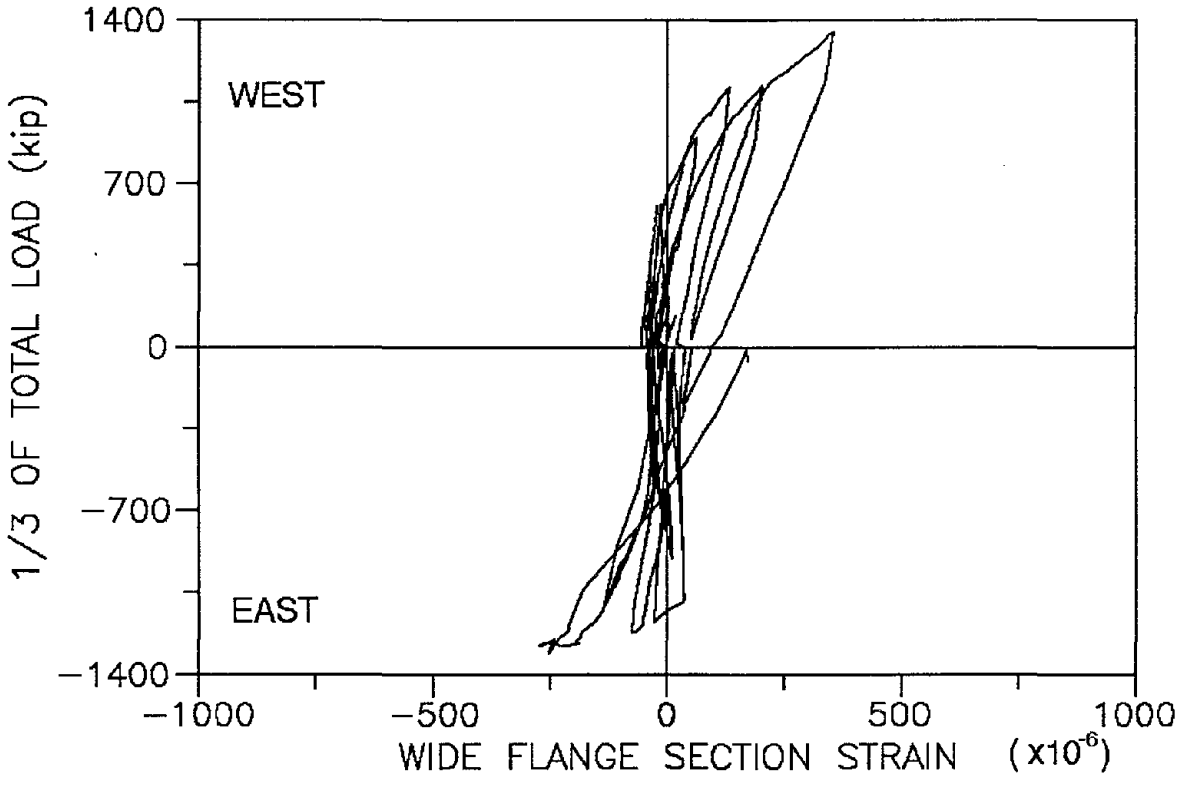
WEST
EAST
1/3 OF TOTAL LOAD (kip)
1400
700
0
−700
−1400
−1000
−500
0
500
1000
WIDE FLANGE SECTION STRAIN
(x10-6)

Fig. B.46

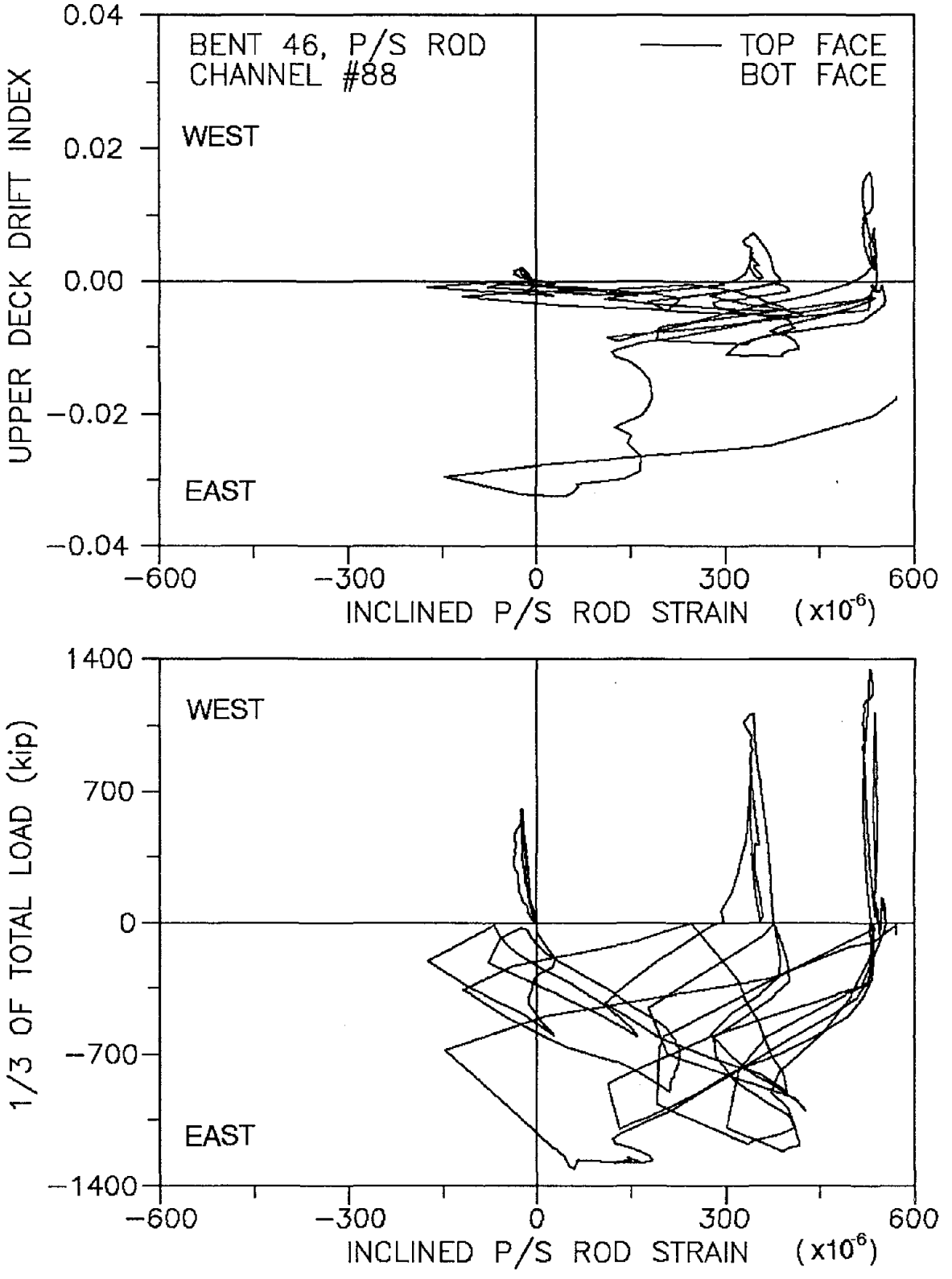
BENT 46, P/S ROD
CHANNEL #88
TOP FACE
BOT FACE
WEST
EAST
UPPER DECK DRIFT INDEX
0.04
0.02
0.00
-0.02
-0.04
-600
-300
0
300
600
INCLINED P/S ROD STRAIN (x10-6)
1/3 OF TOTAL LOAD (kip)
1400
700
0
-700
-1400

Fig. B.47

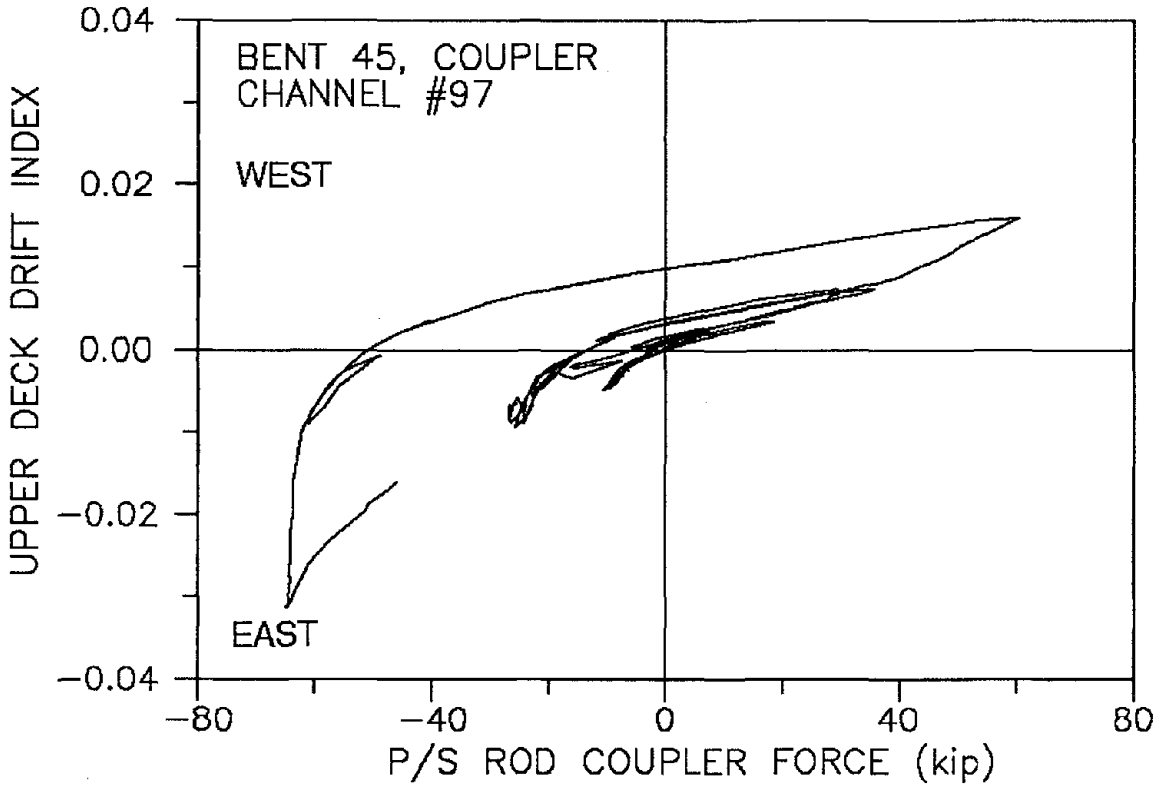
BENT 45, COUPLER
CHANNEL #97
WEST
EAST
UPPER DECK DRIFT INDEX
0.04
0.02
0.00
−0.02
−0.04
−80
−40
0
40
80
P/S ROD COUPLER FORCE (kip)

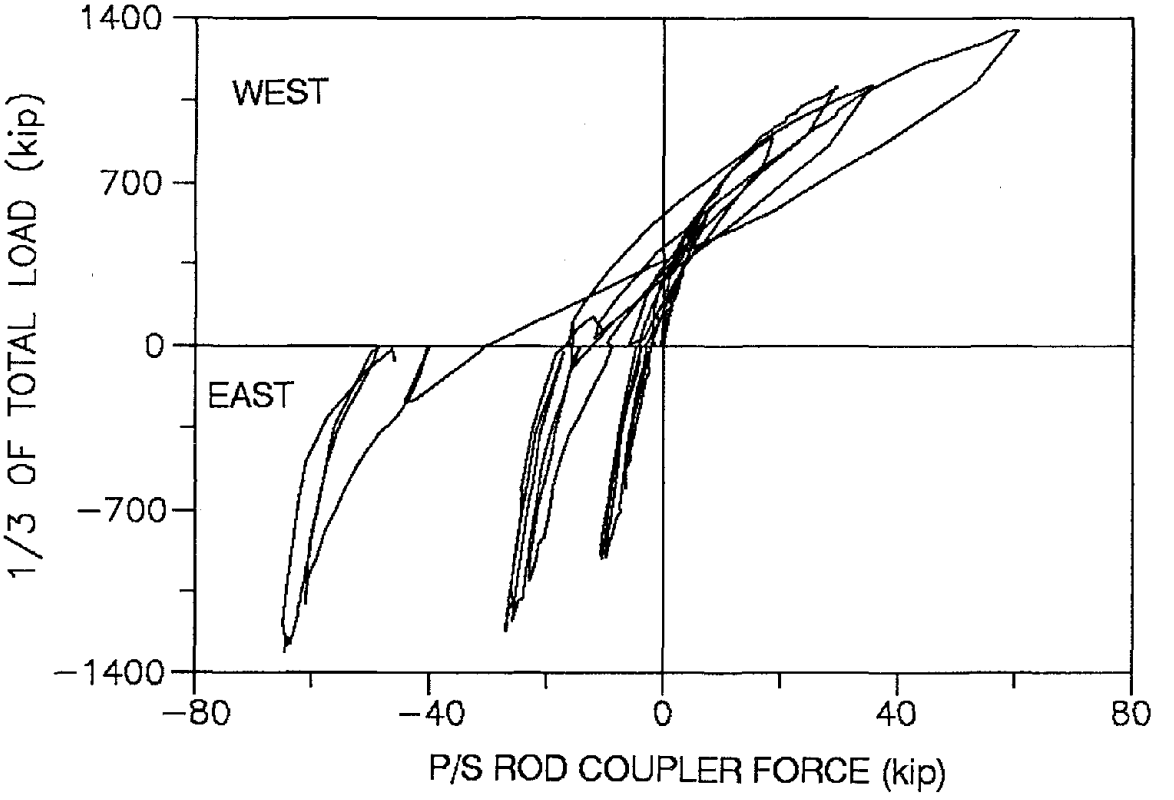
WEST
EAST
1/3 OF TOTAL LOAD (kip)
1400
700
0
−700
−1400
−80
−40
0
40
80
P/S ROD COUPLER FORCE (kip)

Fig. B.48

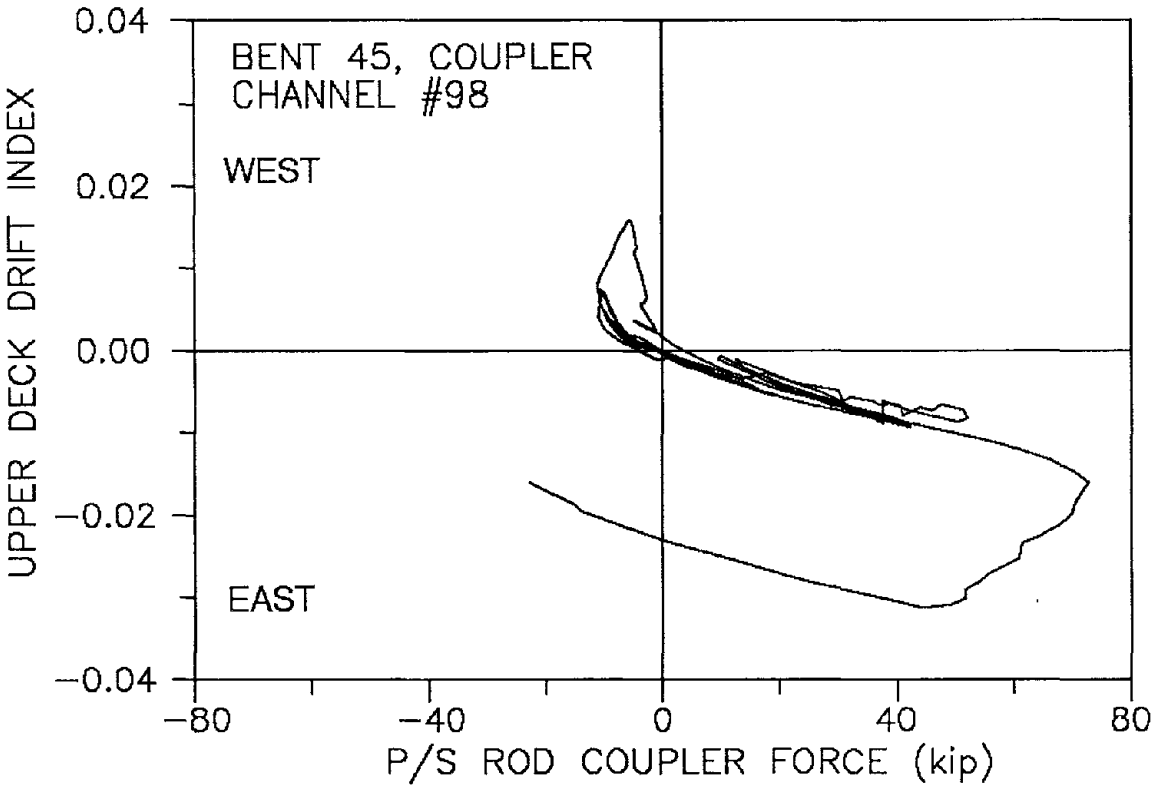
BENT 45, COUPLER
CHANNEL #98
WEST
EAST
UPPER DECK DRIFT INDEX
0.04
0.02
0.00
−0.02
−0.04
−80
−40
0
40
80
P/S ROD COUPLER FORCE (kip)

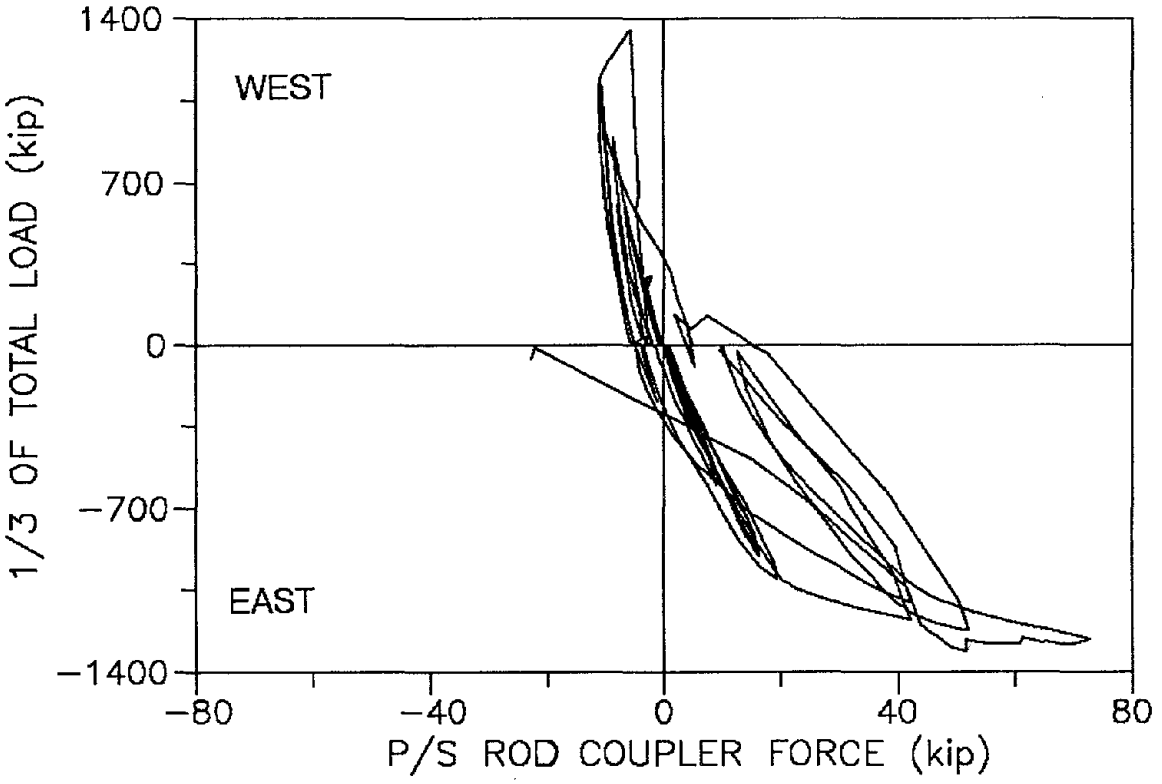
WEST
EAST
1/3 OF TOTAL LOAD (kip)
1400
700
0
−700
−1400
−80
−40
0
40
80
P/S ROD COUPLER FORCE (kip)

Fig. B.49

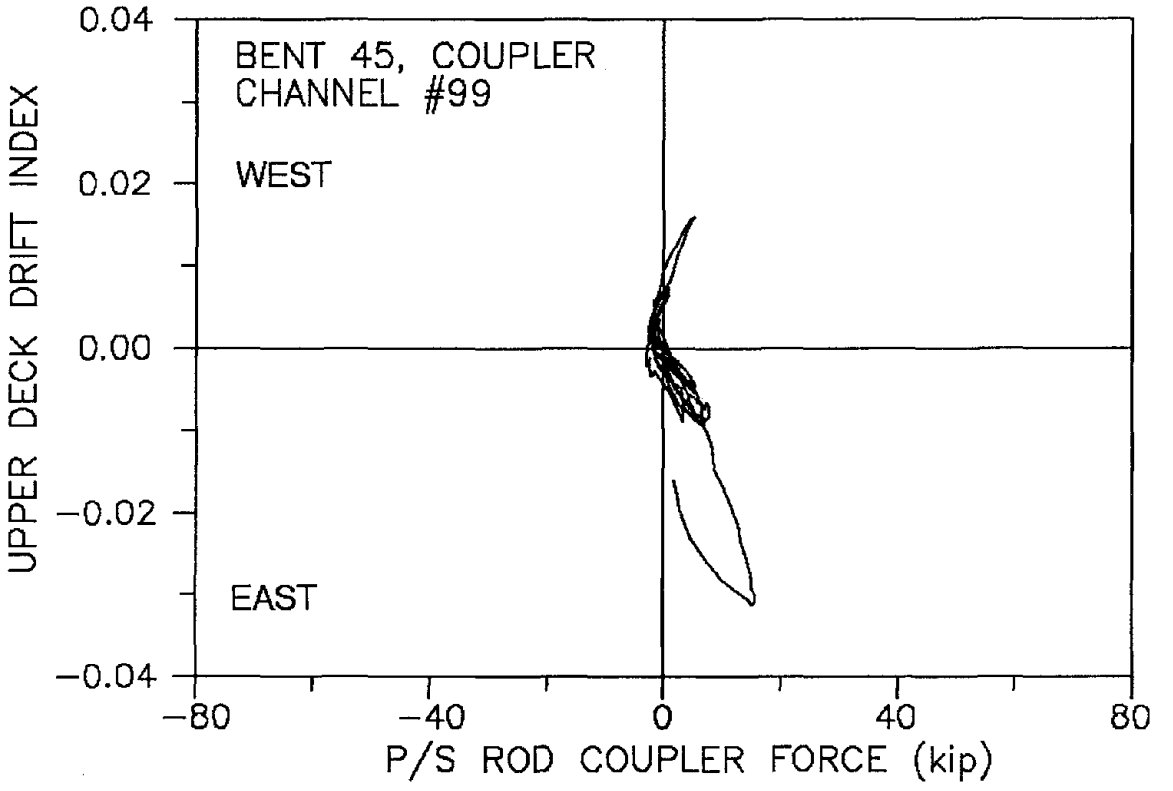
BENT 45, COUPLER
CHANNEL #99
WEST
EAST
UPPER DECK DRIFT INDEX
0.04
0.02
0.00
−0.02
−0.04
−80
−40
0
40
80
P/S ROD COUPLER FORCE (kip)

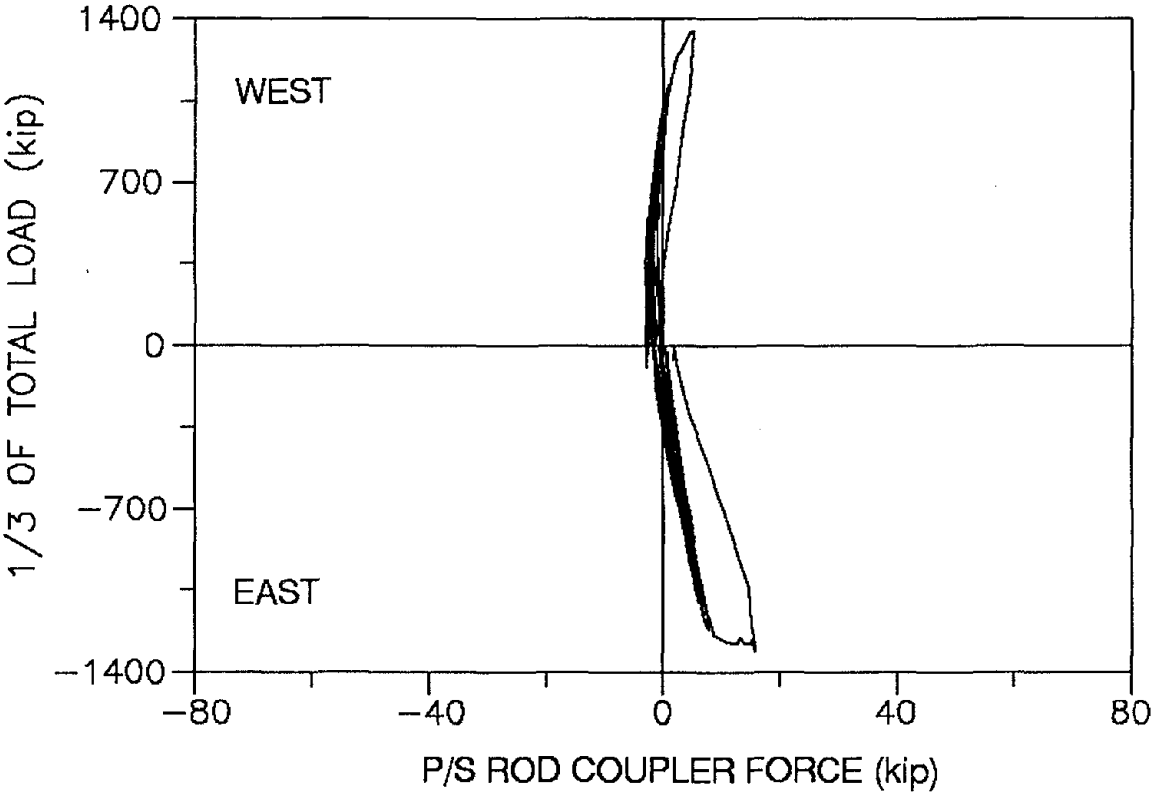
WEST
EAST
1/3 OF TOTAL LOAD (kip)
1400
700
0
−700
−1400
−80
−40
0
40
80
P/S ROD COUPLER FORCE (kip)

Fig. B.50

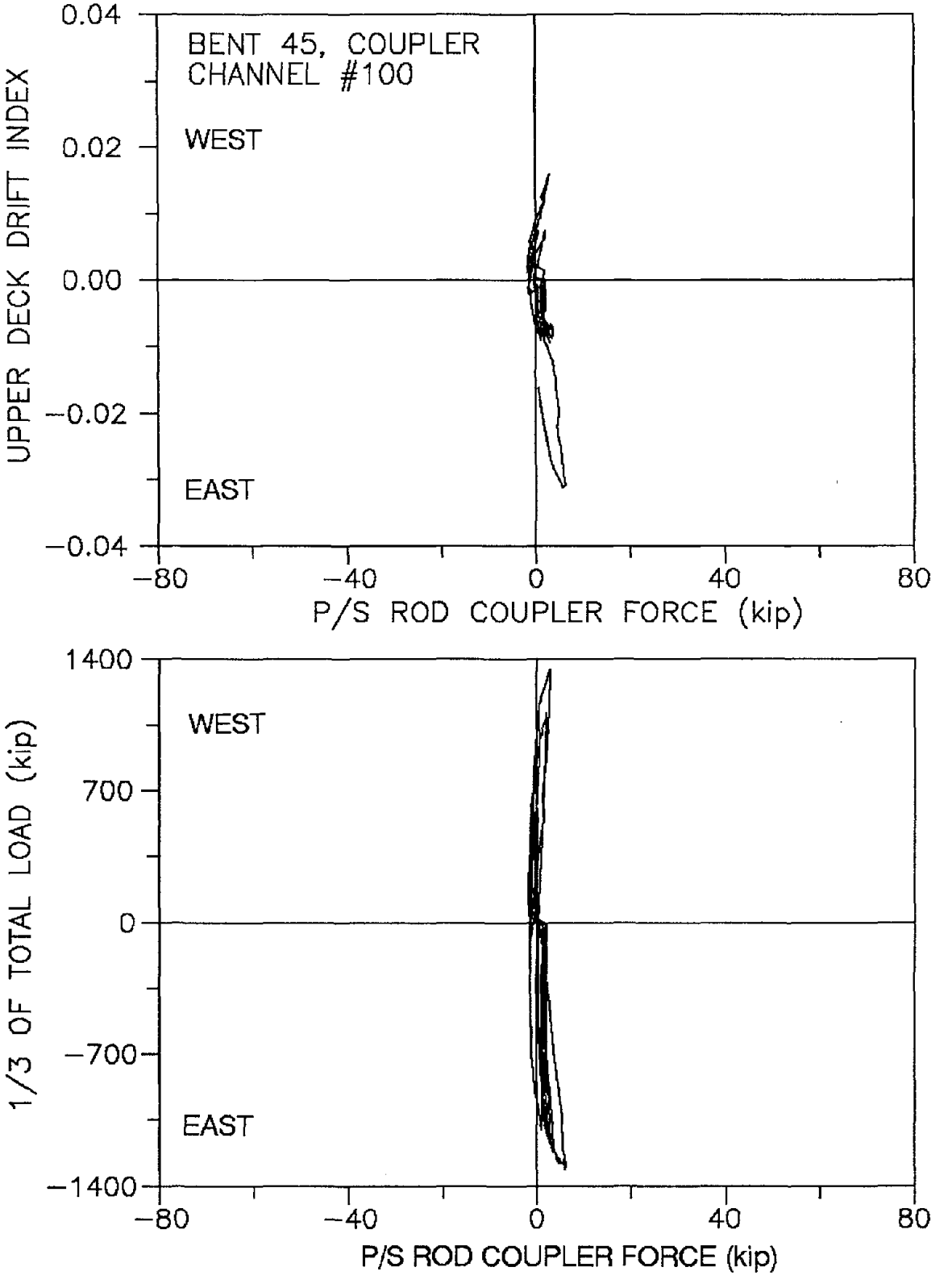
BENT 45, COUPLER
CHANNEL #100
WEST
EAST
UPPER DECK DRIFT INDEX
0.04
0.02
0.00
−0.02
−0.04
−80
−40
0
40
80
P/S ROD COUPLER FORCE (kip)
WEST
EAST
1/3 OF TOTAL LOAD (kip)
1400
700
0
−700
−1400
−80
−40
0
40
80
P/S ROD COUPLER FORCE (kip)

Fig. B.51

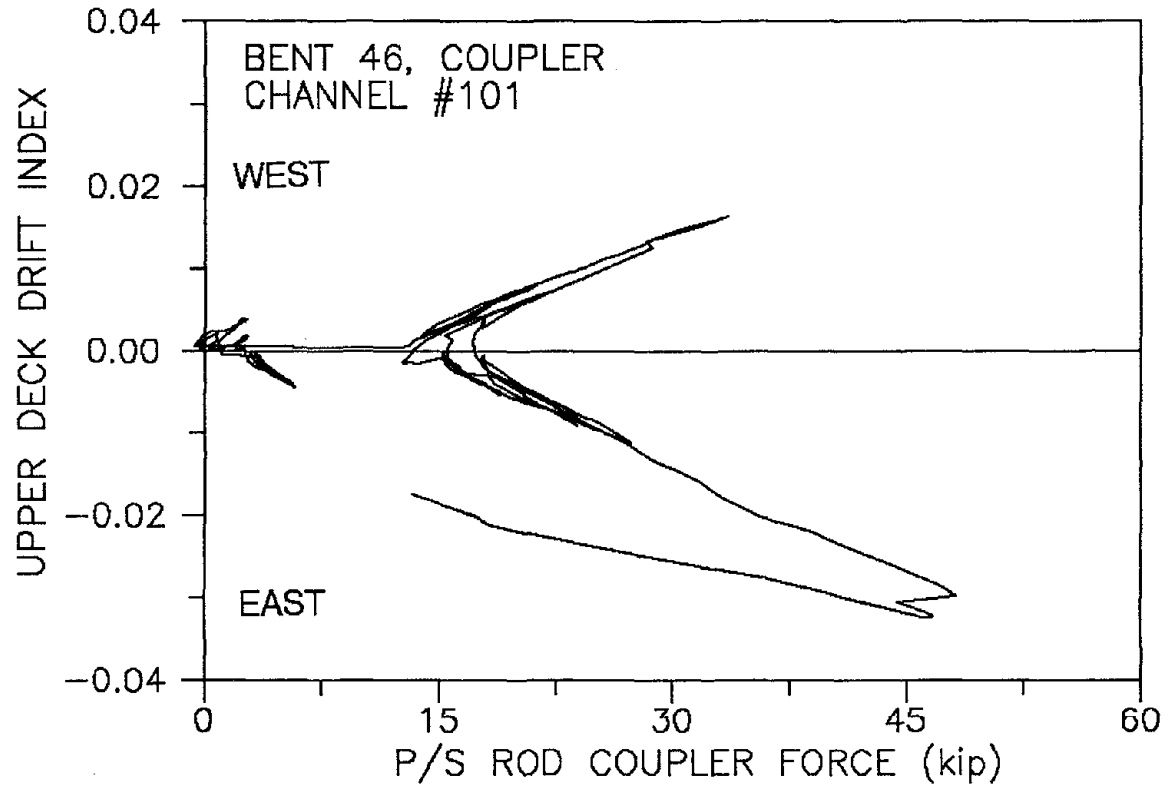
BENT 46, COUPLER
CHANNEL #101
WEST
EAST
UPPER DECK DRIFT INDEX
0.04
0.02
0.00
-0.02
-0.04
0
15
30
45
60
P/S ROD COUPLER FORCE (kip)

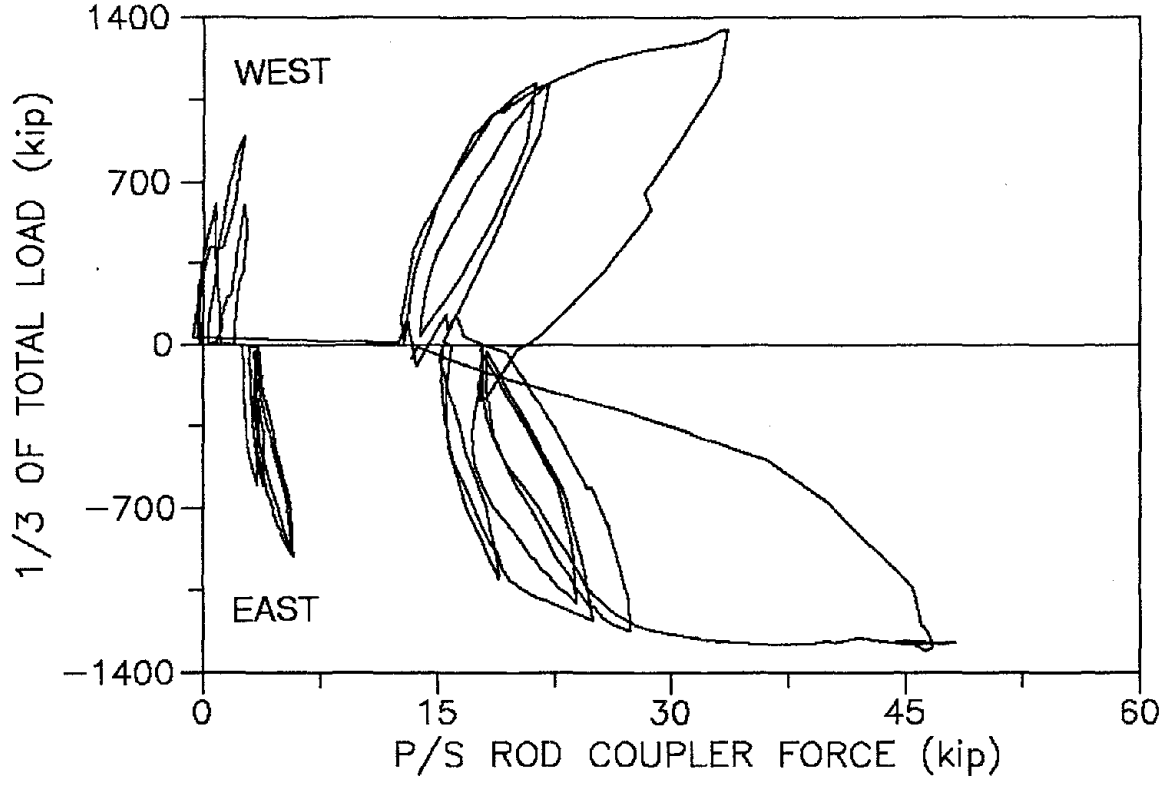
WEST
EAST
1/3 OF TOTAL LOAD (kip)
1400
700
0
-700
-1400
0
15
30
45
60
P/S ROD COUPLER FORCE (kip)

Fig. B.52

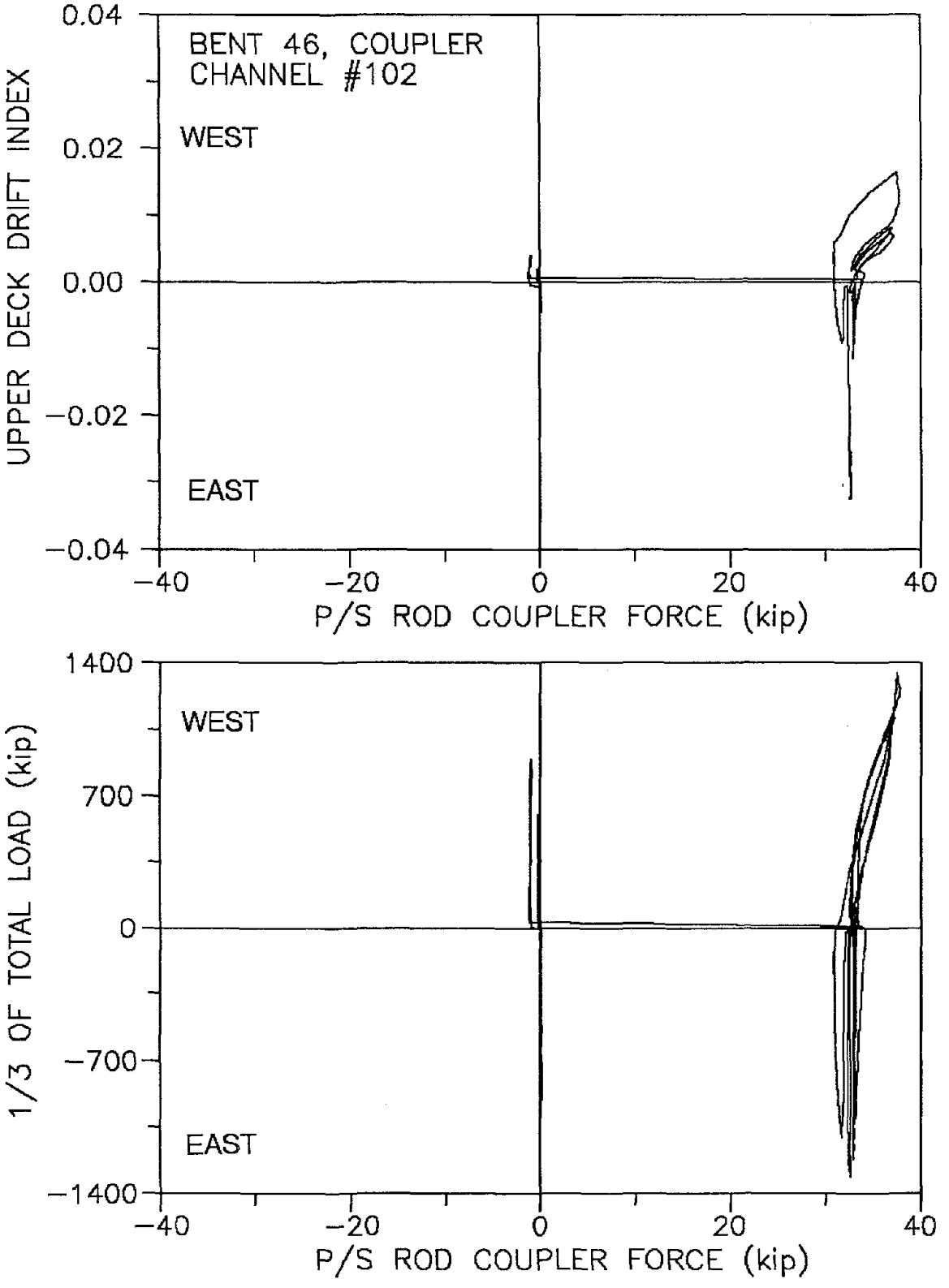
BENT 46, COUPLER
CHANNEL #102
WEST
EAST
UPPER DECK DRIFT INDEX
0.04
0.02
0.00
−0.02
−0.04
−40
−20
0
20
40
P/S ROD COUPLER FORCE (kip)
1/3 OF TOTAL LOAD (kip)
1400
700
0
−700
−1400
WEST
EAST
−40
−20
0
20
40
P/S ROD COUPLER FORCE (kip)

Fig. B.53

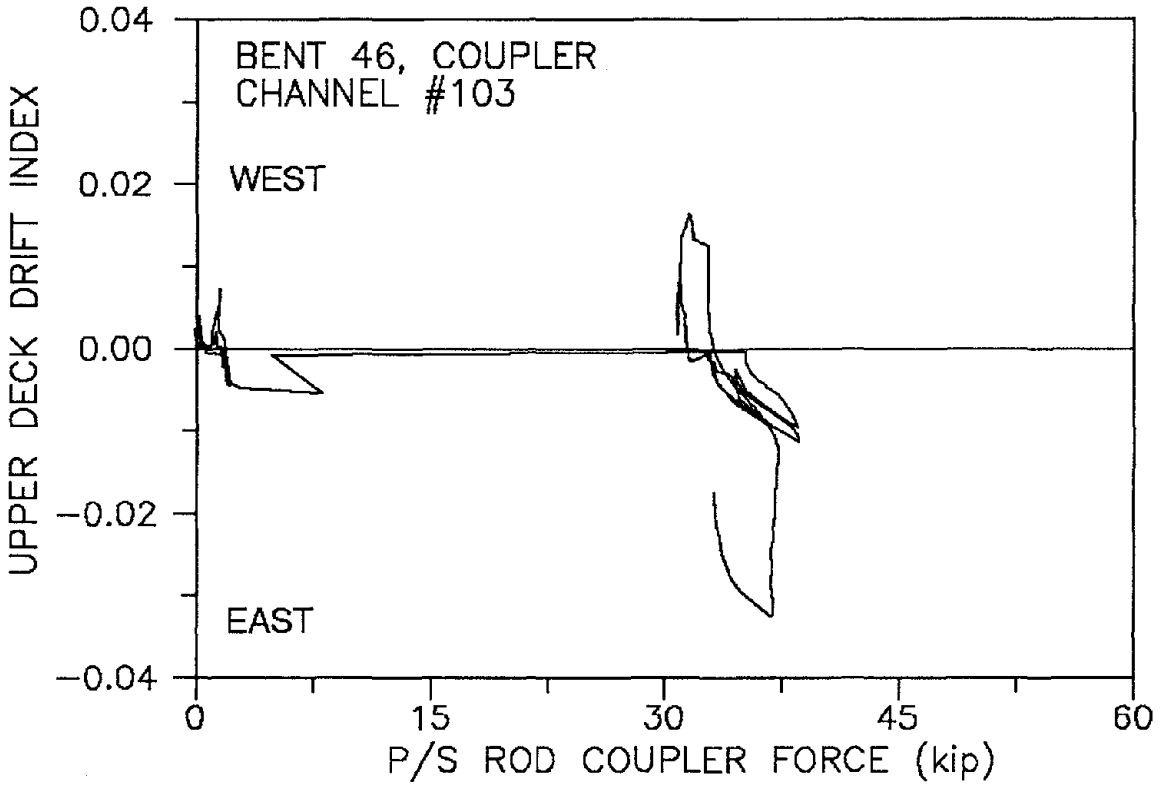
BENT 46, COUPLER
CHANNEL #103
WEST
EAST
UPPER DECK DRIFT INDEX
0.04
0.02
0.00
−0.02
−0.04
0
15
30
45
60
P/S ROD COUPLER FORCE (kip)

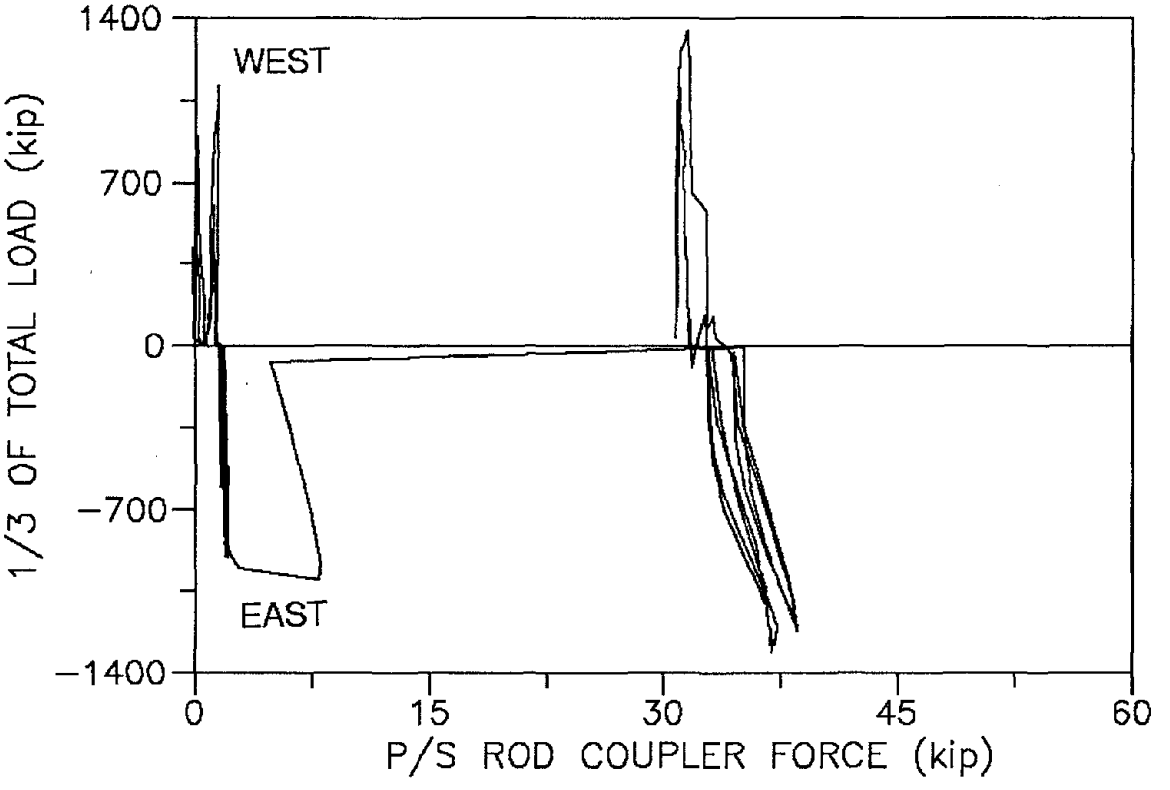
WEST
EAST
1/3 OF TOTAL LOAD (kip)
1400
700
0
−700
−1400
0
15
30
45
60
P/S ROD COUPLER FORCE (kip)

Fig. B.54

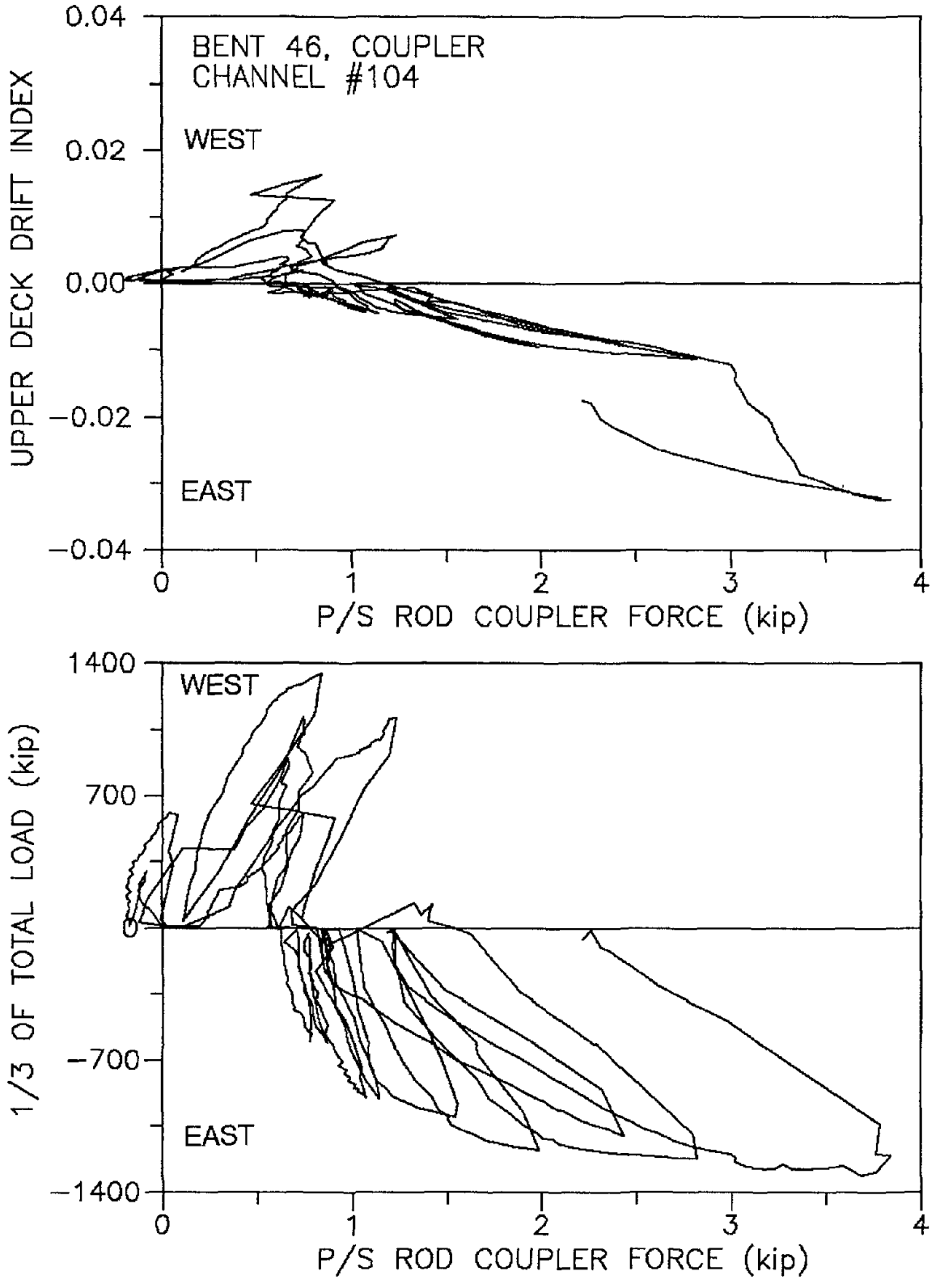
BENT 46, COUPLER
CHANNEL #104
WEST
EAST
UPPER DECK DRIFT INDEX
0.04
0.02
0.00
-0.02
-0.04
0
1
2
3
4
P/S ROD COUPLER FORCE (kip)
1400
700
0
-700
-1400
1/3 OF TOTAL LOAD (kip)

Fig. B.55

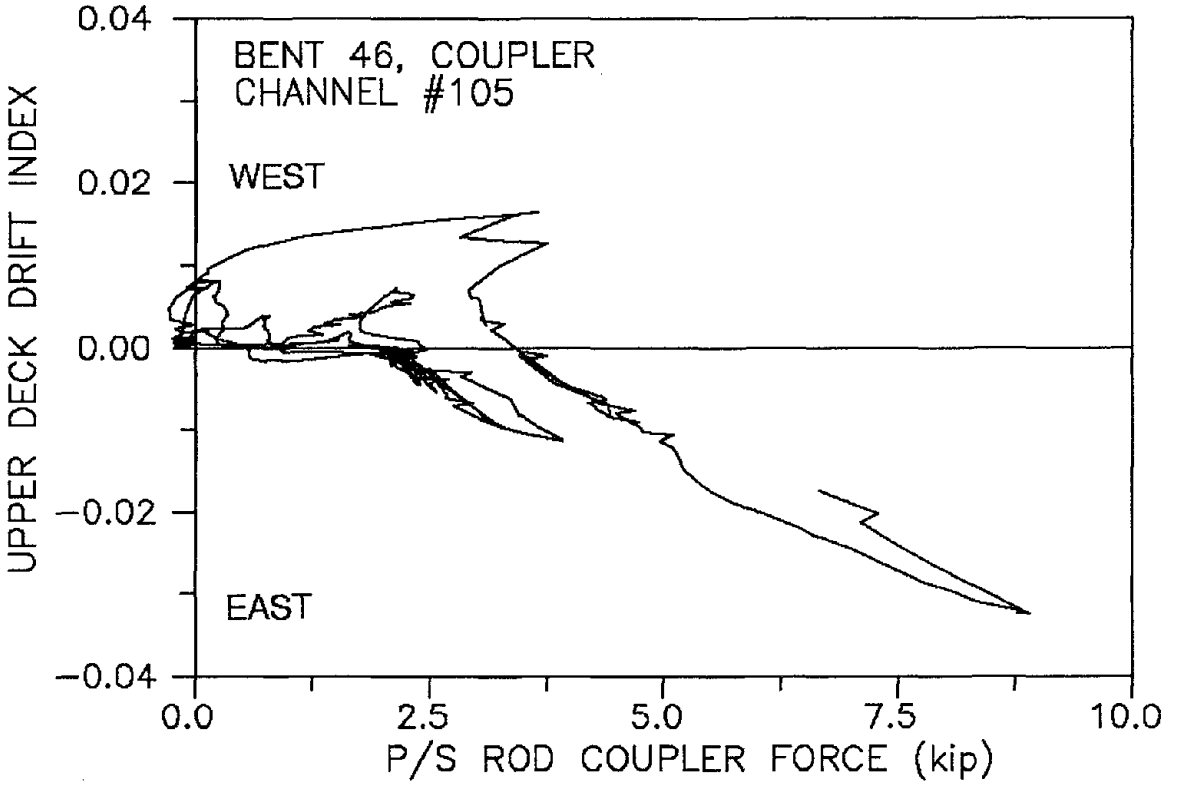
BENT 46, COUPLER
CHANNEL #105
WEST
EAST
UPPER DECK DRIFT INDEX
0.04
0.02
0.00
−0.02
−0.04
0.0
2.5
5.0
7.5
10.0
P/S ROD COUPLER FORCE (kip)

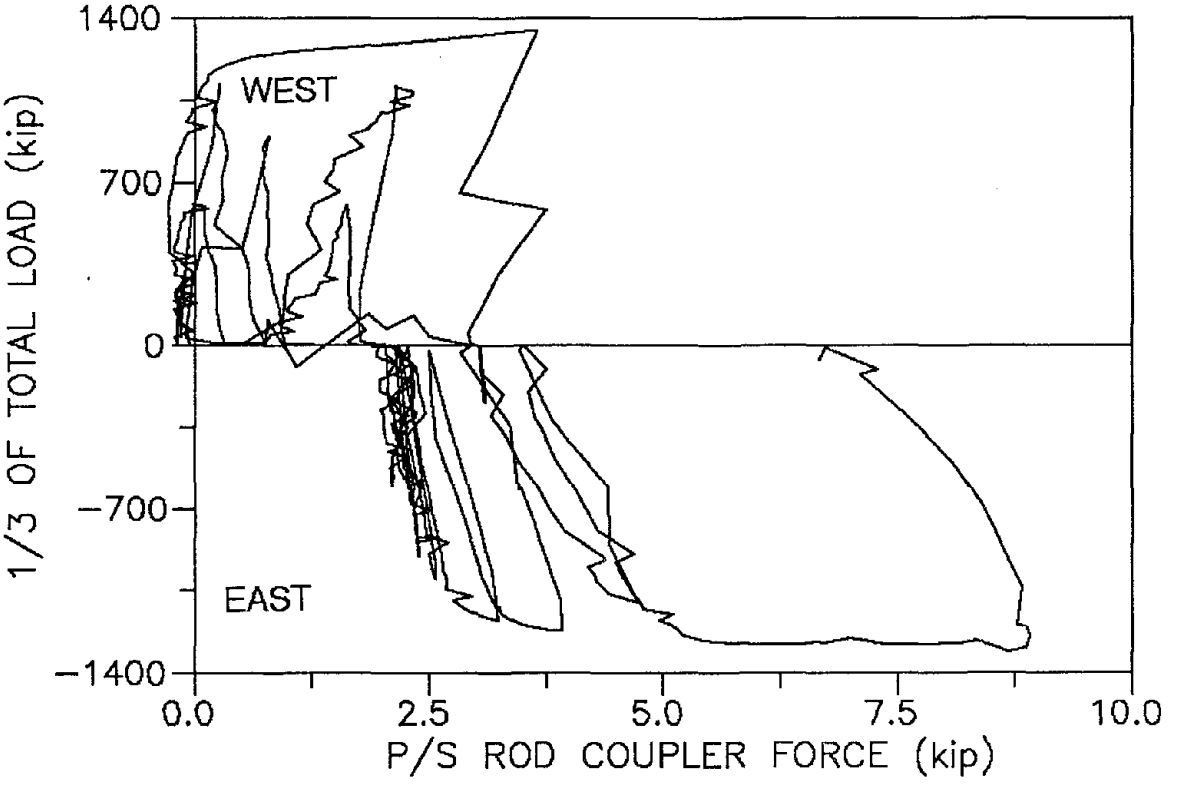
WEST
EAST
1/3 OF TOTAL LOAD (kip)
1400
700
0
−700
−1400
0.0
2.5
5.0
7.5
10.0
P/S ROD COUPLER FORCE (kip)

Fig. B.56

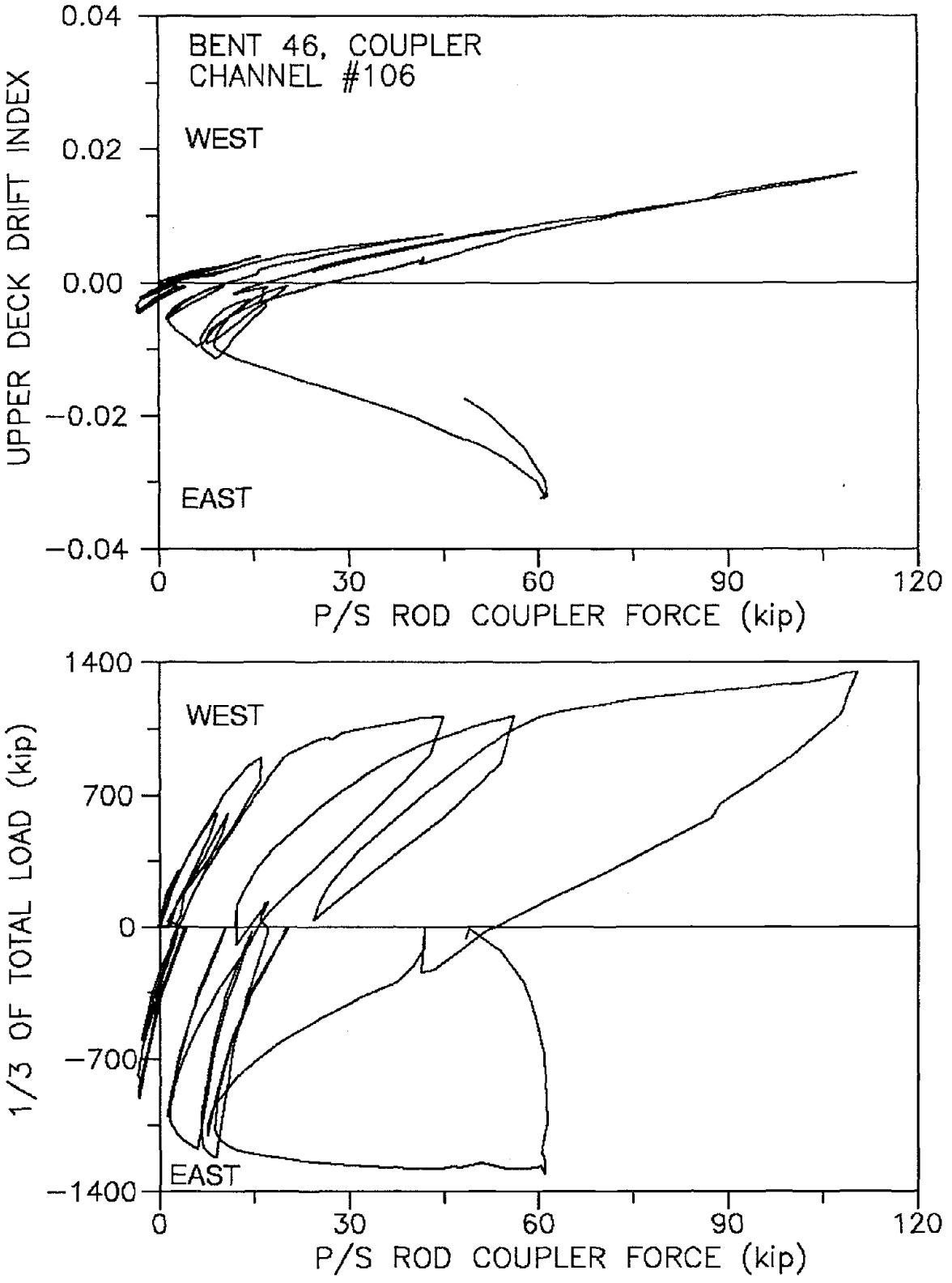
BENT 46, COUPLER
CHANNEL #106
WEST
EAST
UPPER DECK DRIFT INDEX
0.04
0.02
0.00
−0.02
−0.04
0
30
60
90
120
P/S ROD COUPLER FORCE (kip)
WEST
EAST
1/3 OF TOTAL LOAD (kip)
1400
700
0
−700
−1400
0
30
60
90
120
P/S ROD COUPLER FORCE (kip)

Fig. B.57

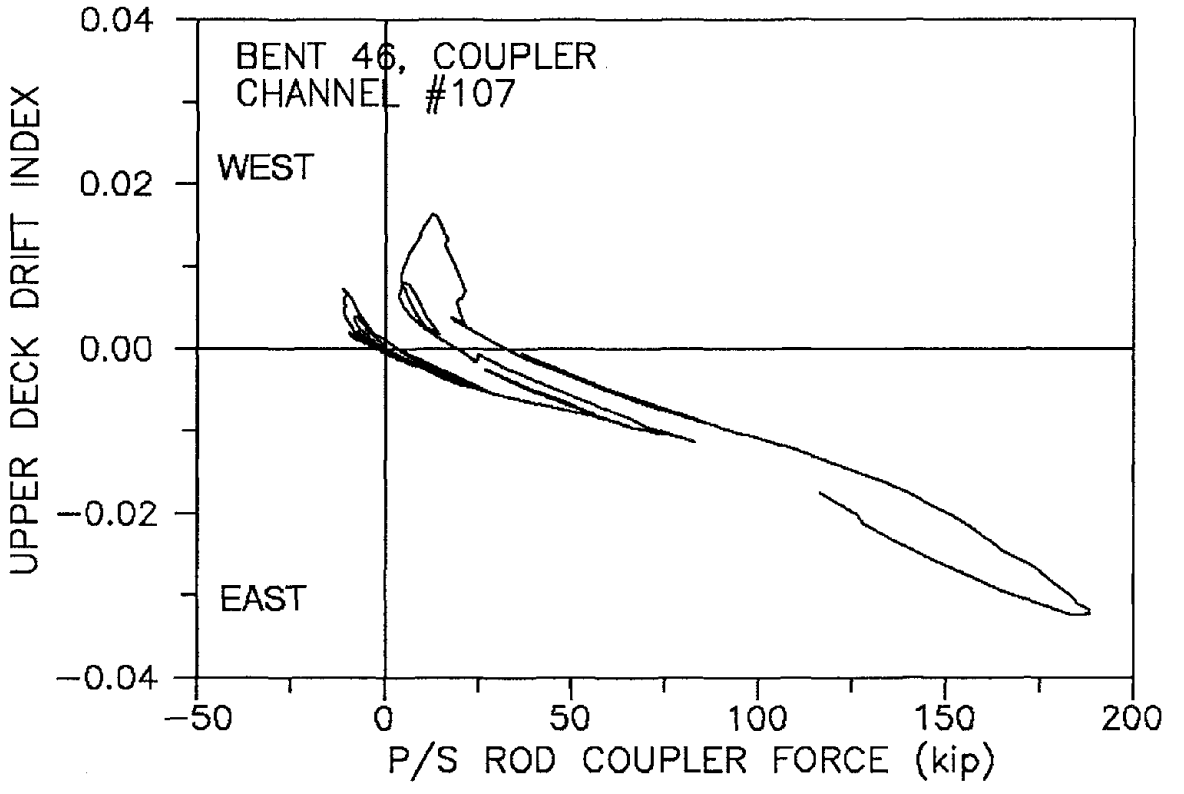
BENT 46, COUPLER
CHANNEL #107
WEST
EAST
UPPER DECK DRIFT INDEX
0.04
0.02
0.00
−0.02
−0.04
−50
0
50
100
150
200
P/S ROD COUPLER FORCE (kip)

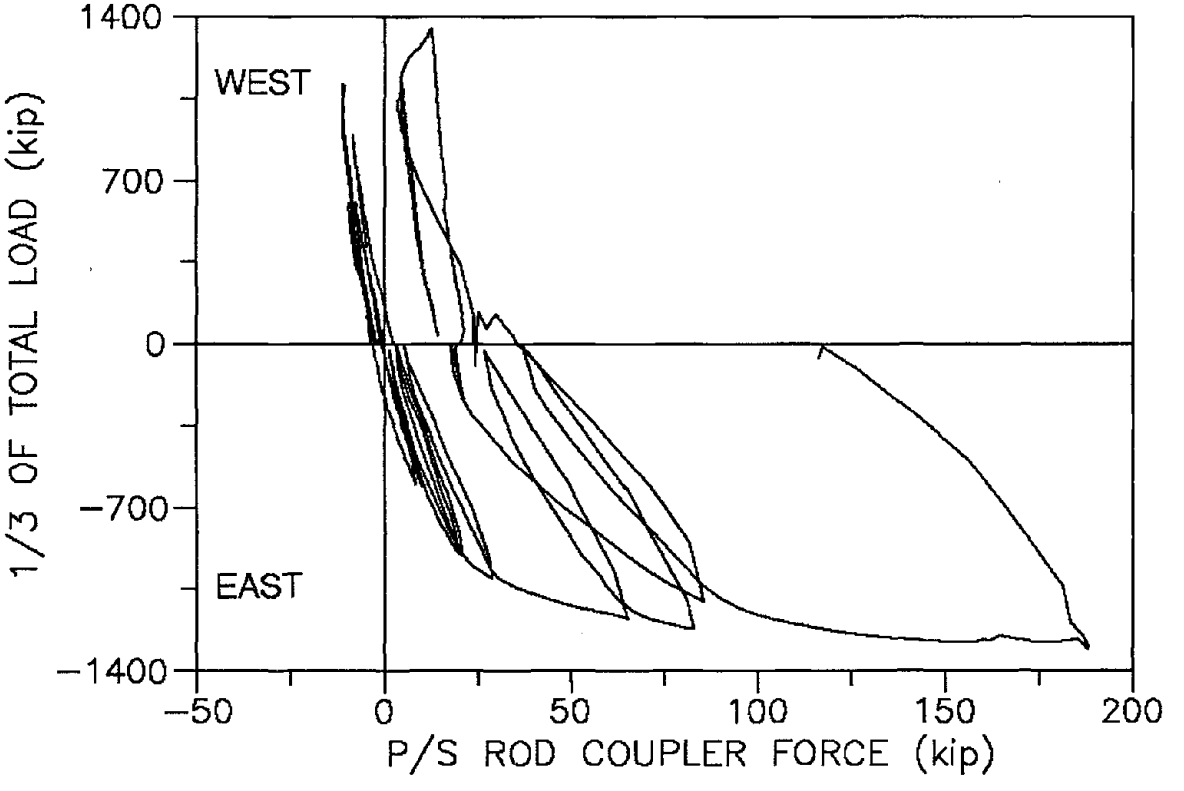
WEST
EAST
1/3 OF TOTAL LOAD (kip)
1400
700
0
−700
−1400
−50
0
50
100
150
200
P/S ROD COUPLER FORCE (kip)

Fig. B.58

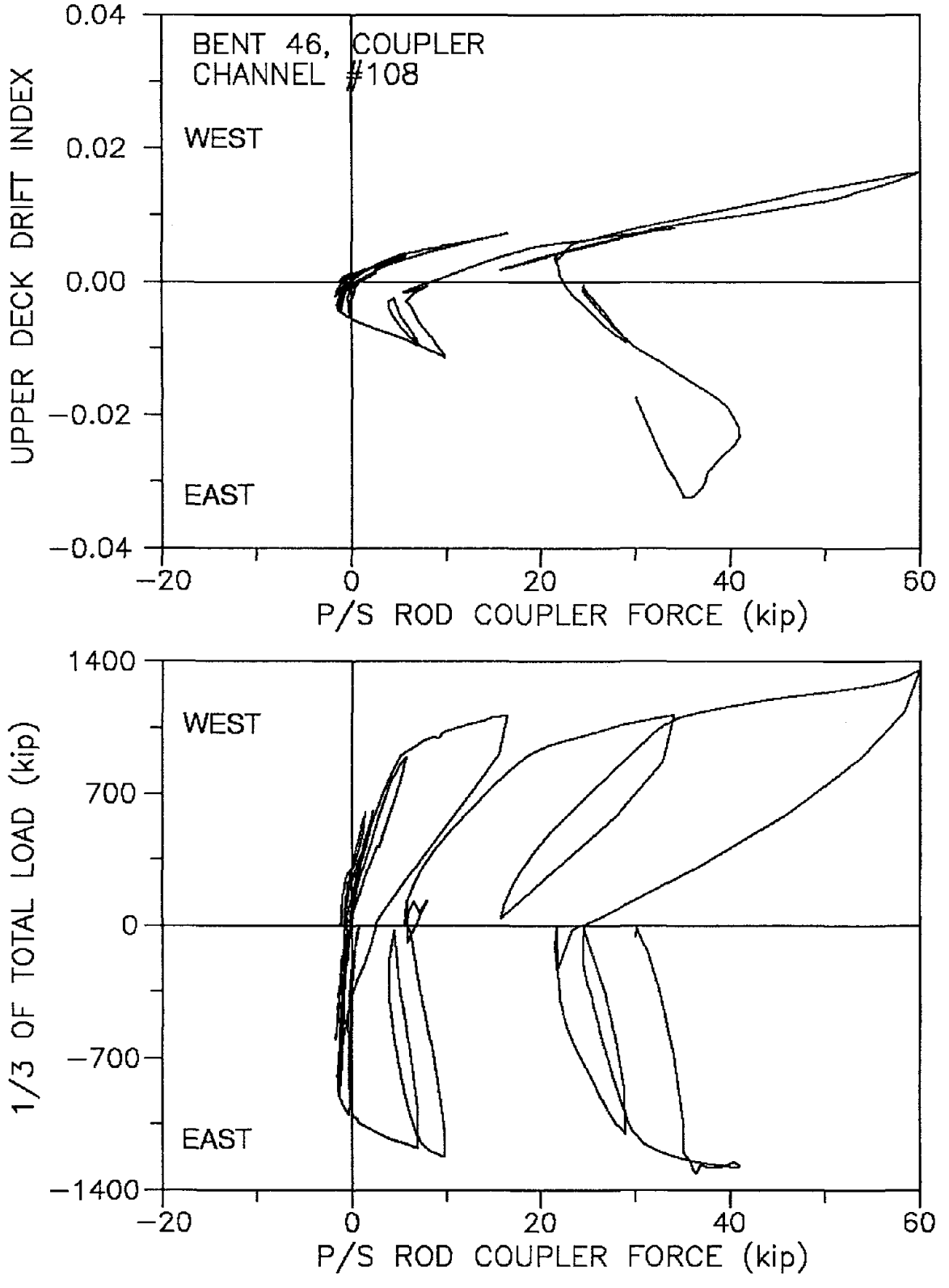
BENT 46, COUPLER
CHANNEL #108
WEST
EAST
UPPER DECK DRIFT INDEX
0.04
0.02
0.00
−0.02
−0.04
−20
0
20
40
60
P/S ROD COUPLER FORCE (kip)
WEST
EAST
1/3 OF TOTAL LOAD (kip)
1400
700
0
−700
−1400
−20
0
20
40
60
P/S ROD COUPLER FORCE (kip)

Fig. B.59

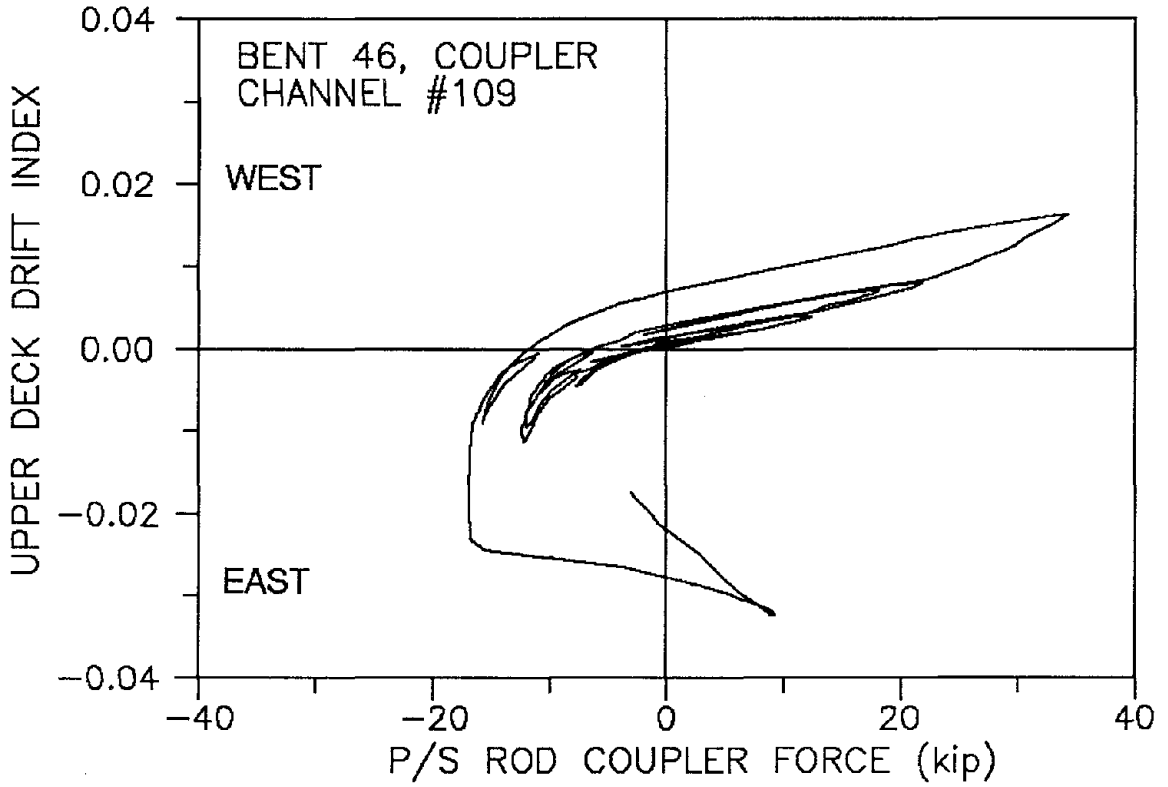
BENT 46, COUPLER
CHANNEL #109
WEST
EAST
UPPER DECK DRIFT INDEX
0.04
0.02
0.00
−0.02
−0.04
−40
−20
0
20
40
P/S ROD COUPLER FORCE (kip)

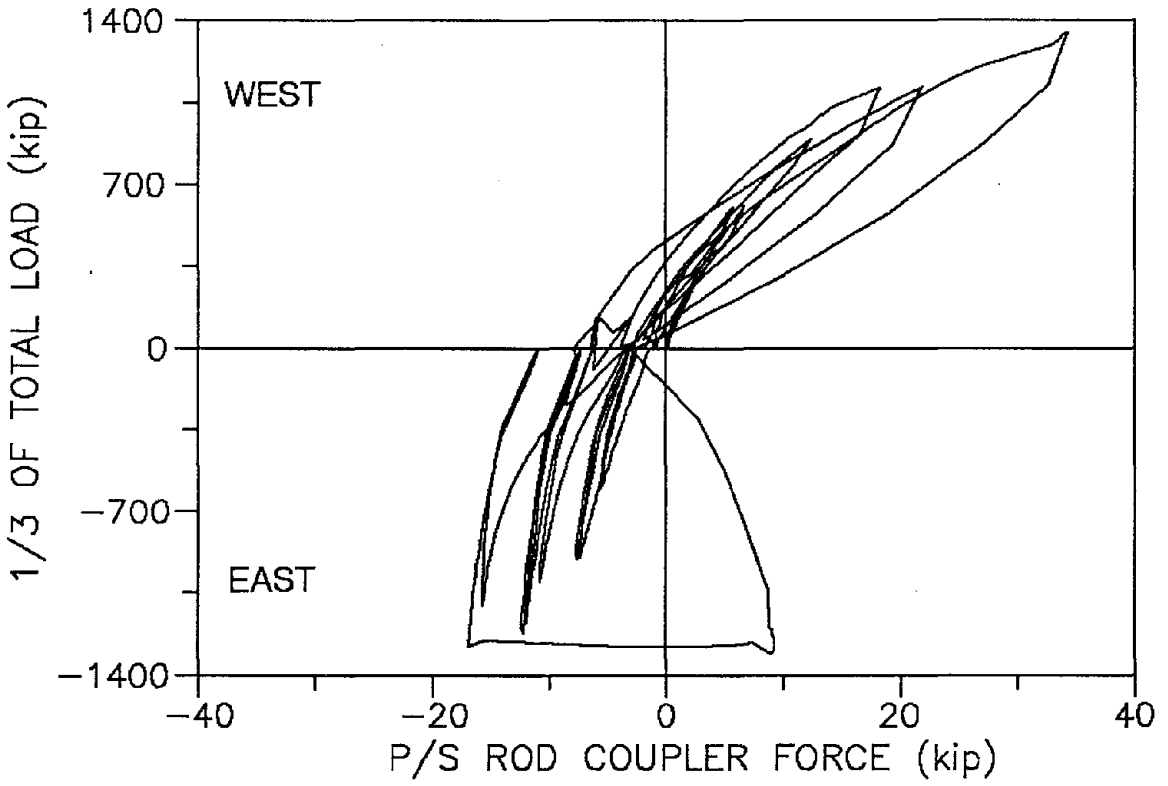
WEST
EAST
1/3 OF TOTAL LOAD (kip)
1400
700
0
−700
−1400
−40
−20
0
20
40
P/S ROD COUPLER FORCE (kip)

Fig. B.60

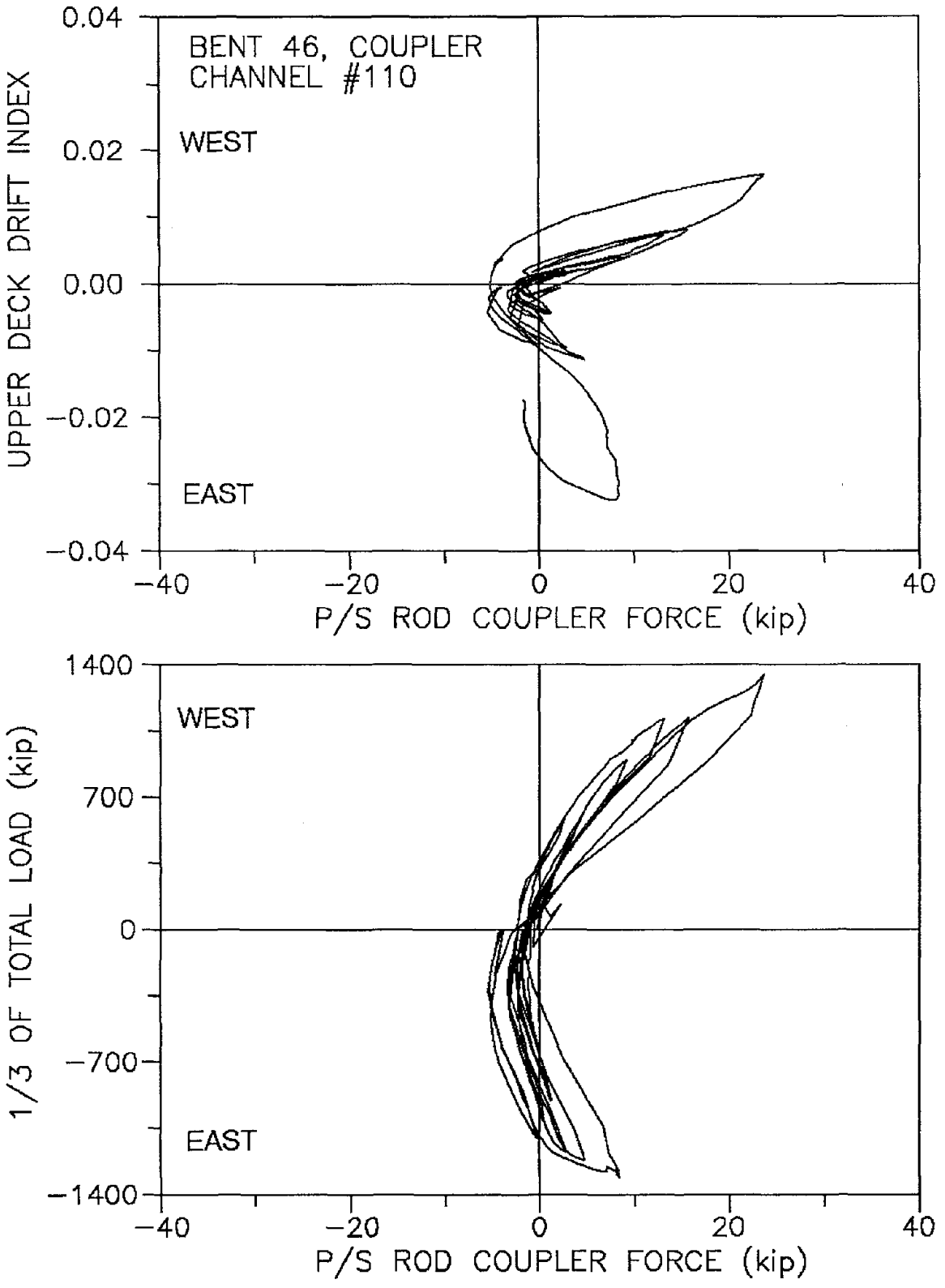
BENT 46, COUPLER
CHANNEL #110
WEST
EAST
UPPER DECK DRIFT INDEX
0.04
0.02
0.00
−0.02
−0.04
−40
−20
0
20
40
P/S ROD COUPLER FORCE (kip)
WEST
EAST
1/3 OF TOTAL LOAD (kip)
1400
700
0
−700
−1400
−40
−20
0
20
40
P/S ROD COUPLER FORCE (kip)

Fig. B.61

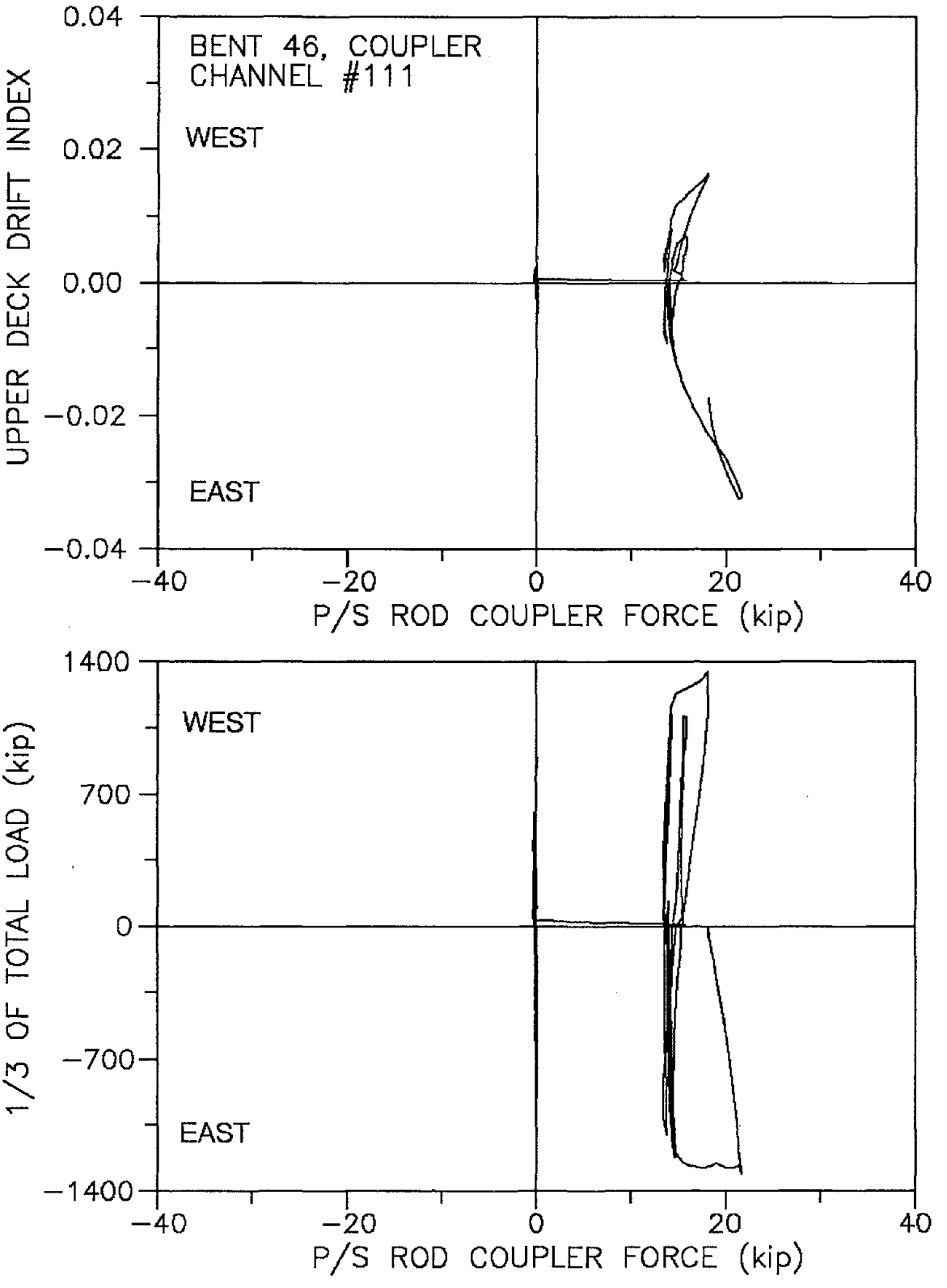
BENT 46, COUPLER
CHANNEL #111
WEST
EAST
UPPER DECK DRIFT INDEX
0.04
0.02
0.00
−0.02
−0.04
−40
−20
0
20
40
P/S ROD COUPLER FORCE (kip)
1/3 OF TOTAL LOAD (kip)
1400
700
0
−700
−1400
WEST
EAST
−40
−20
0
20
40
P/S ROD COUPLER FORCE (kip)

Fig. B.62

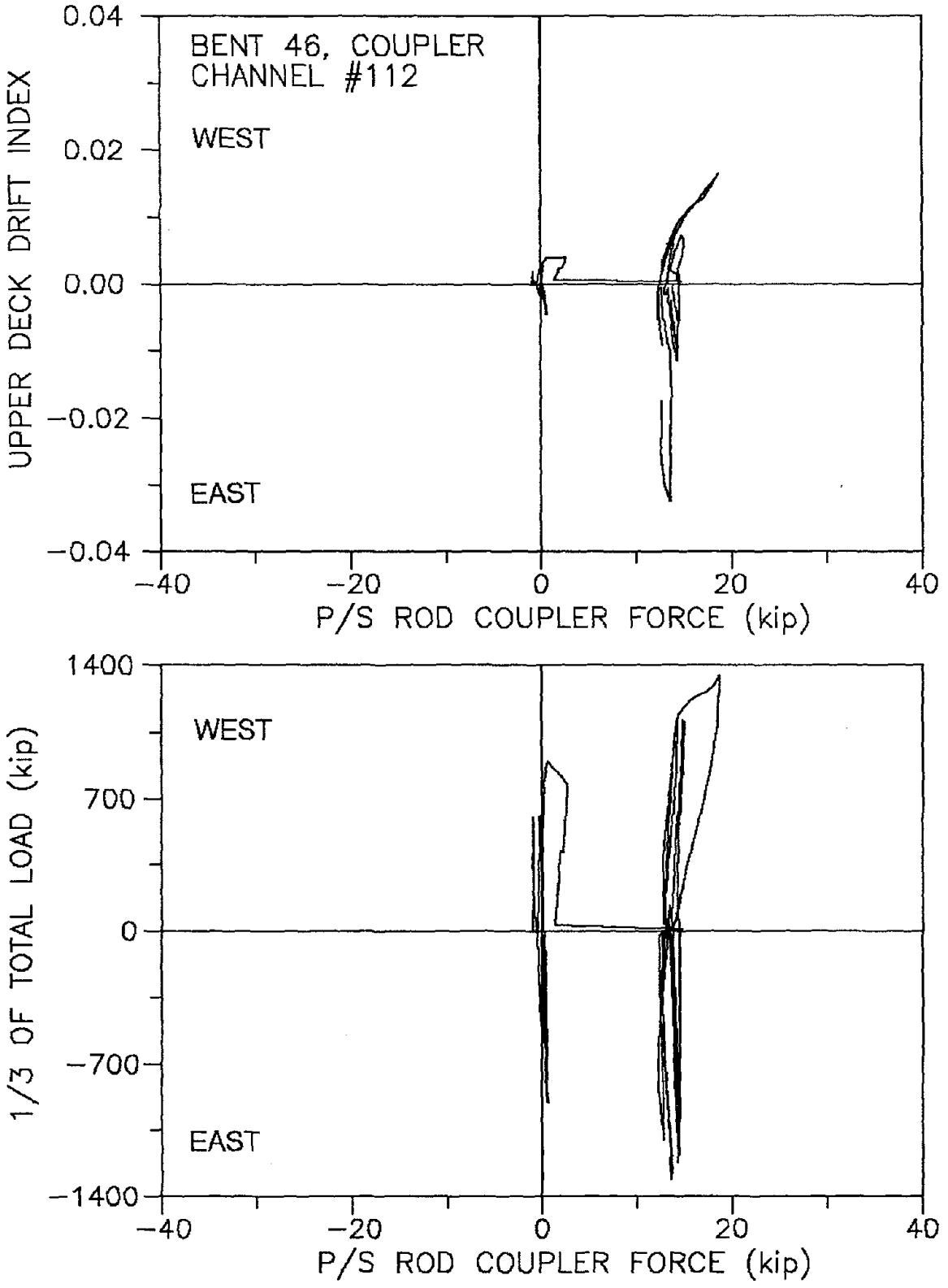
BENT 46, COUPLER
CHANNEL #112
WEST
EAST
UPPER DECK DRIFT INDEX
0.04
0.02
0.00
-0.02
-0.04
-40
-20
0
20
40
P/S ROD COUPLER FORCE (kip)
WEST
EAST
1/3 OF TOTAL LOAD (kip)
1400
700
0
-700
-1400
-40
-20
0
20
40
P/S ROD COUPLER FORCE (kip)

Fig. B.63

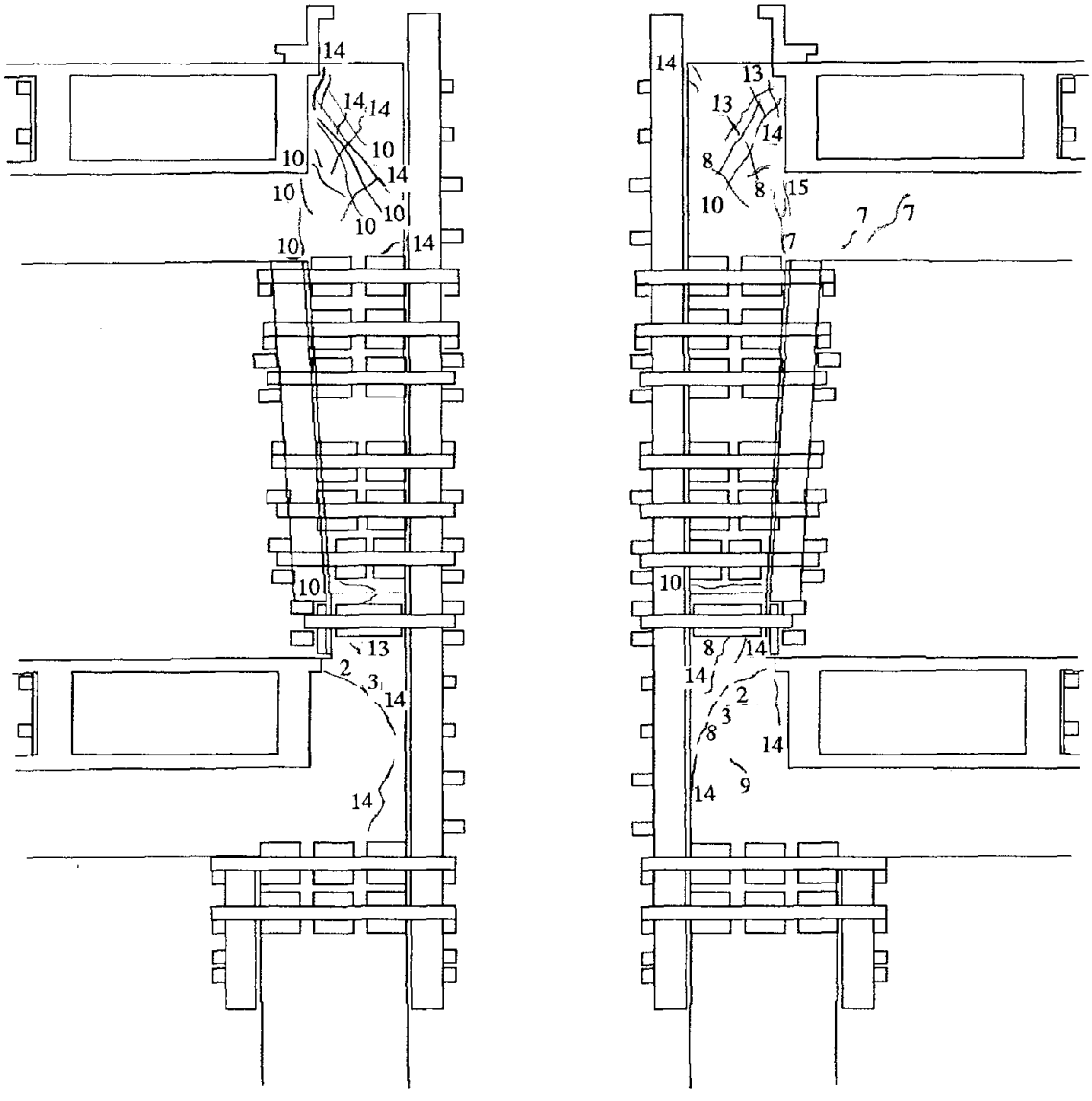

Fig. C.1

Bent 45 West End Crack Formations

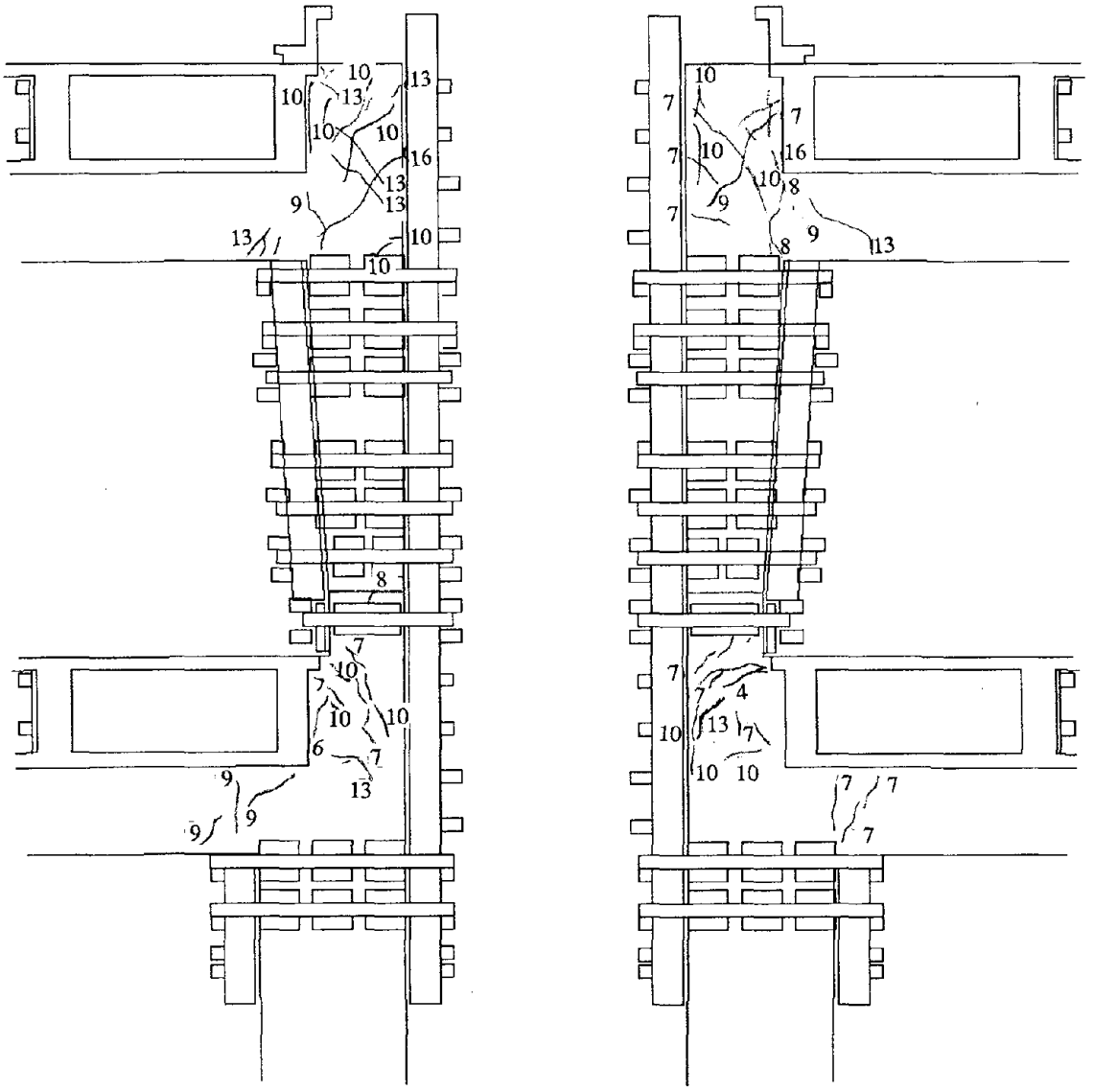

Fig. C.2

Bent 45 East End Crack Formations

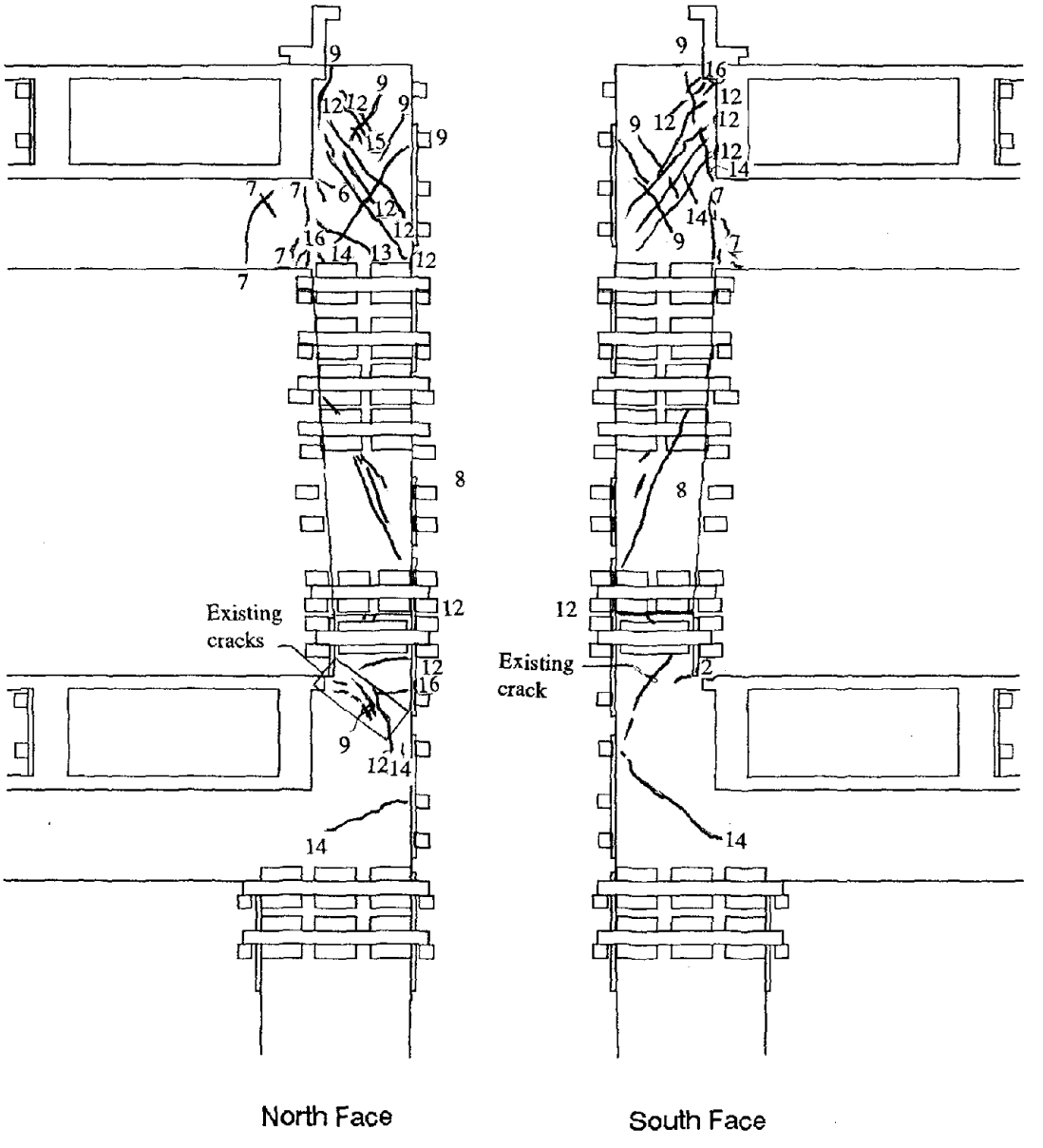

Fig. C.3

Bent 46 West End Crack Formations

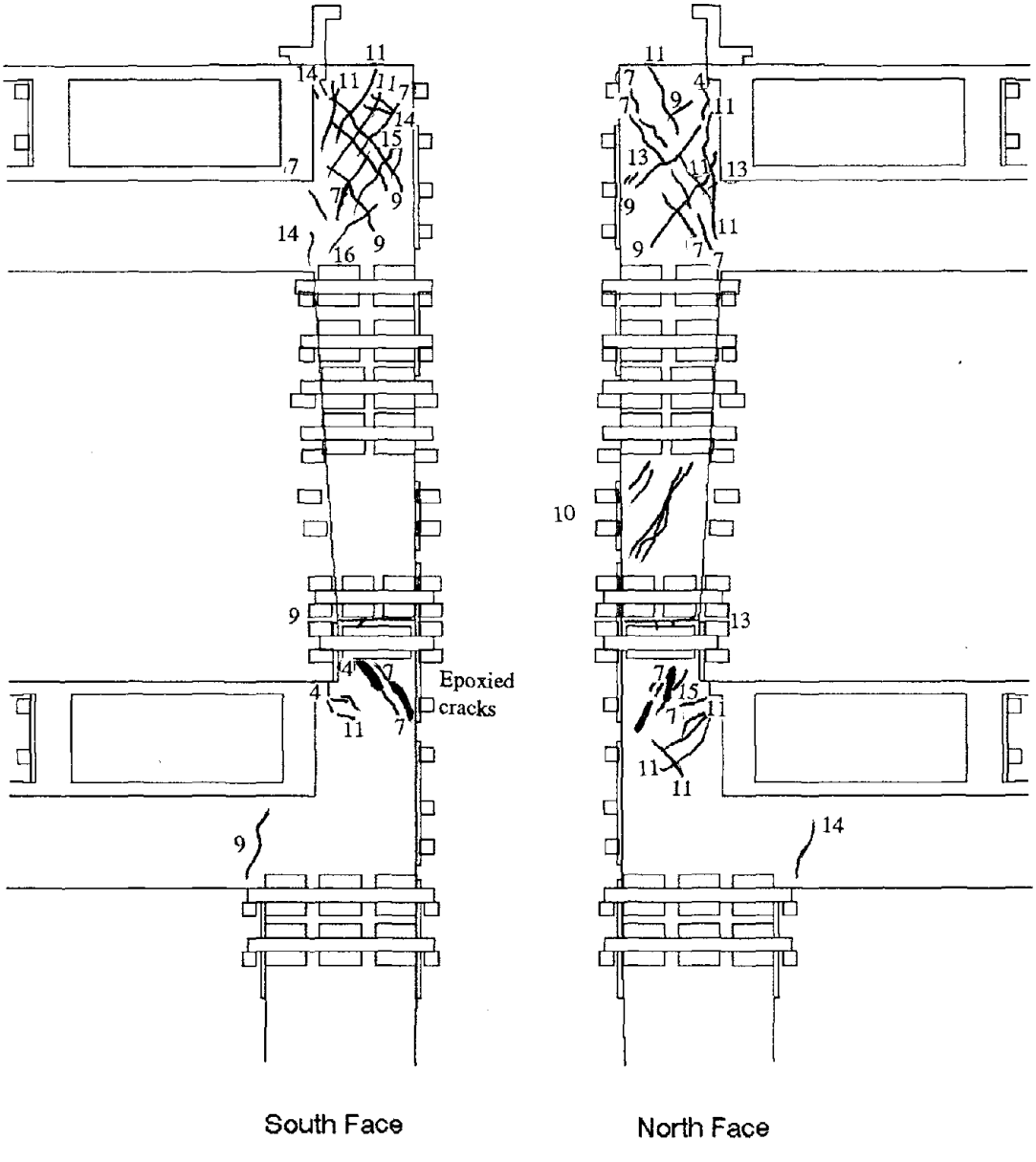

Fig. C.4

Bent 46 East End Crack Formations

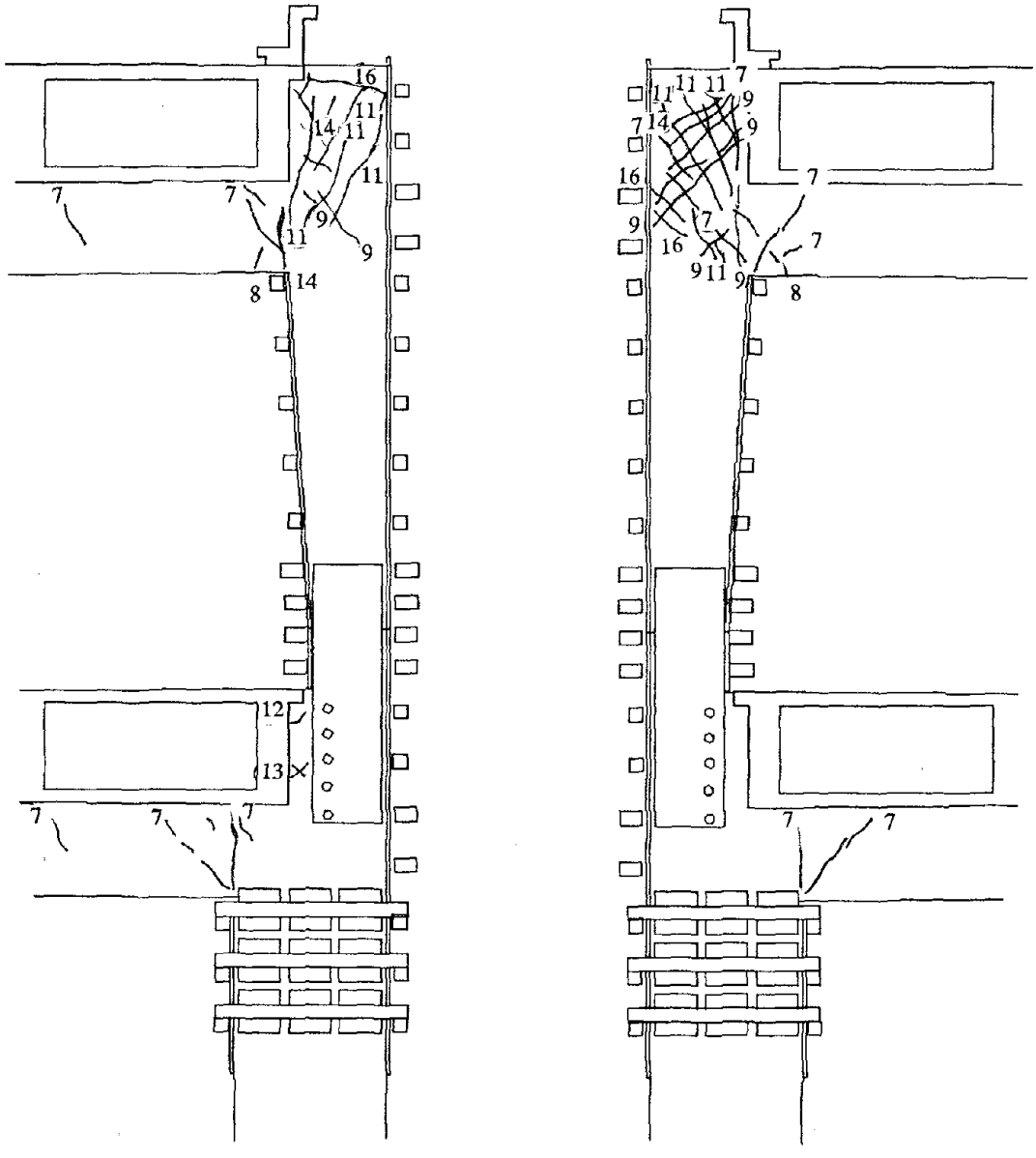

Fig. C.5

Bent 47 East End Crack Formations

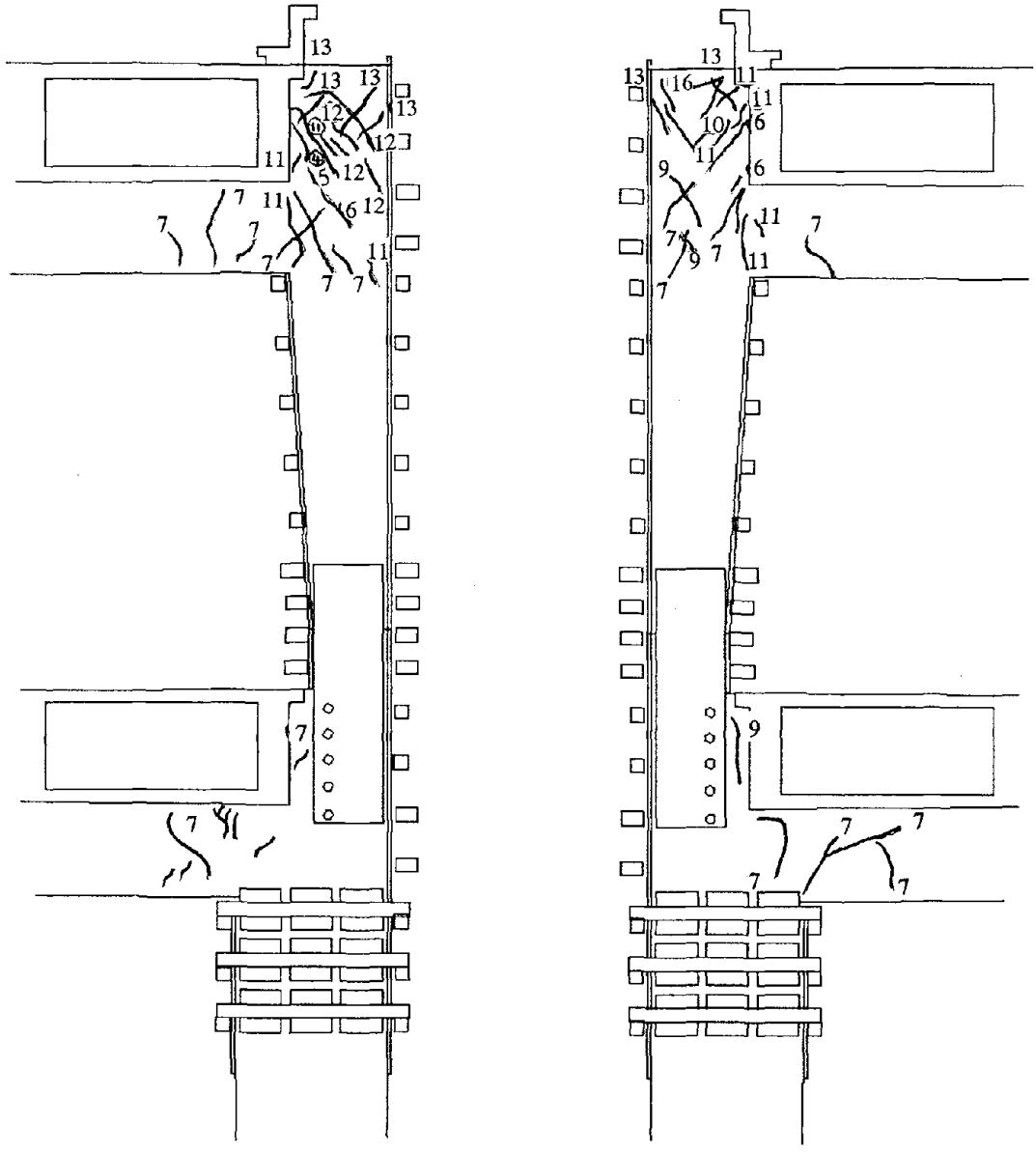

Fig. C.6

Bent 47 West End Crack Formations

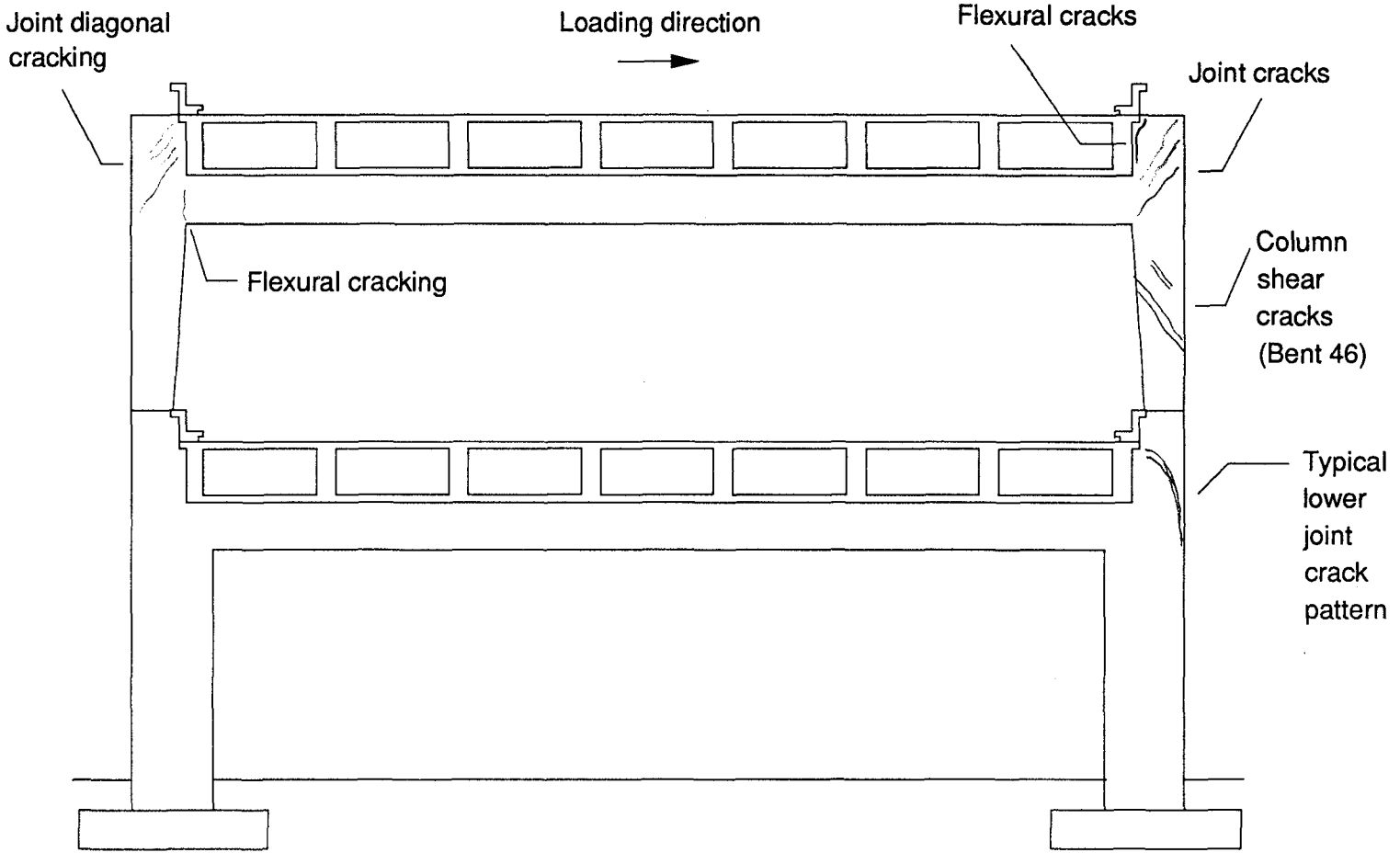

Fig. C.7

Typical crack formation patterns and orientations under lateral loading

EARTHQUAKE ENGINEERING RESEARCH CENTER REPORT SERIES

EERC reports are available from the National Information Service for Earthquake Engineering(NISEE) and from the National Technical Information Service(NTIS). Numbers in parentheses are Accession Numbers assigned by the National Technical Information Service; these are followed by a price code. Contact NTIS, 5285 Port Royal Road, Springfield Virginia, 22161 for more information. Reports without Accession Numbers were not available from NTIS at the time of printing. *For a current complete list of EERC reports (from EERC 67-1) and availablity information, please contact University of California,* EERC, NISEE, 1301 South 46th Street, Richmond, California 94804.

UCB/EERC-81/01 "Control of Seismic Response of Piping Systems and Other Structures by Base Isolation," by Kelly, J.M., January 1981, (PB81 200 735)A05.

UCB/EERC-81/02 "OPTNSR- An Interactive Software System for Optimal Design of Statically and Dynamically Loaded Structures with Nonlinear Response," by Bhatti, M.A., Ciampi, V. and Pister, K.S., January 1981, (PB81 218 851)A09.

UCB/EERC-81/03 "Analysis of Local Variations in Free Field Seismic Ground Motions," by Chen, J.-C., Lysmer, J. and Seed, H.B., January 1981, (AD-A099508)A13.

UCB/EERC-81/04 "Inelastic Structural Modeling of Braced Offshore Platforms for Seismic Loading," by Zayas, V.A., Shing, P.-S.B., Mahin, S.A. and Popov, E.P., January 1981, INEL4, (PB82 138 777)A07.

UCB/EERC-81/05 "Dynamic Response of Light Equipment in Structures," by Der Kiureghian, A., Sackman, J.L. and Nour-Omid, B., April 1981, (PB81 218 497)A04.

UCB/EERC-81/06 "Preliminary Experimental Investigation of a Broad Base Liquid Storage Tank," by Bouwkamp, J.G., Kollegger, J.P. and Stephen, R.M., May 1981, (PB82 140 385)A03.

UCB/EERC-81/07 "The Seismic Resistant Design of Reinforced Concrete Coupled Structural Walls," by Aktan, A.E. and Bertero, V.V., June 1981, (PB82 113 358)A11.

UCB/EERC-81/08 "Unassigned," by Unassigned, 1981.

UCB/EERC-81/09 "Experimental Behavior of a Spatial Piping System with Steel Energy Absorbers Subjected to a Simulated Differential Seismic Input," by Stiemer, S.F., Godden, W.G. and Kelly, J.M., July 1981, (PB82 201 898)A04.

UCB/EERC-81/10 "Evaluation of Seismic Design Provisions for Masonry in the United States," by Sveinsson, B.I., Mayes, R.L. and McNiven, H.D., August 1981, (PB82 166 075)A08.

UCB/EERC-81/11 "Two-Dimensional Hybrid Modelling of Soil-Structure Interaction," by Tzong, T.-J., Gupta, S. and Penzien, J., August 1981, (PB82 142 118)A04.

UCB/EERC-81/12 "Studies on Effects of Infills in Seismic Resistant R/C Construction," by Brokken, S. and Bertero, V.V., October 1981, (PB82 166 190)A09.

UCB/EERC-81/13 "Linear Models to Predict the Nonlinear Seismic Behavior of a One-Story Steel Frame," by Valdimarsson, H., Shah, A.H. and McNiven, H.D., September 1981, (PB82 138 793)A07.

UCB/EERC-81/14 "TLUSH: A Computer Program for the Three-Dimensional Dynamic Analysis of Earth Dams," by Kagawa, T., Mejia, L.H., Seed, H.B. and Lysmer, J., September 1981, (PB82 139 940)A06.

UCB/EERC-81/15 "Three Dimensional Dynamic Response Analysis of Earth Dams," by Mejia, L.H. and Seed, H.B., September 1981, (PB82 137 274)A12.

UCB/EERC-81/16 "Experimental Study of Lead and Elastomeric Dampers for Base Isolation Systems," by Kelly, J.M. and Hodder, S.B., October 1981, (PB82 166 182)A05.

UCB/EERC-81/17 "The Influence of Base Isolation on the Seismic Response of Light Secondary Equipment," by Kelly, J.M., April 1981, (PB82 255 266)A04.

UCB/EERC-81/18 "Studies on Evaluation of Shaking Table Response Analysis Procedures," by Blondet, J. M., November 1981, (PB82 197 278)A10.

UCB/EERC-81/19 "DELIGHT.STRUCT: A Computer-Aided Design Environment for Structural Engineering," by Balling, R.J., Pister, K.S. and Polak, E., December 1981, (PB82 218 496)A07.

UCB/EERC-81/20 "Optimal Design of Seismic-Resistant Planar Steel Frames," by Balling, R.J., Ciampi, V. and Pister, K.S., December 1981, (PB82 220 179)A07.

UCB/EERC-82/01 "Dynamic Behavior of Ground for Seismic Analysis of Lifeline Systems," by Sato, T. and Der Kiureghian, A., January 1982, (PB82 218 926)A05.

UCB/EERC-82/02 "Shaking Table Tests of a Tubular Steel Frame Model," by Ghanaat, Y. and Clough, R.W., January 1982, (PB82 220 161)A07.

UCB/EERC-82/03 "Behavior of a Piping System under Seismic Excitation: Experimental Investigations of a Spatial Piping System supported by Mechanical Shock Arrestors," by Schneider, S., Lee, H.-M. and Godden, W. G., May 1982, (PB83 172 544)A09.

UCB/EERC-82/04 "New Approaches for the Dynamic Analysis of Large Structural Systems," by Wilson, E.L., June 1982, (PB83 148 080)A05.

UCB/EERC-82/05 "Model Study of Effects of Damage on the Vibration Properties of Steel Offshore Platforms," by Shahrivar, F. and Bouwkamp, J.G., June 1982, (PB83 148 742)A10.

UCB/EERC-82/06 "States of the Art and Pratice in the Optimum Seismic Design and Analytical Response Prediction of R/C Frame Wall Structures," by Aktan, A.E. and Bertero, V.V., July 1982, (PB83 147 736)A05.

UCB/EERC-82/07 "Further Study of the Earthquake Response of a Broad Cylindrical Liquid-Storage Tank Model," by Manos, G.C. and Clough, R.W., July 1982, (PB83 147 744)A11.

UCB/EERC-82/08 "An Evaluation of the Design and Analytical Seismic Response of a Seven Story Reinforced Concrete Frame," by Charney, F.A. and Bertero, V.V., July 1982, (PB83 157 628)A09.

UCB/EERC-82/09 "Fluid-Structure Interactions: Added Mass Computations for Incompressible Fluid," by Kuo, J.S.-H., August 1982, (PB83 156 281)A07.

UCB/EERC-82/10 "Joint-Opening Nonlinear Mechanism: Interface Smeared Crack Model," by Kuo, J.S.-H., August 1982, (PB83 149 195)A05.

UCB/EERC-82/11 "Dynamic Response Analysis of Techi Dam," by Clough, R.W., Stephen, R.M. and Kuo, J.S.-H., August 1982, (PB83 147 496)A06.

UCB/EERC-82/12 "Prediction of the Seismic Response of R/C Frame-Coupled Wall Structures," by Aktan, A.E., Bertero, V.V. and Piazzo, M., August 1982, (PB83 149 203)A09.

UCB/EERC-82/13 "Preliminary Report on the Smart 1 Strong Motion Array in Taiwan," by Bolt, B.A., Loh, C.H., Penzien, J. and Tsai, Y.B., August 1982, (PB83 159 400)A10.

UCB/EERC-82/14 "Seismic Behavior of an Eccentrically X-Braced Steel Structure," by Yang, M.S., September 1982, (PB83 260 778)A12.

UCB/EERC-82/15 "The Performance of Stairways in Earthquakes," by Roha, C., Axley, J.W. and Bertero, V.V., September 1982, (PB83 157 693)A07.

UCB/EERC-82/16 "The Behavior of Submerged Multiple Bodies in Earthquakes," by Liao, W.-G., September 1982, (PB83 158 709)A07.

UCB/EERC-82/17 "Effects of Concrete Types and Loading Conditions on Local Bond-Slip Relationships," by Cowell, A.D., Popov, E.P. and Bertero, V.V., September 1982, (PB83 153 577)A04.

UCB/EERC-82/18 "Mechanical Behavior of Shear Wall Vertical Boundary Members: An Experimental Investigation," by Wagner, M.T. and Bertero, V.V., October 1982, (PB83 159 764)A05.

UCB/EERC-82/19 "Experimental Studies of Multi-support Seismic Loading on Piping Systems," by Kelly, J.M. and Cowell, A.D., November 1982, (PB90 262 684)A07.

UCB/EERC-82/20 "Generalized Plastic Hinge Concepts for 3D Beam-Column Elements," by Chen, P. F.-S. and Powell, G.H., November 1982, (PB83 247 981)A13.

UCB/EERC-82/21 "ANSR-II: General Computer Program for Nonlinear Structural Analysis," by Oughourlian, C.V. and Powell, G.H., November 1982, (PB83 251 330)A12.

UCB/EERC-82/22 "Solution Strategies for Statically Loaded Nonlinear Structures," by Simons, J.W. and Powell, G.H., November 1982, (PB83 197 970)A06.

UCB/EERC-82/23 "Analytical Model of Deformed Bar Anchorages under Generalized Excitations," by Ciampi, V., Eligehausen, R., Bertero, V.V. and Popov, E.P., November 1982, (PB83 169 532)A06.

UCB/EERC-82/24 "A Mathematical Model for the Response of Masonry Walls to Dynamic Excitations," by Sucuoglu, H., Mengi, Y. and McNiven, H.D., November 1982, (PB83 169 011)A07.

UCB/EERC-82/25 "Earthquake Response Considerations of Broad Liquid Storage Tanks," by Cambra, F.J., November 1982, (PB83 251 215)A09.

UCB/EERC-82/26 "Computational Models for Cyclic Plasticity, Rate Dependence and Creep," by Mosaddad, B. and Powell, G.H., November 1982, (PB83 245 829)A08.

UCB/EERC-82/27 "Inelastic Analysis of Piping and Tubular Structures," by Mahasuverachai, M. and Powell, G.H., November 1982, (PB83 249 987)A07.

UCB/EERC-83/01 "The Economic Feasibility of Seismic Rehabilitation of Buildings by Base Isolation," by Kelly, J.M., January 1983, (PB83 197 988)A05.

UCB/EERC-83/02 "Seismic Moment Connections for Moment-Resisting Steel Frames.," by Popov, E.P., January 1983, (PB83 195 412)A04.

UCB/EERC-83/03 "Design of Links and Beam-to-Column Connections for Eccentrically Braced Steel Frames," by Popov, E.P. and Malley, J.O., January 1983, (PB83 194 811)A04.

UCB/EERC-83/04 "Numerical Techniques for the Evaluation of Soil-Structure Interaction Effects in the Time Domain," by Bayo, E. and Wilson, E.L., February 1983, (PB83 245 605)A09.

UCB/EERC-83/05 "A Transducer for Measuring the Internal Forces in the Columns of a Frame-Wall Reinforced Concrete Structure," by Sause, R. and Bertero, V.V., May 1983, (PB84 119 494)A06.

UCB/EERC-83/06 "Dynamic Interactions Between Floating Ice and Offshore Structures," by Croteau, P., May 1983, (PB84 119 486)A16.

UCB/EERC-83/07 "Dynamic Analysis of Multiply Tuned and Arbitrarily Supported Secondary Systems," by Igusa, T. and Der Kiureghian, A., July 1983, (PB84 118 272)A11.

UCB/EERC-83/08 "A Laboratory Study of Submerged Multi-body Systems in Earthquakes," by Ansari, G.R., June 1983, (PB83 261 842)A17.

UCB/EERC-83/09 "Effects of Transient Foundation Uplift on Earthquake Response of Structures," by Yim, C.-S. and Chopra, A.K., June 1983, (PB83 261 396)A07.

UCB/EERC-83/10 "Optimal Design of Friction-Braced Frames under Seismic Loading," by Austin, M.A. and Pister, K.S., June 1983, (PB84 119 288)A06.

UCB/EERC-83/11 "Shaking Table Study of Single-Story Masonry Houses: Dynamic Performance under Three Component Seismic Input and Recommendations," by Manos, G.C., Clough, R.W. and Mayes, R.L., July 1983, (UCB/EERC-83/11)A08.

UCB/EERC-83/12 "Experimental Error Propagation in Pseudodynamic Testing," by Shiing, P.B. and Mahin, S.A., June 1983, (PB84 119 270)A09.

UCB/EERC-83/13 "Experimental and Analytical Predictions of the Mechanical Characteristics of a 1/5-scale Model of a 7-story R/C Frame-Wall Building Structure," by Aktan, A.E., Bertero, V.V., Chowdhury, A.A. and Nagashima, T., June 1983, (PB84 119 213)A07.

UCB/EERC-83/14 "Shaking Table Tests of Large-Panel Precast Concrete Building System Assemblages," by Oliva, M.G. and Clough, R.W., June 1983, (PB86 110 210/AS)A11.

UCB/EERC-83/15 "Seismic Behavior of Active Beam Links in Eccentrically Braced Frames," by Hjelmstad, K.D. and Popov, E.P., July 1983, (PB84 119 676)A09.

UCB/EERC-83/16 "System Identification of Structures with Joint Rotation," by Dimsdale, J.S., July 1983, (PB84 192 210)A06.

UCB/EERC-83/17 "Construction of Inelastic Response Spectra for Single-Degree-of-Freedom Systems," by Mahin, S. and Lin, J., June 1983, (PB84 208 834)A05.

UCB/EERC-83/18 "Interactive Computer Analysis Methods for Predicting the Inelastic Cyclic Behaviour of Structural Sections," by Kaba, S. and Mahin, S., July 1983, (PB84 192 012)A06.

UCB/EERC-83/19 "Effects of Bond Deterioration on Hysteretic Behavior of Reinforced Concrete Joints," by Filippou, F.C., Popov, E.P. and Bertero, V.V., August 1983, (PB84 192 020)A10.

UCB/EERC-83/20 "Correlation of Analytical and Experimental Responses of Large-Panel Precast Building Systems," by Oliva, M.G., Clough, R.W., Velkov, M. and Gavrilovic, P., May 1988, (PB90 262 692)A06.

UCB/EERC-83/21 "Mechanical Characteristics of Materials Used in a 1/5 Scale Model of a 7-Story Reinforced Concrete Test Structure," by Bertero, V.V., Aktan, A.E., Harris, H.G. and Chowdhury, A.A., October 1983, (PB84 193 697)A05.

UCB/EERC-83/22 "Hybrid Modelling of Soil-Structure Interaction in Layered Media," by Tzong, T.-J. and Penzien, J., October 1983, (PB84 192 178)A08.

UCB/EERC-83/23 "Local Bond Stress-Slip Relationships of Deformed Bars under Generalized Excitations," by Eligehausen, R., Popov, E.P. and Bertero, V.V., October 1983, (PB84 192 848)A09.

UCB/EERC-83/24 "Design Considerations for Shear Links in Eccentrically Braced Frames," by Malley, J.O. and Popov, E.P., November 1983, (PB84 192 186)A07.

UCB/EERC-84/01 "Pseudodynamic Test Method for Seismic Performance Evaluation: Theory and Implementation," by Shing, P.-S.B. and Mahin, S.A., January 1984, (PB84 190 644)A08.

UCB/EERC-84/02 "Dynamic Response Behavior of Kiang Hong Dian Dam," by Clough, R.W., Chang, K.-T., Chen, H.-Q. and Stephen, R.M., April 1984, (PB84 209 402)A08.

UCB/EERC-84/03 "Refined Modelling of Reinforced Concrete Columns for Seismic Analysis," by Kaba, S.A. and Mahin, S.A., April 1984, (PB84 234 384)A06.

UCB/EERC-84/04 "A New Floor Response Spectrum Method for Seismic Analysis of Multiply Supported Secondary Systems," by Asfura, A. and Der Kiureghian, A., June 1984, (PB84 239 417)A06.

UCB/EERC-84/05 "Earthquake Simulation Tests and Associated Studies of a 1/5th-scale Model of a 7-Story R/C Frame-Wall Test Structure," by Bertero, V.V., Aktan, A.E., Charney, F.A. and Sause, R., June 1984, (PB84 239 409)A09.

UCB/EERC-84/06 "R/C Structural Walls: Seismic Design for Shear," by Aktan, A.E. and Bertero, V.V., 1984.

UCB/EERC-84/07 "Behavior of Interior and Exterior Flat-Plate Connections subjected to Inelastic Load Reversals," by Zee, H.L. and Moehle, J.P., August 1984, (PB86 117 629/AS)A07.

UCB/EERC-84/08 "Experimental Study of the Seismic Behavior of a Two-Story Flat-Plate Structure," by Moehle, J.P. and Diebold, J.W., August 1984, (PB86 122 553/AS)A12.

UCB/EERC-84/09 "Phenomenological Modeling of Steel Braces under Cyclic Loading," by Ikeda, K., Mahin, S.A. and Dermitzakis, S.N., May 1984, (PB86 132 198/AS)A08.

UCB/EERC-84/10 "Earthquake Analysis and Response of Concrete Gravity Dams," by Fenves, G. and Chopra, A.K., August 1984, (PB85 193 902/AS)A11.

UCB/EERC-84/11 "EAGD-84: A Computer Program for Earthquake Analysis of Concrete Gravity Dams," by Fenves, G. and Chopra, A.K., August 1984, (PB85 193 613/AS)A05.

UCB/EERC-84/12 "A Refined Physical Theory Model for Predicting the Seismic Behavior of Braced Steel Frames," by Ikeda, K. and Mahin, S.A., July 1984, (PB85 191 450/AS)A09.

UCB/EERC-84/13 "Earthquake Engineering Research at Berkeley - 1984," by , August 1984, (PB85 197 341/AS)A10.

UCB/EERC-84/14 "Moduli and Damping Factors for Dynamic Analyses of Cohesionless Soils," by Seed, H.B., Wong, R.T., Idriss, I.M. and Tokimatsu, K., September 1984, (PB85 191 468/AS)A04.

UCB/EERC-84/15 "The Influence of SPT Procedures in Soil Liquefaction Resistance Evaluations," by Seed, H.B., Tokimatsu, K., Harder, L.F. and Chung, R.M., October 1984, (PB85 191 732/AS)A04.

UCB/EERC-84/16 "Simplified Procedures for the Evaluation of Settlements in Sands Due to Earthquake Shaking," by Tokimatsu, K. and Seed, H.B., October 1984, (PB85 197 887/AS)A03.

UCB/EERC-84/17 "Evaluation of Energy Absorption Characteristics of Highway Bridges Under Seismic Conditions - Volume I (PB90 262 627)A16 and Volume II (Appendices) (PB90 262 635)A13," by Imbsen, R.A. and Penzien, J., September 1986.

UCB/EERC-84/18 "Structure-Foundation Interactions under Dynamic Loads," by Liu, W.D. and Penzien, J., November 1984, (PB87 124 889/AS)A11.

UCB/EERC-84/19 "Seismic Modelling of Deep Foundations," by Chen, C.-H. and Penzien, J., November 1984, (PB87 124 798/AS)A07.

UCB/EERC-84/20 "Dynamic Response Behavior of Quan Shui Dam," by Clough, R.W., Chang, K.-T., Chen, H.-Q., Stephen, R.M., Ghanaat, Y. and Qi, J.-H., November 1984, (PB86 115177/AS)A07.

UCB/EERC-85/01 "Simplified Methods of Analysis for Earthquake Resistant Design of Buildings," by Cruz, E.F. and Chopra, A.K., February 1985, (PB86 112299/AS)A12.

UCB/EERC-85/02 "Estimation of Seismic Wave Coherency and Rupture Velocity using the SMART 1 Strong-Motion Array Recordings," by Abrahamson, N.A., March 1985. (PB86 214 343)A07.

UCB/EERC-85/03 "Dynamic Properties of a Thirty Story Condominium Tower Building," by Stephen, R.M., Wilson, E.L. and Stander, N., April 1985, (PB86 118965/AS)A06.

UCB/EERC-85/04 "Development of Substructuring Techniques for On-Line Computer Controlled Seismic Performance Testing," by Dermitzakis, S. and Mahin, S., February 1985, (PB86 132941/AS)A08.

UCB/EERC-85/05 "A Simple Model for Reinforcing Bar Anchorages under Cyclic Excitations," by Filippou, F.C., March 1985, (PB86 112 919/AS)A05.

UCB/EERC-85/06 "Racking Behavior of Wood-framed Gypsum Panels under Dynamic Load," by Oliva, M.G., June 1985, (PB90 262 643)A04.

UCB/EERC-85/07 "Earthquake Analysis and Response of Concrete Arch Dams," by Fok, K.-L. and Chopra, A.K., June 1985, (PB86 139672/AS)A10.

UCB/EERC-85/08 "Effect of Inelastic Behavior on the Analysis and Design of Earthquake Resistant Structures," by Lin, J.P. and Mahin, S.A., June 1985, (PB86 135340/AS)A08.

UCB/EERC-85/09 "Earthquake Simulator Testing of a Base-Isolated Bridge Deck," by Kelly, J.M., Buckle, I.G. and Tsai, H.-C., January 1986, (PB87 124 152/AS)A06.

UCB/EERC-85/10 "Simplified Analysis for Earthquake Resistant Design of Concrete Gravity Dams," by Fenves, G. and Chopra, A.K., June 1986, (PB87 124 160/AS)A08.

UCB/EERC-85/11 "Dynamic Interaction Effects in Arch Dams," by Clough, R.W., Chang, K.-T., Chen, H.-Q. and Ghanaat, Y., October 1985, (PB86 135027/AS)A05.

UCB/EERC-85/12 "Dynamic Response of Long Valley Dam in the Mammoth Lake Earthquake Series of May 25-27, 1980," by Lai, S. and Seed, H.B., November 1985, (PB86 142304/AS)A05.

UCB/EERC-85/13 "A Methodology for Computer-Aided Design of Earthquake-Resistant Steel Structures," by Austin, M.A., Pister, K.S. and Mahin, S.A., December 1985, (PB86 159480/AS)A10 .

UCB/EERC-85/14 "Response of Tension-Leg Platforms to Vertical Seismic Excitations," by Liou, G.-S., Penzien, J. and Yeung, R.W., December 1985, (PB87 124 871/AS)A08.

UCB/EERC-85/15 "Cyclic Loading Tests of Masonry Single Piers: Volume 4 - Additional Tests with Height to Width Ratio of 1," by Sveinsson, B., McNiven, H.D. and Sucuoglu, H., December 1985.

UCB/EERC-85/16 "An Experimental Program for Studying the Dynamic Response of a Steel Frame with a Variety of Infill Partitions," by Yanev, B. and McNiven, H.D., December 1985, (PB90 262 676)A05.

UCB/EERC-86/01 "A Study of Seismically Resistant Eccentrically Braced Steel Frame Systems," by Kasai, K. and Popov, E.P., January 1986, (PB87 124 178/AS)A14.

UCB/EERC-86/02 "Design Problems in Soil Liquefaction," by Seed, H.B., February 1986, (PB87 124 186/AS)A03.

UCB/EERC-86/03 "Implications of Recent Earthquakes and Research on Earthquake-Resistant Design and Construction of Buildings," by Bertero, V.V., March 1986, (PB87 124 194/AS)A05.

UCB/EERC-86/04 "The Use of Load Dependent Vectors for Dynamic and Earthquake Analyses," by Leger, P., Wilson, E.L. and Clough, R.W., March 1986, (PB87 124 202/AS)A12.

UCB/EERC-86/05 "Two Beam-To-Column Web Connections," by Tsai, K.-C. and Popov, E.P., April 1986, (PB87 124 301/AS)A04.

UCB/EERC-86/06 "Determination of Penetration Resistance for Coarse-Grained Soils using the Becker Hammer Drill," by Harder, L.F. and Seed, H.B., May 1986, (PB87 124 210/AS)A07.

UCB/EERC-86/07 "A Mathematical Model for Predicting the Nonlinear Response of Unreinforced Masonry Walls to In-Plane Earthquake Excitations," by Mengi, Y. and McNiven, H.D., May 1986, (PB87 124 780/AS)A06.

UCB/EERC-86/08 "The 19 September 1985 Mexico Earthquake: Building Behavior," by Bertero, V.V., July 1986.

UCB/EERC-86/09 "EACD-3D: A Computer Program for Three-Dimensional Earthquake Analysis of Concrete Dams," by Fok, K.-L., Hall, J.F. and Chopra, A.K., July 1986, (PB87 124 228/AS)A08.

UCB/EERC-86/10 "Earthquake Simulation Tests and Associated Studies of a 0.3-Scale Model of a Six-Story Concentrically Braced Steel Structure," by Uang, C.-M. and Bertero, V.V., December 1986, (PB87 163 564/AS)A17.

UCB/EERC-86/11 "Mechanical Characteristics of Base Isolation Bearings for a Bridge Deck Model Test," by Kelly, J.M., Buckle, I.G. and Koh, C.-G., November 1987, (PB90 262 668)A04.

UCB/EERC-86/12 "Effects of Axial Load on Elastomeric Isolation Bearings," by Koh, C.-G. and Kelly, J.M., November 1987.

UCB/EERC-87/01 "The FPS Earthquake Resisting System: Experimental Report," by Zayas, V.A., Low, S.S. and Mahin, S.A., June 1987.

UCB/EERC-87/02 "Earthquake Simulator Tests and Associated Studies of a 0.3-Scale Model of a Six-Story Eccentrically Braced Steel Structure," by Whittaker, A., Uang, C.-M. and Bertero, V.V., July 1987.

UCB/EERC-87/03 "A Displacement Control and Uplift Restraint Device for Base-Isolated Structures," by Kelly, J.M., Griffith, M.C. and Aiken, I.D., April 1987.

UCB/EERC-87/04 "Earthquake Simulator Testing of a Combined Sliding Bearing and Rubber Bearing Isolation System," by Kelly, J.M. and Chalhoub, M.S., 1987.

UCB/EERC-87/05 "Three-Dimensional Inelastic Analysis of Reinforced Concrete Frame-Wall Structures," by Moazzami, S. and Bertero, V.V., May 1987.

UCB/EERC-87/06 "Experiments on Eccentrically Braced Frames with Composite Floors," by Ricles, J. and Popov, E., June 1987.

UCB/EERC-87/07 "Dynamic Analysis of Seismically Resistant Eccentrically Braced Frames," by Ricles, J. and Popov, E., June 1987.

UCB/EERC-87/08 "Undrained Cyclic Triaxial Testing of Gravels-The Effect of Membrane Compliance," by Evans, M.D. and Seed, H.B., July 1987.

UCB/EERC-87/09 "Hybrid Solution Techniques for Generalized Pseudo-Dynamic Testing," by Thewalt, C. and Mahin, S.A., July 1987.

UCB/EERC-87/10 "Ultimate Behavior of Butt Welded Splices in Heavy Rolled Steel Sections," by Bruneau, M., Mahin, S.A. and Popov, E.P., September 1987.

UCB/EERC-87/11 "Residual Strength of Sand from Dam Failures in the Chilean Earthquake of March 3, 1985," by De Alba, P., Seed, H.B., Retamal, E. and Seed, R.B., September 1987.

UCB/EERC-87/12 "Inelastic Seismic Response of Structures with Mass or Stiffness Eccentricities in Plan," by Bruneau, M. and Mahin, S.A., September 1987, (PB90 262 650)A14.

UCB/EERC-87/13 "CSTRUCT: An Interactive Computer Environment for the Design and Analysis of Earthquake Resistant Steel Structures," by Austin, M.A., Mahin, S.A. and Pister, K.S., September 1987.

UCB/EERC-87/14 "Experimental Study of Reinforced Concrete Columns Subjected to Multi-Axial Loading," by Low, S.S. and Moehle, J.P., September 1987.

UCB/EERC-87/15 "Relationships between Soil Conditions and Earthquake Ground Motions in Mexico City in the Earthquake of Sept. 19, 1985," by Seed, H.B., Romo, M.P., Sun, J., Jaime, A. and Lysmer, J., October 1987.

UCB/EERC-87/16 "Experimental Study of Seismic Response of R. C. Setback Buildings," by Shahrooz, B.M. and Moehle, J.P., October 1987.

UCB/EERC-87/17 "The Effect of Slabs on the Flexural Behavior of Beams," by Pantazopoulou, S.J. and Moehle, J.P., October 1987, (PB90 262 700)A07.

UCB/EERC-87/18 "Design Procedure for R-FBI Bearings," by Mostaghel, N. and Kelly, J.M., November 1987, (PB90 262 718)A04.

UCB/EERC-87/19 "Analytical Models for Predicting the Lateral Response of R C Shear Walls: Evaluation of their Reliability," by Vulcano, A. and Bertero, V.V., November 1987.

UCB/EERC-87/20 "Earthquake Response of Torsionally-Coupled Buildings," by Hejal, R. and Chopra, A.K., December 1987.

UCB/EERC-87/21 "Dynamic Reservoir Interaction with Monticello Dam," by Clough, R.W., Ghanaat, Y. and Qiu, X-F., December 1987.

UCB/EERC-87/22 "Strength Evaluation of Coarse-Grained Soils," by Siddiqi, F.H., Seed, R.B., Chan, C.K., Seed, H.B. and Pyke, R.M., December 1987.

UCB/EERC-88/01 "Seismic Behavior of Concentrically Braced Steel Frames," by Khatib, I., Mahin, S.A. and Pister, K.S., January 1988.

UCB/EERC-88/02 "Experimental Evaluation of Seismic Isolation of Medium-Rise Structures Subject to Uplift," by Griffith, M.C., Kelly, J.M., Coveney, V.A. and Koh, C.G., January 1988.

UCB/EERC-88/03 "Cyclic Behavior of Steel Double Angle Connections," by Astaneh-Asl, A. and Nader, M.N., January 1988.

UCB/EERC-88/04 "Re-evaluation of the Slide in the Lower San Fernando Dam in the Earthquake of Feb. 9, 1971," by Seed, H.B., Seed, R.B., Harder, L.F. and Jong, H.-L., April 1988.

UCB/EERC-88/05 "Experimental Evaluation of Seismic Isolation of a Nine-Story Braced Steel Frame Subject to Uplift," by Griffith, M.C., Kelly, J.M. and Aiken, I.D., May 1988.

UCB/EERC-88/06 "DRAIN-2DX User Guide.," by Allahabadi, R. and Powell, G.H., March 1988.

UCB/EERC-88/07 "Cylindrical Fluid Containers in Base-Isolated Structures," by Chalhoub, M.S. and Kelly, J.M. , April 1988.

UCB/EERC-88/08 "Analysis of Near-Source Waves: Separation of Wave Types using Strong Motion Array Recordings," by Darragh, R.B., June 1988.

UCB/EERC-88/09 "Alternatives to Standard Mode Superposition for Analysis of Non-Classically Damped Systems," by Kusainov, A.A. and Clough, R.W., June 1988.

UCB/EERC-88/10 "The Landslide at the Port of Nice on October 16, 1979," by Seed, H.B., Seed, R.B., Schlosser, F., Blondeau, F. and Juran, I., June 1988.

UCB/EERC-88/11 "Liquefaction Potential of Sand Deposits Under Low Levels of Excitation," by Carter, D.P. and Seed, H.B., August 1988.

UCB/EERC-88/12 "Nonlinear Analysis of Reinforced Concrete Frames Under Cyclic Load Reversals," by Filippou, F.C. and Issa, A., September 1988.

UCB/EERC-88/13 "Implications of Recorded Earthquake Ground Motions on Seismic Design of Building Structures," by Uang, C.-M. and Bertero, V.V., November 1988.

UCB/EERC-88/14 "An Experimental Study of the Behavior of Dual Steel Systems," by Whittaker, A.S. , Uang, C.-M. and Bertero, V.V., September 1988.

UCB/EERC-88/15 "Dynamic Moduli and Damping Ratios for Cohesive Soils," by Sun, J.I., Golesorkhi, R. and Seed, H.B., August 1988.

UCB/EERC-88/16 "Reinforced Concrete Flat Plates Under Lateral Load: An Experimental Study Including Biaxial Effects," by Pan, A. and Moehle, J., October 1988.

UCB/EERC-88/17 "Earthquake Engineering Research at Berkeley - 1988," by EERC, November 1988.

UCB/EERC-88/18 "Use of Energy as a Design Criterion in Earthquake-Resistant Design," by Uang, C.-M. and Bertero, V.V., November 1988.

UCB/EERC-88/19 "Steel Beam-Column Joints in Seismic Moment Resisting Frames," by Tsai, K.-C. and Popov, E.P., November 1988.

UCB/EERC-88/20 "Base Isolation in Japan, 1988," by Kelly, J.M., December 1988.

UCB/EERC-89/01 "Behavior of Long Links in Eccentrically Braced Frames," by Engelhardt, M.D. and Popov, E.P., January 1989.

UCB/EERC-89/02 "Earthquake Simulator Testing of Steel Plate Added Damping and Stiffness Elements," by Whittaker, A., Bertero, V.V., Alonso, J. and Thompson, C., January 1989.

UCB/EERC-89/03 "Implications of Site Effects in the Mexico City Earthquake of Sept. 19, 1985 for Earthquake-Resistant Design Criteria in the San Francisco Bay Area of California," by Seed, H.B. and Sun, J.I., March 1989.

UCB/EERC-89/04 "Earthquake Analysis and Response of Intake-Outlet Towers," by Goyal, A. and Chopra, A.K., July 1989.

UCB/EERC-89/05 "The 1985 Chile Earthquake: An Evaluation of Structural Requirements for Bearing Wall Buildings," by Wallace, J.W. and Moehle, J.P., July 1989.

UCB/EERC-89/06 "Effects of Spatial Variation of Ground Motions on Large Multiply-Supported Structures," by Hao, H., July 1989.

UCB/EERC-89/07 "EADAP - Enhanced Arch Dam Analysis Program: Users's Manual," by Ghanaat, Y. and Clough, R.W., August 1989.

UCB/EERC-89/08 "Seismic Performance of Steel Moment Frames Plastically Designed by Least Squares Stress Fields," by Ohi, K. and Mahin, S.A., August 1989.

UCB/EERC-89/09 "Feasibility and Performance Studies on Improving the Earthquake Resistance of New and Existing Buildings Using the Friction Pendulum System," by Zayas, V., Low, S., Mahin, S.A. and Bozzo, L., July 1989.

UCB/EERC-89/10 "Measurement and Elimination of Membrane Compliance Effects in Undrained Triaxial Testing," by Nicholson, P.G., Seed, R.B. and Anwar, H., September 1989.

UCB/EERC-89/11 "Static Tilt Behavior of Unanchored Cylindrical Tanks," by Lau, D.T. and Clough, R.W., September 1989.

UCB/EERC-89/12 "ADAP-88: A Computer Program for Nonlinear Earthquake Analysis of Concrete Arch Dams," by Fenves, G.L., Mojtahedi, S. and Reimer, R.B., September 1989.

UCB/EERC-89/13 "Mechanics of Low Shape Factor Elastomeric Seismic Isolation Bearings," by Aiken, I.D., Kelly, J.M. and Tajirian, F., December 1989.

UCB/EERC-89/14 "Preliminary Report on the Seismological and Engineering Aspects of the October 17, 1989 Santa Cruz (Loma Prieta) Earthquake," by EERC, October 1989.

UCB/EERC-89/15 "Experimental Studies of a Single Story Steel Structure Tested with Fixed, Semi-Rigid and Flexible Connections," by Nader, M.N. and Astaneh-Asl, A., August 1989.

UCB/EERC-89/16 "Collapse of the Cypress Street Viaduct as a Result of the Loma Prieta Earthquake," by Nims, D.K., Miranda, E., Aiken, I.D., Whittaker, A.S. and Bertero, V.V., November 1989.

UCB/EERC-90/01 "Mechanics of High-Shape Factor Elastomeric Seismic Isolation Bearings," by Kelly, J.M., Aiken, I.D. and Tajirian, F.F., March 1990.

UCB/EERC-90/02 "Javid's Paradox: The Influence of Preform on the Modes of Vibrating Beams," by Kelly, J.M., Sackman, J.L. and Javid, A., May 1990.

UCB/EERC-90/03 "Earthquake Simulator Testing and Analytical Studies of Two Energy-Absorbing Systems for Multistory Structures," by Aiken, I.D. and Kelly, J.M., October 1990.

UCB/EERC-90/04 "Damage to the San Francisco-Oakland Bay Bridge During the October 17, 1989 Earthquake," by Astaneh, A., June 1990.

UCB/EERC-90/05 "Preliminary Report on the Principal Geotechnical Aspects of the October 17, 1989 Loma Prieta Earthquake," by Seed, R.B., Dickenson, S.E., Riemer, M.F., Bray, J.D., Sitar, N., Mitchell, J.K., Idriss, I.M., Kayen, R.E., Kropp, A., Harder, L.F., Jr. and Power, M.S., April 1990.

UCB/EERC-90/06 "Models of Critical Regions in Reinforced Concrete Frames Under Seismic Excitations," by Zulfiqar, N. and Filippou, F., May 1990.

UCB/EERC-90/07 "A Unified Earthquake-Resistant Design Method for Steel Frames Using ARMA Models," by Takewaki, I., Conte, J.P., Mahin, S.A. and Pister, K.S., June 1990.

UCB/EERC-90/08 "Soil Conditions and Earthquake Hazard Mitigation in the Marina District of San Francisco," by Mitchell, J.K., Masood, T., Kayen, R.E. and Seed, R.B., May 1990.

UCB/EERC-90/09 "Influence of the Earthquake Ground Motion Process and Structural Properties on Response Characteristics of Simple Structures," by Conte, J.P., Pister, K.S. and Mahin, S.A., July 1990.

UCB/EERC-90/10 "Experimental Testing of the Resilient-Friction Base Isolation System," by Clark, P.W. and Kelly, J.M., July 1990.

UCB/EERC-90/11 "Seismic Hazard Analysis: Improved Models, Uncertainties and Sensitivities," by Araya, R. and Der Kiureghian, A., March 1988.

UCB/EERC-90/12 "Effects of Torsion on the Linear and Nonlinear Seismic Response of Structures," by Sedarat, H. and Bertero, V.V., September 1989.

UCB/EERC-90/13 "The Effects of Tectonic Movements on Stresses and Deformations in Earth Embankments," by Bray, J. D., Seed, R. B. and Seed, H. B., September 1989.

UCB/EERC-90/14 "Inelastic Seismic Response of One-Story, Asymmetric-Plan Systems," by Goel, R.K. and Chopra, A.K., October 1990.

UCB/EERC-90/15 "Dynamic Crack Propagation: A Model for Near-Field Ground Motion.," by Seyyedian, H. and Kelly, J.M., 1990.

UCB/EERC-90/16 "Sensitivity of Long-Period Response Spectra to System Initial Conditions," by Blasquez, R., Ventura, C. and Kelly, J.M., 1990.

UCB/EERC-90/17 "Behavior of Peak Values and Spectral Ordinates of Near-Source Strong Ground-Motion over a Dense Array," by Niazi, M., June 1990.

UCB/EERC-90/18 "Material Characterization of Elastomers used in Earthquake Base Isolation," by Papoulia, K.D. and Kelly, J.M., 1990.

UCB/EERC-90/19 "Cyclic Behavior of Steel Top-and-Bottom Plate Moment Connections," by Harriott, J.D. and Astaneh, A., August 1990.

UCB/EERC-90/20 "Seismic Response Evaluation of an Instrumented Six Story Steel Building," by Shen, J.-H. and Astaneh, A., December 1990.

UCB/EERC-90/21 "Observations and Implications of Tests on the Cypress Street Viaduct Test Structure," by Bollo, M. E., Mahin, S.A., Moehle, J.P., Stephen, R.M., and Qi, X., December 1990.